

1
H41-90
SUP

STATIC AND DYNAMIC ANALYSIS OF EARTH AND ROCKFILL DAMS

A THESIS

*submitted in fulfilment of the
requirements for the award of the degree
of*

DOCTOR OF PHILOSOPHY

in

EARTHQUAKE ENGINEERING

By

S. SUPPIAH



DEPARTMENT OF EARTHQUAKE ENGINEERING
UNIVERSITY OF ROORKEE
ROORKEE-247 667 (INDIA)

JUNE, 1990

CANDIDATE'S DECLARATION


I hereby certify that the work which is being presented in the thesis entitled, **STATIC AND DYNAMIC ANALYSIS OF EARTH AND ROCKFILL DAMS** in fulfillment of the requirement for the award of the Degree of Doctor of Philosophy submitted in the Department of Earthquake Engineering of the University is an authentic record of my own work carried out during the period from June 1981 to June 1990 under the supervision of Dr. A. R. Chandrasekaran, Dr. B. V. K. Lavania and Dr. K. G. Sharma.

This matter embodied in this thesis has not been submitted by me for the award of any other Degree.

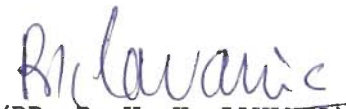


(SUBRAMANIAM SUPPIAH)
Candidate's Signature


This is to certify that the above statement made by the candidate is correct to the best of our knowledge.



(DR. A. R. CHANDRASEKARAN)
Professor
Department of Earthquake
Engineering
University of Roorkee
Roorkee - 247 667
(U. P) - India.



(DR. B. V. K. LAVANIA)
Professor and Head
Department of Earthquake
Engineering
University of Roorkee
Roorkee - 247 667
(U. P) - India.



(DR. K. G. SHARMA)
Professor
Civil Engineering
Department
I. I. T.
Hauz Khas
New Delhi - 110 016.

[Signature(s) of Supervisor(s)]

Date :

The Ph. D. Viva-Voce examination of Shri
Research Scholar has been held on

Signature of Guide(s)

Signature of External Examiner(s)

SYNOPSIS

The frequent occurrence of destructive earthquakes in the past in various places such as, Santa Barbara, USA (1906); Koyna, India (1967); San Fernando, USA (1971); Chile (1985) and other places, causing loss of thousands of lives and damage to dams and earth structures has demonstrated the need for earthquake resistant design of these structures. Failure of a dam during an earthquake would be very catastrophic and hence extreme care should be exercised in their design with respect to earthquake resistance. An earth and rockfill dam is considered to be a desirable type of dam in seismic regions due to its flexibility. Nevertheless, its design needs numerous considerations due to complex stress-strain characteristics of soil and rock which is generally not applicable for other types of dam. This has amply been demonstrated by the total collapse of the Sheffield Dam during the Santa Barbara earthquake of 1906 (Seed, Lee and Idriss, 1968), and the deformations and settlement that occurred in the near catastrophic failure of the Lower San Fernando Dam in California (USA), during the San Fernando earthquake of February 9, 1971 (Seed et al., 1973). In recent years, high rockfill dams of height of the order of more than 250 m are being increasingly constructed all over the world in regions of moderate to very strong seismicity. With the increase in the height of the rockfill

dam, proneness to failure and complexity in design also increase. This is due to the increase in height with an increase in the magnitude of confining pressure and due to the strength-deformation characteristics of the fill materials becoming nonlinear. In such cases, the stress-strain behaviour of the materials constituting the dam is essentially nonlinear (Dibaj and Penzien, 1969) and any attempt to evaluate the safety of a rockfill dam, based on a linear analysis, either in the static or dynamic condition, will only be misleading about the actual behaviour. In general, an embankment dam is a three-dimensional continuum composed of anisotropic, nonhomogenous, nonlinear, inelastic materials with rather complicated geometry, that is difficult to model accurately. The analysis of the dam becomes more complicated, when it is subjected to a severe earthquake with a peak ground acceleration of the order of $0.25g$ (g is the acceleration due to gravity) and above, since, its behaviour depends on the dynamic response of the different materials constituting the dam and the characteristics of the input motion. The shear modulus and damping ratios of the fill materials are strain dependent (Hardin and Drnevich, 1970a, 1970b; Seed and Idriss, 1970; Ishihara, 1971, 1982). Therefore, for a rational dynamic response evaluation of an earth and rockfill dam, the strain dependency of all the materials constituting the dam should effectively be implemented in a computer program using the finite element method, based on eight-noded isoparametric elements with

reduced integration technique (Ergatoudis, Irons and Zienkiewicz, 1968). This computer coding should be capable of modelling the nonlinear stress-strain behaviour of each of the materials as a function of strain. The nonlinear model adopted should predict the behaviour of the dam as closely as possible to the actual situation for an event of a strong ground shaking. The nonlinear stress-strain characteristics of each soil, as a function of strain, ranging between 10^{-6} to 1.0 percent or more could be achieved by carrying out extensive tests in the field and in the laboratory. To achieve this, the following procedures have been suggested/recommended in the available literature:

- 1 Using empirical equations proposed by Hardin and Drnevich (1970a, 1970b) for cohesive and cohesionless fill materials.
- 2 Determining the low-amplitude shear modulus in the field or in the laboratory and using modulus reduction factors as proposed by Seed and Idriss (1970), and Seed et al. (1984), to extrapolate high-amplitude shear moduli for clay, sand and cohesionless soils and using the normalized shear modulus curve for silty soils as proposed by Grant and Brown (1981).
- 3 Assuming the dynamic properties of gravels and boulders, based on the properties of sand (Seed and Idriss, 1970).
- 4 Classifying the different materials constituting the dam into two categories only, namely, clay and sand,

and arriving at the dynamic properties of these two type of materials (Seed and Idriss, 1970).

- 5 Assuming arbitrary and constant values for dynamic properties and neglecting the associated level of strain therein (Chandrasekaran, Paul and Suppiah, 1984, 1985; Chandrasekaran and Prakash, 1989b).

In the dynamic analysis, evaluating the dynamic properties of different soils, as mentioned above would never represent the true situation. The very few cases of nonlinear dynamic analyses performed in the recent years are limited to hydraulic fill dams (Seed, Lee and Idriss, 1968; Seed et al., 1973; Marcuson and Krinitzsky, 1976) and rockfill dams of medium height (Lai and Seed, 1985) only. Further, in these studies, the level of strain considered lies in the medium range and at the threshold values of large strain levels only. A limited number of dynamic analyses carried out in India (Chandrasekaran, Paul and Suppiah, 1984, 1985; Chandrasekaran and Prakash, 1989b), are based on linear and strain independent material characteristics only.

When a high rockfill dam is subjected to a strong earthquake, the induced level of strain would be in the range of large to failure strain values. Thus, an appropriate model, which could predict the actual behaviour of a high rockfill dam, supplemented by field tests is essential.

In view of the numerous shortcomings as mentioned above it was decided to carry out different types of tests in

the field, such as wave propagation test, block vibration test and cyclic plate load test, to establish the in-situ shear modulus values as a function of strain varying from low-strain level to medium strain level and then to large strain values for four different types of soils, namely, silt, clay, sand and gravel. Out of these four different types of materials, the last three types of soils typically represent the materials constituting a rockfill dam. These different types of field test are frequently carried out in India, to establish the strain dependent dynamic material properties (Prakash and his co-workers, 1968a, 1968b, 1970, 1971, 1972, 1973, 1974, 1975, 1976a, 1976b, 1980; IS: 5249, 1977; Nandakumaran et al., 1977, 1979, 1980; Prakash, 1981).

Shear modulus values have also been determined in the laboratory at high-amplitude strain levels only. The influence of secondary time effects on shear modulus values of three different types of soils has been established. Due to secondary time effects, an appreciable increase in the shear modulus values has been observed for clay and silty soils. The increase in shear moduli, due to secondary time effects is of the order of 4 to 28 percent, depending upon the type of soil. The percentage increase in shear moduli is higher for fine grained soils. The reported values are in close agreement with the values reported by other researchers (Affifi and Richart, 1973; Woods and Affifi, 1976; Anderson and Stokoe, 1978).

The high-amplitude shear modulus values obtained

in the field and in the laboratory corresponding to a particular value of strain have been compared and a relationship between these two values as a function of strain is presented. Based on this relationship, a factor, named as the disturbance factor (Suppiah, 1986) has been established. Using this factor, high-amplitude field shear modulus has been predicted for a particular site consisting of sand, for which in-situ shear modulus value is not available. The predicted value of shear modulus using the disturbance factor has been compared with the values obtained using other methods of prediction, presently used in the Geotechnical-Earthquake Engineering profession, such as the arithmetic method and the percentage method (Richart, Anderson and Stokoe, 1977; Anderson and Stokoe, 1978). The merits and demerits of the disturbance factor method have also been presented.

Using the field and laboratory determined shear moduli, shear modulus curves as a function of shear strain for the four different types of soils have been presented. Further, from these shear moduli, the Ramberg-Osgood model (Ramberg and Osgood, 1943) constants have been evaluated for all the four different types of soil based on the method originally proposed by Jennings (1964). The Ramberg-Osgood model parameters thus evaluated have been used to obtain modulus reduction curves as a function of strain for all the soils, through a computer program based on the Newton-Raphson root finding technique (Hinton and Owen, 1986). Using the

same constants of the Ramberg-Osgood model, damping ratio curves have also been presented, independent of the experimentally determined values of damping. The null value of damping obtained at the normalized shear modulus ratio ($G/G_{\max} = 1$) in the Ramberg-Osgood model, has been replaced by the experimentally determined value of damping, which had been interpolated from the medium strain levels to low strain values. The modulus reduction curves and the damping ratio curves presented for clay and sandy soils have been compared with the corresponding curves proposed by Seed and Idriss (1970), and with the modulus reduction curve of silty soil, as proposed by Grant and Brown (1981). From the comparison, it has been observed that the method proposed by Seed and Idriss (1970), which is widely being used in today's Geotechnical-Earthquake Engineering profession, yields low values of modulus reduction factors and low values of damping compared to the experimentally determined values reported in this thesis. Nevertheless, a close agreement has been noticed between the modulus reduction curve for silt as presented by Grant and Brown (1981), and the normalized shear modulus curve obtained for silty soil in the present study.

From the curve fitting of experimental data, it has been observed that the Ramberg-Osgood model can be best utilized for deriving the parameters for the curve that simulates the field determined values of shear modulus as closely as possible. Using the Ramberg-Osgood model parameters, damping values can also be obtained as a function

of strain without conducting experiments to evaluate damping. To verify the applicability of the shear modulus reduction curves and damping ratio curves obtained based on the Ramberg-Osgood model parameters of the present study, a case-history study has been performed. For the case-history analysis, the extensively instrumented El Infiernillo rock-fill Dam (Mexico) of height 146 m has been chosen and the dynamic stress-strain characteristics have been simulated based on the Ramberg-Osgood model as proposed in the present thesis.

Prior to the dynamic analysis, the pre-earthquake stresses in the El Infiernillo Dam have been evaluated using the nonlinear model based on the hyperbolic law (Kondner, 1963; Kondner and Zelasko, 1963), as proposed by Duncan and Chang, 1970; Duncan et al. (1980). This model has been implemented in a computer coding based on the finite element method, with the versatile, stable eight-noded isoparametric elements and reduced integration (2x2) technique as proposed by Ergatoudis, Irons and Zienkiewicz (1968). This computer coding can account for layer-wise construction sequence operation as well. The computed nonlinear static stresses have been used as the initial condition for the dynamic analysis (Kulhawy, Duncan and Seed, 1969; Lai and Seed, 1985).

For the dynamic analysis of the El Infiernillo Dam, three different accelerograms, namely, GM1, GM2 and GM3 have been selected as the base input motion. Accelerogram,

GM1 has been recorded during a recent earthquake in the North-Eastern Region of India (Chandrasekaran and Das, 1989), GM2 is an artificially generated record (Srivastava et al., 1983) and GM3 is the Taft (Kern County) earthquake record of 1952 (Idriss et al., 1973). The total durations of the three ground motions are 120, 38 and 30 seconds respectively. In the literature, an accelerogram with a total duration of 120 seconds has not been used till today for the dynamic analysis of an embankment dam (Prater and Studer, 1979). All the three ground motions have been normalized to a peak ground acceleration value of 0.25g. This has been done since the intensity of the base input motion of the March 14, 1979, Mexico earthquake record was also of the order of 0.25g only.

For performing the dynamic analysis, a computer coding based on the finite element method using the same type of eight-noded elements with reduced integration technique has been developed. The Ramberg-Osgood model, Hardin-Drnevich model and the Seed-Idriss method of simulating the stress-strain characteristics have been implemented in this computer coding. This program performs the dynamic analysis in the time domain based on the step-by-step integration scheme, as proposed by Newmark (1959). The variable damping technique, as proposed by Idriss et al. (1973), has also been implemented in the same computer program.

From the case-history study of the El Infiernillo Dam, based on the strain dependent modulus reduction curves obtained from experiments and the Ramberg-Osgood model

parameters as evaluated in the present thesis, the resulting values of crest accelerations, for the three ground motions, GM1, GM2 and GM3 are respectively of the order of 0.13g, 0.34g and 0.35g. Whereas, the recorded value of acceleration at the crest of the El Infiernillo Dam, due to the March 14, 1979, Mexico earthquake (Resendiz, Romo and Moreno, 1980) is of the order of 0.36g only. The peak ground acceleration value of the March 14, 1979, Mexico earthquake was 0.25g only. This demonstrates that the dynamic analysis as performed in the present thesis based on the Ramberg-Osgood model, predicts a behaviour that is very close to the actual situation in the event of a strong ground shaking. The material properties used in the present analysis are the same as that adopted by Romo et al. (1980).

Similar to the acceleration values, the computed displacement by the present analysis and the measured displacement at the crest, during the March 14, 1979, Mexico earthquake have been compared. For the Taft earthquake waveform, the computed displacement value at the crest by the analysis based on the Ramberg-Osgood model is 13.13 cm.

On the other hand, the measured value of crest displacement during the March 14, 1979, Mexico earthquake was approximately, 13 cm only (Resendiz, Romo and Moreno, 1980).

The close agreement between the computed value of crest displacement (= 13.13 cm) from the analysis based on the Ramberg-Osgood model and the measured displacement value (approximately, 13 cm) at the crest of the El Infiernillo

Dam, during the March 14, 1979, Mexico earthquake merits comments and demonstrates that the Ramberg-Osgood model is the most appropriate model to simulate nonlinear stress-strain characteristics of different soils subjected to seismic forces.

Using the Ramberg-Osgood model the displacement at the crest is of the order of 5.20 and 20.37 cm respectively for the other two ground motions (GM1 and GM2) adopted in the analysis.

For the purpose of comparison, the nonlinear dynamic analysis of the El Infiernillo Dam has been carried out by the Hardin-Drnevich model and the very widely used Seed-Idriss method as well. The computed values of the crest acceleration for the El Infiernillo rockfill Dam using the Hardin-Drnevich model and the Seed-Idriss method for the three ground motions respectively are 0.14g, 0.17g and 0.20g, and 0.79g, 0.41g and 0.51g. From the crest acceleration values obtained for the three ground motions, it can be noticed, that the Hardin-Drnevich model predicts extremely low values. This is perhaps, because the Hardin-Drnevich model converges to an excessively large value of damping of the order of 63.7 percent at large and failure levels of strain (Ishihara, 1982; Shamoto, 1984). On the other hand, the Seed-Idriss method yields very high values of crest acceleration for all the three ground motions. This could possibly be due to the usage of low values of damping.

Identically, the Hardin-Drnevich model yields

crest displacement of the order of 3.22, 14.17 and 7.39 cm respectively corresponding to the three ground motions. The Seed-Idriss method gives displacement values at the crest of the order of 8.38, 13.22 and 11.12 cm respectively, for the three ground motions. As can be seen from the computed and the measured displacement values, the Hardin-Drnevich model and the Seed-Idriss method do not predict the behaviour that is close to the actual situation. Therefore, as mentioned earlier the Ramberg-Osgood model is the most suitable method for the evaluation of dynamic response analysis of earth and earthfill structures.

In the dynamic analysis of the El Infiernillo Dam, the peak values of dynamic shear strain obtained using the Ramberg-Osgood model for the three ground motions are of the order of 1.097, 3.247 and 2.435 percent respectively and the values of total (= static + dynamic) shear strain are respectively of the order of 2.425, 4.434 and 3.734 percent, and occurring at 135.7 m from the base, under the postulated ground motion of 0.25g as the peak ground acceleration value. Using the Hardin-Drnevich model the maximum values of dynamic shear strain for the three ground motions are 1.930, 2.021 and 1.707 percent and the values of total shear strain are 2.450, 2.865 and 2.551 percent respectively. Based on the Seed-Idriss method the maximum values of dynamic shear strain are of the order of 1.782, 2.419 and 2.170 percent and the total values of shear strain are 2.459, 3.096 and 2.847 percent respectively, for the three ground motions and

occurring at element 242.

From the dynamic analysis of El Infiernillo Dam, it is seen that the artificial accelerogram is more severe followed by the Taft earthquake waveform and the North-Eastern earthquake record.

Under the postulated three ground motions with a peak ground acceleration of 0.25g, it has been observed that no portion of the El Infiernillo Dam reaches a five percent shear strain value which is the threshold level of failure (Marcuson and Krinitzsky, 1976). Therefore, the intensity of the artificial waveform has been modified to yield higher peak ground acceleration value of the order of 0.40g. Subsequently, dynamic analysis has been carried out with the re-generated ground motion as the base input motion. In the revised dynamic analysis, it has been observed, that the El Infiernillo Dam reaches a maximum value of dynamic shear strain of 13.016 percent and the peak value of total shear strain of the order of 13.860 percent and occurring at element 241. These values of shear strain lie in the threshold level of failure criteria based on the 5 to 15 percent shear strain phenomenon. This conclusion is qualitative in nature, since for an accurate prediction of the failure criteria, the laboratory determined cyclic shear stress values are inevitable and these values were not available for comparison.

To investigate the influence of the foundation on the stability of the El Infiernillo Dam, the initial maximum

section of this dam has been appended with a stiffer foundation of depth equal to 6.0 m. This modified section of the El Infiernillo Dam has subsequently been analysed to obtain the dynamic response using the artificial (GM2) accelerogram with a peak ground acceleration of 0.25g. The modified section inclusive of the foundation, resulted in marginally lower values of shear strain, in comparison to the shear strain values obtained from the analysis based on the dam without the foundation. Neglecting the minor differences in the values of shear strain between the two cases (with and without the foundation) of analyses, it was concluded, that the presence of a stiff foundation, practically has no influence on the stability of the dam.

The previously mentioned nonlinear static and nonlinear dynamic methods of analysis have been extended to evaluate the dynamic response of two other rockfill dams of height 108 m (Dam DB) and 336 m (Dam DC) inclusive of their respective foundations. These two rockfill dams (DB and DC) were proposed to be built in India, in two different regions with moderate and high seismicity respectively.

The base of the dam DB has been extended in the upstream and in the downstream by one time the width of the dam at the base (without the foundation). Thus the ratio of the width of the dam DB at the base (without the foundation) to that of the width at the bottom inclusive of the foundation was 1:3 (Franklin, 1987). Identically, the same proportion was adopted in the case of the dam DC as well. The

two dams DB and DC have been analysed using the Ramberg-Osgood model with the previously mentioned three ground motions as the earthquake load vectors. As before, for comparison purposes, the dynamic analysis has been done using the Hardin-Drnevich model and the Seed-Idriss method as well. Out of these two dams (DB and DC), the dam DC was the tallest (336 m) and was proposed to be constructed in a region with severe seismicity. The existing literature on the dynamic analysis of such a high rockfill dam is scanty, therefore, this dam has been subjected to an extensive dynamic response evaluation by computing the time-histories of acceleration, displacement and shear stress at a few important locations, using only the synthetic accelerogram as the base input motion, since, the artificial earthquake record was more severe than the other two actual earthquake records. As mentioned earlier, the dynamic analysis has been done using the Ramberg-Osgood and the Hardin-Drnevich models and the Seed-Idriss method.

From the dynamic analysis of the dam DB the values of the crest acceleration obtained using the Ramberg-Osgood model corresponding to the three ground motions are 0.39g, 0.42g and 0.40g respectively. Using the Hardin-Drnevich model the acceleration values obtained at the crest are 0.28g, 0.31g and 0.27g and that for the Seed-Idriss method of analysis these values are 0.46g, 0.50g and 0.56g respectively for the three ground motions.

The maximum values of dynamic shear strain

obtained using the Ramberg-Osgood model for the dam DB are 0.175, 0.342 and 0.242 percent and the total values of shear strain are 1.875, 2.042 and 1.942 percent, respectively and taking place at element 84, for the three ground motions. Using the Hardin-Drnevich model the maximum dynamic shear strain values are 0.140, 0.308 and 0.201 percent and the total values of shear strain are 1.840, 2.008 and 1.901 percent respectively, for the three ground motions and occurring at the same location as in the case of the Ramberg-Osgood model.

Using the Seed-Idriss method the maximum values of dynamic shear strain are of the order of 0.200, 0.324 and 0.198 percent and the total values of shear strain are 1.854, 1.978 and 1.852 percent respectively, corresponding to the three ground motions and occurring at element 94, unlike in the other two models.

The displacement at the crest of the dam DB by the Ramberg-Osgood model using the three ground motions are 7.10, 12.27 and 10.59 cm respectively. Using the Hardin-Drnevich model and the Seed-Idriss method, the displacement at the crest for the three ground motions are 4.11, 8.42 and 6.57 cm and 9.83, 17.43 and 11.72 cm respectively.

In all the three ground motions, except in one case (the Seed-Idriss method and the Taft accelerogram), it was noticed that the maximum value of acceleration, maximum value of shear strain and the maximum displacement value are obtained corresponding to the artificial waveform as the base

input motion with a peak ground acceleration of 0.25g.

Since the dam DB did not undergo any excessive deformation at any part under the postulated three ground motions with a peak ground acceleration of 0.25g and the artificial accelerogram is more stronger than the other two actually recorded accelerograms, as before a revised dynamic analysis has been performed using the Ramberg-Osgood model and the modified artificial waveform as the base input motion with a peak ground acceleration of 0.40g. From the revised dynamic analysis the peak values of dynamic shear strain and the total shear strain are of the order of 3.680 and 5.380 percent respectively and taking place at element 84. Thus, it has been observed that the dam DB is generally safe under the postulated peak ground acceleration of 0.40g as well, based on the 5 percent shear strain failure criteria (Marcuson and Krinitzsky, 1976).

However, this conclusion is qualitative only, since for an exact prediction of failure criterion, the laboratory determined cyclic shear stress values were not available.

Similarly, from the dynamic analysis of dam DC the maximum values of crest acceleration using the Ramberg-Osgood model for the three ground motions with peak ground acceleration as 0.25g are 0.17g, 0.33g and 0.32g respectively, obtained at node 48 which is lying along the axis of the dam and is just below the crest. For the Hardin-Drnevich model these values are 0.12g, 0.16g and 0.17g respectively for the

three ground motions occurring at the same location as in the case of the Ramberg-Osgood model. Using the Seed-Idriss method, the crest acceleration values are of the order of 0.32g, 0.37g and 0.36g respectively for the three ground motions, obtained at node 23 lying along the crest (downstream).

The maximum values of dynamic shear strain using the Ramberg-Osgood model for the three ground motions with peak ground acceleration as 0.25g are of the order of 0.542, 8.491 and 3.265 percent respectively and the values of total shear strain are 4.013, 10.162 and 4.936 percent respectively occurring at the same elevation. Using the Hardin-Drnevich model the maximum values of dynamic shear strain for the three ground motions are 1.829, 2.739 and 2.251 percent respectively and the total values of shear strain are 3.918, 4.757 and 4.269 percent respectively.

Based on the Seed-Idriss method of analysis the maximum values of dynamic shear strain are 2.712, 6.137 and 3.067 percent and the total values of shear strain are 4.383, 7.808 and 4.738 percent respectively for the three base input motions and occurring at element 199 which is at a height of 328.0 metres from the base.

The displacement at the crest of the dam DC, using the Ramberg-Osgood model for the three ground motions with peak ground acceleration as 0.25g are 6.91, 49.26 and 20.50 cm respectively. For the Hardin-Drnevich model using the three ground motions the crest displacement is of the order

of 5.99, 27.55 and 13.66 cm respectively. The displacement using the Seed-Idriss method of analysis is of the order of 9.02, 20.85 and 15.69 cm for the three ground motions respectively.

From the dynamic analysis of the dam DC irrespective of the method of analysis adopted, it is seen that the artificial accelerogram is more severe than the other two actually recorded waveforms.

Since the dam DC did not reach the threshold level of failure under the postulated peak ground acceleration value of 0.25g for the three ground motions and as before the artificial waveform was more severe than the other two accelerograms, to evaluate the stability of the dam DC a revised dynamic analysis has been performed using the Ramberg-Osgood model and the synthetic accelerogram as base input motion modified to yield a peak ground acceleration value of 0.40g. In this revised analysis the peak values of dynamic shear strain and total shear strain obtained are of the order of 12.325 and 13.996 percent respectively and taking place at the same elevation as before (element 199). In this dynamic analysis, it has been observed that under the postulated artificial accelerogram with the peak ground acceleration value of 0.40g, a major portion of the dam DC reaches the threshold level of failure (value of shear strain is between 5 to 15 percent, Marcuson and Krinitzsky, 1976).

From the extensive dynamic analysis performed on three different dam sections of varying geometry, three diff-

erent ground motions of varying durations and three different methods of analysis, it is again demonstrated that the Hardin-Drnevich model yields very low values of crest acceleration and the Seed-Idriss method of analysis gives excessively high values of acceleration as compared to the proposed method of analysis based on the Ramberg-Osgood model which predicts crest acceleration values and displacement values which are in close agreement with the actually recorded/measured values of acceleration/displacement during the March 14, 1979, Mexico earthquake as demonstrated in the case-history analysis of the El Infiernillo Dam.

Also, as far as the cost of the computer time is concerned, the Ramberg-Osgood and Hardin-Drnevich models need approximately 50 percent less time than the Seed-Idriss method, which shows that the latter method is uneconomical as well.

From the extensive dynamic analysis carried out, it has been observed that the Hardin-Drnevich model which is based on the hyperbolic law is not suitable for the dynamic response evaluation of embankment dams and as well the Seed-Idriss method based on empirical equations for predicting the strain dependent shear moduli and damping ratios does not provide a rational solution.

The Ramberg-Osgood model represents the nonlinear material properties, such as the strain dependent shear modulus and damping values in a functional form which is very essential for a nonlinear dynamic analysis based on the step-

by-step integration technique. However, the Seed-Idriss method does not employ a functional expression to represent these dynamic properties and therefore, may not be utilized efficiently for a nonlinear dynamic analysis of an earth or earthfill structure.

As noticed previously, the response of an earth and rockfill dam is a function of the geometry of the structure, nature of the foundation material, zoning of the dam body, strain dependent dynamic properties of the various constituting materials and the characteristics of the base input motion. Thus, to outline an approach that could predict the response of a complicated structure, such as an earth and rockfill dam as closely as possible to the actual situation, in the event of a severe ground shaking is a tedious effort.

The investigation presented in this thesis demonstrates that in the event of a strong ground motion, the proposed method based on the versatile Ramberg-Osgood model can predict the dynamic behaviour of an earth and rockfill dam as closely as possible to the actual condition.

Therefore, in view of the findings of the present thesis, for a rational dynamic response evaluation of an earth structure, only the Ramberg-Osgood model should be used.

ACKNOWLEDGEMENT

At the outset, I wish to thank Dr. B. K. Gairola, Additional Director, National Informatics Centre, New Delhi, for his unlimited help and advice, without which the present study is impossible. Dr. Gairola, a philosopher and an excellent guide. My sincere thanks are due to Professors, A. R. Chandrasekaran, B. V. K. Lavania and K. G. Sharma for their constant help during the course of this investigation.

Sincere thanks are also accorded to Dr. P. Nandakumaran (formerly Professor, Department of Earthquake Engineering, Roorkee), Dr. V. K. Puri (formerly Reader, Department of Earthquake Engineering, Roorkee), Professor Mani Kant Gupta and Mr. S. Mukerjee with whom I have participated/worked in various projects, since I was a student at the Department of Earthquake Engineering, University of Roorkee, Roorkee, and for their kind generosity to use experimental data in this investigation.

Sincere thanks are due to Mr. Messon, Mr. Subodh Jain, Mr. G. R. Agrawal and Mr. Rajendar Kumar of the Soil Dynamics Laboratory and all the staff of the Workshop of the Department of Earthquake Engineering, Roorkee, for their unconditional help during the field and laboratory investigations. Also, thanks are due to Mr. S. C. Sharma, Mr. Lax Man Singh and Mr. Jagdish Prasad of the Drawing Section of the Department of Earthquake Engineering, Roorkee.

My Sincere gratitude is accorded to the following professionals who have rendered unlimited help during the course of this thesis.

Dr. F. Nadim of Norwegian Geotechnical Institute, Norway; Professor Kenji Ishihara of University of Tokyo, Tokyo (Japan); Professor (late) H. B. Seed of University of California, Berkeley (USA); Professor James M. Duncan of University of California, Berkeley (USA); Professor W. O. Keightley of Montana State University (USA); Dr. Arney G. Franklin of Waterways Experiment Station (USA); Professors Kenneth H. Stokoe II and Vincent P. Hardin of University of Kentucky, Kentucky (USA); Dr. R. Kuberan and Mr. A. K. Dhawan of Central Soils and Materials Research Station, Hauz Khas, New Delhi, Professor Shamsheer Pakash of University of Missouri, Rolla (USA); Professor G. I. Prajapati of the Department of Earthquake Engineering and Mr. A. B. Palaniappan, Scientist, National Institute of Hydrology.

My sincere gratitude is accorded to Mr. A. D. Pandey, Reader, Department of Earthquake Engineering, University of Roorkee, Roorkee, for preparing numerous figures.

Finally, my sincere thanks are accorded to Mr. Om Prakash, Mrs. B. Kuberan, Mrs. S. Seema, Mrs. G. Palaniappan, Mrs. Dhawan and others who have rendered their help either directly or indirectly during the course of this investigation.

CONTENTS

SYNOPSIS	(i)
ACKNOWLEDGEMENT	(xxii)
CONTENTS	(xxiv)
List of Figures	(xxxii)
List of Tables	(xlili)
CHAPTER 1 - INTRODUCTION	1
1.1 GENERAL	1
1.2 STRESS-STRAIN CHARACTERISTICS	3
1.2.1 Simulation of Stress-Strain Characteristics of Soils	5
1.3 EARTH AND ROCKFILL DAMS	6
1.3.1 Static Analysis	6
1.3.2 Dynamic Analysis	7
1.4 OBJECTIVES	8
1.5 ORGANIZATION OF THE THESIS	9
CHAPTER 2 - PREVIOUS WORK	12
2.1 GENERAL	12
2.2 SHEAR MODULUS	12
2.2.1 Factors Affecting Shear Modulus	12
2.3.6 Field and Laboratory Determination of Shear Moduli	26
2.4 DAMPING OF SOILS	30
2.4.1 Parameters Affecting Damping of Soils	30
2.4.2 Damping from Empirical Equations	30
2.5 SECONDARY TIME EFFECTS ON SHEAR MODULUS	34
2.5.1 Secondary Time Effects on Clay Minerals	34
2.5.2 Influence of Duration of Confining Pressure	36
2.6 PREDICTION OF IN-SITU SHEAR MODULUS	38
2.7 NONLINEAR STRESS-STRAIN MODELS	41

2.7.1	Hardin-Drnevich Model	43
2.7.2	Ramberg-Osgood Model	47
2.7.3	Hysteresis Loop Criteria	48
2.7.4	Ramberg-Osgood Hysteretic Damping Value	49
2.7.5	Application of Ramberg-Osgood Model	49
2.7.6	Modifications to Ramberg-Osgood Model	50
2.7.7	Comparison Between Hardin-Drnevich and Ramberg-Osgood Models	52
2.8	ANALYSIS OF EMBANKMENT DAMS USING FINITE ELEMENT METHOD	57
2.8.1	Static Analysis	57
2.8.2	Dynamic Analysis	60
2.9	CLOSURE	74
CHAPTER 3 - FIELD AND LABORATORY TESTS		77
3.1	GENERAL	77
3.2	FIELD TESTS	78
3.2.1	Wave Propagation Test	78
3.2.2	Block Vibration Test	79
3.2.2.1	Forced vertical vibration test	81
3.2.2.2	Forced horizontal vibration test	81
3.2.3	Free Vibration Test	81
3.2.4	Cyclic Plate Load Test	82
3.3	LABORATORY TESTS	83
3.3.1	Oscillatory Shear Test	84
3.2.3	Simple Shear Test	85
3.4	DAMPING RATIO	85
3.5	CLOSURE	87

CHAPTER 4 - PRESENTATION OF TEST RESULTS	88
4.1 GENERAL	88
4.1 RESULTS OF FIELD TESTS	88
4.2.1 Wave Propagation Test	89
4.2.2 Block Vibration Test	90
4.2.2.1 Forced vertical vibration test	90
4.2.2.2 Forced horizontal vibration test	102
4.2.2.3 Free vibration test in the vertical direction	107
4.2.2.4 Free vibration test in horizontal direction	108
4.2.3 Cyclic Plate Load Test	108
4.2.4 Damping Values from Field Tests	110
4.2.4.1 Damping values from forced-vibration test	111
4.2.4.2 Damping from forced horizontal vibration test	112
4.2.6 Damping from Free-Vibration Tests	113
4.3 RESULTS OF LABORATORY TESTS	113
4.3.1 Oscillatory Shear Test	115
4.3.2 Simple Shear Test	116
4.5 CLOSURE	119
CHAPTER 5 - DISCUSSION AND INTERPRETATION OF TEST RESULTS	120
5.1 GENERAL	120
5.2 SHEAR MODULUS	121
5.2.1 Relation between Field and Laboratory Shear Moduli	121
5.2.2 Verification of the Disturbance Factor Method	127
5.2.2.1 Methods proposed by Anderson and Stokoe	129
(a) Arithmetic method	130
(b) Percentage method	130
5.2.2.2 Method proposed in the present study	131

5.2.3	Advantages and Disadvantages of the Disturbance Factor Method	134
5.3	DAMPING VALUE	134
5.4	SECONDARY TIME EFFECTS ON SHEAR MODULUS	136
5.5	RAMBERG-OSGOOD MODEL	136
5.5.1	Ramberg-Osgood Curve Theory	137
5.5.2	Least-Squares Curve Fitting Technique	140
5.5.3	Normalized Values of Shear Modulus	140
5.5.4	Comparison with Other Available Data	143
5.5.5	Damping Values	145
5.6	CLOSURE	147
CHAPTER 6 - FINITE ELEMENT FORMULATION		148
6.1	GENERAL	148
6.2	FINITE ELEMENT METHOD	149
	(a) Static analysis	150
	(b) Dynamic analysis	150
6.2.1	Eight-Noded Isoparametric Element	150
6.2.2	Selection of Displacement or Interpolation Function	151
6.2.3	Strain-Displacement Relationship	155
6.2.4	Stress-Strain Relationship	156
6.2.5	Equilibrium Equations	157
6.2.6	Jacobian Matrix	159
6.2.7	Element Stiffness Matrix	159
6.2.9	Global Stiffness Matrix	161
6.3	FINITE ELEMENT FORMULATION OF NONLINEAR STATIC PROBLEM	161

6.3.1	Successive Approximation or Secant Modulus Method	162
6.3.2	Successive Increment or Tangent Modulus Method	162
6.3.4	Sequential or Incremental Construction Method	168
6.4	FORMULATION WITH RESPECT TO DYNAMIC ANALYSIS	172
6.4.1	Stiffness Matrix	173
6.4.2	Mass Matrix	173
6.4.3	Damping Matrix	175
6.4.5	Step-by-Step Integration Scheme	178
6.5	CLOSURE	183
CHAPTER 7 - DEVELOPMENT OF COMPUTER PROGRAMS		184
7.1	GENERAL	184
7.2	COMPUTER PROGRAM FOR STATIC ANALYSIS	186
7.2.1	Program Operation	186
7.2.2	Verification of FEABANS	189
7.3	COMPUTER PROGRAM FOR DYNAMIC ANALYSIS	190
7.3.1	Organization of FEADYNS	196
7.3.2	Verification of FEADYNS	198
7.4	CLOSURE	205
CHAPTER 8 - ANALYSIS		206
8.1	GENERAL	206
8.2	DESCRIPTION OF THE THREE ROCKFILL DAMS	207
8.2.1	El Infiernillo Dam (Dam DA)	207
8.3	NONLINEAR STATIC ANALYSIS	208
8.3.1	Discretization	208
8.4	DYNAMIC ANALYSIS	213

8.4.1	Material Properties for Dynamic Analysis	213
8.4.2	Earthquake Records for Dynamic Analysis	213
8.4.3	Dynamic Analysis Based on Ramberg-Osgood Model	215
8.4.4	Dynamic Analysis Based on Hardin-Drnevich Model	222
8.4.5	Dynamic Analysis Based on Seed-Idriss Method	224
8.5	RESPONSE EVALUATION OF EL INFIERNILLO DAM	226
8.6	ANALYSIS AND DISCUSSION OF RESULTS	231
8.6.1	Acceleration Values	231
8.6.1.1	Acceleration values using Ramberg-Osgood model	231
8.6.1.2	Acceleration values using Hardin-Drnevich model	238
8.6.1.3	Acceleration values using Seed-Idriss method	242
8.6.2	Shear Strain Values	246
8.6.2.1	Analysis by Ramberg-Osgood model	250
8.6.2.2	Analysis by Hardin-Drnevich model	250
8.6.2.3	Analysis by Seed-Idriss method	251
8.6.3	Displacement	251
8.6.4	Discussion	252
8.6.4.1	Acceleration values	252
8.6.4.2	Comparison of computed and recorded acceleration values	
8.6.4.3	Shear strain values	264
8.6.4.4	Comparison of computed and measured crest displacement	265
8.7	EVALUATION OF STABILITY OF EI INFIERNILLO DAM	266
8.8	EFFECT OF FOUNDATION	268
8.8.1	Shear Strain Values	269
8.9	COMMENTS ON THE ANALYSIS OF EI INFIERNILLO DAM	272
8.10	ANALYSIS OF ROCKFILL DAM DB	275

8.10.1 Nonlinear Static Analysis of Dam DB	275
8.10.2 Finite Element Idealization	278
8.10.3 Dynamic Analysis of Dam DB	278
8.10.4 Results and Discussion on Dam DB	282
8.10.4.1 Acceleration values	292
8.10.4.2 Shear strain values	302
8.10.4.3 Displacement	307
8.10.5 Comments on the Analysis of Dam DB	318
8.11 ANALYSIS OF ROCKFILL DAM DC	320
8.11.1 Description of Dam DC	321
8.11.2 Nonlinear Static Analysis	321
8.11.3 Discretization	321
8.11.4 Material Properties	323
8.11.5 Results of Nonlinear Static Analysis	327
8.11.6 Dynamic Analysis of Dam DC	327
8.11.7 Results of Dynamic Analysis	335
8.11.8 Discussion	344
8.11.8.1 Acceleration	382
8.11.8.2 Shear strain	392
8.11.8.3 Displacement	400
8.11.8.4 Time-history of acceleration	400
8.11.8.5 Time-history of shear stress	412
8.11.9 Comments on the Analysis of Dam DC	415
8.12 CLOSURE	418

CHAPTER 9 - CONCLUSIONS AND RECOMMENDATIONS	426
9.1 GENERAL	426
9.2 CONCLUSIONS	430
9.2.1 Shear Modulus	430
9.2.1.1 Secondary time effects on shear modulus	430
9.2.1.2 Relation between field and laboratory determined shear moduli	431
9.2.1.3 Prediction of in-situ high-amplitude shear modulus	431
9.2.2 Nonlinear Dynamic Stress-Strain Relationship	432
9.2.2.1 Ramberg-Osgood model	432
9.2.2.2 Hardin-Drnevich model	433
9.2.2.3 Seed-Idriss method	433
9.2.3 Computer Programs	434
9.2.4 Nonlinear Static Analysis	434
9.2.5 Nonlinear Dynamic Analysis	435
9.3 SUGGESTIONS FOR FURTHER WORK	438
9.3.1 Dynamic Properties of Soils	438
9.3.2 Nonlinear Static Stress-Strain Models	438
9.3.3 Nonlinear Dynamic Stress-Strain Model	440
9.4 SIGNIFICANT CONTRIBUTIONS	440
9.5 MISCELLANEOUS	442
9.5.1 Shear Wave Velocity in Rockfill Dams	442
9.5.2 Shape of Valley	442
9.5.3 Three-Dimensional Analysis	442
REFERENCES	443
VITA	475

Figure	Description	Page
1.1	Influence of Strain on Various Factors	4
2.1	Shear Moduli of Sands at Different Relative Densities	18
2.2	Normalized Shear Modulus Curve for Sand	19
2.3	Shear Modulus for Clay Soils	21
2.4	Modulus Reduction Curve for Clay Soils	22
2.5	Modulus Reduction Curves for Granular Materials	23
2.6	Normalized Shear Moduli for Stiff Clay/Silt	24
2.7	Normalized Shear Moduli for Hard Clay/Silt	25
2.8	Dynamic Shear Modulus Curve	28
2.9	Shear Modulus Curves for Different Sites in India	29
2.10	Damping Ratio Curves for Sand	32
2.11	Damping Ratio Curves for Saturated Clays	33
2.12	Variation of Shear Wave Velocity with Time at Constant Confining Pressures	37
2.13	Predicted Field Curve	42
2.14	Comparison of Predicted Shear Modulus Values	42
2.15	Basic Parameters for Hyperbolic Model	45
2.16	Hyperbolic Stress-Strain Curves for Sand and Clay	45
2.17	Hyperbolic Strain Relating Normalized Values of Shear Modulus and Damping	46
2.18	Fit of Hardin-Drnevich and Ramberg-Osgood Models	53
2.19	Approximate Values of Reference Strain and Failure Strain	56
2.20	Sheffield Dam Cross Section	62
2.21	Embankment Dams Analysed	65
3.1	Block Vibration Test Set-up	80
3.2	Oscillatory Shear Box Apparatus	86
4.1	Wave Propagation Test Record (Site A)	91

4.2	Travel Time Versus Distance Relationship (Site A)	91
4.3	Vertical Vibration Test Record (Site A)	96
4.4	Amplitude Versus Frequency Relationship from Forced Vertical Vibration Test (Site A)	98
4.5	Amplitude Versus Frequency Relationship from Forced Horizontal Vibration Test (Site A)	104
4.6	Free-Vibration Test Record: Vertical Direction (Site A)	107
4.7	Load Versus Settlement Relationship (Site A)	109
4.8	Elastic Settlement Versus Intensity of Loading (Site A)	109
4.9	Oscillatory Shear Test Record (Site A)	116
5.1	Shear Moduli from Field and Laboratory Tests (Site A)	123
5.2	Disturbance Factors Determined Before the Beginning of Primary Consolidation	126
5.3	Disturbance Factors Determined at the end of Primary Consolidation	126
5.4	Problem Considered by Anderson and Stokoe	128
5.5	Damping Ratio Based on Experiments	135
5.6	Ramberg-Osgood Curve Theory	138
5.7	Comparison of Normalized Values of Shear Modulus	144
5.8	Comparison of Damping Values	146
6.1	An Eight-Noded Element with Shape Functions	154
6.2	Hyperbolic Representation of Stress-Strain Curve	164
6.3	Transformed Hyperbolic Representation	164
6.4	In-situ Stresses at Initial State	171
6.5	Stresses at the End of First Lift	171
6.6	Stresses at the End of i th Layer	171
6.7	Newmark's Constant Average Acceleration Method	179
7.1	Flow Chart for FEABANS	187

7.2	Finite Element Idealization using 4- Noded Elements	191
7.3	Finite Element Idealization using 8- Noded Elements	193
7.4	Flow Chart for FEADYNS	195
7.5	Finite Element Idealization of the Soil Column based 4- and 8- Noded Elements	199
7.6	Damping and Modulus Values Used in the Soil Column	200
7.7	Comparison of Shear Stress and Acceleration Values of the Soil Column	204
8.1	Maximum Section of El Infiernillo Dam	209
8.2	Idealized Maximum Section of El Infiernillo Dam	210
8.3	Finite Element Idealization of El Infiernillo Dam	212
8.4	Accelerogram of GM1	216
8.5	Response Spectra for GM1	217
8.6	Accelerogram of GM2	218
8.7	Response Spectra for GM2	219
8.8	Accelerogram of GM3	220
8.9	Response Spectra for GM3	221
8.10	Concept of Reference Strain	223
8.11	El Infiernillo Dam; Node Numbers at which Acceleration Values are Tabulated	227
8.12	El Infiernillo Dam; Element Numbers at which Shear Strain Values are Tabulated	232
8.13	El Infiernillo Dam; Amplified Acceleration Values at a few Locations; R-O Model; GM1	239
8.14	El Infiernillo Dam; Amplified Acceleration Values at a few Locations; R-O Model; GM2	240
8.15	El Infiernillo Dam; Amplified Acceleration Values at a few Locations; R-O Model; GM3	241
8.16	El Infiernillo Dam; Amplified Acceleration Values at a few Locations; H-D Model; GM1	243

8.17	El Infiernillo Dam; Amplified Acceleration Values at a few Locations; H-D Model; GM2	244
8.18	El Infiernillo Dam; Amplified Acceleration Values at a few Locations; H-D Model; GM3	245
8.19	El Infiernillo Dam; Amplified Acceleration Values at a few Locations; S-I Method; GM1	247
8.20	El Infiernillo Dam; Amplified Acceleration Values at a few Locations; S-I Method; GM2	248
8.21	El Infiernillo Dam; Amplified Acceleration Values at a few Locations; S-I Method; GM3	249
8.22	El Infiernillo Dam; Displacement Values at a few Locations; R-O Model; GM1	253
8.23	El Infiernillo Dam; Displacement Values at a few Locations; R-O Model; GM2	254
8.24	El Infiernillo Dam; Displacement Values at a few Locations; R-O Model; GM3	255
8.25	El Infiernillo Dam; Displacement Values at a few Locations; H-D Model; GM1	256
8.26	El Infiernillo Dam; Displacement Values at a few Locations; H-D Model; GM2	257
8.27	El Infiernillo Dam; Displacement Values at a few Locations; H-D Model; GM3	258
8.28	El Infiernillo Dam; Displacement Values at a few Locations; S-I Method; GM1	259
8.29	El Infiernillo Dam; Displacement Values at a few Locations; S-I Method; GM2	260
8.30	El Infiernillo Dam; Displacement Values at a few Locations; S-I Method; GM3	261
8.31	El Infiernillo Dam Discretization with its Foundation	270
8.32	Maximum Section of Dam DB	276
8.33	Finite Element Idealization of Dam DB	279
8.34	Dam DB; Nodes at which Acceleration Values are Tabulated	284

8.35	Dam DB; Elements at which Shear Strain Values are Tabulated	285
8.36	Dam DB; Amplified Acceleration Values at a few Locations; R-O Model; GM1	295
8.37	Dam DB; Amplified Acceleration Values at a few Locations; R-O Model; GM2	296
8.38	Dam DB; Amplified Acceleration Values at a few Locations; R-O Model; GM3	297
8.39	Dam DB; Amplified Acceleration Values at a few Locations; H-D Model; GM1	299
8.40	Dam DB; Amplified Acceleration Values at a few Locations; H-D Model; GM2	300
8.41	Dam DB; Amplified Acceleration Values at a few Locations; H-D Model; GM3	301
8.42	Dam DB; Amplified Acceleration Values at a few Locations; S-I Method; GM1	303
8.43	Dam DB; Amplified Acceleration Values at a few Locations; S-I Method; GM2	304
8.44	Dam DB; Amplified Acceleration Values at a few Locations; S-I Method; GM3	305
8.45	Dam DB; Displacement Values at a few Locations; R-O Model; GM1	309
8.46	Dam DB; Displacement Values at a few Locations; R-O Model; GM2	310
8.47	Dam DB; Displacement Values at a few Locations; R-O Model; GM3	311
8.48	Dam DB; Displacement Values at a few Locations; H-D Model; GM1	312
8.49	Dam DB; Displacement Values at a few Locations; H-D Model; GM2	313
8.50	Dam DB; Displacement Values at a few Locations; H-D Model; GM3	314
8.51	Dam DB; Displacement Values at a few Locations; S-I Method; GM1	315

8.52	Dam DB; Displacement Values at a few Locations; S-I Method; GM2	316
8.53	Dam DB; Displacement Values at a few Locations; S-I Method; GM3	317
8.54	Maximum Section of Dam DC	322
8.55	Finite Element Idealization of Dam DC	324
8.56	Material Type Identification of Dam DC	328
8.57	Horizontal Stress Contours of Dam DC (Static Analysis)	329
8.58	Vertical Stress Contours of Dam DC (Static Analysis)	330
8.59	Shear Stress Contours of Dam DC (Static Analysis)	331
8.60	Major Principal Stress Contours of Dam DC (Static Analysis)	332
8.61	Minor Principal Stress Contours of Dam DC (Static Analysis)	333
8.62	Stress Ratio Contours of Dam DC (Static Analysis)	334
8.63	Dam DC; Nodes at which Acceleration Values are Tabulated	336
8.64	Dam DC; Elements at which Shear Strain Values are Tabulated	337
8.65	Dam DC; Typical Nodes at which Time-Histories of Acceleration and Displacement have been Computed	346
8.66	Dam DC; Typical Elements at which Time-Histories of Shear Strain have been Computed	347
8.67	Horizontal Acceleration Time-History at Node 13; R-O Model	348
8.68	Horizontal Acceleration Time-History at Node 13; H-D Model	348
8.69	Horizontal Acceleration Time-History at Node 13; S-I Method	348
8.70	Horizontal Acceleration Time-History at Node 48; R-O Model	349
8.71	Horizontal Acceleration Time-History at Node 48; H-D Model	349

8.72	Horizontal Acceleration Time-History at Node 48; S-I Method	349
8.73	Horizontal Acceleration Time-History at Node 223; R-O Model	350
8.74	Horizontal Acceleration Time-History at Node 223; H-D Model	350
8.75	Horizontal Acceleration Time-History at Node 223; S-I Method	350
8.76	Horizontal Acceleration Time-History at Node 328; R-O Model	351
8.77	Horizontal Acceleration Time-History at Node 328; H-D Model	351
8.78	Horizontal Acceleration Time-History at Node 328; S-I Method	351
8.79	Horizontal Acceleration Time-History at Node 468; R-O Model	352
8.80	Horizontal Acceleration Time-History at Node 468; H-D Model	352
8.81	Horizontal Acceleration Time-History at Node 468; S-I Method	352
8.82	Vertical Acceleration Time-History at Node 13; R-O Model	353
8.83	Vertical Acceleration Time-History at Node 13; H-D Model	353
8.84	Vertical Acceleration Time-History at Node 13; S-I Method	353
8.85	Vertical Acceleration Time-History at Node 48; R-O Model	354
8.86	Vertical Acceleration Time-History at Node 48; H-D Model	354
8.87	Vertical Acceleration Time-History at Node 48; S-I Method	354
8.88	Vertical Acceleration Time-History at Node 223; R-O Model	355
8.89	Vertical Acceleration Time-History at Node 223; H-D Model	355
8.90	Vertical Acceleration Time-History at Node 223; S-I Method	355
8.91	Vertical Acceleration Time-History at Node 328; R-O Model	356
8.92	Vertical Acceleration Time-History at Node 328; H-D Model	356
8.93	Vertical Acceleration Time-History at Node 328; S-I Method	356
8.94	Vertical Acceleration Time-History at Node 468; R-O Model	357
8.95	Vertical Acceleration Time-History at Node 468; H-D Model	357
8.96	Vertical Acceleration Time-History at Node 468; S-I Method	357
8.97	Horizontal Displacement Time-History at Node 13; R-O Model	358

8.98	Horizontal Displacement Time-History at Node 13; H-D Model	358
8.99	Horizontal Displacement Time-History at Node 13; S-I Method	358
8.100	Horizontal Displacement Time-History at Node 48; R-O Model	359
8.101	Horizontal Displacement Time-History at Node 48; H-D Model	359
8.102	Horizontal Displacement Time-History at Node 48; S-I Method	359
8.103	Horizontal Displacement Time-History at Node 223; R-O Model	360
8.104	Horizontal Displacement Time-History at Node 223; H-D Model	360
8.105	Horizontal Displacement Time-History at Node 223; S-I Method	360
8.106	Horizontal Displacement Time-History at Node 328; R-O Model	361
8.107	Horizontal Displacement Time-History at Node 328; H-D Model	361
8.108	Horizontal Displacement Time-History at Node 328; S-I Method	361
8.109	Horizontal Displacement Time-History at Node 468; R-O Model	362
8.110	Horizontal Displacement Time-History at Node 468; H-D Model	362
8.111	Horizontal Displacement Time-History at Node 468; S-I Method	362
8.112	Vertical Displacement Time-History at Node 13; R-O Model	363
8.113	Vertical Displacement Time-History at Node 13; H-D Model	363
8.114	Vertical Displacement Time-History at Node 13; S-I Method	363
8.115	Vertical Displacement Time-History at Node 48; R-O Model	364
8.116	Vertical Displacement Time-History at Node 48; H-D Model	364
8.117	Vertical Displacement Time-History at Node 48; S-I Method	364
8.118	Vertical Displacement Time-History at Node 223; R-O Model	365
8.119	Vertical Displacement Time-History at Node 223; H-D Model	365
8.120	Vertical Displacement Time-History at Node 223; S-I Method	365
8.121	Vertical Displacement Time-History at Node 328; R-O Model	366
8.122	Vertical Displacement Time-History at Node 328; H-D Model	366
8.123	Vertical Displacement Time-History at Node 328; S-I Method	366

8.124	Vertical Displacement Time-History at Node 468; R-O Model	367
8.125	Vertical Displacement Time-History at Node 468; H-D Model	367
8.126	Vertical Displacement Time-History at Node 468; S-I Method	367
8.127	Shear Stress Time-History at Element 63; R-O Model	368
8.128	Shear Stress Time-History at Element 63; H-D Model	368
8.129	Shear Stress Time-History at Element 63; S-I Method	368
8.130	Shear Stress Time-History at Element 66; R-O Model	369
8.131	Shear Stress Time-History at Element 66; H-D Model	369
8.132	Shear Stress Time-History at Element 66; S-I Method	369
8.133	Shear Stress Time-History at Element 67; R-O Model	370
8.134	Shear Stress Time-History at Element 67; H-D Model	370
8.135	Shear Stress Time-History at Element 67; S-I Method	370
8.136	Shear Stress Time-History at Element 68; R-O Model	371
8.137	Shear Stress Time-History at Element 68; H-D Model	371
8.138	Shear Stress Time-History at Element 68; S-I Method	371
8.139	Shear Stress Time-History at Element 69; R-O Model	372
8.140	Shear Stress Time-History at Element 69; H-D Model	372
8.141	Shear Stress Time-History at Element 69; S-I Method	372
8.142	Shear Stress Time-History at Element 70; R-O Model	373
8.143	Shear Stress Time-History at Element 70; H-D Model	373
8.144	Shear Stress Time-History at Element 70; S-I Method	373
8.145	Shear Stress Time-History at Element 132; R-O Model	374
8.146	Shear Stress Time-History at Element 132; H-D Model	374
8.147	Shear Stress Time-History at Element 132; S-I Method	374
8.148	Shear Stress Time-History at Element 133; R-O Model	375
8.149	Shear Stress Time-History at Element 133; H-D Model	375

8.150	Shear Stress Time-History at Element 133; S-I Method	375
8.151	Shear Stress Time-History at Element 134; R-O Model	376
8.152	Shear Stress Time-History at Element 134; H-D Model	376
8.153	Shear Stress Time-History at Element 134; S-I Method	376
8.154	Shear Stress Time-History at Element 135; R-O Model	377
8.155	Shear Stress Time-History at Element 135; H-D Model	377
8.156	Shear Stress Time-History at Element 135; S-I Method	377
8.157	Shear Stress Time-History at Element 198; R-O Model	378
8.158	Shear Stress Time-History at Element 198; H-D Model	378
8.159	Shear Stress Time-History at Element 198; S-I Method	378
8.160	Shear Stress Time-History at Element 199; R-O Model	379
8.161	Shear Stress Time-History at Element 199; H-D Model	379
8.162	Shear Stress Time-History at Element 199; S-I Method	379
8.163	Shear Stress Time-History at Element 200; R-O Model	380
8.164	Shear Stress Time-History at Element 200; H-D Model	380
8.165	Shear Stress Time-History at Element 200; S-I Method	380
8.166	Shear Stress Time-History at Element 201; R-O Model	381
8.167	Shear Stress Time-History at Element 201; H-D Model	381
8.168	Shear Stress Time-History at Element 201; S-I Method	381
8.169	Dam DC; Amplified Acceleration Values at a few Locations; R-O Model; GM1	385
8.170	Dam DC; Amplified Acceleration Values at a few Locations; R-O Model; GM2	386
8.171	Dam DC; Amplified Acceleration Values at a few Locations; R-O Model; GM3	387
8.172	Dam DC; Amplified Acceleration Values at a few Locations; H-D Model; GM1	389

8.173	Dam DC; Amplified Acceleration Values at a few Locations; H-D Model; GM2	390
8.174	Dam DC; Amplified Acceleration Values at a few Locations; H-D Model; GM3	391
8.175	Dam DC; Amplified Acceleration Values at a few Locations; S-I Method; GM1	393
8.176	Dam DC; Amplified Acceleration Values at a few Locations; S-I Method; GM2	394
8.177	Dam DC; Amplified Acceleration Values at a few Locations; S-I Method; GM3	395
8.178	Dam DC; Displacement Values at a few Locations; R-O Model; GM1	402
8.179	Dam DC; Displacement Values at a few Locations; R-O Model; GM2	403
8.180	Dam DC; Displacement Values at a few Locations; R-O Model; GM3	404
8.181	Dam DC; Displacement Values at a few Locations; H-D Model; GM1	405
8.182	Dam DC; Displacement Values at a few Locations; H-D Model; GM2	406
8.183	Dam DC; Displacement Values at a few Locations; H-D Model; GM3	407
8.184	Dam DC; Displacement Values at a few Locations; S-I Method; GM1	408
8.185	Dam DC; Displacement Values at a few Locations; S-I Method; GM2	409
8.186	Dam DC; Displacement Values at a few Locations; S-I Method; GM3	410

Table	Description	Page
2.1	Values of k versus Plasticity Index	14
2.2	Approximate Values of Damping Ratio at Large Strains	56
4.1	Shear Modulus and Shear Strain Values for all the Sites	92
4.2	Shear Modulus from Vertical Vibration Test (Site A)	101
4.3	Shear Modulus from Forced Horizontal Vibration Test (Site A)	106
4.4	Shear Modulus Values from Cyclic Plate Load Test	111
4.5	Damping Values for Different Soils (Sites A, B, C and D)	114
4.6	Shear Modulus Values from Oscillatory Shear Test (Sites A, B and C)	117
4.7	Shear Modulus Values from Simple Shear Test (Sites A, B and C)	118
5.1	Values of Disturbance Factors B _b and B _a	124
5.2	Values of Constants in Eqs. 5.3 and 5.4	127
5.3	Values of a and R for Different Type of Soils	141
6.1	Different Parameters of the Hyperbolic Model	169
7.1	Values of Different Stress Vectors	192
7.2	Values of Different Stress Vectors (using FEABANS)	194
7.3	Distribution of Shear Stress in the Soil Column	202
7.4	Distribution of Acceleration in the Soil Column	203
8.1	Material Properties Used in the Static Analysis	211
8.2	Material Properties Used in the Dynamic Analysis	214
8.3	Characteristics of the Three Ground Motions	215
8.4	Strain Compatible Dynamic Soil Properties	225
8.5	Maximum Acceleration Values at a few Nodes Ramberg-Osgood Model; PGA = 0.25g	228
8.6	Maximum Acceleration Values at a few Nodes Hardin-Drnevich Model; PGA = 0.25g	229

8.7	Maximum Acceleration Values at a few Nodes Seed-Idriss Method; PGA = 0.25g	230
8.8	Shear Strain Values at a few Elements; Ramberg-Osgood Model El Infiernillo Dam; PGA = 0.25g	233
8.9	Shear Strain Values at a few Elements; Hardin-Drnevich Model El Infiernillo Dam; PGA = 0.25g	234
8.10	Shear Strain Values at a few Elements; Seed-Idriss Method El Infiernillo Dam; PGA = 0.25g	235
8.11	Displacement at the Crest; El Infiernillo Dam	252
8.12	Shear Strain Values at a few Elements R-O Model; PGA = 0.40g; GM2	267
8.13	Comparison of Shear Strain Values Including Foundation; R-O Model	271
8.14	Material Properties Used in the Static Analysis; Dam DC	277
8.15	Shear Wave Velocity for Different Materials	281
8.16	Maximum Acceleration Values at a few Nodes Ramberg-Osgood Model; Dam DB; PGA = 0.25g	286
8.17	Maximum Acceleration Values at a few Nodes Hardin-Drnevich Model; Dam DB; PGA = 0.25g	287
8.18	Maximum Acceleration Values at a few Nodes Seed-Idriss Method; Dam DB; PGA = 0.25g	288
8.19	Shear Strain Values at a few Elements; Ramberg-Osgood Model Dam DB; PGA = 0.25g	289
8.20	Shear Strain Values at a few Elements; Hardin-Drnevich Model Dam DB; PGA = 0.25g	290
8.21	Shear Strain Values at a few Elements; Seed-Idriss Method Dam DB; PGA = 0.25g	291
8.22	Shear Strain Values at a few Elements R-O Model; Dam DB; PGA = 0.40g; GM2	293
8.23	Displacement at the Crest; Dam DB	308
8.24	Physical Properties for Nonlinear Static Analysis	325
8.25	Nonlinear Parameters Used for the Duncan-Chang Model	326

8.26	Maximum Acceleration Values at a few Nodes Ramberg-Osgood Model; Dam DC; PGA = 0.25g	338
8.27	Maximum Acceleration Values at a few Nodes Hardin-Drnevich Model; Dam DC; PGA = 0.25g	339
8.28	Maximum Acceleration Values at a few Nodes Seed-Idriss Method; Dam DC; PGA = 0.25g	340
8.29	Shear Strain Values at a few Elements; R-O Model Dam DC; PGA = 0.25g	341
8.30	Shear Strain Values at a few Elements; H-D Model Dam DC; PGA = 0.25g	342
8.31	Shear Strain Values at a few Elements; S-I Method Dam DC; PGA = 0.25g	343
8.32	Shear Strain Values at a few Elements R-O Model; Dam DC; PGA = 0.40g; GM2	345
8.33	Displacement at the Crest; Dam DC	401

CHAPTER 1

INTRODUCTION

1.1 GENERAL

Destructive earthquakes occurred in the recent past in Santa Barbara, USA (1906); Koyna, India (1967); San Fernando, USA (1971); Chile (1985) and other places causing heavy loss of life in thousands and severe, irreparable damage or total collapse to dams and earth structures have demonstrated the need for earthquake resistant design of these structures. As a result of these natural disasters, much attention has been given to the research in the field of Geotechnical-Earthquake Engineering, to minimize the damages due to the future earthquakes.

With the recent advances in the method of analysis to evaluate the response of soil-structure interaction problems and with the development of high speed digital computers, it has become possible to carry out detailed investigations in Soil Dynamics related applications.

In support of the above methods of analysis, experiments have been conducted to determine the shear modulus and damping values of undisturbed soils in the field and on remoulded or disturbed soils in the laboratory. In the field, the cross-hole test device or the surface wave

propagation method is frequently used to determine the in-situ shear modulus. The level of shear strain, induced in these type of tests is of the order of 10^{-6} percent. In the laboratory, the shear modulus is often determined, using the cyclic triaxial shear test apparatus (Woods, 1978), on 'undisturbed' samples, in which the associated level of strain is in the range of 10^{-3} to 10^{-1} percent.

The field determined shear modulus and the laboratory determined shear modulus values are combined together and interpolated/extrapolated to obtain the shear modulus values as a function of shear strain ranging between 10^{-6} or 10^{-4} to 1.0 or 10 percent. In such a combination the laboratory determined shear modulus value is adjusted to the field value by multiplying an arbitrary factor known as correction factor varying between 1 and 2.5 (Seed and Idriss, 1970), irrespective of the level of strain under consideration. Adjusting the laboratory determined shear modulus to the field value of shear modulus is based on the meager data available on in-situ high amplitude shear modulus.

In the dynamic response evaluation of a soil deposit or an earth and rockfill structure subjected to ground motion, the in-situ shear modulus values ranging between $\gamma = 10^{-3}$ to $\gamma = 1.0$ percent should be available to obtain any meaningful results. This is possible, only by conducting different type of field tests, such as wave propagation test, free and forced block vibration tests and

cyclic plate load test, covering a large range of shear strain ($\gamma = 10^{-6}$ to 1.0 percent, IS: 5249, 1977; Nandakumaran et al., 1977; Prakash, 1981). As shown in Fig. 1.1, today no unique method of testing is available which can be used to determine the shear modulus values ranging between the strain level of 10^{-6} to 1.0 percent or more. Further, the shear modulus data, as a function of strain for coarse grained materials such as gravels is very scanty, and efforts are being made to establish the relationship between shear modulus versus shear strain for gravels and crushed rocks (Ishihara, 1982).

Similar to the shear modulus values, the damping value is also strain dependent (Hardin and Drnevich, 1970a; Seed and Idriss, 1970). Once these two parameters, namely, shear modulus and damping ratio are available as a function of strain, it is possible to evaluate the dynamic response of soil deposits and earth structures, subjected to any ground motion or other vibratory forces.

1.2 STRESS-STRAIN CHARACTERISTICS

The stress-strain behaviour of soils subjected to dynamic loading depends on the induced level of strain. Only at very low values of strain ($\gamma \leq 5.0 \times 10^{-5}$ percent), the soil is linearly elastic as shown in Fig. 1.1. At medium range of strain, γ varying between 10^{-5} to 10^{-3} percent the behaviour of soil is elasto-plastic. When the soil is subjected to a strong ground motion the induced strain value

Shear Strain (percent)	10 ⁻⁶	10 ⁻⁵	10 ⁻⁴	10 ⁻³	10 ⁻²	10 ⁻¹
	Small	Medium		Large		Failure
Laboratory Tests	Resonance Column Test			Cyclic Triaxial Test	Simple Shear Test	
Field Tests	Wave Propagation Test		Block Vibration Test	Impulse Test	Plate Load Test	Ground Vibration
Elastic						
Elasto-Plastic						
Failure						
Effect of Loading Rate and Repetition						
Model	Linear Elastic		Visco-Elastic		Load-History Tracing Type	
Method of Response Analysis	Linear		Equivalent Linear		Step-by-Step Integration	

Fig. 1.1 Influence of Strain on Various Factors
(Suppiah, 1986)

is large, nearing failure condition, the behaviour of soil is nonlinear and the method of analysis also drastically changes. In such cases, the step-by-step time integration scheme is the only method that can take into account the nonlinearity of the soil (Ishihara, 1982, 1985, 1987).

1.2.1 Simulation of Stress-Strain Characteristics of Soils

To account for the stress-strain characteristics of soils when subjected to earthquake or vibratory loading, presently, the Hardin-Drnevich model (1970b), which is based on the hyperbolic law (Kondner, 1963; Kondner and Zelasko, 1963), is widely used. However, in recent years, the Ramberg-Osgood model has been increasingly used to represent the stress-strain behaviour of soils (Constantopoulos, 1973; Richart, 1975; Richart and Wylie, 1975; Desai, 1977; Roësset, 1977; Ishihara, 1982, 1985, 1987; Shamoto, 1984). The Hardin-Drnevich model (1970b), based on two parameters, namely, (a) the low-amplitude shear modulus, G_{\max} and (b) the shear strength, τ_f corresponding to low-amplitude shear modulus, predicts an extremely large value of damping, of the order of 63.7 percent at large strain levels, which is not experienced in actual situation (Ishihara, 1982, 1985). The Ramberg-Osgood model based on four parameters, namely, (a) low-amplitude shear modulus, (b) the shear strength corresponding to low-amplitude shear modulus and (c) the two constants, α and R gives zero value of damping at a point where G/G_{\max} is unity. However, this deficiency can be

overcome by adjusting the damping value at G/G_{\max} equal to unity, to that of the experimental value, or an assumed value of damping of very low order in magnitude at G/G_{\max} equal to unity. Thus, the Ramberg-Osgood model permits a better degree of freedom to fit the experimentally obtained values of shear modulus and damping (Ishihara, 1982; Shamoto, 1984).

1.3 EARTH AND ROCKFILL DAMS

1.3.1 Static Analysis

Clough and Woodward (1967), were the first to apply the finite element method to carry out a linear elastic analysis of an earth dam. Clough and Woodward (1967). in their analysis, demonstrated the layer-wise sequential construction operation. However, the linear elastic analysis, as performed by Clough and Woodward (1967), does not predict the true behaviour of the earth dam due to nonlinear characteristics of soils. Duncan and Chang (1970), developed a method to account for the nonlinear stress-strain behaviour of soils, based on the hyperbolic model (Kondner, 1963; Kondner and Zelasko, 1963). Duncan et al. (1980), added a revision to account for volume change characteristics of soils in the hyperbolic model. Since, the introduction of the hyperbolic model by Duncan and Chang (1970), and Duncan et al. (1980), embankment dams are increasingly being analysed with nonlinear stress-strain characteristics of soils, and also, considering the incremental analysis (Kondner, 1963; Duncan and Chang, 1970; Kramer, 1972:

Kulwahy, Duncan and Seed, 1975; Sharma, 1976; Lai and Seed, 1985). A nonlinear, sequential construction analysis is essential to understand the pre-earthquake or the initial stresses developed in the embankment, due to self-weight and water loads (Seed et al., 1976; Lai and Seed, 1985).

1.3.2 Dynamic Analysis

Clough and Chopra (1966), extended the finite element method of analysis for the first time to analyse a homogeneous earth dam subjected to dynamic loading. They performed a linear dynamic analysis based on the mode superposition method. After the investigation of Clough and Chopra (1966), the finite element method is being increasingly used for the dynamic analysis of earth and rockfill dams (Idriss, 1968; Seed, Lee and Idriss, 1968; Dibaj and Penzien, 1969; Duncan and Clough, 1971; Clough, 1972; Idriss et al., 1973; Lefebvre, Duncan and Wilson, 1973; Seed et al., 1973; Lysmer et al., 1974, 1975; Sharma, 1976; Chandrasekaran, Paul and Suppiah, 1984, 1985; Chandrasekaran and Prakash, 1989b).

Since, the complete failure of the Sheffield dam (Seed, Lee and Idriss, 1968) and the near catastrophic failure that occurred in the Lower San Fernando (hydraulic fill) dam during the San Fernando earthquake of February 9, 1971 (Seed et al., 1973), much efforts are being made to analyse and construct high earth and rockfill dams with improved techniques/method (Dihang Dam (proposed): 276 m; Nurek dam:

310 m; Oroville Dam: 240 m; Tehri Dam: 265 m) in severe seismic regions for ground motions with peak ground acceleration values of the order of 0.25g (g is the acceleration due to gravity) or more. The successful application of the improved techniques is dependent on the efficient incorporation of representative dam-material properties, such as the strain dependent shear modulus and damping values in the analysis. Since, the behaviour of earth and rockfill dams during earthquakes is governed by the dynamic response characteristics of the materials constituting the dam. When an earth structure is subjected to a strong earthquake, the induced level of strain is large and the dynamic characteristics of the dam-materials are not linear. This factor is more pronounced in high rockfill dams, in which the height is of the order of 200 m or more, due to the presence of large amount of confining pressure. In an earthquake resistant analysis of such a high rockfill dam, the nonlinear stress-strain characteristics of all the materials constituting the dam should be considered, using an appropriate model, such as the Ramberg-Osgood model, based on the step-by-step time integration scheme supplemented with experimental results.

1.4 OBJECTIVES

Today, in most of the aseismic analyses related to earth and rockfill dams and soil deposits the strain

dependent shear modulus and damping properties are considered only for sand and clay materials (Seed et al., 1973, 1974, 1975), and recently to account for gravel materials as well (Seed et al., 1984; Lai and Seed, 1985). Due to the meager data available on gravel or boulder materials the stress-strain behaviour of these materials are approximated to that of sand. Nevertheless, experience shows (Prater and Struder, 1979), that the seismic analysis of a rockfill dam involves more complexities than that of a homogeneous (earth) dam, due to the presence of different type of materials and pronounced nonlinearity of these materials. Therefore, a realistic seismic analysis, considering the nonlinear behaviour of all the materials constituting the dam by an appropriate nonlinear model supplemented by field investigation on these dam-materials is essential to assess the safety of a rockfill dam during a strong ground shaking and to establish improved analysis/design techniques and to demonstrate the suitability of the chosen model through a case-history study. This is the main objective of the present thesis.

1.5 ORGANIZATION OF THE THESIS

The presentation of the thesis is made in nine chapters. The literature survey on the dynamic characteristics of different materials, low-amplitude and high-amplitude shear moduli, secondary time effects on shear modulus, damping values and models to represent nonlinear stress-strain characteristics of different soils are

presented in Chapter 2. In the same chapter, static and dynamic analysis of a few of the embankment dams, carried out by different investigators based on the finite element method is also reviewed.

Chapter 3 describes the different type of tests carried out in the field and in the laboratory to determine the dynamic properties of soils as a function of strain.

The results of experimentally determined shear moduli along with the associated strain levels are presented in Chapter 4.

Interpretation of the different test results. Newton-Raphson iterative technique, evaluation of Ramberg-Osgood model constants, modulus reduction curves and damping values for different types of soils as a function of strain are described in Chapter 5.

Chapter 6 describes the formulation of the finite element method with respect to the eight-noded isoparametric element. The hyperbolic model as applicable to nonlinear static case and the method of sequential construction are presented in this chapter. Formulation of stiffness matrix, mass matrix and damping matrix, and an implicit time integration scheme are also described in Chapter 6.

In Chapter 7, the computer programs based on the finite element method and applicable for nonlinear static analysis and nonlinear dynamic analysis are discussed. The verification of the developed computer codings has been done by solving two standard examples, namely, an embankment dam

and a soil column.

The case history analysis results of the 146 m high El Infiernillo Dam and dynamic response evaluation of two other rockfill dams of height 108 m and 336 m including their respective foundations subjected to three different ground motions are presented in Chapter 8. The dynamic analysis of each dam based on the Ramberg-Osgood model, Hardin-Drnevich model and the widely used Seed-Idriss method is described as well. In the same chapter, the comparison of all the three methods of analysis is also made.

Chapter 9 gives the important conclusions drawn and the significant contributions made in the present work.

CHAPTER 2

PREVIOUS WORK

2.1 GENERAL

A survey of past studies, with emphasis on the determination of field and laboratory shear moduli and damping ratios of different type of soils, the influence of secondary time effects on shear moduli; the determination of different parameters pertaining to nonlinear stress strain characteristics of various soils, nonlinear static and nonlinear dynamic analysis of a few embankment dams based on the finite element method are reviewed in this chapter.

2.2 SHEAR MODULUS

Almost all type of soils exhibit nonlinearity. The response of soils subjected to dynamic or earthquake loads varies from linear elastic behaviour at low shear strain values ($\gamma \leq 10^{-4}$ percent) to highly nonlinear behaviour at large strain values (Fig. 1.1). Therefore, the shear modulus should be estimated with extreme care due to its significant influence on any dynamic soil-structure interaction problems.

2.2.1 Factors Affecting Shear Modulus

As many as eleven parameters are found to affect

the shear modulus values of soils (Hardin and Black, 1968; Hardin and Drnevich, 1970a; Richart, Hall and Woods, 1970).

These different parameters are:

- 1 Strain amplitude, γ
- 2 Mean effective principal stress, σ'_m
- 3 Void ratio, e , or relative density, D_r
for cohesionless soils
- 4 Number of cycles of loading, N
- 5 Secondary time effects for fine grained soils
- 6 Octahedral shear stress
- 7 Overconsolidation ratio, OCR
- 8 Degree of saturation, S
- 9 Effective strength parameters, c' and ϕ'
- 10 Ambient stress history and vibration history, and
- 11 Temperature effects including freezing.

Out of these eleven factors, the shear modulus of any soil is greatly affected by the first two parameters listed above.

2.2.2 Shear Modulus from Empirical Equations

Hardin and Black (1968), conducted a parametric study and proposed an expression to estimate the shear modulus at low-amplitude strain levels from:

$$G_{\max} = \frac{1230(2.973-e)^2 (\text{OCR})^k (\sigma'_m)^{0.5}}{(1+e)} \quad (2.1)$$

where

(G_{\max} in pounds/square inch and

1 pound/square inch = 0.703 tonne/sq. m)

G_{\max} = low-amplitude shear modulus at $\tau \leq 10^{-4}$ percent

e = void ratio

OCR = over consolidation ratio

σ'_m = mean effective principal stress.

The value of k (Eq. 2.1), which is given in Table 2.1, is related to the plasticity index, PI of the soil (Hardin and Drnevich, 1970a) .

Table 2.1 Values of k

k (1)	PI (2)
0.00	0
0.18	20
0.30	40
0.41	60
0.48	80
0.50	>100

Eq. 2.1 was formulated from tests, carried out on sands and low plasticity clays. This equation is applicable.

over a range of void ratio values between 0.4 and 1.2 and the resulting value of shear modulus is in pounds per square inch.

Hardin and Drnevich (1970a), proposed identical expression (Eq. 2.2), to compute the values of maximum shear modulus, at essentially zero strain for some soils, as given by:

$$G_{\max} = \frac{14760(2.973-e)^2 (\text{OCR})^k (\sigma'_m)^{0.5}}{(1+e)} \quad (2.2)$$

in which

(G_{\max} is in pounds/sq. foot and
1 pound/sq. foot = 0.0048 tonne/sq. m.)

All notations remain as defined in Eq. (2.1), except that the constant here is 14760. Hardin and Drnevich (1970a), further, proposed empirical equations, to calculate high-amplitude shear modulus. These equations are:

$$G = \frac{G_{\max}}{1+\Gamma/\Gamma_r} \quad (2.3)$$

where

$$\Gamma_r = \tau_{\max}/G_{\max} \quad (2.4)$$

$$\tau_{\max} = \left[\left(\frac{1+K_0}{2} \sigma'_v \sin \phi' + c' \cos \phi' \right)^2 \left(\frac{1-K_0}{2} \sigma'_v \right)^2 \right]^{1/2} \quad (2.4a)$$

K_0 = coefficient of earth pressure at rest

σ'_v = vertical effective stress

c' , ϕ' = effective strength parameters.

Hardin (1978), proposed a modification in Eqs. 2.1 and 2.2, to take into account a wide range of void ratio for different soils and suggested the following expression:

$$G_{\max} = \frac{A (\text{OCR})^k (p_a)^{1-n} (\sigma'_m)^n}{F(e)} \quad (2.5)$$

in which

A = dimensionless coefficient

p_a = atmospheric pressure

n = elastic parameter defining the power to which stress is raised in the stress range where the soil is normally consolidated.

The parameter, $F(e)$ is given by:

$$F(e) = 0.3 + 0.7e^2 \quad (2.6)$$

Eq. (2.5) is applicable for all type of soils.

Seed and Idriss (1970), conducted a very extensive survey on strain dependent dynamic soil properties. Based on the type of soil, they classified the shear modulus values and proposed empirical equations. These empirical equations are being widely used, in evaluating the dynamic response of soil-structure interaction problems. Most of the data they

collected were from laboratory tests, conducted at high strain levels, ranging between 10^{-3} and 10^{-1} percent. From this range of data, Seed and Idriss (1970), extrapolated the low-amplitude shear modulus values. The work done by them is briefly presented herein.

From the extensive data collected by Seed and Idriss (1970), they proposed an expression for cohesionless soils, relating the shear modulus and confining pressure as given by:

$$G = 1000 K_2 (\sigma'_m)^{0.5} \quad (2.7)$$

where

G = high-amplitude shear modulus, in pounds/square feet

K_2 = a parameter which accounts for the influence of void ratio or relative density and strain amplitude.

The variation of K_2 with shear strain at different relative density values is shown in Fig. 2.1. Seed and Idriss (1970), further presented modulus reduction factors, to obtain shear modulus values at high-amplitude strain level for sandy soils, knowing the low-amplitude shear modulus value. This relationship is shown in Fig. 2.2.

Seed and Idriss (1970), attempted to generalize the shear modulus values of clay soils as a function of shear strain. From the large volume of data collected, they normalized the shear modulus of clay soils with respect to the undrained shear strength, S_u . This relationship is shown

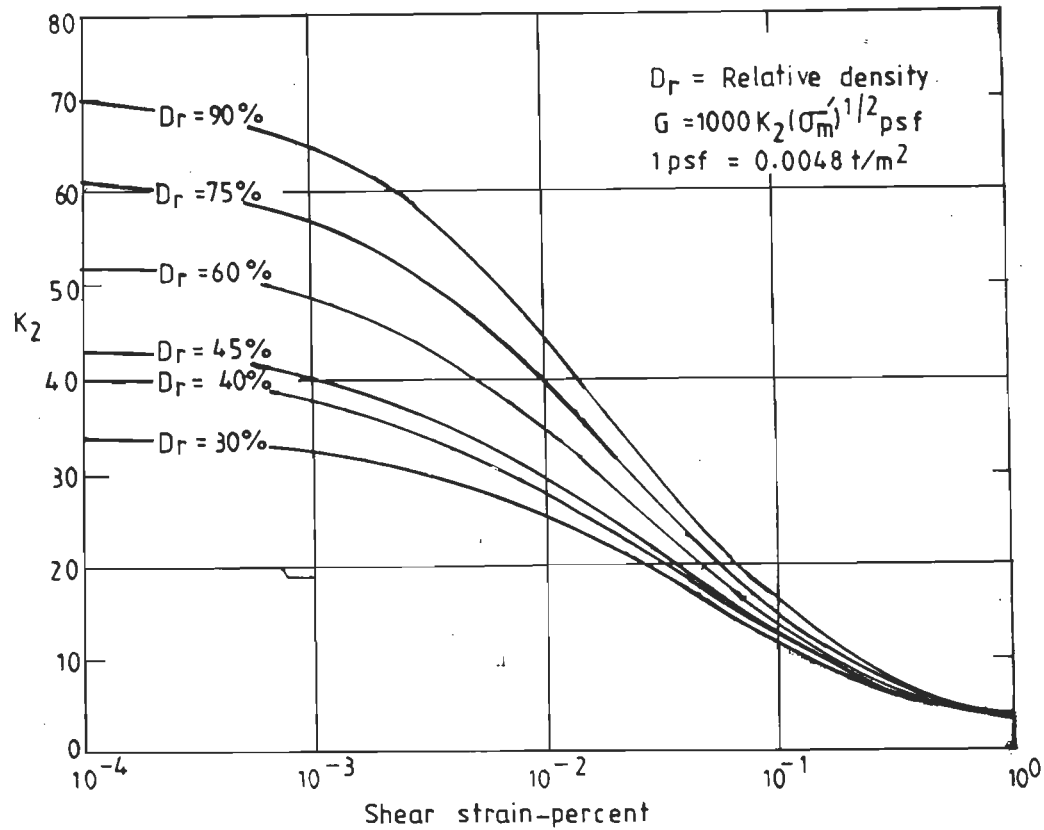


Fig. 2.1 Shear Moduli of Sands at Different Relative Densities
 (Seed and Idriss, 1970)

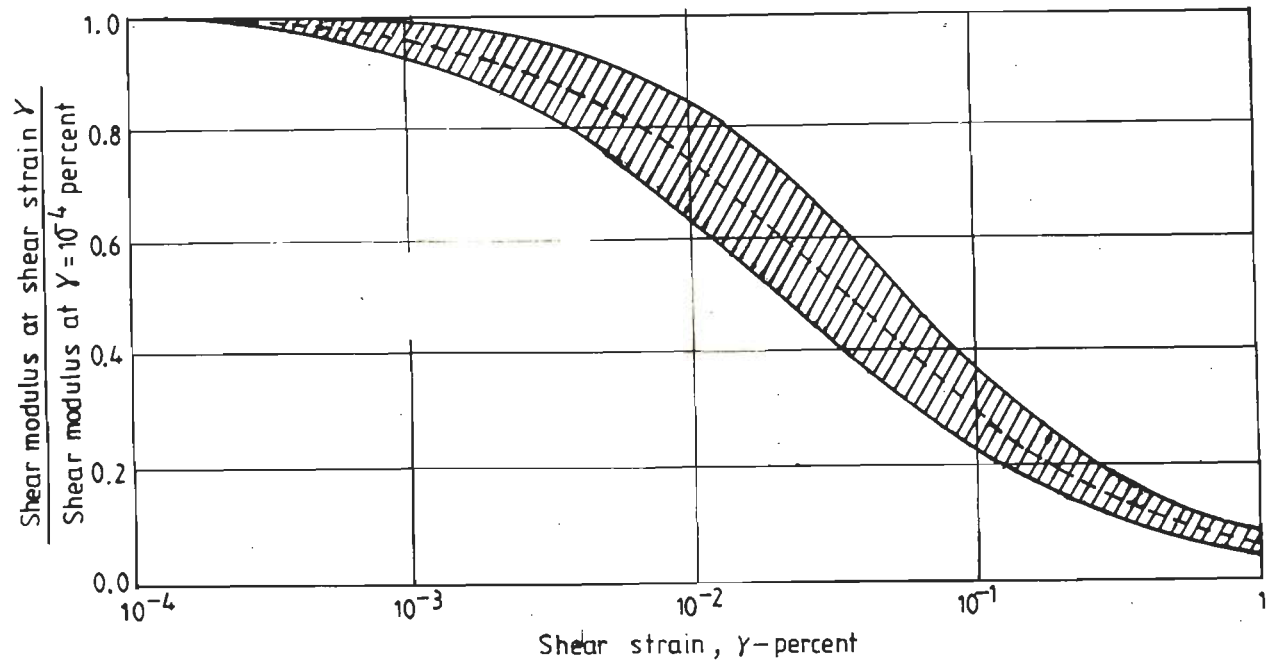


Fig. 2.2 Normalized Shear Modulus Curve for Sand
(Seed and Idriss, 1970)

in Fig. 2.3.

Similar to the modulus reduction curve of sand (Fig. 2.2), for clay soils also, Seed and Idriss (1970), recommended a modulus reduction curve as shown in Fig. 2.4. Seed and Idriss (1970), concluded from their literature survey, that the shear modulus of peaty soils was similar to that of clay soils, as shown in Fig. 2.3, except that the ratio of G/S_u is of the order of 150.

Seed et al. (1984), made a revision on their earlier investigation (Seed and Idriss, 1970), by providing shear modulus values for gravel materials as a function of shear strain. Seed et al. (1984), in their latest study, proposed modulus attenuation curve for gravels and made a comparison with the modulus reduction curve of sand as shown in Fig. 2.5.

Grant and Brown (1981), carried out field and laboratory tests to determine shear moduli of silty soils at six different sites. In the field, they employed geophysical methods to determine the low-amplitude shear moduli and in the laboratory, they used the resonant column test and cyclic triaxial test equipments. Grant and Brown (1981), have proposed, normalized shear modulus curves as a function of shear strain for silty soils. These curves are shown in Figs. 2.6 and 2.7, in which they have compared their proposed curves with the curves given by Seed and Idriss (1970), for clay and rock.

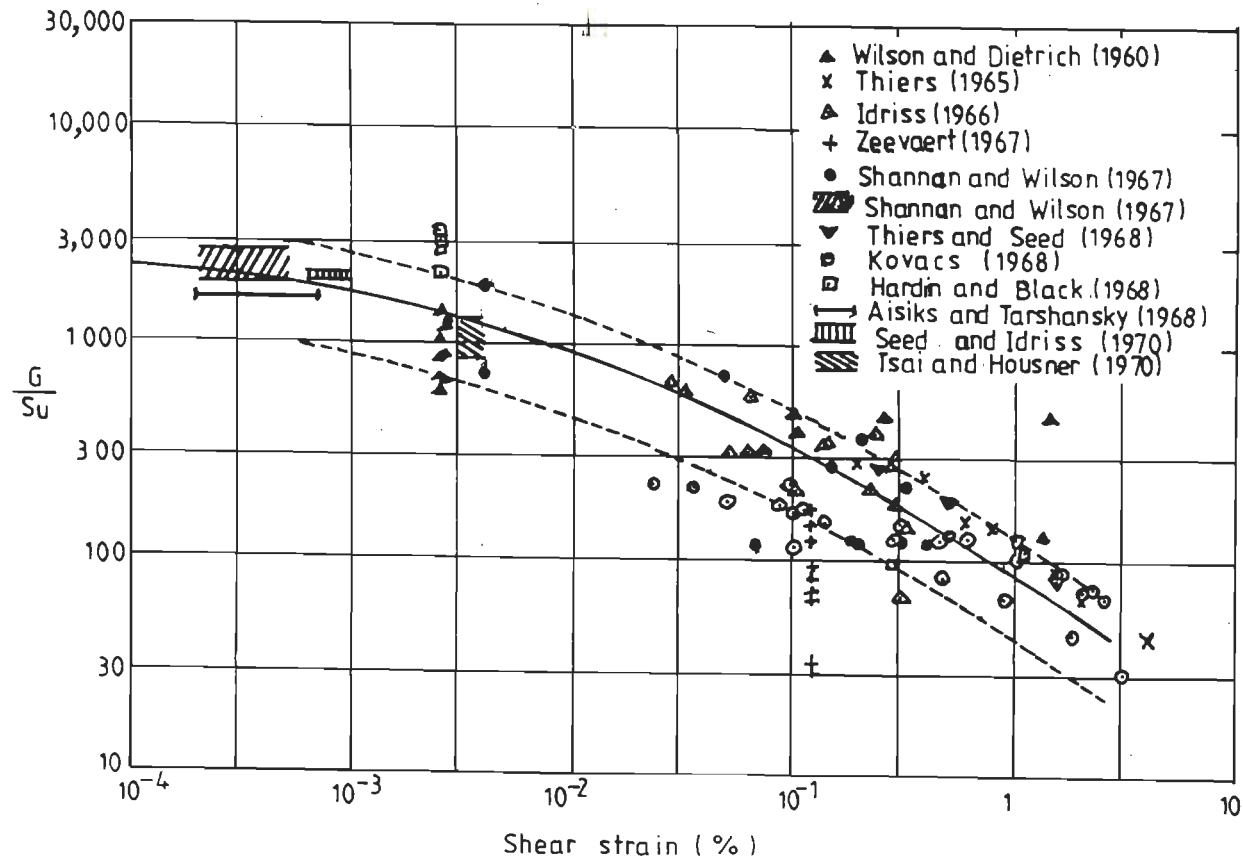


Fig. 2.3 Shear Modulus for Clay Soils
(Seed and Idriss, 1970)

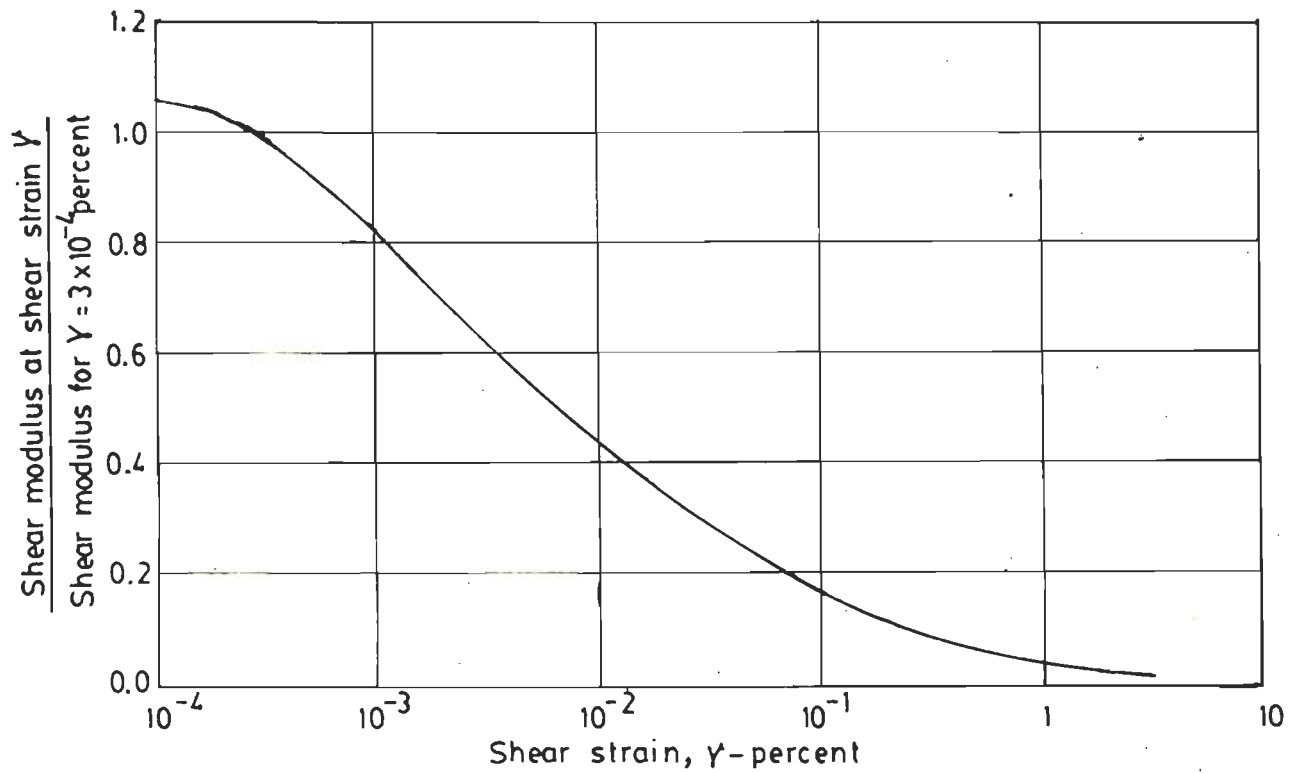


Fig. 2.4 Modulus Reduction Curve for Clay Soils
(Seed and Idriss, 1970)

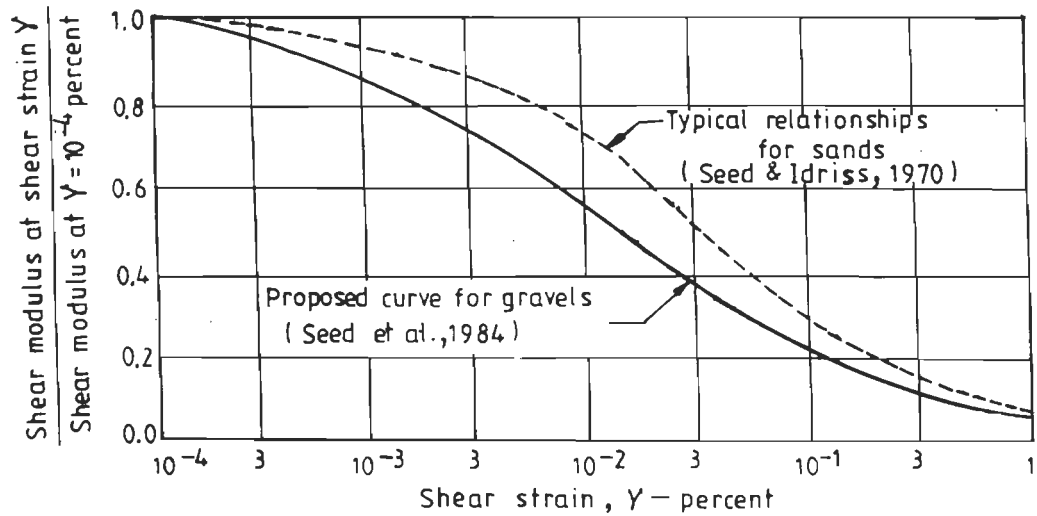
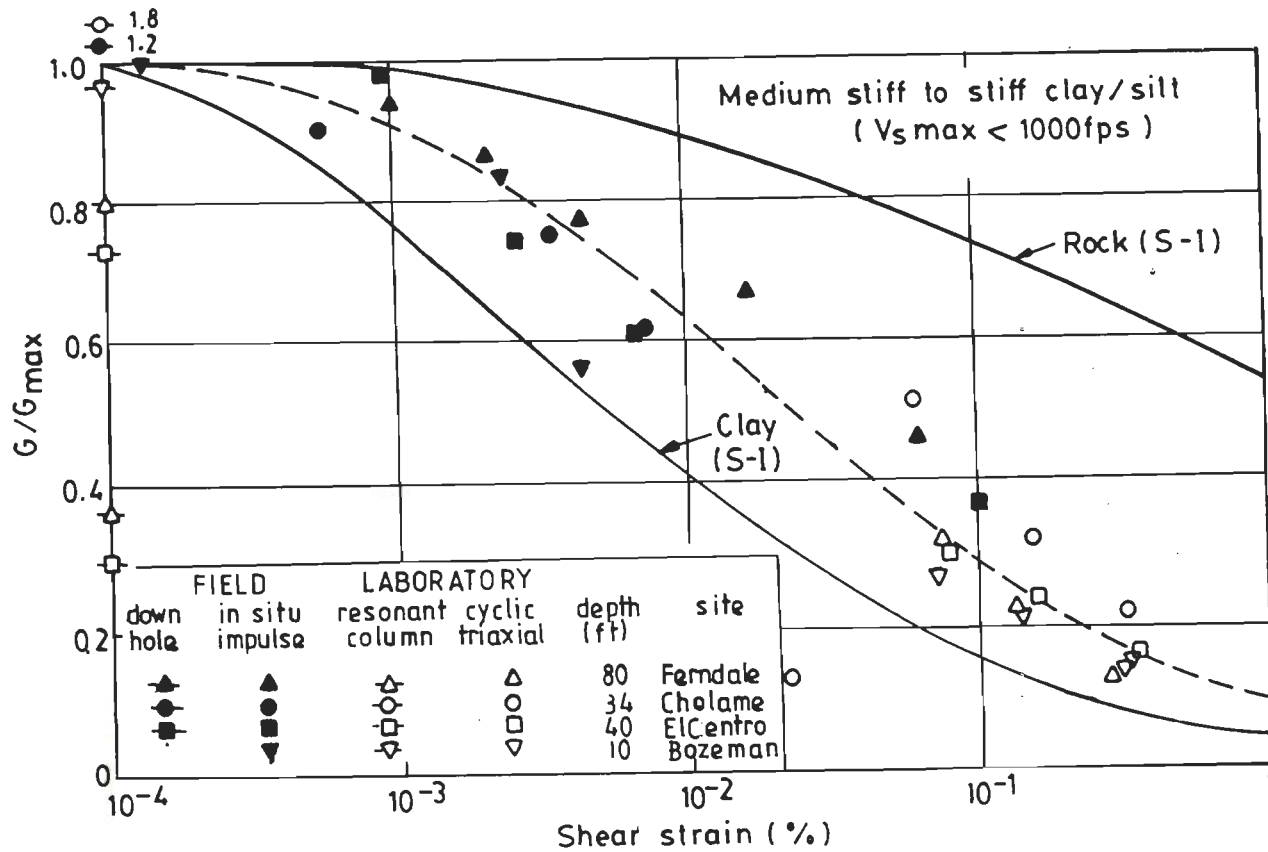
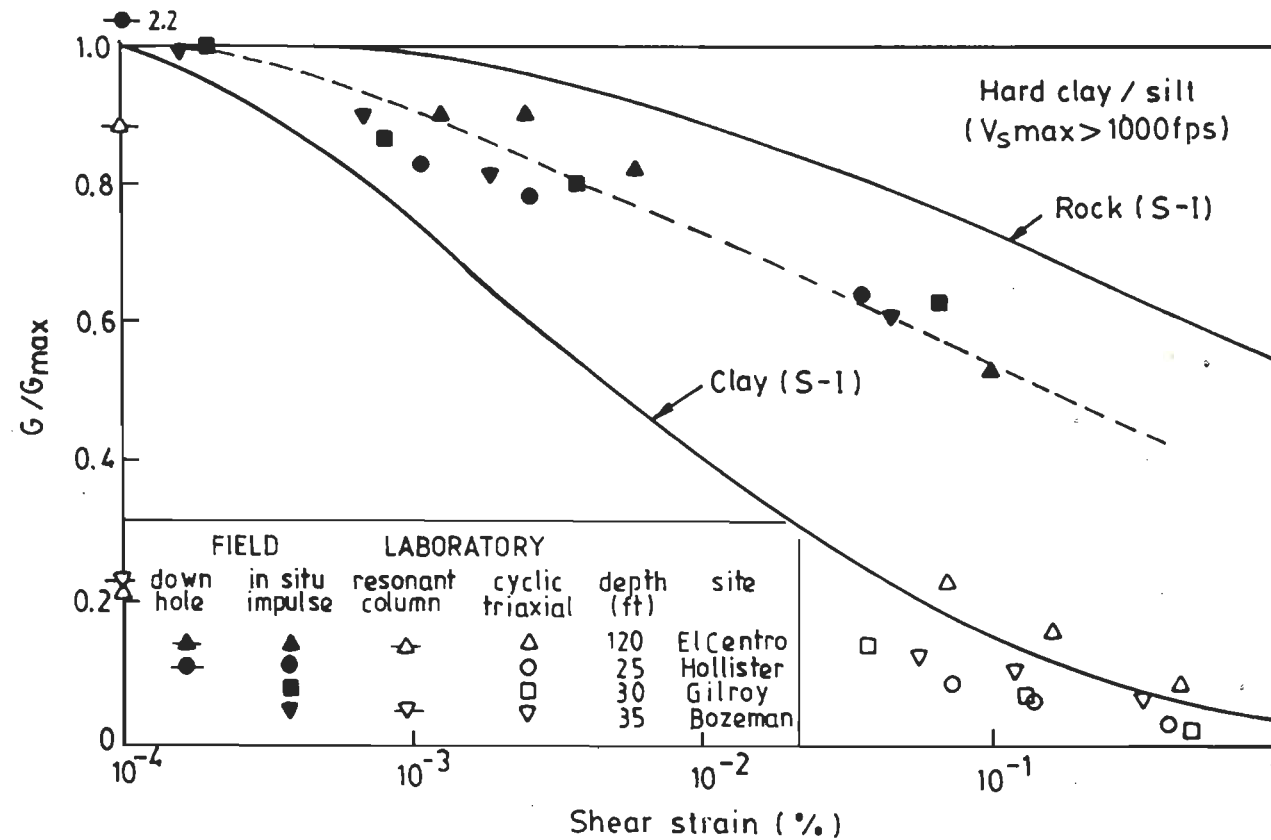


Fig. 2.5 Modulus Reduction Curves for Granular Materials
(Lai and Seed, 1985)



1 ft = 0.3048 m

Fig. 2.6 Normalized Shear Moduli for Stiff Clay/Silt
(Grant and Brown, 1981)



1 ft = 0.3048 m

Fig. 2.7 Normalized Shear Moduli for Hard Clay/Silt
(Grant and Brown, 1981)

2.3.6 Field and Laboratory Determination of Shear Modulii

Several investigators have studied the variation of shear modulus between the field and laboratory tested values. The work done by few researchers, who have conducted tests both in the field and in the laboratory to determine shear modulus is summarized below:

Cunny and Fry (1973), conducted in-situ and laboratory tests at fourteen sites, consisting of different type of soils. They made a comparative study between the shear modulii obtained in the field and in the laboratory. Cunny and Fry (1973), reported a variation of as much as ± 50 percent, in the shear modulus values, determined in the field and in the laboratory for a particular site. They further suggested to carry out additional tests, whenever the observed variation between the two shear modulus values was very large. One of the reasons, they cited for the difference between field and laboratory shear modulii was the confining pressure.

In India, Prakash and his co-workers (1968a, 1968b, 1970, 1971, 1972, 1973, 1974, 1975, 1976a, 1976b, 1981); Nandakumaran et al. (1977, 1979, 1980), have carried out extensive in-situ tests to establish the shear modulus of different soils as a function of shear strain ranging between 10^{-6} to 1.0 percent, at major project sites, including nuclear power plant sites and different dam sites. Prakash (1981), has summarized the different type of tests

carried out in India and presented the absolute values of shear moduli for at least seven sites. These investigators have employed the following type of tests for evaluating the dynamic properties of different soils:

- 1 hammer (or wave propagation) test
- 2 block vibration test
- 3 cyclic plate load test
- 4 passive pressure test.

Two sets of plots between the shear modulus and shear strain, presented by Nandakumaran et al. (1977), and Prakash (1981), are shown in Figs. 2.8 and 2.9 respectively. These investigators have recommended that the shear modulus versus shear strain relationship should be established based on a variety of tests and not from a single test.

Arango, Moriwaki and Brown (1978), performed a comparative study by conducting numerous tests in the field and in the laboratory to determine shear modulus values. They employed down-hole and cross-hole methods of testing in the field and cyclic and static triaxial compression tests and resonant column test in the laboratory. They observed the difference between the field shear wave velocity, obtained at $\gamma = 10^{-4}$ percent and the laboratory shear wave velocity, obtained at $\gamma = 10^{-1}$ percent, to be of the order of 100 to 25 percent respectively. Arango, Moriwaki and Brown (1978), cautioned against the method of obtaining modulus reduction curves by combining field test data and

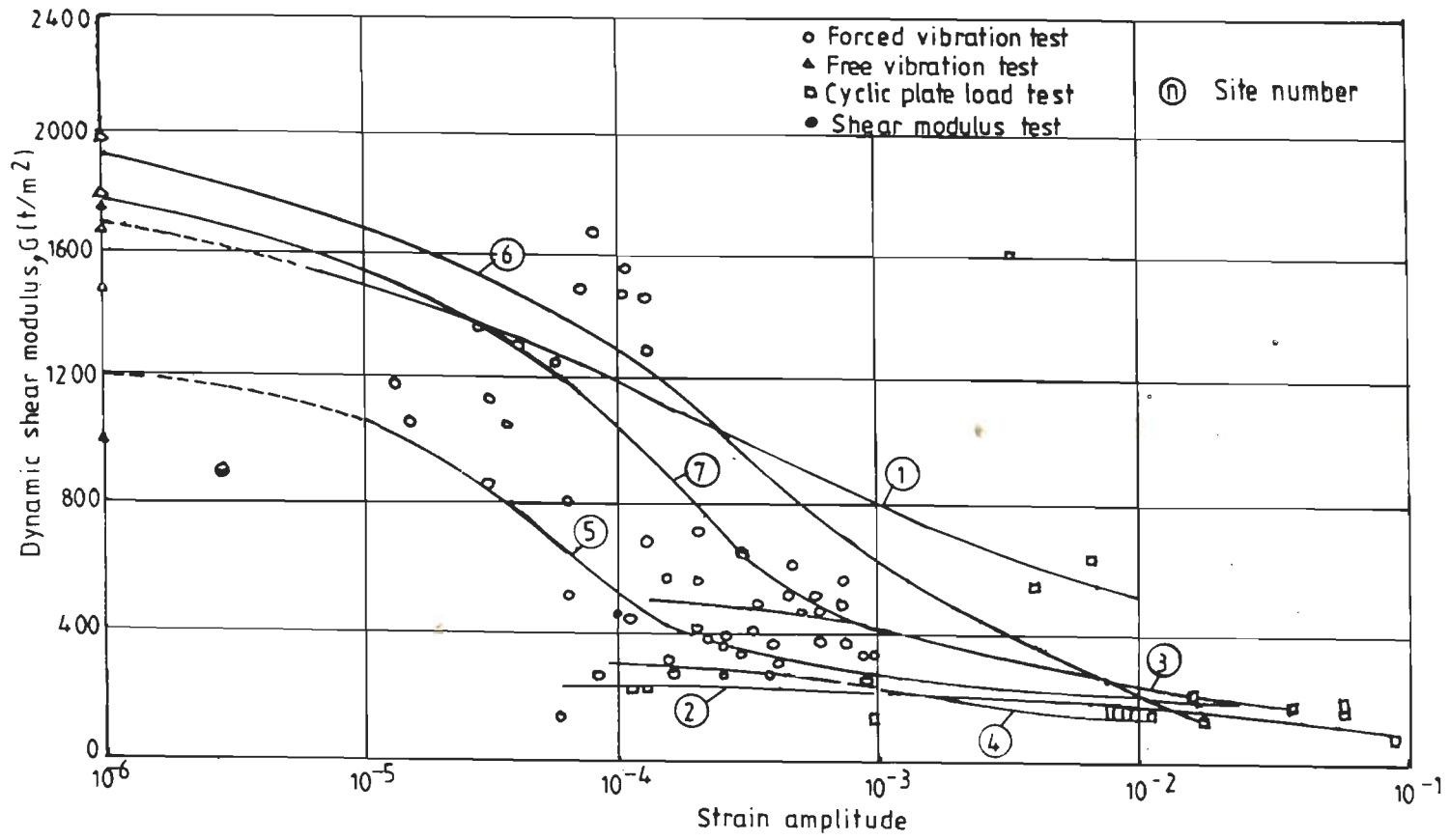


Fig. 2.9 Shear Modulus Curves for Different Sites in India
 (Prakash, 1981)

laboratory test data, since this resulted in significant errors.

2.4 DAMPING OF SOILS

As reported earlier, similar to shear moduli of soils, the damping parameter also has a major influence in the behaviour of soil-structure interaction problems subjected to dynamic loads.

2.4.1 Parameters Affecting Damping of Soils

Hardin and Drnevich (1970a), reported that the same factors affecting shear moduli of soils are found to influence the damping ratio of soils as well. These parameters are listed in Sec. 2.2.1.

2.4.2 Damping from Empirical Equations

Hardin and Drnevich (1970a), from their extensive research on shear modulus and damping of soils, proposed the following empirical equation to compute the damping ratio, D of soils:

$$D = D_{\max} \frac{\tau/\tau_r}{1 + \tau/\tau_r} \quad (2.8)$$

in which

D_{\max} = maximum damping ratio corresponding to large strain value.

Hardin and Drnevich (1970a), from their study found that the shear strain amplitude, mean effective principal stress, void ratio and number of cycles of loading are the major factors influencing the damping values of sands. From their study, Hardin and Drnevich (1970a), proposed the following equation for computing the maximum damping ratio of sands:

$$D_{\max} = D - 1.5 \log_{10} N \quad (2.9)$$

where

D = damping ratio at low strain levels

N = number of cycles of loading.

Seed and Idriss (1970), from their detailed investigation, presented approximate curves to compute damping ratio of sands, as a function of shear strain. These curves which are shown in Fig. 2.10, have upper and lower bound values of damping ratios for sandy soils.

From the very limited data collected by Seed and Idriss (1970), approximate curves for damping values have been recommended which are similar to that of sand. These curves are shown in Fig. 2.11.

Practically no data on damping values of gravel material was available. However, Seed and Idriss (1970), suggested the same value of damping as that of sands for gravel materials.

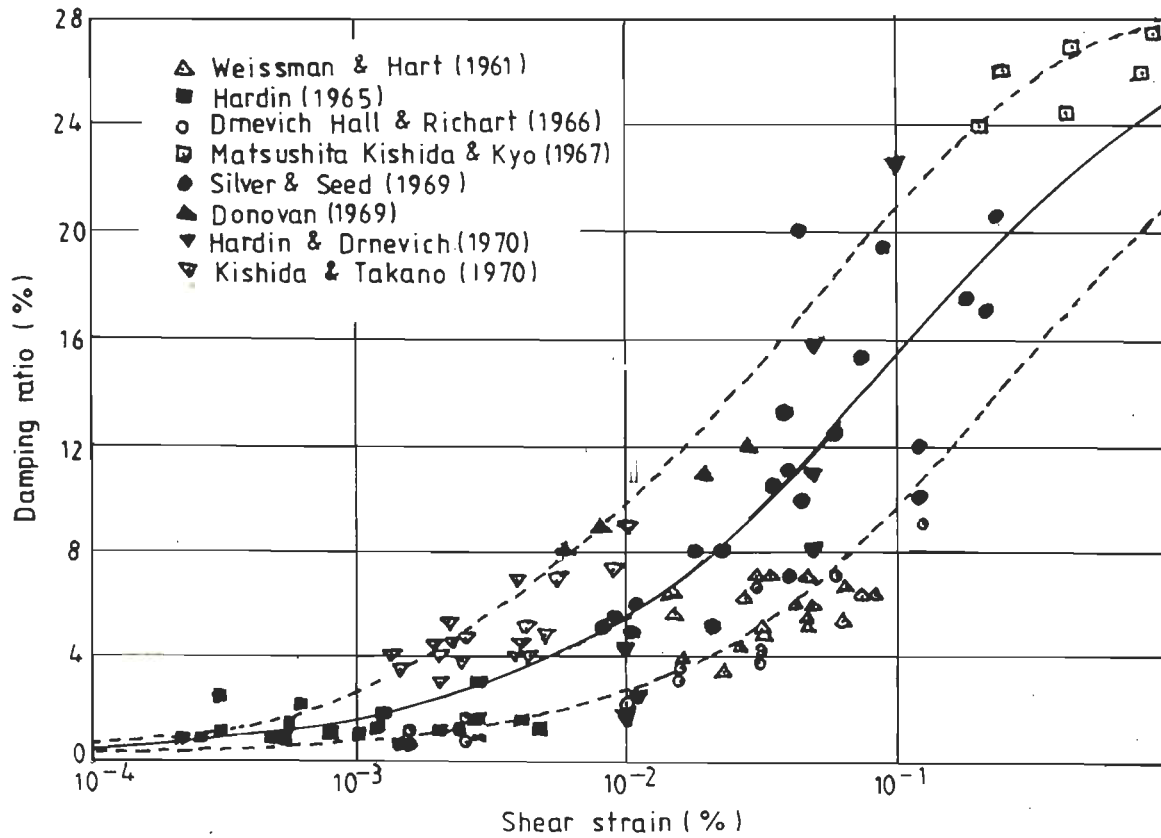


Fig. 2.10 Damping Ratio Curves for Sand
(Seed and Idriss, 1970)

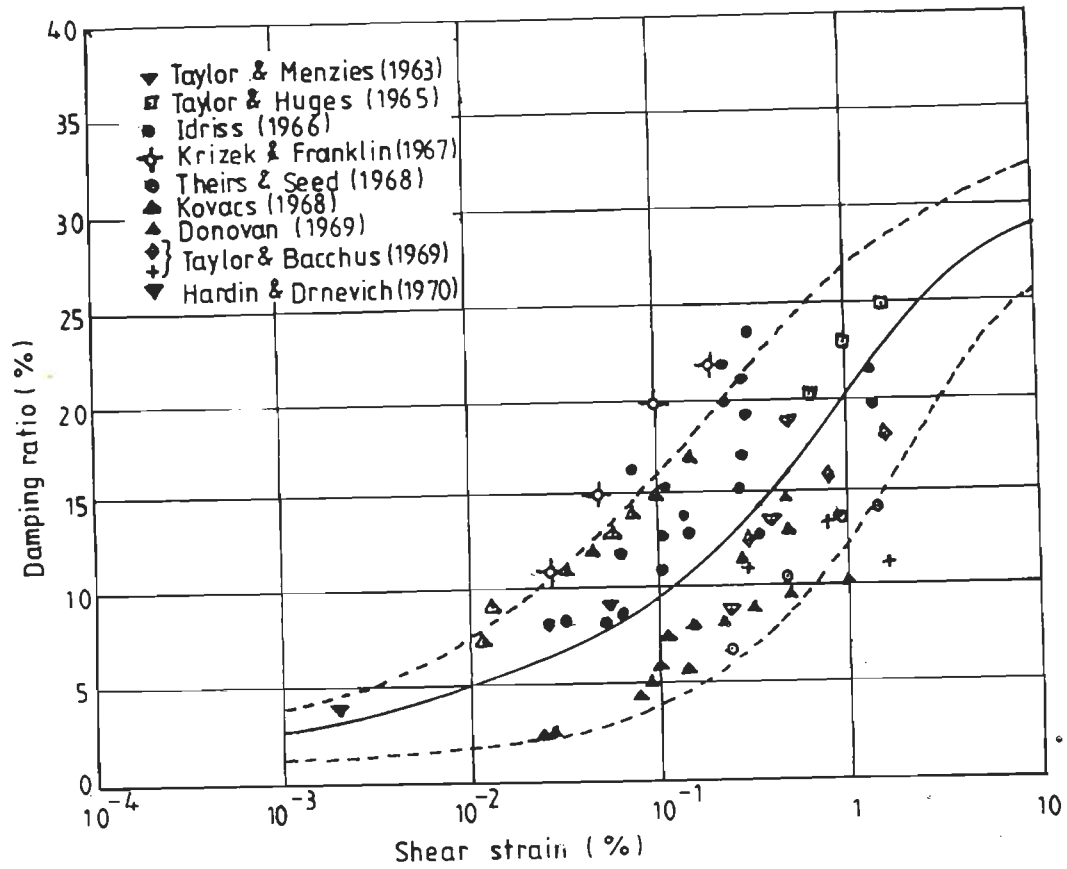


Fig. 2.11 Damping Ratio Curves for Saturated Clays
(Seed and Idriss, 1970)

2.5 SECONDARY TIME EFFECTS ON SHEAR MODULUS

One of the factors affecting shear moduli of soils, namely, secondary time effects or long-term time effects, such as the duration of confining pressure, has been increasingly studied in recent years by a limited number of researchers, Marcuson and Wahls (1972), Afifi and Richart (1973), Anderson and Woods (1976), Stokoe and Abdel (1975), and Anderson and Stokoe (1978).

2.5.1 Secondary Time Effects on Clay Minerals

Marcuson and Wahls (1972), were the only investigators who studied the secondary time effects, on shear modulus of two clay minerals, namely, kaolinite and bentonite. These two minerals were chosen, since kaolinite exhibits a very small amount of secondary consolidation and bentonite exhibits a large amount of secondary consolidation.

In their study, first, the samples were subjected to different magnitudes of consolidation pressure, till the end of primary consolidation. The samples were then tested in resonant column apparatus. Marcuson and Wahls (1972), modified the empirical equation proposed by Hardin and Drnevich (1970a), to take into account the secondary time effects on low-amplitude shear modulus. This modified equation is given by:

$$G = \frac{1709 F(t) (2.973-e)^2 (OCR)^k (\sigma'_m)^{0.5}}{(1+e)} \quad (2.10)$$

where

$$F(t) = 1.0 + 0.046 \log_{10} T \quad (2.11)$$

T accounts for the increase in shear modulus with time.

Afifi and Richart (1973), and Anderson and Woods (1976), performed extensive tests on a variety of soils using resonant column testing equipments. They concluded separately, that for fine grained soils, the increase in low-amplitude shear modulus, due to secondary time effects was of the order of 11 percent or more. These investigators also concluded that:

- 1 the time dependent increase in shear modulus is relatively unimportant for soils having the mean grain diameter, D_{50} greater than 0.04 mm and
- 2 for fine grained soils, the shear modulus values should be estimated only at the end of primary consolidation.

Anderson and Woods (1976), also suggested an empirical relationship between shear wave velocity, V_s , and undrained strength, S_u , for fine grained soils, with a mean grain diameter less than or equal to 0.04 mm. This relationship is given by the following expression:

$$\frac{\Delta V_s}{V_{s1000}} = \exp(1.7 - 0.25S_u + 0.37e) \quad (2.12)$$

in which

ΔV_s = change in shear wave velocity per log cycle of time

V_{s1000} = shear wave velocity determined at the end of primary consolidation.

Eq. 2.12 is applicable, for void ratio and mean grain diameter less than 2.0 and 0.04 mm respectively.

2.5.2 Influence of Duration of Confining Pressure

Stokoe and Abdel (1975), and Anderson and Stokoe (1978), conducted extensive field and laboratory tests, to study the long-term time effects, such as the duration of confining pressure on the shear wave velocities and on shear moduli of soils. They tested 'undisturbed' samples at a constant confining pressure for a long duration of time.

Stokoe and Abdel (1975), plotted the relation between shear wave velocity, V_s , and log of time for each of the tested soils. One of the plots obtained by them is shown in Fig. 2.12. The reason for the first straight line, they cited, was due to changes in void ratio during primary consolidation and that for the second line was due to the result of time effects. Stokoe and Abdel (1975), suggested the following expression to compute the increase in shear wave velocity due to secondary time effects:

$$I_s = \frac{\Delta V_s}{\log_{10}(t_2/t_1)} \quad (2.13)$$

where

I_s = a shear wave velocity coefficient which increases with time

t_1 and t_2 are the durations of times after primary consolidation

ΔV_s = change in shear wave velocity from t_1 to t_2 .

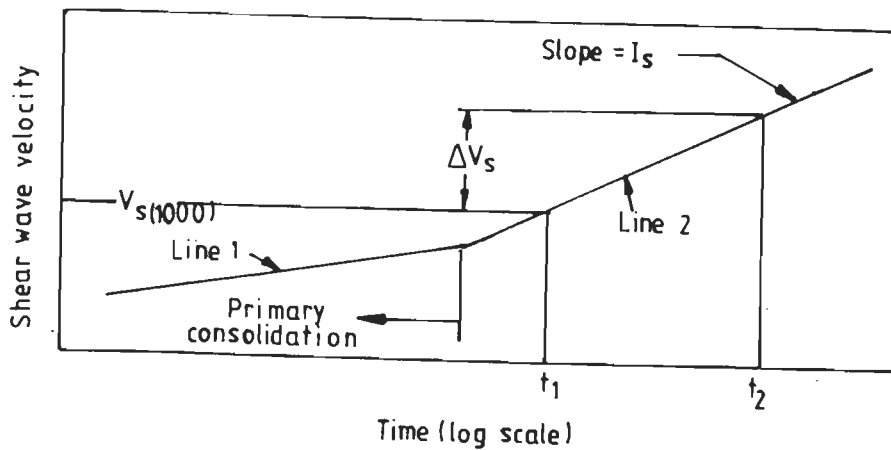


Fig. 2.12 Variation of Shear Wave Velocity with Time at Constant Confining Pressures (Stokoe and Abdel, 1975)

Stokoe and Abdel (1975), concluded that the empirical equation (Eq. 2.2) proposed by Hardin and Drnevich (1970b) could not take into account the secondary increase in the shear moduli of soils.

Anderson and Stokoe (1978), carried out similar tests and they proposed empirical equations in terms of shear modulus, which can take into account the long-term influence of time.

Anderson, Espana and McLamore (1978), performed laboratory tests to determine the shear modulus values on 'undisturbed' samples from four sites. For the same sites, they estimated the shear modulus values based on the Hardin-Drnevich empirical equation (Eq. 2.2) and the Seed-Idriss method of normalized curves. They observed that these two methods under estimated the actual values of shear moduli and the variation was between 25 and 100 percent.

2.6 PREDICTION OF IN-SITU SHEAR MODULUS

Richart, Anderson and Stokoe (1977), and Anderson and Stokoe (1978), attempted to predict the in-situ low-amplitude shear modulus and then the in-situ high-amplitude shear modulus values. The in-situ low-amplitude shear modulus is given by the following expression:

$$G_{mf} = G_{mlp} + F_A \times I_G \quad (2.14)$$

in which

G_{mf} = predicted in-situ low-amplitude shear modulus

G_{mlp} = low-amplitude laboratory determined shear modulus
obtained at the end of primary consolidation

F_A = age factor for the site

I_G = a shear modulus coefficient which increases with time.

The age factor of a particular site is estimated from:

$$F_A = \log_{10}(t_c/t_p) \quad (2.15)$$

where

t_c = time since the start of most recent significant change
in stress history at the site

t_p = time to complete the primary consolidation at the site
as a result of change in stress.

Once the low-amplitude laboratory shear modulus was known, the high-amplitude field shear modulus had been predicted by two methods, namely, the arithmetic method and the percentage method. In the arithmetic method, the high-amplitude field shear modulus, G_f is given by:

$$G_f = G_l + A_r \quad (2.16)$$

in which

G_f = predicted high-amplitude shear modulus

G_l = laboratory determined high-amplitude shear modulus

$$A_r = G_{mf} - G_{mlp} \quad (2.17)$$

In the percentage method, the value of G_f is predicted as given in the expression:

$$\frac{G_f}{G_1} = \frac{G_{mf}}{G_{mlp}} \quad (2.18)$$

The assumption made in Eq. 2.18 is that, the disturbance exhibited on the soil sample in the field and in the laboratory are proportional to each other. The percentage method is widely being used for the prediction of high-amplitude shear modulus in today's Geotechnical-Earthquake Engineering profession.

Anderson and Stokoe (1978), demonstrated the use of the above two methods, for a particular site consisting of dense sand. Fig. 2.13 shows the general trend of the predicted values by both the methods. Anderson and Stokoe (1978), concluded that the arithmetic method and the percentage method yielded upper and lower bound values for the field shear modulus respectively.

Suppiah (1986), proposed a method known as the β -factor method or the disturbance factor method to predict high-amplitude shear modulus values. He conducted field and laboratory tests at two sites to determine shear modulus values of silty soils. To obtain the field curve, wave propagation test, block vibration test, free-vibration test and cyclic plate load test, covering a large range of shear strain (10^{-6} to 1 percent) levels were carried out. Similarly, to obtain the laboratory curve, oscillatory shear test and simple shear test equipments were used, covering a strain range of 3.5×10^{-3} to 1 percent.

According to Suppiah (1986), the value of β at any one value of strain is given by the expression:

$$\beta = \frac{\text{field shear modulus at any strain level, } i}{\text{laboratory shear modulus at the same strain level, } i}$$

He compared the disturbance factor method, which was obtained by conducting field and laboratory tests on silty soils with that of the arithmetic method and the percentage method of prediction, proposed by Anderson and Stokoe (1978), as shown in Fig. 2.14. He further concluded that upto 5.0×10^{-2} percent strain, the β method predicted intermediate values of field shear modulus between the arithmetic and the percentage methods. He further proposed an expression for β as a function of strain for silty soils and given by:

$$\beta = 1.704 - 0.086 \log_{10} \epsilon \quad (2.20)$$

in which

β the disturbance factor corresponding to silty soil.

He further suggested, that at shear strain values smaller than 5×10^{-3} percent, any method of prediction could be adopted.

2.7 NONLINEAR STRESS-STRAIN MODELS

To model the nonlinear stress-strain characteristics of soils, subjected to dynamic or earthquake forces, two models are presently being used. These models are:

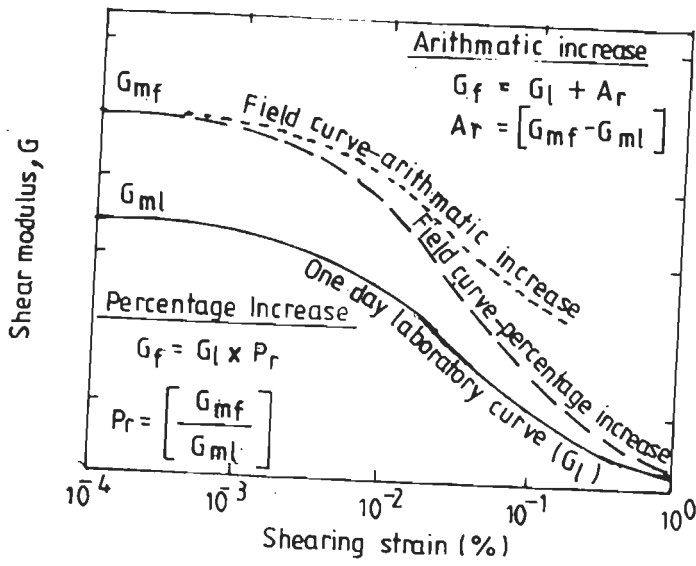


Fig. 2.13 Predicted Field Curve
 (Anderson and Stokoe, 1978)

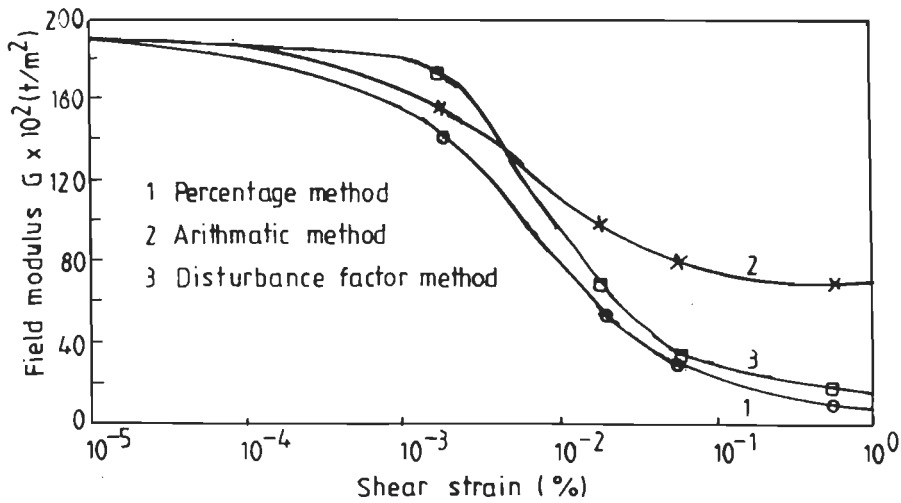


Fig. 2.14 Comparison of Predicted Shear Modulus Values
 (Suppiah, 1986)

- 1 Hardin-Drnevich model proposed by Hardin and Drnevich (1970b)
- 2 Ramberg-Osgood model proposed by Ramberg and Osgood (1943).

These two models are briefly reviewed in the following paragraphs.

2.7.1 Hardin-Drnevich Model

Hardin and Drnevich (1970b), represented the stress-strain relation of the skeleton curve (Fig. 2.15), using the hyperbolic equation, as initially proposed by Kondner (1963), Kondner and Zelasko (1963), and as given by Ishihara (1982):

$$\tau = \frac{G_i \gamma}{1 + (G_i/\tau_m) \gamma} \quad (2.21)$$

where

τ = shear strength of soil

G_i = initial tangent shear modulus, essentially
at $\gamma=0$ and $G_i=G_{\max}$

τ_m = maximum shear stress (at failure).

The different parameters are shown in Fig. 2.15 and γ_r is defined as the reference strain and given by:

$$\gamma_r = \tau_m/G_{\max} \quad (2.22)$$

Hardin and Drnevich (1970b), in an attempt to refine the hyperbolic relation, used a normalized ratio of strain, τ/τ_r . With this normalized value of strain, the stress-strain data collapsed into narrow bands, one for cohesive and the other for cohesionless soils as shown in Fig. 2.16.

Hardin and Drnevich (1970b), further refined the data in Fig. 2.16 and proposed an expression, relating the hyperbolic strain and a few empirical constants. This refined relationship is given by:

$$\tau_h = \tau/\tau_r [1 + a \exp(-b \tau/\tau_r)] \quad (2.23)$$

where

τ_h = hyperbolic strain

a and b are constants, and have to be established depending upon the type of soil.

After establishing the hyperbolic strain, Hardin and Drnevich (1970b), developed one single curve relating the hyperbolic strain to the modulus ratio, G/G_{max} , and damping ratio, D/D_{max} . This relationship is shown in Fig. 2.17.

The different parameters specifying the structure of the Hardin-Drnevich model, as formulated (Ishihara, 1982), are the initial shear modulus, G_i and the shear strength, τ_f . However, it is difficult to specify both the strain dependent shear modulus and damping ratio by the use of only two parameters, since the reference strain, τ_r is once determined from the strain dependent characteristics of the shear

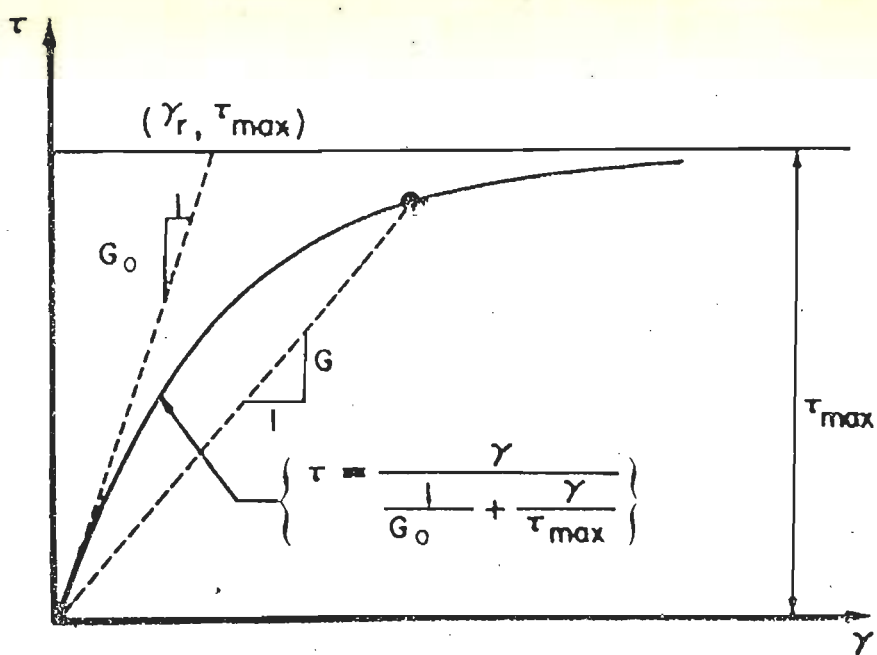


Fig. 2.15 Basic Parameters for Hyperbolic Model

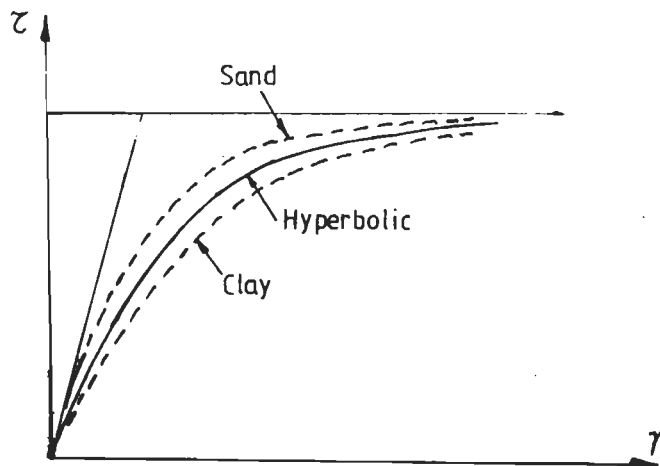


Fig. 2.16 Hyperbolic Stress-Strain Curves for Sand and Clay

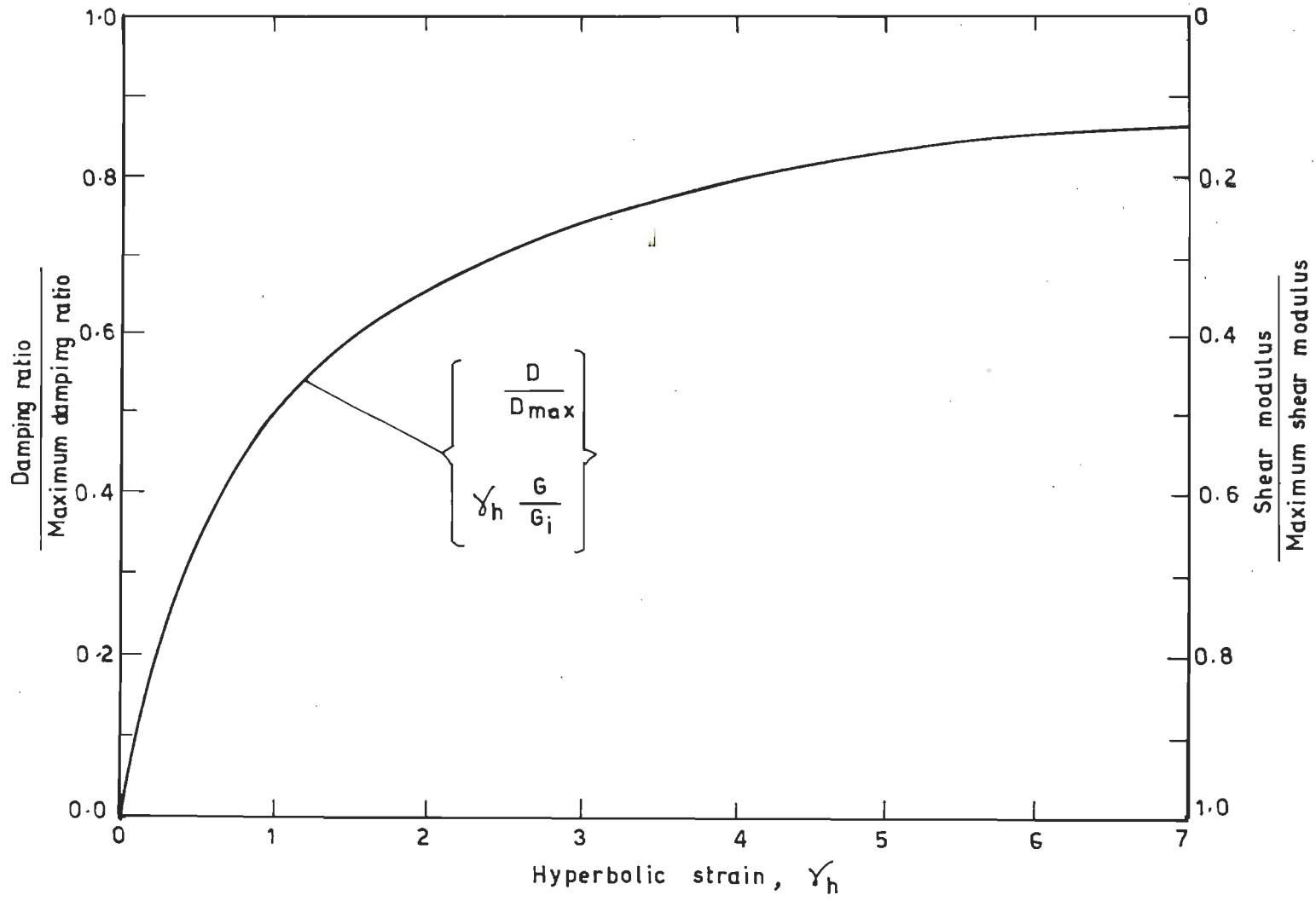


Fig. 2.17 Hyperbolic Strain Relating Normalized Values of Shear Modulus and Damping

modulus, the damping ratio, D/D_{\max} is automatically computed, and the experimentally determined damping values cannot be fitted in the following expression (Ishihara, 1982, 1985):

$$D = \frac{4}{\pi} \frac{1}{1-B} \left[1 - \frac{B}{1-B} \ln \left(\frac{1}{B} \right) \right] - \frac{2}{\pi} \quad (2.24)$$

in which

$$B = G/G_{\max} \text{ or } G/G_i$$

G_i = initial shear modulus.

To avoid this difficulty, Hardin and Drnevich (1970b), proposed the use of the following empirical relationship:

$$D = D_{\max} (1 - B) \quad (2.25)$$

where

D_{\max} = damping value at large strain levels at which G is very small in comparison to G_i or G_{\max} .

Eq. 2.25, gives a better fit to the experimental data, due to the additional parameter, D_{\max} . Nevertheless, this equation is not compatible with the Masing rule and one has to revert to Eq. 2.24, instead of Eq. 2.25 (Ishihara, 1982).

2.7.2 Ramberg-Osgood Model

This model was developed by Ramberg and Osgood (1943), originally to describe the stress-strain characteris-

tics of aircraft metals. However, this model had been applied to simulate the stress-strain characteristics of any strain softening material or structural system. The Ramberg-Osgood model is expressed in a functional form as:

$$\Gamma = \frac{\tau}{G_{\max}} + \alpha \left[\frac{\tau}{G_{\max}} \right]^R \quad (2.26)$$

where

α = dimensionless parameter describing the curvature between the elastic and plastic curves

R = dimensionless parameter describing the amount of break between the elastic and plastic curves.

2.7.3 Hysteresis Loop Criteria

Ramberg and Osgood (1943), described the hysteresis loop, combining Eq. 2.26 and the Masing Criteria (Masing, 1926). The following expression was obtained to describe Ramberg-Osgood hysteresis loop for a material which exhibits the Masing criteria (Masing, 1926):

$$\Gamma_1 - \Gamma_0 = \frac{\tau_1 - \tau_0}{G_{\max}} + \alpha \left[\frac{\tau_1 - \tau_0}{2G_{\max}} \right]^R \quad (2.27)$$

where

Γ_0 and τ_0 denote the point of last load reversal

Γ_1 denotes the shearing strain, corresponding to the shearing stress, τ_1 .

2.7.4 Ramberg-Osgood Hysteretic Damping Value

In the Ramberg-Osgood model, the damping value is given by:

$$D = \frac{2}{\pi} \left[1 - \frac{\tau}{\Gamma G_{max}} + \frac{2\alpha}{\Gamma(R+1)} \left[\frac{\tau}{G_{max}} \right]^R \right] \quad (2.28)$$

2.7.5 Application of Ramberg-Osgood Model

Jennings (1964), first demonstrated the applicability of the Ramberg-Osgood model to structural dynamic problems. In his extensive research, after analysing a single degree of freedom system subjected to sinusoidal excitation Jennings (1964), proposed a general yielding relation.

Constantopoulos, Roësset and Christian (1973), studied the nonlinear dynamic response of a soil deposit. For modelling the nonlinear stress-strain characteristics of the soil deposit, they adopted two methods, namely, a linear visco-elastic model and the Ramberg-Osgood model. From their investigation, they concluded that the Ramberg-Osgood model yielded, displacements and accelerations which were very close to the actual values.

Streeter, Wylie and Richart (1974), and Richart and Wylie (1975), demonstrated the use of the Ramberg-Osgood model to simulate the nonlinear stress-strain characteristics of soils, subjected to earthquake or vibratory loadings. Richart and Wylie (1975), evaluated the dynamic response of a soil deposit, with three different types of model, namely. (1) Ramberg-Osgood model, (2) elastic-slip model and (3) strain compatible visco-elastic model. They concluded, that the Ramberg-Osgood model gave better results in comparison to the other two models.

Papadakis and Wylie (1975), evaluated the dynamic response of an earth dam using the Ramberg-Osgood method to model the nonlinear stress-strain behaviour of the soils involved.

Faccioli and Ramirez (1976), studied the seismic amplification response of horizontally stratified soil deposits using the Ramberg-Osgood stress-strain relationship. They modelled the deposit as a discrete shear beam system.

Idriss, Dobry and Singh (1978), adopted the Ramberg-Osgood model to account for degradation in soft clayey soils due to cyclic loading. They concluded that the Ramberg-Osgood model yielded satisfactory results, which were close to the actual values.

2.7.6 Modifications to Ramberg-Osgood Model

Richart (1975), made a revision of Eq. 2.26 and proposed the following expression:



$$\Gamma = \frac{\tau}{G_{\max}} \left[1 + \alpha \left| \frac{\tau}{C_1 \tau_m} \right|^{R-1} \right] \quad (2.29)$$

in which

C_1 = a factor relating the maximum shear strength and yield shear strength.

Richart (1975), suggested a value for C_1 , as in the following expression:

$$C_1 = \tau_y / \tau_m \quad (2.30)$$

Pyke (1979), proposed a new hypothesis on the hysteretic modelling phenomena. He replaced the constant, C_1 , in Eq. 2.29, by the following expression:

$$C_1 = \left| \pm 1 - \frac{\tau_0}{\tau_y} \right| \quad (2.31)$$

in which

τ_0 = shear stress at the last reversal of loading.

The first term in Eq. 2.31, is negative for unloading and positive for reloading. Hara (1980), recommended the use of the reference strain, Γ_r , in place of Γ , and τ_y , in place of τ in Eq. 2.29. This modification is identical to substituting a value of unity for C_1 in Eq. 2.29.

2.7.7 Comparison Between Hardin-Drnevich and Ramberg-Osgood Models

Very few investigators, for instance, Anderson (1974), Richart and Wylie (1975), Isenhower (1979), Ishihara (1982, 1985, 1987), and Shamoto (1984) have made attempts to model the nonlinear stress strain characteristics of different soils by the Hardin-Drnevich model and the Ramberg-Osgood model. The important findings of these investigators are reported in the following paragraphs.

Anderson (1974), studied the stress-strain relationship of different type of soils, by employing both the models, and reported that the Ramberg-Osgood method could be adopted to predict the high-amplitude behaviour. He found that both the models were inconsistent in predicting the stress-strain characteristics at large strain values. However, Anderson (1974), reported that the Ramberg-Osgood model gave a better fit to shear strains below $\gamma = 0.1$ per cent.

Richart and Wylie (1975), attempted to obtain the Ramberg-Osgood model parameters, for the already available hyperbolic curves of Hardin-Drnevich. The different values for the constants in the Ramberg-Osgood model, obtained by Richart and Wylie (1975), are shown in Fig. 2.18.

Desai (1977), reported the advantages of the Ramberg-Osgood model over the Hardin-Drnevich model and recommended the adoption of the former model, for modelling of Geologic media.

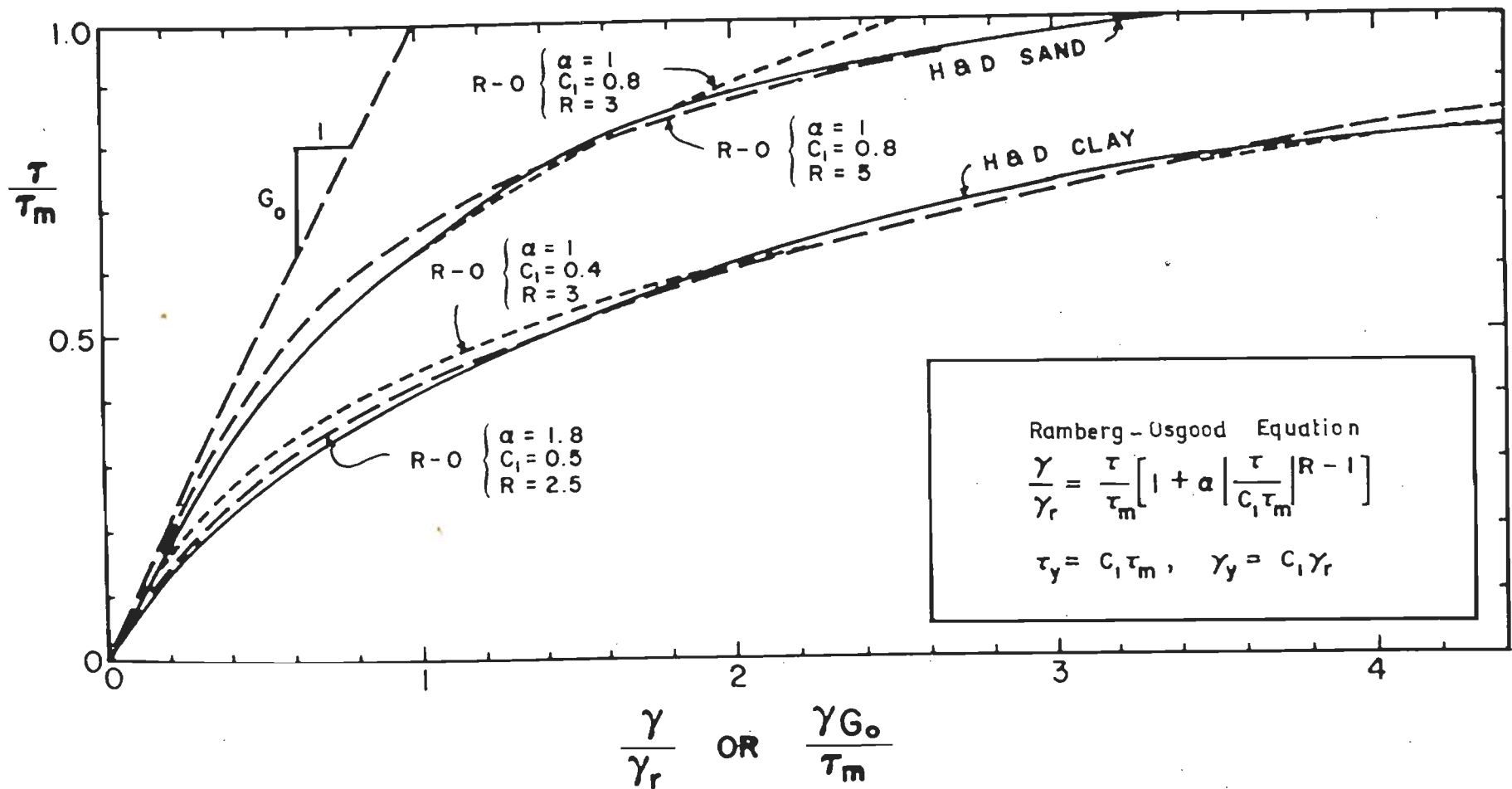


Fig. 2.18 Fit of Hardin-Drnevich and Ramberg-Osgood Models
(Richart and Wylie, 1975)

According to Roësset (1977), the Ramberg-Osgood model provided the most reasonable fit to experimental data.

Isenhower (1979), also attempted to model the stress-strain characteristics of San Francisco bay mud by both the models and found that the Ramberg-Osgood model performed better than the Hardin-Drnevich model.

Ishihara (1982), investigated the suitability of the Hardin-Drnevich and Ramberg-Osgood models, to simulate the nonlinear stress-strain characteristics of soils subjected to dynamic loadings, through extensive test procedures in the field and in the laboratory to determine shear modulus and damping values of various soils.

Ishihara (1982), pointed out the advantages and disadvantages of both the models. The following are some of his significant conclusions:

- 1 The Hardin-Drnevich model can be used only for the response analysis, inducing medium level of shear strains in the soil upto about 1.0 percent, and the Ramberg-Osgood model can be adopted for large and failure strain levels ($\gamma > 1.0$ percent).
- 2 When the shear strain becomes large ($\gamma > 1.0$ percent) the Hardin-Drnevich model tends to converge to a damping value of 63.7 ($= 2/\pi \times 100$) percent, which is excessively large when compared to the experimentally obtained value.
- 3 The Hardin-Drnevich model is formulated, based on two parameters, namely, the initial shear modulus (G_i)

and the shear strength at failure (τ_f). Whereas, the Ramberg-Osgood model is based on four parameters, namely, G_i or G_{max} , τ_f , α and R . Out of these four parameters, the two constants, α and R permit the adjustment of the shape and position of the curve. Thus, the Ramberg-Osgood model gives a better fit to the experimentally observed strain dependent soil properties.

Ishihara (1982), further, summarized the values of reference strain, τ_r , failure strain, τ_f , and the two constants, α and R as applicable to the Ramberg-Osgood model. These values are presented in Fig. 2.19 and in Table 2.2.

Shamoto (1984), conducted cyclic triaxial tests to determine the strain dependent shear moduli and damping values on 'undisturbed' silts and clays. He fitted his experimental values of shear modulus and damping by the Hardin-Drnevich and the Ramberg-Osgood models. He observed that both the models fitted as closely as possible to his experimental values of shear modulus in the strain range of 10^{-4} to 10^{-2} percent. Shamoto (1984), however, observed that the damping values predicted using the Hardin-Drnevich model were very much larger than the actual values at large strain levels, whereas, the Ramberg-Osgood model yielded a better fit to his damping values as well.

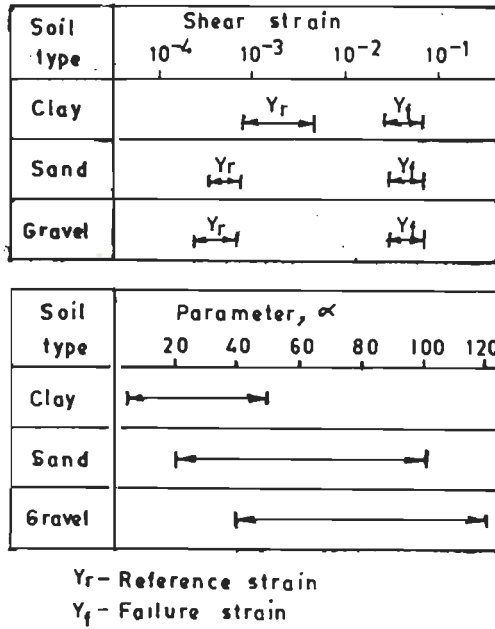


Fig. 2.19 Approximate Values of Reference Strain and Failure Strain (Ishihara, 1982)

Table 2.2 Approximate Values of Damping Ratio at Large Strains (Ishihara, 1982)

Soil Type (1)	Damping Ratio at Large Strain, D_{max} (2)	Parameter R (3)
Clay	0.15 \approx 0.30	1.65 \approx 2.80
Sand	0.25 \approx 0.40	2.30 \approx 4.40
Gravel	0.20 \approx 0.35	1.90 \approx 3.40

2.8 ANALYSIS OF EMBANKMENT DAMS USING FINITE ELEMENT METHOD

The finite element method is being used since 1960, for the static and dynamic analysis of embankment dams. A few of the important work carried out by different researchers is reviewed in this section.

2.8.1 Static Analysis

Clough and Woodward (1967), were the first to apply the finite element method for the analysis of a homogeneous embankment dam of height 30 m, to study the distribution of displacements and stresses obtained by the 'gravity turn-on' method and the incremental construction method. The dam section has been analysed using constant strain triangular elements and linear elastic material properties. From the linear elastic analysis Clough and Woodward (1967), observed that the horizontal displacements are identical in both the cases. However, the vertical displacements were maximum at the crest in the 'gravity turn-on' method. Whereas, in the construction sequence method, the maximum vertical displacement was noticed in the mid-height region of the embankment. They also, concluded that the stresses obtained in both the cases were nearly identical in the linear analysis.

Kulhawy and Duncan (1972), adopted the finite element method using the triangular elements and plane strain condition to evaluate the stresses and movements of the

Oroville Dam of 235 m height, with an inclined core, during construction. The stress-strain characteristics of the different materials were simulated by the nonlinear hyperbolic model (Kondner, 1963; Kondner and Zelasko, 1963; Duncan and Chang, 1970).

Nobari and Duncan (1972), used the finite element method to study the behaviour of the Oroville Dam due to filling of the reservoir. The same finite element mesh used by Kulhawy and Duncan (1972), has been used in this case as well. The stresses obtained at the end-of-construction condition of the Oroville Dam have been adopted as the initial stresses by Nobari and Duncan (1972).

Resendiz and Romo (1972), Alberro (1972), and Skermer (1973), have utilized the finite element method of analysis and sequential construction technique, for the analysis of numerous embankment dams to study the distribution of different type of stresses.

Resendiz and Romo (1972), have used the Kondner's hyperbolic model to simulate the stress-strain characteristics of different soils, to analyse 14 dam sections of different heights and slopes.

Alberro (1972), and Skermer (1973), have analysed separately, the El Infiernillo Dam, assuming the plane strain condition and the concept of construction sequence. In both the analyses the number of lifts used was seven only.

Llyn Brianne rockfill Dam (United Kingdom) has been analysed using the finite element method to study the

constructional deformations by Penman and Charles (1973). The height of the dam was 142 m including a foundation of depth 52 m. The dam has been idealized into 10 layers and the foundation into 3 horizontal layers. The stress-strain relationship used was of linear characteristics.

Skermer (1975), performed an analysis of the Mica Dam based on the finite element method. This dam is of 240 m height and is one of the highest rockfill dams in the world. The dam has been discretized into a total number of 359 elements consisting of constant strain triangles, linear strain rectangles and trapezoidal elements. The analysis has been carried out using construction sequence operation in 16 lifts.

In India, Sharma (1976), carried out the nonlinear static analysis of the proposed 260 m high Tehri rockfill Dam with two different types of cores. One type was the central core and the other was an inclined core. The analysis has been performed assuming plane strain condition and without interaction of the foundation. The stress-strain characteristics of the different materials constituting the dam section under static condition have been simulated using the hyperbolic law (Kondner and Zelasko, 1963; Duncan and Chang, 1970). The construction sequence operation has been considered into account by discretizing the dam into 10 horizontal layers, using isoparametric, numerically integrated curved joint elements. The residual force approach has been used for convergence purpose. The dam

section has been analysed for:

- 1 end-of-construction condition and
- 2 reservoir-full loading case.

The stresses computed in the end-of-construction case have been used as the initial condition for the reservoir-full loading case. The filling of the reservoir was simulated in 5 steps and the upstream shell and transition materials have been assumed to be submerged below the phreatic line. The water pressure was assumed to act along the upstream face of the core.

Sharma (1976), concluded that no separation was noticed in the dam section with vertical core under end-of-construction condition, along the shell-filter-core interfaces in the upstream and the downstream. However, in the inclined core case, separation has been observed along the core-filter interface in zones with high deviatoric stresses.

Larger horizontal and vertical displacements have been noticed in the vertical core case and the inclined core case respectively. Also, along the core-filter interface in the upstream, separation has occurred, due to water loading. However, no such phenomenon has been observed in the downstream. The water loading has increased the horizontal and the vertical stresses in the core.

2.8.2 Dynamic Analysis

Clough and Chopra (1966), were the pioneers to

apply the finite element method to the solution of two dimensional linear elasto-dynamic problems. Since then, the finite element method has been used by many investigators (Chopra, 1967; Idriss and Seed, 1967; Idriss, 1968) to study the different aspects of the behaviour of earth structures subjected to vibratory and earthquake loadings (Dibaj and Penzien, 1969).

Seed, Lee and Idriss (1968), performed the dynamic analysis of the Sheffield hydraulic fill Dam which collapsed during the June 29, 1925, Santa Barbara (California) earthquake, to study the adequacy of the existing analytical methods. The Sheffield Dam was constructed in 1917, in the city of Santa Barbara. A representative section through the dam at its maximum height is shown in Fig. 2.20. The height of the Sheffield Dam was 8.3 metres and composed of silty sand and sandy silt.

The dynamic analysis was carried out by using strain independent Young's modulus values for the embankment and the foundation materials. Finite element method with constant strain triangles and the base input motion was a hypothetical record with a peak ground acceleration of $0.15g$ (g is the acceleration due to gravity) and a total duration of 15 seconds. Based on the dynamic analysis results and cyclic simple shear tests performed in the laboratory, Seed, Lee and Idriss (1968), demonstrated the progressive failure of the dam due to liquefaction phenomenon.

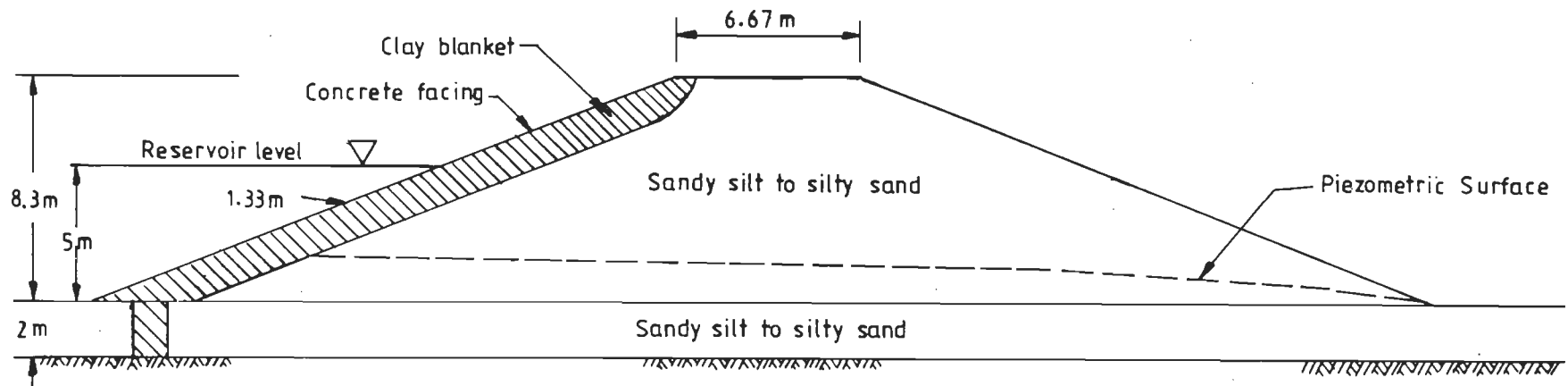


Fig. 2.20 Sheffield Dam Cross Section
(Seed, Lee and Idriss, 1968)

Penzien, Scheffey and Parmelee (1964), were the first to perform a nonlinear dynamic analysis of soil masses using a discrete mathematical model. These investigators developed a one dimensional model with lumped masses to study the response of semi-infinite soil layers having hysteretic bilinear stress-strain characteristics. By dividing the soil layers into a number of sub-layers and replacing every sub-layer by a Kelvin model attached in series to a dashpot representing the creep characteristics of the layer, the semi-infinite solid was reduced to a one-dimensional model with several degrees of freedom. The assumption made was that the spring of the Kelvin model had bilinear hysteretic force-displacement characteristics and that the dashpot represented the internal velocity dependent damping within each sub-layer (Dibaj and Penzien, 1969).

Idriss and Seed (1968), have used the above mentioned Kelvin model to evaluate the response of soil deposits during earthquakes and have proposed a procedure for substituting equivalent linear parameters for the bilinear stress-strain characteristics (Dibaj and Penzien, 1969).

Dibaj and Penzien (1969), have extended the Drucker-Prager yield criterion to include work-hardening effects for materials obeying this criterion. These two researchers have employed the finite element method with triangular elements, Wilson- θ (Bathe and Wilson, 1987) method of step-by-step time integration scheme to develop an incremental procedure for nonlinear earthquake analysis of

earth structures. Two earth structures, one with central core and another without the core have been extensively analysed for nonlinear dynamic responses by computing the time-history of acceleration and displacement at a few important locations. The analysed dam sections along with the finite element discretization is shown in Fig. 2.21.

The discretized finite element mesh consisted of 80 triangular elements and 54 nodal points. In all the analyses, the nonlinear solution has been compared with the linear solution and the pre-earthquake stresses have been computed by a linear analysis. In the numerous dynamic analyses conducted, either the El-Centro earthquake of May 18, 1940 or an artificial accelerogram corresponding to an earthquake of magnitude of 8.3 has been used as the base input motion.

From the very extensive analytical studies carried out, Dibaj and Penzien (1969), arrived at the following significant conclusions:

- 1 The magnitude, distribution and direction of stresses are not adequate for predicting a failure but the magnitude and distribution of strains based on experiments and displacements are the significant factors for predicting failure.
- 2 No significant difference in acceleration response was noticed between linear and nonlinear solutions. However, the maximum displacement obtained in the nonlinear solution was larger than that obtained in

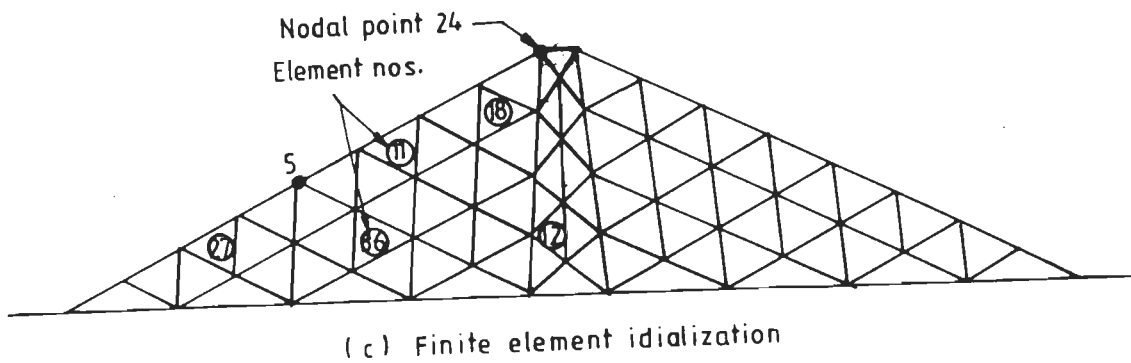
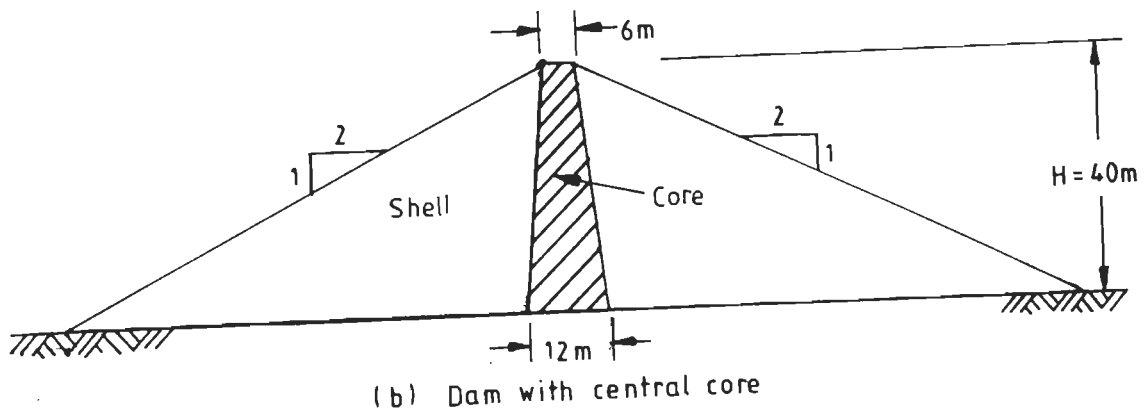
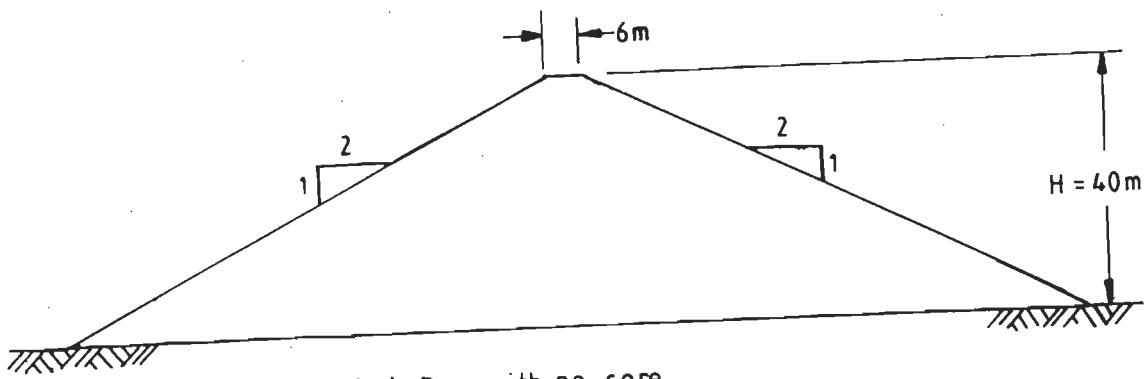


Fig. 2.21 Embankment Dams Analysed
(Dibaj and Penzien, 1969)

the linear solution and in a few cases, it was twice that of the linear case.

- 3 The dynamic response of earth structures is significantly affected by the nonlinear properties of the materials distributed within the structure. The presence of a core in an earth dam alters the dynamic response appreciably.
- 4 The vertical component of the ground motion has an important effect in the overall response of an earth structure when subjected to a nonlinear earthquake analysis. Dibaj and Penzien (1969), finally concluded that the geometry, nonlinear material characteristics, base input motion and other similar factors decide the dynamic response of an earth structure.

Seed et al. (1973), performed the dynamic analysis of the 48 m high Lower San Fernando Dam and the 27 m high Upper San Fernando Dam. These two dams were of hydraulic fill type and the Lower San Fernando Dam failed during the earthquake of February 9, 1971.

Seed et al. (1973), carried out extensive field survey and collected soil samples immediately after the occurrence of the February 9, 1971 earthquake. Numerous laboratory tests, such as cyclic triaxial tests have been conducted to evaluate the strength characteristics of the different dam materials. Using these strength characteris-

tics, the pre-earthquake stresses have been determined using the hyperbolic model (Kulhawy, Duncan and Seed, 1969; Duncan and Chang, 1970). For the dynamic analysis the strain dependent shear modulus and damping characteristics as proposed by Seed and Idriss (1970), have been adopted. The dynamic analysis has been performed using linear triangular elements and a computer coding called QUAD-4 (Idriss et al., 1973) with the Wilson- θ step-by-step time integration scheme (Bathe, 1982; Bathe and Wilson, 1987). The base input motion used was the modified Pacoima record with a peak ground acceleration of 0.60g.

Based on the experimental and analytical studies on the Lower and Upper San Fernando Dams, Seed et al. (1973), concluded that:

- 1 The Lower San Fernando Dam failed due to liquefaction phenomenon.
- 2 The analysis based on QUAD-4 computer coding predicted the behaviour that was very close to the actual condition due to the February 9, 1971 earthquake.

Due to the near catastrophic failure of the Lower San Fernando Dam, during the February 9, 1971 earthquake, the Water Resources Department of California, USA, ordered the investigation of the stability of all the existing dams against future earthquakes. In one such investigation, Marcuson and Krinitzsky (1976), carried out the dynamic

analysis of the 120 m high Fort Peck hydraulic fill Dam. This dam was one of the medium height dams. The initial stresses have been determined based on a nonlinear two-dimensional 'gravity turn-on' finite element static analysis using the Duncan-Chang method. The dynamic analysis procedure was identical to the procedures used in the analysis of the Lower and Upper San Fernando hydraulic fill Dams. The base input motion used was the Helena, Montana, earthquake record of 1935, normalized to a peak ground acceleration of 0.20g.

After conducting extensive in-situ and laboratory tests, Marcuson and Krinitzsky (1976), concluded that the Fort Peck hydraulic fill Dam was safe in the event of an earthquake of magnitude 5.5. From the static and dynamic analysis of the Fort Peck Dam, the investigators concluded that:

- 1 There was no danger of liquefaction or excessive deformation during or after the occurrence of the earthquake, against the postulated event.
- 2 Evaluation of stability against 5 percent strain during the postulated earthquake of 0.20g, indicated that the major portions of the dam section have had factors of safety greater than 1.0. Local areas in the foundation at the upstream side of the core trench were found to have factor of safety less than 1.0 indicating the soils in these areas could deform more than 5 percent. Similar local area was observed at the downstream toe as well.

Similar type of dynamic analyses have been done by Carrera et al. (1979), on the Guri Dam of height 120 m located in the Guyana Region of Venezuela. The time-history of the Parkfield, California, event scaled to 0.20g and without any change in the time scale has been used as the base input motion. The peak horizontal acceleration of 0.20g was expected to result from a magnitude 5.0 earthquake, with epicentre within one or two kilometres of the dam site. Severn et al. (1979), carried out in-situ vibratory tests on Llyn Brianne rockfill Dam and conformed that Nose's method (Nose, Takahashi and Kunii, 1976), of computing the shear wave velocity yielded values very close to the actual values of shear wave velocities.

Romo et al. (1980), have performed dynamic analysis on two rockfill dams, namely, El Infiernillo and La Villita Dams. The former is 146 m high and the latter is 60 m high and situated in the Mexico City.

As mentioned earlier, the initial stresses have been computed using the method proposed by Kulhawy, Duncan and Seed (1969), and Duncan and Chang (1970). The dynamic analyses procedures used were the same as that adopted in the analysis of the Lower and the Upper San Fernando hydraulic fill Dams.

The El Infiernillo and the La villita Dams had been subjected to the March 14, 1979, Mexico earthquake. During the time of the earthquake the two dams had been very extensively instrumented and the actual values of accelera-

tion and displacement have been recorded/measured.

The March 14, 1979 earthquake originated near the coast of the State of Guerrero, Mexico, with epicenter about 40 km from the resort town of Zihvatanejo. The characteristics of the earthquake were:

- 1 Epicenter = 17.823° N; 101.259° W
- 2 Focal depth = 59 km
- 3 Magnitude = 7.6 (Richter scale).

The distances from the epicenter to the El Infiernillo and La Villita Dams were 87 and 108 km respectively (Alonso, Prince and Havskov, 1980).

Due to the March 14, 1979 earthquake, cracks have been noticed at the crests of El Infiernillo and La Villita Dams. The horizontal displacements and the vertical settlements at the crest of El Infiernillo and La Villita Dams were 13 and 5 cms and 4.5 and 8 cms respectively.

The crest accelerations observed at the El Infiernillo and La Villita Dams were of the order of 0.36g and 0.38g respectively. Interestingly, a dam of lower height (La Villita Dam, height = 60 m), experienced larger acceleration value than a taller dam did (El Infiernillo Dam, height is 146 m). This shows that the dynamic response of a rockfill dam is a function of different parameters, such as the geometry and dynamic properties of different materials.

Resendiz, Romo and Moreno (1980), concluded that a finite threshold value of acceleration existed for each dam. The threshold values of acceleration for the El Infiernillo

and the La Villita Dams were:

$$0.21g < a_r \leq 0.36g \quad \text{for El Infiernillo Dam}$$

$$0.31g < a_r \leq 0.38g \quad \text{for La Villita Dam}$$

in which

a_r is the threshold value of acceleration.

From the dynamic analysis carried out on the El Infiernillo and the La Villita Dams, the observed behaviour of these two dams during the March 14, 1979, Mexico earthquake and the comparative study between the observations made after the occurrence of the earthquake and analysis results, Resendiz, Romo and Moreno (1980), arrived at the following conclusions:

- 1 The seismic behaviour of El Infiernillo and La Villita Dams demonstrated that strong earthquakes acting on modern embankment dams are capable of producing permanent deformations, which are not negligible as compared to that occurred during construction, first filling of the reservoir, or decades of normal operation after first filling. And no high embankment dam should be considered intrinsically safe against earthquakes. Thus, every important dam in seismic zones should explicitly be designed against earthquake damage.
- 2 For every dam a threshold for input rock acceleration and for maximum response acceleration seems to exist below which no significant damage or permanent

deformation occurs.

- 3 The behaviour of the El Infiernillo and the La Villita Dams during the earthquake of March 14, 1979, generally conforms to the trend expected from the best of the current knowledge. The main deformation pattern and type of damage, including cracking were those associated with shear distortion (spreading) of the embankment under dynamic shaking.
- 4 The existing two-dimensional, nonlinear finite element models are capable of reproducing the spectra of the observed dynamic response, provided the parameters of the relationship between strain dependent shear modulus as a function of confining pressure and strain dependent damping values are properly selected.
- 5 Stiffening of the embankment materials seems to be induced by strong earthquakes in El Infiernillo and La Villita Dams.

Lai and Seed (1985), carried out the dynamic analysis of Long Valley Dam, which was subjected to the Mammoth Lake Earthquake Series of May 25-27, 1980, using 2- and 3- dimensional finite element models (FLUSH and TLUSH computer packages respectively), taking into account strain dependent dynamic material properties.

The Long Valley Dam is supported on bedrock and has a maximum height of 40 m with a crest length of 200 m.

The dam is a homogeneous section with the main compacted fill consisting of sand and gravel with sufficient fines to produce a permeability somewhat less than 7×10^{-6} cm/sec, and with outer shell consisting of dumped-sluiced small rock and coarse fines.

The Long Valley Dam is situated in a high seismicity region. Due to May 25-27, 1980, earthquake no significant damage was noticed in the dam, but water was observed to flow out of the soil just downstream of the toe of the dam and continued to flow for several minutes after the earthquake shaking ceased. In this region the materials were dumped and loosely compacted. Interestingly, a moderate earthquake (magnitude = 6.2) with peak acceleration of 0.20g in bedrock, reduced the volume and developed excess pore pressures sufficient to cause liquefaction and expulsion of water.

From the 2- and 3- dimensional dynamic analyses. Lai and Seed (1985), concluded that the analysis results were in close conformity to the observed values of acceleration due to the May 25-27, 1980, Mammoth Valley earthquake, with the computed values being larger than the observed values.

In India, a number of two dimensional dynamic analyses of earth and rockfill dams have been conducted using the finite element method based on eight-noded isoparametric elements by Chandrasekaran, Paul and Suppiah (1984, 1985); Chandrasekaran and Prakash (1989a, 1989b). The pre-earthquake stresses have been computed using a two-

dimensional linear 'gravity turn-on' analysis. In all the dynamic analyses, only linear (strain in-dependent) properties of moduli, constant values of modal damping and mode-superposition method have been used. Interestingly, based on the linear analysis alone, Chandrasekaran and Prakash (1989a), concluded that rockfill dams can withstand earthquake forces.

2.9 CLOSURE

From the brief review of literature presented it is observed that the shear modulus and damping ratio of different soils are strain dependent. Empirical equations for determination of low-amplitude shear modulus are available mostly for clay and sandy soils only. These empirical equations do not yield precise values of dynamic properties. Modulus attenuation curves and damping ratio curves, as a function of strain are available for clay and sand materials only. These curves are meagerly available for gravel and silty soils.

For the prediction of in-situ high-amplitude shear modulus, presently arithmetic method and percentage method are available. These two methods are strain independent and yield upper and lower bound values of shear moduli respectively.

The shear modulus of fine grained soils in addition to the mean confining pressure and the void ratio, is significantly influenced by the secondary time effects.

Also, from the brief review of literature it is noticed that the finite element method is being widely used in Geotechnical Engineering profession. The pre-earthquake stresses in an embankment dam are computed using the nonlinear analysis procedure as proposed by Duncan and his co-workers, either in the sequential or 'gravity turn-on' method. The nonlinear dynamic analysis of embankment dams are done using the popular computer codings, such as QUAD-4, LUSH, FLUSH or TLUSH which are based on the Seed-Idriss method of modulus reduction curves and damping ratio curves only. These computer programs use either linear triangular or four-noded rectangular elements only and not the versatile and stable eight-noded isoparametric elements with reduced integration.

In India, most of the static and dynamic analysis of different embankment dams carried out till today are based on the linear analysis with strain in dependent moduli and constant values of modal damping only.

In view of the aforesaid limitations, there is a need to investigate the following:

- 1 The influence of long-term or secondary time effects on shear moduli of different type of soils, by conducting different types of field and laboratory tests.
- 2 To predict the high-amplitude in-situ shear modulus value for sites wherein the shear modulus values are not available.

- 3 To establish modulus attenuation curves for silt and gravel materials, in addition to clay and sandy soils, and to compare these attenuation curves with the curves very widely used in today's Geotechnical Earthquake Engineering profession.
- 4 To determine the appropriate parameters of the Ramberg-Osgood model depending upon the type of soil.
- 5 To implement the Ramberg-Osgood model and Hardin-Drnevich model in a computer coding based on the finite element method with eight-noded isoparametric elements, that is capable of analysing dynamic soil-structure interaction problems in the time domain using the step-by-step integration scheme.
- 6 To apply the computer coding developed in Step 5, for the case-history study of a well instrumented rockfill dam and for the dynamic analysis of two other rockfill dams of medium and large height including the interaction of foundation and to compare the dynamic responses with that of the Hardin-Drnevich model and the very widely used Seed-Idriss method of analysis.

CHAPTER 3

FIELD AND LABORATORY TESTS

3.1 GENERAL

The influence of secondary time effects on shear moduli of different soils can be evaluated only by conducting tests in the laboratory. The Ramberg-Osgood model parameters, namely, α and R as mentioned in Chapter 2, can be computed by establishing shear modulus as a function of strain. Therefore, different type of field tests, which are very frequently carried out in India, at the School of Research and Training in Earthquake Engineering (Prakash and his co-workers 1968a, 1968b, 1970, 1971, 1972, 1973, 1974, 1975, 1976a, 1976b, 1980; Nandakumaran et al. 1977, 1979, 1980; IS: 5249, 1977; Prakash, 1981), of the University of Roorkee, Roorkee (India), have been used to obtain the shear modulus value as a function of strain, varying from small strain value to large strain value. Field tests have been conducted at four different sites consisting of different types of soils.

In addition to different field tests, laboratory tests have also been carried out in the range of medium strain level to large strain levels, on 'undisturbed' soils borrowed from the first three sites. The various type of field tests and laboratory tests, which were performed are

described in this chapter.

3.2 FIELD TESTS

The different types of field tests, conducted in the four different sites to establish the relationship between shear modulus and shear strain are (Barkan, 1962; IS: 5249, 1977; Nandakumaran et al., 1977; Prakash, 1981):

- 1 wave propagation test
- 2 block vibration test
- 3 free vibration test
- 4 cyclic plate load test.

These tests are briefly described in the following sub-sections.

3.2.1 Wave Propagation Test

For the determination of low-amplitude field shear modulus values (shear strain ranging between 10^{-6} to 10^{-5} percent), hammer test was conducted. In the hammer test, arbitrary radial lines were ranged out from the origin (the point at which impact was given), for a distance of 30-40 m. At every 2 metre interval marking was done along these arbitrary radial lines. At the origin, a geophone was embedded at a depth of 0.15 m from the surface. Waves were generated at the origin by the impact of a 5 kg hammer falling from a height of 2 m on a 0.15 m thick steel plate resting on the ground surface at the origin. Similarly, a second geophone was fixed at a known distance along one of

the radial lines. The time taken by the waves to travel a known distance was determined. The test was repeated for other different known distances between the pick-ups along each of the radial line.

The various values of the travel times for the compression waves and the corresponding distances along the pre-selected lines were plotted. From the plot, the average value of the compression wave velocity was calculated. Knowing the value of compression wave velocity and Poisson's ratio, the shear modulus corresponding to low-amplitude strain level was determined.

3.2.2 Block Vibration Test

For the determination of in-situ shear modulus at medium strain ranges, block vibration test was conducted in the vertical and horizontal directions. In this test, a standard plane concrete block of size 3.0 m x 1.5 m x 0.70 m (length, width and height respectively) was cast at the site, at a depth of 1.0 m from the ground surface as shown in Fig. 3.1 (IS: 5249, 1977).

The block was excited to resonance with the help of a mechanical oscillator mounted on the top surface of the block and driven by a speed controlled direct current motor. The vibrations were sensed using acceleration pick-ups, the signal of which was amplified through a universal amplifier and recorded directly on an ink writing oscillograph.

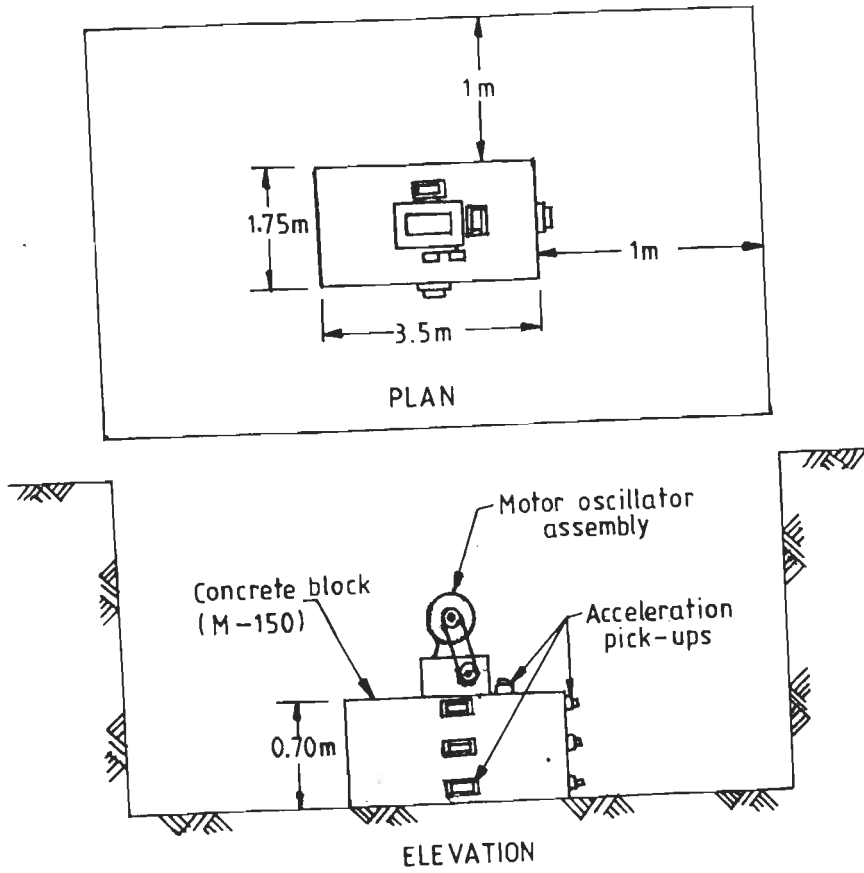


Fig. 3.1 Block Vibration Test Set-up
(IS: 5249, 1977)

3.2.2.1 Forced vertical vibration test

For the vertical vibration mode, two acceleration pick-ups were fixed on the top of the block, such that the pick-ups could sense vertical vibration only. The mechanical oscillator, which works on the principle of eccentric masses, mounted on two shafts rotating in opposite directions on the block was used to generate sinusoidal vibrations, in the vertical direction only. The amplitudes of motion of the block at different frequencies were recorded using acceleration pick-ups. The block was excited with varying magnitudes of sinusoidal forces.

3.2.2.2 Forced horizontal vibration test

The forced horizontal vibration test was conducted by mounting the oscillator in such a direction, that sinusoidal vibrations were produced in the horizontal direction only. The response was recorded as described in Sec. 3.2.2.1.

3.2.3 Free Vibration Test

Free vibration test was performed by striking the block with a hammer in the vertical direction and by pulling the block and releasing it in the longitudinal direction. Knowing the natural frequency in both the directions, the shear modulus values were calculated.

3.2.4 Cyclic Plate Load Test

For the determination of in-situ shear modulus values at large strain levels, cyclic plate load test was performed. The various equipments and accessories used were same as those required to carry out a static plate load test as described in IS: 1888, (1971). To perform the plate load test, a pit was dug to a depth of 1.0 m from the ground surface. A square steel plate of size 0.60 m x 0.60 m, was placed at the centre of the pit, after levelling the top surface of the pit. The lateral dimensions of the pit were kept as more than 5 times the largest size of the steel plate.

Kentledge was used as loading for the plate load test. A hydraulic jack with an attached pressure gauge was kept in between the kentledge and the test plate. The settlement of the plate was measured with the help of four dial gauges resting at the four corners of the test plate and fixed to an independent datum bar. Once the whole assembly was ready, the initial readings of the dial gauges were noted and the first increment of the static load was applied to the plate. The initial loading was applied for a shorter duration, until the rate of settlement became negligible. The final readings of the dial gauges were then recorded. The entire load was removed and the plate was allowed to rebound. When the rebound had ceased, the dial gauge readings were again observed. The load was then gradually

increased until its magnitude was equal to the next step of loading. The magnitude of load was maintained constant and the final dial gauge readings were recorded. The total load applied was released and the final dial gauge readings were noted, when the rebound rate was negligible.

The loading, unloading and the reloading cycles were continued until the loading reached the estimated ultimate load. The dial gauge readings were observed at each step. The magnitude of each load increment was equal to $1/3$ to $1/6$ th of the ultimate load. The elastic rebound of the plate corresponding to each intensity of loading was obtained.

3.3 LABORATORY TESTS

To investigate the influence of secondary time effects on shear modulus and to obtain a relationship between field shear moduli and laboratory shear moduli at the same strain level, laboratory tests were carried out on 'undisturbed' samples collected from the first three sites where field tests were performed. The different physical properties were determined on the 'undisturbed' soils brought from the four sites.

Laboratory shear modulus values were determined on samples borrowed from the first three sites, A, B and C only, since, the facilities to evaluate shear modulus on gravel materials (Site D) in the laboratory were inadequate. To study the influence of secondary time effects on shear

modulus few specimen samples were consolidated under a consolidation pressure of magnitude that was equal to the in-situ over-burden pressure. Depending on the type of soil the consolidation pressure was applied for a period of 24 hours or till the completion of primary consolidation. At the end of this duration, the specimens were tested to obtain the shear modulus, values in the range of medium to large strain levels using different type of tests. In this respect the following tests were carried out in the laboratory.

- 1 Oscillatory shear box test
- 2 Simple shear test.

These tests are briefly described in the following subsections.

3.3.1 Oscillatory Shear Test

For the determination of laboratory shear modulus in the medium strain ranges, tests were conducted using the oscillatory shear test apparatus. This equipment was developed at the School of Research and Training in Earthquake Engineering, University of Roorkee, Roorkee, India (Joshi, 1970; Nandakumaran et al., 1977).

In this test, a specimen of size 6 cm x 6 cm x 2 cm which had previously been subjected to primary consolidation was enclosed in a rubber membrane. The shear box consists of a top plate resting on a pair of ball trains, two fixed vertical sides and two tilting side plates capable of rotating in either directions from their mean

vertical position and hinged to the fixed vertical sides as shown in Fig. 3.2.

Normal stress was applied on the sample by weights placed on the hanger of a yoke resting on the top plate. Oscillatory shear stress was applied by hanging weights on the flexible cords. The applied shear loads and shear deformations were measured using strain gauge mounted load and displacement transducers connected to universal amplifiers and ink-writing oscillographs. Different values of normal stress and shear stress were used and the corresponding shear strain was measured. The computed shear strain was in the range of 10^{-2} to 10^{-1} percent. The oscillatory shear tests were carried out on the 'undisturbed' soils borrowed from the first three sites only.

3.2.3 Simple Shear Test

As in the oscillatory shear box test, specimen of the same size was prepared. At the end of primary consolidation or after a duration of 24 hours depending on the type of soil, simple shear test was conducted at different values of normal stress and shear stress. The value of shear strain in this case varied between 10^{-2} to 1.0 percent.

3.4 DAMPING RATIO

The damping values of the different soils were determined from the forced- and free- vibration tests carried out in the field. In the free-vibration test, the logarith-

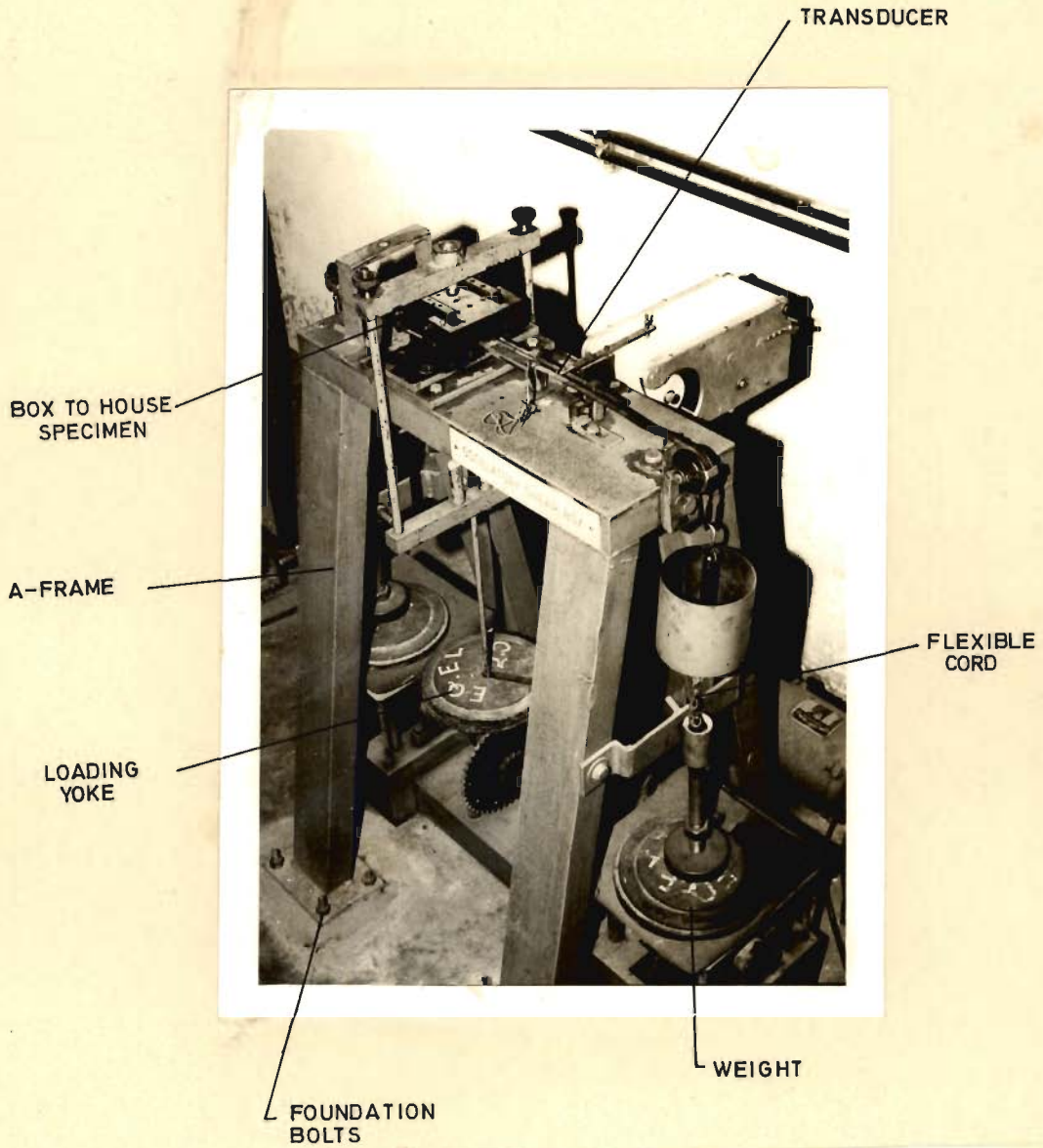


Fig. 3.2 Oscillatory Shear Box Apparatus
(Nandakumaran et al., 1977)

mic decrement and in the forced-vibration tests the half-power method were used to compute the damping values of different soils.

3.5 CLOSURE

For determination of in-situ shear modulus as a function of strain, ranging between low strain value to large strain value, different types of field tests have been performed at four sites consisting of varying types of soils. In the laboratory, tests have been carried out to determine high-amplitude shear moduli on 'undisturbed' samples. These 'undisturbed' samples have been borrowed from the same locations at which field tests have been conducted.

CHAPTER 4

PRESENTATION OF TEST RESULTS

4.1 GENERAL

The results of the different field tests conducted at the four sites and the laboratory tests carried out on 'undisturbed' samples borrowed from the first three sites to evaluate the shear modulus, as described in Chapter 3 are presented in this chapter. For each type of test performed, either in the field or in the laboratory, the shear modulus value and the associated shear strain value have been computed. Damping values are calculated from forced- and free-vibration tests carried out in the field. The computed values of shear modulus, damping ratio and the associated shear strain values are presented as a function of strain. At a given strain level, for which the field shear modulus and the laboratory shear modulus values are available, the ratio between these two shear moduli is expressed as a function of strain. The percentage difference between the shear modulus values determined at the completion of primary consolidation and before the beginning of primary consolidation are also presented in this chapter.

4.1 RESULTS OF FIELD TESTS

The results of the different field tests

conducted are described in this section. For performing the block vibration test, a block of size 3.50 m x 1.75 m x 0.70 m and for carrying out the cyclic plate load test, a steel plate of size 0.60 m x 0.60 m have been used. The specimen calculations involved in computing the shear modulus, damping and the corresponding shear strain values are presented for site A only. For the other sites these values are presented in tabular form.

4.2.1 Wave Propagation Test

Generally, from the wave propagation test records obtained, the time of travel of the compression waves is easily calculated (Nandakumaran et al., 1977). In this study, from the records obtained during the wave propagation tests at site A as shown in Fig. 4.1, the time taken by the compression wave to travel a known distance, is calculated. By plotting the relation between the time and distance, the value of the compression wave velocity, V_p as given by the slope of the time-distance curve is obtained. Once the compression wave velocity is known, the shear modulus is computed from the expression:

$$G_{\max} = j \frac{v_p^2}{p} \frac{(1-2\mu)}{(1-\mu)} \quad (4.1)$$

in which

$j = r/g$

$r = \text{unit weight}$

g = acceleration due to gravity

V_p = compression wave velocity

μ = Poisson's ratio.

For site A, the travel time versus distance relationship is shown in Fig. 4.2, from which the compression wave velocity, V_p is obtained as 363.6 m/sec. Substituting the other known quantities,

$$\mu = 0.40 \quad (\text{assumed for silt})$$

$$r = 1.83 \quad \text{t/m}^3$$

$$g = 9.81 \quad \text{m/sec}^2$$

in Eq. 4.1, the value of shear modulus is obtained as:

$$\begin{aligned} G_{\max} &= \frac{1.83}{9.81} \times 363.6^2 \frac{\{1 - 2(0.4)\}}{(1 - 0.4)} \\ &= 8222.3 \text{ t/m}^2 \end{aligned}$$

The associated value of shear strain is assumed to be 1.0×10^{-5} percent (Woods, 1978). Similarly, for the other sites, namely, B, C and D the computed shear modulus values are given in Table 4.1.

4.2.2 Block Vibration Test

4.2.2.1 Forced vertical vibration test

In the forced vertical vibration, the soil-foundation system is subjected to a single-degree of freedom system. One of the test records obtained during the vertical

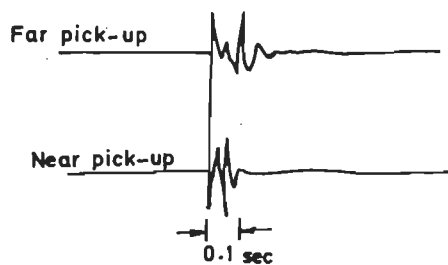


Fig. 4.1 Wave Propagation Test Record (Site A)

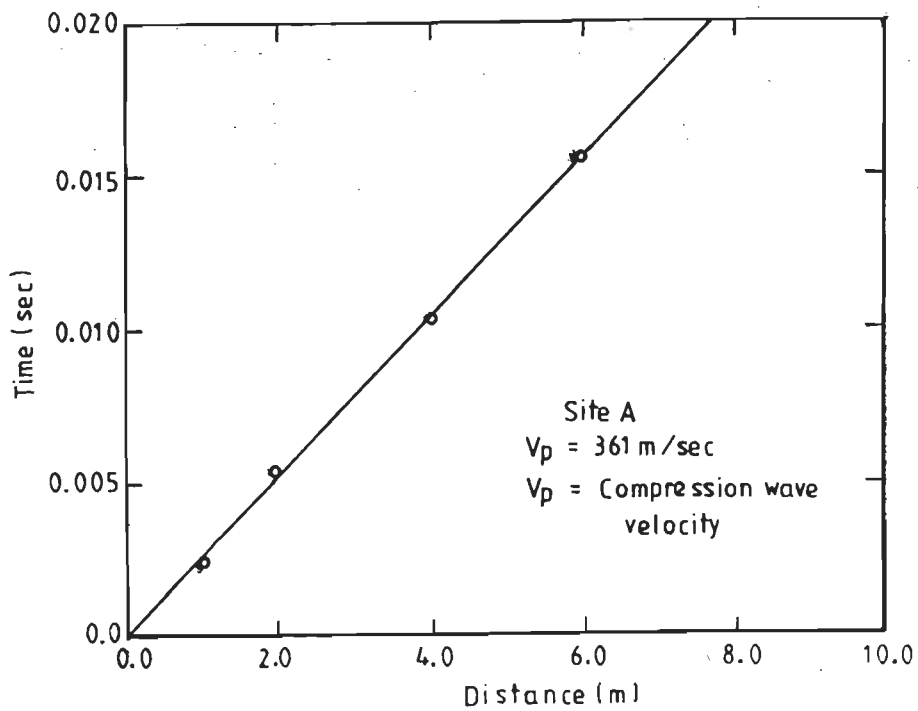


Fig. 4.2 Travel Time Versus Distance Relationship (Site A)

Table 4.1 Shear Modulus and Shear Strain Values for all the Sites

Type of test (1)	Size of block/ plate (2)	G (t/m ²) (3)	γ (%) (4)	Remarks (5)
WPT	-	8222.3	1.00x10 ⁻⁵	Site A
BVT	3.50 m 1.75 m 0.70 m	7852.5 7841.9 7702.3 7443.6 7296.4 4056.7	2.10x10 ⁻⁵ 4.56x10 ⁻⁵ 9.51x10 ⁻⁵ 1.15x10 ⁻⁴ 3.11x10 ⁻⁴ 1.34x10 ⁻³	Fine silty soil φ = 30° C = 2.5 t/m ² forced vertical vibration test free vibration test
BVT	3.50 m 1.75 m 0.70 m	6228.3 6124.9 6004.6 5201.4 3198.5 1981.6	5.50x10 ⁻⁴ 7.51x10 ⁻⁴ 9.50x10 ⁻⁴ 1.50x10 ⁻³ 5.61x10 ⁻³ 2.00x10 ⁻³	forced horizontal vibration test free vibration test
CPLT	0.60 m 0.60 m	2344.1 2009.8 1145.3 855.0	1.05x10 ⁻² 2.30x10 ⁻² 1.51x10 ⁻² 5.00x10 ⁻¹	

(continued)

Table 4.1 Shear Modulus and Shear Strain Values for all the Sites

Type of test (1)	Size of block/ plate (2)	G (t/m ²) (3)	Γ (%) (4)	Remarks (5)
WPT	-	7982.1	1.00x10 ⁻⁵	Site B
BVT	3.50 m 1.75 m 0.70 m	7694.2 7552.8 7329.4 7392.6 7098.6 6094.2	1.51x10 ⁻⁵ 3.91x10 ⁻⁵ 6.25x10 ⁻⁵ 9.15x10 ⁻⁵ 1.61x10 ⁻⁴ 1.51x10 ⁻³	Clay soil ϕ = 0° C = 5.0 t/m ² forced vertical vibration test free vibration test
BVT	3.50 m 1.75 m 0.70 m	6121.4 5651.8 5011.4 4476.6 3452.6 3028.2	3.05x10 ⁻⁴ 4.12x10 ⁻⁴ 6.25x10 ⁻⁴ 1.01x10 ⁻³ 2.23x10 ⁻³ 2.00x10 ⁻³	forced horizontal vibration test free vibration test
CPLT	0.60 m 0.60 m	2213.6 1575.2 1126.4 1003.2	9.21x10 ⁻³ 2.72x10 ⁻² 6.96x10 ⁻² 1.15x10 ⁻¹	

(continued)

Table 4.1 Shear Modulus and Shear Strain Values for all the Sites

Type of test (1)	Size of block/ plate (2)	G (t/m ²) (3)	γ (%) (4)	Remarks (5)
WPT	-	15385.3	1.00×10^{-5}	Site C
BVT	3.50 m 1.75 m 0.70 m	15174.2 15009.2 14628.3 14574.4 14944.6 14951.2	1.20×10^{-5} 2.01×10^{-5} 4.02×10^{-5} 6.55×10^{-5} 1.21×10^{-4} 2.49×10^{-4}	Sand φ = 38.5° C = 0.0 forced vertical vibration test free vibration test
BVT	3.50 m 1.75 m 0.70 m	14006.4 13648.6 13798.5 13046.4 12109.3 12576.1	1.91×10^{-4} 3.01×10^{-4} 4.01×10^{-4} 7.81×10^{-3} 1.11×10^{-3} 1.76×10^{-3}	forced horizontal vibration test free vibration test
CPLT	0.60 m 0.60 m	8622.4 7236.3 3611.5 2451.6	4.01×10^{-3} 8.96×10^{-3} 5.15×10^{-3} 1.79×10^{-2}	

(continued)

Table 4.1 Shear Modulus and Shear Strain Values for all the Sites

Type of test (1)	Size of block/ plate (2)	G (t/m ²) (3)	γ (%) (4)	Remarks (5)
WPT	-	18921.6	1.00×10^{-5}	Site D
BVT	3.50 m 1.75 m 0.70 m	18796.1 18621.4 18799.2 17848.6 17602.9 17955.7	1.45×10^{-5} 2.43×10^{-5} 4.56×10^{-5} 7.31×10^{-5} 1.10×10^{-4} 4.01×10^{-4}	Gravel ϕ = 42.5° forced vertical vibration test free vibration test
BVT	3.50 m 1.75 m 0.70 m	17622.5 17095.1 16051.5 14795.3 13821.5 15952.6	1.79×10^{-4} 2.81×10^{-4} 5.95×10^{-4} 9.01×10^{-3} 2.15×10^{-3} 1.19×10^{-3}	forced horizontal vibration test free vibration test
CPLT	0.60 m 0.60 m	7021.4	3.21×10^{-3}	

Note:

G = shear modulus

γ = shear strain

WPT = wave propagation test

BVT = block vibration test

CPLT = cyclic plate load test.

vibration test for site A is shown in Fig. 4.3. The test record gives the forcing frequency and the recorded value of acceleration, a_{rc} during the vibration test. Since the speed of the paper is known, the forcing frequency is calculated by counting the number of cycles, N , recorded in a specified length of the test record. The amplitude of vibration, A is given by:

$$A = \frac{a_{rc}}{(2\pi f)^2} \quad (4.2)$$

where

a_{rc} = recorded acceleration (Fig. 4.3)

f = forcing frequency in Hz.



a_{rc} = Recorded acceleration
Speed of paper = 125 mm/sec

Fig. 4.3 Vertical Vibration Test Record (Site A)

Eq. 4.2 is solved using a computer coding, called BLOCK (Suppiah and Palaniappan, 1982), since voluminous data handling is needed even for a single value of eccentricity (= angle between the eccentric masses of the oscillator). For the program BLOCK, the recorded acceleration, a_{rc} and forcing frequency, f are given as input data. The program gives frequency versus amplitude relationship in a graphical form as output as shown in Fig. 4.4. From this output knowing the value of natural frequency in the vertical direction, f_z , the coefficient of elastic uniform compression, C_u is computed using the expression (Barkan, 1962; IS: 5249, 1977; Nandakumaran et al., 1977; Prakash, 1981):

$$C_u = \frac{4\pi^2 f_z^2 m_b}{A_b} \quad (4.3)$$

in which

C_u = is the compressive stress causing unit elastic uniform compression for a given area

m_b = mass of the block, motor, oscillator and other accessories

A_b = contact area of the block

f_z = natural frequency in the vertical direction.

Once the value of C_u is known from Eq. 4.3, the value of Young's modulus, E , and the shear modulus, G respectively are evaluated from the following expressions

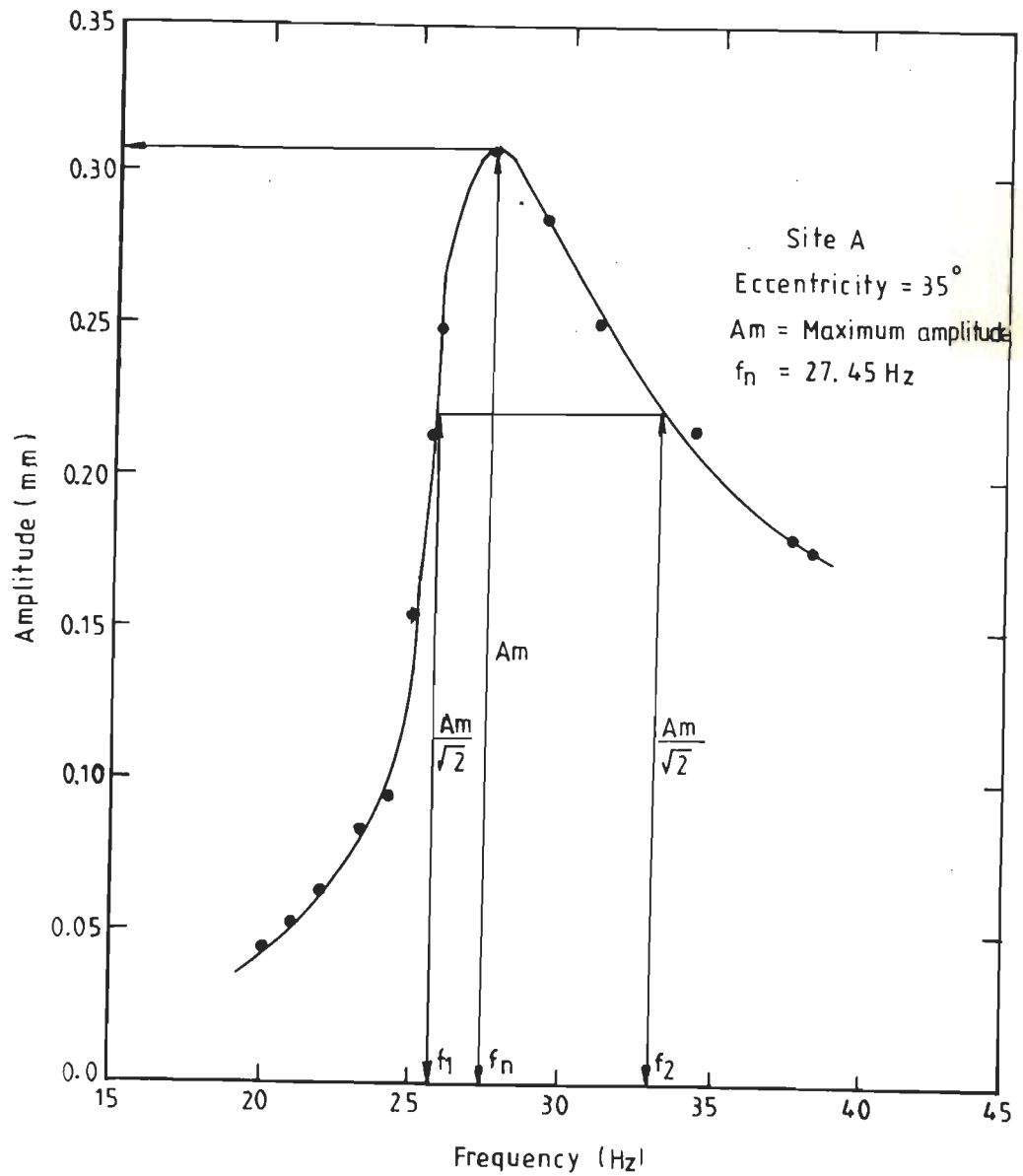


Fig. 4.4 Amplitude Versus Frequency Relationship from Forced Vertical Vibration Test (Site A)

(Barkan, 1962; Nandakumaran et al., 1977; Prakash, 1981):

$$E = \frac{C_u (1 - \mu^2) A_b}{1.13} \quad (4.4)$$

and

$$G = \frac{E}{2(1 + \mu)} \quad (4.5)$$

in which

E = Young's modulus

G = shear modulus.

The associated value of shear strain is given by:

$$\Gamma = A_m / B_w \quad (4.6)$$

where

A_m = maximum amplitude corresponding to the vertical natural frequency, f_z as shown in Fig. 4.4

B_w = width of the test block used.

At site A, a block of size 3.50 m x 1.75 m x 0.70 m has been used for the determination of in-situ shear modulus. For an eccentricity of 30 degrees (angle of setting between the eccentric masses, IS: 5249, 1977), the specimen calculations are as follow:

$$\begin{aligned} \text{Contact area of the block, } A_b &= 3.5 \times 1.75 \text{ m}^2 \\ &= 6.125 \text{ m}^2 \end{aligned}$$

$$\begin{aligned} \text{Mass of the block, motor} \\ \text{and other accessories, } m_b &= \frac{(3.5 \times 1.75 \times 0.7) 2.24 + 0.15}{9.81} \\ &= 0.9943 \text{ t} \cdot \text{sec}^2/\text{m} \end{aligned}$$

From Fig. 4.4, the vertical natural frequency, $f_z = 27.45$ Hz.

Substituting, these values (A_b , m_b , f_z), in Eq. 4.3, the value of C_u is obtained as:

$$\begin{aligned} C_u &= \frac{(2\pi \times 27.45)^2 \times 0.9943}{6.125} \\ &= 4828.98 \text{ t/m}^3 \end{aligned}$$

Assuming, $\mu = 0.40$ for the silty soil at site A,

the value of Young's modulus, E (Eq. 4.4) = 21986.4 t/m^2

and

the value of shear modulus, G (Eq. 4.5) = 7852.5 t/m^2

The associated value of shear strain, $\gamma = 0.0315/1500$

$$= 2.1 \times 10^{-5} \text{ percent}$$

Table 4.2 gives the values of coefficient of elastic uniform compression, C_u , shear modulus, G and the corresponding values of shear strain, γ at different eccentricities for site A.

Similarly, the values of shear modulus and associated shear strain values are calculated for other sites and these values are presented in Table 4.1.

Table 4.2 Shear Modulus from Vertical Vibration Tests
(Site A)

Sl. No.	θ (deg)	f_z (Hz)	C_u (t/m ³)	G (t/m ²)	$\Gamma \times 10^{-5}$ (%)
(1)	(2)	(3)	(4)	(5)	(6)
1	60	27.43	4822.50	7841.90	4.56
2	90	24.91	4736.65	7702.30	9.51
3	120	24.49	4577.56	7443.60	11.50
4	150	24.25	4487.03	7296.40	31.10

Note:

θ = eccentricity (= angle of setting between eccentric masses)

f_z = natural frequency in the vertical direction

C_u = coefficient of elastic uniform compression

G = shear modulus

Γ = shear strain.

4.2.2.2 Forced horizontal vibration test

In the forced horizontal vibration test, the soil-foundation system is subjected to a two-degree-of freedom system. Thus, in this system, two resonant frequencies are present; the first one corresponding to rocking mode, w_x , and the other pertaining to sliding mode, w_ϕ . The combined equation is expressed as (Barkan, 1962):

$$w^4 - \frac{w_x^2 + w_\phi^2}{w_r} w^2 + \frac{w_x^2 \times w_\phi^2}{w_r} = 0 \quad (4.7)$$

in which

w = resonant frequency

$$w_x = \sqrt{(C_T A_b / m_b)} \quad (4.8)$$

$$w_\phi = \sqrt{(C_\phi I / M_{m0})} \quad (4.9)$$

C_T = ratio of the shear stress to elastic uniform shear displacement for a given area

C_ϕ = ratio of compressive stress and elastic non-uniform compressive deformation for a given area

I = mass moment of inertia of the base of the contact area about the axis of rotation

M_m = mass moment of inertia of the block and motor-oscillator assembly about an axis passing through the centre of gravity of the block and motor-oscillator assembly and perpendicular to the plane of vibration

M_{m0} = mass moment of inertia of the block and motor-oscillator assembly about an axis passing through the centroid

of the base contact area and perpendicular to the plane of vibration (IS: 5249, 1977)

$$w_r = M_m/M_{m0}. \quad (4.10)$$

As before the computer program, BLOCK (Suppiah and Palaniappan, 1982) has been employed for the reduction of data obtained in the forced horizontal vibration test. By entering the necessary input data as in Sub-Sec. 4.2.2.1, the output shown in Fig. 4.5 is obtained.

For a foundation-block with a length to width ratio of 2, the values of C_ϕ and C_u are given by (Barkan, 1962):

$$C_\phi = 3.46 C_T \quad (4.11)$$

$$C_u = 2.00 C_T \quad (4.12)$$

Substituting, Eqs. 4.8, 4.9 and 4.11 in Eq. 4.7, the resulting equation is given by:

$$w^4 - \frac{A_1 + A_2}{w_r} w^2 + \frac{A_1 \times A_2}{w_r} = 0 \quad (4.13)$$

where

$$A_1 = C_T A_b/m_b \quad (4.14)$$

$$A_2 = 3.46 C_T I/M_{m0} \quad (4.15)$$

I = moment of inertia.

For site A, substituting the values of A_b , m_b , I , M_{m0} and w_r in Eqs. 4.13 to 4.15 and solving for C_T , one gets

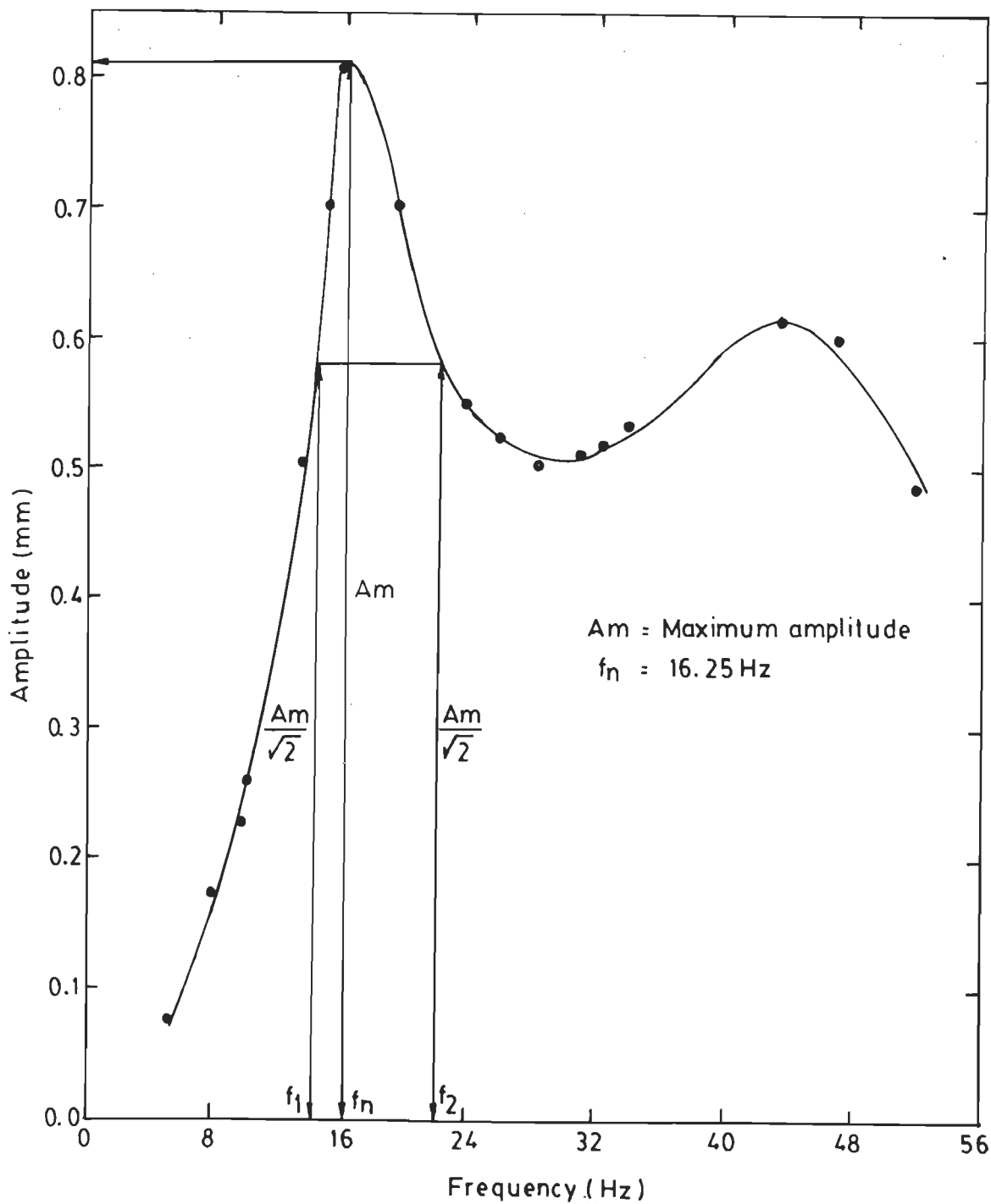


Fig. 4.5 Amplitude Versus Frequency Relationship from Forced Horizontal Vibration Test (Site A)

$$C_T = 0.1837 w^2 \quad (4.16)$$

since,

$$w = 2\pi f_x \quad (4.17)$$

Therefore, Eq. 4.16 can be written as:

$$C_T = 7.25 f_x^2 \quad (4.18)$$

in which

f_x = natural or resonant frequency in the horizontal direction.

From Fig. 4.5, for an eccentricity of 30° , $f_x = 16.25$ Hz.

Substituting the value of f_x in Eq. 4.18,

$$C_T = 1915.1 \text{ t/m}^3$$

Using Poisson's ratio, $\mu = 0.4$, the values of C_U and G from Eqs. 4.12 and 4.5, respectively are computed as:

$$C_U = 3830.2 \text{ t/m}^3$$

and

$$G = 6228.3 \text{ t/m}^2$$

The associated value of shear strain, $\gamma = 5.50 \times 10^{-4}$ percent (from Eq. 4.6).

The computed values of C_T , C_U , G and γ corresponding to different eccentricities are shown in Table 4.3 for site A.

For all the sites, the shear modulus values and the corresponding shear strain values are given in Table 4.1.

Table 4.3 Shear Modulus from Forced Horizontal Vibration Test (Site A)

Sl. No.	θ (deg)	f_x (Hz)	C_r (t/m ³)	$C_u = 2C_r$ (t/m ³)	G (t/m ²)	$\gamma \times 10^{-4}$ (%)
(1)	(2)	(3)	(4)	(5)	(6)	(7)
1	60	16.12	1883.30	3766.60	6124.9	7.51
2	90	15.96	1846.31	3692.63	6004.6	9.50
3	120	14.85	1599.34	3198.68	5201.4	15.00
4	150	11.65	983.49	1966.97	3198.5	56.10

Note:

θ = eccentricity

f_x = natural frequency in the horizontal direction

C_r = coefficient of elastic uniform shear

C_u = coefficient of elastic uniform compression

G = shear modulus

γ = shear strain.

4.2.2.3 Free vibration test in the vertical direction

From the free-vibration test record corresponding to the vertical direction, shown in Fig. 4.6, knowing the speed of the paper, and counting the number of cycles, N the vertical natural frequency for site A is obtained as 19.73 Hz. Substituting, this value in Eqs. 4.3 and 4.5, the following values of C_u and G are obtained:

$$C_u = 2496.47 \text{ t/m}^3$$

$$G = 4056.71 \text{ t/m}^2$$

and the corresponding shear strain, γ is 1.34×10^{-3} percent (Eq. 4.6).

As before, for all the sites, the shear modulus and shear strain values are given in Table 4.1.



Fig. 4.6 Free-Vibration Test Record: Vertical Direction (Site A)

4.2.2.4 Free vibration test in horizontal direction

A record similar to that shown in Fig. 4.6 was obtained in the horizontal direction, corresponding to the free-vibration test conducted at site A. Following the same procedure of Sec. 4.2.2.3, the shear modulus value and the corresponding shear strain are computed as:

$$G = 1981.6 \text{ t/m}^2$$

$$\gamma = 2 \times 10^{-3} \text{ percent.}$$

For all the sites the shear modulus and the shear strain values are given in Table 4.1.

4.2.3 Cyclic Plate Load Test

Load versus settlement curve obtained during the cyclic plate load test at site A, is shown in Fig. 4.7. Using this plot, another curve is plotted between the elastic-settlement, S_e , and the intensity of loading, p as shown in Fig. 4.8. The slope of the curve in this figure (Fig. 4.8), gives the value of coefficient of elastic uniform compression, C_u . Thus,

$$C_u = p/S_e \quad (4.19)$$

As before, the values of Young's modulus and the shear modulus values are evaluated from Eqs. 4.4 and 4.5 respectively.

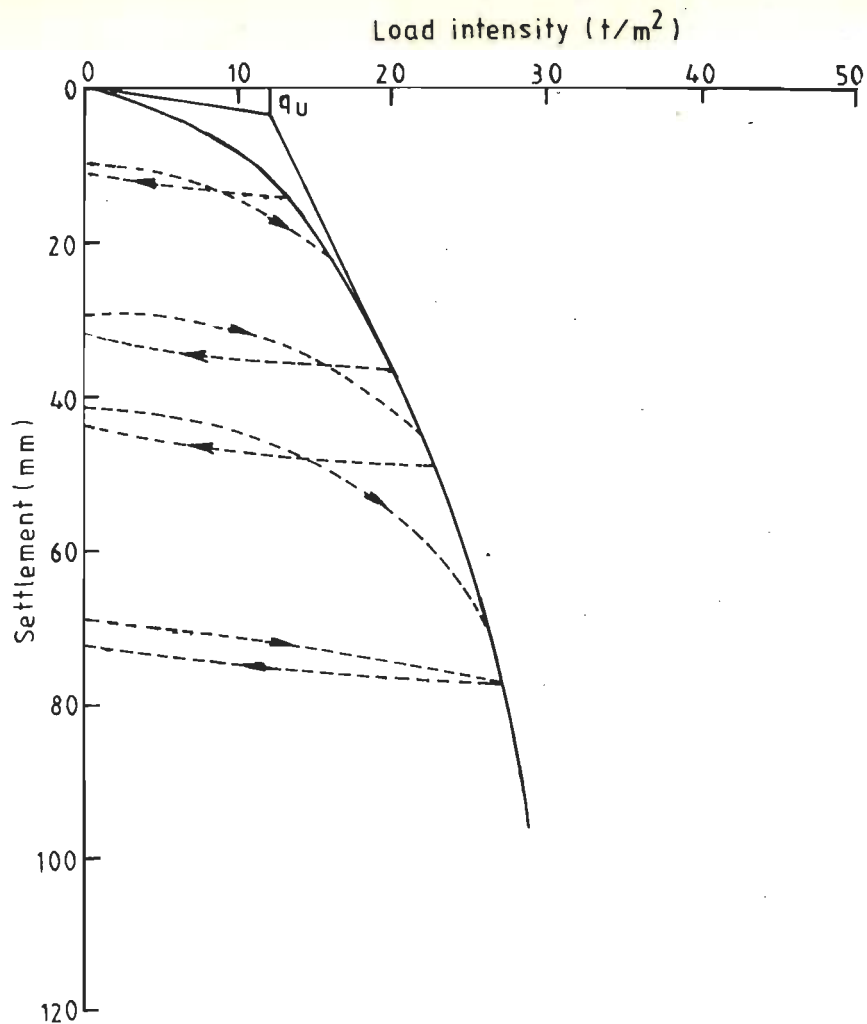


Fig. 4.7 Load Versus Settlement Relationship (Site A)

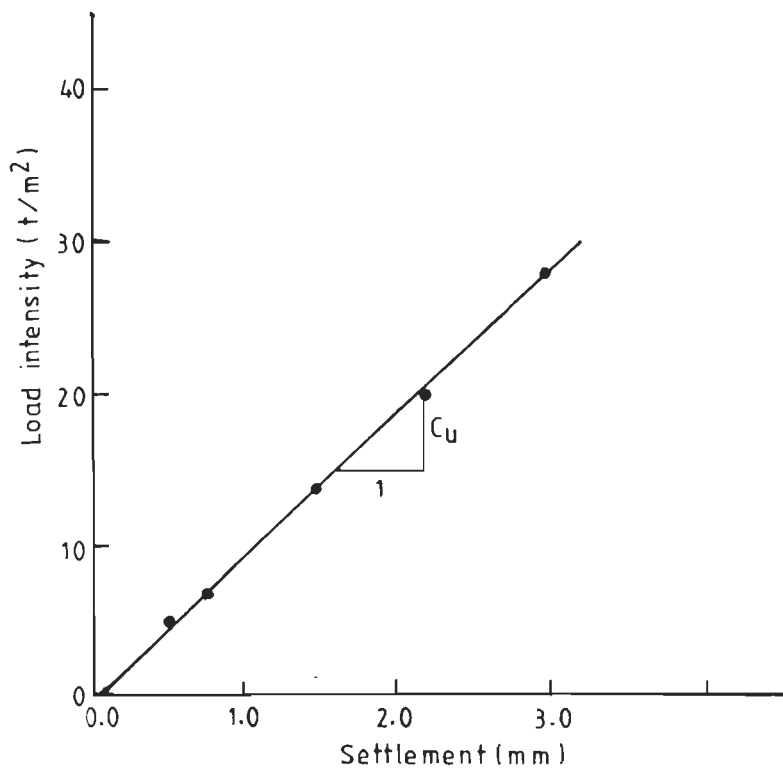


Fig. 4.8 Elastic Settlement Versus Intensity of Loading (Site A)

From Fig. 4.8,

$$C_u = 8947.4 \text{ t/m}^3$$

and using Eq. 4.5, shear modulus is obtained as:

$$G = 855.0 \text{ t/m}^2$$

And the associated value of shear strain is given by (Prakash, 1981):

$$\gamma = \frac{\text{elastic settlement}}{\text{width of the plate}}$$

in the present case,

$$\begin{aligned} \gamma &= \frac{3.0}{600} \\ &= 0.5 \text{ percent.} \end{aligned}$$

Table 4.4 shows the shear modulus values determined at different locations for site A.

The shear modulus and the corresponding shear strain values obtained during the cyclic plate load tests are given in Table 4.1 for all the sites.

4.2.4 Damping Values from Field Tests

The damping ratio, D is evaluated from the forced- and free- vibration tests conducted in the field as described in the following sub-sections.

Table 4.4 Shear Modulus Values from Cyclic Plate Load Test

Sl. No.	C_u (t/m ³)	G (t/m ²)	$\Gamma \times 10^{-2}$ (%)
(1)	(2)	(3)	(4)
1	24526.23	2344.10	1.05
2	21028.46	2009.80	2.30
3	11983.23	1145.30	15.10
4	8945.84	855.00	50.00

Note:

C_u = coefficient elastic uniform compression

G = shear modulus

Γ = shear strain.

4.2.4.1 Damping values from forced-vibration test

The response curve drawn between amplitude and frequency is shown in Fig. 4.4. The damping ratio, D is computed using the half-power method as proposed by Clough and Penzien (1975), and is given by the following expression (IS: 5249, 1977):

$$D = \frac{f_2 - f_1}{f_2 + f_1} \times 100 \text{ percent} \quad (4.20)$$

in which

f_1 and f_2 are the two frequencies corresponding to an amplitude of $A_m/\sqrt{2}$

A_m = the maximum amplitude.

For site A, from Fig. 4.4, the following values are available

$$A_m = 0.308 \text{ mm}$$

$$f_1 = 25.75 \text{ Hz}$$

$$f_2 = 33.00 \text{ Hz.}$$

Substituting, these values in Eq. 4.20, the value of damping, D is computed as 12.34 percent, corresponding to the strain value of 2.1×10^{-5} (percent).

4.2.4.2 Damping from forced horizontal vibration test

In this case, the damping value is calculated as described in the Sub-section 4.2.4.1. From Fig. 4.5, the following values are obtained:

$$A_m = 0.815 \text{ mm}$$

$$f_1 = 14.50 \text{ Hz}$$

$$f_2 = 22.00 \text{ Hz.}$$

As before, substituting these values in Eq. 4.20, the value of damping is obtained as 20.54 percent. And the corresponding value of strain is evaluated as 5.5×10^{-4} percent. The computed values of damping for different sites are shown in Table 4.5.

4.2.6 Damping from Free-Vibration Tests

From the free-vibration test record as shown in Fig. 4.6, the damping value is given by (Clough and Penzien, 1975):

$$D = \sqrt{[\delta^2 / (4\pi^2 + \delta^2)]} \quad (4.21)$$

in which

δ = logarithmic decrement which is the ratio of the natural logarithm of the amplitude of any two successive cycles.

For site A, from Fig. 4.6, the value of δ is 1.25 and the value of damping, D is 19.5 percent using Eq. 4.21. The damping values obtained for all the sites are presented in Table 4.5.

4.3 RESULTS OF LABORATORY TESTS

The results of the different laboratory tests performed on 'undisturbed' samples, from the first three sites, namely, A, B and C to determine shear moduli are presented in this section. To study the secondary time effects on shear modulus, two types of tests were conducted. In the first type, shear modulus values were determined at the end of primary consolidation. For this purpose, each specimen had been subjected to a consolidation pressure that was equal to the in-situ effective over-burden pressure. This pressure was maintained for a duration of 24 hours or till the completion of primary consolidation. In the second type of

Table 4.5 Damping Values for Different Soils
(Sites A, B, C and D)

Sl. No. (1)	Shear Strain - γ (%) (2)	Damping Value - D (%) (3)	Type of Soil (4)
1	2.1×10^{-5}	12.50	Silt
2	5.4×10^{-4}	20.50	Silt
3	5.5×10^{-3}	30.00	Silt
4	3.5×10^{-5}	15.00	Clay
5	6.0×10^{-4}	25.00	Clay
6	4.5×10^{-3}	30.00	Clay
7	3.0×10^{-5}	10.00	Sand
8	5.1×10^{-4}	14.80	Sand
9	4.0×10^{-3}	22.10	Sand
10	1.0×10^{-5}	8.00	Gravel
11	1.0×10^{-4}	12.20	Gravel
12	5.4×10^{-3}	15.00	Gravel

tests, shear modulus was determined, as soon as the specimen has been prepared from the 'undisturbed' samples without allowing for primary consolidation.

As site D, consisted of gravel materials, laboratory shear modulus values could not be determined due to inadequate laboratory facilities.

4.3.1 Oscillatory Shear Test

From the records of shear load as shown in Fig. 4.9, the shear stress, τ , is calculated, knowing the cross-sectional area of the soil specimen. For each value of shear load, the corresponding shear strain, γ is computed using the expression:

$$\gamma = \frac{\Delta s}{h} \quad (4.22)$$

in which

Δs = shear deformation of the specimen measured using strain gauge

h = height of the soil sample.

The shear modulus is calculated using the expression:

$$G = \tau / \gamma \quad (4.23)$$

where

τ = shear stress

γ = shear strain.

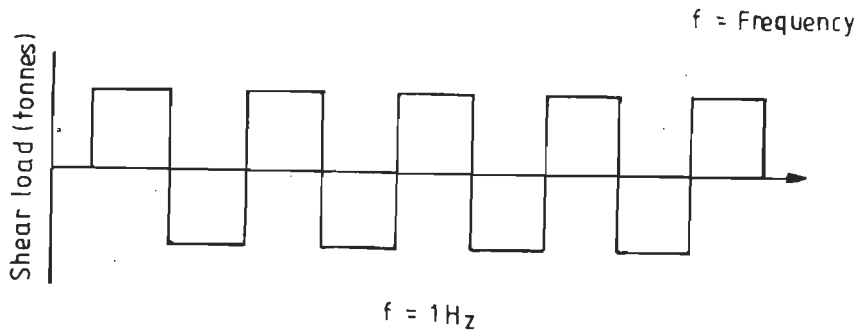


Fig. 4.9 Oscillatory Shear Test Record (Site A)

Table 4.6 shows the different values of shear modulus obtained, before the beginning of primary consolidation and after the completion of primary consolidation and the corresponding shear strain values for the samples borrowed from site A. For sites B and C the shear moduli and the associated shear strain values calculated in the laboratory are also presented in Table 4.6.

4.3.2 Simple Shear Test

The procedure for computation of shear modulus is same as that discussed in Sec. 4.3.1. The shear modulus values obtained for the samples from site A are given in Table 4.7. In the same table, the shear modulus and the

Table 4.6 Shear Modulus Values from Oscillatory Shear Test
(Sites A, B and C)

Sl. No. (1)	G_b (t/m ²) (2)	G_a (t/m ²) (3)	Percent Difference between G_a and G_b (4)	$\Gamma \times 10^{-2}$ (%) (5)	Site (6)
1	1483.6	1824.9	23.0	1.00	A
2	1300.8	1603.9	23.3	2.10	A
3	1107.6	1363.4	23.1	3.50	A
4	1020.3	1251.9	22.0	5.20	A
5	1174.7	1500.1	27.7	1.21	B
6	921.2	1179.1	28.0	2.70	B
7	820.9	1044.2	27.2	4.39	B
8	691.9	881.5	27.4	6.94	B
9	4856.6	5055.7	4.1	0.89	C
10	3958.3	4112.7	3.9	1.51	C
11	3165.2	3285.5	3.8	3.20	C
12	2675.2	2771.5	3.6	5.20	C

Note:

G_b = shear modulus determined before the start of primary consolidation

G_a = shear modulus determined after the end of primary consolidation.

Table 4.7 Shear Modulus Values from Simple Shear Test
(Sites A, B and C)

Sl. No. (1)	G_b (t/m^2) (2)	G_a (t/m^2) (3)	Percent Difference between G_a and G_b (4)	$\Gamma \times 10^{-2}$ (%) (5)	Site (6)
1	937.8	1157.2	23.4	7.50	A
2	891.6	1095.8	22.9	9.05	A
3	784.5	950.8	21.2	15.00	A
4	602.1	734.6	22.0	50.00	A
5	630.6	808.9	28.3	11.60	B
6	654.3	831.6	27.1	8.51	B
7	462.2	586.1	26.8	20.10	B
8	354.3	450.3	27.1	35.10	B
9	2288.6	2368.7	3.5	9.21	C
10	1752.4	1817.2	3.7	24.10	C
11	1483.9	1543.3	4.0	34.80	C
12	1426.3	1477.7	3.6	45.10	C

Note:

G_b = shear modulus determined before the start of primary consolidation

G_a = shear modulus determined after the end of primary consolidation.

corresponding shear strain values for the sites B and C are presented as well.

4.5 CLOSURE

The results of the different field tests conducted at four sites and the laboratory tests carried out on samples from the first three sites as described in Chapter 3, have been presented in this chapter. For each type of test, carried out, either in the field or in the laboratory, the shear modulus and the corresponding shear strain values have been computed. Damping values have been calculated from the forced- and free- vibration tests only. The computed values of shear modulus, damping and the associated shear strain have been presented. The percentage difference between the shear modulus values determined before the beginning of primary consolidation and after the completion of primary consolidation have also been presented.

CHAPTER 5

DISCUSSION AND INTERPRETATION OF TEST RESULTS

5.1 GENERAL

The different values of shear modulus and damping reported in the previous chapter are interpreted and discussed here. The variations between (1) field shear modulus and laboratory shear modulus and (2) shear modulus determined at the end of primary consolidation and shear modulus determined before the beginning of primary consolidation are discussed.

The ratio between field and laboratory shear modulus corresponding to a particular strain level has been estimated for silt, clay and sand materials. Using this ratio, called the disturbance factor, the in-situ high-amplitude shear modulus has been predicted for a particular site. The disturbance factor method proposed in this study is compared with the other existing methods of prediction for shear modulus. For gravel material (site D), shear modulus could not be determined in the laboratory due to inadequate testing facilities.

Least squares curve fitting is done to determine the Ramberg-Osgood model parameters, using field shear modulus and the corresponding shear strain values. The Ramberg-Osgood model parameters are subsequently been used to

obtain the damping values and the normalized shear modulus factors as a function of shear strain. These normalized values have been compared with the existing modulus reduction curves proposed by different researchers (Seed and Idriss, 1970; Grant and Brown, 1981).

5.2. SHEAR MODULUS

5.2.1 Relation between Field and Laboratory Shear Moduli

The field determined shear modulus value and the laboratory determined shear modulus value at a particular strain level are not identical as can be seen in Fig. 5.1. In this figure the field and laboratory shear moduli are plotted as a function of shear strain. The ratio between these two values of shear moduli are given by (Suppiah, 1986):

$$\beta_b = \frac{G_f \text{ (at } r=i)}{G_{lb} \text{ (at } r=i)} \quad (5.1)$$

and

$$\beta_a = \frac{G_f \text{ (at } r=i)}{G_{la} \text{ (at } r=i)} \quad (5.2)$$

in which

β_b = disturbance factor corresponding to the shear modulus ratio determined before the start of the primary consolidation

β_a = disturbance factor corresponding to the shear modulus ratio determined after the end of the primary

consolidation

G_f = field shear modulus corresponding to a strain level.

$$\tau = i$$

G_{1b} = laboratory shear modulus determined before the beginning of the primary consolidation, corresponding to the same strain level, $\tau = i$, or $\tau \approx i$ th value of strain

G_{1a} = laboratory shear modulus determined at the end of the primary consolidation, corresponding to the same strain level, $\tau = i$, or $\tau \approx i$.

For site A.

$$G_f = 2344.1 \text{ t/m}^2, \text{ at } \tau = 1.05 \times 10^{-2} \text{ percent}$$

$$G_{1b} = 1483.6 \text{ t/m}^2, \text{ at } \tau = 1.00 \times 10^{-2} \text{ percent}$$

$$G_{1a} = 1824.8 \text{ t/m}^2, \text{ at } \tau = 1.00 \times 10^{-2} \text{ percent}$$

Substituting these values in Eqs. 5.1 and 5.2, the following values of disturbance factors are obtained.

$$\beta_b = 1.580 \text{ at } \tau = 1.0 \times 10^{-2} \text{ percent}$$

and

$$\beta_a = 1.225 \text{ at } \tau = 1.0 \times 10^{-2} \text{ percent}$$

The β_b and β_a values computed at other values of shear strain for the first three sites are shown in Table 5.1. As mentioned in Chapter 4 the laboratory facilities were inadequate to conduct different tests on gravel materials (site D), therefore β_b and β_a factors could not be included in Table 5.1.

From Table 5.1, it is seen that the difference between β_b values and β_a values for sand (site C) is

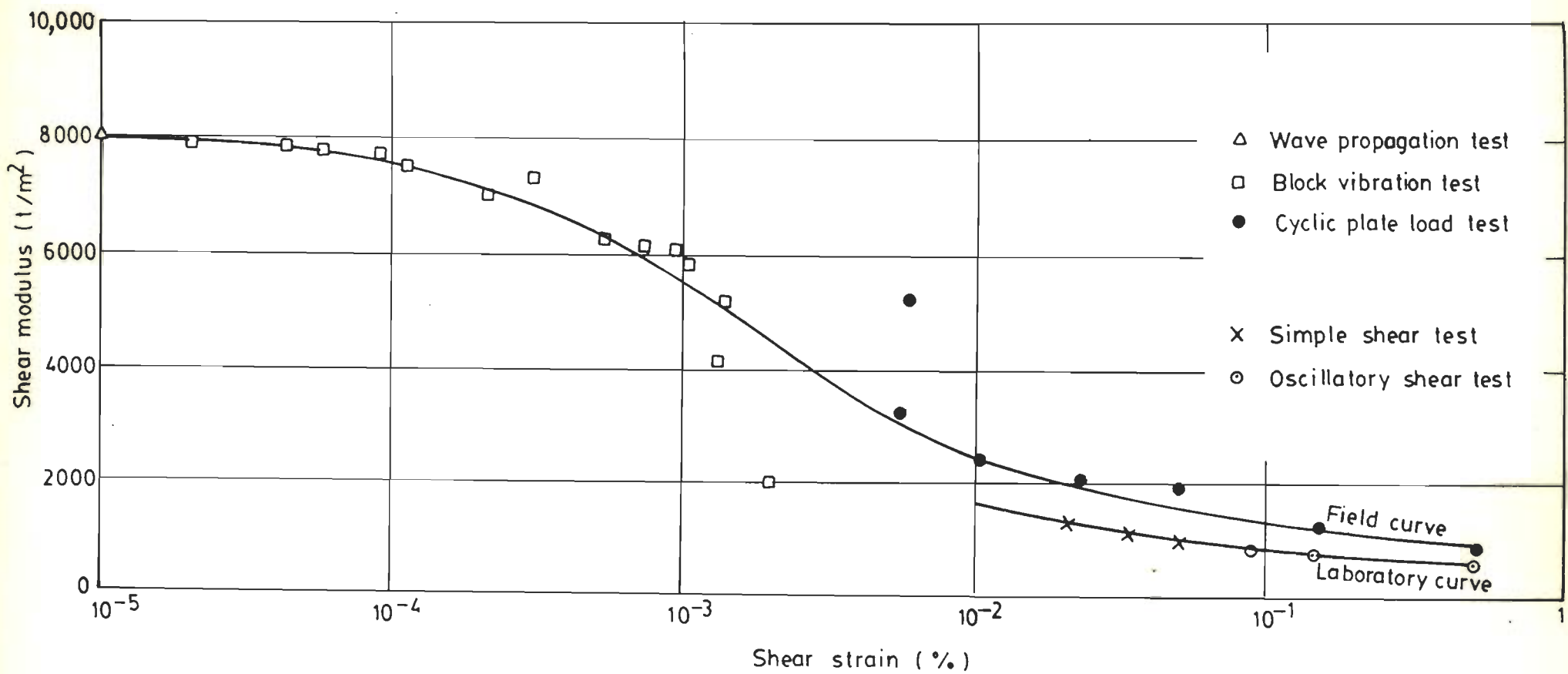


Fig. 5.1 Shear Moduli from Field and Laboratory Tests (Site A)

Table 5.1 Values of Disturbance Factors β_b and β_a

Site	G_{1b} (t/m ²)	G_{1a} (t/m ²)	γ_1	G_f (t/m ²)	γ_f	Percent Increase	β_b	β_a
(1)	(2)	(3)	(4)	(5)	(6)	(7)	(8)	(9)
A	1483.6	1824.8	1.00×10^{-2}	2344.1	1.05×10^{-2}	23.0	1.580	1.28
	1300.8	1603.9	2.10×10^{-2}	2009.8	2.30×10^{-2}	23.3	1.545	1.25
	784.5	950.8	1.50×10^{-1}	1145.3	1.51×10^{-1}	21.2	1.460	1.20
	602.1	734.6	5.00×10^{-1}	855.0	5.00×10^{-1}	22.0	1.420	1.16
B	921.2	1179.1	2.70×10^{-2}	1575.2	2.72×10^{-2}	28.0	1.720	1.33
	671.9	881.5	6.94×10^{-2}	1126.4	6.96×10^{-2}	27.4	1.628	1.27
	630.6	808.9	1.16×10^{-2}	1003.2	1.15×10^{-1}	28.3	1.591	1.24
C	4856.6	5055.7	8.98×10^{-3}	1236.3	8.96×10^{-3}	4.1	1.410	1.43
	2675.2	2771.5	5.20×10^{-2}	3611.5	5.15×10^{-2}	3.6	1.350	1.30
	1961.3	2043.7	1.80×10^{-1}	2451.6	1.79×10^{-1}	4.2	1.250	1.20

Note:

G_{1b} = shear modulus determined in the laboratory before the beginning of the primary consolidation

G_{1a} = shear modulus determined in the laboratory at the end of the primary consolidation

γ_1 = shear strain computed in the laboratory

G_f = shear modulus determined in the field

γ_f = shear strain computed in the field

Percent Increase in Shear Modulus = $\frac{\text{Column (3)} - \text{Column (2)}}{\text{Column (2)}} \times 100$

$\beta_b = G_f/G_{1b}$

$\beta_a = G_f/G_{1a}$

negligible. This shows that the secondary time effects on the shear modulus values of sand is insignificant.

The disturbance factors, β_b and β_a for the first three sites A, B and C are plotted in Figs. 5.2 and 5.3 respectively. From these two figures it is observed, that the β_b values cover a large band whereas, β_a values lie in a narrow range. The variation between the two disturbance factors is due to an appreciable increase in the shear modulus values of fine grained soils due to primary consolidation.

The disturbance factors, β_b and β_a shown in Figs. 5.2 and 5.3, for the first three sites, are obtained by conducting field tests and laboratory tests within a small range of high-amplitude shear strain (γ varying between 8.96×10^{-3} to 0.5 percent). The disturbance factors are extrapolated to other strain values using a least squares curve fitting method and the following equations are obtained:

$$\beta_b = K_1 + K_2 \log_{10} \gamma \quad (5.3)$$

$$\beta_a = K_1' + K_2' \log_{10} \gamma \quad (5.4)$$

in which

K_1 , K_2 , K_1' and K_2' are constants as shown in Table 5.2.

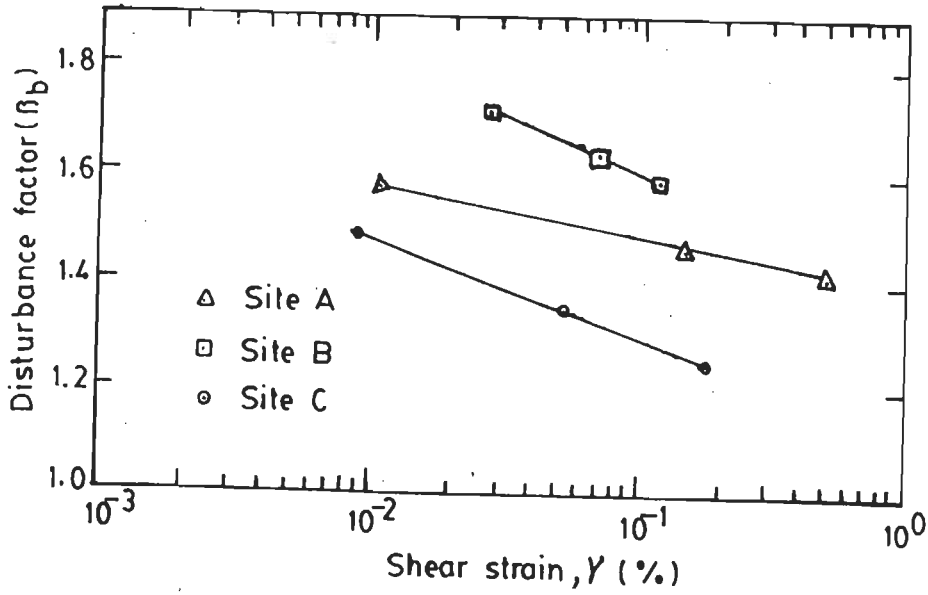


Fig. 5.2 Disturbance Factors Determined Before the Beginning of Primary Consolidation

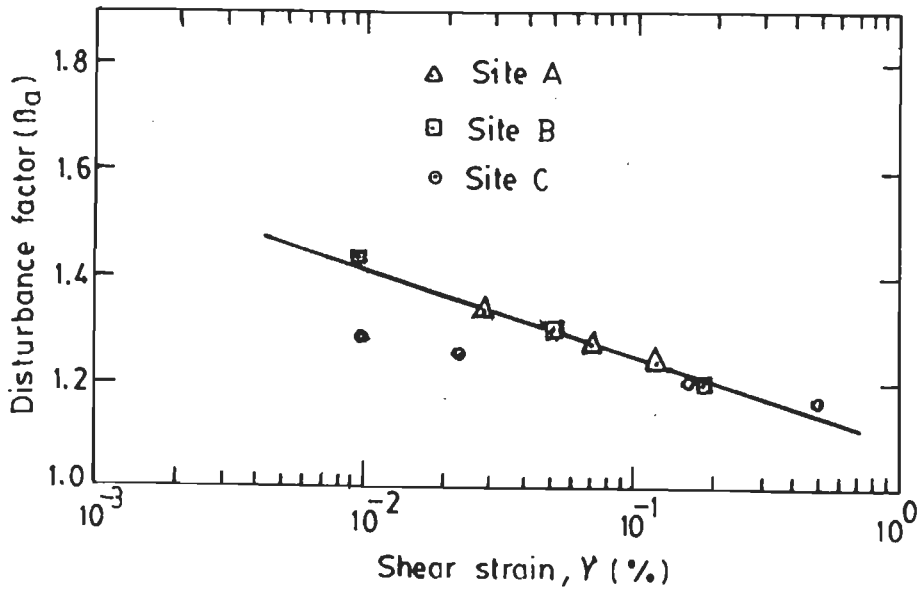


Fig. 5.3 Disturbance Factors Determined at the end of Primary Consolidation

Table 5.2 Values of Constants in Eqs. 5.3 and 5.4

Site (1)	Soil Type (2)	K_1 (3)	K_2 (4)	K_1' (5)	K_2' (6)
A	Silt	1.3867	-0.0967	1.1445	-0.0695
B	Clay	1.3918	-0.2085	1.0993	-0.1519
C	Sand	1.2640	-0.0904	1.2130	-0.0957

5.2.2 Verification of the Disturbance Factor Method

To study the suitability of the disturbance factor method, the problem solved by Anderson and Stokoe (1978), shown in Fig. 5.4 is considered here. Anderson and Stokoe (1978), predicted the high-amplitude in-situ shear modulus at a shear strain value of 0.1 percent, for a site consisting of dense sand for a depth of 6.0 m, using two different methods known as the

- 1 arithmetic method and
- 2 percentage method.

Out of these two methods, the latter method is being widely used to obtain in-situ high-amplitude shear modulus in the Geotechnical-Earthquake Engineering profession (Anderson and Stokoe, 1978). For predicting the in-situ high-amplitude shear modulus at the centre of the clay layer,

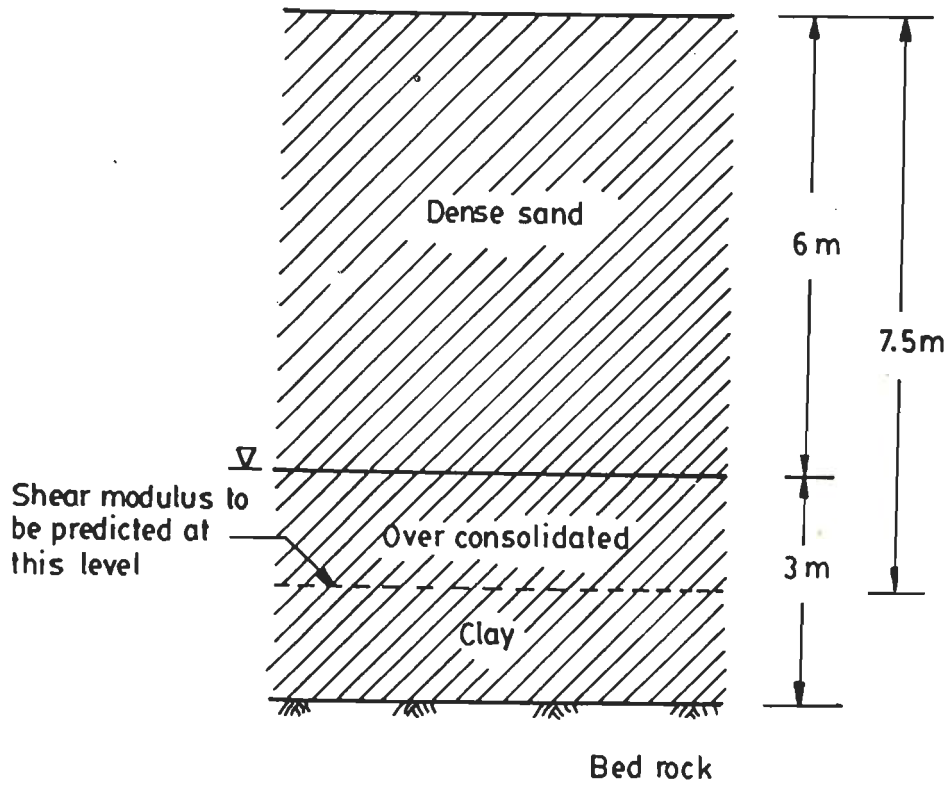


Fig. 5.4 Problem Considered by Anderson and Stokoe

Anderson and Stokoe (1978), used the following data:

Low-amplitude in-situ shear modulus $G_{mf} = 18520 \text{ t/m}^2$
 (estimated empirically based on the
 age factor of the site)

Low-amplitude laboratory shear modulus $G_{mlp} = 12500 \text{ t/m}^2$
 (determined at the end of primary
 consolidation)

High-amplitude laboratory shear modulus $G_1 = 3800 \text{ t/m}^2$
 (determined at the end of primary
 consolidation at $r=0.1$ percent).

It is needed to establish the in-situ shear modulus as a function of strain at the centre of the clay layer (Fig. 5.4). This problem is solved by the different methods proposed by Anderson and Stokoe (1978), and the disturbance factor method (Suppiah, 1986), as proposed in this study. The results obtained by these three methods have been compared. The method proposed by Anderson and Stokoe (1978), is described briefly in the following sub-section.

5.2.2.1 Methods proposed by Anderson and Stokoe

The problem considered in the present study has previously been solved by Anderson and Stokoe (1978), by two different procedures namely, (a) arithmetic method and (b) percentage method. The solution by these two methods are given subsequently:

(a) Arithmetic method

In this method, the high-amplitude field shear modulus, G_f is given by:

$$G_f = G_l + A_r \quad (5.5)$$

where

G_l = high-amplitude laboratory shear modulus determined at the end of primary consolidation

A_r = the arithmetic difference and given by:

$$A_r = G_{mf} - G_{mlp} \quad (5.6)$$

G_{mf} = low-amplitude field shear modulus

G_{mlp} = low-amplitude laboratory shear modulus determined at the end of primary consolidation or after 1000 minutes.

(b) Percentage method

According to this method the in-situ high-amplitude shear modulus is expressed as:

$$G_f = G_l \times P_r \quad (5.7)$$

in which, P_r is given by:

$$P_r = G_{mf}/G_{mlp} \quad (5.8)$$

The assumption made in deriving Eq. 5.7, is that the disturbance caused in the field and in the laboratory are proportional to each other.

Substituting, the known values in Eq. 5.5 to 5.8, the in-situ

shear modulus at a shear strain value of 0.1 percent is obtained as:

$$G_f = 11800 \text{ t/m}^2 \quad (\text{by the arithmetic method})$$

and

$$G_f = 6232 \text{ t/m}^2 \quad (\text{by the percentage method})$$

5.2.2.2 Method proposed in the present study

Suppiah (1986), proposed a method known as the disturbance factor method, for the prediction of high-amplitude field shear modulus using the following expression:

$$G_f = G_1 \times \beta \quad (5.9)$$

in which

$\beta = \beta_b$ or β_a given by Eq. 5.3 or Eq. 5.4 respectively, based on the laboratory determined shear modulus, either before the beginning of the primary consolidation or after the completion of primary consolidation.

Eq. 5.9 is similar to Eq. 5.7, however, the value of β in Eq. 5.9 is a function of strain as given by Eq. 5.3 or Eq. 5.4. Further, the disturbance factor increases, from high-amplitude strain level to low-amplitude strain values, unlike a constant (in-dependent of the strain) as in the two methods proposed by Anderson and Stokoe (1978).

In the absence of field shear modulus values only, the disturbance factor method should be adopted for obtaining the in-situ high-amplitude shear moduli of fine grained

soils. The important steps involved in the disturbance method are:

- 1 obtain 'undisturbed' samples from the site for which shear modulus value is to be evaluated
- 2 subject the soil sample to a consolidation pressure equal to the in-situ effective over-burden pressure till the end of the primary consolidation or for a minimum period of 24 hours
- 3 determine the shear modulus in the laboratory using simple shear test or oscillatory shear test at high-amplitude strain levels
- 4 knowing the value of shear modulus determined in the laboratory obtain the in-situ high-amplitude shear modulus using the disturbance factor, β_a as a function of strain.

Substituting the available values in Eq. 5.9, the field shear modulus at 0.1 percent shear strain is computed as:

$$G_f(\text{at } \gamma=0.1 \%) = 3800 \times \beta_a \quad (5.10)$$

where

$$\begin{aligned} \beta_a &= 1.264 - 0.0904 \log_{10} \tau && \text{(using } \beta_a \text{ for sand)} \\ &= 1.3544 \end{aligned}$$

Substituting the value of β_a in Eq. 5.10, the value of G_f for sand is computed as:

$$G_f(\text{at } \gamma=0.1 \%) = 5146.7 \text{ t/m}^2$$

A comparison of the predicted shear modulus value at 0.1 percent shear strain, by the three methods shows that the disturbance factor method gives the lowest value of shear modulus at $\gamma = 0.1$ percent, compared to the other two methods described by Anderson and Stokoe (1978).

The present investigation is an improved version over the values reported by Suppiah (1986). The previously reported values of shear modulus (Suppiah, 1986) were of intermediate range upto a strain value of between $\gamma = 5 \times 10^{-2}$ to $\gamma = 0.1$ percent, in comparison to the arithmetic and the percentage methods. The deviation in the two reported values (Suppiah, 1986 and the present investigation) is due to the fact that in the present investigation, the disturbance factor corresponds to that of sand. Whereas, in the previous investigation (Suppiah, 1986), the disturbance factor used corresponds to that of the silty soil.

Anderson and Stokoe (1978), observed that the shear modulus values predicted by the arithmetic method possibly resulted an upper bound value and the percentage method yielded a lower bound value. It was further suggested that more investigations were needed in the prediction of in-situ shear modulus values by conducting field tests at high-amplitude strain levels.

The different methods of prediction described in Sec. 5.2.2 may not be applicable to any soil strata consisting of loose sands. Since, while sampling, the stiffness of the loose sandy soil will increase and the prediction of in-situ shear modulus by the foregoing methods

can be misleading.

5.2.3 Advantages and Disadvantages of the Disturbance Factor Method

- 1 The low-amplitude field shear modulus, which is an essential parameter in the methods proposed by Anderson and Stokoe (1978), is not needed.
- 2 The disturbance factor method proposed herein is a function of strain and not a constant as assumed either in the arithmetic method or the percentage method.

One of the major disadvantages of the method is that the disturbance factors have been obtained from a limited number of laboratory tests lying in a narrow range of high-amplitude strain levels. Extrapolation of this method to other strain values should be supplemented by carrying out more laboratory and field tests in the medium and low-strain levels.

5.3 DAMPING VALUE

The different values of damping obtained using forced- and free- vibration tests (Table 4.5) for site A are shown as a function of strain in Fig. 5.5. This damping reduction curve may yield large values of damping in comparison to the reported values in the available literature due to limitations in the experiments used, for instance, the block vibration test.

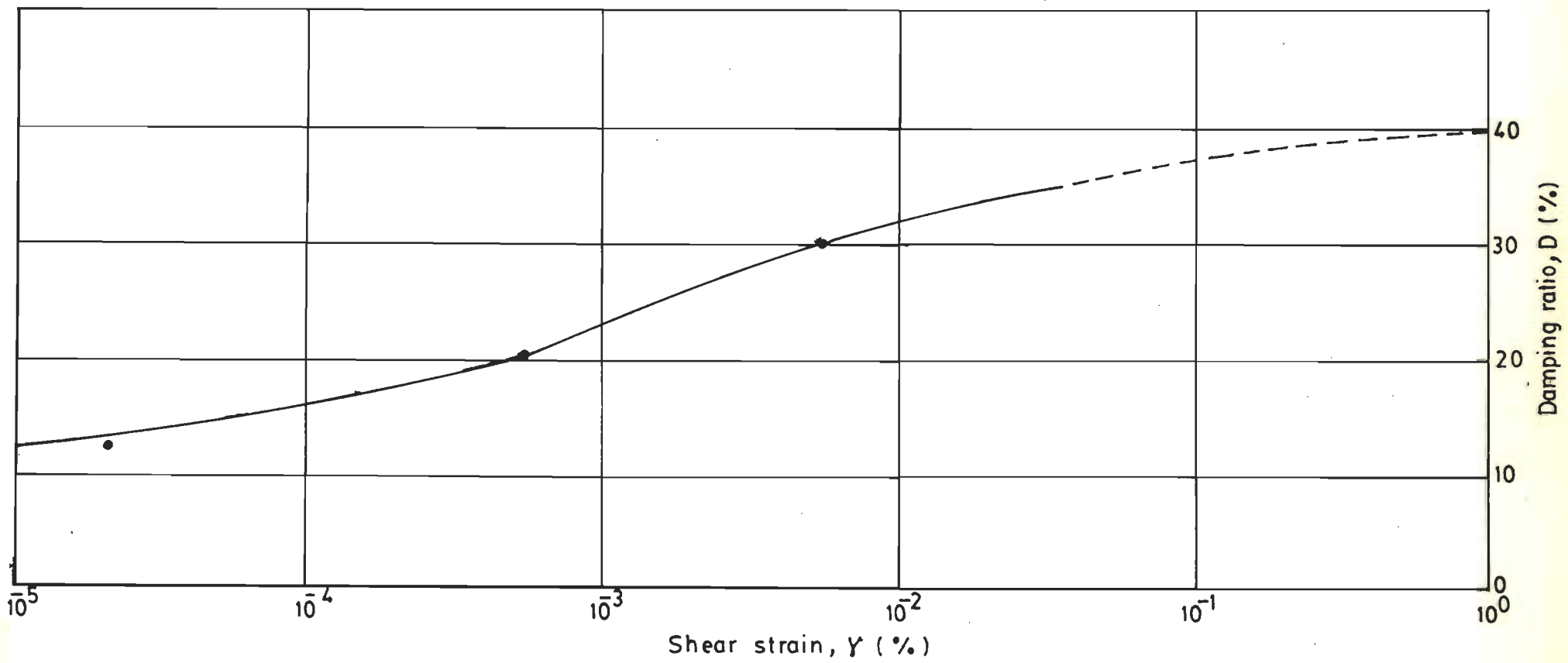


Fig. 5.5 Damping Ratio Based on Experiments

5.4 SECONDARY TIME EFFECTS ON SHEAR MODULUS

From the various laboratory determined shear modulus values presented in Tables 4.7 and 4.8, it is observed that the shear moduli of different soils determined, at the end of primary consolidation are larger than those determined before the beginning of primary consolidation. The variation between these two values of shear modulus is of the order of 3 to 28 percent depending upon the type of soil and agrees reasonably well with the other reported studies (Anderson and Woods, 1976; Afifi and Richart, 1973; Anderson and Stokoe, 1978). The variation in shear modulus is appreciable and increases from coarse grained soil to fine grained soil. The reason for this secondary increase in shear modulus is believed to result largely from a strengthening of physical-chemical bonds in the case of cohesive soils and an increase in particle contact for cohesionless soils (Anderson and Stokoe, 1978).

5.5 RAMBERG-OSGOOD MODEL

To model the nonlinear stress-strain characteristics of soils subjected to dynamic or earthquake loads, the Ramberg-Osgood model is being increasingly used (Streeter, Wylie and Richart, 1974; Papadakis and Wylie, 1975; Richart and Wylie, 1975; Christian and Desai, 1977; Roësset, 1977; Ishenower, 1979; Pyke, 1979; Ishihara, 1982, 1986, 1987; Shamoto, 1984). The Ramberg-Osgood model is briefly explained in the following sub-section.

5.5.1 Ramberg-Osgood Curve Theory

The Ramberg-Osgood curve fitting technique is based on the behaviour of many strain softening materials. The stress-strain curve of such a material is shown on a log-log plot in Fig. 5.6. In this figure line 1 describes the elastic behaviour and line 2 corresponds to the elasto-plastic curve. Combining the elastic and plastic behaviour a mathematical formulation was developed by Ramberg and Osgood (1943), and given by (Richart, 1975):

$$\frac{\Gamma}{\Gamma_y} = \frac{\tau}{\tau_y} \left[1 + \alpha \left| \frac{\tau}{\tau_y} \right|^{R-1} \right] \quad (5.11)$$

in which

τ_y = yield shear stress

Γ_y = shear strain corresponding to τ_y

R = an exponent which accounts for the curvature

α = a parameter to adjust the shape and position of the curve along the strain axis.

Substituting the following values (Richart, 1975), in Eq. 5.11,

$$\tau_y = C_1 \tau_m \quad (5.12)$$

and

$$\Gamma_y = C_1 \Gamma_r \quad (5.13)$$

the resulting expression is:

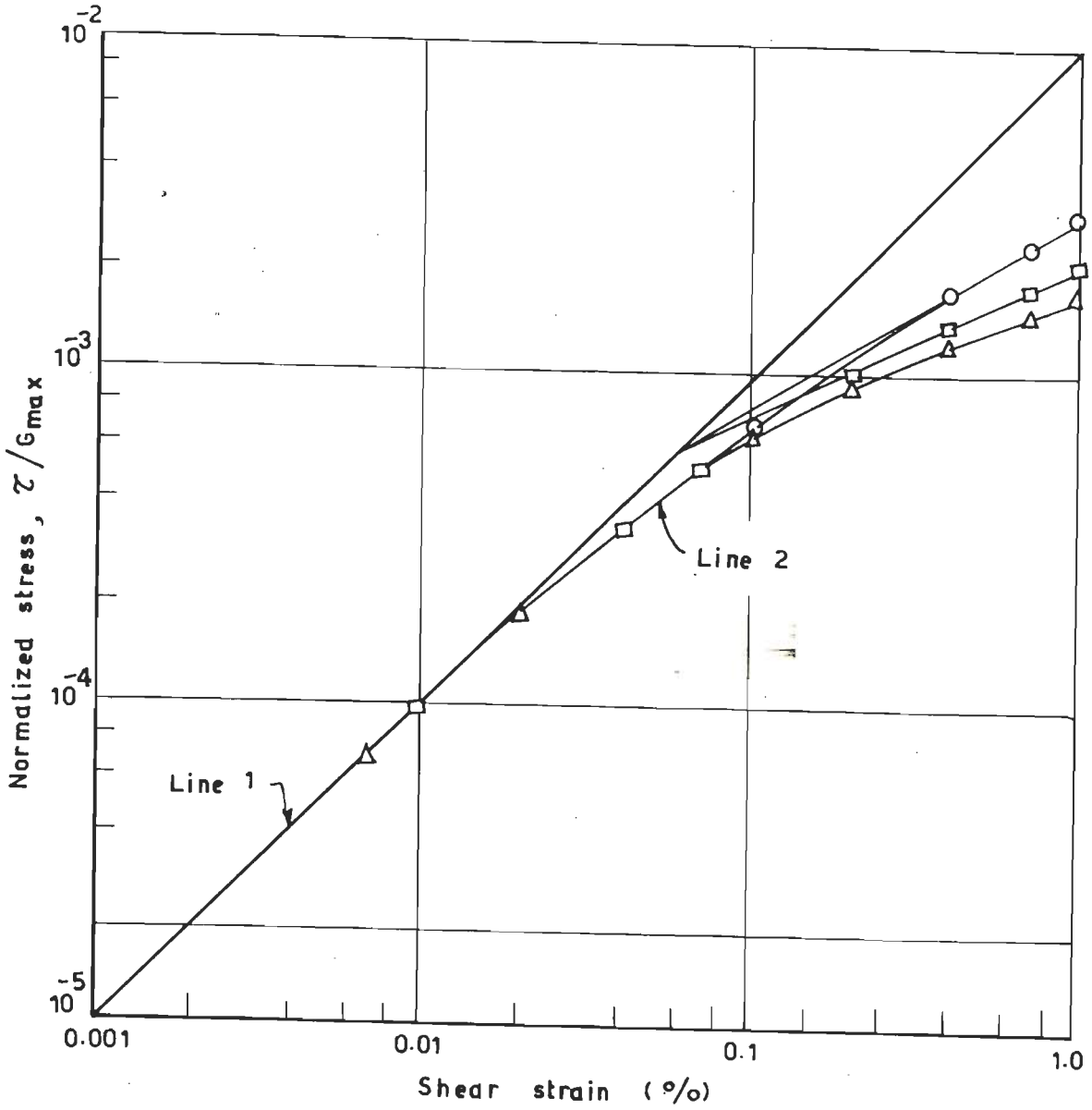


Fig. 5.6 Ramberg-Osgood Curve Theory
(Ishenower, 1979)

$$\frac{\Gamma}{C_1 \Gamma_r} = \frac{\tau}{C_1 \tau_m} \left[1 + \alpha \left| \frac{\tau}{C_1 \tau_m} \right|^{R-1} \right] \quad (5.14)$$

where

τ_m = maximum shear stress

C_1 = a factor relating the maximum shear stress and yield shear stress

$$= \tau_y / \tau_m \quad (5.15)$$

$$= 0.8$$

Γ_r = reference strain

$$= \tau_m / G_{\max} \quad (5.16)$$

Substituting Eq. 5.16 in Eq. 5.14, the following expression is obtained:

$$\frac{\Gamma_{G_{\max}}}{\tau_m} = \frac{\tau}{\tau_m} \left[1 + \alpha \left| \frac{\tau}{C_1 \tau_m} \right|^{R-1} \right] \quad (5.17)$$

Eq. 5.17 describes the shearing strain as the sum of a linear function of shearing stress and a nonlinear function of shearing stress. This equation was primarily developed to describe the stress-strain behaviour of air-craft metals and the Ramberg-Osgood model has been extended to define the non-linear stress-strain characteristics of soils by Richart and his co-workers (Richart, 1975; Richart and Wylie, 1975).

5.5.2 Least-Squares Curve Fitting Technique

The dimensionless parameters of the Ramberg-Osgood model, α and R are evaluated, using a first order least-squares curve fitting algorithm. In this method, a least-squares curve fit is performed using the logarithm of the elastic strain as the abscissa and the logarithm of deviation from the linearity as the ordinate. The procedure adopted in the present study is same as that proposed by Jennings (1964). The parameters, α and R in Eq. 5.17, are the value of the slope and the anti-logarithm of the intercept respectively, from the least-squares fit (Isenhower, 1979).

In the present study a computer program has been written to find the parameters, α and R using the least-squares technique as proposed by Jennings (1964). Input data to the program are the different values of shear modulus and the corresponding shearing strain determined in the field as shown in Table 4.1. The computed values of α and R for different soils are given in Table 5.3.

5.5.3 Normalized Values of Shear Modulus

The brief review of literature on shear modulus indicates that the shear modulus versus shear strain curves available for sand and clay (Hardin and Drnevich, 1970a; Seed and Idriss, 1970), and for silt (Grant and Brown, 1981) are in the form of modulus attenuation curves, in which the shear modulus values are normalized with respect to the low-amplitude shear modulus corresponding to a strain value of $\gamma = 10^{-6}$

or $\gamma = 10^{-4}$ percent as shown in Figs. 2.2, 2.4 and 2.7 or in the form of digitized values (User Manuals of LUSH and FLUSH computer packages). Expressing the normalized values of shear

Table 5.3 Values of α and R for Different Type of Soils

Sl. No. (1)	Soil Type (2)	α (3)	R (4)
1	Silt	133	2.33
2	Clay	249	2.50
3	Sand	288	3.10
4	Gravel	105	2.10

modulus as a function of shear strain has the following advantages:

- 1 Once the low-amplitude shear modulus, G_{\max} is known, any value of shear modulus (one other than, G_{\max}) can be interpolated using the modulus reduction factors.
- 2 Different field tests need not be conducted to obtain the absolute values of shear modulus as a function of strain except for the low-amplitude shear modulus.
- 3 In a nonlinear dynamic soil-structure interaction analysis case the shear modulus should be available at each time step, in a functional form which is an essential requirement.

These advantages are taken into account, by expressing the shear modulus ratio, G/G_{\max} , as given in the following equation:

$$\frac{G}{G_{\max}} = \frac{1}{1 + \alpha \left| \frac{G \Gamma}{C_1 G_{\max} \Gamma_r} \right|^{R-1}} \quad (5.18)$$

where

G/G_{\max} = modulus reduction factor.

In Eq. 5.18, the modulus reduction factor, G/G_{\max} is the unknown quantity and the shear strain is the known quantity for which G/G_{\max} is needed. The reference strain, Γ_r is given as:

$$\Gamma_r = \tau_m / G_{\max} \quad (5.19)$$

where

G_{\max} = low-amplitude shear moduli corresponding to shear strain values ranging between 10^{-6} to 10^{-4} percent

τ_m = maximum shear strength and given by (Hara et al., 1974):

$$\tau_m = \frac{1 + K_0}{2 \sigma'_v \sin \phi + C \cos \phi} \quad (5.20)$$

in which

K_0 = coefficient of earth pressure at rest

σ'_v = effective over-burden pressure

- ϕ = angle of internal friction
 C = cohesion.

The coefficient of earth pressure at rest, K_0 is given by:

$$K_0 = \mu / (1 - \mu) \quad (5.21)$$

where

μ = Poisson's ratio.

In the absence of explicit solution technique (Jennings, 1964), to solve Eq. 5.18, the Newton-Raphson iterative method (Hinton and Owen, 1986), has been implemented in a computer coding. Based on the type of soil, the Ramberg-Osgood model constants, α and R , given in Table 5.3 are used as input to the computer program. The normalized shear modulus ratios obtained for the different types of soils are presented in Fig. 5.7.

5.5.4 Comparison with Other Available Data

The modulus reduction curves obtained in the present study are compared with the widely used modulus attenuation curves, as proposed by Seed and Idriss (1970), in Fig. 5.7. From this figure, it is observed that the normalized values of shear modulus proposed by Seed and Idriss (1970), for the sand and clay soils give lower values of modulus reduction factors than that obtained using the Ramberg-Osgood model from the present study. However, the modulus reduction curve obtained in the present study and that the curve proposed by Grant and Brown (1981), show a

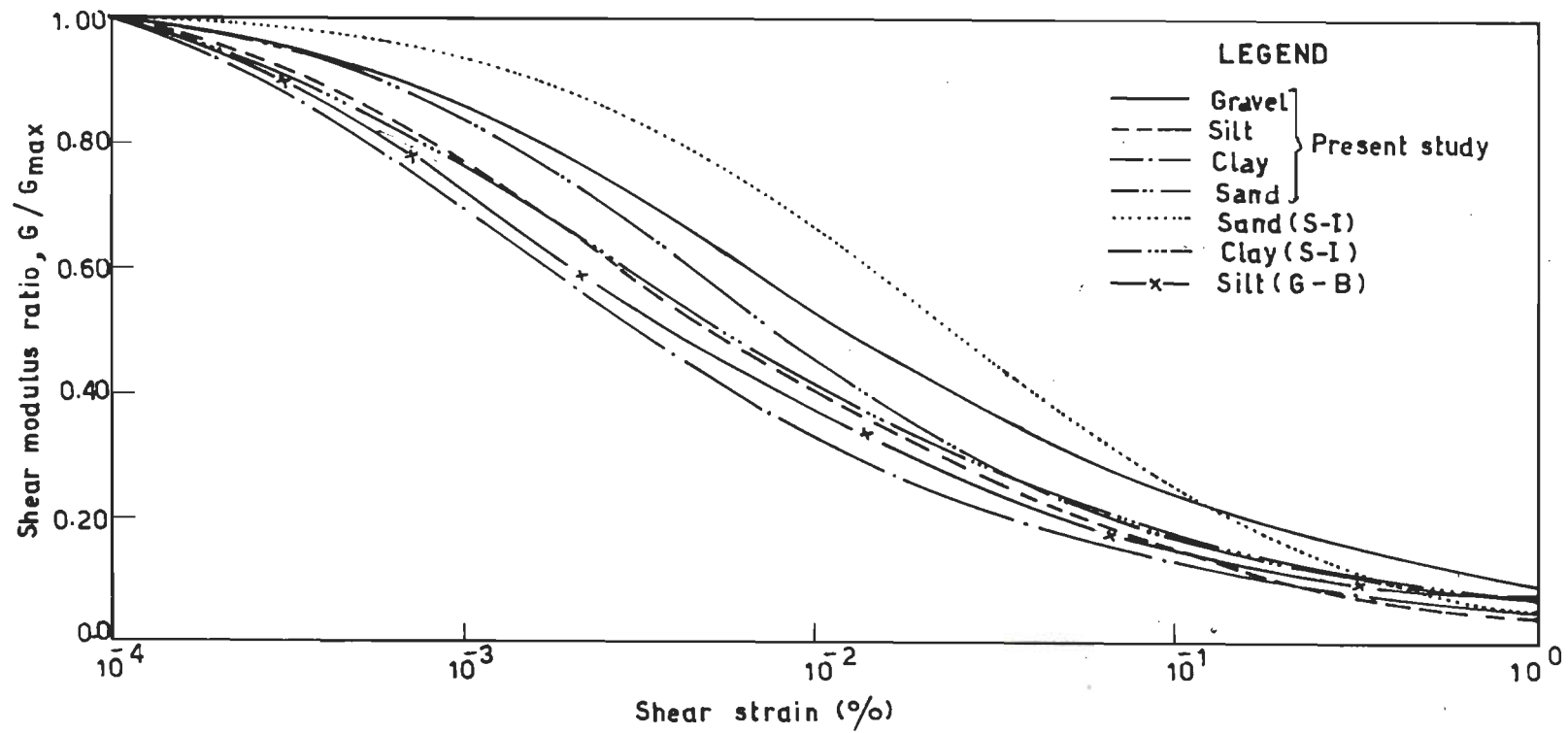


Fig. 5.7 Comparison of Normalized Values of Shear Modulus

close comparison.

5.5.5 Damping Values

The damping values as a function of strain can be expressed in analytical form using the Ramberg-Osgood model as (Ishihara, 1982):

$$D = \frac{2}{\pi} \times \frac{R-1}{R+1} \times \left(1 - \frac{G}{G_{\max}} \right) \quad (5.22)$$

where

D = the value of damping to be computed

R = the same constant shown in Table 5.3.

The G/G_{\max} values needed in solving Eq. 5.22, are obtained by solving Eq. 5.18. Eq. 5.22, is solved for different values of damping, D at different levels of shear strain, for all the four type of soils. The damping values obtained by solving Eq. 5.22 are shown in Fig. 5.8. For the purpose of comparison, the damping ratio curves proposed by Seed and Idriss (1970), are also plotted in the same figure. The damping values presented in Fig. 5.8 using the Ramberg-Osgood model are larger than the values proposed by Seed and Idriss (1970).

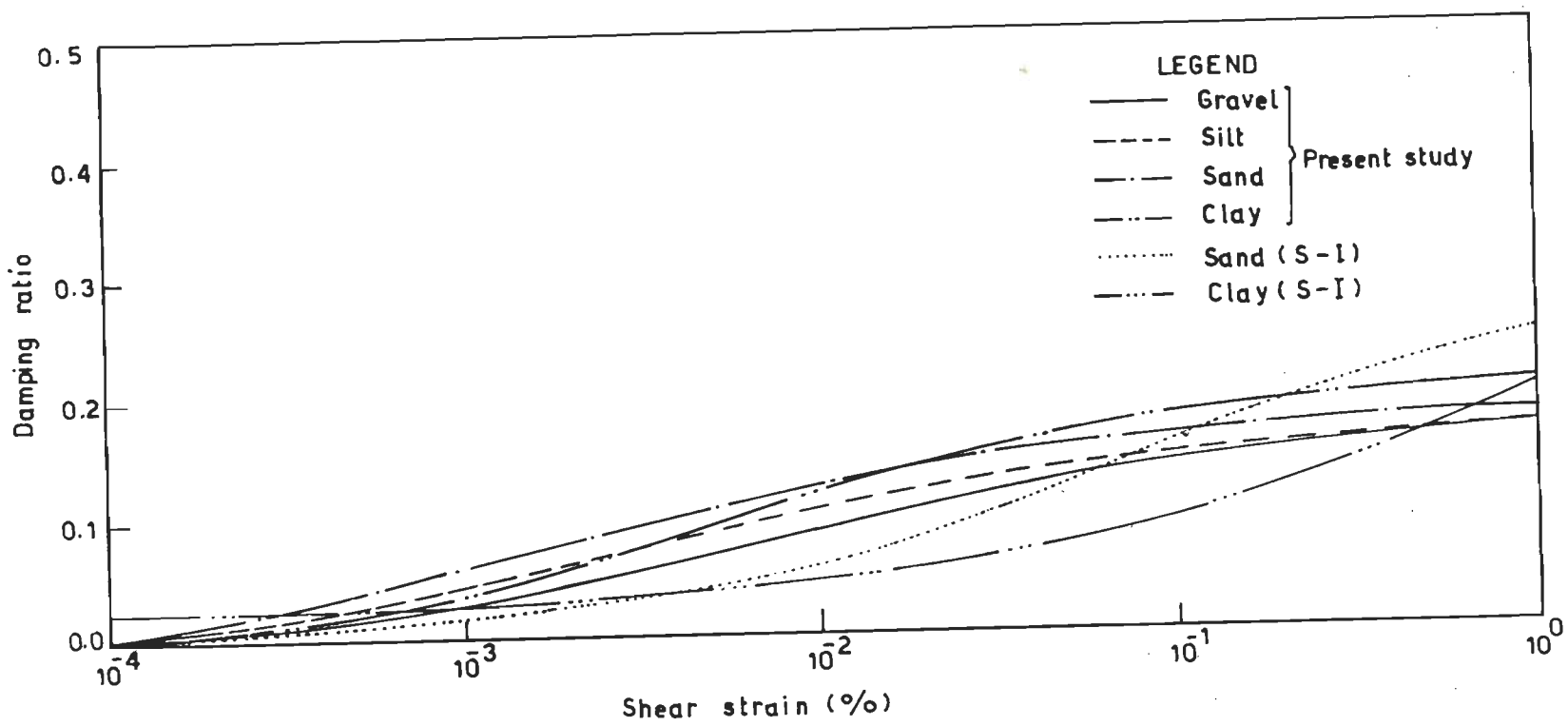


Fig. 5.8 Comparison of Damping Values

5.6 CLOSURE

The absolute values of field and laboratory shear modulus have been plotted as a function of strain. The ratio between field determined shear modulus and laboratory determined shear modulus values at large strain levels have been presented in the form of disturbance factors as a function of shear strain, corresponding to before the start of the primary consolidation and at the end of primary consolidation for three different type of soils. The difference between the shear modulus values determined before the beginning of primary consolidation and after the completion of primary consolidation, for three different types of soils has also been computed. The damping values obtained are larger due to limitations in the experiments adopted.

Using the field shear modulus values obtained at the four sites, the Ramberg-Osgood model constants have been evaluated, using the least-squares curve fitting technique. Using these constants, the modulus reduction factor curves and damping values as a function of strain for four different type of soils have been presented. The different modulus attenuation curves and damping value curves obtained in this study have been compared with the curves, that are very widely being employed in the dynamic analysis of soil-structure interaction problems and embankment dams subjected to seismic forces.

CHAPTER 6

FINITE ELEMENT FORMULATION

6.1 GENERAL

The finite element method of analysis is a powerful technique for the solution of various problems in continuum mechanics. This method has been applied extensively, for the evaluation of the seismic response of soil deposits and earth structures (Clough and Chopra, 1966; Idriss and Seed, 1967; Dibaj and Penzien, 1969; Idriss et al., 1973; Seed et al., 1973; Lysmer et al., 1974, 1975; Seed, Duncan and Idriss, 1975; Marcuson and Krinitzsky, 1976; Kagawa et al., 1981; Chandrasekaran, Paul and Suppiah, 1984, 1985; Chandrasekaran and Prakash, 1989b; Pandey et al., 1990).

The finite element method has been applied to the linear-elastic analysis of earth and rockfill dams by Brown and Goodman (1963), and Clough and Woodward (1967). The method has been used to analyse embankment dams with accounting for nonlinear stress-strain behaviour of soils (Kulhawy, Duncan and Seed, 1969; Duncan and Chang, 1970; Duncan et al., 1980), using the hyperbolic model developed by Kondner (1963), Kondner and Zelasko (1965). In this chapter, the formulation of the finite element method as applicable to

the analysis of embankment dams subjected to static and dynamic loading cases with material nonlinearity under plane strain condition is presented.

In the static nonlinear elastic case, the hyperbolic model as presented by Duncan et al. (1980), and in the dynamic analysis, the Ramberg-Osgood (1943), model as presented by Richart (1975), have been considered in this study.

6.2 FINITE ELEMENT METHOD

The finite element method may be described as a numerical discretization procedure, in which a continuum is idealized as an assemblage of discrete elements. The finite element method has been described in detail by a number of authors (Desai and Abel, 1972; Bathe, 1982; Bathe and Wilson, 1987; Hinton and Owen, 1977, 1979, 1986; Zienkiewicz, 1978; Craig, 1981; Naylor and Pande, 1983; Desai, 1984).

Three different approaches are available to solve any problem when the finite element method is employed. They are the stiffness or displacement, force and the hybrid or mixed methods. Out of these three methods the displacement method of formulation is commonly used, due to its versatility, and this method has been adopted in the present work. In this approach, the displacement is the primary unknown. The strains and stresses constitute the secondary unknowns. The important steps involved in a static analysis and in a dynamic analysis respectively, using the finite element method are presented subsequently.

(a) Static analysis

The different steps involved in a static analysis are:

- 1 Discretization of the elastic continuum or body
- 2 Selection of displacement or interpolation function
- 3 Formulation and assembly of stiffness matrix with the introduction of boundary conditions
- 4 Solving for displacement
- 5 Computation of stresses and strains.

(b) Dynamic analysis

The different steps involved in a dynamic analysis are:

- 1 Discretization of the elastic continuum or body
- 2 Selection of displacement or interpolation function
- 3 Formulation and assembly of stiffness matrix with the introduction of boundary conditions
- 4 Formulation and assembly of mass matrix
- 5 Formulation and assembly of damping matrix
- 6 Selection of the base input motion
- 7 Selection of the time interval for the step-by-step integration scheme
- 8 Computation of acceleration, velocity and displacement
- 9 Evaluation of stresses and strains

6.2.1 Eight-Noded Isoparametric Element

The problems considered in this study, are three rockfill dams of plane strain case in which the number of

degrees of freedom for each node is two. The eight-noded isoparametric elements with reduced integration scheme are used in the present study, since they are numerically stable and versatile (Ergatoudis, Irons and Zienkiewicz, 1968; Hinton and Owen, 1977, 1979).

The important steps involved in the formulation of finite element method with respect to eight-noded isoparametric elements are discussed below:

6.2.2 Selection of Displacement or Interpolation Function

The accuracy of the solution of any problem, using the finite element method depends upon the selected displacement function. An interpolation function is that which inter-relates either the displacement or the coordinates within an element to that at the nodal points.

Thus, at any point within an element, e the displacement components are defined in terms of the nodal displacements by the expression:

$$\{U\} = [N]\{q_e\} \quad (6.1)$$

in which

$\{U\}$ = the nodal displacement vector

$[N]$ = the shape function defined by a suitable polynomial expressing the displacement at any point, as a function of its coordinates

$\{q_e\}$ = vector of nodal displacements for an element, e .

Eq. 6.1 can be written as

$$\{U\} = \begin{Bmatrix} U \\ V \end{Bmatrix} = \begin{bmatrix} [N_1] & \dots & [N_1] & \dots & [N_8] \end{bmatrix} \begin{Bmatrix} U_1 \\ V_1 \\ \vdots \\ U_1 \\ V_1 \\ \vdots \\ U_8 \\ V_8 \end{Bmatrix} \quad (6.2)$$

where

U and V are horizontal and vertical displacements at a point within the element respectively

$[N_i]$ = the shape function sub-matrix, for the node, i

U_i and V_i are the horizontal and vertical displacements at node, i.

The sub-matrix, $[N_i]$, for the i th node is given by:

$$[N_i] = \begin{bmatrix} N_i & 0 \\ 0 & N_i \end{bmatrix} \quad (6.3)$$

where

N_i = shape function for node i.

The interpolation function employs a local coordinate system (ξ, η) , which permits the use of elements with curvilinear shape. The dimensionless local coordinates lie between the interval of -1 to +1, which makes it convenient to carry out numerical integration. The parabolic shape

functions corresponding to the eight nodes are shown in Fig. 6.1. For a 2-dimensional case with eight-noded isoparametric element the displacement function becomes:

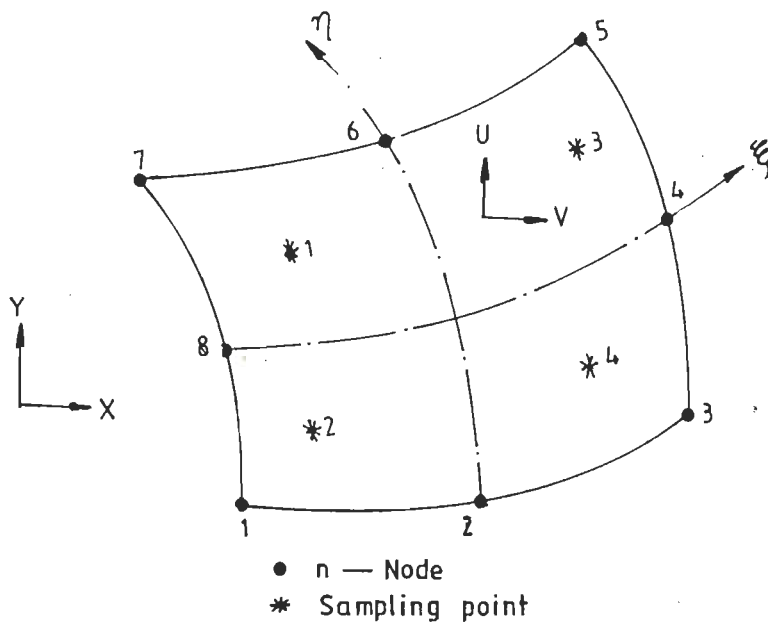
$$\begin{Bmatrix} U \\ V \end{Bmatrix} = \begin{bmatrix} N_1 & 0 & \dots & N_1 & 0 & \dots & N_8 & 0 \\ 0 & N_1 & \dots & 0 & N_1 & \dots & 0 & N_8 \end{bmatrix} \begin{Bmatrix} U_1 \\ V_1 \\ \vdots \\ U_1 \\ V_1 \\ \vdots \\ U_8 \\ V_8 \end{Bmatrix} \quad (6.4)$$

Using the isoparametric concept, the geometry and the displacement field are expressed by the same shape functions. Therefore, the x and y coordinates at any point within an eight-noded element are given as:

$$\begin{Bmatrix} x \\ y \end{Bmatrix} = [N] \begin{Bmatrix} x_1 \\ y_1 \\ \vdots \\ x_i \\ y_i \\ \vdots \\ x_8 \\ y_8 \end{Bmatrix} \quad (6.5)$$

where

x_i and y_i are the x and y coordinates of the i th node respectively.



$$N_1(\xi, \eta) = -0.25(1-\xi)(1-\eta)(1+\xi+\eta)$$

$$N_2(\xi, \eta) = 0.50(1-\xi^2)(1-\eta)$$

$$N_3(\xi, \eta) = 0.25(1+\xi)(1-\eta)(\xi-\eta-1)$$

$$N_4(\xi, \eta) = 0.50(1+\xi)(1-\eta^2)$$

$$N_5(\xi, \eta) = 0.25(1+\xi)(1+\eta)(\xi+\eta-1)$$

$$N_6(\xi, \eta) = 0.50(1-\xi^2)(1+\eta)$$

$$N_7(\xi, \eta) = 0.25(1-\xi)(1+\eta)(-\xi+\eta-1)$$

$$N_8(\xi, \eta) = 0.50(1-\xi)(1-\eta^2)$$

Fig. 6.1 An Eight-Noded Element with Shape Functions

6.2.3 Strain-Displacement Relationship

The components of strain at any point within an element for a two-dimensional case are related to the displacements as given by:

$$\{\varepsilon\} = \begin{Bmatrix} \varepsilon_x \\ \varepsilon_y \\ \gamma_{xy} \end{Bmatrix} = \begin{bmatrix} \frac{\partial U}{\partial x} \\ \frac{\partial V}{\partial y} \\ \frac{\partial V}{\partial x} + \frac{\partial U}{\partial y} \end{bmatrix} \quad (6.6)$$

$$= [L] \begin{Bmatrix} U \\ V \end{Bmatrix} \quad (6.7)$$

where

$\{\varepsilon\}$ = strain vector

ε_x = strain in x-direction

ε_y = strain in y-direction

γ_{xy} = shear strain

$[L]$ = the differential operator and given by:

$$[L] = \begin{bmatrix} \frac{\partial}{\partial x} & 0 \\ 0 & \frac{\partial}{\partial y} \\ \frac{\partial}{\partial y} & \frac{\partial}{\partial x} \end{bmatrix} \quad (6.8)$$

Substituting Eq. 6.1 in Eq. 6.8, the strain-displacement relationship is obtained as:

$$\{\varepsilon\} = [L][N]\{q_e\}$$

or

$$\{\varepsilon\} = [B]\{q_e\} \quad (6.9)$$

where

$[B] = [L][N]$ is the strain-displacement matrix and is given by:

$$[B] = \left[[B_1], \dots [B_i], \dots [B_s] \right] \quad (6.10)$$

in which

$[B_i]$ is the sub-matrix for the i th node and is equal to:

$$[B_i] = \begin{bmatrix} \frac{\partial N_i}{\partial x} & 0 \\ 0 & \frac{\partial N_i}{\partial y} \\ \frac{\partial N_i}{\partial y} & \frac{\partial N_i}{\partial x} \end{bmatrix} \quad (6.11)$$

6.2.4 Stress-Strain Relationship

The stresses are determined from the strains using the expression:

$$\{\sigma\} = [D]\{\varepsilon\} + \{\sigma_0\} \quad (6.12)$$

where

$\{\sigma\}$ = stress vector

$\{\sigma_0\}$ = initial stress vector

$[D]$ = elasticity matrix for the material.

The elasticity matrix, $[D]$ for a two-dimensional plane strain case ($\epsilon_z = 0$) is given as (Hinton and Owen, 1977):

$$[D] = \frac{E(1-\mu)}{(1+\mu)(1-2\mu)} \begin{bmatrix} 1 & \frac{\mu}{1-\mu} & 0 \\ \frac{\mu}{1-\mu} & 1 & 0 \\ 0 & 0 & \frac{1-2\mu}{2(1-\mu)} \end{bmatrix} \quad (6.13)$$

where

E = Young's modulus

μ = Poisson's ratio.



Substituting the value of $\{\epsilon\}$, from Eq. 6.9 in Eq. 6.12, one obtains

$$\{\sigma\} = [D][B]\{q_e\} + \{\sigma_0\} \quad (6.14)$$

6.2.5 Equilibrium Equations

The equilibrium equation based on the principle of virtual work for an element is given as:

$$\frac{\partial \Pi_e}{\partial \mathbf{q}_e} = \int_V [\mathbf{B}]^T [\mathbf{D}] [\mathbf{B}] \{\mathbf{q}_e\} dV - \int_V [\mathbf{N}]^T \{\mathbf{b}\} dV - \int_S [\mathbf{N}]^T \{\mathbf{T}\} dS \quad (6.15)$$

where

$\{\mathbf{b}\}$ = body force vector

$\{\mathbf{T}\}$ = surface traction vector

V = elemental volume.

Without the forces due to surface traction, Eq. 6.15 can be written as:

$$\int_V [\mathbf{B}]^T [\mathbf{D}] [\mathbf{B}] dV \{\mathbf{q}_e\} = \{\mathbf{R}_e\} \quad (6.16)$$

in which

$\{\mathbf{q}_e\}$ = displacement vector of an element, e

$$\{\mathbf{R}_e\} = \int_V [\mathbf{N}]^T \{\mathbf{b}\} dV \quad (6.17a)$$

is the equivalent nodal forces

$$\{\mathbf{k}_e\} = \int_V [\mathbf{B}]^T [\mathbf{D}] [\mathbf{B}] dV \quad (6.17b)$$

is the element stiffness matrix of an element, e

and the integration is carried out over the elemental volume, V .

Eq. 6.16 can be written as:

$$[k_e]\{q_e\} = \{R_e\} \quad (6.18)$$

6.2.6 Jacobian Matrix

The Jacobian Matrix, $J(\xi, \eta)$, for a two-dimensional case is given by:

$$J = \begin{bmatrix} \frac{\partial x}{\partial \xi} & \frac{\partial y}{\partial \eta} \\ \frac{\partial x}{\partial \xi} & \frac{\partial y}{\partial \eta} \end{bmatrix} \quad (6.19a)$$

and for an eight-noded element, Eq. 6.19a is given as:

$$J = \sum_{i=1}^8 \begin{bmatrix} \frac{\partial N_i}{\partial \xi} x_i & \frac{\partial N_i}{\partial \xi} y_i \\ \frac{\partial N_i}{\partial \eta} x_i & \frac{\partial N_i}{\partial \eta} y_i \end{bmatrix} \quad (6.19b)$$

6.2.7 Element Stiffness Matrix

The stiffness matrix of an element, e , given in Eq. 6.17b can be written as

$$[k_e] = \iint [B]^T [D] [B] t [J] d\xi d\eta \quad (6.19c)$$

where

t = thickness

$$dx dy = |J| d\xi d\eta$$

$|J|$ = determinant of the Jacobian matrix

For a two-dimensional plane strain situation in which the thickness, t is unity, then Eq. 6.19c can be written as:

$$[k_e] = \iint [B]^T [D] [B] [J] d\xi d\eta \quad (6.19d)$$

Eq. 6.19d is evaluated using the numerical integration techniques which are described subsequently.

6.2.8 Numerical Integration

The Gauss-Legendre formula for performing numerical integration which is needed to solve Eq. 6.19d is given by:

$$I = \int_{-1}^{+1} \int_{-1}^{+1} \phi(\xi, \eta) d\xi d\eta \quad (6.19e)$$

Integrating Eq. 6.19e, the following expression is obtained:

$$I = \sum_{i=1} \sum_{j=1} W_i W_j \phi(\xi_i, \eta_j) \quad (6.19f)$$

in which

ϕ = the numerical value of the function

W_i, W_j = weighting factors

ξ_i, η_j = sampling points.

For a 2-point numerical integration scheme, the value of weighting factors are equal to ± 0.57777775 . Substituting the different values in Eq. 6.19d, the element stiffness matrix is evaluated.

6.2.9 Global Stiffness Matrix

The global stiffness matrix, $[K]$ of the whole assembly is obtained from the individual element matrix using the direct stiffness method. The assembled global stiffness matrix is of size, $2NN \times 2NN$, in which NN is the total number of nodes. Since this matrix is symmetric and banded in nature, it can be stored in the computer, as an array of size $2NN \times MB$, in which MB is the semi-band width of the global stiffness matrix. This storage scheme is used in the present study. The global stiffness matrix is expressed as:

$$[K]\{q\} = \{R\} \quad (6.20)$$

where

$[K]$ = the assembled stiffness matrix

$\{q\}$ = the unknown displacement vector

$\{R\}$ = the global load vector.

6.3 FINITE ELEMENT FORMULATION OF NONLINEAR STATIC PROBLEM

The formulation of the finite element method with respect to nonlinear elasticity and sequential construction analysis of embankment dams is briefly explained in this section.

As mentioned in Chapter 2, the stress-strain characteristics of soils are nonlinear. It is essential, therefore, that nonlinearity should be taken into consideration in the analysis of earth and earthfill structures. Two methods, namely, (1) successive approximation method and (2) successive increment method are presently available to model the nonlinear stress-strain behaviour of soils, under static loading conditions. These two methods are briefly summarized below:

6.3.1 Successive Approximation or Secant Modulus Method

In this method, the same loading is applied repeatedly throughout the analysis, adjusting the modulus values assigned to each element, every time until the computed values of stress and strain are consistent with the assumed nonlinear model. This method has severe limitations, which have been highlighted by Dunlop and Duncan (1970). The advantage of this method is that, strain softening or reduction in shear resistance beyond the peak value can be approximated. One of the limitations is that, non-zero initial stresses, which are a characteristic of all geotechnical problems, cannot be approximated (Kuberan, 1978).

6.3.2 Successive Increment or Tangent Modulus Method

In this method, the stiffness of each element is selected in accordance with the existing state of stress in that element (Clough and Woodward, 1967). The construction

sequence can be simulated using this method and the nonlinear behaviour is approximated by a series of linear increments.

Successive increment or tangent modulus method is used in the present study to simulate the static nonlinear material behaviour. The nonlinear stress-strain curve is represented by a hyperbolic equation. The hyperbolic model is presented in the next section.

6.3.3 Hyperbolic Model

Kondner and his co-workers (Kondner, 1963; Kondner and Zelasko, 1963a, 1963b; Kondner and Horner, 1965), have proposed a simplified model to represent the nonlinear stress-strain behaviour of different soils. In this method the nonlinear stress-strain law is expressed by a hyperbola in the following form (Duncan et al., 1980):

$$\frac{(\sigma_1 - \sigma_3)}{1 - 3} = \frac{\epsilon}{\frac{1}{E_i} + \frac{\epsilon}{(\sigma_1 - \sigma_3)_{ult}}} \quad (6.21)$$

where

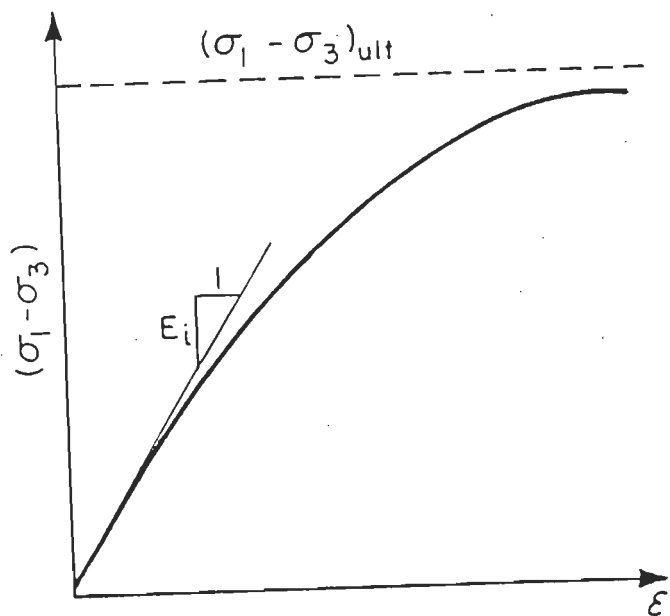
$(\sigma_1 - \sigma_3)$ = deviator stress

ϵ = axial strain

E_i = initial tangent modulus

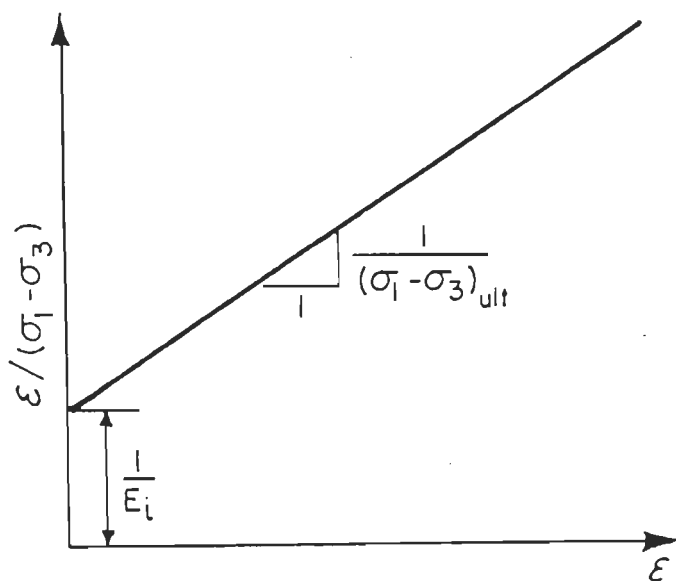
$(\sigma_1 - \sigma_3)_{ult}$ = asymptotic deviator stress.

The hyperbolic expression (Eq. 6.21) is shown in Fig. 6.2. When Eq. 6.21 is transformed, a linear relationship is obtained between $\epsilon / (\sigma_1 - \sigma_3)$ and ϵ as shown in Fig. 6.3.



$$(\sigma_1 - \sigma_3) = \frac{\text{Real } \epsilon}{\frac{1}{E_i} + \frac{\epsilon}{(\sigma_1 - \sigma_3)_{ult}}}$$

Fig. 6.2 Hyperbolic Representation of Stress-Strain Curve
(Duncan et al., 1980)



$$\frac{\epsilon}{(\sigma_1 - \sigma_3)} = \frac{1}{E_i} + \frac{\epsilon}{(\sigma_1 - \sigma_3)_{ult}}$$

Fig. 6.3 Transformed Hyperbolic Representation
(Duncan et al., 1980)

The stress-strain characteristics of most of the soils, depend on the confining pressure. The influence of confining pressure on the stress-strain characteristics of soils may be incorporated in the stress-strain relationship by relating the values of the initial tangent modulus, E_i and the soil strength, $(\sigma_1 - \sigma_3)_{ult}$ with confining pressure. The variation of initial tangent modulus with confining pressure is empirically expressed as (Janbu, 1963):

$$E_i = K p_a (\sigma_3 / p_a)^{n_h} \quad (6.22)$$

where

E_i = initial tangent modulus

σ_3 = minor principal stress

p_a = atmospheric pressure expressed in the same units as E_i and σ_3

K = a modulus number

n_h = an exponent determining the rate of variation of E_i with σ_3 .

The variation of $(\sigma_1 - \sigma_3)_{ult}$ with σ_3 is accounted by relating $(\sigma_1 - \sigma_3)_{ult}$ to the compressive strength or stress difference at failure, $(\sigma_1 - \sigma_3)_f$ and then using the Mohr-Coulomb strength criterion. The relation between $(\sigma_1 - \sigma_3)_f$ with σ_3 is obtained as:

$$(\sigma_1 - \sigma_3)_f = \frac{2 (C \cos \phi + \sigma_3 \sin \phi)}{1 - \sin \phi} \quad (6.23)$$

in which

C = cohesion and

ϕ = angle of internal friction are the Mohr-Coulomb strength parameters.

The asymptotic deviator stress, $(\sigma_1 - \sigma_3)_{ult}$, shown in Fig. 6.2, and the deviator stress at failure, $(\sigma_1 - \sigma_3)_f$, are related by the following expression:

$$(\sigma_1 - \sigma_3)_f = R_f (\sigma_1 - \sigma_3)_{ult} \quad (6.24)$$

where

R_f = a correlation factor called the failure ratio, with a value less than unity.

The tangent modulus, E_i corresponding to any point on the stress-strain curve (Fig. 6.2), is expressed in the form:

$$E_i = \frac{d(\sigma_1 - \sigma_3)}{d\varepsilon} \quad (6.25)$$

Differentiating, Eq. 6.21, as indicated in Eq. 6.25 and substituting the other parameters given in Eqs. 6.22 and 6.23, the following expression is obtained:

$$E_i = \left[1 - \frac{R_f (1 - \sin \phi) (\sigma_1 - \sigma_3)}{2(C \cos \phi + \sigma_3 \sin \phi)} \right]^2 K p_a (\sigma_3 / p_a)^{n_h} \quad (6.26)$$

Eq. 6.26 can be employed, either in an effective or a total stress analysis using the finite element method.

The value of bulk modulus, B is defined as (Duncan et al., 1980):

$$B = \frac{\Delta\sigma_1 + \Delta\sigma_2 + \Delta\sigma_3}{3\varepsilon_v} \quad (6.27)$$

in which

$\Delta\sigma_1$, $\Delta\sigma_2$ and $\Delta\sigma_3$ are the changes in the values of the three principal stresses

ε_v = the corresponding change in volumetric strain.

In a triaxial test, keeping the confining pressure constant and increasing the deviator stress, $(\sigma_1 - \sigma_3)$, then Eq. 6.27 can be written as:

$$B = \frac{\sigma_1 - \sigma_3}{3\varepsilon_v} \quad (6.28)$$

Duncan et al. (1980), observed that the bulk modulus is directly proportional to the confining pressure. The variation between bulk modulus and confining pressure is given empirically, in the form:

$$B = K_b p_a (\sigma_3 / p_a)^{m_h} \quad (6.29)$$

where

K_b = bulk modulus number

m_h = bulk modulus exponent.

In all, the hyperbolic method involves eight different parameters to simulate the nonlinear stress-strain behaviour of soils under static condition and these parameters are listed in Table 6.1 (Duncan et al., 1980). In the present study, the different parameters given in Table 6.1, have been adopted to account for the material nonlinearity of different soils. Duncan et al. (1980), have discussed the advantages and the disadvantages of the hyperbolic model in detail.

6.3.4 Sequential or Incremental Construction Method

Brown and Goodman (1963), have shown that for an accurate analysis of embankments, the simulation of the placement of successive layers of embankment material is necessary. Clough and Woodward (1967), compared the usefulness of the incremental finite element analysis in which the placement of successive layers is simulated with the 'gravity turn-on' method, in which the gravity body forces are applied to the entire structure at one time only. Their studies indicate that the incremental method of analysis predicts the actual behaviour of an embankment under static case.

In the incremental analysis the load is divided into a number of small increments and the soil behaviour is assumed to be linear within each increment.

The stress-strain relationship for an isotropic material, under plane strain condition is given by (Duncan et al., 1980):

Table 6.1 Different Parameters of the Hyperbolic Model
(Duncan et al., 1980)

Parameter (1)	Name (2)	Function (3)
K	Modulus number	Relate E_i to σ_3
n_h	Modulus exponent	
C	Cohesion intercept	Relate $(\sigma_1 - \sigma_3)_f$ to σ_3
$\phi, \lambda/\phi$	Friction angle parameters	
R_f	Failure ratio	Relates $(\sigma_1 - \sigma_3)_{ult}$ to $(\sigma_1 - \sigma_3)_f$
K_b	Bulk modulus number	Value of B/p_a at $\sigma_3 = p_a$
m_h	Bulk modulus exponent	Change in B/p_a for ten-fold increase in σ_3

$$\begin{Bmatrix} \Delta\sigma_x \\ \Delta\sigma_y \\ \Delta\tau_{xy} \end{Bmatrix} = \frac{3B}{9B-E} \begin{bmatrix} (3B+E) & (3B-E) & 0 \\ (3B-E) & (3B+E) & 0 \\ 0 & 0 & E \end{bmatrix} \begin{Bmatrix} \Delta\varepsilon_x \\ \Delta\varepsilon_y \\ \Delta\gamma_{xy} \end{Bmatrix} \quad (6.30)$$

where

$\Delta\sigma_x$ = normal stress increment

$\Delta\sigma_y$ = normal stress increment

$\Delta\tau_{xy}$ = shear stress increment

$\Delta\varepsilon_x$ = normal strain increment

$\Delta\varepsilon_y$ = normal strain increment

$\Delta\gamma_{xy}$ = shear strain increment

E = Young's modulus

B = bulk modulus.

Before the starting of the sequential construction, the initial or in-situ stress, $\{\sigma_0\}$, in the initial ground surface is computed as shown in Fig. 6.4. The first layer of soil mass is placed over the initial ground surface as shown in Fig. 6.5, and the resulting increment in stress, $\{\Delta\sigma_1\}$, is computed. The total stresses at the completion of the first layer are given by:

$$\{\sigma_1\} = \{\sigma_0\} + \{\Delta\sigma_1\} \quad (6.31)$$

At the end of placing of the i th layer as shown in Fig. 6.6, the stresses are computed using a recursive formula as (Desai and Abel, 1972):

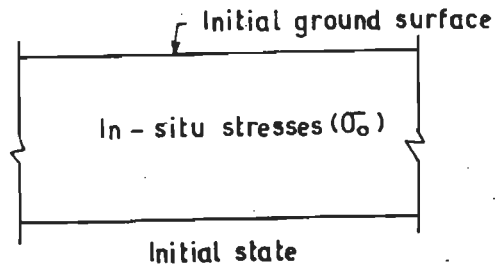


Fig. 6.4 In-situ Stresses at Initial State
(Desai and Abel, 1972)

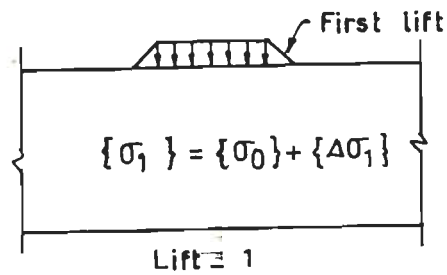


Fig. 6.5 Stresses at the End of First Lift
(Desai and Abel, 1972)

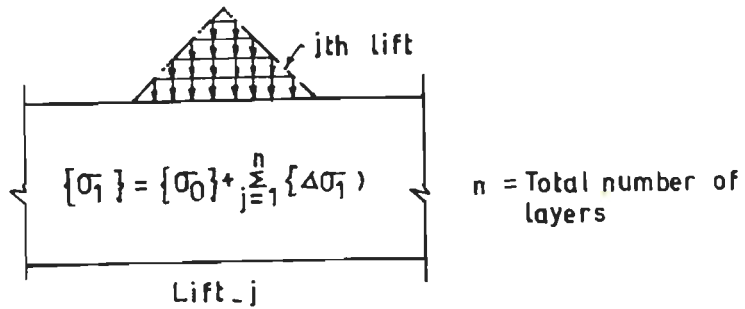


Fig. 6.6 Stresses at the End of i th Layer
(Desai and Abel, 1972)

$$\{\sigma_i\} = \{\sigma_0\} + \sum_{j=1}^i \{\Delta \sigma_j\} \quad (6.32)$$

Similarly, the displacements are computed by:

$$\{u_i\} = \sum_{j=1}^i \{\Delta u_j\} \quad (6.33)$$

where

$\{u_i\}$ = total displacement vector at the end of placing of the i th layer

$\{\sigma_i\}$ = stress vector at the end of placing of the i th layer

$\{\Delta u\}$ = increment in displacement.

In the present work, the incremental method of analysis has been used to obtain the pre-earthquake stresses in embankment dams analysed.

6.4 FORMULATION WITH RESPECT TO DYNAMIC ANALYSIS

The formulation of the finite element method, related to seismic or earthquake loading is described in this section. The equilibrium equation for evaluating the earthquake response is (Dibaj and Penzien, 1969):

$$[M]\ddot{\{r\}} + [C]\dot{\{r\}} + [K]\{r\} = \{R(t)\} \quad (6.34)$$

in which

$[M]$ = global mass matrix

$[C]$ = global damping matrix

$[K]$ = global stiffness matrix

$\{\ddot{r}\}$ = nodal acceleration vector
 $\{\dot{r}\}$ = nodal velocity vector
 $\{r\}$ = nodal displacement vector
 $\{R(t)\}$ = earthquake load vector.

Expanding the vector, $\{r\}$, into component form,

$$\{r\}^T = [U_1 \ V_1, \dots, U_i \ V_i, \dots, U_{NN} \ V_{NN}] \quad (6.35)$$

in which

U_i and V_i are the x and y components of the displacement of nodal point, i and NN represents the total number of nodal points.

For a lumped-mass system, the earthquake force excitation vector, $\{R\}$ is given by:

$$\{R\} = -[M]\{\ddot{y}_g\} \quad (6.36)$$

where

$\{\ddot{y}_g\}$ = ground acceleration vector.

6.4.1 Stiffness Matrix

The assembly and storage scheme used in this case is identical to that described in Secs. 6.2.7 to 6.2.9.

6.4.2 Mass Matrix

In the formulation of the mass matrix, the diagonal mass system is adopted, since the problem considered in the present study is of wave propagation category (Desai

and Abel, 1972). The element mass matrix, $[m_e]$ is given by (Cook, 1981):

$$[m_e] = \int_V \rho [N]^T [N] dV \quad (6.37)$$

where

ρ = mass density

$[N]$ = shape function, N_i with unit value at the node i and zero elsewhere.

Eq. 6.37 represents the consistent mass matrix. Test cases to date show that the accuracy of the diagonal mass matrix is excellent, often surpassing that of the consistent mass matrix (Cook, 1981). The diagonal mass matrix which is more sophisticated than a lumped mass matrix is derived from the consistent mass matrix as mentioned below (Cook, 1981):

- a Compute only the diagonal coefficients of the consistent mass matrix.
- b Compute m , the total mass of the element.
- c Compute a number, s_1 by adding the diagonal coefficients, m_{ii} associated with translation (but not rotation).
- d Scale the diagonal coefficients, m_{ii} by multiplying them by the ratio m/s_1 , thus preserving the translational mass of the element.

The assembly of the mass matrix is analogous to that of the stiffness matrix as described in Sec. 6.2.7. The global mass matrix remains diagonal and is given by:

$$[M] = \sum_{e=1}^L [m_e] \quad (6.38)$$

where

$[M]$ = the assembled mass matrix which is diagonal and the summation is done upto to the total number of elements L .

The consistent mass matrix system leads to more computer time and memory.

6.4.3 Damping Matrix

Dissipation of energy with time or distance is called damping. The damping term shown in Eq. 6.34 is the viscous damping, which is directly proportional to the velocity. In general, a simplified form of damping is used in seismic studies, which is known as the Rayleigh damping and is given by (Dibaj and Penzien, 1969; Idriss et al., 1973):

$$[C] = \alpha_1 [M] + \beta_1 [K] \quad (6.39)$$

where

α_1 and β_1 are constants.

In Eq. 6.39, the damping matrix contains a component proportional to the mass matrix and a component proportional to the stiffness matrix. Assigning the damping value in the above form has the advantage, that the numerical values of α_1 and β_1 , only need to be stored (Dibaj and

Penzien, 1969). Eq. 6.39 is applicable for constant damping cases only (Idriss et al., 1973).

However, as shown in Chapters 2 and 5, the damping induced in soils is a function of strain and is not a constant. Thus, Eq. 6.39 should be modified to account for variable damping. This is described in the next sub-section.

6.4.4 Variable Damping Method

In this method, the damping matrix is formulated for each individual element and these matrices are added together for the entire assemblage of elements (Idriss et al., 1973). For any element, e the damping matrix is stated as:

$$[C_e] = \alpha_e [m_e] + \beta_e [k_e] \quad (6.40)$$

in which

$[C_e]$ = damping matrix for element e

$[m_e]$ = mass matrix for element e

$[k_e]$ = stiffness matrix for element e

α_e and β_e are functions of the mass and stiffness characteristics of element, e respectively.

The parameters α_e and β_e are given by:

$$\alpha_e = D_e \times w_1 \quad (6.41)$$

$$\beta_e = D_e / w_1 \quad (6.42)$$

in which

D_e = the damping ratio for element, e and is selected on the basis of the strain developed in the element under consideration (Chapter 5)

w_1 = the fundamental frequency in rad/sec of the system and given by (Idriss et al., 1973):

$$w_1^2 = \frac{\{\phi'\}^T [K] \{\phi'\}}{\{\phi'\}^T [M] \{\phi'\}} \quad (6.43)$$

in which

$\{\phi'\}$ = mode shape of the system corresponding to the fundamental mode and obtained using the method of inverse iteration

$[K]$ = the modified stiffness matrix.

If c_{ij} represents the (ij) th term of the damping sub-matrix $[C]$, then the (IJ) th term of the damping matrix of the whole system is stated as (Idriss et al., 1973):

$$C_{IJ} = \sum_e^L c_{ij} \quad (6.44)$$

wherein

$C_{IJ} \neq 0$, only if $I = J$ or I is adjacent to J and

L is the total number of elements.

The final damping matrix $[C]$ is symmetric and banded in nature and the assembly is same as that of stiffness and mass matrices. In the present work the variable damping solution, as proposed by Idriss et al. (1973), is adopted.

6.4.5 Step-by-Step Integration Scheme

The dynamic response of the system subjected to earthquake loading is evaluated by solving Eq. 6.34. To solve this equation, a direct time integration scheme, known as the step-by-step method, as proposed by Newmark (1959), (Bathe, 1982; Bathe and Wilson, 1987; Craig, 1981) has been used in the present work.

In the Newmark's method of step-by-step time integration scheme the following assumptions are made (Bathe, 1982; Bathe and Wilson, 1987).

$$\dot{r}_{t+\Delta t} = \dot{r}_t + [(1-\delta)\ddot{r}_t + \delta \ddot{r}_{t+\Delta t}] \Delta t \quad (6.45)$$

and

$$r_{t+\Delta t} = r_t + \dot{r}_t \Delta t + [(\frac{1}{2}-\alpha_3)\ddot{r}_t + \alpha_3 \ddot{r}_{t+\Delta t}] \Delta t^2 \quad (6.46)$$

where

$r_{t+\Delta t}$ = the displacement at time $t + \Delta t$

$\dot{r}_{t+\Delta t}$ = the velocity at time $t + \Delta t$

α_3 and δ = parameters used to achieve integration accuracy and stability

Δt = the time step required in the integration scheme.

Newmark (1959), proposed an unconditionally stable scheme, which is called the constant-average-acceleration method as shown in Fig. 6.7, and the values of α_3 and δ are 0.25 and 0.5 respectively.

The equation of motion (Eq. 6.34), at time, $t + \Delta t$, can be expressed as:

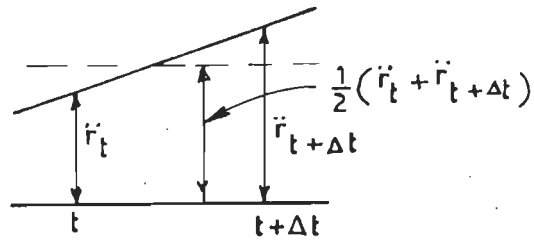


Fig. 6.7 Newmark's Constant Average Acceleration Method

$$M \ddot{r}_{t+\Delta t} + C \dot{r}_{t+\Delta t} + K r_{t+\Delta t} = R_{t+\Delta t} \quad (6.47)$$

Solving for $\ddot{r}_{t+\Delta t}$ from Eq. 6.46,

$$\ddot{r}_{t+\Delta t} = \frac{1}{\alpha_3 \Delta t^2} \left[r_{t+\Delta t} - r_t - \dot{r}_t \Delta t - \frac{1}{2} \ddot{r}_t \Delta t^2 + \alpha_3 \ddot{r}_t \Delta t^2 \right] \quad (6.48)$$

Substituting Eq. 6.48 in Eq. 6.45 and solving for $\dot{r}_{t+\Delta t}$,

$$\dot{r}_{t+\Delta t} = \dot{r}_t + \Delta t \ddot{r}_t - \delta \Delta t \ddot{r}_t + \frac{\delta \Delta t}{\alpha_3 \Delta t^2} \left[r_{t+\Delta t} - r_t - \dot{r}_t \Delta t - \frac{1}{2} \ddot{r}_t \Delta t^2 + \alpha_3 \ddot{r}_t \Delta t^2 \right]$$

$$\dot{r}_{t+\Delta t} = \dot{r}_t + \Delta t \ddot{r}_t (1-\delta) +$$

$$\frac{\delta}{\alpha_3 \Delta t} \left[r_{t+\Delta t} - r_t - \dot{r}_t \Delta t + \ddot{r}_t \Delta t^2 (\alpha_3 - \frac{1}{2}) \right]$$

$$\dot{r}_{t+\Delta t} = \dot{r}_t + \Delta t \ddot{r}_t (1-\delta) +$$

$$\frac{\delta}{\alpha_3 \Delta t} \left[r_{t+\Delta t} - r_t - \dot{r}_t \Delta t + \ddot{r}_t \Delta t^2 \left\{ 1 - \frac{1}{2\alpha_3} \right\} \right]$$

$$\dot{r}_{t+\Delta t} = \dot{r}_t \left(1 - \frac{\delta}{\alpha_3} \right) + \Delta t \ddot{r}_t (1-\delta) +$$

$$\frac{\delta}{\alpha_3 \Delta t} \left[\ddot{r}_t \Delta t^2 \left\{ 1 - \frac{1}{2\alpha_3} \right\} + \frac{\delta}{\alpha_3 \Delta t} (r_{t+\Delta t} - r_t) \right] \quad (6.49)$$

Substituting Eqs. 6.48 and 6.49 in 6.47 the following expression is obtained:

$$[M] \frac{1}{\alpha_3 \Delta t^2} \left[r_{t+\Delta t} - r_t - \dot{r}_t \Delta t + \ddot{r}_t \Delta t^2 \left\{ 1 - \frac{1}{2\alpha_3} \right\} \right] +$$

$$[C] \left[\dot{r}_t \left\{ 1 - \frac{\delta}{\alpha_3} \right\} + \Delta t \ddot{r}_t \left\{ 1 - \delta + \frac{\delta}{\alpha_3} - \frac{\delta}{2\alpha_3^2} \right\} +$$

$$\frac{\delta}{\alpha_3 \Delta t} (r_{t+\Delta t} - r_t) \right] + K r_{t+\Delta t} = R_{t+\Delta t} \quad (6.50)$$

in which

[C] = is the damping matrix as given by Eq. 6.44.

The important steps involved in solving Eq. 6.47 are (Bathe, 1982; Bathe and Wilson, 1987):

- (a) 1 Formation of stiffness matrix, K , mass matrix, M and damping matrix, C as discussed in Secs. 6.4.1 to 6.4.4.
- 2 Initialization of displacement, r , velocity, \dot{r} , and acceleration, \ddot{r}
- 3 Calculation of integration constants and selection of time step, Δt
- 4 Formation of effective matrix, \bar{K} where

$$\bar{K} = K + a_0 M + a_1 C \quad (6.51)$$

$$a_0 = \frac{1}{\alpha_3 \Delta t^2}; \quad a_1 = \frac{\delta}{\alpha_3 \Delta t}$$

- 5 Triangularization of \bar{K}

(b) For each time step, Δt ,

- 1 Computation of effective load at time, $t + \Delta t$, is given by:

$$\bar{R}_{t+\Delta t} = R_{t+\Delta t} + M(a_0 \ddot{r}_t + a_2 \dot{r}_t + a_3 r_t) + C(a_4 \dot{r}_t + a_5 r_t) \quad (6.52)$$

where

$$a_2 = \frac{1}{\alpha_3 \Delta t}; \quad a_3 = \frac{1}{2\alpha_3} - 1; \quad a_4 = \frac{\delta}{\alpha_3} - 1;$$

$$a_5 = \frac{\Delta t}{2} \left[\frac{\delta}{\alpha_3} - 2 \right]$$

- 2 Solving for displacement at time, $t + \Delta t$.
- 3 Calculation of acceleration and velocity at time, $t + \Delta t$, using the following expressions:

$$\ddot{r}_{t+\Delta t} = a_0(r_{t+\Delta t} - r_t) - a_2\dot{r}_t - a_3\ddot{r}_t \quad (6.53)$$

$$\dot{r}_{t+\Delta t} = \dot{r}_t + a_6\ddot{r}_t + a_7\ddot{r}_{t+\Delta t} \quad (6.54)$$

where

$$a_6 = \Delta t(1-\delta) \quad \text{and} \quad a_7 = \delta \Delta t.$$

Using the above mentioned procedure, Eq. 6.47 has been solved in the present study.

6.4.6 Dynamic Nonlinear Stress-Strain Behaviour of Soils

The nonlinear stress-strain characteristics of different soils subjected to dynamic loads can be appropriately represented by the Ramberg-Osgood model (Constantopoulos, Roësset and Christian, 1973; Papadakis, Streeter and Wylie, 1974; Streeter, Wylie and Richart, 1974; Richart and Wylie, 1975; Desai, 1977; Roësset, 1977; Ishenower, 1979; Pyke, 1979; Ishihara, 1982, 1985, 1987; Shamoto, 1984). The normalized curves between shear modulus and shear strain and the damping ratios as a function of strain obtained in Chapter 5, have been represented by the

Ramberg-Osgood model (Eqs. 5.18 and 5.22), to account for the nonlinear behaviour of soils under dynamic loading conditions in the present study. The different values of the Ramberg-Osgood model constants, namely, α and R , presented in Chapter 5, for the different types of soils have been used in modelling the stress-strain characteristics of different soils.

6.5 CLOSURE

The formulation of the finite element method with respect to eight-noded isoparametric element and reduced integration scheme has been described briefly in this chapter. The assembly of element stiffness matrix, mass matrix and the damping matrix have also been discussed. The Newmark method of implicit, step-by-step time integration scheme is briefly presented. Material nonlinearity as applicable to static case with incremental construction sequence analysis of embankment dams and in the dynamic case the nonlinear stress-strain characteristics of the different types of soils have been represented using the Ramberg-Osgood model.

CHAPTER 7

DEVELOPMENT OF COMPUTER PROGRAMS

7.1 GENERAL

The different steps involved in the formulation of the finite element method as applicable to nonlinear static and nonlinear dynamic cases, which have been described in the previous chapter need to be implemented efficiently in computer programs for solving practical problems.

This chapter describes the development of two computer codings, namely, (1) FEABANS (Finite Element Analysis of EmBANKment Dams), which can take into account the nonlinear elastic stress-strain behaviour of soils under static case, with the simulation of sequential construction operation and (2) FEADYNS (Finite Element Analysis of DYNamic Soil-structure Interaction Problems), which is capable of analysing earth and earthfill structures subjected to earthquake or vibratory loading, considering the nonlinear stress-strain characteristics of different materials constituting the earth structure as a function of strain.

The computer program FEABANS has originally been developed by Duncan, Wong and Ozawa (1980), using constant strain triangular elements and four-noded quadrilateral elements. This computer coding is based on the hyperbolic

model, considering the volume change characteristics and as incorporated by Duncan et al. (1980). In the dynamic case, the nonlinear, strain dependent material property curves of different soils developed in Chapter 5, based on the (1) Ramberg-Osgood model as described by Jennings (1964), Richart (1975), and Ishihara (1982), (2) Hardin-Drnevich model as described by Hardin and Drnevich (1970b), and Ishihara (1982), and (3) Seed-Idriss method as described by Lysmer et al. (1974), have been implemented in the computer coding, FEADYNS. This coding has initially been written by Idriss et al. (1973), based on constant strain triangular elements and four-noded quadrilateral elements. These two computer programs have been developed using the standard FORTRAN IV language, in the DEC 2050 Computer System, at the Roorkee University Regional Computer Centre, Roorkee (India). The development of these two computer programs and the associated subroutines therein, as applicable to the present study have been described in detail in this chapter.

Also, the analysis results of a 55 feet high embankment dam evaluated through FEABANS have been compared with the results reported by Duncan, Wong and Ozawa (1980), using constant strain triangles and four-noded quadrilateral elements.

In the dynamic case the analysis results of a soil column of depth, 100 feet as presented by Idriss et al. (1973), have been compared with that of the results using the FEADYNS coding.

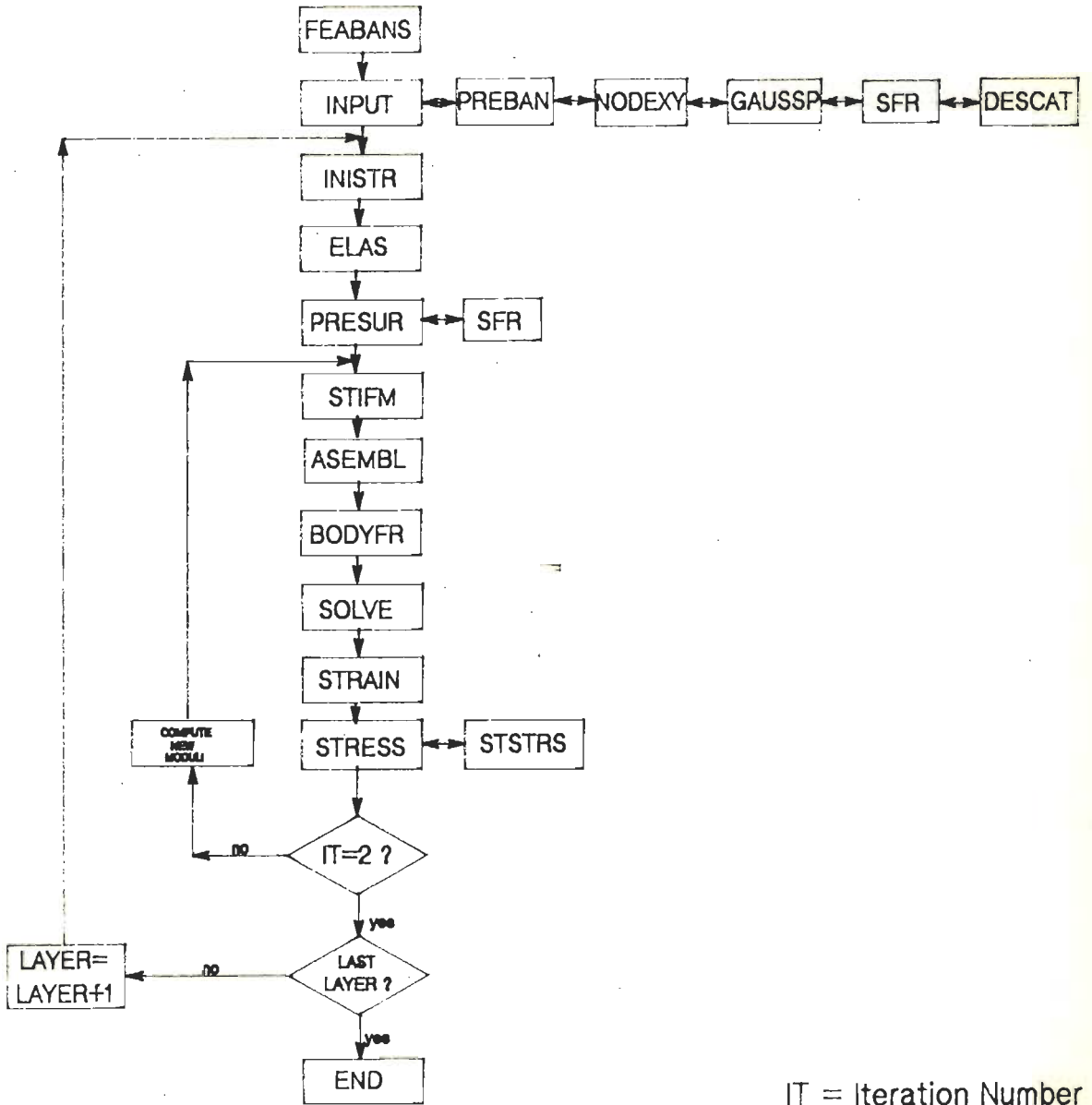
7.2 COMPUTER PROGRAM FOR STATIC ANALYSIS

The computer program FEABANS is capable of simulating the actual construction sequence operations of embankment dams under static case (Chapter 6), based on the hyperbolic law. The computer coding written by Duncan, Wong and Ozawa (1980), has been modified to accommodate eight-noded isoparametric elements with Gauss-Legendre reduced integration scheme and graphic display facilities using a CALCOMP PLOTTER. A CALCOMP PLOTTER is a peripheral, in which the hard-copy of the graphic display can be obtained. The essential sequences of operation involved in the FEABANS computer coding are shown in Fig. 7.1

7.2.1 Program Operation

The computer program developed to carry out nonlinear static analysis consists of a main segment called FEABANS and 15 subroutines and is coded in standard FORTRAN IV language. The main program (FEABANS) reads and prints all the control data and monitors all operations by calling the different subroutines in the specified order as shown in Fig. 7.1. The function of each subroutine is briefly described subsequently.

- 1 Subroutine INPUT reads and prints the element connectivity data and the coordinates of all the corner nodes. The boundary conditions of all the nodes and the different material properties are also read here.
- 2 Subroutine PREBAN calls subroutine NODEXY to obtain the



IT = Iteration Number

Fig. 7.1 Flow Chart for FEABANS

coordinates of the mid nodes using the method of linear interpolation. With the topology data, PREBAN gives a graphical output based on the CALCOMP PLOTTER library routines, such as, PLOT, NUMBER and AXIS. The graphical display permits corrections in the input data.

- 3 Based on the method of linear interpolation. subroutine NODEXY evaluates the coordinates of the mid nodes using the coordinates of the corner nodes of each element.
- 4 Subroutine GAUSSP sets the sampling point positions and weighting factors needed for numerical integration. This subroutine is called by subroutine INPUT.
- 5 Subroutine SFR which is called by subroutine GAUSSP, calculates the values of the shape functions and their derivatives at the Gauss points with respect to ξ and η local coordinate system as shown in Chapter 6.
- 6 Subroutine DESCAT calculates the cartesian derivatives of shape functions using the Jacobian matrix and its inverse at the Gaussian points. This subroutine is called by subroutine INPUT.
- 7 Subroutine INISTR computes the initial stresses at the Gauss sampling points of the elements.
- 8 Subroutine ELAS calculates the modulus values needed in the analysis.
- 9 Subroutine PRESUR computes the equivalent nodal loads due to boundary pressure or water load.
- 10 Subroutine STIFM calculates the element stiffness matrix.
- 11 Subroutine ASEMBL assembles the global stiffness matrix

- from element stiffness matrix.
- 12 Subroutine **SOLVE** evaluates the solution of simultaneous equations involving the stiffness matrix, displacement vector and load vector arrays using the Gauss elimination technique, considering the banded property of the assembled matrix. The solution is obtained for the unknown nodal displacements.
 - 13 Subroutine **STRAIN** computes the different components of strain at the Gaussian points using the nodal displacements computed by the subroutine **SOLVE**.
 - 14 Subroutine **STRESS** calculates the stresses at the Gaussian points using the strains which are computed by subroutine **STRAIN**.
 - 15 Subroutine **STSTRS** stores the different stresses at the completion of the nonlinear static analysis. These static stresses are the initial conditions for the dynamic analysis.

7.2.2 Verification of FEABANS

To evaluate the applicability of FEABANS, the results obtained using this computer coding have been compared with the results reported by Duncan, Wong and Ozawa (1980). For the purpose of verification, an embankment dam of height 55 feet has been selected. This embankment dam has previously been analysed by Duncan, Wong and Ozawa (1980), using constant strain triangles and four-noded quadrilateral elements. The finite element idealization consisting of a

total of 28 (25 four-noded quadrilaterals plus 3 triangular constant strain) elements and 39 nodes as used by Duncan, Wong and Ozawa (1980), is shown in Fig. 7.2. The values of different stress vectors, such as horizontal stress (σ_{xx}), vertical stress (σ_{yy}), shear stress (τ_{xy}), major principal stress (σ_1) and minor principal stress (σ_3) computed at the centre of each element and reported by Duncan, Wong and Ozawa (1980), are shown in Table 7.1.

The finite element mesh as produced by FEABANS using eight-noded isoparametric elements and the numbering of the Gauss points are shown in Fig. 7.3. The finite element mesh shown in Fig. 7.3, consists of 28 eight-noded elements and 105 nodes. The corresponding values of different stress vectors obtained using FEABANS are given in Table 7.2.

It can be noticed from Tables 7.1 and 7.2 that the values of different stress vectors obtained by Duncan, Wong and Ozawa (1980), and in the present study using eight-noded isoparametric elements through FEABANS are in close agreement.

7.3 COMPUTER PROGRAM FOR DYNAMIC ANALYSIS

The computer program FEADYNS, is capable of analysing soil-structure interaction problems and earth structures subjected to seismic forces in the time domain. The nonlinear stress-strain behaviour of different soils is represented by the Ramberg-Osgood model, Hardin-Drnevich model and the Seed-Idriss method (Chapter 5). Fig. 7.4 gives the flow chart of the computer coding FEADYNS.

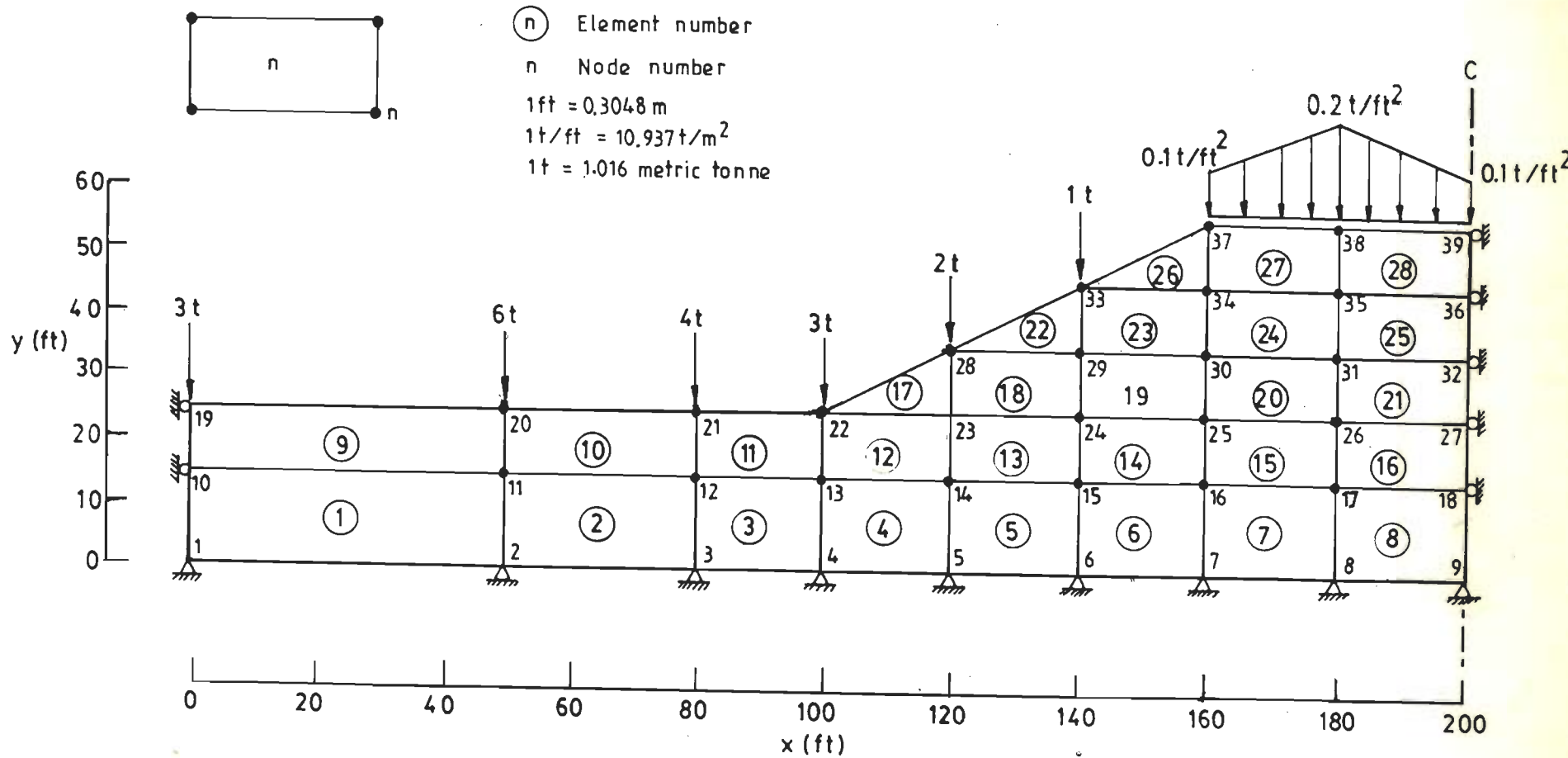


Fig. 7.2 Finite Element Idealization using 4- Noded Elements
 (Duncan et al., 1980)

Table 7.1 Values of Different Stress Vectors
(Duncan, Wong and Ozawa, 1980)

E1. No.	σ_{xx}	σ_{yy}	τ_{xy}	σ_1	σ_3	θ	σ_1/σ_3	τ_{xy}/σ_{yy}
(1)	(2)	(3)	(4)	(5)	(6)	(7)	(8)	(9)
1	0.419	0.748	0.019	0.749	0.418	3.32	1.793	0.026
2	0.484	0.801	0.064	0.814	0.472	11.06	1.725	0.080
3	0.573	0.830	0.144	0.894	0.509	24.13	1.757	0.173
4	0.772	1.154	0.257	1.283	0.643	26.66	1.995	0.222
5	0.957	1.635	0.277	1.734	0.858	19.63	2.021	0.170
6	1.193	2.101	0.240	2.161	1.134	13.93	1.905	0.114
7	1.331	2.374	0.150	2.395	1.310	8.01	1.828	0.063
8	1.416	2.611	0.047	2.513	1.414	2.43	1.776	0.019
9	0.207	0.302	0.008	0.303	0.206	4.81	1.468	0.027
10	0.294	0.341	0.017	0.347	0.288	18.15	1.203	0.051
11	0.451	0.361	0.055	0.477	0.334	64.53	1.427	0.154
12	0.509	0.632	0.162	0.744	0.397	34.68	1.873	0.257
13	0.779	1.260	0.150	1.303	0.736	16.00	1.770	0.119
14	0.889	1.651	0.133	1.673	0.866	9.60	1.932	0.080
15	1.066	2.015	0.070	2.020	1.061	4.22	1.904	0.035
16	1.132	2.115	0.023	2.116	1.131	1.35	1.870	0.011
17	0.365	0.304	0.001	0.365	0.304	89.37	1.199	0.002
18	0.358	0.726	0.163	0.787	0.296	20.75	2.658	0.224
19	0.376	1.287	0.096	1.297	0.366	5.93	3.543	0.074
20	0.288	1.492	0.033	1.493	0.287	1.56	5.200	0.022
21	0.345	1.668	-0.003	1.668	0.345	-0.14	4.833	-0.002
22	0.063	0.236	-0.006	0.236	0.063	-2.08	3.766	-0.027
23	0.236	0.660	0.127	0.695	0.201	15.41	3.460	0.192
24	0.315	1.013	0.029	1.014	0.314	2.35	3.233	0.028
25	0.289	1.034	-0.007	1.034	0.289	-0.54	3.990	-0.007
26	0.061	0.191	0.022	0.195	0.057	9.42	3.396	0.116
27	0.185	0.425	0.030	0.429	0.181	6.97	2.368	0.070
28	0.213	0.454	-0.012	0.455	0.212	-2.93	2.142	-0.027

Note:

Stresses are in tons/ft²

1 ton/ft² = 10.76 tonne/m²

= 105.50 kN/m²

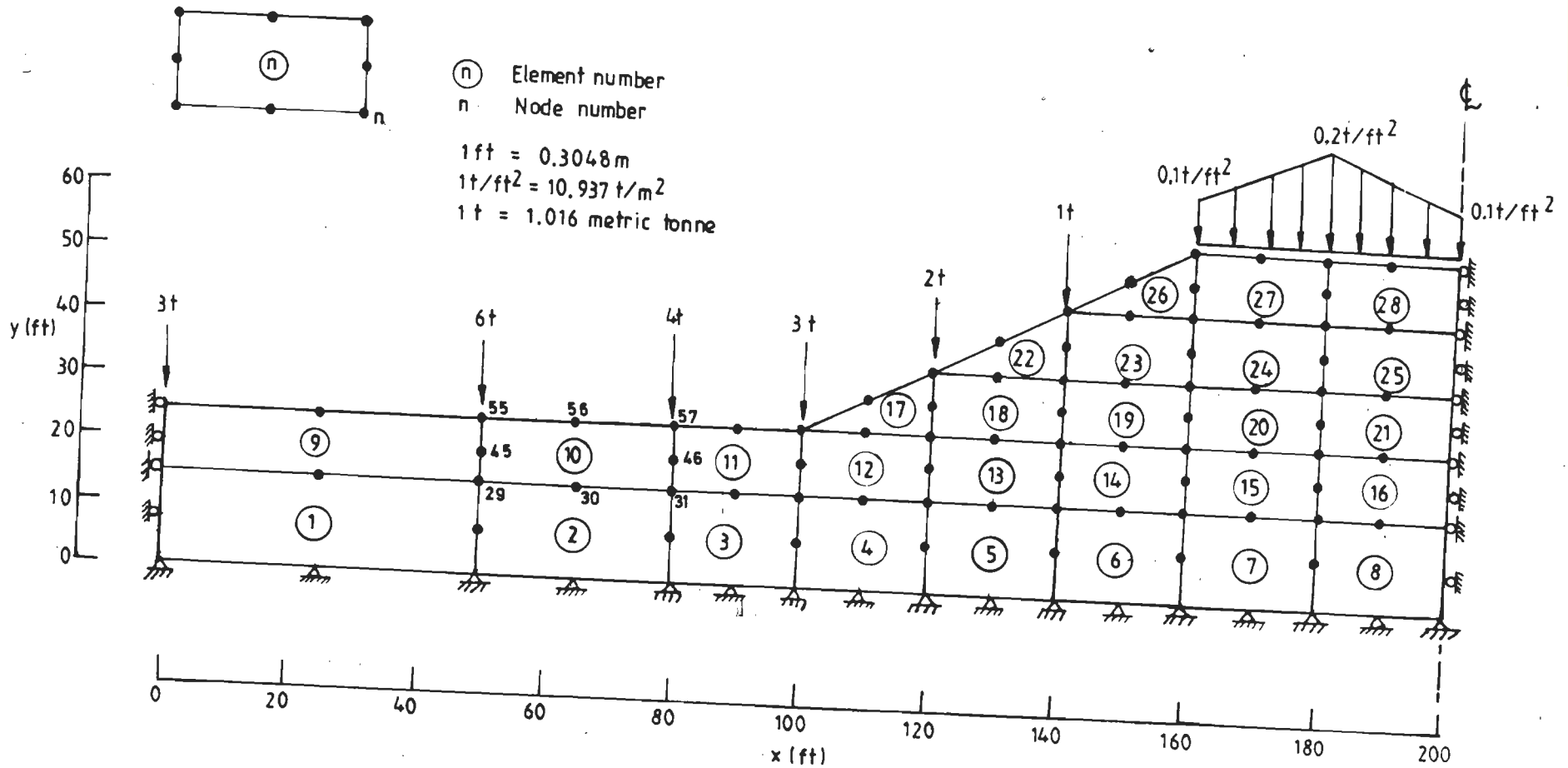


Fig. 7.3 Finite Element Idealization using 8- Noded Elements

Table 7.2 Values of Different Stress Vectors
(using FEABANS)

E1. No.	σ_{xx}	σ_{yy}	τ_{xy}	σ_1	σ_3	θ	σ_1/σ_3	τ_{xy}/σ_{yy}
(1)	(2)	(3)	(4)	(5)	(6)	(7)	(8)	(9)
1	0.409	0.704	-0.014	0.705	0.408	-2.77	1.728	-0.020
2	0.532	0.891	0.039	0.895	0.528	6.12	1.695	0.044
3	0.604	0.834	0.186	0.938	0.500	29.20	1.876	0.223
4	0.753	1.150	0.260	1.280	0.625	26.20	2.048	0.226
5	0.966	1.620	0.293	1.730	0.855	20.90	2.023	0.181
6	1.170	2.100	0.250	2.160	1.110	14.20	1.946	0.119
7	1.320	2.400	0.154	2.420	1.300	7.97	1.862	0.064
8	1.390	2.470	0.048	2.470	1.390	2.51	1.777	0.019
9	0.170	0.212	-0.003	0.212	0.170	-4.15	1.247	-0.014
10	0.207	0.377	0.036	0.384	0.200	11.50	1.920	0.096
11	0.386	0.417	-0.025	0.431	0.372	-28.70	1.159	-0.060
12	0.616	0.763	0.139	0.847	0.532	31.20	1.592	0.182
13	0.750	1.230	0.184	1.290	0.688	18.80	1.875	0.150
14	0.917	1.700	0.144	1.730	0.891	10.10	1.942	0.085
15	1.050	2.020	0.088	2.020	1.040	5.14	1.942	0.044
16	1.110	2.080	0.028	2.080	1.110	1.63	1.874	0.014
17	0.098	0.396	0.087	0.420	0.074	15.00	5.676	0.220
18	0.360	0.759	0.119	0.792	0.327	15.40	2.422	0.157
19	0.337	1.260	0.115	1.270	0.323	7.01	3.932	0.091
20	0.305	1.570	0.058	1.570	0.302	2.60	5.199	0.037
21	0.334	1.610	0.012	1.610	0.333	0.53	4.835	0.007
22	0.063	0.261	0.052	0.273	0.050	13.80	5.460	0.199
23	0.261	0.685	0.102	0.708	0.237	12.90	2.987	0.149
24	0.295	1.020	0.064	1.020	0.289	5.06	3.529	0.063
25	0.256	1.020	0.010	1.020	0.255	0.75	4.000	0.009
26	0.186	0.348	0.111	0.405	0.130	26.90	3.115	0.319
27	0.366	0.746	0.027	0.748	0.364	4.10	2.055	0.036
28	0.460	0.740	-0.010	0.740	0.460	-2.14	1.609	-0.134

Note:

Stresses are in tons/ft²

$$1 \text{ ton/ft}^2 = 10.76 \text{ tonne/m}^2$$

$$= 105.50 \text{ kN/m}^2$$

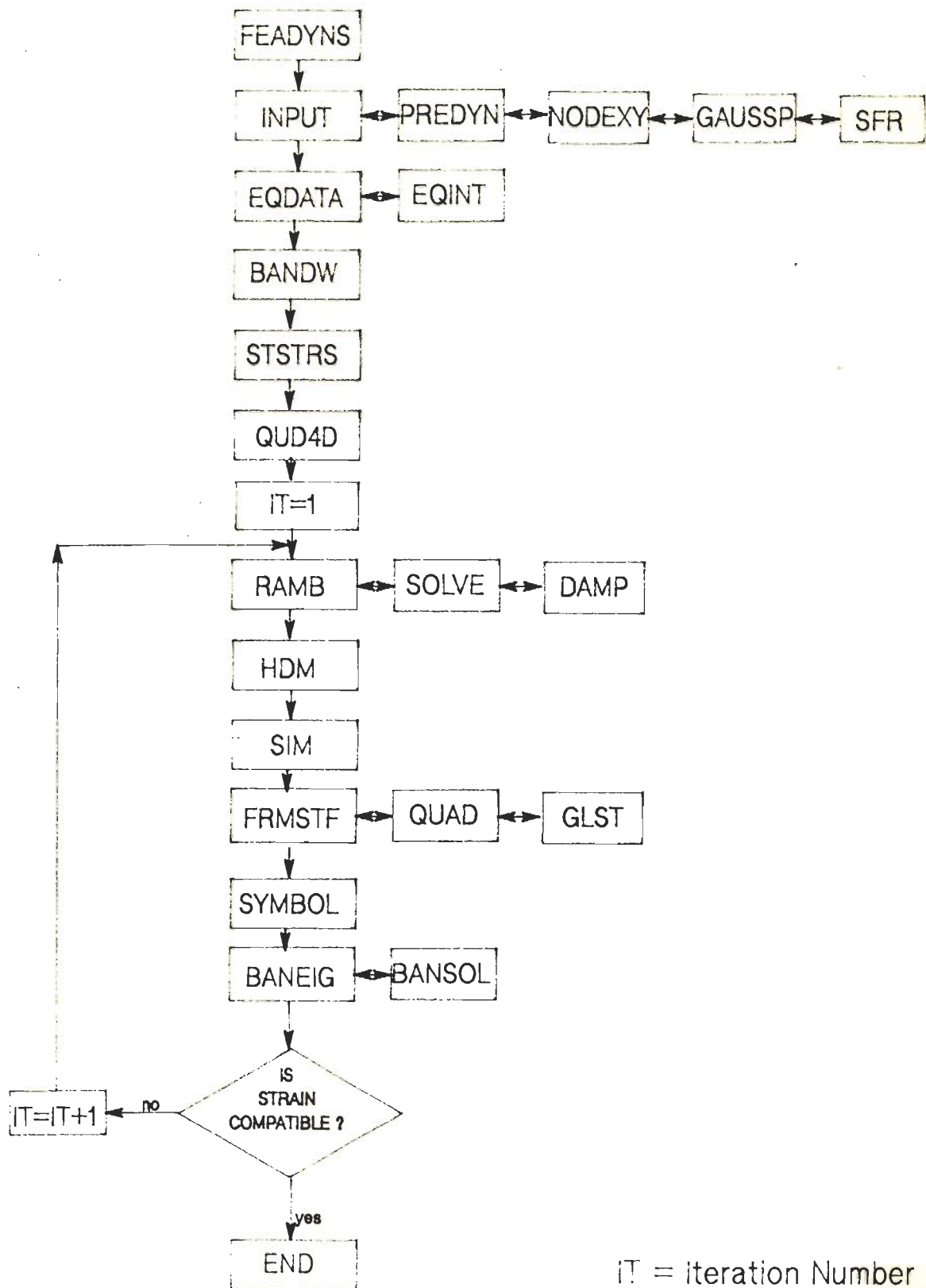


Fig. 7.4 Flow Chart for FEADYNS

7.3.1 Organization of FEADYNS

The nonlinear dynamic analysis computer program developed in the present study consists of a main segment called FEADYNS and 21 subroutines. As in the static case, the main program reads and prints the control data and monitors all operations by calling the different subroutines in the specified order. The functions of the first five subroutines, namely, INPT, PREDYN, NODEXY, GAUSSP and SFR are identically same as that of the first five subroutines in the nonlinear static analysis computer program FEABANS. The functions of the remaining subroutines are briefly explained subsequently.

- 1 Subroutine EQDATA reads and stores the digitized values of acceleration of the selected ground motion.
- 2 Subroutine EQINT modifies and regenerates the design accelerogram based on the peak ground acceleration value of the initial input motion.
- 3 Subroutine BANDW computes the band width of each individual element and stores the largest value.
- 4 Subroutine STSTRS reads the pre-earthquake or static initial stresses obtained from the nonlinear static analysis carried out using FEABANS.
- 5 Subroutine QUD4D consists of the Newmark method of time integration scheme and sets up the equation of motion after calling subroutine FRMSTF. Subroutines RAMB, SOLVE and DAMP which evaluate the shear modulus and damping

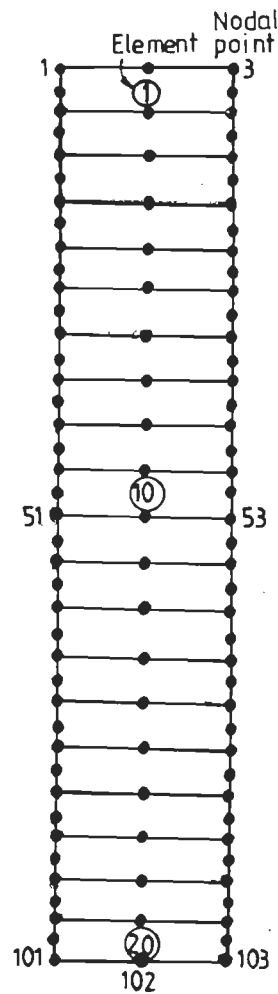
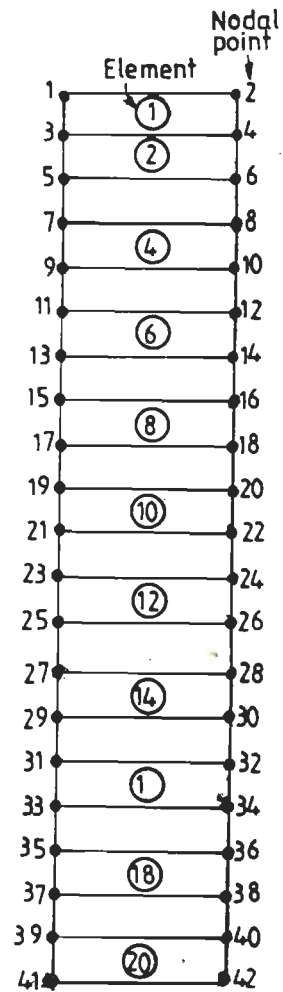
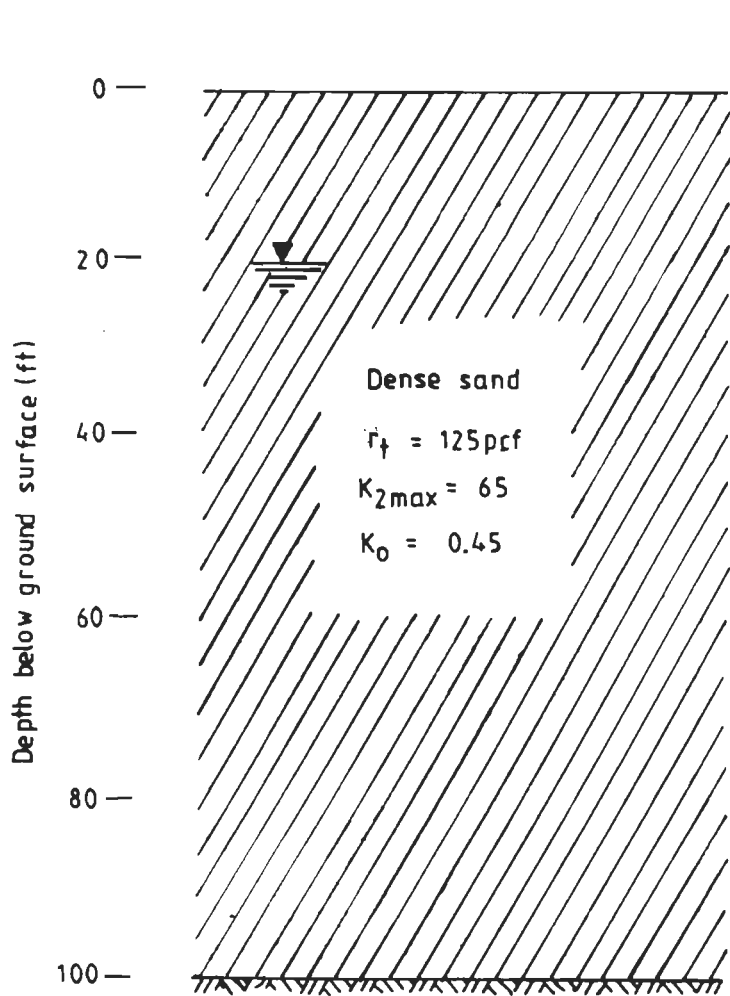
- ratio as a function of strain based on the Ramberg-Osgood model are also called here. The time-histories of acceleration, displacement and shear stresses are also evaluated in subroutine QUD4D.
- 6 Subroutine **RAMB** incorporates the Ramberg-Osgood model as described in Chapters 5 and 6 to obtain shear modulus values as a function of strain. This subroutine calls two other subroutines, namely, **SOLVE** and **DAMP** to obtain the damping values as a function of strain.
 - 7 Subroutine **SOLVE** evaluates the G/G_{\max} values as a function of strain, based on the Newton-Raphson root finding technique.
 - 8 Subroutine **DAMP** evaluates the damping values as a function of strain using the Ramberg-Osgood model.
 - 9 Subroutine **HDM** computes the shear modulus ratio and the damping values using Eqs. 2.23 and 2.24 respectively, which are based on the Hardin-Drnevich model.
 - 10 Subroutine **SIM** stores the modulus reduction factors and the damping ratios as a function of strain corresponding to a few selected strain levels as recommended in the Seed-Idriss method.
 - 11 Subroutine **FRMSTF** forms the element stiffness matrix, mass matrix and the damping matrix. Subsequently, these matrices are assembled into the global matrices. Subroutine **QUAD** is also, being called by subroutine **FRMSTF**.
 - 12 Subroutine **QUAD** forms the stress-strain relationship.
 - 13 Subroutine **GLST** computes the cartesian shape function

derivatives using the Jacobian matrix and its inverse. This subroutine is called by subroutine QUAD.

- 14 Subroutine SYMBOL evaluates the simultaneous equations involved in the system by calling the subroutine BANSOL.
- 15 Subroutine BANSOL takes into account the banded property of the different global matrices.
- 16 Subroutine BANEIG computes the natural frequency and the time period of the system by solving the standard eigen value problem.

7.3.2 Verification of FEADYNS

As described in Sec. 7.2.2. to evaluate the suitability of FEADYNS, the dynamic response of a soil column of depth, 100 feet has been performed using numerically integrated eight-noded isoparametric elements. This soil column has previously been studied by Idriss et al. (1973), and the finite element mesh adopted by them using four-noded quadrilateral elements is shown in Fig. 7.5. As can be seen from this figure, the finite element digitization consists a total of 20 four-noded quadrilateral elements and 42 nodes, in which node 41 is the first node on the rigid base. The damping and shear modulus values used for the dynamic analysis by Idriss et al. (1973), are shown in Fig. 7.6. The Taft accelerogram, recorded at Kern County in 1952. and normalized to a peak ground acceleration of 0.15g has been applied as the base input motion at node 41.



1 ft = 0.3048 m
 1 pcf = 0.016 t/m²

Fig. 7.5 Finite Element Idealization of the Soil Column based 4- and 8- Noded Elements

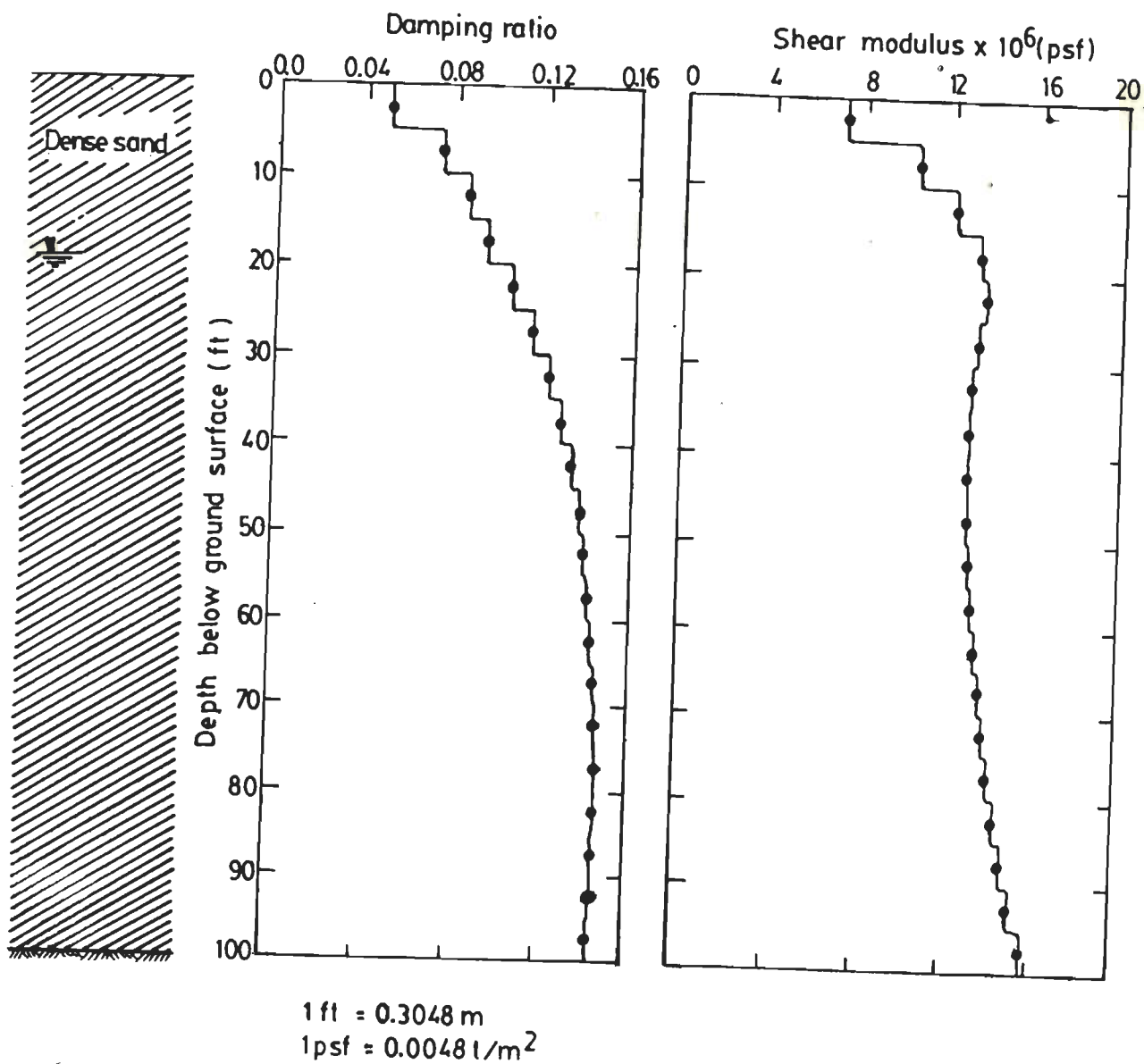


Fig. 7.6 Damping and Modulus Values Used in the Soil Column (Idriss et al., 1973)

The different values of stress vectors computed at the centre of each element and the values of horizontal (x) acceleration computed at all the nodal points (except on the rigid base), by Idriss et al. (1973), are given in Tables 7.3 and 7.4.

The finite element idealization generated by FEADYNS is also shown in Fig. 7.5. The total number of elements are 20 as adopted by Idriss et al. (1973), and the total number of nodes are 103, in which the first node on the rigid base is 101. As before, the different stress vectors obtained using eight-noded isoparametric elements and the resulting acceleration values at the corresponding corner nodes (except at the nodes lying on the rigid base) are as well shown in Tables 7.3 and 7.4. The distribution of shear stress and acceleration values plotted along the depth of the soil column are as well presented in Fig. 7.7.

It can be seen from Table 7.3, that the magnitude of shear stress in the two cases (using 4-noded quadrilateral elements and 8-noded isoparametric elements) yield nearly identical values, except at the base (elements 18 to 20) in which, slightly lower values of shear stress are noticed in the present case (Fig. 7.7) in comparison with the shear stress values reported by Idriss et al. (1973).

From Table 7.4 the occurrence of deamplification to a small extent is seen in the distribution of acceleration along the depth of the soil column, below 60 feet from the ground level, when 4-noded quadrilateral elements are used. The lowest value of acceleration of the order of 0.1310g is

Table 7.3 Distribution of Shear Stress in the Soil Column

4 - Noded Quadrilateral Elements (after Idriss et al., 1973)					8 - Noded Isoparametric Elements (using FEADYNS)				
El. No.	σ_{xx}	σ_{yy}	τ_{xy}	Γ_{max}	El. No.	σ_{xx}	σ_{yy}	τ_{xy}	Γ_{max}
(1)	(2)	(3)	(4)	(5)	(6)	(7)	(8)	(9)	(10)
1	0.0	0.0	83.0	0.012	1	0.0	0.0	82.8	0.012
2	0.0	0.0	247.1	0.022	2	0.0	0.0	247.1	0.022
3	0.0	0.0	407.4	0.027	3	0.0	0.0	408.0	0.027
4	0.0	0.0	563.0	0.038	4	0.0	0.0	564.7	0.038
5	0.0	0.0	714.6	0.048	5	0.0	0.0	715.6	0.048
6	0.0	0.0	859.6	0.057	6	0.0	0.0	860.4	0.057
7	0.0	0.0	996.7	0.066	7	0.0	0.0	998.5	0.067
8	0.0	0.0	1125.0	0.075	8	0.0	0.0	1128.0	0.075
9	0.0	0.0	1244.9	0.083	9	0.0	0.0	1248.0	0.083
10	0.0	0.0	1357.8	0.091	10	0.0	0.0	1360.4	0.091
11	0.0	0.0	1458.8	0.097	11	0.0	0.0	1460.1	0.097
12	0.0	0.0	1550.8	0.103	12	0.0	0.0	1552.1	0.103
13	0.0	0.0	1631.8	0.109	13	0.0	0.0	1633.4	0.109
14	0.0	0.0	1708.3	0.114	14	0.0	0.0	1706.7	0.114
15	0.0	0.0	1786.7	0.119	15	0.0	0.0	1784.1	0.119
16	0.0	0.0	1852.5	0.123	16	0.0	0.0	1851.1	0.123
17	0.0	0.0	1904.8	0.127	17	0.0	0.0	1904.8	0.127
18	0.0	0.0	1947.5	0.130	18	0.0	0.0	1944.8	0.130
19	0.0	0.0	1976.7	0.132	19	0.0	0.0	1970.5	0.131
20	0.0	0.0	1991.7	0.133	20	0.0	0.0	1985.5	0.132

Note:

Stresses in pounds/ft²

1 pound/ft² = 0.0048 tonne/m²

= 0.0470 kN/m²

Table 7.4 Distribution of Acceleration in the Soil Column
(Maximum input base acceleration = 0.15g)

4 - Noded Element				8 - Noded Element	
Node No.	Coordinate (ft)		Acceleration (g)	Corresponding Node	Acceleration (g)
	X	Y			
(1)	(2)	(3)	(4)	(5)	(6)
1	0.0	0.0	0.2600	1	0.2639
2	10.0	0.0	0.2600	3	0.2639
3	0.0	-5.0	0.2580	6	0.2612
4	10.0	-5.0	0.2580	8	0.2612
5	0.0	-10.0	0.2539	11	0.2563
6	10.0	-10.0	0.2539	13	0.2563
7	0.0	-15.0	0.2482	16	0.2504
8	10.0	-15.0	0.2482	18	0.2504
9	0.0	-20.0	0.2410	21	0.2424
10	10.0	-20.0	0.2410	23	0.2424
11	0.0	-25.0	0.2320	26	0.2326
12	10.0	-25.0	0.2320	28	0.2326
13	0.0	-30.0	0.2211	31	0.2211
14	10.0	-30.0	0.2211	33	0.2211
15	0.0	-35.0	0.2153	36	0.2136
16	10.0	-35.0	0.2153	38	0.2136
17	0.0	-40.0	0.2087	41	0.2074
18	10.0	-40.0	0.2087	43	0.2074
19	0.0	-45.0	0.1998	46	0.1995
20	10.0	-45.0	0.1998	48	0.1995
21	0.0	-50.0	0.1893	51	0.1897
22	10.0	-50.0	0.1893	53	0.1898
23	0.0	-55.0	0.1766	56	0.1779
24	10.0	-55.0	0.1766	58	0.1779
25	0.0	-60.0	0.1619	61	0.1639
26	10.0	-60.0	0.1619	63	0.1639
27	0.0	-65.0	0.1472	66	0.1492
28	10.0	-65.0	0.1472	68	0.1492
29	0.0	-70.0	0.1359	71	0.1335
30	10.0	-70.0	0.1359	73	0.1335
31	0.0	-75.0	0.1310	76	0.1187
32	10.0	-75.0	0.1310	78	0.1187
33	0.0	-80.0	0.1345	81	0.1210
34	10.0	-80.0	0.1345	83	0.1210
35	0.0	-85.0	0.1369	86	0.1254
36	10.0	-85.0	0.1369	88	0.1254
37	0.0	-90.0	0.1408	91	0.1324
38	10.0	-90.0	0.1408	93	0.1324
39	0.0	-95.0	0.1412	96	0.1412
40	10.0	-95.0	0.1412	98	0.1412

Note:

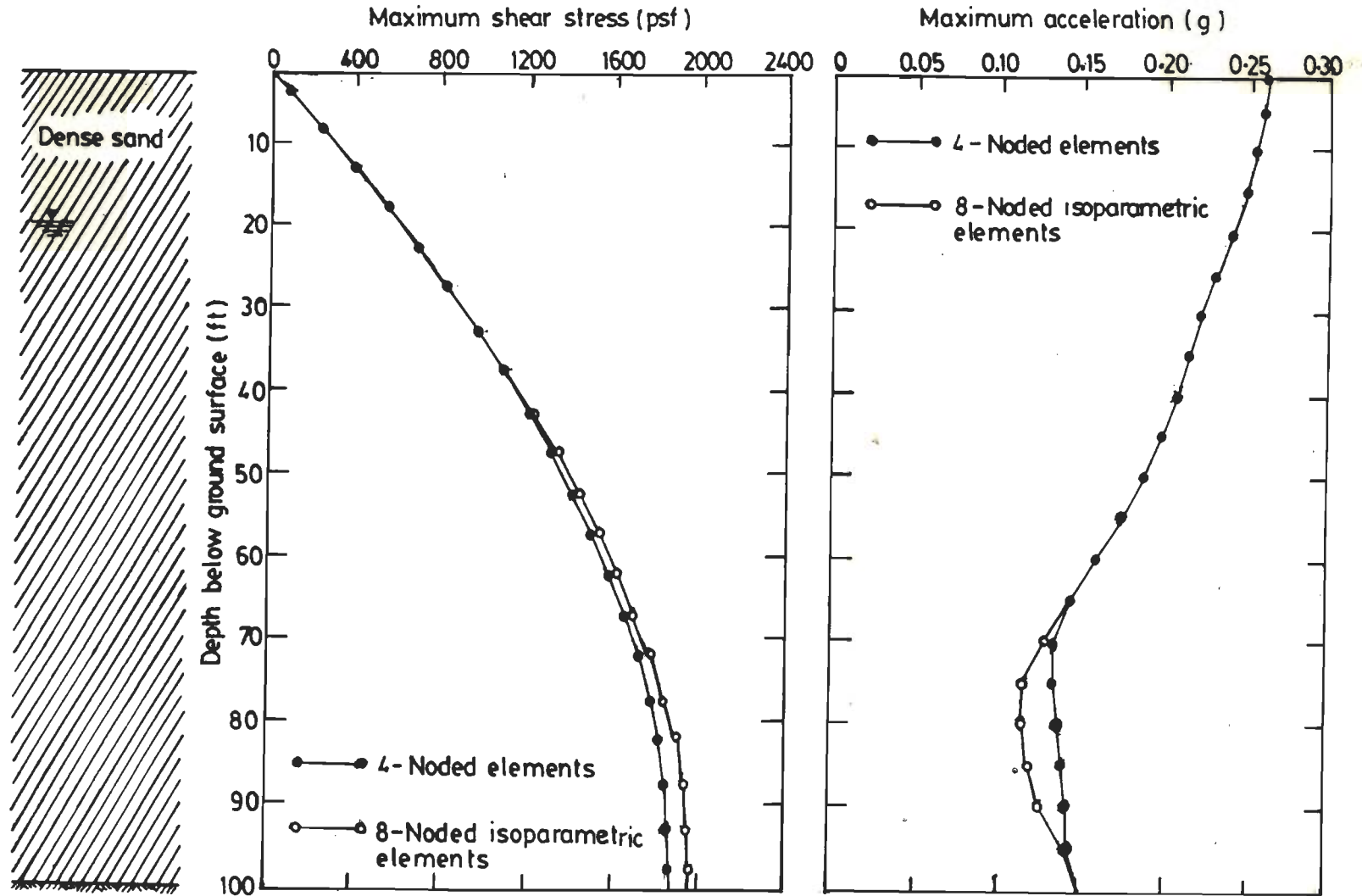


Fig. 7.7 Comparison of Shear Stress and Acceleration Values of the Soil Column

observed at a depth of 75 feet from the ground level (nodes 31 and 32).

However, when 8-noded isoparametric elements are used the deamplification phenomenon to a larger extent is noticed at the same depth from the ground level. The lowest value of acceleration of the order of 0.1187g is observed at nodes 76 and 78. Except at these locations, a close agreement in the distribution of acceleration is seen between the two cases (using 4- and 8- noded elements) of analysis.

7.4 CLOSURE

The capabilities of the two computer programs, namely, FEABANS and FEADYNS, performing nonlinear static incremental analysis with the construction sequence operation and nonlinear dynamic analysis based on three different methods of analysis in the time domain respectively, have been presented in this chapter. The flow charts for these two computer programs have also been presented separately. The two codings are based on eight-noded isoparametric elements with the reduced integration scheme. The function of every subroutine in both the computer codings has been individually and briefly described. The verification of the two computer codings has also been carried out by solving two standard examples, namely, an embankment dam and a soil column, and the obtained results have been compared with the earlier reported values in both the analysis cases.

CHAPTER 8

ANALYSIS

8.1 GENERAL

The computer program FEABANS which is capable of performing nonlinear static analysis with the construction sequence operation has been used for the evaluation of the pre-earthquake or initial stresses of three rockfill dams, namely, El Infiernillo Dam (146 m high), and of two other dams including their respective foundations of total height 108 m and 336 m respectively. These computed static stresses have been used as the initial conditions for the nonlinear dynamic analysis using FEADYNS computer coding, described in the previous chapter.

The dynamic analysis results of the El Infiernillo Dam as performed in the present study, have been compared with the actually recorded/measured response values at the crest, during the March 14, 1979, Mexico earthquake. For the dynamic analysis three different ground motions, namely, GM1, which was recorded during the recent earthquake in the North-Eastern Region of India, GM2 which was an artificially generated accelerogram and GM3 which was the Taft accelerogram recorded during the 1952, Kern County earthquake were used. In all the accelerograms the peak ground accele-

ration has been taken as $0.25g$ (g is the gravity constant) since, the value of the peak ground acceleration of the March 14, 1979, Mexico earthquake was also $0.25g$. The total durations of the three ground motions were 120, 38 and 30 seconds respectively.

The extensive dynamic analysis of the 336 m high dam with acceleration, displacement and shear stress time-histories at a few important locations subjected to the artificial earthquake record have been presented. The nonlinear stress-strain characteristics of the different materials constituting the three dams have been simulated using the Ramberg-Osgood model described in Chapter 5. For the purpose of comparison the dynamic analyses of the three dams have been carried out using the Hardin-Drnevich model and the Seed-Idriss method as well. The results obtained for the three rockfill dams by all the three methods of analyses using three ground motions have been compared.

8.2 DESCRIPTION OF THE THREE ROCKFILL DAMS

8.2.1 El Infiernillo Dam (Dam DA)

The El Infiernillo Dam is located on the Balsas River (Mexico) and impounds 12000 million cubic metres of water. The rockfill dam with a central impervious core of compacted clay has a maximum height of 146 m above the foundation rock. The dam is a slender embankment with an average slope of 1.8:1 in the upstream and the downstream, and a symmetrical thin core with 0.089:1 slope. The width of

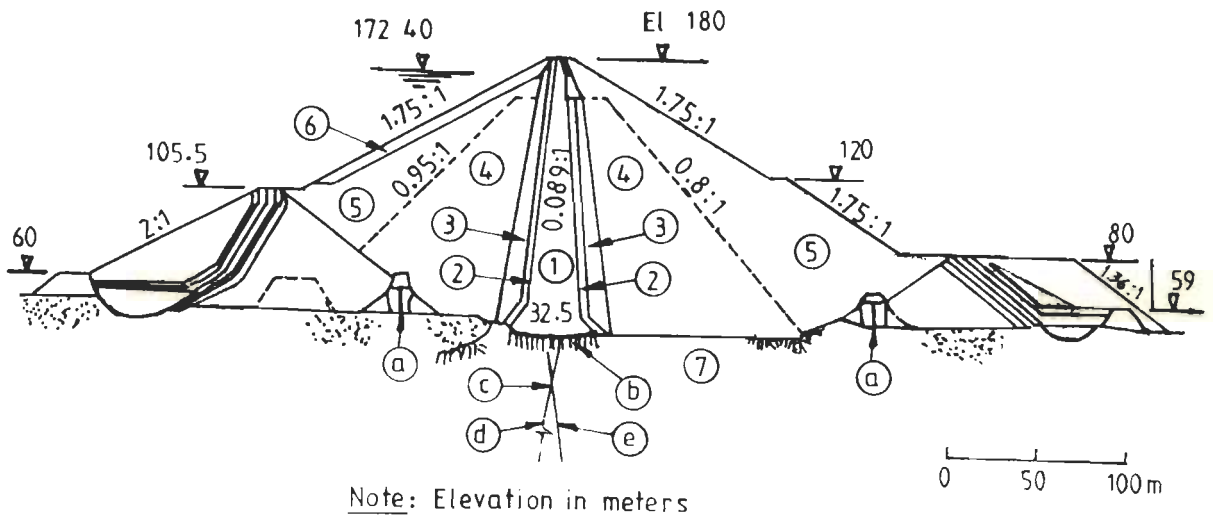
the core corresponds to only 22 percent of the hydraulic head as shown in Fig. 8.1 (Moreno, 1980).

8.3 NONLINEAR STATIC ANALYSIS

The El Infiernillo rockfill Dam has been analysed to evaluate the pre-earthquake or initial stresses using the FEABANS coding. As described in Chapter 5, the hyperbolic model (Kondner, 1963; Kondner and Zelasko, 1963) which can simulate the nonlinear stress-strain behaviour of soils considering the volume change characteristics and accounting for sequential construction (Duncan and Chang, 1970; Duncan et al., 1980), has been adopted for the analysis. These initial stresses have subsequently been used as the initial condition for the dynamic analysis of the El Infiernillo Dam.

8.3.1 Discretization

The idealized maximum cross-section of the El Infiernillo Dam as adopted by Romo et al. (1980), is shown in Fig. 8.2. The rockfill dam has been discretized into 17 layers, resulting in a total of 263 eight-noded isoparametric elements and 864 nodes. The effective number of degrees of freedom was 1646 in the plane strain ($\epsilon_z=0$) case of analysis. The finite element discretization has been done using the PREBAN subroutine described in the previous chapter to perform construction sequence analysis. The different material properties used in the static analysis are shown in Table 8.1 and the material type identifications are described in Fig. 8.2. The finite element discretization is shown in



Note: Elevation in meters

- | | |
|----------------------|--------------------------------|
| ① Imperious core | ④ Cut-off walls (secant piles) |
| ② Filters | ⑤ Grout blanket |
| ③ Transition zones | ⑥ Gallery G-4 |
| ④ Compacted rockfill | ⑦ Grout holes |
| ⑤ Dumped rockfill | ⑧ Drainage holes |
| ⑥ Riprap | |
| ⑦ Sound rock | |

Fig. 8.1 Maximum Section of El Infiernillo Dam
(Moreno, 1980)

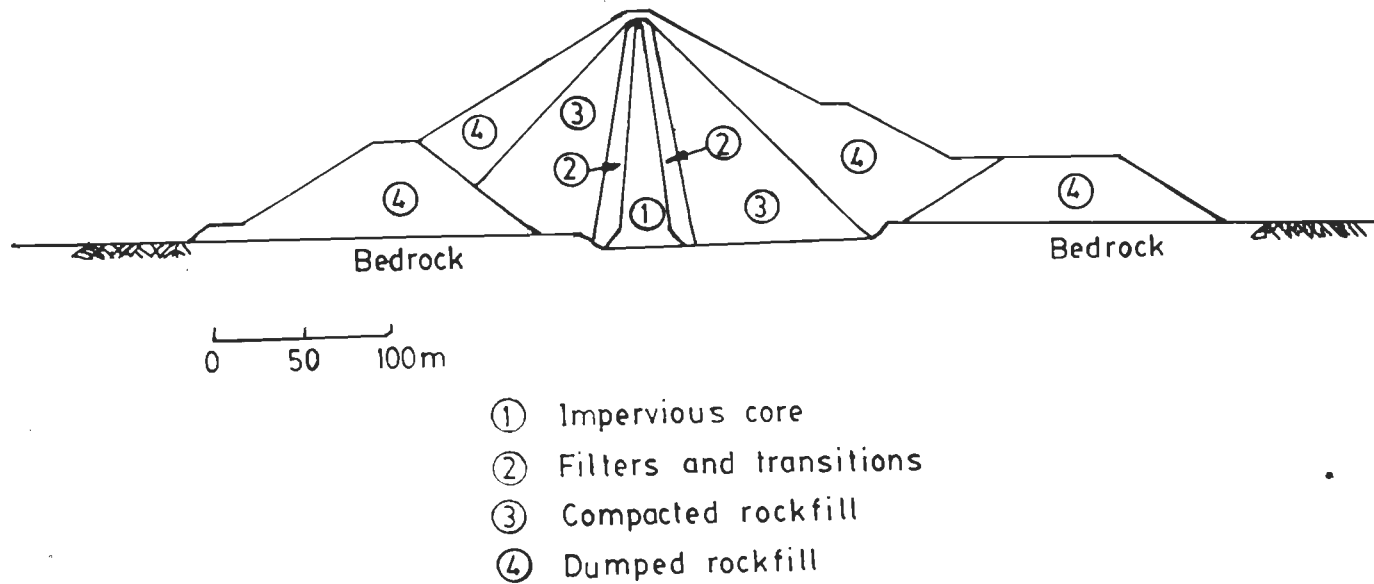


Fig. 8.2 Idealized Maximum Section of El Infiernillo Dam
 (Romo et al., 1980)

Fig. 8.3.

Table 8.1 Material Properties Used in the Static Analysis
(Romo et al., 1980)

Mat. No.	Material Identification	Unit Weight (t/m ³)		C (t/m ²)	φ (deg)
		Dry	Saturated		
(1)	(2)	(3)	(4)	(5)	(6)
1	Clay core	1.58	2.00	3	0
2	Filter	1.87	2.19	0	35
3	Compacted rockfill	1.85	2.16	0	45
4	Dumped rockfill	1.76	2.10	0	45

The shell and filter materials below the full reservoir level have been assumed to be submerged and the clay core below the phreatic line to be saturated. The materials above the maximum water level have been considered as moist and the different materials in the downstream to be dry. The water pressure has been considered to act vertically along the top surface of the bed-rock and normal to the upstream face of the core, as shown in Fig. 8.3. The computed pre-earthquake stresses have been stored in the subroutine STSTRS (Chapter 7) for subsequent dynamic analysis.

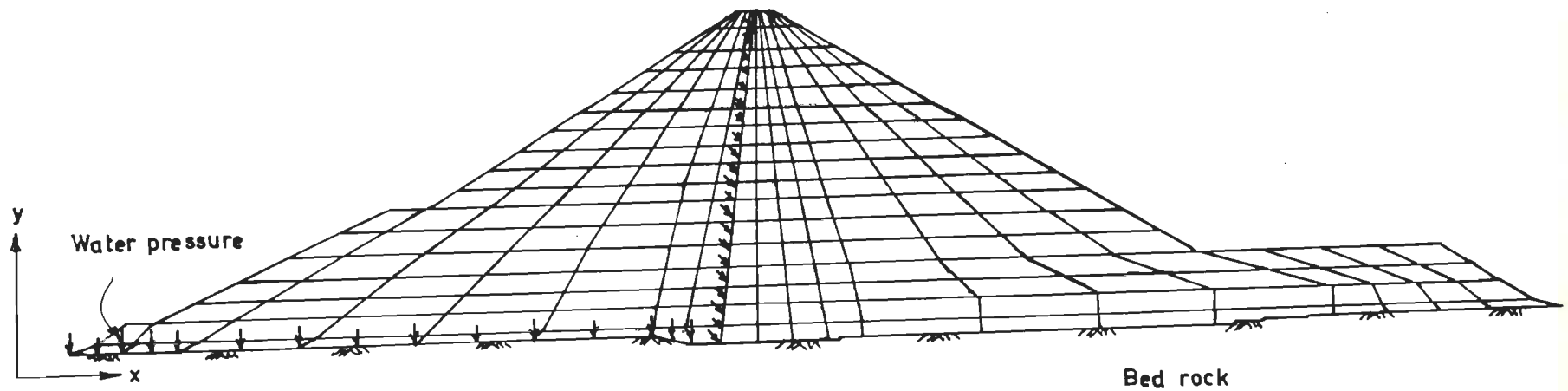


Fig. 8.3 Finite Element Idealization of El Infiernillo Dam

8.4 DYNAMIC ANALYSIS

Dynamic analysis has been performed on the El Infiernillo Dam using the same finite element mesh shown in Fig. 8.3 with a change in numbering of nodes. The nonlinear static stresses stored through the subroutine STSTRS of FEABANS have been used as the initial condition in the dynamic analysis.

8.4.1 Material Properties for Dynamic Analysis

For the dynamic analysis the different material properties used are shown in Table 8.2. These properties have been used in addition to the properties shown in Table 8.1 and are same as that adopted by Romo et al. (1980). These properties have been used for estimating the low-amplitude shear modulus values as suggested by Seed and Idriss (1970). The damping values have also been adopted from the same reference (Seed and Idriss, 1970).

8.4.2 Earthquake Records for Dynamic Analysis

In the absence of the March 14, 1979, Mexico earthquake record, three ground motions namely, GM1, GM2 and GM3 have been selected as base input motions for the dynamic analysis of the El Infiernillo Dam. Out of these three accelerograms, GM1 corresponds to the record of the recent earthquake that took place in the North-East Region of India (Chandrasekaran and Das, 1989). GM2 is an artificially generated accelerogram (Srivastava et al., 1983) and GM3 is

the Taft earthquake record, which was obtained during the 1952, Kern County earthquake (Idriss et al., 1973). Some of the important parameters of the three ground motions are given in Table 8.3. From this table it can be observed that the selected accelerograms vary between a shortest duration of 30 seconds to a longest duration of the order of 120 seconds. Existing literature on the dynamic analysis of rockfill dams subjected to such a long duration earthquake record is scanty (Prater and Studer, 1979). The three ground motions and the respective spectra are given in Figs. 8.4 to 8.9.

Table 8.2 Material Properties Used in the Dynamic Analysis (Romo et al., 1980)

Mat. No.	Material Identification	μ	S_u (t/m ²)	k_2 (at $r=10^{-6}$)	G/S_u
(1)	(2)	(3)	(4)	(5)	(6)
1	Clay core	0.49	5.5-9.0	-	2150-2640
2	Filter	0.33	-	150	-
3	Compacted rockfill	0.33	-	150	-
4	Dumped rockfill	0.33	-	100	-

Note:

μ = Poisson's ratio

S_u = undrained strength

k_2 = a constant

G/S_u = normalized value of shear modulus.

Table 8.3 Characteristics of the Three Ground Motions

Sl. No.	GMI	PGA (g)	TD (secs)	Description
(1)	(2)	(3)	(4)	(5)
1	GM1	0.25	120	Recorded in the North-East Region of India
2	GM2	0.25	38	Synthetic accelerogram
3	GM3	0.25	30	Recorded at Taft, Kern County(1952)

Note:

GMI = Ground Motion Identification

PGA = Peak Ground Acceleration

TD = Total Duration.

8.4.3 Dynamic Analysis Based on Ramberg-Osgood Model

Once the low-amplitude ($\gamma=10^{-6}$ or 10^{-4} percent) shear moduli and the corresponding damping values are established as mentioned in Sec. 8.4.1, the shear modulus values and damping values at other values of shear strain ($\gamma>10^{-4}$ percent) are evaluated using the Ramberg-Osgood model as given by Eqs. 5.18 and 5.22 respectively (Chapter 5, Sec. 5.4.3). The respective values of α and R , for different types of soils shown in Table 5.3, have been used in solving Eq. 5.18. The constant, C_1 in Eq. 5.18 has been assigned unity.

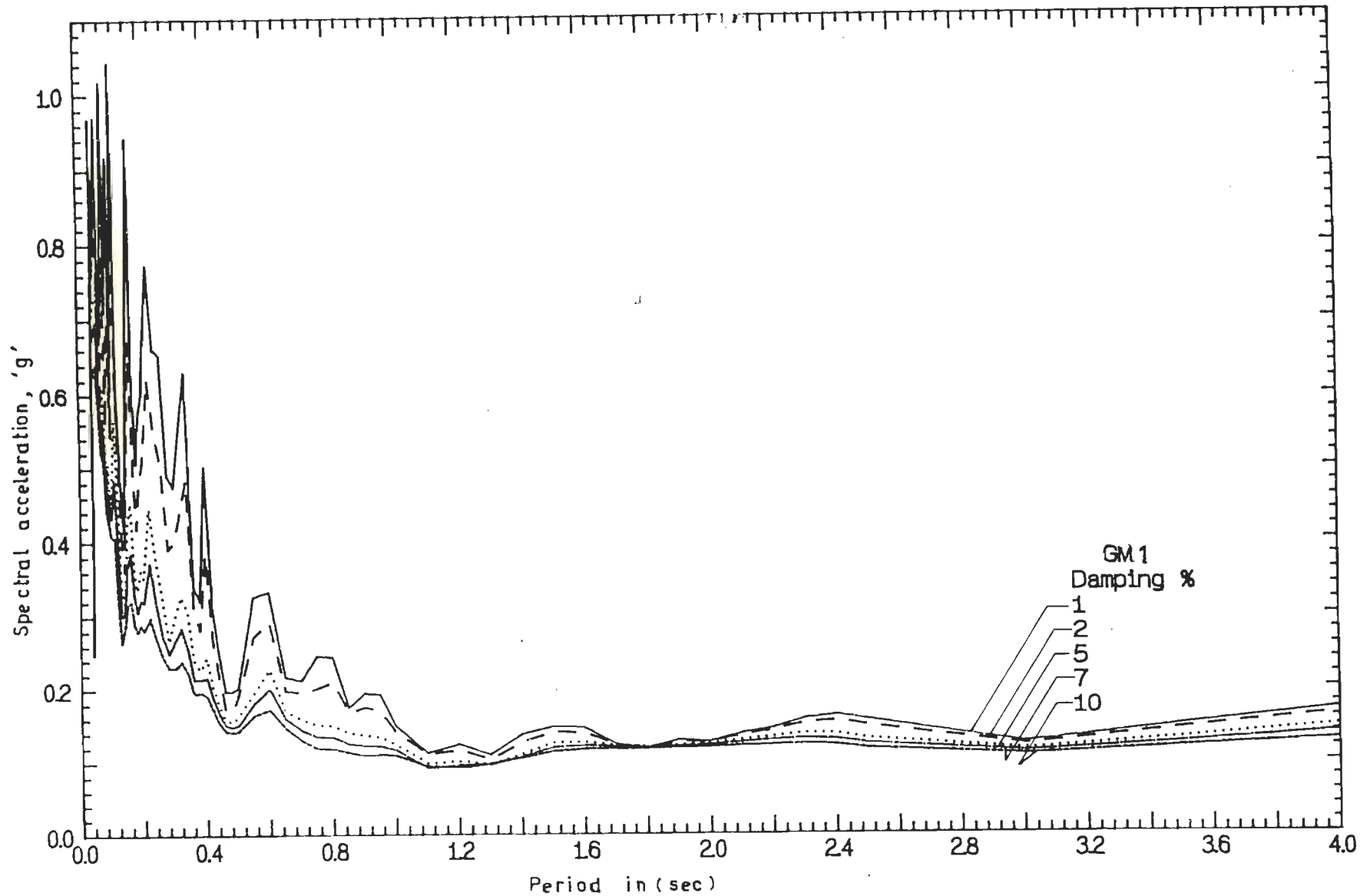


Fig. 8.5 Response Spectra for GM1

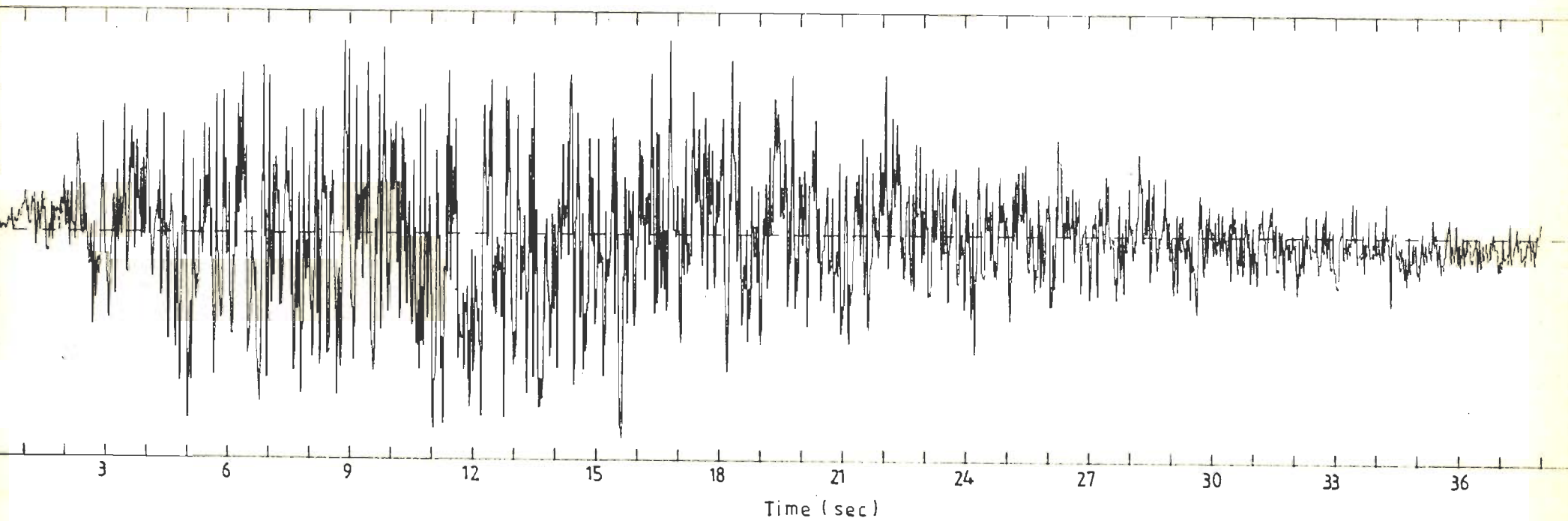


Fig. 8.6 Accelerogram of GM2

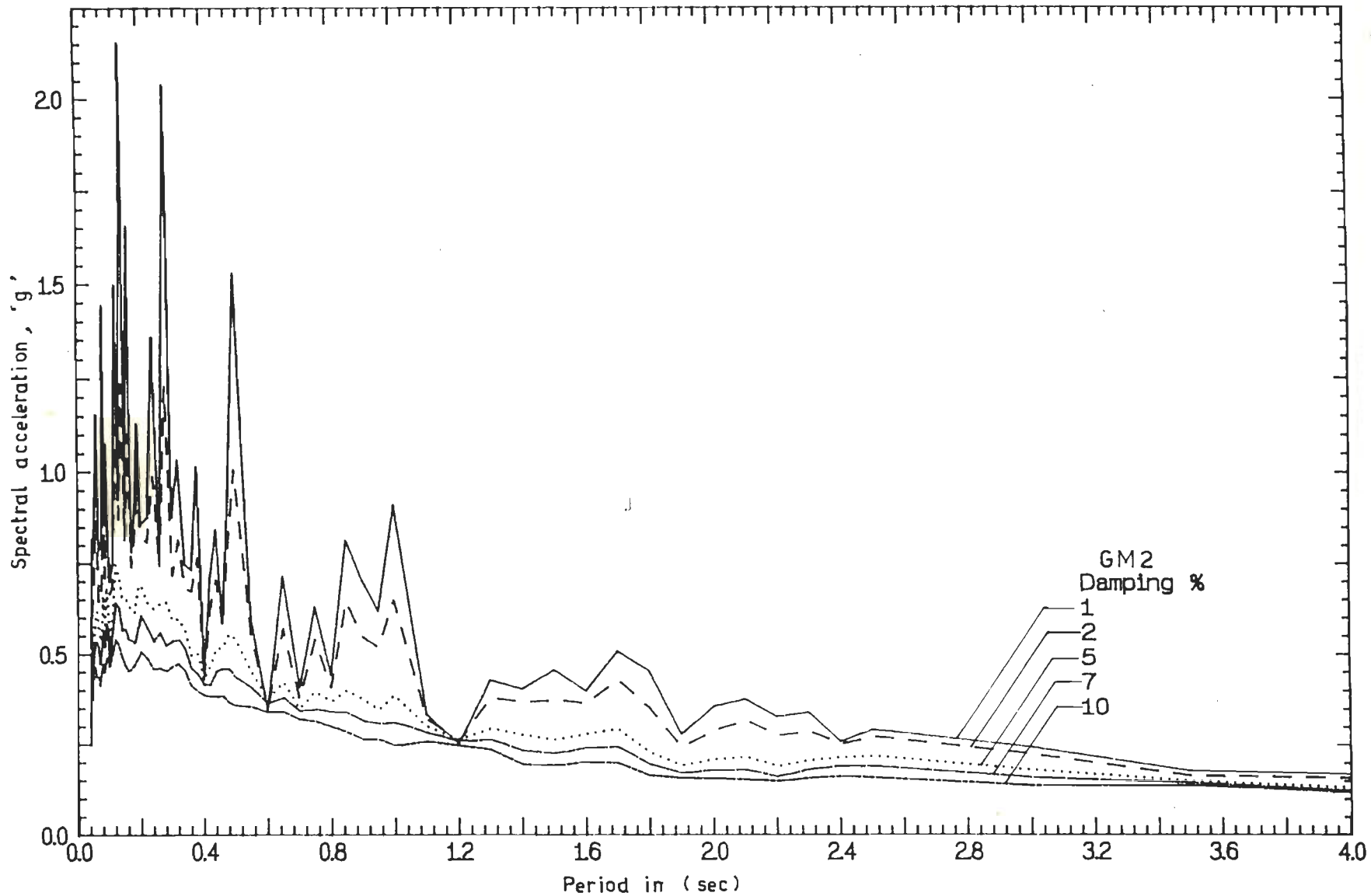


Fig. 8.7 Response Spectra for GM2

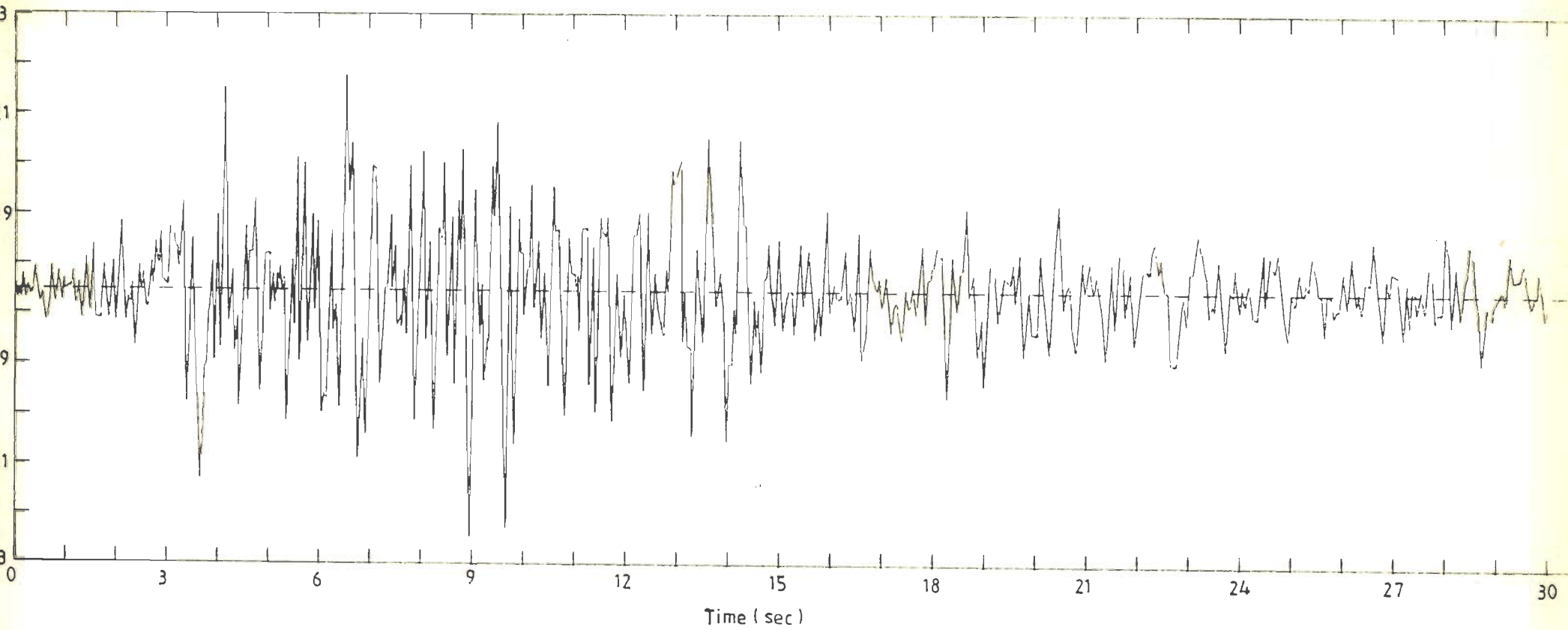


Fig. 8.8 Accelerogram of GM3

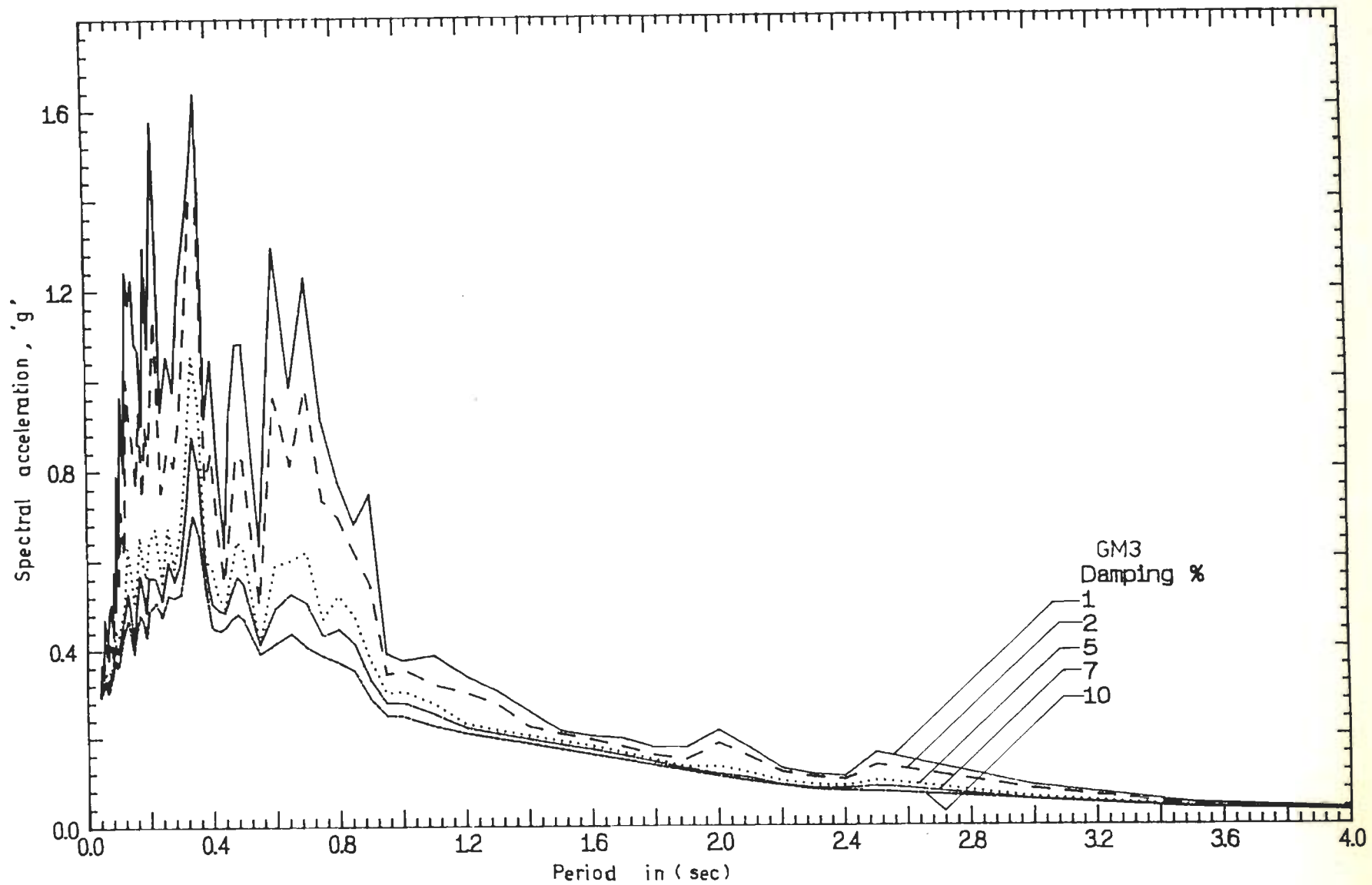


Fig. 8.9 Response Spectra for GM3

Knowing all the material properties and low-amplitude shear modulus and damping ratio as a function of strain, the dynamic analysis of El Infiernillo Dam has been performed by the three methods of analysis using the computer coding FEADYNS, for all the three ground motions as the earthquake load vectors.

8.4.4 Dynamic Analysis Based on Hardin-Drnevich Model

As mentioned in the previous section, the dynamic analysis of the El Infiernillo Dam has been carried out using the Hardin-Drnevich model. The shear modulus values and damping values respectively, at strain levels other than the unit value of shear modulus ratio, have been interpolated using the following expressions:

$$\frac{G}{G_{\max}} = \frac{1}{1 + r/r_r} \quad (8.1)$$

(for shear modulus)

$$D = \frac{4}{\pi} \times \frac{1}{A} \left[1 - \frac{B}{A} \ln\left\{\frac{1}{B}\right\} \right] - \frac{2}{\pi} \quad (8.2)$$

(for damping)

in which

r_r = reference strain

A = $1 - G/G_{\max}$

B = G/G_{\max} .

The reference strain is that value of shear strain corresponding to the shear modulus when reduced to half of its initial shear modulus. The definition of reference strain is shown in Fig. 8.10 and as before the dynamic analysis is done using FEADYNS.

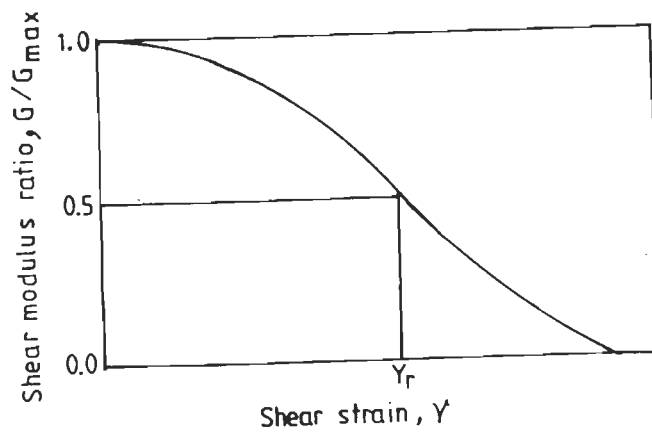


Fig. 8.10 Concept of Reference Strain
(Ishihara, 1982)

8.4.5 Dynamic Analysis Based on Seed-Idriss Method

The modulus reduction curves and damping curves proposed by Seed and Idriss (1970), are at present being widely used in today's Geotechnical-Earthquake Engineering profession, for the evaluation of response of soil profiles (Idriss et al., 1973), earth and earthfill dams (Seed et al., 1973; Marcuson and Krinitzsky, 1976; Lai and Seed, 1985). A few of the computer codings, namely, QUAD-4 (Idriss et al., 1973), LUSH (Lysmer, et al., 1974), FLUSH (Lysmer et al., 1975), and TLUSH (Kagawa et al., 1981) based on the Seed-Idriss method are widely being employed in different parts of the world for the dynamic analysis of different earth structures including foundations of nuclear power plants. Any dynamic analysis of an earth structure performed by any other method should essentially be compared with an analysis based on any one of the above mentioned computer programs, as exercised by Marcuson and Krinitzsky (1976), in the case of Fort Peck Dam.

The Seed-Idriss method uses a limited number of digitized values of modulus reduction factors, unlike the Ramberg-Osgood or Hardin-Drnevich models, in which the modulus and damping values are expressed in a functional form. The digitized values of reduction factors and damping values as proposed by Seed-Idriss (1970), are given in Table 8.4. These values have been used in FEADYNS for the analysis of the El Infiernillo Dam.

Table 8.4 Strain-Compatible Dynamic Soil Properties
(after Seed and Idriss, 1970)

Effective Shear Strain γ_{eff} (%)	$\log(\gamma_{eff})$	Shear Modulus Reduction Factor		Fraction of Critical Damping (%)	
		Clay	Sand	Clay	Sand
(1)	(2)	(3)	(4)	(5)	(6)
$\leq 1.00 \times 10^{-4}$	-4.0	1.000	1.000	2.50	0.50
3.16×10^{-4}	-3.5	0.913	0.984	2.50	0.80
1.00×10^{-3}	-3.0	0.761	0.934	2.50	1.70
3.16×10^{-3}	-2.5	0.565	0.826	3.50	3.20
1.00×10^{-2}	-2.0	0.400	0.656	4.75	5.60
3.16×10^{-2}	-1.5	0.261	0.443	6.50	10.00
1.00×10^{-1}	-1.0	0.152	0.246	9.25	15.50
0.316	-0.5	0.076	0.115	13.80	21.00
1.00	0.0	0.037	0.049	20.00	24.60
3.16	0.5	0.013	0.049	26.00	24.60
$\geq 1.00 \times 10$	1.0	0.004	0.049	29.00	24.60

Note:

γ_{eff} = Effective value of shear strain.

8.5 RESPONSE EVALUATION OF EL INFIERNILLO DAM

From the dynamic analysis of the El Infiernillo Dam, based on the Ramberg-Osgood model, Hardin-Drnevich model and Seed-Idriss method and subjected to the three ground motions, the computed maximum acceleration values at a few pre-determined nodal points as shown in Fig. 8.11 are given in Tables 8.5 to 8.7 with the respective locations.

The nodes at which the acceleration values are displayed in Tables 8.5 to 8.7 correspond to specified elevations, for instance, the crest, approximately $3/4$ th the height, half the height, $1/4$ th the height from the base and the base of the dam (top surface of the foundation). At each elevation three nodes have been selected, the first node lying on the upstream slope surface or the upstream toe, the second node along the axis of the dam and the third node along the downstream slope surface or the downstream toe in sequence.

Similarly, the peak values of shear strain shown in Tables 8.8 to 8.10 correspond to specific zones in which a variation in stiffness exists. The few selected elements lie in the upstream, the impervious core and in the downstream.

In order to assess the stability of the El Infiernillo Dam, the stresses must be compared with the corresponding strengths. However, in the absence of laboratory cyclic triaxial test results, a 5 percent shear strain criterion has been adopted as the failure phenomenon. If a shear strain of 5 percent is used and if the dam is stable

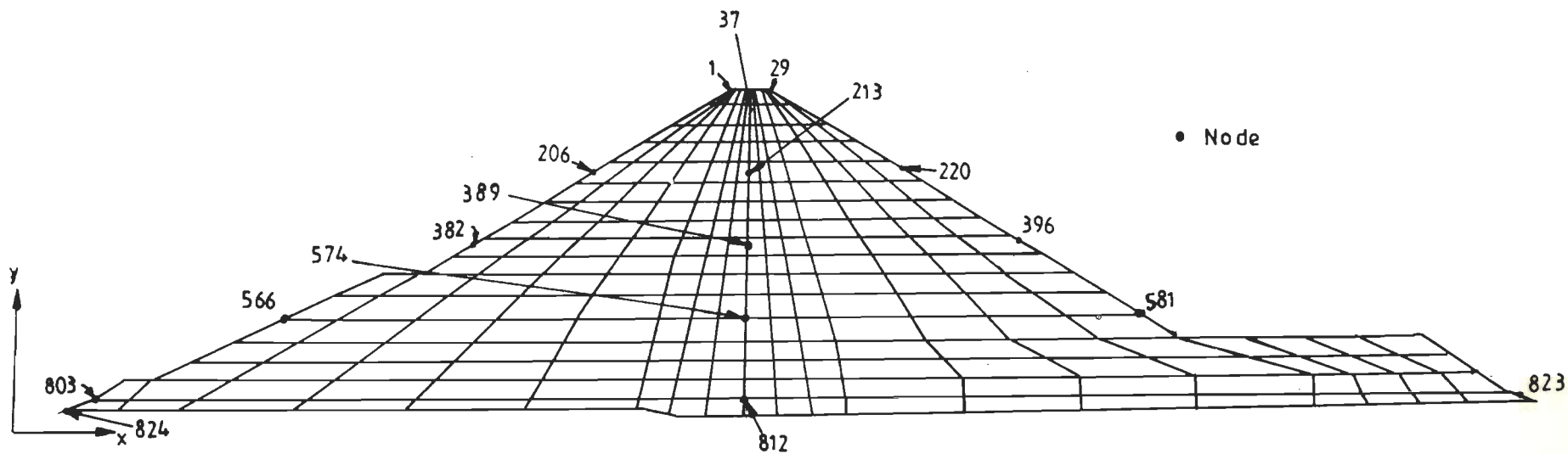


Fig. 8.11 El Infiernillo Dam; Node Numbers at which Acceleration Values are Tabulated

Table 8.5 Maximum Acceleration Values at a few Nodes
 Ramberg-Osgood Model; PGA = 0.25g

Node No.	Coordinate (m)		Maximum Acceleration (g)			Location
	X	Y	Applied Ground Motion			
			GM1	GM2	GM3	
(1)	(2)	(3)	(4)	(5)	(6)	(7)
1	283.0	146.0	0.15	0.29	0.29	U/s Crest
15	290.0	146.0	0.15	0.26	0.29	Crest, along axis
29	297.0	146.0	0.16	0.30	0.30	D/s Crest
37	291.5	142.8	0.13	0.34	0.35	Axis, below crest (Maximum value)
206	224.0	109.8	0.07	0.16	0.13	0.75H from base
213	288.9	109.8	0.07	0.18	0.15	0.75H from base
220	352.8	109.8	0.08	0.15	0.13	0.75H from base
382	171.7	75.8	0.12	0.18	0.18	0.50H from base
389	287.9	75.8	0.07	0.17	0.14	0.50H from base
396	402.4	75.8	0.13	0.18	0.18	0.50H from base
566	82.7	38.0	0.23	0.24	0.24	0.25H from base
574	286.9	38.0	0.05	0.16	0.15	0.25H from base
581	461.8	38.0	0.19	0.22	0.21	0.25H from base
803	6.3	4.0	0.25	0.25	0.25	U/s toe
812	285.6	4.0	0.11	0.15	0.15	bottom of axis
823	613.8	4.0	0.25	0.25	0.25	D/s toe

Note:

H = Height of the dam from the base

Table 8.6 Maximum Acceleration Values at a few Nodes
Hardin-Drnevich Model; PGA = 0.25g

Node No.	Coordinate (m)		Maximum Acceleration (g)			Location
	X	Y	Applied Ground Motion			
			GM1	GM2	GM3	
(1)	(2)	(3)	(4)	(5)	(6)	(7)
1	283.0	146.0	0.11	0.14	0.14	U/s Crest
15	290.0	146.0	0.10	0.13	0.13	Crest, along axis
29	297.0	146.0	0.12	0.14	0.15	D/s Crest
37	291.5	142.8	0.14	0.17	0.20	Axis, below crest (Maximum value)
206	224.0	109.8	0.08	0.12	0.12	0.75H from base
213	288.9	109.8	0.07	0.12	0.12	0.75H from base
220	352.8	109.8	0.08	0.12	0.12	0.75H from base
382	171.7	75.8	0.17	0.14	0.15	0.50H from base
389	287.9	75.8	0.08	0.13	0.11	0.50H from base
396	402.4	75.8	0.17	0.15	0.15	0.50H from base
566	82.7	38.0	0.27	0.21	0.20	0.25H from base
574	286.9	38.0	0.09	0.13	0.12	0.25H from base
581	441.8	38.0	0.24	0.19	0.19	0.25H from base
803	6.3	4.0	0.25	0.25	0.25	U/s toe
812	285.6	4.0	0.18	0.25	0.14	bottom of axis
823	613.8	4.0	0.25	0.25	0.25	D/s toe

Note:

H = Height of the dam from the base

Table 8.7 Maximum Acceleration Values at a few Nodes
Seed-Idriss Method; PGA = 0.25g

Node No.	Coordinate (m)		Maximum Acceleration (g)			Location
	X	Y	Applied Ground Motion			
			GM1	GM2	GM3	
(1)	(2)	(3)	(4)	(5)	(6)	(7)
1	283.0	146.0	0.76	0.40	0.52	U/s Crest
15	290.0	146.0	0.78	0.41	0.51	Crest, along axis
29	297.0	146.0	0.79	0.43	0.55	O/s Crest
37	291.5	142.8	0.73	0.49	0.58	Axis, below crest
206	224.0	109.8	0.27	0.24	0.19	0.75H from base
213	288.9	109.8	0.30	0.24	0.24	0.75H from base
220	352.8	109.8	0.26	0.24	0.20	0.75H from base
382	171.7	75.8	0.31	0.26	0.27	0.50H from base
389	287.9	75.8	0.23	0.22	0.22	0.50H from base
396	402.4	75.8	0.31	0.26	0.27	0.50H from base
566	82.7	38.0	0.30	0.33	0.32	0.25H from base
574	286.9	38.0	0.18	0.20	0.19	0.25H from base
581	461.8	38.0	0.30	0.30	0.30	0.25H from base
803	6.3	4.0	0.25	0.25	0.25	U/s toe
812	285.6	4.0	0.20	0.16	0.15	bottom of axis
823	613.8	4.0	0.25	0.25	0.25	O/s toe

Note:

H = Height of the dam from the base

against this criterion, it can be assumed safe against the stipulated ground motion (Marcuson and Krinitzsky, 1976). Therefore, the static shear strain values and the corresponding dynamic shear strain values computed at a few pre-determined elements (centre of each element) as shown in Fig. 8.12 are given in Tables 8.8 to 8.10 for the Ramberg-Osgood model, Hardin-Drnevich model and the Seed-Idriss method respectively. The static shear strain values have been evaluated knowing the Young's modulus, Poisson's ratio, shear modulus and the shear stress values at the centre of each element evaluated using FEABANS. In the same tables the values of total shear strain (static + dynamic) for the three methods of analysis are also presented. The computed crest displacement (node 15) by the three methods of analysis and for the three ground motions are shown in Table 8.11.

8.6 ANALYSIS AND DISCUSSION OF RESULTS

8.6.1 Acceleration Values

8.6.1.1 Acceleration values using Ramberg-Osgood model

From the maximum acceleration values shown at some important locations in Column 4 of Table 8.5, by the Ramberg-Osgood model and subjected to the three input motions, it is seen that the crest acceleration (nodes: 1, 15 and 29) values corresponding to GM1 are less than the base input motion (= 0.25g), which shows the occurrence of deamplification phenomenon of the order of 40 percent. Immediately below the crest and along the axis (node 37) more deamplification is seen of the order of approximately 50 percent. At 3/4 th the

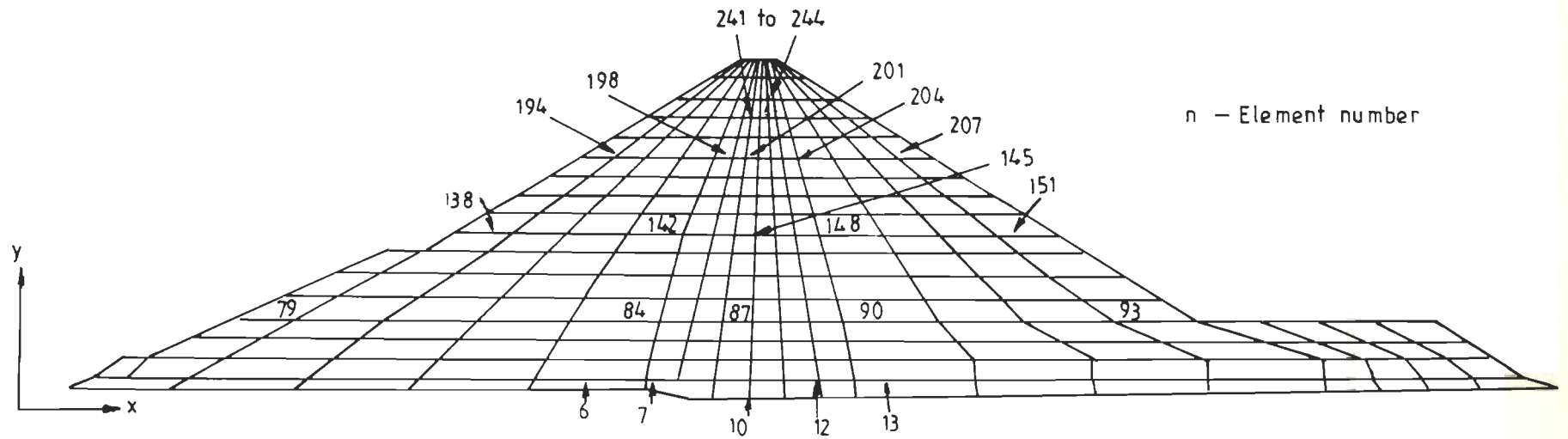


Fig. 8.12 El Infiernillo Dam; Element Numbers at which Shear Strain Values are Tabulated

Table 8.8 Shear Strain Values at a few Elements; Ramberg-Osgood Model
El Infiernillo Dam; PGA = 0.25g

El. No.	Coordinate (m)		Shear Strain (%)						
	X	Y	Static	Dynamic			Total		
				GM1	GM2	GM3	GM1	GM2	GM3
(1)	(2)	(3)	(4)	(5)	(6)	(7)	(8)	(9)	(10)
6	219.5	4.0	0.070	0.039	0.067	0.046	0.109	0.137	0.116
7	250.2	4.0	0.942	0.035	0.108	0.056	0.977	1.050	0.998
10	292.8	4.0	0.159	0.355	0.988	0.615	0.514	1.147	0.774
12	322.1	4.0	2.376	0.037	0.111	0.055	2.413	2.487	2.431
13	354.0	4.0	1.277	0.041	0.072	0.050	1.318	1.349	1.327
79	94.4	38.0	0.120	0.041	0.050	0.040	0.161	0.170	0.160
84	257.8	38.0	1.346	0.036	0.099	0.065	1.382	1.445	1.411
87	292.4	38.0	0.147	0.117	0.323	0.181	0.264	0.470	0.328
90	341.1	38.0	0.801	0.033	0.062	0.042	0.834	0.863	0.843
93	444.6	38.0	1.264	0.035	0.066	0.046	1.299	1.330	1.310
138	182.8	75.7	0.579	0.054	0.169	0.096	0.633	0.748	0.675
142	266.6	75.7	2.144	0.038	0.093	0.072	2.182	2.237	2.216
145	291.7	75.7	0.248	0.341	0.953	0.732	0.589	1.201	0.980
148	325.4	75.7	0.517	0.025	0.061	0.039	0.542	0.578	0.556
151	391.4	75.7	0.873	0.067	0.212	0.120	0.940	1.085	0.993
194	230.1	109.7	0.215	0.068	0.187	0.137	0.283	0.402	0.352
198	276.2	109.7	0.097	0.037	0.063	0.070	0.134	0.160	0.167
201	291.1	109.7	0.306	0.804	2.006	1.680	1.110	2.312	1.986
204	310.8	109.7	0.319	0.034	0.071	0.061	0.353	0.390	0.380
207	346.8	109.7	0.485	0.074	0.202	0.153	0.559	0.687	0.638
241	286.4	135.7	0.844	0.926	3.247	2.223	1.770	4.091	3.067
242	288.5	135.7	0.677	1.091	3.140	2.435	1.768	3.817	3.112
243	290.7	135.7	1.328	1.097	3.106	2.406	2.425	4.434	3.734
244	292.9	135.7	0.520	0.918	3.156	2.180	1.438	3.676	2.700
250	277.5	142.2	0.687	0.192	0.460	0.326	0.879	1.147	1.013
254	285.8	142.2	0.033	0.195	0.668	0.475	0.228	0.701	0.508
257	290.6	142.2	0.176	0.433	1.429	1.070	0.609	1.605	1.246
260	296.2	142.2	0.203	0.098	0.235	0.153	0.301	0.438	0.356
263	302.2	142.2	0.028	0.236	0.572	0.383	0.264	0.600	0.411

Note:

Total strain = static + dynamic strain.

Table 8.9 Shear Strain Values at a few Elements; Hardin-Drnevich Model
 El Infiernillo Dam; PGA = 0.25g

El. No.	Coordinate (m)		Shear Strain (%)						
	X	Y	Static	Dynamic			Total		
				GM1	GM2	GM3	GM1	GM2	GM3
(1)	(2)	(3)	(4)	(5)	(6)	(7)	(8)	(9)	(10)
6	219.5	4.0	0.070	0.036	0.063	0.041	0.106	0.133	0.111
7	250.2	4.0	0.942	0.035	0.104	0.048	0.977	1.046	0.990
10	292.8	4.0	0.159	0.241	0.670	0.355	0.400	0.829	0.514
12	322.1	4.0	2.376	0.036	0.110	0.049	2.412	2.486	2.425
13	354.0	4.0	1.277	0.038	0.067	0.044	1.315	1.344	1.321
79	94.4	38.0	0.120	0.029	0.043	0.030	0.149	0.163	0.150
84	257.8	38.0	1.346	0.025	0.063	0.044	1.371	1.409	1.390
87	292.4	38.0	0.147	0.062	0.197	0.107	0.209	0.344	0.254
90	341.1	38.0	0.801	0.029	0.057	0.036	0.830	0.858	0.837
93	444.6	38.0	1.264	0.029	0.062	0.036	1.293	1.326	1.300
138	182.8	75.7	0.579	0.043	0.124	0.066	0.622	0.703	0.645
142	266.6	75.7	2.144	0.027	0.053	0.046	2.171	2.197	2.190
145	291.7	75.7	0.248	0.196	0.560	0.392	0.444	0.808	0.640
148	325.4	75.7	0.517	0.019	0.040	0.026	0.536	0.557	0.543
151	391.4	75.7	0.873	0.053	0.155	0.080	0.926	1.028	0.953
194	230.1	109.7	0.215	0.045	0.110	0.091	0.260	0.325	0.306
198	276.2	109.7	0.097	0.024	0.039	0.041	0.121	0.136	0.138
201	291.1	109.7	0.306	0.434	1.113	0.874	0.740	1.419	1.180
204	310.8	109.7	0.319	0.022	0.043	0.040	0.341	0.362	0.359
207	346.8	109.7	0.485	0.048	0.118	0.100	0.533	0.603	0.585
241	286.4	135.7	0.844	0.665	2.021	1.707	1.509	2.865	2.551
242	288.5	135.7	0.677	0.669	1.861	1.430	1.346	2.538	2.107
243	290.7	135.7	1.328	0.673	1.105	0.681	2.001	2.433	2.009
244	292.9	135.7	0.520	1.930	1.989	1.463	2.450	2.509	1.983
250	277.5	142.2	0.687	0.131	0.288	0.228	0.818	0.975	0.915
254	285.8	142.2	0.033	0.127	0.405	0.288	0.160	0.438	0.321
257	290.6	142.2	0.176	0.256	0.846	0.596	0.432	1.022	0.772
260	296.2	142.2	0.203	0.070	0.159	0.123	0.273	0.362	0.326
263	302.2	142.2	0.028	0.161	0.368	0.281	0.189	0.396	0.309

Note:

Total strain = static + dynamic strain.

Table 8.10 Shear Strain Values at a few Elements; Seed-Idriss Method
El Infiernillo Dam; PGA = 0.25g

El. No.	Coordinate (m)		Shear Strain (%)						
	X	Y	Static	Dynamic			Total		
				GM1	GM2	GM3	GM1	GM2	GM3
(1)	(2)	(3)	(4)	(5)	(6)	(7)	(8)	(9)	(10)
6	219.5	4.0	0.070	0.023	0.022	0.015	0.093	0.092	0.085
7	250.2	4.0	0.942	0.036	0.055	0.041	0.978	0.997	0.983
10	292.8	4.0	0.159	0.461	0.993	0.753	0.620	1.152	0.912
12	322.1	4.0	2.376	0.034	0.056	0.041	2.410	2.432	2.417
13	354.0	4.0	1.277	0.028	0.023	0.016	1.305	1.300	1.293
79	94.4	38.0	0.120	0.017	0.021	0.014	0.137	0.141	0.134
84	257.8	38.0	1.346	0.037	0.054	0.044	1.383	1.400	1.390
87	292.4	38.0	0.147	0.155	0.298	0.165	0.302	0.445	0.312
90	341.1	38.0	0.801	0.020	0.022	0.016	0.821	0.823	0.817
93	444.6	38.0	1.264	0.022	0.030	0.020	1.286	1.294	1.284
138	182.8	75.7	0.579	0.042	0.069	0.053	0.621	0.648	0.632
142	266.6	75.7	2.144	0.047	0.065	0.052	2.191	2.209	2.196
145	291.7	75.7	0.248	0.430	0.500	0.427	0.678	0.748	0.675
148	325.4	75.7	0.517	0.025	0.027	0.023	0.542	0.544	0.540
151	391.4	75.7	0.873	0.050	0.086	0.065	0.923	0.959	0.938
194	230.1	109.7	0.215	0.062	0.089	0.075	0.277	0.304	0.290
198	276.2	109.7	0.097	0.051	0.056	0.054	0.148	0.153	0.151
201	291.1	109.7	0.306	0.926	1.546	1.138	1.232	1.852	1.444
204	310.8	109.7	0.319	0.028	0.030	0.027	0.347	0.349	0.346
207	346.8	109.7	0.485	0.068	0.094	0.082	0.553	0.579	0.567
241	286.4	135.7	0.844	1.343	1.852	1.699	2.187	2.696	2.543
242	288.5	135.7	0.677	1.782	2.419	2.170	2.459	3.096	2.847
243	290.7	135.7	1.328	1.028	1.557	1.378	2.356	2.885	2.706
244	292.9	135.7	0.520	1.679	1.679	1.658	2.199	2.199	2.178
250	277.5	142.2	0.687	0.141	0.096	0.097	0.828	0.783	0.784
254	285.8	142.2	0.033	0.251	0.350	0.296	0.284	0.383	0.329
257	290.6	142.2	0.176	1.257	1.728	1.548	1.433	1.904	1.724
260	296.2	142.2	0.203	0.054	0.043	0.039	0.257	0.246	0.242
263	302.2	142.2	0.028	0.173	0.115	0.106	0.201	0.143	0.134

Note:

Total strain = static + dynamic strain.

height of the dam (nodes 206, 213 and 220) from the base approximately 75 percent deamplification occurs. At half the height of the dam (nodes 382, 389 and 396), nearly 50 percent deamplification takes place. At 1/4 th the height of the dam from the base on the upstream (node 566, 0.23g), only 8 percent deamplification occurs. At the same height along the axis (node 574, 0.05g), more than 99 percent deamplification takes place. And at the same height on the downstream (node 581, 0.19g), only 24 percent deamplification is noticed. At the two extreme slope surfaces, namely on the upstream and downstream, along the base (nodes 803 and 823, 0.25g), no deamplification takes place, showing that the free-field motion remains unchanged. At the base along the axis (node 812, 0.11g), 56 percent amplification is observed.

However, the acceleration values observed at a few locations, using the Ramberg-Osgood model with the earthquake record obtained in the North-Eastern Region of India, show deamplification to a greater extent.

As seen in Column 5 of Table 8.5, the crest acceleration values at nodes 1, 15 and 29 are 0.29g, 0.26g and 0.30g respectively which is more than the base input motion. Larger acceleration values are noticed at the two extreme nodes along the crest (nodes 1 and 29), than that at the top of the axis (node 15, 0.26g). Immediately below the crest, along the axis (node 37), the maximum value of acceleration of the order of 0.34g is noticed. At 3/4 th height from the base, the values of acceleration observed at the three locations (nodes 206, 213 and 220) are 0.16g, 0.18g and 0.15g

respectively. At these locations deamplification varying between 28 and 40 percent respectively is seen. Along the axis higher value of acceleration (node 213, 0.18g) is noticed. At half the height of the dam (nodes 382, 389 and 396), the computed values of acceleration are 0.18g, 0.17g and 0.18g respectively. At these locations the magnitude of deamplification is of the order of 28 to 32 percent. The value of acceleration computed along the axis is lower than the values computed at the upstream and the downstream slope surfaces. At 1/4 th the height from the base of the dam, the computed values of acceleration at the three locations (nodes 566, 574 and 581) are 0.24g, 0.16g and 0.22g and the corresponding magnitude of deamplification are 4, 36 and 12 percent respectively. The computed value of acceleration along the axis (node 574) is lower than the corresponding values at the two extreme slope surfaces. At the base (nodes 803, 812 and 823), the computed values of acceleration are 0.25g, 0.15g and 0.25g. At the two extreme faces (nodes 803 and 823) the acceleration values are equal to that of the base motion which demonstrates again that the free-field motion remains unaltered. However, along the axis at the base (node 812), the value is only 0.15g which shows deamplification of the order of 40 percent.

As seen in Column 6 of Table 8.5, the acceleration values (corresponding to the Taft accelerogram) observed at different nodes are same as the values shown in Column 5 of Table 8.5, except a slight variation at a few locations. The maximum value of acceleration, 0.35g is observed just

below the crest, along the axis. The actual value of acceleration recorded during the March 14, 1979, Mexico earthquake, at the crest was 0.36g (Resendiz, Romo and Moreno, 1980) only. At other locations the same trend is valid as mentioned before.

The acceleration values shown in Table 8.5 have been obtained at the end of the fourth iteration, since convergence criteria have been noticed between the third and fourth iterations while using the Ramberg-Osgood model.

In Figs. 8.13 to 8.15, based on the Ramberg-Osgood model corresponding to the three ground motions at a few locations where only amplification is noticed, the values of absolute acceleration are plotted. The presentation of the magnitude of acceleration in this form has been reported by Lai and Seed (1985).

8.6.1.2 Acceleration values using Hardin-Drnevich model

From the acceleration values computed at the few nodes shown in Table 8.6, corresponding to the three accelerograms, the same behaviour as described in Sec. 8.6.1.1 is noticed, except at 1/4 th the height from the base corresponding to GM1. In this case, the maximum value of acceleration of the order of 0.27g is obtained due to the input motion, GM1. At other locations, except at the base a larger degree of deamplification is observed (nodes 803 and 823).

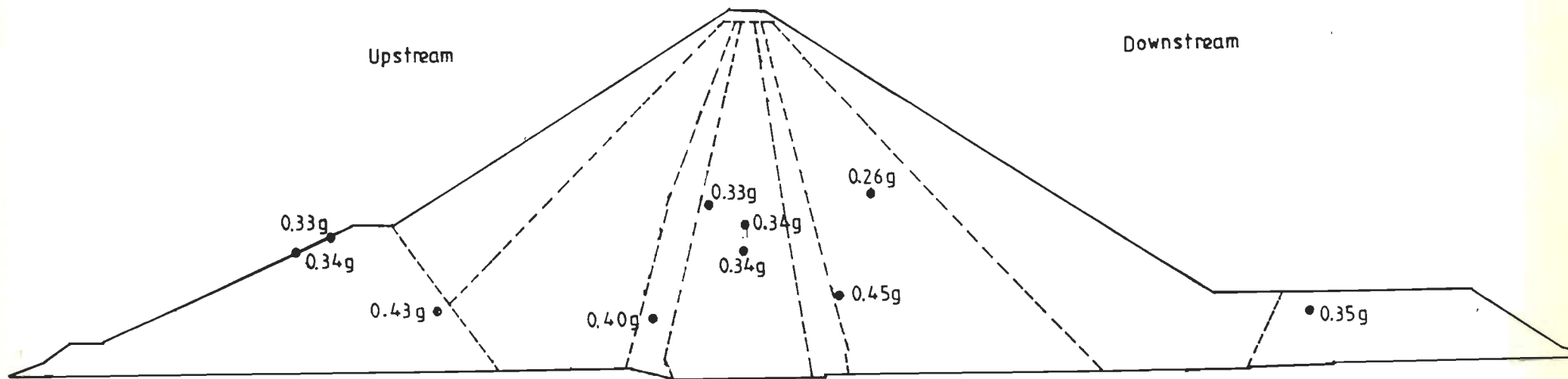


Fig. 8.13 El Infiernillo Dam; Amplified Acceleration Values at a few Locations; R-O Model; GM1

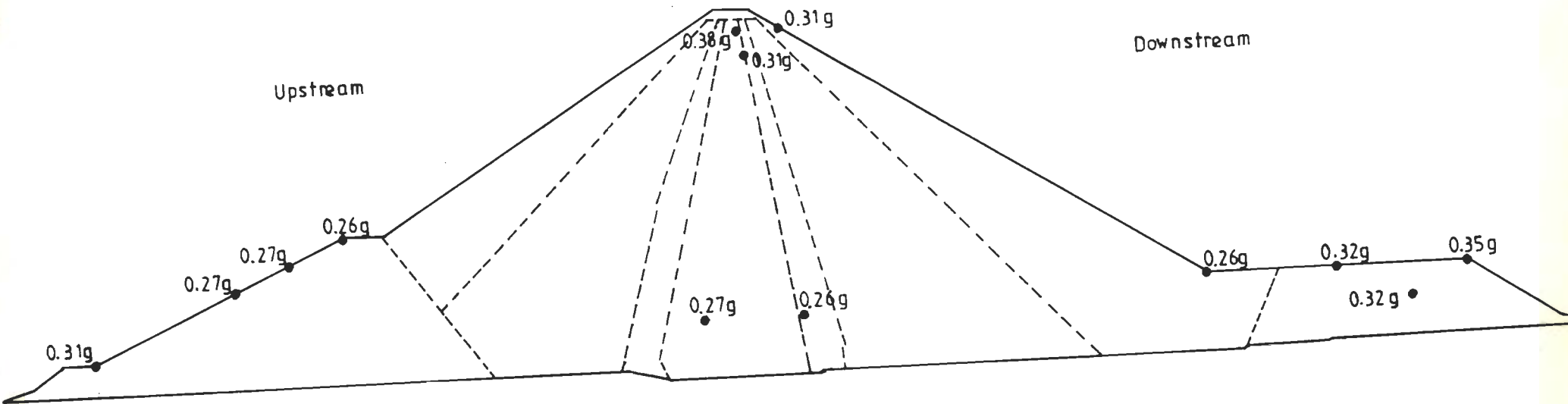


Fig. 8.14 El Infiernillo Dam; Amplified Acceleration Values at a few Locations; R-O Model; GM2

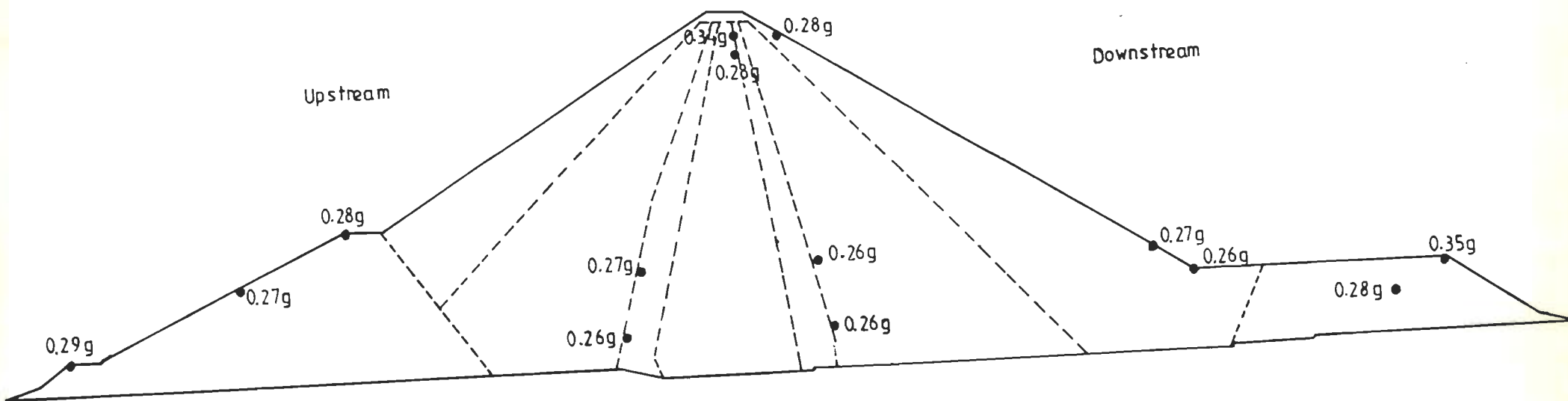


Fig. 8.15 El Infiernillo Dam; Amplified Acceleration Values at a few Locations; R-O Model; GM3

As in Sec. 8.6.1.1, a maximum number of four iterations was sufficient for convergence in the Hardin-Drnevich model as well.

As before, in Figs. 8.16 to 8.18, based on the Hardin-Drnevich model corresponding to the three ground motions at a few locations where only amplification has taken place, the values of absolute acceleration are plotted.

8.6.1.3 Acceleration values using Seed-Idriss method

As seen from the acceleration values shown in Column 4 of Table 8.7, corresponding to GM1, deamplification is noticed upto half the height of the dam from the base along the axis (nodes 389, 574 and 812). At all other locations, only amplification is observed, and the maximum value of acceleration of the order of 0.79g occurs at node 29 which is lying along the crest.

From Column 5 of Table 8.7, the acceleration values corresponding to GM2 (the synthetic accelerogram), as before no deamplification is observed near the crest and immediately below the crest. The maximum value of acceleration, 0.49g is observed at node 37. At 3/4 th height from the base deamplification is observed of the order of 4 percent only. From the base to the 3/4 th height along the axis deamplification is noticed at nodes 213, 389, 574 and 812. However, at the two extreme slope surfaces, from the base to half the height of the dam no deamplification is noticed.

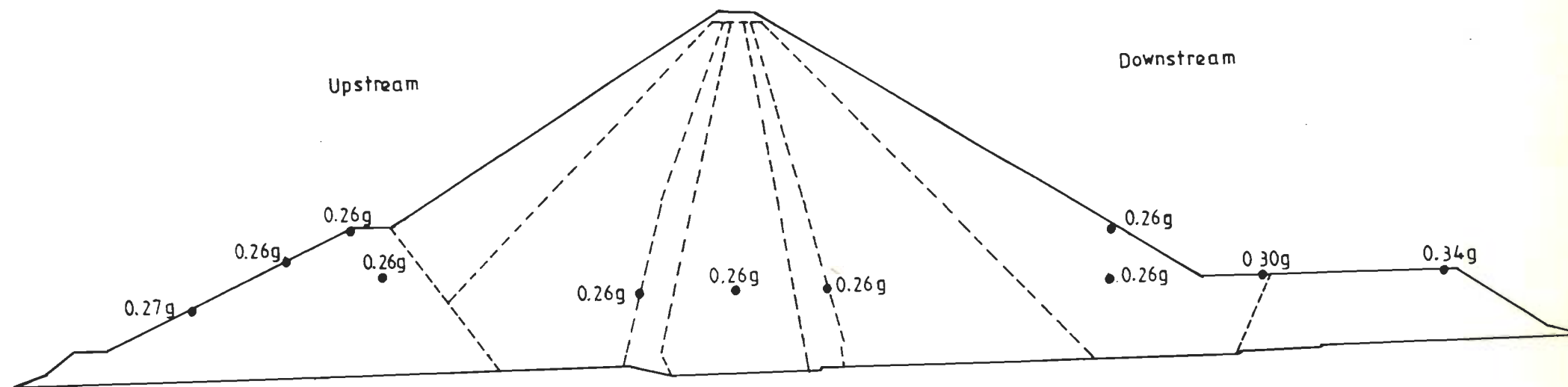


Fig. 8.16 El Infiernillo Dam; Amplified Acceleration Values at a few Locations; H-D Model; GM1

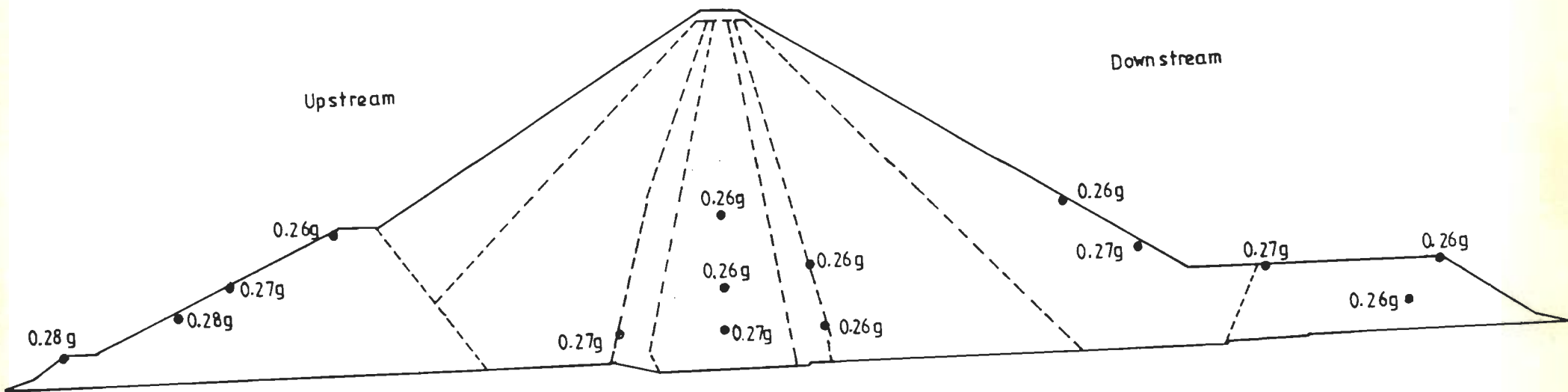


Fig. 8.17 El Infiernillo Dam; Amplified Acceleration Values at a few Locations; H-D Model; GM2

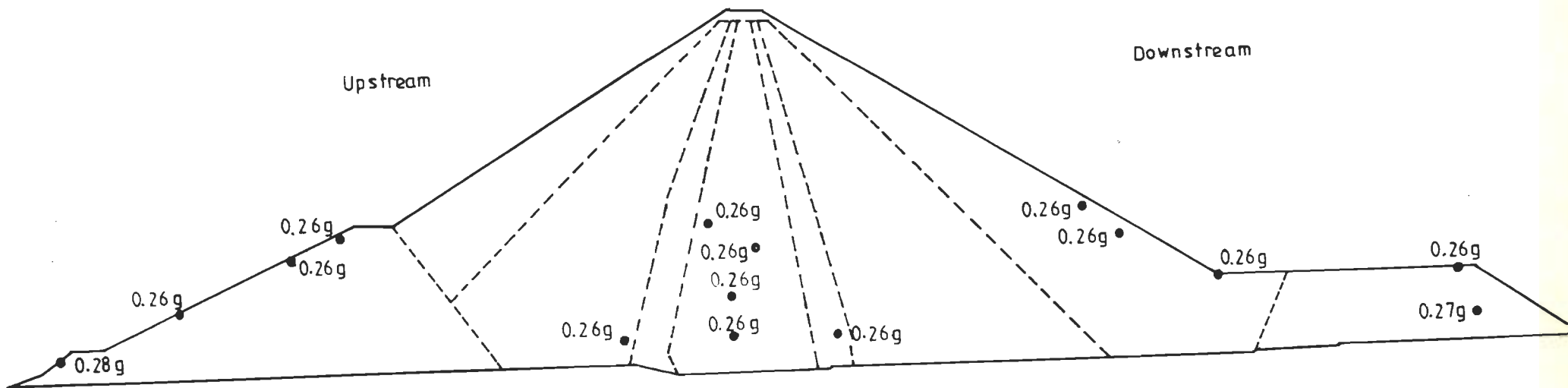


Fig. 8.18 El Infiernillo Dam; Amplified Acceleration Values at a few Locations; H-D Model; GM3

Identically, the same response, similar to that explained in the previous paragraph is observed from Column 6 of Table 8.7, using the Taft ground motion (GM3). As before, the maximum value of acceleration as 0.58g is obtained along the axis immediately below the crest.

In general, when the analysis is performed using the Seed-Idriss method no deamplification is noticed at the crest, for all the three ground motions. Except at the two extreme nodes (803 and 823) in the upstream and the downstream, the computed values of acceleration are larger than the corresponding values obtained by the Ramberg-Osgood and Hardin-Drnevich models.

Unlike in the Ramberg-Osgood and Hardin-Drnevich models, the number of iterations required was six, which is uneconomical in terms of computer time.

Based on the Seed-Idriss method, corresponding to the three ground motions the acceleration values at a few locations at which only amplification has occurred are shown in Figs. 8.19 to 8.21.

8.6.2 Shear Strain Values

The static shear strain values obtained from the nonlinear (static) analysis and the dynamic shear strain values computed at the centre of a few selected elements using the three ground motions (normalized to a peak ground acceleration value of 0.25g) are shown in Tables 8.8 to 8.10 by the three methods of analysis. The total (= static + dynamic) shear strain values are also been presented in these

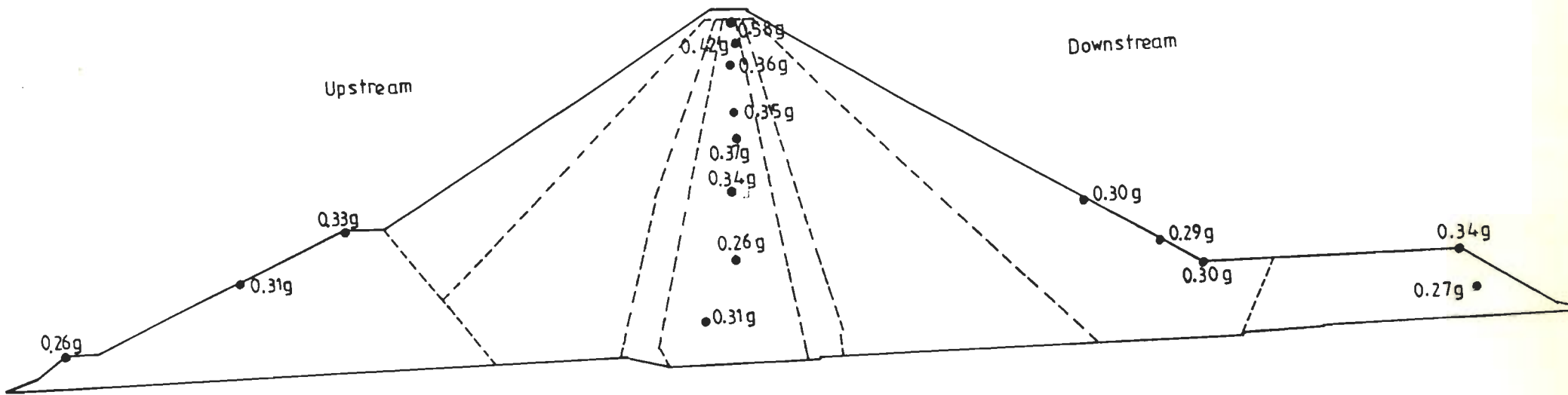


Fig. 8.19 El Infiernillo Dam; Amplified Acceleration Values at a few Locations; S-I Method; GM1

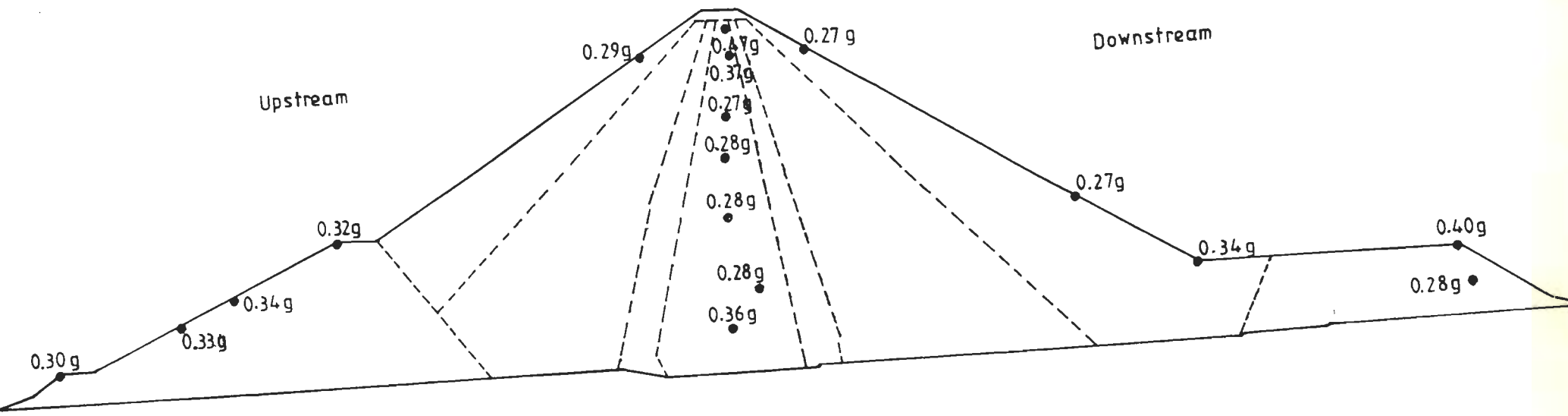


Fig. 8.20 El Infiernillo Dam; Amplified Acceleration Values at a few Locations; S-I Method; GM2

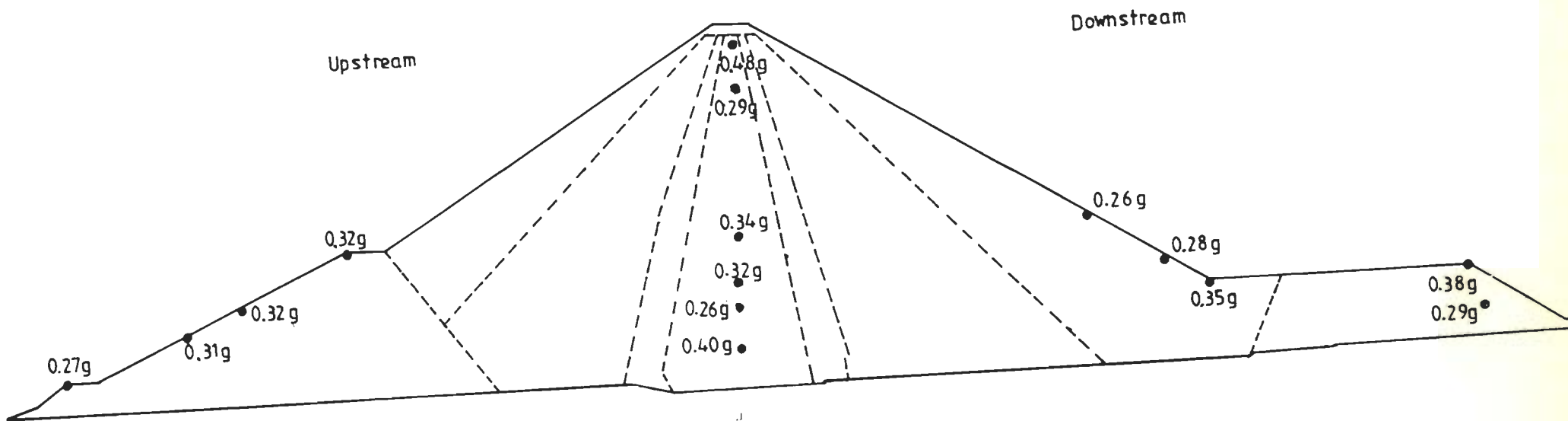


Fig. 8.21 El Infiernillo Dam; Amplified Acceleration Values at a few Locations; S-I Method; GM3

tables.

8.6.2.1 Analysis by Ramberg-Osgood model

The dynamic shear strain values using the Ramberg-Osgood model for the three ground motions are shown in Table 8.8. It can be seen that the maximum values of dynamic shear strain are of the order of 1.097, 3.247 and 2.435 percent corresponding to the three ground motions and occurring at elements 243, 241 and 242 respectively. Interestingly, all the three elements lie in the impervious core and at the same elevation (135.7 m from the base or 10.3 m from the crest in Fig. 8.12). The full reservoir level is at 138.4 m from the base.

The total shear strain values are of the order of 2.425, 4.434 and 3.734 percent occurring at the same location (element 243) for the three ground motions (Table 8.8).

8.6.2.2 Analysis by Hardin-Drnevich model

Using the Hardin-Drnevich model, it can be seen from Table 8.9 that the maximum values of dynamic shear strain for the three ground motions as the earthquake load vectors are of the order of 1.930, 2.021 and 1.707 percent, and taking place at elements 244, 241 and 241 respectively, which are at the same elevation (135.7 m from the base). And the values of total shear strain for the three ground motions are of the order of 2.450, 2.865 and 2.551 percent respectively occurring at the same location as noticed in the peak

values of dynamic shear strain.

8.6.2.3 Analysis by Seed-Idriss method

In the Seed-Idriss method of analysis, the computed values of dynamic shear strain corresponding to the three ground motions are 1.782, 2.419 and 2.170 (Table 8.10) respectively and occurring at the same elevation (=135.7 m from the base). The values of total shear strain are of the order of 2.459, 3.096 and 2.847 percent respectively for the three ground motions, and taking place at the same elevation as before. Interestingly, these maximum values of dynamic shear strain and the total shear strain are seen only at element 242, unlike in the Ramberg-Osgood and Hardin-Drnevich models.

8.6.3 Displacement

The displacement obtained at the crest (node 15) by the three methods of analysis for the three ground motions are given in Table 8.11. When the North-Eastern earthquake record is used, the crest displacement obtained corresponding to Ramberg-Osgood and Hardin-Drnevich models and the Seed-Idriss method are 5.20, 3.22 and 8.38 cm respectively. For the artificial earthquake record these values are of the order of 20.37, 14.27 and 13.22 cm and that for the Taft earthquake record are 13.13, 7.39 and 11.12 cm respectively. The deformed shape of the El Infiernillo Dam, subjected to the three ground motions, for the three methods of analysis are shown in Figs. 8.22 to 8.30.

Table 8.11 Displacement at the Crest
El Infiernillo Dam; PGA = 0.25g

Sl. No.	Crest Displacement (cm)			Method of Analysis
	Applied Ground Motion			
	GM1 (2)	GM2 (3)	GM3 (4)	
1	5.20	20.37	13.13	Ramberg-Osgood Model
2	3.22	14.27	7.39	Hardin-Drnevich Model
3	8.38	13.22	11.12	Seed-Idriss Method

8.6.4 Discussion

8.6.4.1 Acceleration values

From the acceleration values computed at different nodes for the three input ground motions, the Ramberg-Osgood and Hardin-Drnevich models show deamplification at a number of nodes. The responses due to the synthetic ground motion and the Taft ground motion as earthquake load vectors are more or less identical when the Ramberg-Osgood and the Hardin-Drnevich models are adopted.

Whereas, when the Seed-Idriss method is used for the analysis, the largest value of acceleration at the crest (node 29, 0.79g) is observed for GM1 (recorded in the North-Eastern Region of India) only. Corresponding to GM2 and GM3

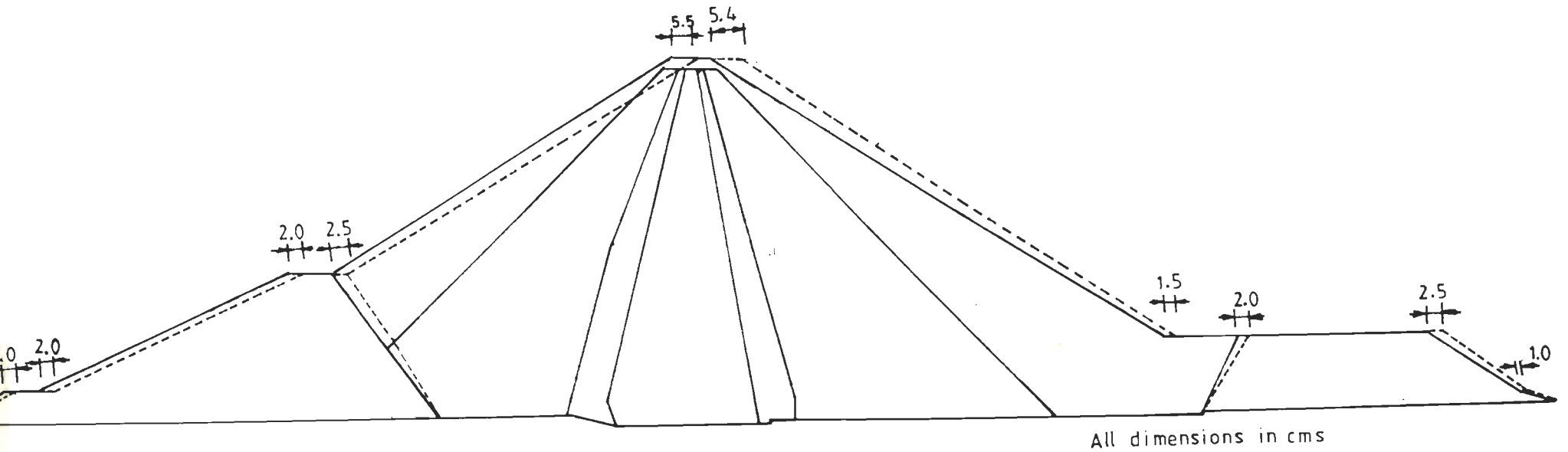


Fig. 8.22 El Infiernillo Dam; Displacement Values at a few Locations; R-O Model; GM1

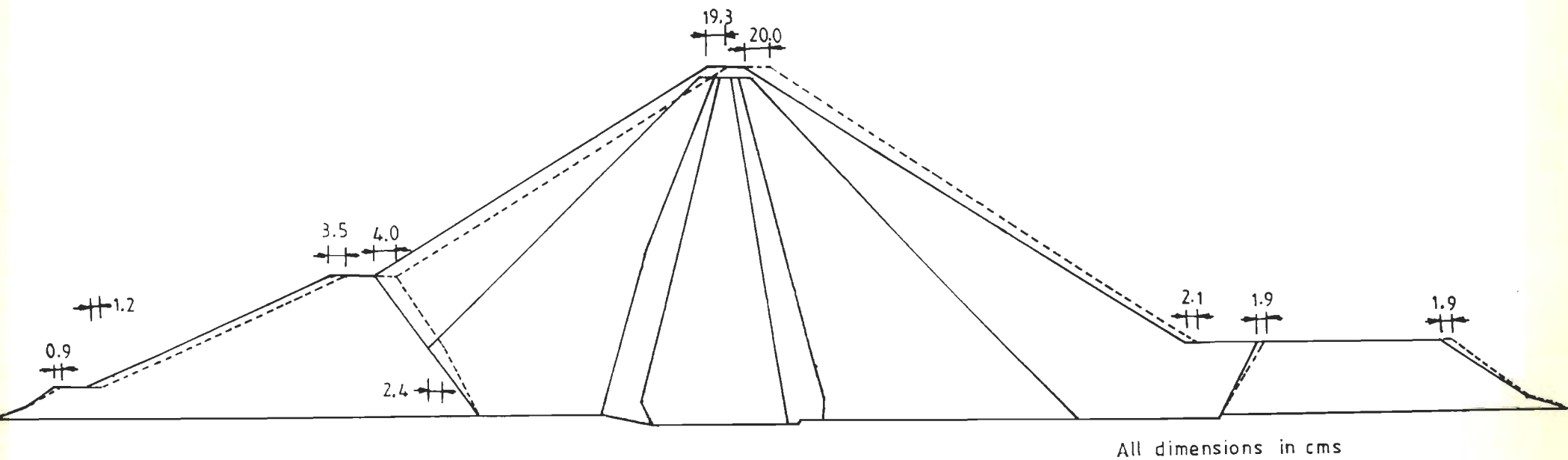


Fig. 8.23 El Infiernillo Dam; Displacement Values at a few Locations; R-O Model; GM2

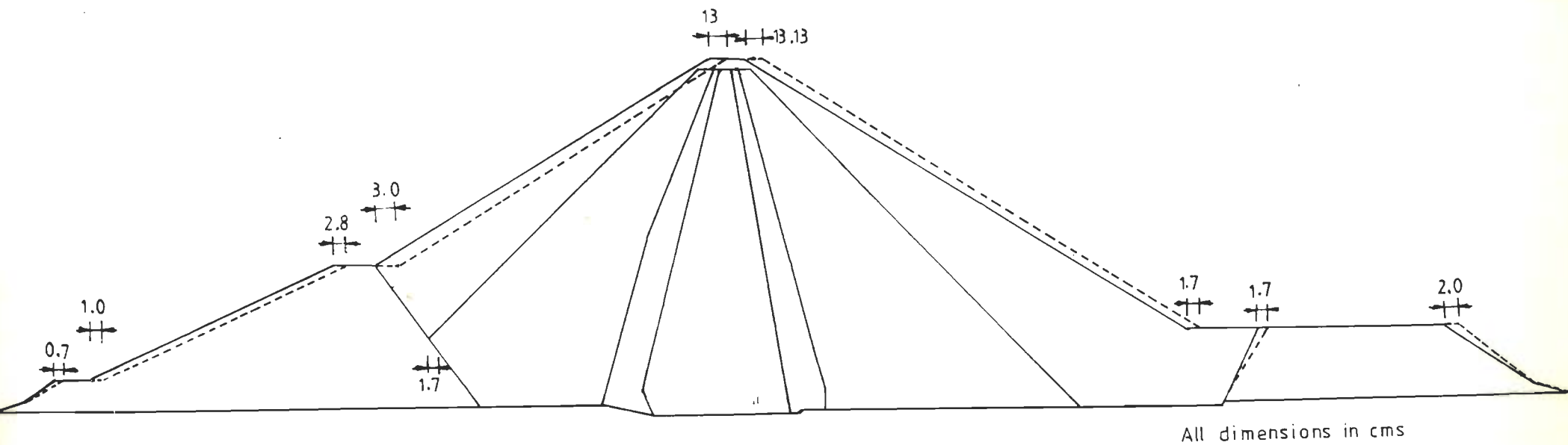


Fig. 8.24 El Infiernillo Dam; Displacement Values at a few Locations; R-O Model; GM3

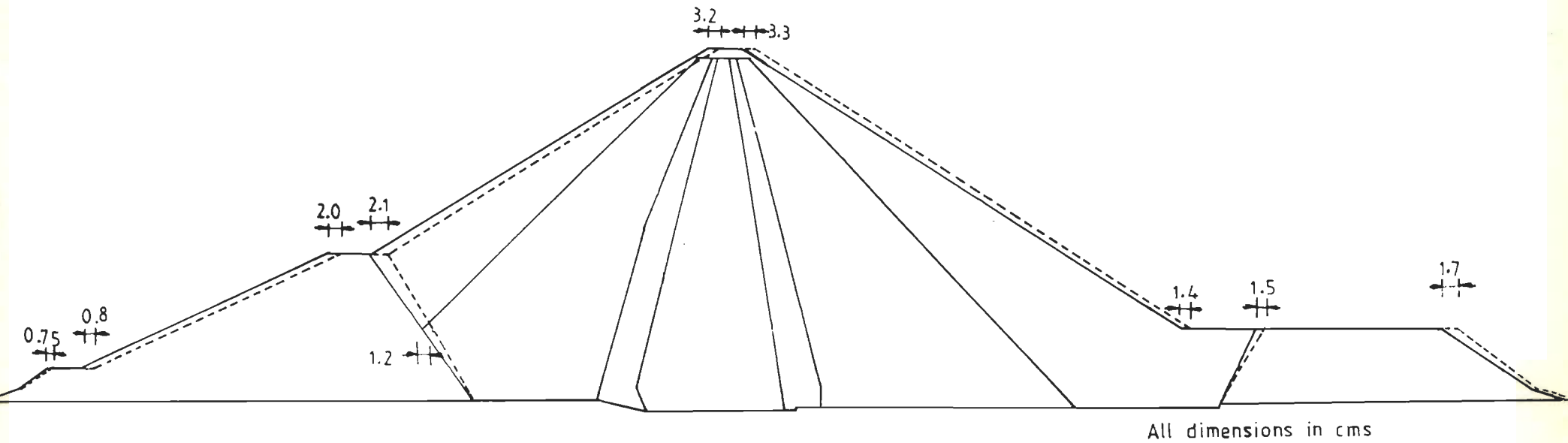


Fig. 8.25 El Infiernillo Dam; Displacement Values at a few Locations; H-D Model; GM1

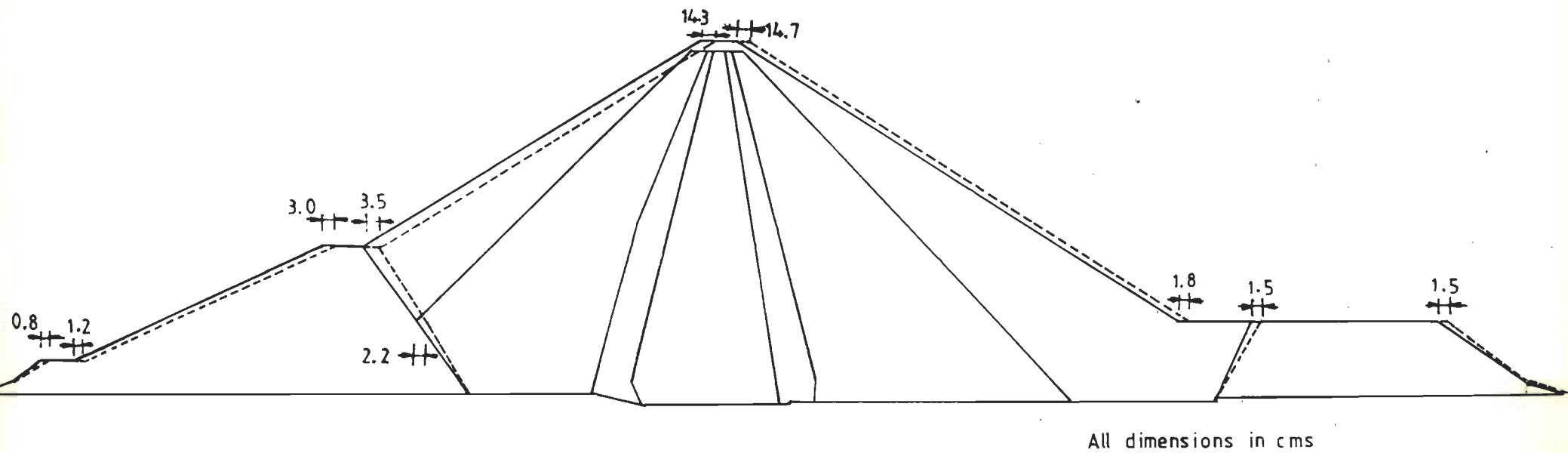
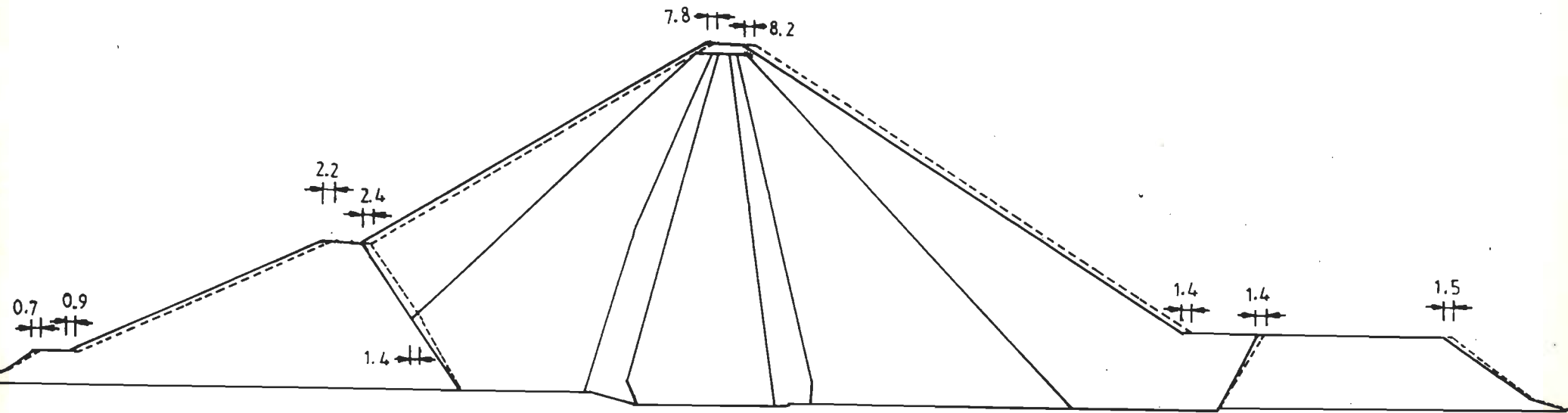


Fig. 8.26 El Infiernillo Dam; Displacement Values at a few Locations; H-D Model; GM2



All dimensions in cms

Fig. 8.27 El Infiernillo Dam; Displacement Values at a few Locations; H-D Model; GM3

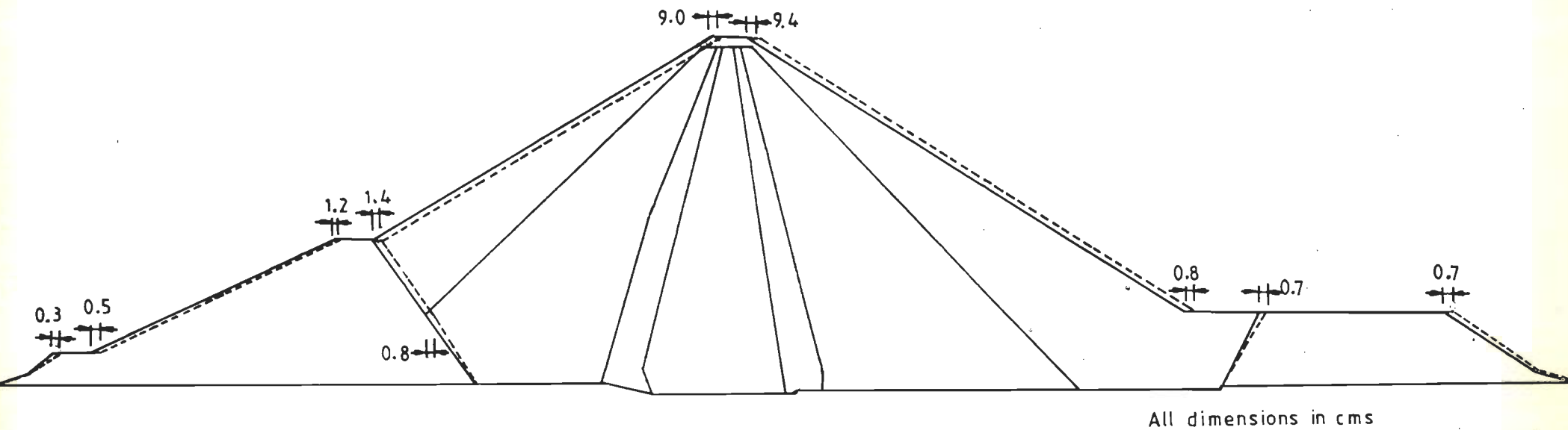
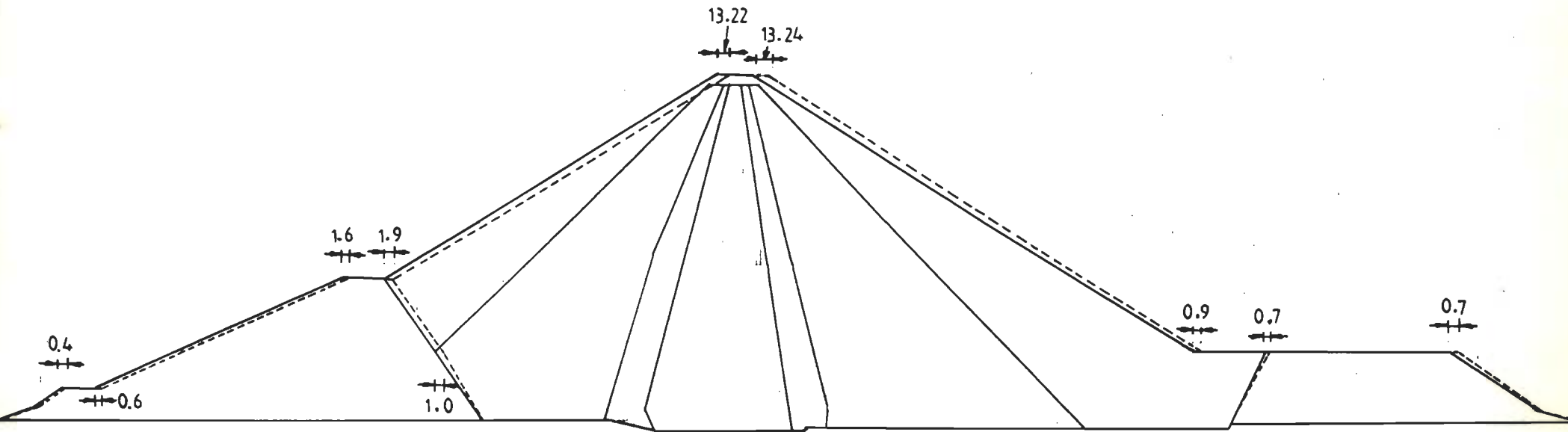
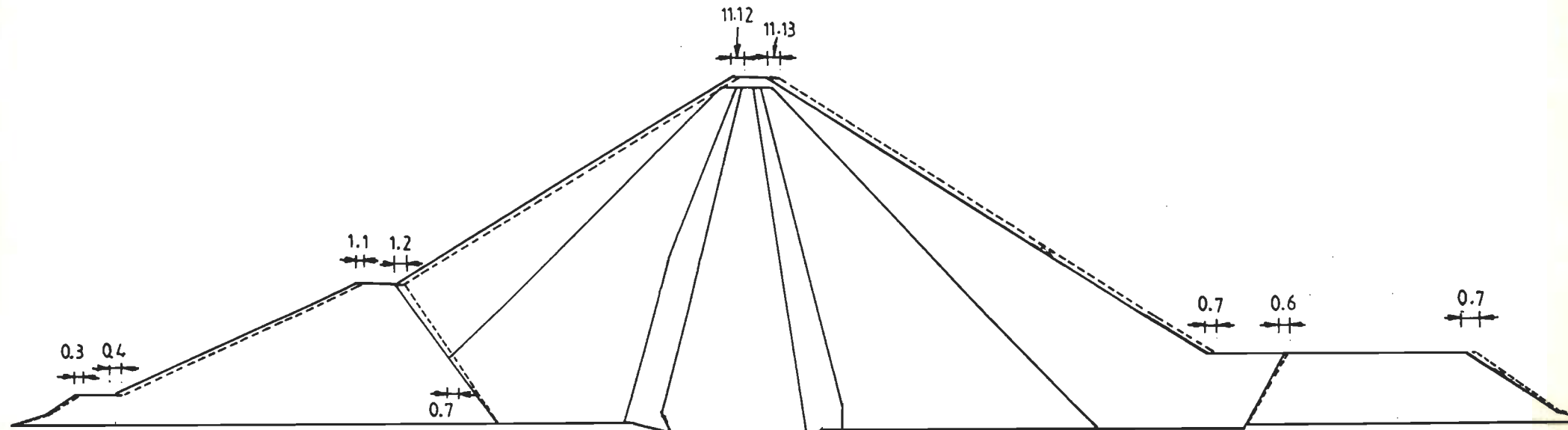


Fig. 8.28 El Infiernillo Dam; Displacement Values at a few Locations; S-I Method; GM1



All dimensions in cms

Fig. 8.29 El Infiernillo Dam; Displacement Values at a few Locations; S-I Method; GM2



All dimensions in cms

Fig. 8.30 El Infiernillo Dam; Displacement Values at a few Locations; S-I Method; GM3

accelerograms, identically the same behaviour is observed, except at the crest, when the analysis is done using the Seed-Idriss method. However, in all the cases of analysis, the free-field motion remains unchanged.

Generally, from the extensive dynamic analysis carried out, it can be seen that the lowest and the highest values of acceleration are respectively obtained, when the Hardin-Drnevich model and the Seed-Idriss method are used and the reverse is true in the phenomenon of deamplification. At present, it is difficult to attribute any reason for the occurrence of deamplification, in the case of Ramberg-Osgood and the Hardin-Drnevich models. Possibly, this may be because the Seed-Idriss method does not represent the strain dependent dynamic properties in a functional form at every step of time integration, as in the case of Ramberg-Osgood and the Hardin-Drnevich models. Essentially, the strain dependent dynamic soil properties should be available in a functional form at every time step of increment in a step-by-step nonlinear analysis technique (Ishihara, 1982).

8.6.4.2 Comparison of computed and recorded acceleration values

The computed values of acceleration at the crest and immediately below the crest by the Ramberg-Osgood and Hardin-Drnevich models and the Seed-Idriss method corresponding to the three base input motions are shown in Tables 8.5 to 8.7. From which it is seen, that the maximum values of acceleration occur either, along the crest (top of

the dam) or immediately below the crest (along the axis) except in one case (Hardin-Drnevich model, GM1; node 566, 0.27g).

During the March 14, 1979, Mexico earthquake the recorded value of acceleration at the crest was 0.36g (Resendiz, Romo and Moreno, 1980). In the present study a value of 0.35g, corresponding to the Taft earthquake record is obtained using the Ramberg-Osgood model. Therefore, the close agreement between the computed and the recorded values of acceleration demonstrates that the analysis based on the Ramberg-Osgood model and as used in the present investigation, predicts the behaviour that is fairly close to the actual situation.

On the other hand, the Hardin-Drnevich model yields appreciably very low values of crest acceleration in comparison to the actually recorded value. This could possibly be because the Hardin-Drnevich model uses a very high value of damping, of the order of 63.7 percent, which is not experienced in practical situation.

On the other hand, the Seed-Idriss method predicts excessively large values of acceleration compared to the actually recorded value during the March 14, 1979, Mexico earthquake. This could perhaps be due to the use of the strain dependent properties, at a pre-determined values of strain and low values of damping (Chapter 5). Thus, out of all the three methods of analysis, the Ramberg-Osgood model is the best model to simulate the nonlinear stress-strain characteristics of different soils subject to dynamic or

earthquake loading cases.

8.6.4.3 Shear strain values

In the dynamic analysis of the El Infiernillo Dam for the three ground motions and the three methods of analysis, the maximum value dynamic of shear strain of the order of 3.247 percent is observed at element 241 which is at the top of the core at a height of 135.7 m from the base, corresponding to the Ramberg-Osgood model and the synthetic ground motion. At the same location a maximum value of dynamic shear strain of the order of 2.021 percent is noticed using the Hardin-Drnevich model and the synthetic ground motion. And by the Seed-Idriss method, using the same ground motion the maximum value of dynamic shear strain of the order of 2.419 percent is obtained at element 242. The maximum values of total shear strain of the order of 4.434, 2.865 and 3.096 percent are obtained for the Ramberg-Osgood model, Hardin-Drnevich model and the Seed-Idriss method of analysis, and occurring at the impervious material. This shows that deformation is likely to take place in the less stiff material. In this case, the impervious core is the least stiff material than the shell material. Such a behaviour has been noticed by Carrera et al. (1979), in the analysis of Guri embankment Dam. Among the three methods of analysis, the Ramberg-Osgood model predicts the highest value of shear strain. The Hardin-Drnevich model yields the lowest value of shear strain and the Seed-Idriss method predicts intermediate values. Significantly, all the three methods of analysis

predict the maximum values of shear strain at the same elevation which is in the impervious material.

In general, no portion of the dam reaches the threshold value of failure, assuming a 5 percent shear strain as the failure criterion, subjected to the three ground motions with the peak ground acceleration value of 0.25g.

8.6.4.4 Comparison of computed and measured crest displacement

The computed values of crest displacements in the present study given in Table 8.11 have been compared with the actually measured displacement during the March 14, 1979, Mexico earthquake.

As in the case of comparison of the computed acceleration due to Taft ground motion and the recorded value of acceleration due to the March 14, 1979, Mexico earthquake the corresponding values of the computed displacement for the Taft accelerogram based on the Ramberg-Osgood model and the March 14, 1979, Mexico earthquake are of the order of 13.13 cm (Column 4, Table 8.11) and approximately 13 cm (Resendiz, Romo and Moreno, 1980) respectively. This very close agreement is noteworthy and demonstrates that the analysis based on the Ramberg-Osgood model and as proposed in the present study can predict a behaviour which is close to the actual situation of a rockfill dam subject to a strong ground shaking.

At the same location (crest, node 15), the Hardin-Drnevich model and the Seed-Idriss method yield a crest

displacement of the order of 7.39 cm and 11.12 cm respectively. The latter two methods of analysis do not predict any such displacement value which is close to the actual situation.

8.7 EVALUATION OF STABILITY OF EL INFIERNILLO DAM

Since, no portion of the El Infiernillo Dam experienced the threshold level of failure (on the basis of 5 percent shear strain), under the postulated earthquake with a peak ground acceleration value of 0.25g, to evaluate the stability of this dam, the intensity of the synthetic earthquake record was modified to yield a peak ground acceleration value of 0.40g. This modified accelerogram was used as the base input motion for the revised dynamic analysis of the El Infiernillo Dam, based on the Ramberg-Osgood model. The Ramberg-Osgood model and the artificial ground motion have been selected since, the response to this ground motion using the Ramberg-Osgood model is severe. And among all the three methods of analysis, the Ramberg-Osgood model predicted the highest value of shear strain.

In the revised dynamic analysis the maximum values of shear strain obtained at specific locations are given in Table 8.12 corresponding to the peak ground acceleration of 0.40g of the re-generated artificial accelerogram using FEADYNS. It can be seen from Table 8.12, that the maximum value of total shear strain of the order of 6.048 percent is obtained at element 250.

Table 8.12 Shear Strain Values at a few Elements
R-O Model; PGA = 0.40g; GM2

El. No.	Coordinate (m)		Shear Strain (%)		
	X	Y	Static	Dynamic	Total
(1)	(2)	(3)	(4)	(5)	(6)
6	219.5	4.0	0.070	0.151	0.221
7	250.2	4.0	0.942	0.225	1.167
10	292.8	4.0	0.159	1.654	1.813
12	322.1	4.0	2.376	0.238	2.614
13	354.0	4.0	1.277	0.156	1.433
79	94.4	38.0	0.120	0.119	0.239
84	257.8	38.0	1.346	0.197	1.543
87	292.4	38.0	0.147	0.751	0.898
90	341.1	38.0	0.801	0.145	0.946
93	444.6	38.0	1.264	0.155	1.419
138	182.8	75.7	0.579	0.356	0.935
142	266.5	75.7	2.144	0.147	2.291
145	291.7	75.7	0.248	2.012	2.260
148	325.4	75.7	0.517	0.142	0.659
151	391.4	75.7	0.873	0.437	1.310
194	230.1	109.7	0.215	0.375	0.590
198	276.2	109.7	0.097	0.128	0.225
201	291.1	109.7	0.306	3.858	4.164
204	310.8	109.7	0.319	0.160	0.479
207	346.8	109.7	0.485	0.394	0.879
250	277.5	142.2	0.687	6.048	6.735
254	285.8	142.2	0.033	5.848	5.881
257	290.6	142.2	0.176	5.812	5.988
260	296.2	142.2	0.203	5.955	6.158
263	302.2	142.2	0.028	6.012	6.040

Note:

Total strain = static + dynamic strain.

Thus, the El Infiernillo Dam is likely to undergo excessive deformation at a few elements based on an analysis with the modified synthetic waveform as the input motion. However, this conclusion is qualitative in nature, since it can only be verified with the laboratory tested cyclic shear stress values. The verification between the computed and the laboratory tested cyclic shear stress values could not be done due to non-availability of laboratory test results.

8.8 EFFECT OF FOUNDATION

To investigate the influence of the presence of foundation on stability, the finite element idealization of the El Infiernillo Dam shown in Fig. 8.3 has been extended only below the base of the dam in the direction of depth. An arbitrary depth of foundation of approximately 6 meters has been added since, the exact details of the foundation were not available. The revised finite element mesh with the foundation is shown in Fig. 8.31. The enhanced finite element mesh consists of a total of 283 eight-noded isoparametric elements and 926 nodes. The foundation layer alone constitutes 20 eight-noded elements. The effective number of degrees of freedom is 1762 and the free-field motion has been applied at the base of the foundation (node 884) instead at the base of the dam (node 824). In this case, the bottom of the foundation is the new rigid base and the coordinates of the nodes in the foundation alone lie in the fourth quadrant. The first element and the last element

Table 8.13 Comparison of Shear Strain Values; Ramberg-Osgood Model
(Inclusive of Foundation); PGA = 0.25g; GM2

El. No.	Shear Strain (%)			El. No.	Shear Strain (%)		
	Without Foundation				With Foundation		
	Static	Dynamic	Total		Static	Dynamic	Total
(1)	(2)	(3)	(4)	(5)	(6)	(7)	(8)
6	0.070	0.067	0.137	26	0.085	0.046	0.131
7	0.942	0.108	1.050	27	1.100	0.056	1.156
10	0.159	0.988	1.147	30	0.516	0.615	1.131
12	2.376	0.111	2.487	32	2.330	0.055	2.385
13	1.277	0.072	1.349	33	1.275	0.050	1.325
79	0.120	0.050	0.170	99	0.050	0.040	0.090
84	1.346	0.099	1.445	104	1.340	0.065	1.405
87	0.147	0.323	0.470	107	0.311	0.181	0.492
90	0.801	0.062	0.863	110	0.575	0.042	0.617
93	1.264	0.066	1.330	113	1.079	0.046	1.125
138	0.579	0.169	0.748	158	0.602	0.096	0.698
142	2.144	0.093	2.237	162	2.143	0.072	2.215
145	0.248	0.953	1.201	165	0.373	0.732	1.105
148	0.517	0.061	0.578	168	0.373	0.039	0.412
151	0.873	0.212	1.085	161	0.901	0.120	1.021
194	0.215	0.187	0.402	214	0.235	0.137	0.372
198	0.097	0.063	0.160	218	0.069	0.070	0.139
201	0.306	2.006	2.312	221	0.426	1.680	2.106
204	0.319	0.071	0.390	224	0.211	0.061	0.272
207	0.485	0.202	0.687	227	0.329	0.153	0.482
241	0.844	3.247	4.091	261	1.646	2.250	3.896
242	0.677	3.140	3.817	262	1.005	2.612	3.617
243	1.328	3.106	4.434	263	0.891	2.630	3.521
244	0.520	3.156	3.676	264	1.222	2.190	3.412

Note:

Total strain = static + dynamic strain.

shown in Fig. 8.3 now become the 21 st element and 283 rd element in Fig. 8.31. This procedure is adopted to simplify the comparison of analysis results between the two cases (Figs. 8.3 and 8.31).

As before, the nonlinear static and dynamic analysis have been performed on the El Infiernillo Dam including its foundation (Fig. 8.31). In the revised dynamic analysis only the artificial accelerogram (GM2) normalized to 0.25g and the Ramberg-Osgood model were used. The material in the foundation have been assumed to be strain independent and stiffer than any other material present in the whole structure.

8.8.1 Shear Strain Values

Based on the revised dynamic analysis of the El Infiernillo Dam to evaluate the stability inclusive its foundation, the computed shear strain values at the same locations as in the case, without the foundation (Table 8.8) are shown in Table 8.13. As seen from this table, marginally lower values of shear strain are obtained for the analysis including the foundation. In the analysis, excluding the foundation, the maximum value of total shear strain corresponding to the artificial earthquake record is 4.434 percent (element 243). At the same location (element 263) the value of total shear strain is 3.521 percent for the case with the foundation. Neglecting the minor difference in the values of shear strain obtained in the two cases of dynamic analysis, namely, the first case without the

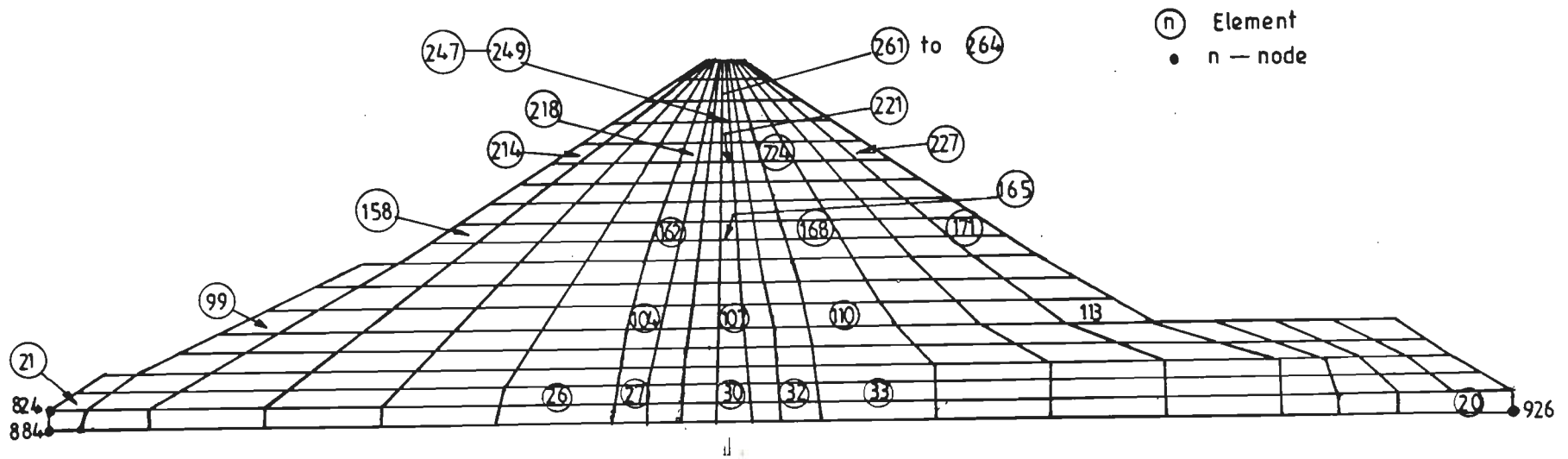


Fig. 8.31 El Infiernillo Dam Discretization with its Foundation

Table 8.13 Comparison of Shear Strain Values; Ramberg-Osgood Model (Inclusive of Foundation); PGA = 0.25g; GM2

El. No.	Shear Strain (%)			El. No.	Shear Strain (%)		
	Without Foundation				With Foundation		
	Static	Dynamic	Total		Static	Dynamic	Total
(1)	(2)	(3)	(4)	(5)	(6)	(7)	(8)
6	0.070	0.067	0.137	26	0.085	0.046	0.131
7	0.942	0.108	1.050	27	1.100	0.056	1.156
10	0.159	0.988	1.147	30	0.516	0.615	1.131
12	2.376	0.111	2.487	32	2.330	0.055	2.385
13	1.277	0.072	1.349	33	1.275	0.050	1.325
79	0.120	0.050	0.170	99	0.050	0.040	0.090
84	1.346	0.099	1.445	104	1.340	0.065	1.405
87	0.147	0.323	0.470	107	0.311	0.181	0.492
90	0.801	0.062	0.863	110	0.575	0.042	0.617
93	1.264	0.066	1.330	113	1.079	0.046	1.125
138	0.579	0.169	0.748	158	0.602	0.096	0.698
142	2.144	0.093	2.237	162	2.143	0.072	2.215
145	0.248	0.953	1.201	165	0.373	0.732	1.105
148	0.517	0.061	0.578	168	0.373	0.039	0.412
151	0.873	0.212	1.085	161	0.901	0.120	1.021
194	0.215	0.187	0.402	214	0.235	0.137	0.372
198	0.097	0.063	0.160	218	0.069	0.070	0.139
201	0.306	2.006	2.312	221	0.426	1.680	2.106
204	0.319	0.071	0.390	224	0.211	0.061	0.272
207	0.485	0.202	0.687	227	0.329	0.153	0.482
241	0.844	3.247	4.091	261	1.646	2.250	3.896
242	0.677	3.140	3.817	262	1.005	2.612	3.617
243	1.328	3.106	4.434	263	0.891	2.630	3.521
244	0.520	3.156	3.676	264	1.222	2.190	3.412

Note:

Total strain = static + dynamic strain.

foundation and the second case including a stiff foundation, it can be concluded that a stiff foundation has practically no influence on the stability of the El Infiernillo Dam.

8.9 COMMENTS ON THE ANALYSIS OF EL INFIERNILLO DAM

Based on the detailed dynamic analysis of the well instrumented El Infiernillo Dam, without the foundation and with the foundation the following conclusions are drawn:

- 1 Among the three methods of analysis using the three ground motions, the Ramberg-Osgood model yields the crest acceleration value of the order of 0.34g and 0.35g corresponding to the artificial and the Taft accelerograms respectively. These computed crest acceleration values are very close to the recorded value of crest acceleration during the March 14, 1979, Mexico earthquake which was of the order of 0.36g. Thus, the Ramberg-Osgood model based on the experimental work of the present investigation predicts a behaviour which is close to the actual situation. The response of the Ramberg-Osgood model to the North-Eastern earthquake record shows deamplification to an appreciable amount compared to the other two ground motions.
- 2 The Hardin-Drnevich model gives the lowest values of acceleration and the highest degree of deamplification at different locations of the dam, for all the three ground motions. This is possibly because, at large strain levels, this model converges towards

a damping ratio of 63.7 percent, which is not experienced in practical conditions.

- 3 The Seed-Idriss method gives the highest values of acceleration at different locations of the dam and the lowest degree of deamplification for all the three ground motions. The largest crest acceleration of the order of 0.79g which is more than three times the base input motion was obtained with the North-Eastern Region (India) earthquake record as the base input motion.
- 4 As far as the computational cost is concerned, the Ramberg-Osgood and the Hardin-Drnevich models are more economical than the Seed-Idriss method, since the latter method needs as much as 50 percent more computer time in comparison to the former two models.
- 5 No portion of the El Infiernillo Dam reaches the threshold level of failure, based on the 5 percent shear strain criterion under the postulated base input motion with the peak ground acceleration value of 0.25g. This conclusion is qualitative in nature since, for the exact stability evaluation of the dam, the laboratory determined cyclic shear stress test results are essential.
- 6 From the computed values of shear strain, the Ramberg-Osgood model, Hardin-Drnevich model and the Seed-Idriss method give the maximum value of dynamic shear strain of the order of 3.247, 2.021 and 2.419 percent and the peak value of total shear

strain as 4.434, 2.865 and 3.096 percent respectively, corresponding to the artificial ground motion only. These maximum shear strain values occur at the top of the impervious core, at an elevation equal to 135.7 m from the base and 2.7 m below the full reservoir level. All the three methods of analysis predict the maximum value of shear strain at the same elevation. Among the three methods of analysis, the Ramberg-Osgood model predicts the highest value of shear strain.

- 7 The analysis of the dam including a stiff foundation does not alter the response of the dam.
- 8 In all the three methods of analysis, the Ramberg-Osgood model simulates the nonlinear stress-strain characteristics of the materials constituting the dam as closely as possible to the actual situation as seen from the comparison of recorded/measured acceleration/displacement and the computed values.

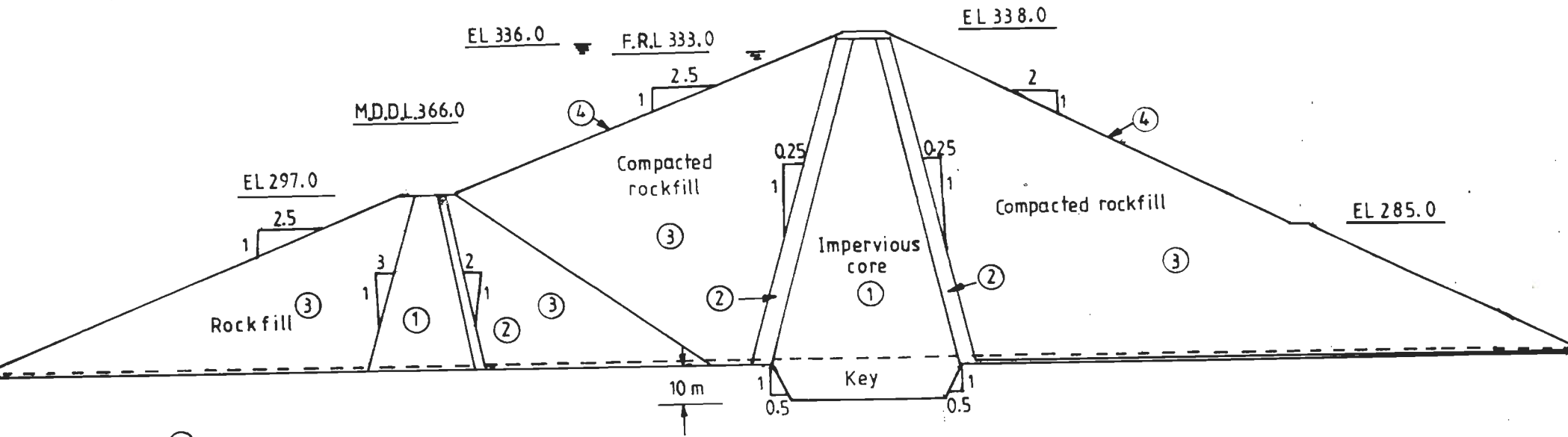
8.10 ANALYSIS OF ROCKFILL DAM DB

The dynamic response evaluation of the El Infiernillo Dam by the three methods of analysis as described in the previous section (Sec. 8.9) demonstrates that the Ramberg-Osgood model parameters evaluated on the basis of experimental values as done in the present thesis, predicts the dynamic response which is close to the actual behaviour recorded/measured during the March 14, 1979, Mexico earthquake.

Therefore, the Ramberg-Osgood model has been used for the dynamic response evaluation of the rockfill dam, DB which is of medium height and proposed to be built in India, in a region of moderate seismicity. Nevertheless, for comparison of the dynamic response, the analysis has been done using the Hardin-Drnevich model and the Seed-Idriss method as well. The height of the dam, DB is 88 metres, above the top surface of the foundation. The maximum section of the dam with a central core and other details are shown in Fig. 8.32. However, in the analysis of this medium height dam the foundation has also been included for a complete response evaluation.

8.10.1 Nonlinear Static Analysis of Dam DB

The nonlinear static analysis of the dam, DB has been carried out following the same procedure and the same computer coding described in Sec. 8.3. The different material properties used in the nonlinear static analysis of the



- ① Impervious
- ② Filters
- ③ Compacted rockfill
- ④ Riprap

Note: Elevation in meters

fig. 8.32 Maximum Section of Dam DB

dam DB are given in Table 8.14 and the material type identifications are shown in Fig. 8.32. Identically, the same assumptions have been made as in Sec. 8.3, except that in the present case, the water pressure is considered to act vertically downwards along the top surface of the foundation and normal to the upstream face of the core as shown in Fig. 8.33. The computed nonlinear stresses are the pre-earthquake stresses used as the initial condition for the dynamic analysis.

Table 8.14 Material Properties Used in the Static Analysis

Mat. No.	Material Identification	Unit Weight (t/m ³)		C (t/m ²)	φ (deg)
		Dry	Saturated		
(1)	(2)	(3)	(4)	(5)	(6)
1	Clay core	1.58	2.00	3	0
2	Filter	1.87	2.19	0	35
3	Compacted rockfill	1.85	2.16	0	45
4	Foundation and Hard-rock	1.76	2.10	0	45

Note:

C = Cohesion

φ = Angle of internal friction.

8.10.2 Finite Element Idealization

The finite element discretization of the dam, DB is shown in Fig. 8.33. A stiff foundation of depth 20 m has been included at the base of the dam. The depth of the foundation below the key is 10 m. The width of the foundation in the upstream and in the downstream have been extended by one time the width of the dam at the base (without the foundation, Franklin, 1986; 1987). This leads to an approximate total width of three times the width of the dam at the base, corresponding the base width which is without the foundation (Fig. 8.33).

The discretized dam consists of 7 horizontal layers and 67 eight-noded isoparametric elements including that of the key. The foundation consists of two horizontal layers and 76 eight-noded isoparametric elements excluding that in the key. The total number of elements and nodes in the whole structure are 143 and 528 respectively of which 447 nodes are effective ones. The first node on the rigid base is 448, at which the base input motion is applied for the dynamic response analysis.

8.10.3 Dynamic Analysis of Dam DB

In the dynamic analysis, the same finite element mesh, shown in Fig. 8.33 has been adopted. To reduce the band-width, the nodes have been numbered along the shorter direction (in the direction of height) of the dam. In addition to the static material properties given in Table 8.14,

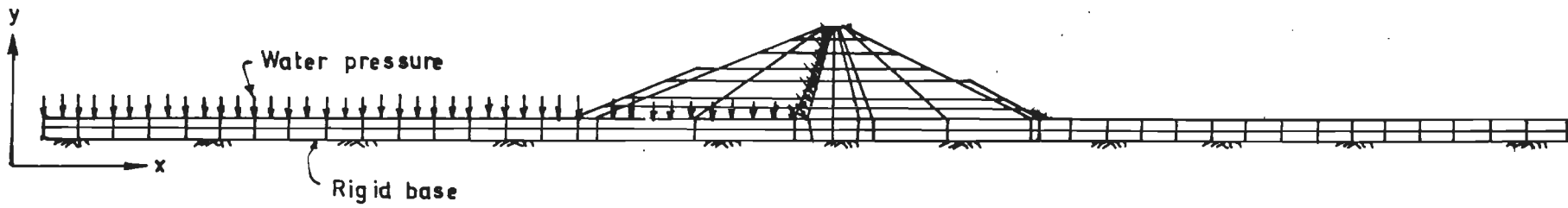


Fig. 8.33 Finite Element Idealization of Dam DB

the value of Poisson's ratio of different materials considered in the analysis of the El Infiernillo Dam have been assumed.

Due to the uncertainties involved in using the empirical expressions as given by Eqs. 2.1, 2.2, 2.5 and 2.7 to compute the low-amplitude shear modulus (Stokoe and Abdel-razzak, 1975; Arango et al., 1978), the low-amplitude shear wave velocities of different materials constituting the dam, DB have been computed using the method proposed by Nose, Takahashi and Kunii (1976), as given by the equation:

$$V_s = Z_1 H_c^{Z_2} \quad (8.3)$$

where

V_s = shear wave velocity corresponding to low-amplitude ($\epsilon \leq 10^{-4}$ percent) shear strain

Z_1 and Z_2 are empirical constants.

On the basis of extensive prototype field tests performed on a number of medium height earth and rockfill dams in Japan, Nose, Takahashi and Kunii (1976), recommended Eq. 8.3 for estimating the low-amplitude shear modulus value. The validity of Eq. 8.3, has subsequently been demonstrated by Sawada and Takahashi (1975), and Baba and Watanabe (1979), and its excellent agreement with the analytical results by Severn et al. (1979), in the dynamic response evaluation of the Llyn Brianne rockfill Dam of United Kingdom. Chandrasekaran, Paul and Suppiah (1985), and Chandrasekaran

and Prakash (1989b), have also adopted the Nose's method for evaluating the low-amplitude shear modulus, in the linear dynamic analyses of Dihang Dam (276 m, Arunachal Pradesh, India) and the Thein Dam (Punjab, India) respectively. The parameters used in computing the shear wave velocities of different materials are given in Table 8.15.

Table 8.15 Shear Wave Velocity for Different Materials
(Baba and Watanabe, 1979)

Zone Height H_c (m) (1)	Shear Wave Velocity, V_s (m/sec)				
	Core (2)	Filter (3)	Shell (4)	Founda- tion (5)	Hard Rock (6)
0-5 m	210	245	245	-	-
5-30 m	$140H_c^{0.34}$	$220H_c^{0.20}$	$250H_c^{0.20}$	-	-
30 m to base of the dam	$140H_c^{0.34}$	$220H_c^{0.20}$	$200H_c^{0.30}$	-	-
Founda- tion	-	-	-	875	-
Hard Rock	-	-	-	-	900

Note:

H_c = Height from the crest of the dam.

Upto a depth of 5 m from the crest of the dam, constant values of shear wave velocities have been assumed (Nose, Takahashi and Kunii, 1976) as shown in Table 8.15. In the foundation and in the hard rock constant values of shear wave velocities of the order of 875 and 900 m/sec (Marcuson and Krinitzsky, 1976) respectively have been adopted. Assuming the axis of the dam as the reference line, shear wave velocities have been evaluated at the centre of each element through a separate computer program.

Once the shear wave velocity is known the corresponding shear modulus is expressed by:

$$G_{\max} = \rho v_s^2 \quad (8.4)$$

in which

G_{\max} = low-amplitude shear modulus

ρ = mass density (= r/g)

r = unit weight

g = acceleration due to gravity.

Similar to the shear modulus values, the damping ratios of different materials constituting the dam, corresponding to the low-amplitude shear strain levels ($\gamma \leq 10^{-4}$ percent) have been adopted from the damping curves recommended by Seed and Idriss (1970), which are shown in Figs. 2.10 and 2.11 (Chapter 2) for sand and clay materials.

8.10.4 Results and Discussion on Dam DB

Following the same procedure given in Sec. 8.4,

the dynamic analysis of dam DB has been performed using the three methods of analysis and the three ground motions as earthquake load vector. From the dynamic analysis, the acceleration values at a few important nodal points as shown in Fig. 8.34, the shear strain values at a few element centres as given in Fig. 8.35, and the displacement at the crest, for the different methods of analysis have been presented in Tables 8.16 to 8.23 respectively.

As before, the nodes at which acceleration values are displayed in Tables 8.16 to 8.18, lie at specified elevations. These specified elevations are the crest, approximately $3/4$ th the height, half the height, $1/4$ th the height from the base and the base of the dam (top surface of the foundation). At each elevation three nodes have been chosen, the first node lying on the upstream slope surface or the toe at the upstream, the second node along the axis and the third node on the downstream slope surface or the toe at the downstream in sequence.

Identically, the maximum shear strain values shown in Tables 8.19 to 8.21 correspond to specific zones at which a sudden change in stiffness takes place. The few selected elements lie in the upstream filter, the impervious core and the downstream filter of the dam only. These elements are from the base of the core upto 5 layers and each layer consists of 4 elements only. The maximum shear strain values have been observed at these elements only, since across these elements a change in stiffness exists. The maximum shear strain values obtained using the Ramberg-Osgood model and the

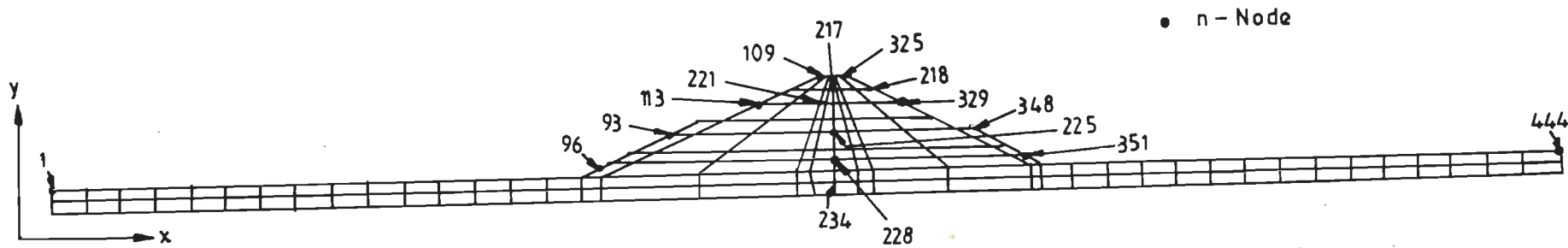


Fig. 8.34 Dam DB; Nodes at which Acceleration Values are Tabulated

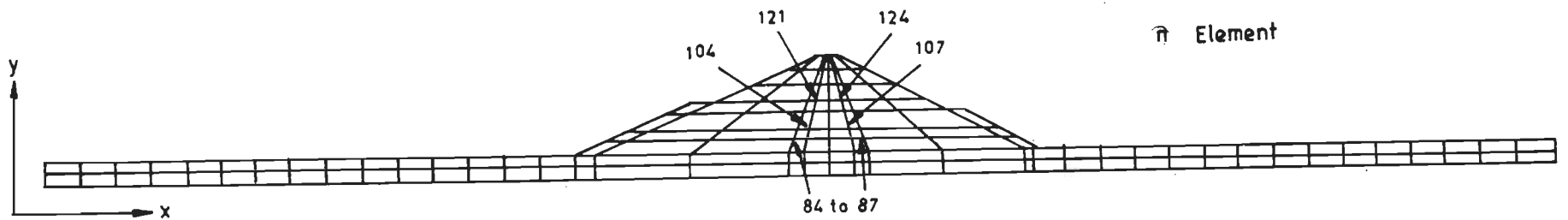


Fig. 8.35 Dam DB; Elements at which Shear Strain Values are Tabulated

Table 8.16 Maximum Acceleration Values at a few Nodes
 Ramberg-Osgood Model; Dam DB; PGA = 0.25g

Node No.	Coordinate (m)		Maximum Acceleration (g)			Location
	X	Y	Applied Ground Motion			
			GM1	GM2	GM3	
(1)	(2)	(3)	(4)	(5)	(6)	(7)
109	735.0	108.0	0.38	0.40	0.39	U/s Crest
217	740.0	108.0	0.38	0.40	0.39	Crest of axis
325	745.0	108.0	0.38	0.40	0.39	D/s Crest
218	740.0	101.0	0.39	0.42	0.40	Axis, below crest
113	666.7	80.7	0.28	0.29	0.30	U/s 0.75H from base
221	740.0	80.7	0.29	0.34	0.32	Axis 0.75H from base
329	800.0	80.7	0.26	0.31	0.31	D/s 0.75H from base
93	587.5	55.0	0.26	0.22	0.20	U/s 0.50H from base
225	740.0	55.0	0.12	0.20	0.15	Axis 0.50H from base
348	856.0	55.0	0.26	0.22	0.19	D/s 0.50H from base
96	525.6	30.2	0.26	0.27	0.25	U/s 0.25H from base
228	740.0	30.2	0.19	0.19	0.16	Axis 0.25H from base
351	905.5	30.2	0.26	0.27	0.25	D/s 0.25H from base
1	0.0	20.0	0.25	0.25	0.25	U/s top of foundation
234	740.0	20.0	0.25	0.26	0.25	Along the axis
444	1426.0	20.0	0.25	0.25	0.25	D/s top of foundation

Note:

H = Height of the dam from the base.

Table 8.17 Maximum Acceleration Values at a few Nodes
Hardin-Drnevich Model; Dam DB; PGA = 0.25g

Node No.	Coordinate (m)		Maximum Acceleration (g)			Location
	X	Y	Applied Ground Motion			
			GM1	GM2	GM3	
(1)	(2)	(3)	(4)	(5)	(6)	(7)
109	735.0	108.0	0.25	0.29	0.28	U/s Crest
217	740.0	108.0	0.25	0.29	0.28	Crest of axis
325	745.0	108.0	0.25	0.29	0.28	D/s Crest
218	740.0	101.0	0.25	0.31	0.30	Axis, below crest
113	666.7	80.7	0.12	0.16	0.16	U/s 0.75H from base
221	740.0	80.7	0.13	0.18	0.17	Axis 0.75H from base
329	800.0	80.7	0.12	0.16	0.15	D/s 0.75H from base
93	587.5	55.0	0.22	0.18	0.17	U/s 0.50H from base
225	740.0	55.0	0.11	0.15	0.14	Axis 0.50H from base
348	856.0	55.0	0.21	0.18	0.16	D/s 0.50H from base
96	525.6	30.2	0.26	0.27	0.25	U/s 0.25H from base
228	740.0	30.2	0.20	0.18	0.16	Axis 0.25H from base
351	905.5	30.2	0.26	0.27	0.24	D/s 0.25H from base
1	0.0	20.0	0.25	0.25	0.25	U/s top of foundation
234	740.0	20.0	0.25	0.26	0.25	Along the axis
444	1426.0	20.0	0.25	0.25	0.25	D/s top of foundation

Note:

H = Height of the dam from the base.

Table 8.18 Maximum Acceleration Values at a few Nodes
Seed-Idriss Method; Dam DB; PGA = 0.25g

Node No.	Coordinate (m)		Maximum Acceleration (g)			Location
	X	Y	Applied Ground Motion			
			GM1	GM2	GM3	
(1)	(2)	(3)	(4)	(5)	(6)	(7)
109	735.0	108.0	0.46	0.50	0.56	U/s Crest
217	740.0	108.0	0.45	0.50	0.55	Crest of axis
325	745.0	108.0	0.46	0.50	0.56	D/s Crest
218	740.0	101.0	0.45	0.49	0.53	Axis, below crest
113	666.7	80.7	0.23	0.25	0.28	U/s 0.75H from base
221	740.0	80.7	0.27	0.34	0.27	Axis 0.75H from base
329	800.0	80.7	0.21	0.29	0.27	D/s 0.75H from base
93	587.5	55.0	0.37	0.28	0.30	U/s 0.50H from base
225	740.0	55.0	0.16	0.20	0.17	Axis 0.50H from base
348	856.0	55.0	0.37	0.30	0.29	D/s 0.50H from base
96	525.6	30.2	0.26	0.30	0.29	U/s 0.25H from base
228	740.0	30.2	0.22	0.21	0.20	Axis 0.25H from base
351	905.5	30.2	0.28	0.28	0.28	D/s 0.25H from base
1	0.0	20.0	0.25	0.25	0.25	U/s top of foundation
234	740.0	20.0	0.25	0.26	0.25	Along the axis
444	1426.0	20.0	0.25	0.25	0.25	D/s top of foundation

Note:

H = Height of the dam from the base.

Table 8.19 Shear Strain Values at a few Elements; Ramberg-Osgood Model
Dam DB; PGA = 0.25g

El. No.	Coordinate (m)		Shear Strain (%)						
	X	Y	Static	Dynamic			Total		
				GM1	GM2	GM3	GM1	GM2	GM3
(1)	(2)	(3)	(4)	(5)	(6)	(7)	(8)	(9)	(10)
84	714.6	25.0	1.700	0.175	0.342	0.242	1.875	2.042	1.942
85	727.8	25.0	1.607	0.095	0.175	0.130	1.702	1.782	1.737
86	752.2	25.0	0.765	0.094	0.172	0.128	0.859	0.937	0.893
87	765.4	25.0	0.141	0.170	0.321	0.227	0.311	0.462	0.368
94	717.1	30.3	1.654	0.140	0.264	0.218	1.794	1.918	1.872
95	729.1	30.3	0.423	0.100	0.186	0.148	0.523	0.609	0.571
96	751.0	30.3	0.674	0.099	0.180	0.145	0.773	0.854	0.819
97	762.9	30.3	0.492	0.136	0.251	0.208	0.628	0.743	0.700
104	720.9	46.8	1.381	0.155	0.269	0.225	1.536	1.650	1.606
105	730.5	46.8	0.084	0.102	0.174	0.145	0.186	0.258	0.229
106	749.1	46.8	0.382	0.100	0.169	0.142	0.482	0.551	0.524
107	759.1	46.8	0.495	0.149	0.262	0.221	0.644	0.757	0.716
114	724.3	61.0	1.254	0.122	0.193	0.169	1.376	1.447	1.423
115	732.6	61.0	0.301	0.082	0.125	0.111	0.383	0.426	0.412
116	747.4	61.0	0.241	0.082	0.124	0.110	0.323	0.365	0.351
117	755.8	61.0	0.314	0.124	0.197	0.174	0.438	0.511	0.488
122	727.8	73.8	1.061	0.078	0.119	0.109	1.139	1.180	1.170
123	734.4	73.8	0.141	0.053	0.077	0.072	0.194	0.218	0.213
124	745.6	73.8	0.144	0.054	0.076	0.072	0.198	0.220	0.216
125	752.2	73.8	0.165	0.083	0.122	0.115	0.248	0.287	0.280

Note:

Total strain = static + dynamic strain.

Table 8.20 Shear Strain Values at a few Elements; Hardin-Drnevich Model
Dam DB; PGA = 0.25g

El. No.	Coordinate (m)		Shear Strain (%)						
	X	Y	Static	Dynamic			Total		
				GM1	GM2	GM3	GM1	GM2	GM3
(1)	(2)	(3)	(4)	(5)	(6)	(7)	(8)	(9)	(10)
84	714.6	25.0	1.700	0.140	0.308	0.201	1.840	2.008	1.901
85	727.8	25.0	1.607	0.071	0.160	0.108	1.678	1.767	1.715
86	752.2	25.0	0.765	0.071	0.158	0.106	0.836	0.923	0.871
87	765.4	25.0	0.141	0.132	0.293	0.190	0.273	0.434	0.331
94	717.1	30.3	1.654	0.092	0.210	0.150	1.746	1.864	1.804
95	729.1	30.3	0.423	0.071	0.157	0.112	0.494	0.580	0.535
96	751.0	30.3	0.674	0.070	0.154	0.110	0.744	0.828	0.784
97	762.9	30.3	0.492	0.089	0.205	0.146	0.581	0.697	0.638
104	720.9	46.8	1.381	0.087	0.177	0.138	1.468	1.558	1.519
105	730.5	46.8	0.084	0.061	0.118	0.094	0.145	0.202	0.178
106	749.1	46.8	0.382	0.060	0.116	0.093	0.442	0.498	0.475
107	759.1	46.8	0.495	0.085	0.175	0.136	0.580	0.670	0.631
114	724.3	61.0	1.254	0.061	0.113	0.096	1.315	1.367	1.350
115	732.6	61.0	0.301	0.044	0.076	0.066	0.345	0.377	0.367
116	747.4	61.0	0.241	0.044	0.076	0.066	0.285	0.317	0.307
117	755.8	61.0	0.314	0.062	0.115	0.098	0.376	0.429	0.412
122	727.8	73.8	1.061	0.038	0.066	0.060	1.099	1.127	1.121
123	734.4	73.8	0.141	0.027	0.044	0.041	0.168	0.185	0.182
124	745.6	73.8	0.144	0.027	0.044	0.041	0.171	0.188	0.185
125	752.2	73.8	0.165	0.040	0.068	0.062	0.205	0.233	0.227

Note:

Total strain = static + dynamic strain.

Table 8.21 Shear Strain Values at a few Elements; Seed-Idriss Method
Dam DB; PGA = 0.25g

El. No.	Coordinate (m)		Shear Strain (%)						
	X	Y	Static	Dynamic			Total		
				GM1	GM2	GM3	GM1	GM2	GM3
(1)	(2)	(3)	(4)	(5)	(6)	(7)	(8)	(9)	(10)
84	714.6	25.0	1.700	0.149	0.227	0.147	1.849	1.927	1.847
85	727.8	25.0	1.607	0.068	0.110	0.069	1.675	1.717	1.676
86	752.2	25.0	0.765	0.067	0.103	0.068	0.832	0.868	0.833
87	765.4	25.0	0.141	0.138	0.211	0.138	0.279	0.352	0.279
94	717.1	30.3	1.654	0.200	0.324	0.198	1.854	1.978	1.852
95	729.1	30.3	0.423	0.081	0.150	0.088	0.504	0.573	0.511
96	751.0	30.3	0.674	0.082	0.136	0.085	0.756	0.810	0.759
97	762.9	30.3	0.492	0.187	0.297	0.190	0.679	0.789	0.682
104	720.9	46.8	1.381	0.155	0.273	0.170	1.536	1.654	1.551
105	730.5	46.8	0.084	0.071	0.133	0.081	0.155	0.217	0.165
106	749.1	46.8	0.382	0.069	0.120	0.077	0.451	0.502	0.459
107	759.1	46.8	0.495	0.136	0.273	0.166	0.631	0.768	0.661
114	724.3	61.0	1.254	0.092	0.161	0.109	1.346	1.415	1.363
115	732.6	61.0	0.301	0.048	0.081	0.057	0.349	0.382	0.358
116	747.4	61.0	0.241	0.046	0.075	0.053	0.287	0.316	0.294
117	755.8	61.0	0.314	0.092	0.179	0.116	0.406	0.493	0.430
122	727.8	73.8	1.061	0.052	0.083	0.067	1.113	1.144	1.128
123	734.4	73.8	0.141	0.026	0.041	0.035	0.167	0.182	0.176
124	745.6	73.8	0.144	0.025	0.038	0.033	0.169	0.182	0.177
125	752.2	73.8	0.165	0.058	0.097	0.071	0.223	0.262	0.236

Note:

Total strain = static + dynamic strain.

regenerated artificial ground motion with a peak ground acceleration value of 0.40g are given in Table 8.22. As before, the displacement of the crest is shown in Table 8.23 corresponding to the three ground motions and the three methods of analysis.

8.10.4.1 Acceleration values

From the acceleration values shown in Table 8.16 by the Ramberg-Osgood model, it can be noticed that at the crest, the acceleration is of the order of 0.38g, 0.40g and 0.39g corresponding to GM1, GM2 and GM3 respectively, which is greater than the peak ground acceleration (= 0.25g). Thus no deamplification is observed at the crest in all the three ground motions. However, the largest value of acceleration is seen at node 218 which is immediately below the crest and not at the crest. The maximum values of acceleration by the Ramberg-Osgood model, corresponding to the three ground motions are 0.39g, 0.42g and 0.40g respectively, out of which the artificial ground motion produces the highest value (node 218, 0.42g).

In all the three ground motions, between 0.25H and 0.50H (H = height of the dam from the base), the two extreme slope surfaces experience identically the same value of acceleration. However, along the axis, lower values of acceleration are noticed, which indicates that the body of the dam at the centre between 0.25H to 0.50H experiences lower acceleration values than the two slope surfaces. The upstream experiences more acceleration values than the

Table 8.22 Shear Strain Values at a few Elements
R-O Model; Dam DB; PGA = 0.40g; GM2

El. No.	Coordinate (m)		Shear Strain (%)		
	X	Y	Static	Dynamic	Total
(1)	(2)	(3)	(4)	(5)	(6)
84	714.6	25.0	1.700	3.680	5.380
85	727.8	25.0	1.607	3.330	4.937
86	752.2	25.0	0.765	3.330	4.095
87	765.4	25.0	0.141	1.532	1.673
94	717.1	30.3	1.654	3.500	5.154
95	729.1	30.3	0.423	3.340	3.763
96	751.0	30.3	0.674	3.330	4.004
97	762.9	30.3	0.492	3.489	3.981
104	720.9	46.8	1.381	3.462	4.843
105	730.5	46.8	0.084	3.280	3.364
106	749.1	46.8	0.382	3.271	3.653
107	759.1	46.8	0.495	3.450	3.945
114	724.3	61.0	1.254	3.350	4.604
115	732.6	61.0	0.301	2.910	3.211
116	747.4	61.0	0.241	3.210	3.451
117	755.8	61.0	0.314	3.360	3.674
122	727.8	73.8	1.061	3.220	4.281
123	734.4	73.8	0.141	3.030	3.171
124	745.6	73.8	0.144	3.130	3.274
125	752.2	73.8	0.165	3.230	3.395

Note:

Total strain = static + dynamic strain.

downstream at this elevation.

At an elevation $0.75H$ from the base, the two extreme slope surfaces experience lower values of acceleration than that along the axis. As before, the locations in the upstream show higher values of acceleration than of the corresponding locations in the downstream.

At the two extreme toes on the top of foundation (nodes 1 and 444) and along the axis more or less the same value of acceleration ($= 0.25g$), that is equal to the base input motion is noticed. As discussed in the analysis of El Infiernillo Dam, the free-field motion remains unaltered in this case as well. The acceleration values at nodes 1, 234 and 444 are lower than at the elevation of $0.75H$ (nodes 113, 221 and 329), which shows that the foundation of the dam experiences less acceleration values than the body of the dam at this elevation.

As done in Sec. 8.6.1, a few of the locations at which only amplification of acceleration has occurred are displayed in Figs. 8.36 to 8.38 based on the Ramberg-Osgood model for the three ground motions.

Similar to the Ramberg-Osgood model, the Hardin-Drnevich model also shows the same trend as can be seen in Table 8.17, except for a larger degree of deamplification from $0.50H$ to the crest. Unlike in the Ramberg-Osgood model, the maximum value of acceleration of the order of $0.31g$ is noticed at node 218 which is located immediately below the crest (Column 5, Table 8.17), corresponding to the artificial ground motion. As before, the locations in the upstream show

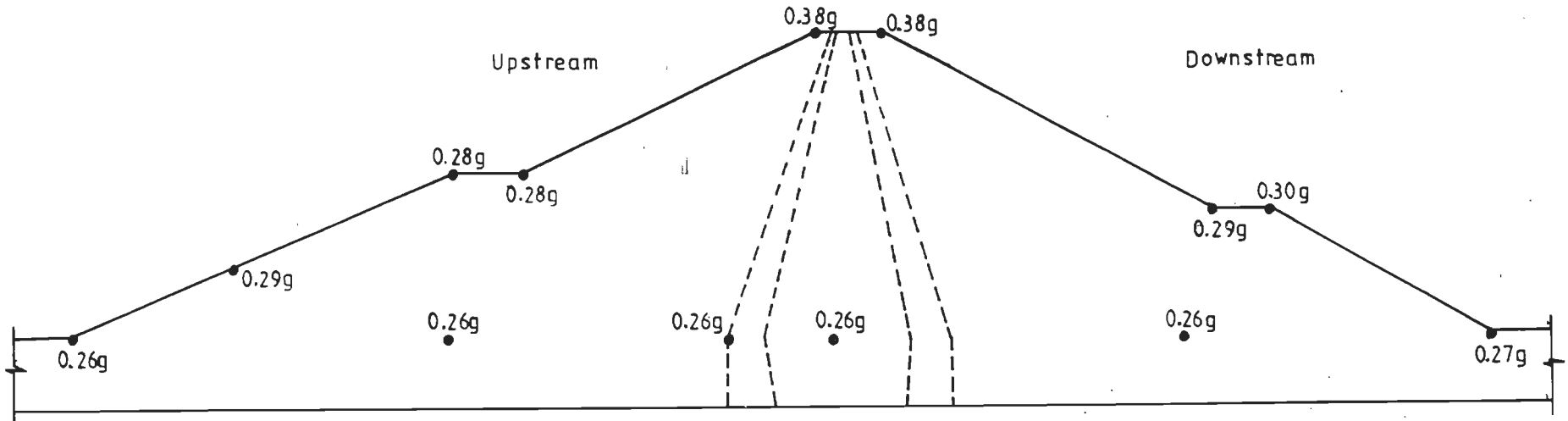


Fig. 8.36 Dam DB; Amplified Acceleration Values at a few Locations; R-O Model; GM1

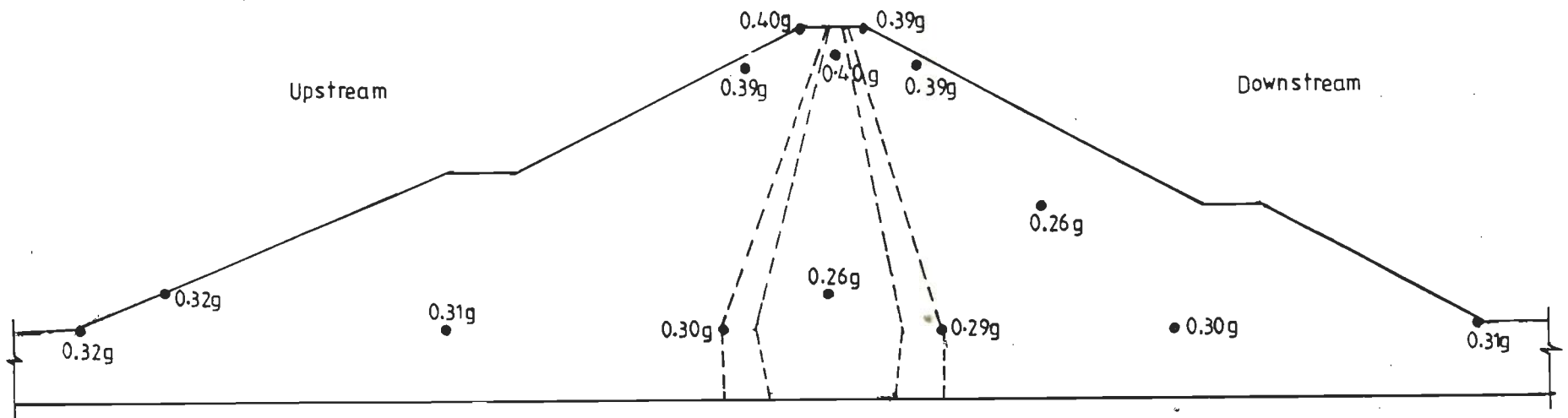


Fig. 8.37 Dam DB; Amplified Acceleration Values at a few Locations; R-O Model; GM2

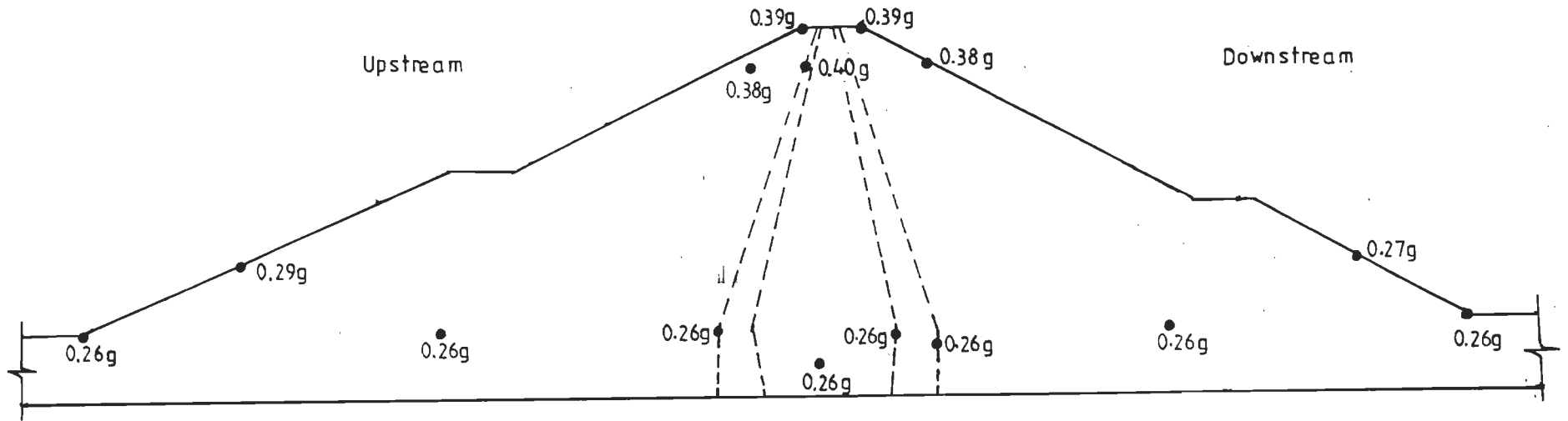


Fig. 8.38 Dam DB; Amplified Acceleration Values at a few Locations; R-O Model; GM3

larger acceleration values than the downstream locations due to the presence of water on the upstream.

Using the Hardin-Drnevich model, a few of the locations where no deamplification of acceleration is noticed are shown in Figs. 8.39 to 8.41 for the three ground motions respectively.

The Seed-Idriss method also, identically follows the same trend of distribution of acceleration as the other two models with the least degree of deamplification. The maximum values of acceleration, as seen in Table 8.18, are obtained at the crest for all the three input motions. The highest value of acceleration of the order of 0.56g is seen at the crest (nodes 109 and 325) corresponding to the Taft earthquake record. The Seed-Idriss method yields larger values of acceleration at all nodal points except at the base.

In the Seed-Idriss method of analysis, the acceleration response at 0.50H and 0.75H corresponding to the artificial accelerogram shows that the downstream (nodes 348 and 329, Column 5, Table 8.18) experiences larger values than the corresponding values at the upstream (nodes 93 and 113).

Figs. 8.42 to 8.44 show the locations at which only amplification of acceleration is noticed for the three ground motions based on the Seed-Idriss method of analysis.

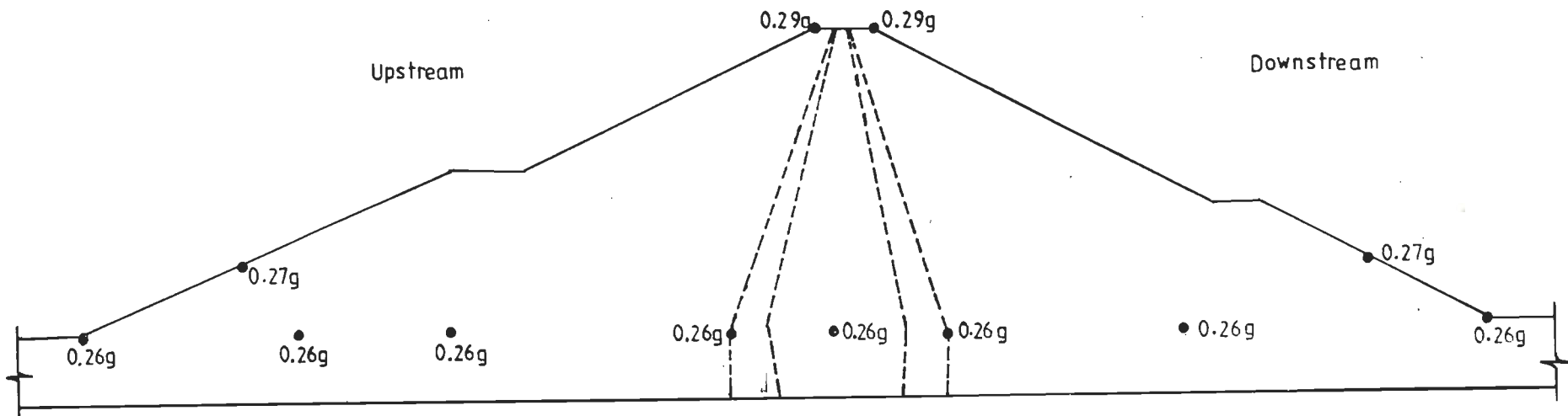


Fig. 8.39 Dam DB; Amplified Acceleration Values at a few Locations; H-D Model; GM1

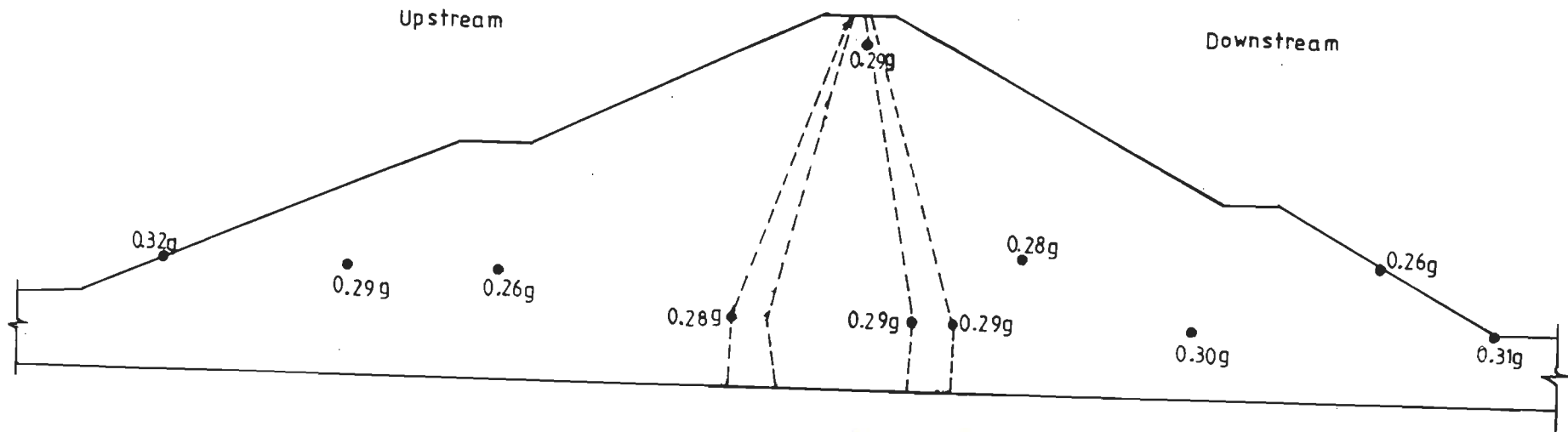


Fig. 8.40 Dam DB; Amplified Acceleration Values at a few Locations; H-D Model; GM2

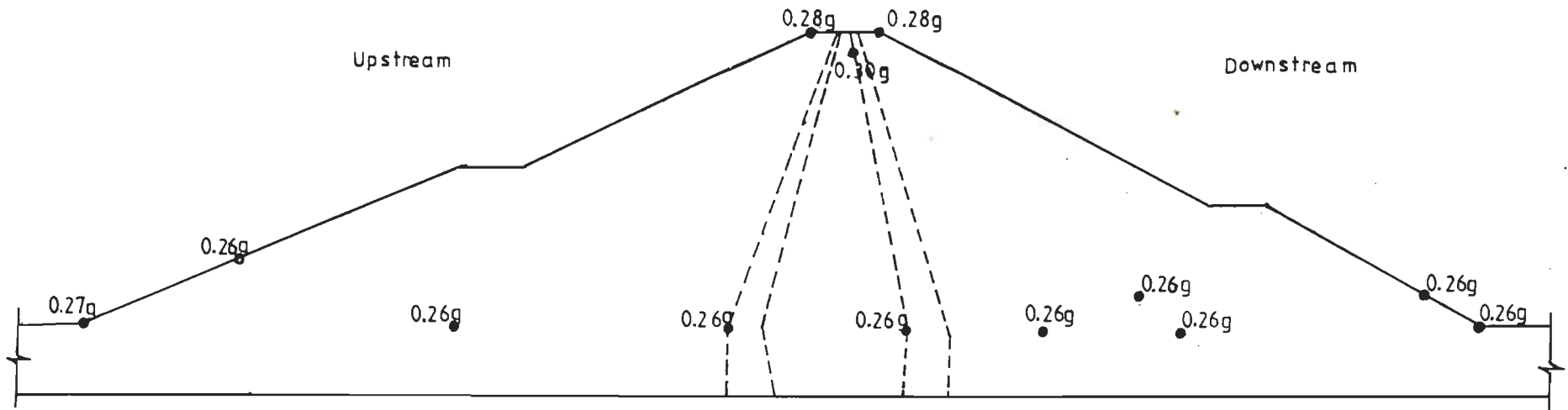


Fig. 8.41 Dam DB; Amplified Acceleration Values at a few Locations; H-D Model; GM3

8.10.4.2 Shear strain values

From the maximum values of dynamic and total shear strain shown in Tables 8.19 to 8.21 for the three methods of analysis it can be seen that the Ramberg-Osgood model yields the highest values of dynamic shear strain of the order of 0.342 percent at element 84 for the artificial accelerogram as the input motion. The dynamic shear strain values for the same ground motion by the Hardin-Drnevich model and the Seed-Idriss method are 0.308 and 0.324 percent respectively and occurring at elements 84 and 94.

In all the cases, the synthetic accelerogram yields the highest values of dynamic shear strain, followed by the Taft and the North-Eastern Region (India) earthquake records in sequence, when these three ground motions have been used as the earthquake load vectors. As far as the method of analysis is concerned, as before, the Ramberg-Osgood model gives the highest values of shear strain and the Hardin-Drnevich model gives the lowest values and the Seed-Idriss method yields intermediate values corresponding to the North-Eastern (GM1), synthetic (GM2) and the Taft (GM3) earthquake records respectively. For the Taft accelerogram, the Hardin-Drnevich model gives higher values of shear strain than the values obtained by the Seed-Idriss method at elements 84 to 87.

At all elevations, for all the three ground motions and the three methods of analysis, the value of

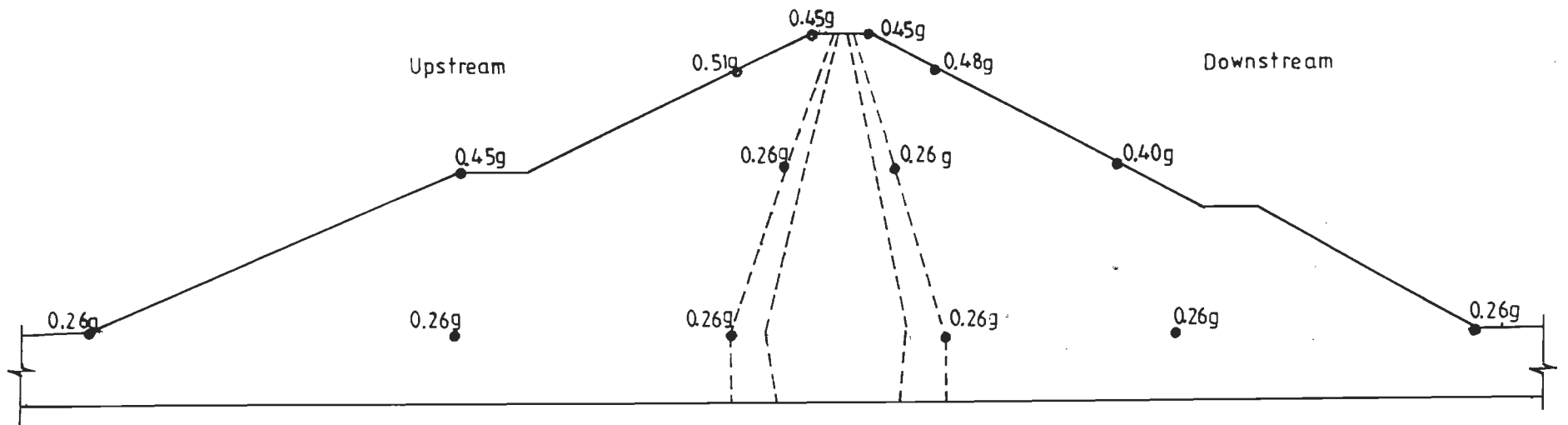


Fig. 8.42 Dam DB; Amplified Acceleration Values at a few Locations; S-I Method; GM1

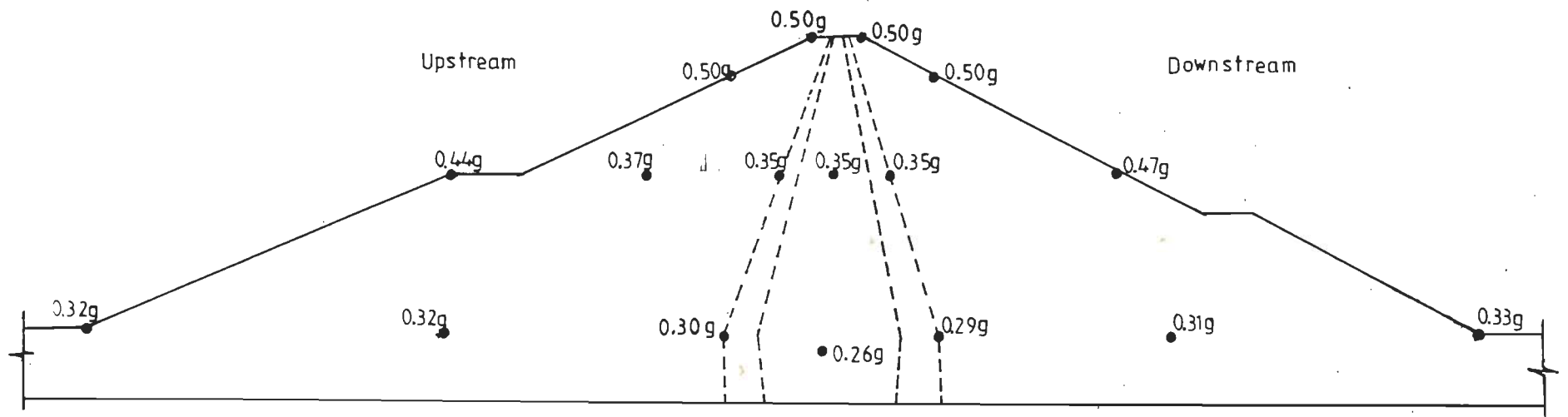


Fig. 8.43 Dam DB; Amplified Acceleration Values at a few Locations; S-I Method; GM2

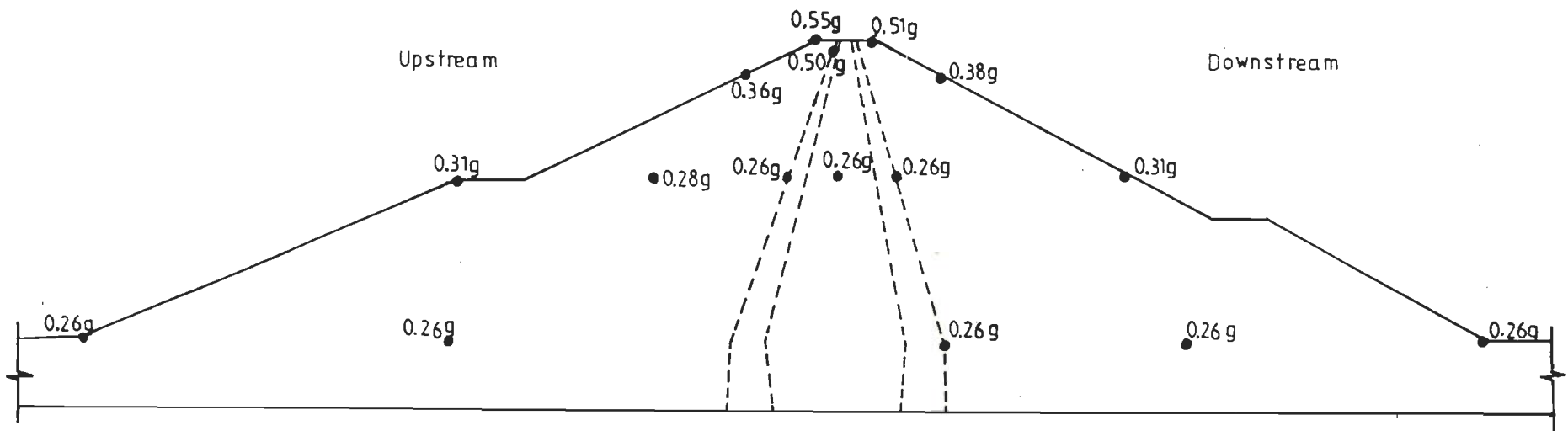


Fig. 8.44 Dam DB; Amplified Acceleration Values at a few Locations; S-I Method; GM3

dynamic shear strain is larger in the upstream filter and decreases in the core and again increases in the downstream filter zone. This behaviour is because the filter zones in the upstream and the downstream consists of relatively less stiff materials in comparison to the adjacent shell and core materials.

The total values of shear strain for the Ramberg-Osgood model are of the order of 1.875, 2.042 and 1.942 percent occurring at element number 84, and for the Hardin-Drnevich model, these values are of the order of 1.840, 2.008 and 1.901 percent occurring at the same location and for the Seed-Idriss method, the total values of shear strain are 1.854, 1.978 and 1.852 percent occurring at element 94.

In general, the lowest values of total shear strain (less than 2.1 percent) obtained in the analysis of the dam DB could perhaps, be due to the nonavailability of the actual material properties. Keeping the 5 percent shear strain limit as the failure phenomenon, no portion of the dam DB attains the threshold level of failure. The analysis results show that the dam DB is safe against the postulated three ground motions with the peak ground acceleration value of 0.25g.

Since the dam DB did not show any portion undergoing excessive deformation under the postulated earthquake motions with peak ground acceleration value of 0.25g, the shear strain values have been computed from an analysis based on the artificial accelerogram modified to yield a peak

ground acceleration value of 0.40g as the base motion. In the revised dynamic analysis only the Ramberg-Osgood model has been used. The static, dynamic and the total values of shear strain obtained in this analysis are shown in Table 8.22. The maximum value of dynamic shear strain and total shear strain are of the order of 3.680 and 5.380 percent and occurring at element 84.

It is seen from Table 8.22 that the highest value of total shear strain is 5.380 (occurring at element 84) percent indicating that the dam DB is safe against the postulated earthquake as well with the intensity of 0.40g as the peak ground acceleration. As before, this conclusion is qualitative only due to the non-availability of laboratory tested cyclic shear stress values.

8.10.4.3 Displacement

From the displacement values of the crest (node 109) corresponding to the top of the axis shown in Table 8.23, it can be seen that all the three methods of analysis give the maximum values of displacement when the synthetic accelerogram was adopted as the base input motion. These values are of the order of 12.27, 8.43 and 17.43 cm corresponding to the Ramberg-Osgood model, Hardin-Drnevich model and the Seed-Idriss method respectively. The lowest values of displacement are noticed corresponding to the

Table 8.23 Displacement at the Crest
Dam DB; PGA = 0.25g

Sl. No.	Crest Displacement (cm)			Method of Analysis
	Applied Ground Motion			
	GM1	GM2	GM3	
(1)	(2)	(3)	(4)	(5)
1	7.10	12.27	10.59	Ramberg-Osgood Model
2	4.11	8.42	6.57	Hardin-Drnevich Model
3	9.83	17.43	11.72	Seed-Idriss Method

North-Eastern Region (India) earthquake record and the Taft accelerogram yields displacement values which are intermediate in nature.

The deformed shape of the dam DB subjected to the three ground motions, using the Ramberg-Osgood model are shown in Figs. 8.45 to 8.47. For the Hardin-Drnevich model and the three ground motions the deformed plots are shown in Figs. 8.48 to 8.50 and using the Seed-Idriss method the deformed shape for the three ground motions are displayed in Figs. 8.51 to 8.53.

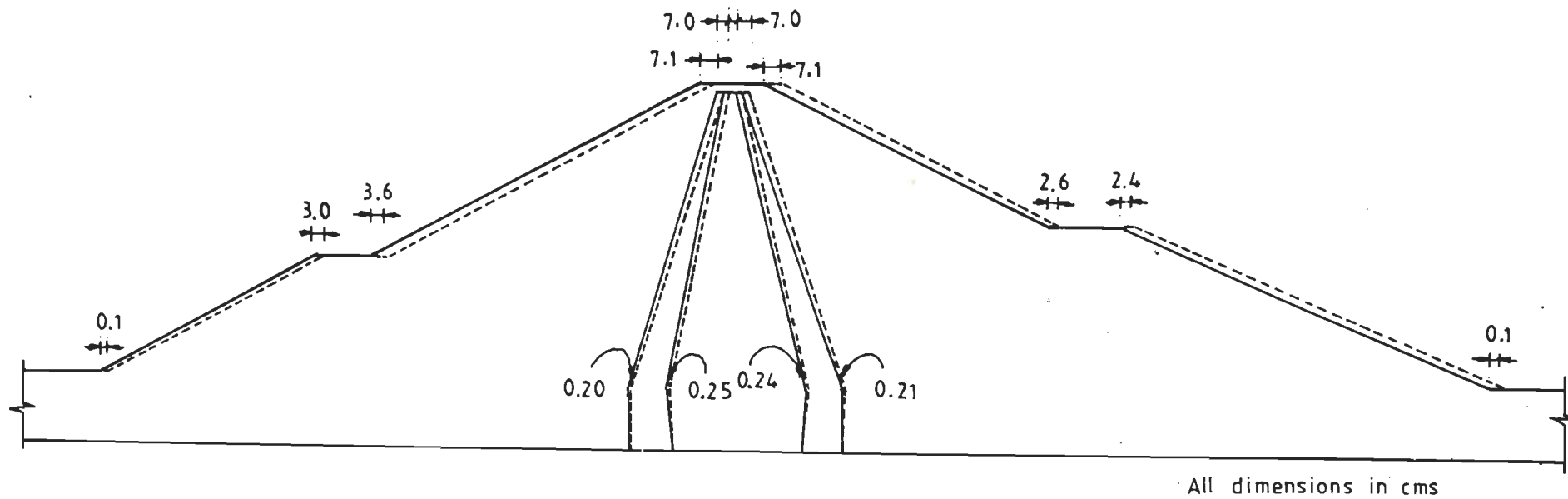


Fig. 8.45 Dam DB; Displacement Values at a few Locations; R-O Model; GM1

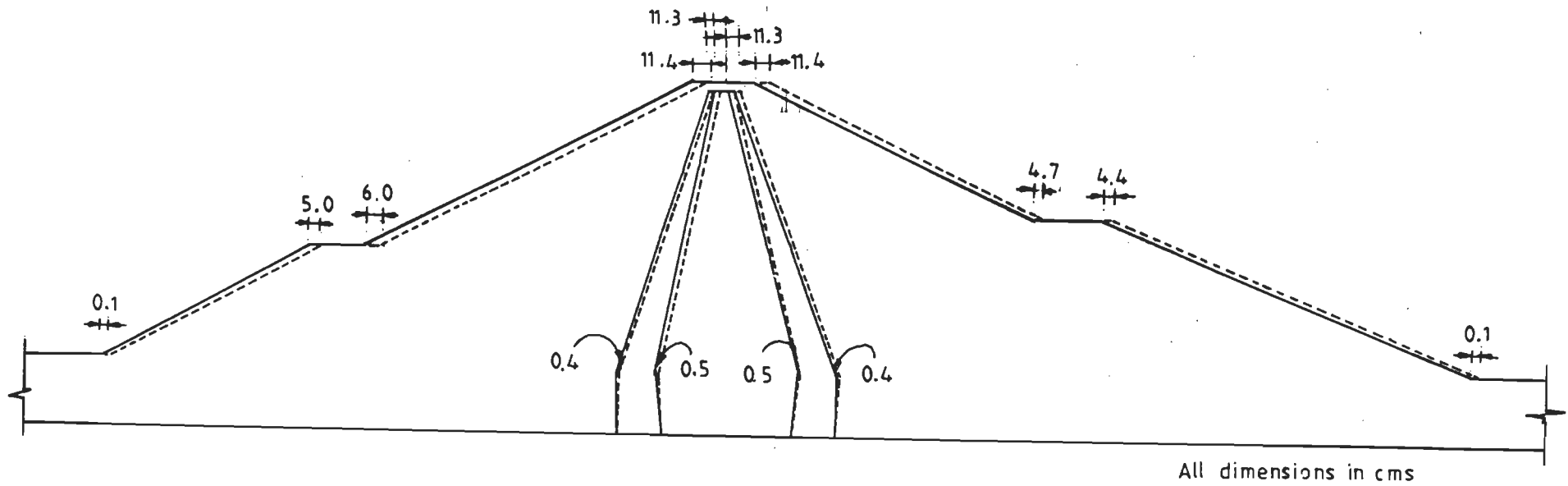


Fig. 8.46 Dam DB; Displacement Values at a few Locations; R-O Model; GM2

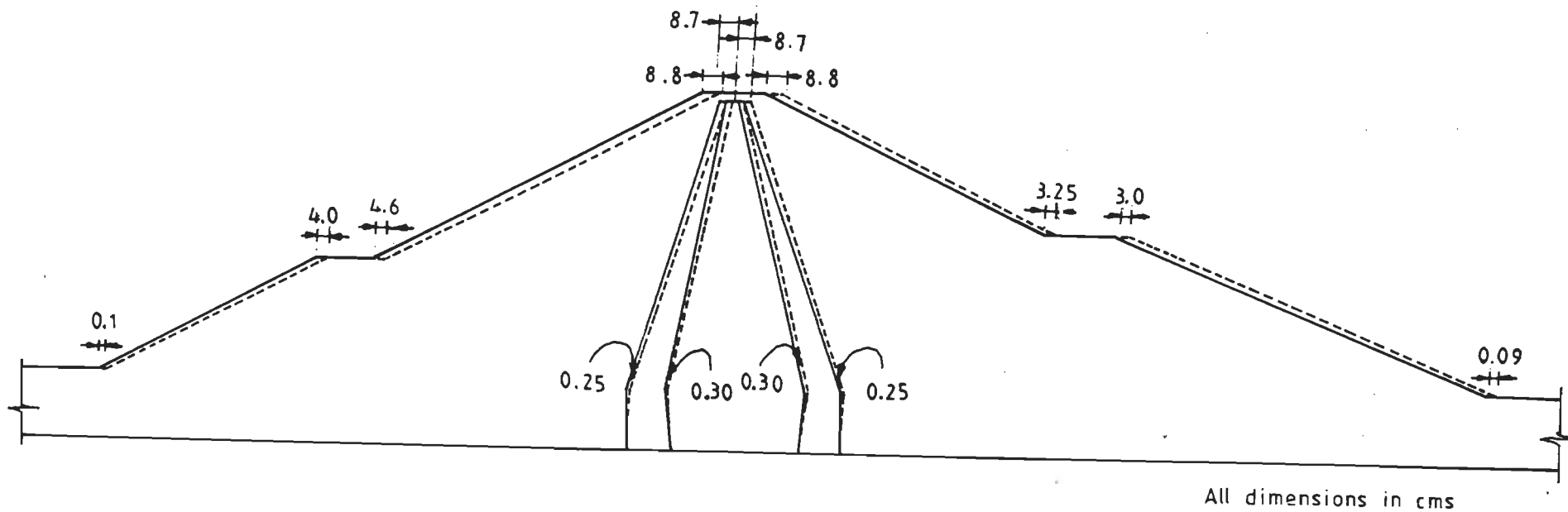


Fig. 8.47 Dam DB; Displacement Values at a few Locations; R-O Model; GM3

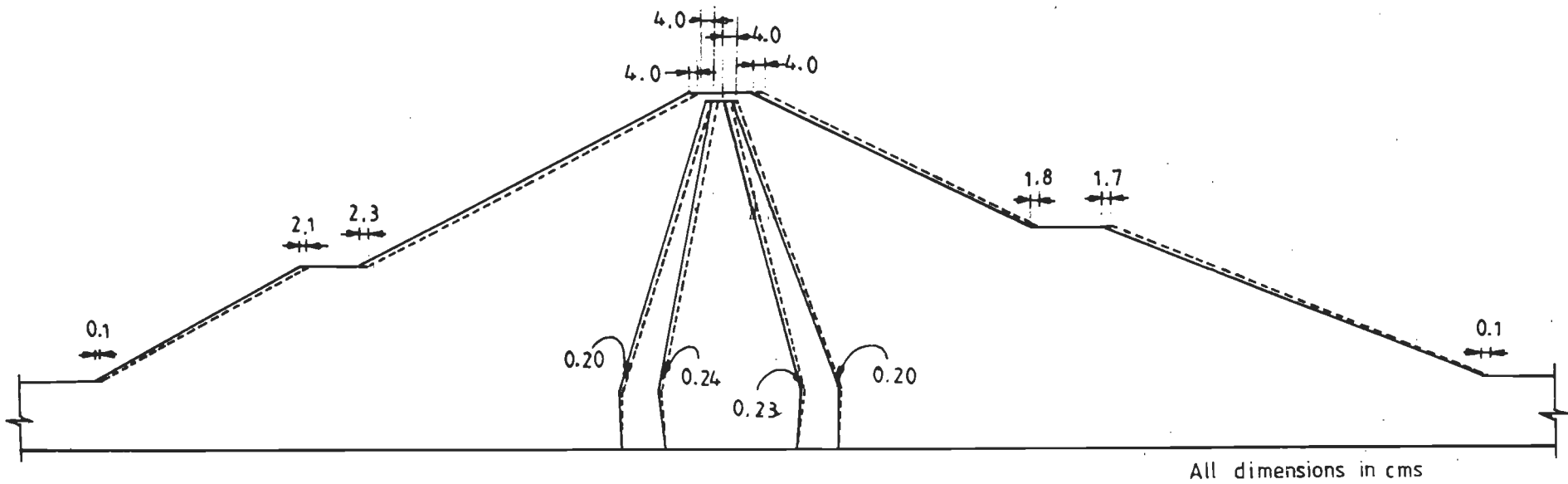


Fig. 8.48 Dam DB; Displacement Values at a few Locations; H-D Model; GM1

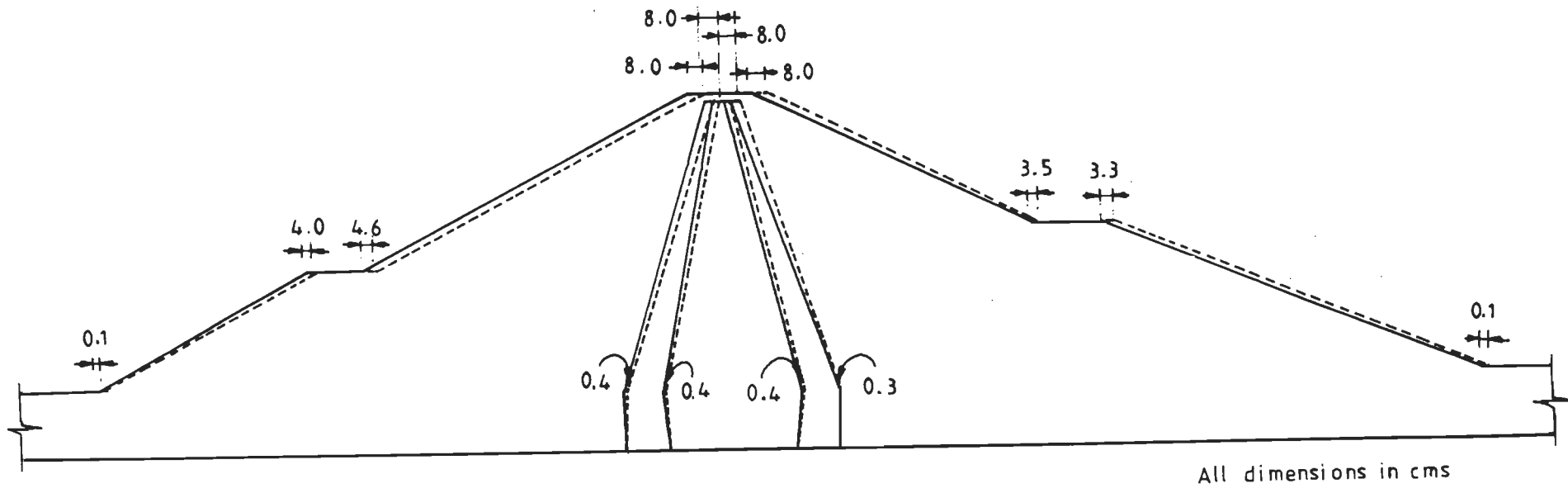


Fig. 8.49 Dam DB; Displacement Values at a few Locations; H-D Model; GM2

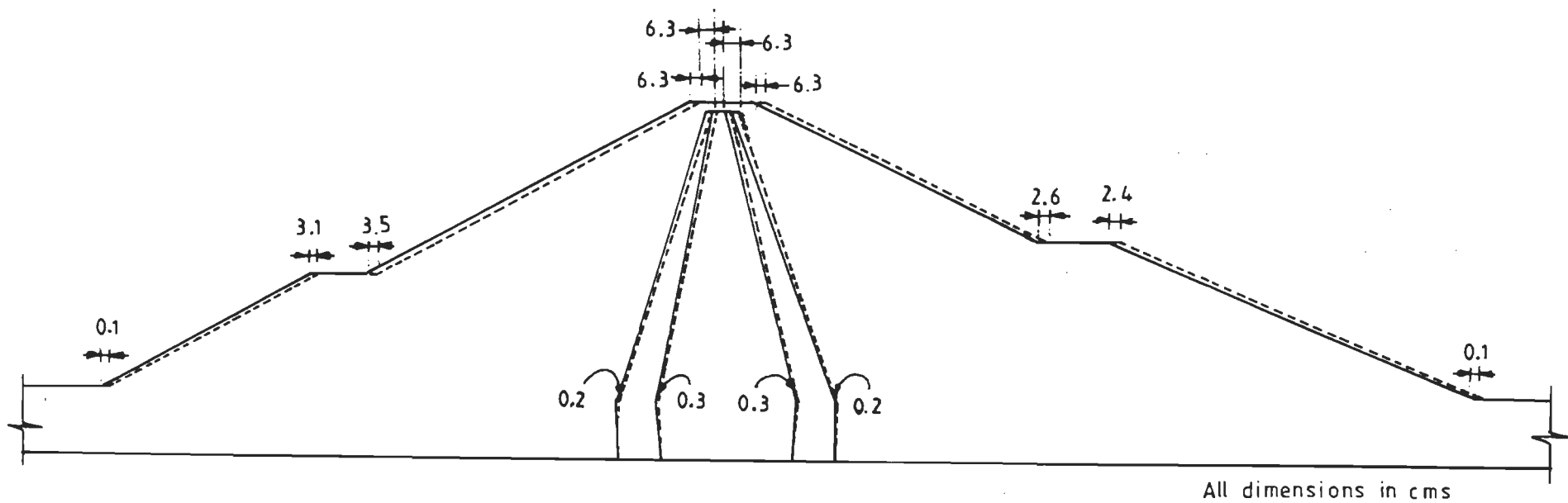


Fig. 8.50 Dam DB; Displacement Values at a few Locations; H-D Model; GM3

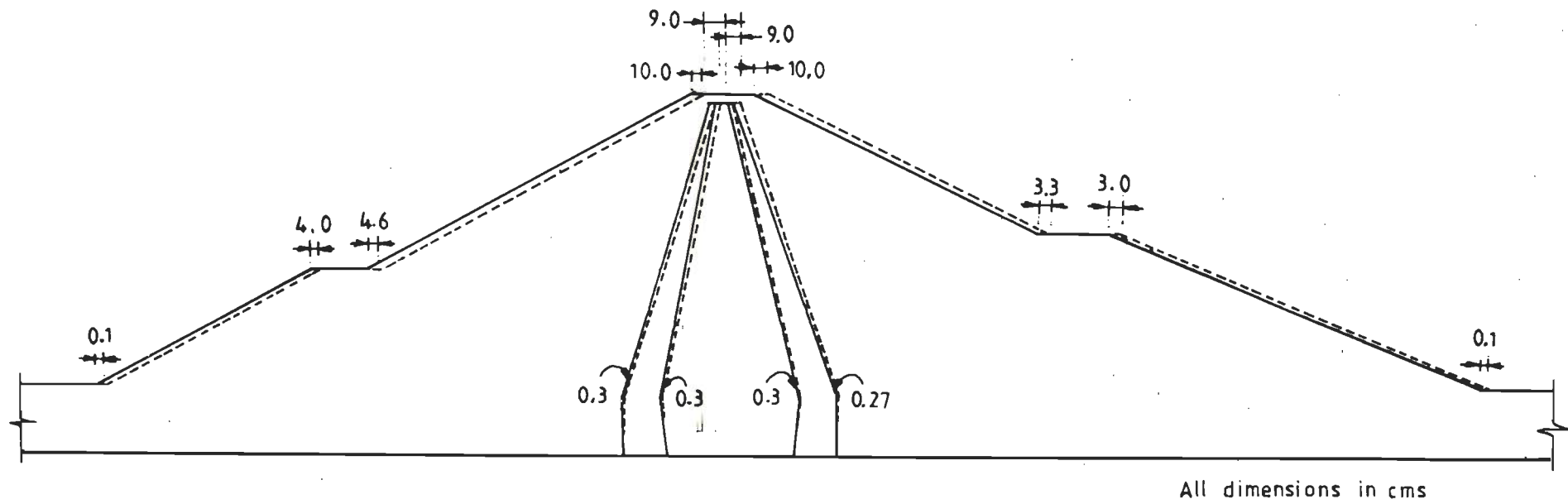


Fig. 8.51 Dam DB; Displacement Values at a few Locations; S-I Method; GM1

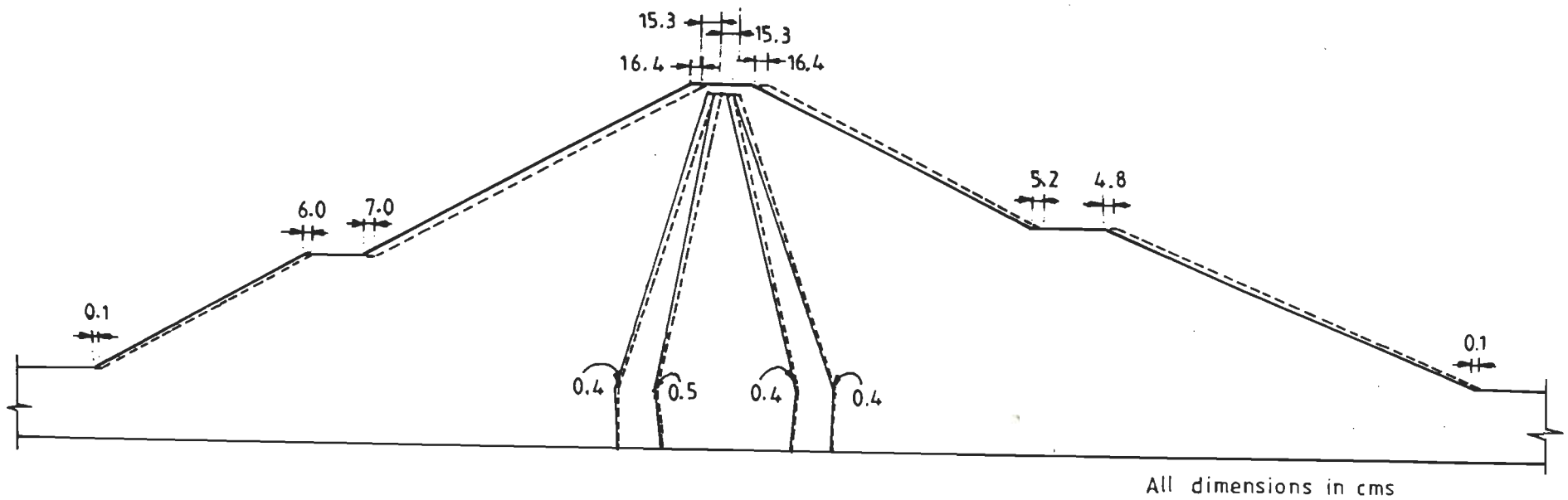


Fig. 8.52 Dam DB; Displacement Values at a few Locations; S-I Method; GM2

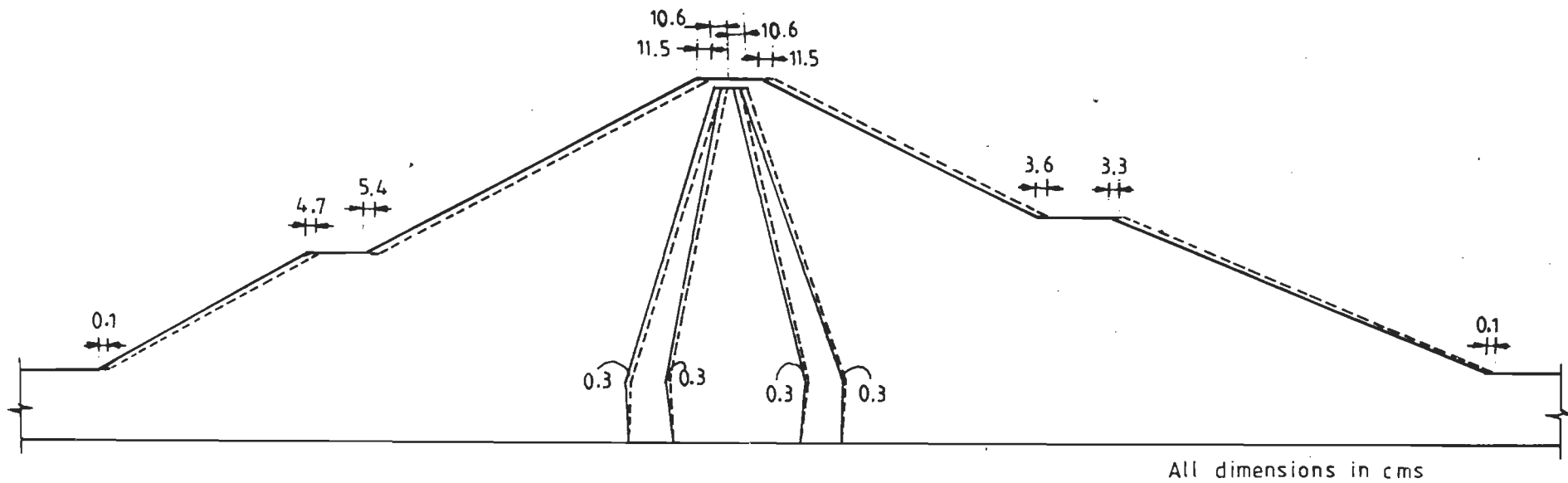


Fig. 8.53 Dam DB; Displacement Values at a few Locations; S-I Method; GM3

8.10.5 Comments on the Analysis of Dam DB

From the dynamic analysis of the 108 m high dam, including its foundation which is of medium height category, based on the Ramberg-Osgood and Hardin-Drnevich models and the Seed-Idriss method and the three different ground motions, the following conclusions are drawn:

- 1 The maximum value of crest acceleration is 0.42g using the Ramberg-Osgood model which is 1.68 times the peak ground acceleration. This takes place immediately below the crest corresponding to the artificial ground motion. The Hardin-Drnevich model yields a maximum value of 0.31g which is 1.24 times as the peak ground acceleration and occurs at immediately below the crest (node 218) corresponding to the artificial earthquake record as the base input motion. In the Seed-Idriss method of analysis, the maximum value of crest acceleration is of the order of 0.56g, which is 2.24 times the peak ground acceleration corresponding to the Taft ground motion. In this case also, the Hardin-Drnevich model shows deamplification to a greater extent followed by the Ramberg-Osgood model. The Seed-Idriss method shows the least degree of deamplification and higher magnitude of acceleration.
- 2 From the acceleration response obtained by the Ramberg-Osgood and Hardin-Drnevich models, the artificial waveform is more severe than the other two

actually recorded ground motions. In the case of the Seed-Idriss method of analysis, the Taft earthquake record is more stronger than the other two ground motions.

- 3 The upstream of the dam is more critical under the reservoir full condition than the downstream.
- 4 The foundation experiences more acceleration values than the centre portion of the dam along the axis.
- 5 The Ramberg-Osgood model yields the highest values of shear strain.
- 6 The Seed-Idriss method yields excessively large values of acceleration compared to the other two models.
- 7 The maximum values of the computed shear strain occur in the relatively low stiff regions such as the filter zones in the upstream and the downstream of the dam.
- 8 The very low values of shear strain obtained in all the analyses with peak ground acceleration values as 0.25g and 0.40g, could possibly be due to the non-availability of the actual dynamic properties of the different materials constituting the dam DB.
- 9 The stability of the dam DB, under the postulated base input motions with peak ground accelerations corresponding to 0.25g and 0.40g as obtained in the present study should be evaluated based on the laboratory tested cyclic shear stress values only.

8.11 ANALYSIS OF ROCKFILL DAM DC

The dynamic response evaluation of the El Infiernillo Dam by the Ramberg-Osgood model as used in the present thesis, this model has further been applied for the nonlinear dynamic analysis of a 336 m high rockfill dam (Dam DC), including its foundation. This tall dam was proposed to be constructed in India, in a region with severe seismicity. When the construction of this dam is completed, it would be one among the first ten tallest (height more than 250 metres) rockfill dams of the world.

Therefore, in view of the significant importance of this tall dam and existing literature on the dynamic analysis on such a tall dam being very meager, an extensive dynamic response analysis has been performed on dam DC, by evaluating the time-histories of acceleration and displacement at a few important nodal points and time-histories of shear stress at a few element centres using the Ramberg-Osgood model and the artificial accelerogram as the base input motion. The synthetic ground motion has been chosen because of its severity compared to the other two actually recorded ground motions. For the purpose of comparison, the time-histories of the different vectors have been obtained using the Hardin-Drnevich model and the Seed-Idriss method as well corresponding to the same input motion only. However, the maximum values of absolute acceleration at some important nodal points, the maximum shear strain values at a few element centres, the crest displacement and the deformed

shape of the dam for three base input motions using the three methods of analysis have been presented in this case as well. The static and dynamic analysis procedures adopted are same as that described in Sec. 8.10.

8.11.1 Description of Dam DC

The maximum section and other details of the dam DC, without the foundation are shown in Fig. 8.54. The height of the dam DC is 270 m and that of the foundation is 22 m. The full reservoir level is 6 m below the crest of the dam. The dam has a composite section consisting of three different groups of materials, namely, core, transition and shell. The impervious core is inclined to the vertical in the ratio of 1:0.506, in the upstream face, and surrounded by crushed and compacted cohesionless soil, filter and shell materials.

8.11.2 Nonlinear Static Analysis

As mentioned in Sec. 8.10.1, the initial static stresses have been evaluated using the hyperbolic model as proposed by Duncan et al. (1980). In the analysis twice the depth of the foundation has been included as the depth of the base rock (Duncan et al., 1980; Franklin, 1987). Thus the total depth of the foundation including the hard rock is 66 metres and the total height of the dam is 336 metres.

8.11.3 Discretization

The foundation in the upstream and the downstream

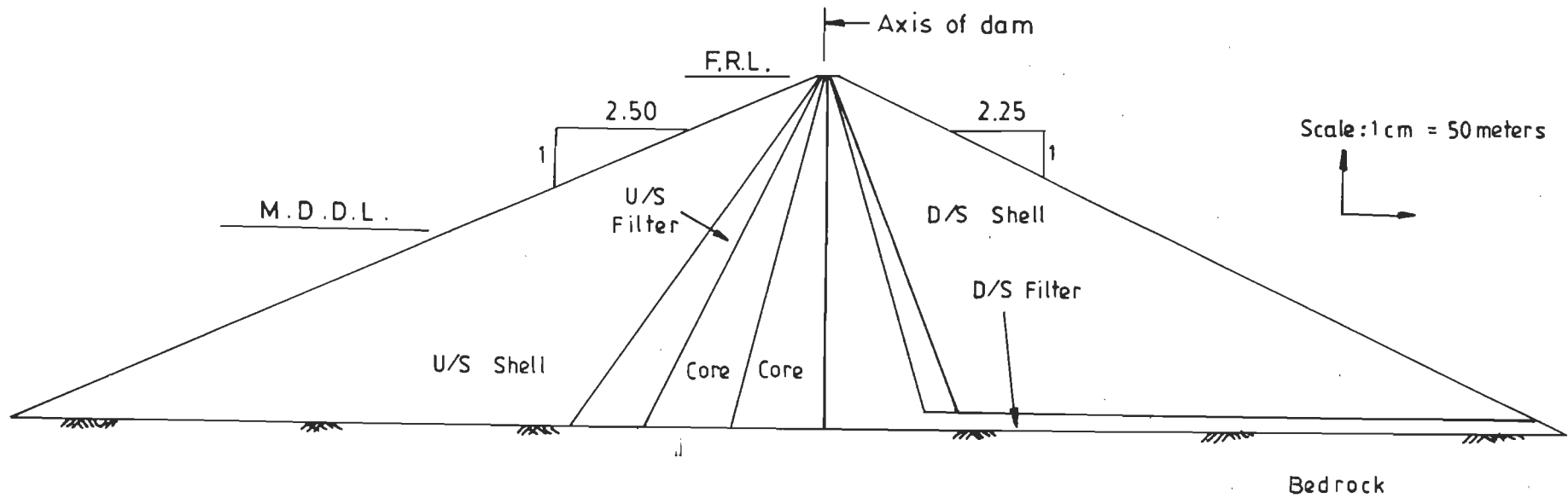


Fig. 8.54 Maximum Section of Dam DC

have been extended by one time the base width of the dam that is on the top surface of the foundation. This leads to a total width of approximately 3 km, which is three times the width of the dam at the base of the dam corresponding to the dam without the foundation.

The dam (superstructure) has been discretized into 14 horizontal layers and each layer consisting of 11 eight-noded isoparametric elements using the PREBAN subroutine described in Chapter 7. Similarly, the foundation including the hard rock has been divided into 2 horizontal layers and each layer into 31 eight-noded elements. Thus the dam and its foundation have been idealized into 154 and 62 eight-noded elements respectively. The finite element mesh adopted for the analysis is shown in Fig. 8.55 and consists of a total number of 216 eight-noded elements and 743 nodes out of which 679 nodes are the effective ones.

8.11.4 Material Properties

The different material properties and the non-linear parameters adopted for the nonlinear static analysis of the dam DC are given in Tables 8.24 and 8.25 respectively. In the upstream, submerged unit weights for shell and filter materials below the phreatic line and in the downstream for these materials, either, dry or moist unit weights have been considered. In the impervious core, saturated unit weight below the phreatic line and dry or moist unit weights above this line have been adopted. The water pressure is considered to act in the same manner as described in Sec. 8.10.1 and is

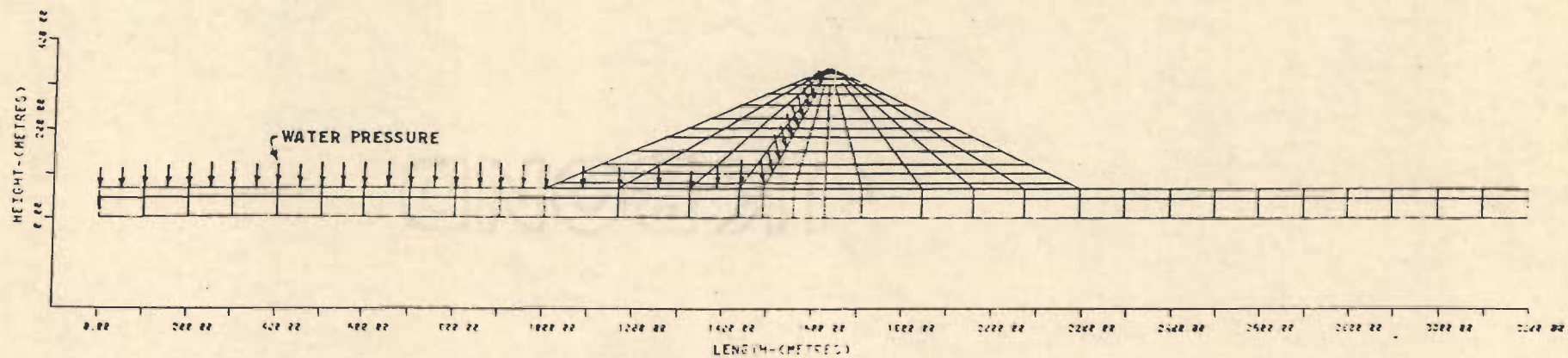


Fig. 8.55 - Finite element Idealization of Dam DC

Table 8.24 Physical Properties for Nonlinear Static Analysis

Mat. No. (1)	Description (2)	γ (t/m ³) (3)	K_0 (4)	ϕ (deg) (5)	C (t/m ²) (6)
1	U/s Shell (submerged)	1.250	0.33	42	0
2	U/s Filter (submerged)	1.100	0.36	42	0
3	Core (saturated)	1.989	0.44	30.5	5
4	D/s Filter (moist)	1.850	0.36	42	0
5	D/s Shell (moist)	2.068	0.33	42	0
6	Core (dry)	1.619	0.38	30.5	5
7	Foundation (submerged)	1.160	0.38	42	0
8	Hard rock (saturated)	2.250	0.33	44	0

Note:

γ = unit weight

K_0 = coefficient of earth pressure at rest

ϕ = angle of internal friction

C = cohesion.

Table 8.25 Nonlinear Parameters Used for the Duncan-Chang Model

Mat. No.	Description	K	n_h	R_f	$\Delta \phi$	K_b	m_h
(1)	(2)	(3)	(4)	(5)	(6)	(7)	(8)
1	U/s Shell (submerged)	3780	0.19	0.76	7	1300	0.16
2	U/s Filter (submerged)	3350	0.19	0.76	7	470	0.52
3	Core (saturated)	345	0.76	0.88	0	280	0.19
4	D/s Filter (moist)	3350	0.19	0.76	7	470	0.52
5	D/s Shell (moist)	3780	0.19	0.76	7	1300	0.16
6	Core (dry)	345	0.76	0.88	0	280	0.19
7	Foundation (submerged)	3780	0.19	0.76	7	1300	0.16
8	Hard rock (saturated)	4000	0.18	0.64	6	1400	0.22

Note:

K = modulus number

n_h = modulus exponent

R_f = failure ratio

$\Delta \phi$ = decrease in friction angle

K_b = bulk modulus number

m_h = bulk modulus exponent.

shown in Fig. 8.55. The different material type identifications used are shown in Fig. 8.56.

8.11.5 Results of Nonlinear Static Analysis

The different static stresses, such as the horizontal stress (σ_{xx}), vertical stress (σ_{yy}), shear stress (τ_{xy}), major principal stress (σ_1) and minor principal stress (σ_3) obtained from the nonlinear analysis based on the Duncan-Chang model, are displayed in the form of stress contours in Figs. 8.57 to 8.61.

The stress ratio contours between the minor principal stress (σ_3) and the major principal stress (σ_1) are also shown in Fig. 8.62. The different stress values are computed at the Gauss sampling points. The horizontal stress, vertical stress and the shear stress vectors have been stored in the computer memory for subsequent dynamic analysis.

8.11.6 Dynamic Analysis of Dam DC

The dynamic analysis of the dam DC has been carried out adopting the same procedure described in Sec. 8.10.3. The finite element mesh shown in Fig. 8.55, has been adopted for the dynamic analysis as well. The dynamic material properties, namely, the low-amplitude shear modulus and damping values have also been evaluated using the same procedure described in Sec. 8.10.3. These dynamic material properties have been used in addition to the physical

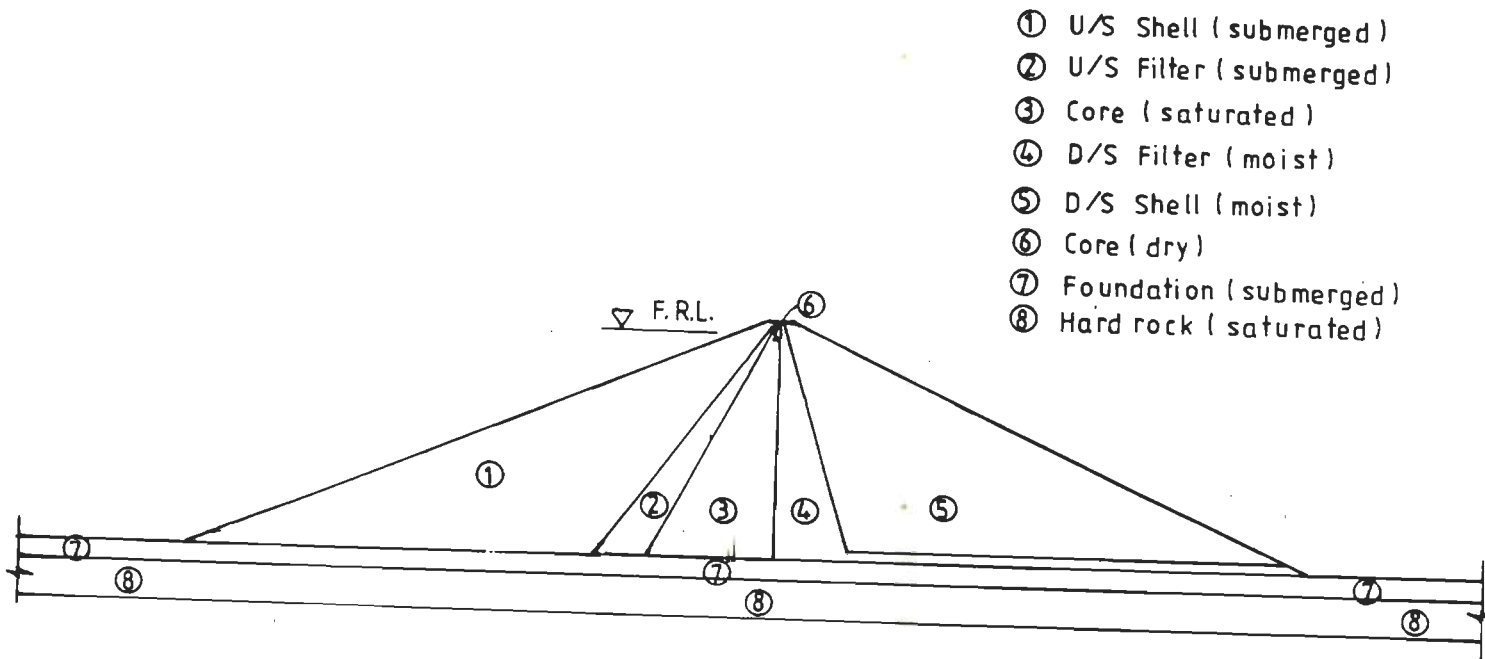


Fig. 8.56 Material Type Identification of Dam DC

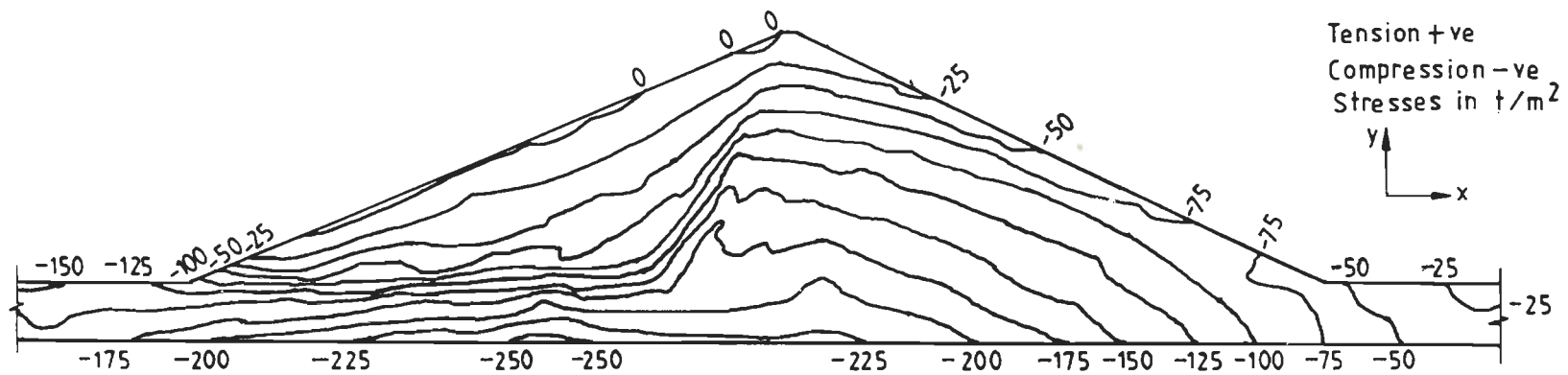


Fig. 8.57 Horizontal Stress Contours of Dam DC (Static Analysis)

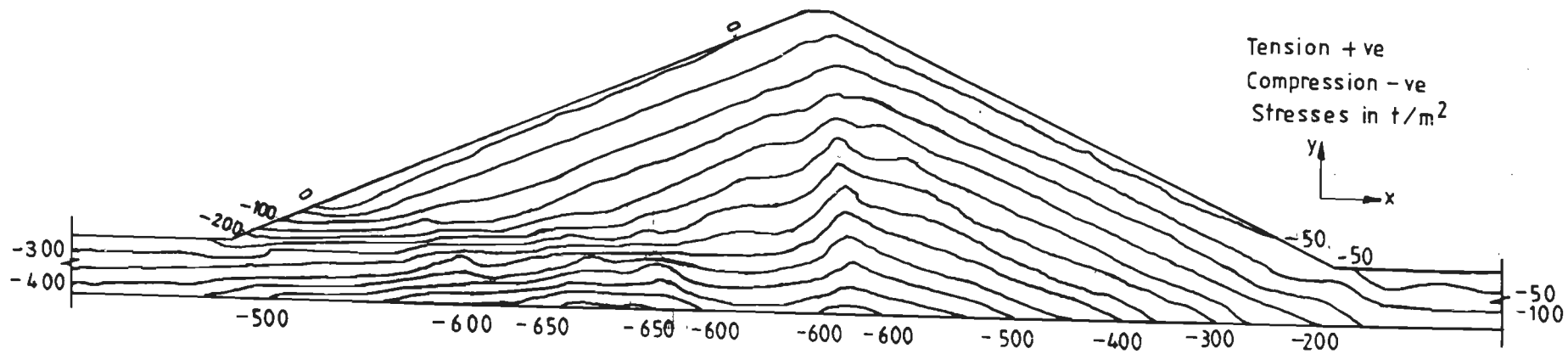


Fig. 8.58 Vertical Stress Contours of Dam DC
 (Static Analysis)

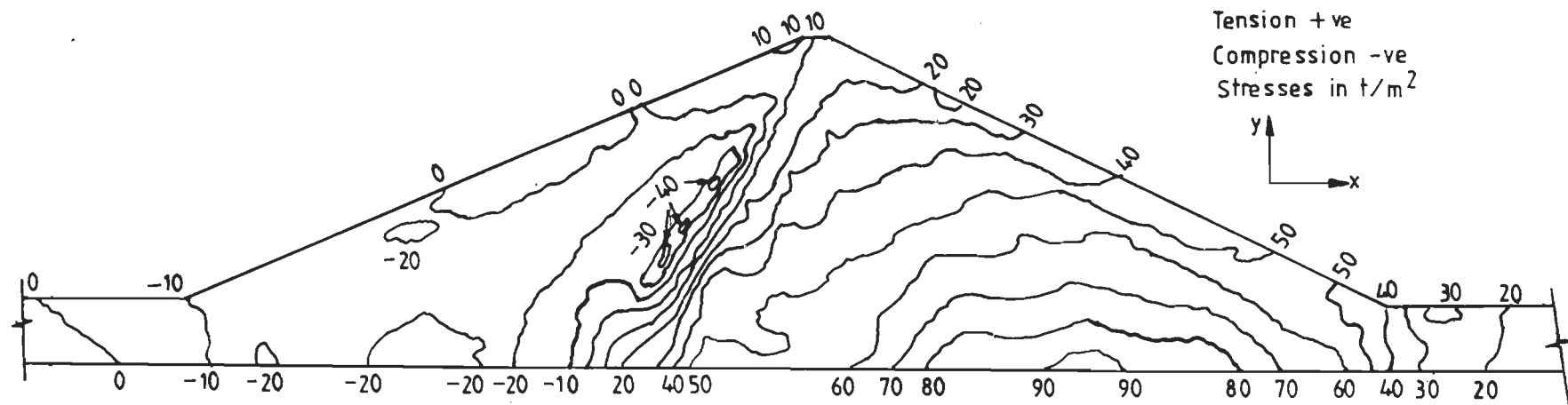


Fig. 8.59 Shear Stress Contours of Dam DC
 (Static Analysis)

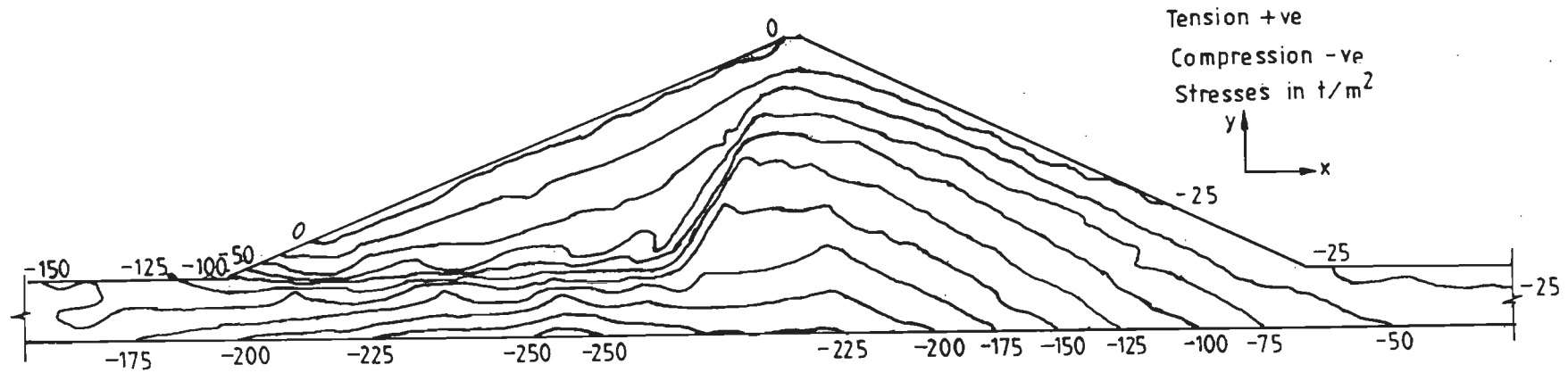


Fig. 8.60 Major Principal Stress Contours of Dam DC
(Static Analysis)

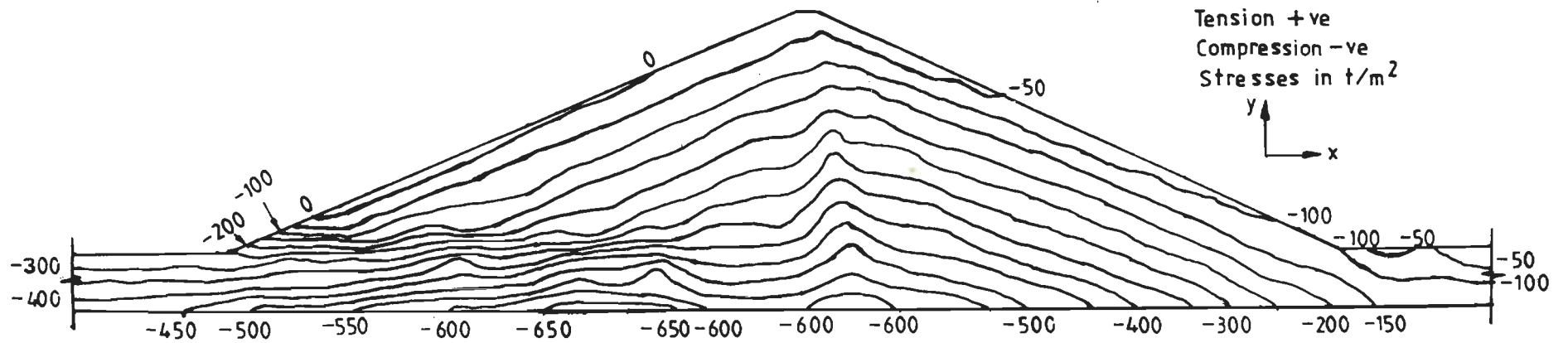


Fig. 8.61 Minor Principal Stress Contours of Dam DC
(Static Analysis)

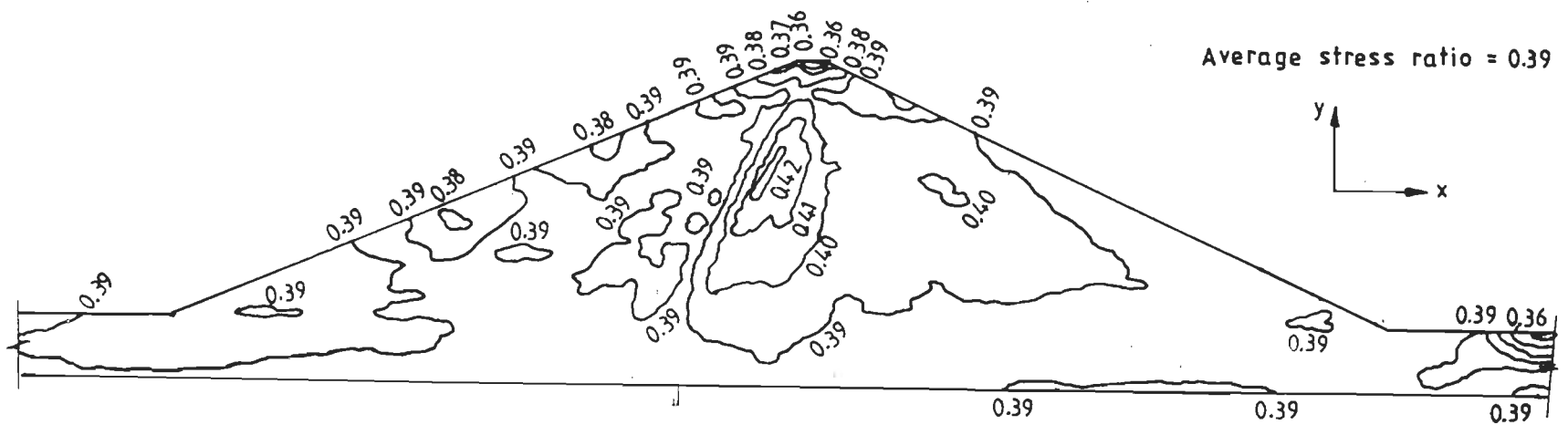


Fig. 8.62 Stress Ratio Contours of Dam DC
(Static Analysis)

properties shown in Table 8.24. As before, the dynamic analysis has been carried out using the three methods of analysis and the three ground motions as earthquake load vectors. The different ground motions have been applied at the rigid base (node 680) as the earthquake load vectors.

8.11.7 Results of Dynamic Analysis

From the dynamic analysis of the dam DC, performed using the Ramberg-Osgood model, Hardin-Drnevich model and the Seed-Idriss method, the peak acceleration values at a few selected node points as shown in Fig. 8.63 and the maximum values of shear strain at a few element centres as shown in Fig. 8.64 are evaluated. As mentioned in Sec. 8.10.4, the nodes shown in Fig. 8.63 lie in the crest, $0.75H$, $0.50H$, $0.25H$ and immediately above the base (in the foundation). Approximately, at the same locations the shear strain values have also been displayed at a few element centres. The chosen elements at each elevation correspond to critical stiffness zones, namely, across the upstream transition, the impervious core and the downstream transition.

The peak acceleration values corresponding to the nodes shown in Fig. 8.63 and the maximum shear strain values at the elements shown in Fig. 8.64, for the three methods of analysis and for the three ground motions under the postulated earthquakes with peak ground acceleration value of $0.25g$ are given in Tables 8.26 to 8.28 and Tables 8.29 to 8.31 respectively. The shear strain values obtained

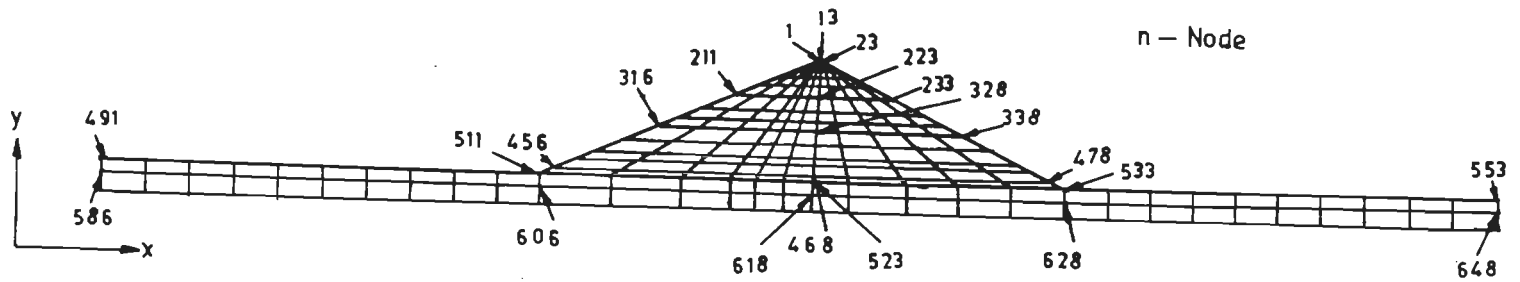


Fig. 8.63 Dam DC; Nodes at which Acceleration Values are Tabulated

Table 8.26 Maximum Acceleration Values at a few Nodes
 Ramberg-Osgood Model; Dam DC; PGA = 0.25g

Node No.	Coordinate (m)		Maximum Acceleration (g)			Location
	X	Y	Applied Ground Motion			
			GM1	GM2	GM3	
(1)	(2)	(3)	(4)	(5)	(6)	(7)
1	1619.3	336.0	0.15	0.25	0.25	U/s Crest
13	1627.2	336.0	0.15	0.25	0.25	Crest of axis
23	1634.3	336.0	0.16	0.25	0.25	D/s Crest
48	1627.2	330.0	0.17	0.33	0.32	Axis, below crest
211	1431.2	254.0	0.13	0.17	0.14	U/s 0.75H from base
223	1626.4	254.0	0.07	0.15	0.10	Axis 0.75H from base
233	1803.0	254.0	0.10	0.16	0.13	D/s 0.75H from base
316	1266.1	182.0	0.22	0.21	0.21	U/s 0.50H from base
328	1625.6	182.0	0.09	0.13	0.09	Axis 0.50H from base
338	1951.2	182.0	0.15	0.17	0.18	D/s 0.50H from base
456	1027.5	78.0	0.32	0.28	0.30	U/s 0.25H from base
468	1624.4	78.0	0.23	0.20	0.19	Axis 0.25H from base
478	2165.2	78.0	0.31	0.25	0.26	D/s 0.25H from base
491	0.0	66.0	0.25	0.25	0.25	U/s top of foundation
511	1000.0	66.0	0.30	0.32	0.31	U/s slope surface
523	1624.4	66.0	0.25	0.25	0.22	Axis, bottom of dam
533	2190.0	66.0	0.29	0.31	0.31	D/s slope surface
553	3190.0	66.0	0.25	0.25	0.25	D/s top of foundation
586	0.0	44.0	0.25	0.25	0.25	U/s top of foundation
606	1000.0	44.0	0.31	0.33	0.32	U/s extreme left
618	1624.4	44.0	0.26	0.26	0.23	Axis, bottom of dam
628	2190.0	44.0	0.30	0.32	0.31	D/s slope surface
648	3190.0	44.0	0.25	0.25	0.25	D/s top of foundation

Note:

H = Height of the dam from the base.

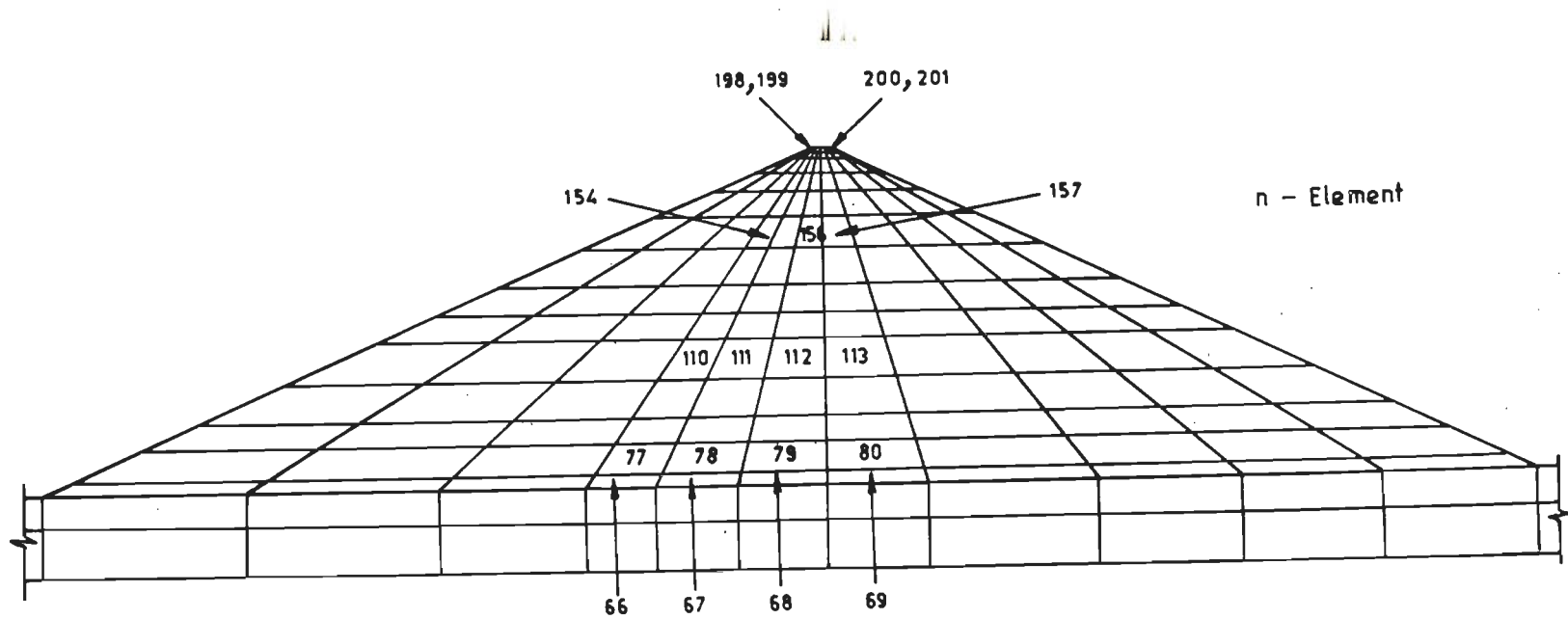


Fig. 8.64 Dam DC; Elements at which Shear Strain Values are Tabulated

Table 8.27 Maximum Acceleration Values at a few Nodes
Hardin-Drnevich Model; Dam DC; PGA = 0.25g

Node No.	Coordinate (m)		Maximum Acceleration (g)			Location
	X	Y	Applied Ground Motion			
			GM1	GM2	GM3	
(1)	(2)	(3)	(4)	(5)	(6)	(7)
1	1619.3	336.0	0.11	0.16	0.17	U/s Crest
13	1627.2	336.0	0.11	0.16	0.17	Crest of axis
23	1634.3	336.0	0.11	0.16	0.17	D/s Crest
48	1627.2	330.0	0.12	0.16	0.17	Axis, below crest
211	1431.2	254.0	0.10	0.12	0.12	U/s 0.75H from base
223	1626.4	254.0	0.06	0.12	0.08	Axis 0.75H from base
233	1803.0	254.0	0.08	0.12	0.11	D/s 0.75H from base
316	1266.1	182.0	0.18	0.16	0.17	U/s 0.50H from base
328	1625.6	182.0	0.07	0.10	0.09	Axis 0.50H from base
338	1951.2	182.0	0.12	0.14	0.14	D/s 0.50H from base
456	1027.5	78.0	0.31	0.28	0.29	U/s 0.25H from base
468	1624.4	78.0	0.23	0.20	0.18	Axis 0.25H from base
478	2165.2	78.0	0.29	0.25	0.26	D/s 0.25H from base
491	0.0	66.0	0.25	0.25	0.25	U/s top of foundation
511	1000.0	66.0	0.30	0.32	0.31	U/s slope surface
523	1624.4	66.0	0.25	0.24	0.21	Axis, bottom of dam
533	2190.0	66.0	0.30	0.31	0.30	D/s slope surface
553	3190.0	66.0	0.25	0.25	0.25	D/s top of foundation
586	0.0	44.0	0.25	0.25	0.25	U/s top of foundation
606	1000.0	44.0	0.31	0.33	0.32	U/s extreme left
618	1624.4	44.0	0.26	0.25	0.22	Axis, bottom of dam
628	2190.0	44.0	0.30	0.32	0.30	D/s slope surface
648	3190.0	44.0	0.25	0.25	0.25	D/s top of foundation

Note:

H = Height of the dam from the base.

Table 8.28 Maximum Acceleration Values at a few Nodes
Seed-Idriss Method; Dam DC; PGA = 0.25g

Node No.	Coordinate (m)		Maximum Acceleration (g)			Location
	X	Y	Applied Ground Motion			
			GM1	GM2	GM3	
(1)	(2)	(3)	(4)	(5)	(6)	(7)
1	1619.3	336.0	0.22	0.29	0.27	U/s Crest
13	1627.2	336.0	0.22	0.30	0.28	Crest of axis
23	1634.3	336.0	0.32	0.37	0.36	D/s Crest
48	1627.2	330.0	0.31	0.36	0.35	Axis, below crest
211	1431.2	254.0	0.21	0.21	0.20	U/s 0.75H from base
223	1626.4	254.0	0.20	0.25	0.24	Axis 0.75H from base
233	1803.0	254.0	0.18	0.21	0.21	D/s 0.75H from base
316	1266.1	182.0	0.31	0.25	0.27	U/s 0.50H from base
328	1625.6	182.0	0.15	0.18	0.16	Axis 0.50H from base
338	1951.2	182.0	0.24	0.21	0.24	D/s 0.50H from base
456	1027.5	78.0	0.34	0.31	0.32	U/s 0.25H from base
468	1624.4	78.0	0.22	0.24	0.21	Axis 0.25H from base
478	2165.2	78.0	0.30	0.28	0.28	D/s 0.25H from base
491	0.0	66.0	0.25	0.25	0.25	U/s top of foundation
511	1000.0	66.0	0.31	0.37	0.34	U/s slope surface
523	1624.4	66.0	0.23	0.27	0.24	Axis, bottom of dam
533	2190.0	66.0	0.30	0.34	0.34	D/s slope surface
553	3190.0	66.0	0.25	0.25	0.25	D/s top of foundation
586	0.0	44.0	0.25	0.25	0.25	U/s top of foundation
606	1000.0	44.0	0.32	0.35	0.35	U/s extreme left
618	1624.4	44.0	0.25	0.27	0.24	Axis, bottom of dam
628	2190.0	44.0	0.31	0.34	0.33	D/s slope surface
648	3190.0	44.0	0.25	0.25	0.25	D/s top of foundation

Note:

H = Height of the dam from the base.

Table 8.29 Shear Strain Values at a few Elements; Ramberg-Osgood Model
Dam DC; PGA = 0.25g

El. No.	Coordinate (m)		Shear Strain (%)						
	X	Y	Static	Dynamic			Total		
				GM1	GM2	GM3	GM1	GM2	GM3
(1)	(2)	(3)	(4)	(5)	(6)	(7)	(8)	(9)	(10)
66	1464.2	72.0	2.018	0.530	3.830	0.680	2.548	5.848	2.698
67	1523.7	72.0	1.873	0.430	3.020	0.510	2.303	4.893	2.383
68	1591.0	72.0	1.493	0.410	2.110	0.530	1.903	3.603	2.023
69	1664.7	72.0	0.907	0.400	3.210	0.500	1.307	4.117	1.407
77	1474.7	89.0	3.397	0.380	2.220	0.600	3.777	5.617	3.997
78	1530.5	89.0	1.185	0.330	2.030	0.530	1.515	3.215	1.715
79	1593.5	89.0	1.108	0.350	1.920	0.540	1.458	3.028	1.648
80	1662.5	89.0	0.795	0.320	1.940	0.508	1.115	2.735	1.303
110	1521.5	166.0	3.638	0.340	1.710	0.700	3.978	5.348	4.338
111	1560.2	166.0	0.160	0.262	1.531	0.581	0.422	1.691	0.741
112	1604.0	166.0	0.590	0.290	1.695	0.641	0.880	2.285	1.231
113	1652.0	166.0	0.441	0.240	1.410	0.543	0.681	1.851	0.984
154	1583.0	267.0	0.457	0.462	2.333	1.211	0.919	2.790	1.668
155	1599.2	267.0	0.079	0.432	1.940	1.091	0.511	2.019	1.170
156	1617.7	267.0	0.218	0.462	2.031	1.163	0.680	2.249	1.381
157	1638.5	267.0	0.155	0.384	1.520	0.932	0.539	1.675	1.087
198	1619.7	328.0	0.645	0.361	3.349	0.900	1.006	3.994	1.545
199	1622.7	328.0	1.671	0.352	8.491	3.265	2.023	10.162	4.936
200	1626.2	328.0	3.471	0.542	5.983	1.183	4.013	9.454	4.654
201	1630.2	328.0	0.307	0.331	2.912	0.891	0.638	3.219	1.198

Note:

Total strain = static + dynamic strain.

Table 8.30 Shear Strain Values at a few Elements; Hardin-Drnevich Model
Dam DC; PGA = 0.25g

El. No.	Coordinate (m)		Shear Strain (%)						
	X	Y	Static	Dynamic			Total		
				GM1	GM2	GM3	GM1	GM2	GM3
(1)	(2)	(3)	(4)	(5)	(6)	(7)	(8)	(9)	(10)
66	1464.2	72.0	2.018	1.829	2.739	2.251	3.847	4.757	4.269
67	1523.7	72.0	1.873	0.430	1.220	0.450	2.303	3.093	2.323
68	1591.0	72.0	1.493	0.300	1.160	0.450	1.793	2.653	1.943
69	1664.7	72.0	0.907	0.330	1.150	0.450	1.237	2.057	1.357
77	1474.7	89.0	3.397	0.350	1.340	0.530	3.747	4.737	3.927
78	1530.5	89.0	1.185	0.290	1.190	0.450	1.475	2.375	1.635
79	1593.5	89.0	1.108	0.300	1.130	0.423	1.408	2.238	1.531
80	1662.5	89.0	0.795	0.300	1.100	0.430	1.095	1.895	1.225
110	1521.5	166.0	3.638	0.280	1.080	0.520	3.918	4.718	4.158
111	1560.2	166.0	0.160	0.222	0.931	0.441	0.382	1.091	0.601
112	1604.0	166.0	0.590	0.240	0.950	0.481	0.830	1.540	1.071
113	1652.0	166.0	0.441	0.210	0.760	0.433	0.651	1.201	0.874
154	1583.0	267.0	0.457	0.292	1.113	0.731	0.749	1.570	1.188
155	1599.2	267.0	0.079	0.262	0.930	0.631	0.341	1.009	0.710
156	1617.7	267.0	0.218	0.272	0.951	0.643	0.490	1.169	0.861
157	1638.5	267.0	0.155	0.234	0.761	0.532	0.389	0.916	0.687
198	1619.7	328.0	0.645	0.233	0.591	0.601	0.878	1.236	1.246
199	1622.7	328.0	1.671	0.292	0.747	0.743	1.963	2.418	2.414
200	1626.2	328.0	3.471	0.282	0.653	0.653	3.753	4.124	4.124
201	1630.2	328.0	0.307	0.223	0.522	0.520	0.530	0.829	0.827

Note:

Total strain = static + dynamic strain.

Table 8.31 Shear Strain Values at a few Elements; Seed-Idriss Method
Dam DC; PGA = 0.25g

El. No.	Coordinate (m)		Shear Strain (%)						
	X	Y	Static	Dynamic			Total		
				GM1	GM2	GM3	GM1	GM2	GM3
(1)	(2)	(3)	(4)	(5)	(6)	(7)	(8)	(9)	(10)
66	1464.2	72.0	2.018	0.760	1.820	1.060	2.778	3.838	3.078
67	1523.7	72.0	1.873	0.480	1.400	0.670	2.353	3.273	2.543
68	1591.0	72.0	1.493	0.480	1.500	0.770	1.973	2.993	2.263
69	1664.7	72.0	0.907	0.336	1.400	0.700	1.237	2.307	1.607
77	1474.7	89.0	3.397	0.530	1.310	0.680	3.927	4.707	4.077
78	1530.5	89.0	1.185	0.480	1.230	0.640	1.665	2.415	1.825
79	1593.5	89.0	1.108	0.480	1.210	0.610	1.568	2.318	1.718
80	1662.5	89.0	0.795	0.380	1.060	0.590	1.175	1.855	1.385
110	1521.5	166.0	3.638	0.560	1.180	0.980	4.198	4.838	4.618
111	1560.2	166.0	0.160	0.522	0.951	0.751	0.682	1.111	0.911
112	1604.0	166.0	0.580	0.510	1.100	0.881	1.100	1.690	1.471
113	1652.0	166.0	0.441	0.450	0.760	0.591	0.891	1.201	0.914
154	1583.0	267.0	0.457	0.652	2.521	1.111	1.109	2.078	1.568
155	1599.2	267.0	0.079	1.000	2.360	1.381	1.079	2.439	1.160
156	1617.7	267.0	0.218	1.282	2.283	1.071	1.470	2.501	1.389
157	1638.5	267.0	0.155	0.544	1.150	1.062	0.699	1.405	0.917
198	1619.7	328.0	0.645	1.381	3.031	0.275	2.026	4.456	0.920
199	1622.7	328.0	1.671	2.712	6.147	3.067	4.383	7.808	4.738
200	1626.2	328.0	3.471	2.602	5.513	1.123	6.073	8.984	4.592
201	1630.2	328.0	0.307	1.323	2.822	0.251	1.620	3.139	0.756

Note:

Total strain = static + dynamic strain

corresponding to the artificial accelerogram with a peak ground acceleration value of 0.40g using the Ramberg-Osgood model are presented in Table 8.32. The locations at which the peak acceleration values and the shear strain values are displayed in Tables 8.26 to 8.31 have been chosen at specific locations as mentioned in Secs. 8.9 and 8.10. The crest displacement for the three ground motions are given in Table 8.33.

Further, at a few important nodal points along the axis of the dam DC, as shown in Fig. 8.65, the time-histories of acceleration and displacement in the horizontal and vertical directions and the time-history of shear stress at a few element centres, as shown in Fig. 8.66 are plotted in Figs. 8.67 to 8.168 obtained by the three methods of analysis. In the time-history plots, only the artificial accelerogram has been used as the input motion, due to its severity over the other two actual earthquake records.

The time-histories of continuously varying shear stresses have been converted into an equivalent number of uniform cyclic stress application. This was done by taking the equivalent uniform cyclic stress equal to 65 percent of the maximum peak shear stress (Carrera et al., 1979).

8.11.8 Discussion

From the dynamic analysis of the 336 m high rock-fill dam, based on the three methods of analysis and the three ground motions as the earthquake load vectors, the

Table 8.32 Shear Strain Values at a few Elements
R-O Model; Dam DC; PGA = 0.40g; GM2

El. No.	Coordinate (m)		Shear Strain (%)		
	X (1)	Y (2)	Static (3)	Dynamic (4)	Total (5)
66	1464.2	72.0	2.018	6.216	8.234
67	1523.7	72.0	1.873	4.410	6.283
68	1591.0	72.0	1.493	4.024	5.517
69	1664.7	72.0	0.907	4.224	5.131
77	1474.7	89.0	3.397	4.750	8.147
78	1530.5	89.0	1.185	4.367	5.552
79	1593.5	89.0	1.108	4.076	5.184
80	1662.5	89.0	0.795	4.054	4.849
110	1521.5	166.0	3.638	4.079	7.717
111	1560.2	166.0	0.160	3.380	3.540
112	1604.0	166.0	0.590	3.642	4.232
113	1652.0	166.0	0.441	2.981	3.422
154	1583.0	267.0	0.457	3.694	4.151
155	1599.2	267.0	0.079	3.000	3.079
156	1617.7	267.0	0.218	3.150	3.368
157	1638.5	267.0	0.155	2.404	2.559
198	1619.7	328.0	0.645	4.324	4.969
199	1622.7	328.0	1.671	12.325	13.996
200	1626.2	328.0	3.471	11.915	15.386
201	1630.2	328.0	0.307	4.106	4.413

Note:

Total strain = static + dynamic strain.

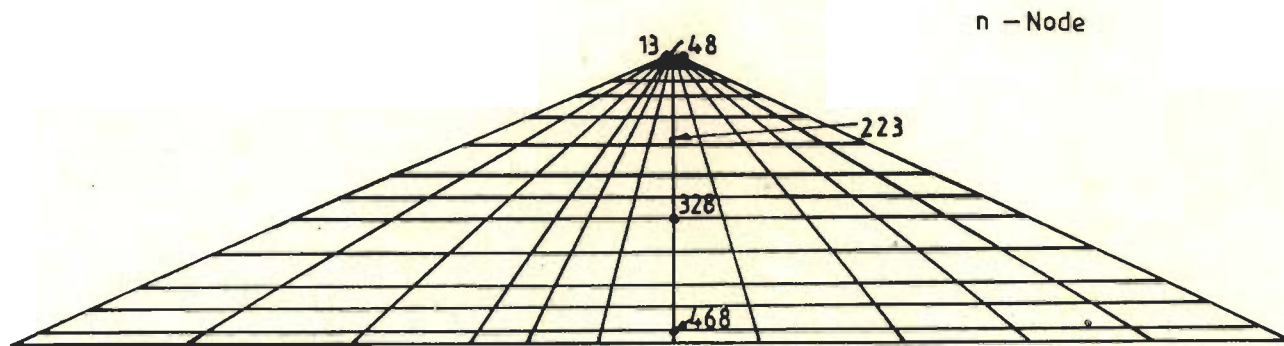


Fig. 8.65 Dam DC; Typical Nodes at which Time-Histories of Acceleration and Displacement have been Computed

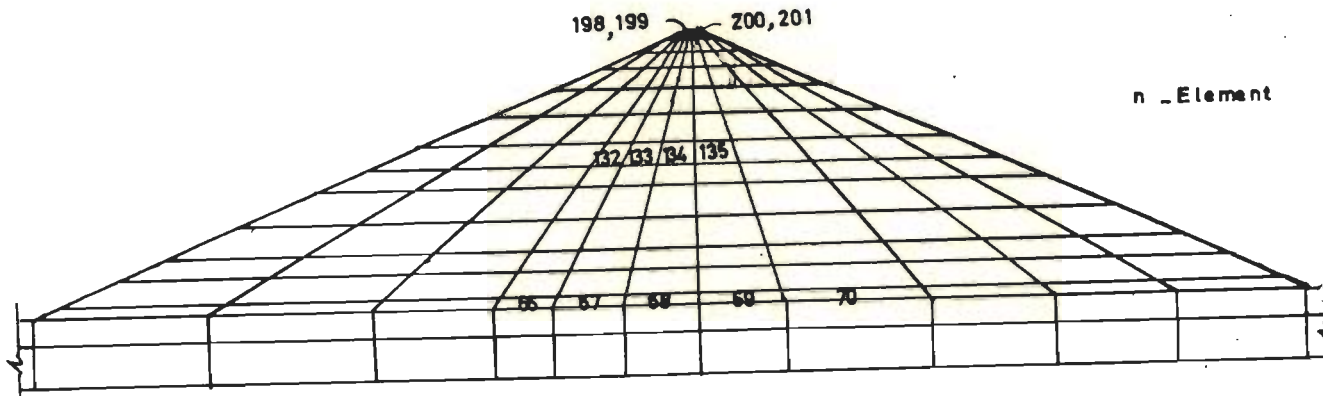


Fig. 8.66 Dam DC; Typical Elements at which Time-Histories of Shear Strain have been Computed

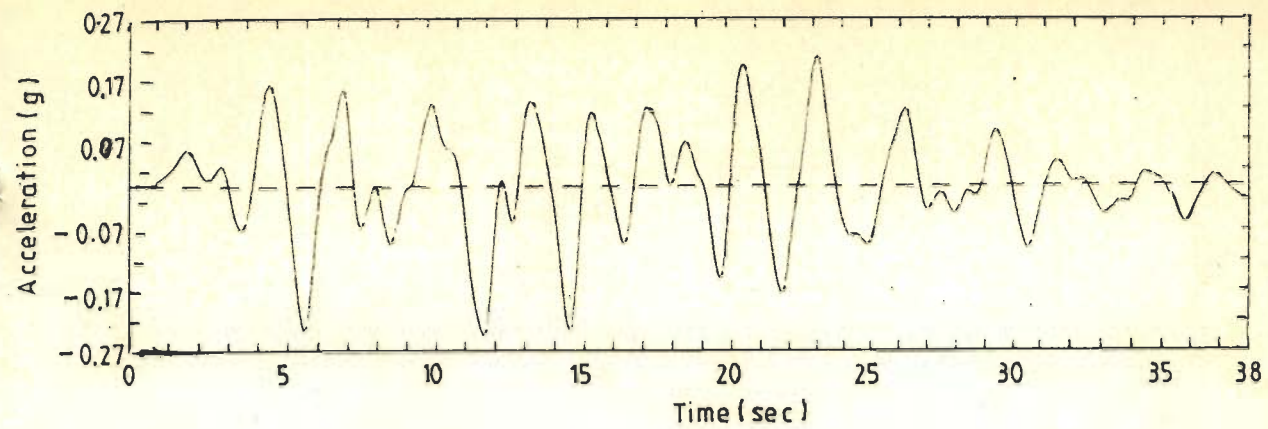


Fig. 8.67 Horizontal Acceleration Time-History at Node 13; R-O Model

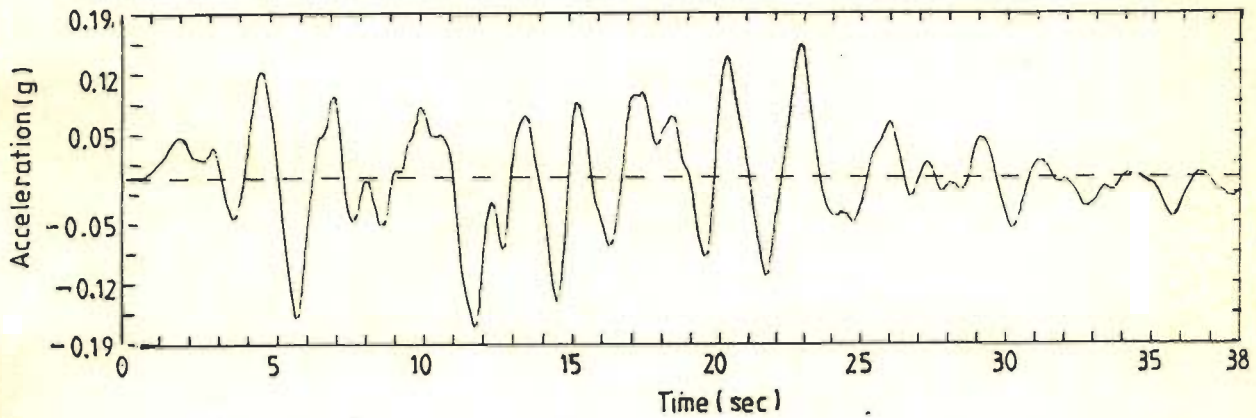


Fig. 8.68 Horizontal Acceleration Time-History at Node 13; H-D Model

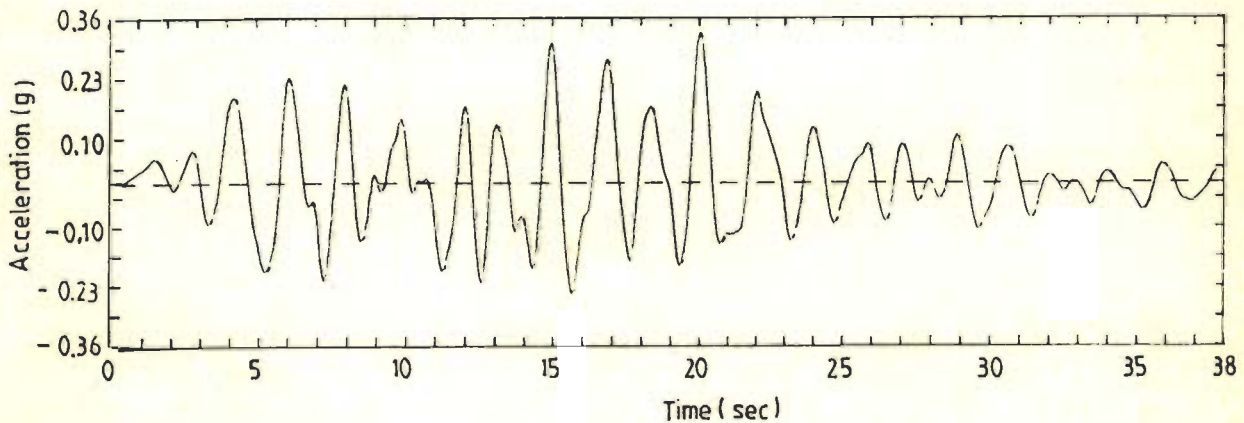


Fig. 8.69 Horizontal Acceleration Time-History at Node 13; S-I Method

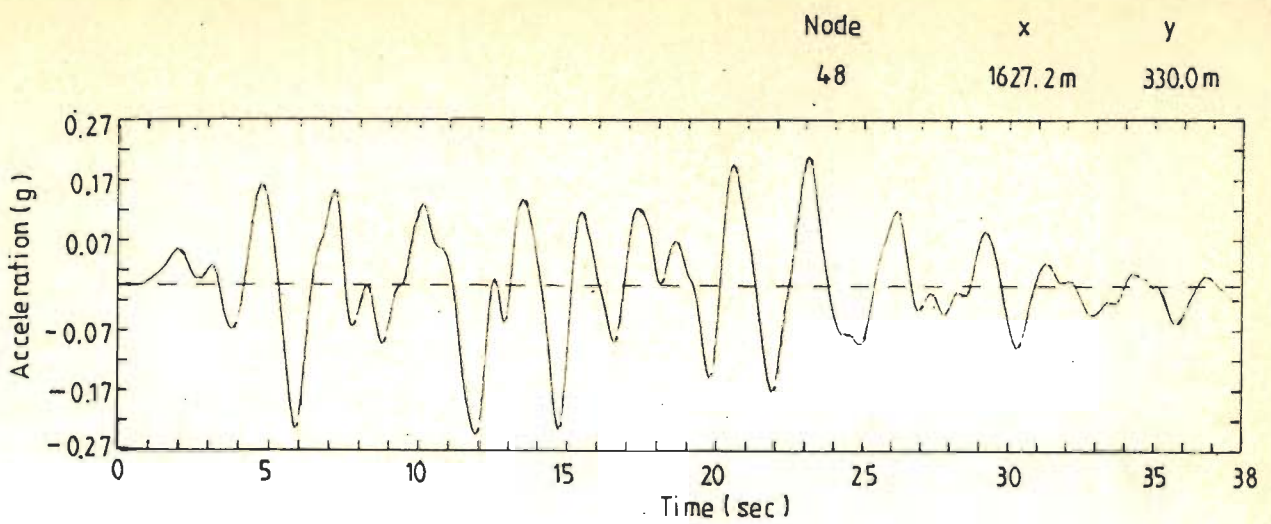


Fig. 8.70 Horizontal Acceleration Time-History at Node 48; R-O Model

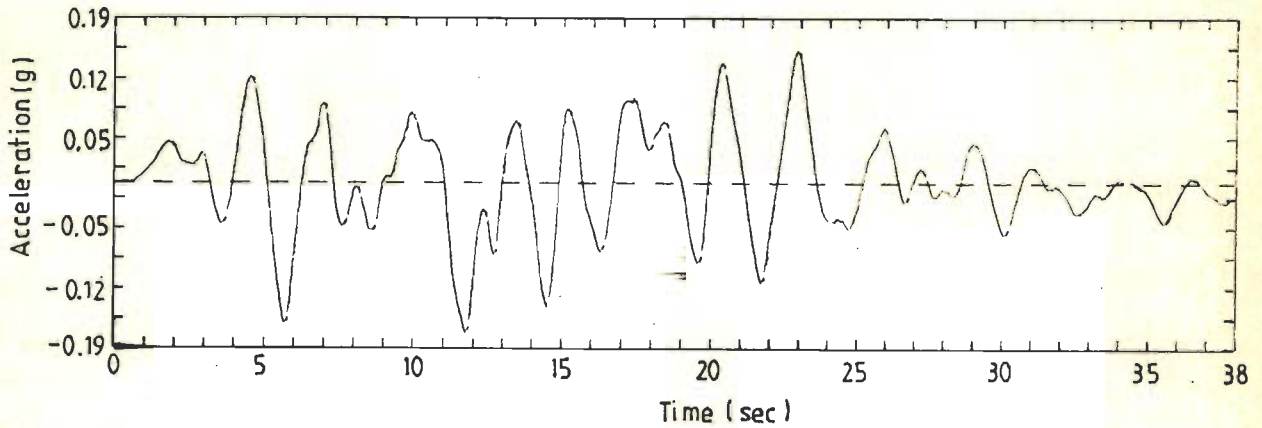


Fig. 8.71 Horizontal Acceleration Time-History at Node 48; H-D Model

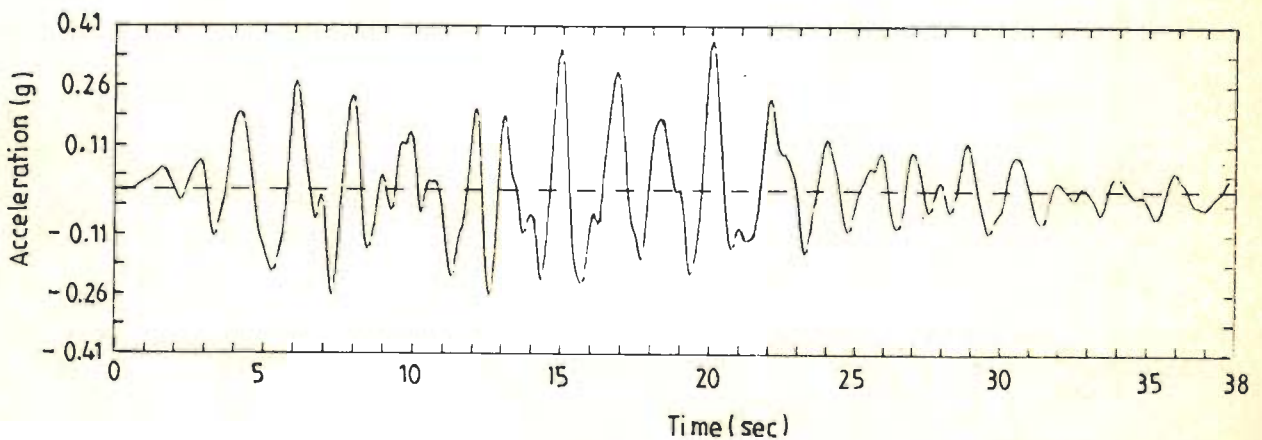


Fig. 8.72 Horizontal Acceleration Time-History at Node 48; S-I Method

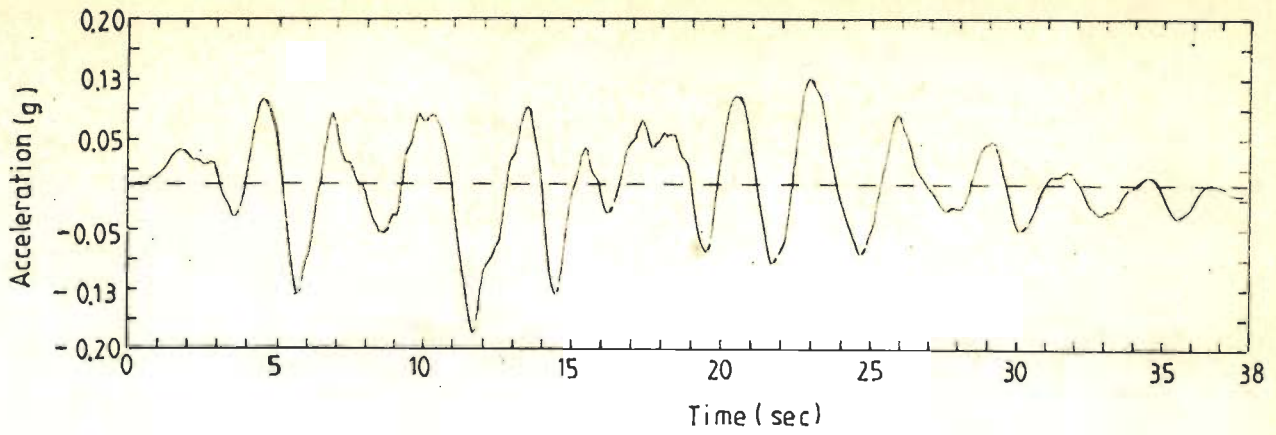


Fig. 8.73 Horizontal Acceleration Time-History at Node 223; R-O Model

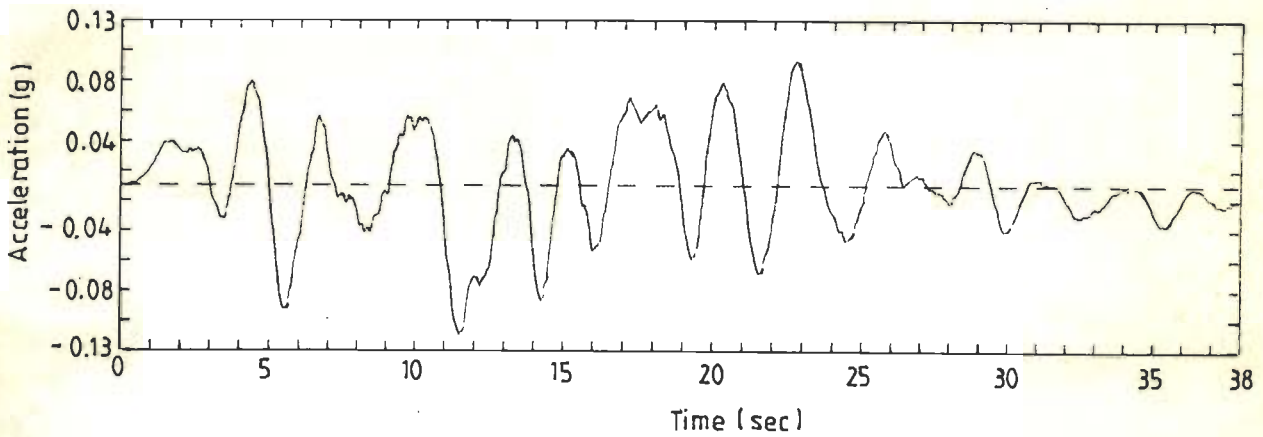


Fig. 8.74 Horizontal Acceleration Time-History at Node 223; H-D Model

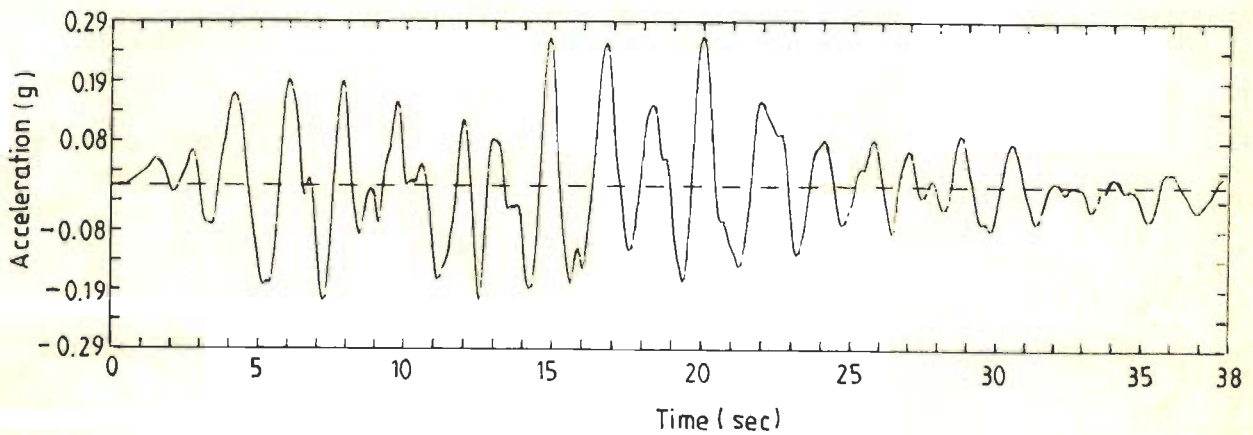


Fig. 8.75 Horizontal Acceleration Time-History at Node 223; S-I Method

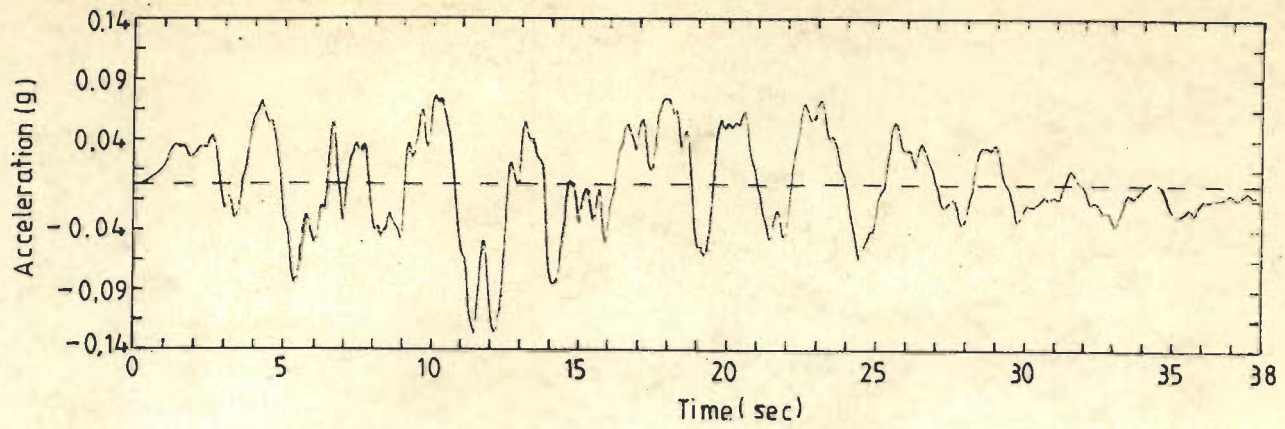


Fig. 8.76 Horizontal Acceleration Time-History at Node 328; R-O Model

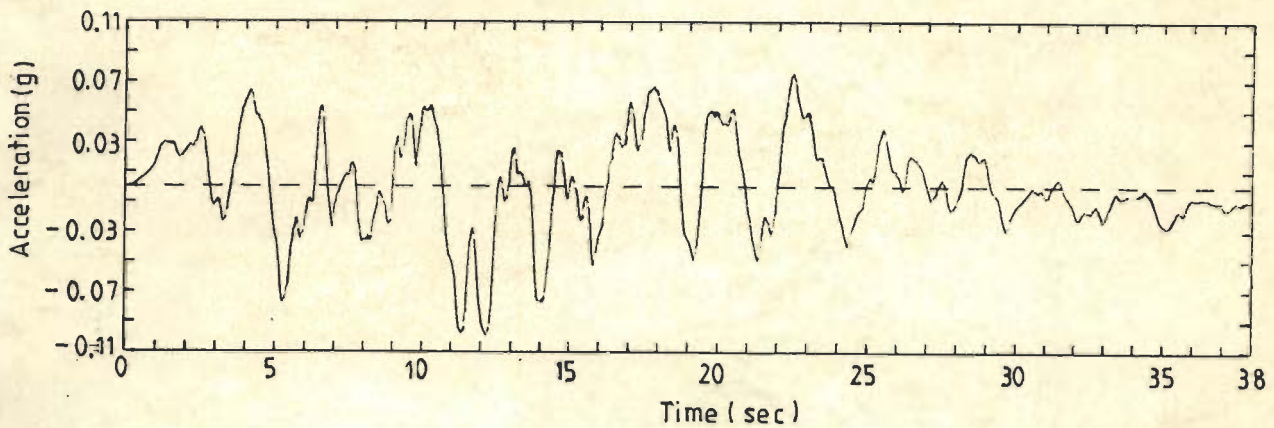


Fig. 8.77 Horizontal Acceleration Time-History at Node 328; H-D Model

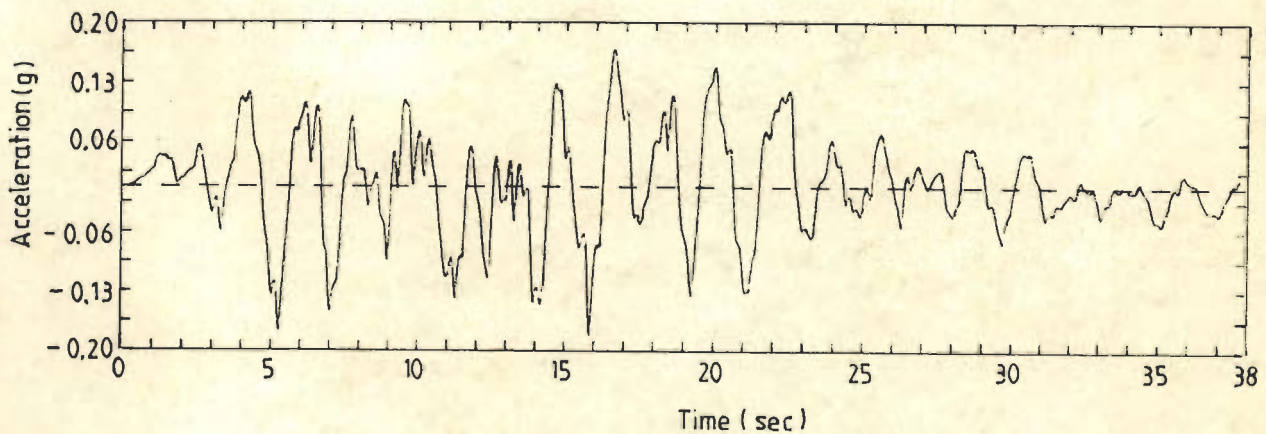


Fig. 8.78 Horizontal Acceleration Time-History at Node 328; S-I Method

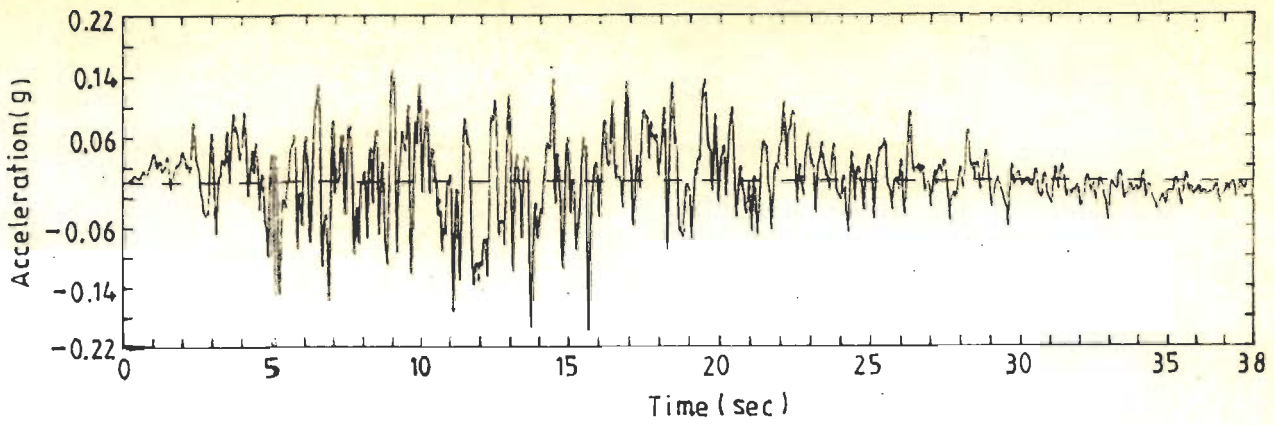


Fig. 8.79 Horizontal Acceleration Time-History at Node 468; R-O Model

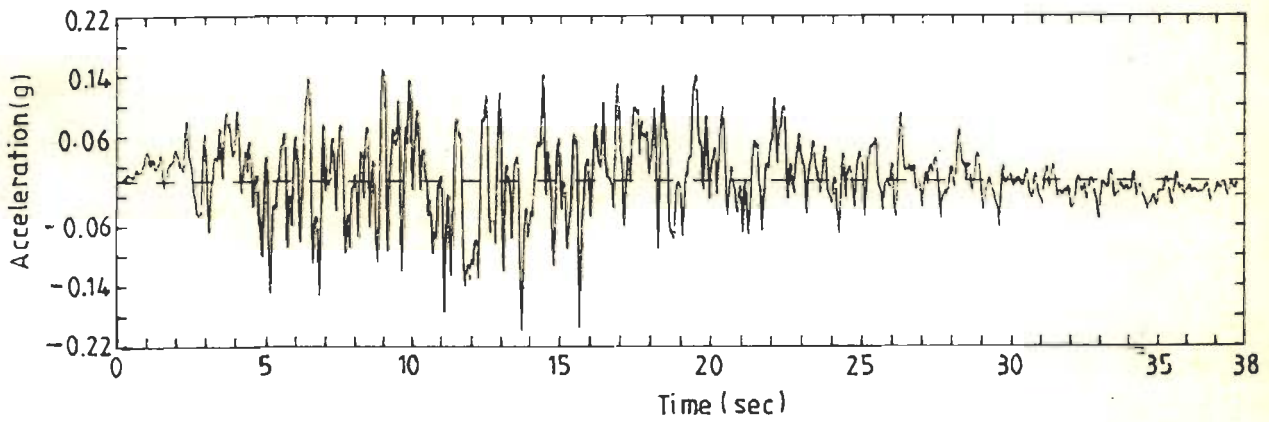


Fig. 8.80 Horizontal Acceleration Time-History at Node 468; H-D Model

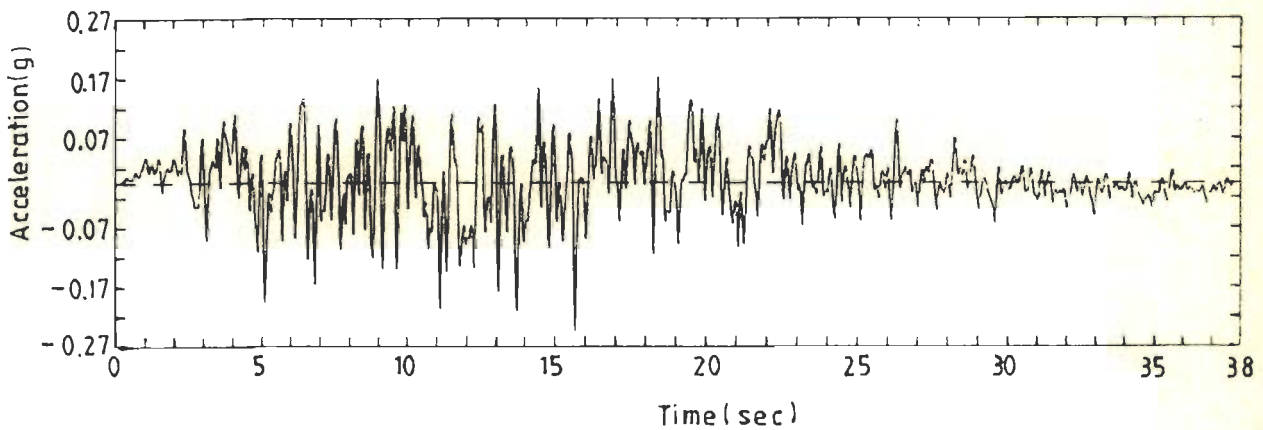


Fig. 8.81 Horizontal Acceleration Time-History at Node 468; S-I Method

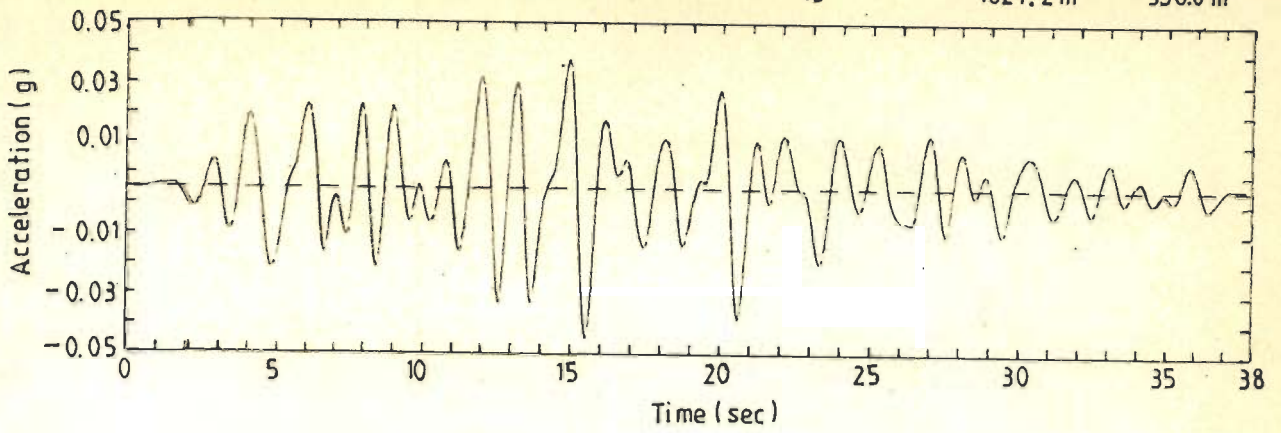


Fig. 8.82 Vertical Acceleration Time-History at Node 13; R-O Model

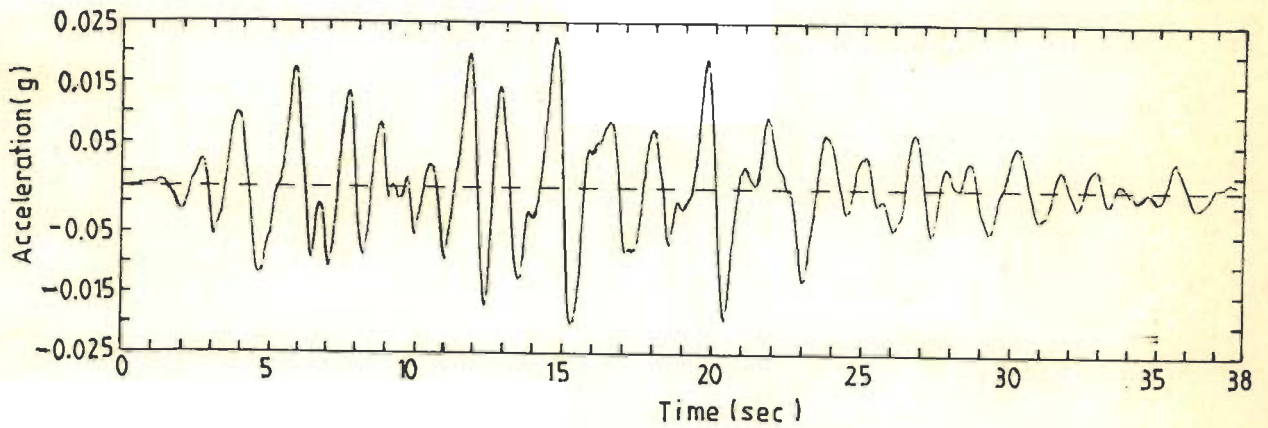


Fig. 8.83 Vertical Acceleration Time-History at Node 13; H-D Model

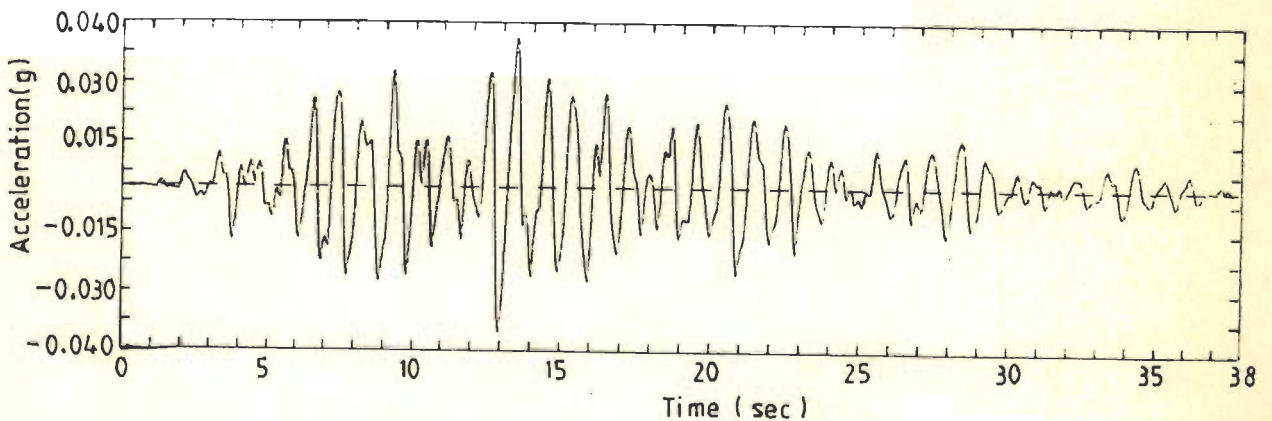


Fig. 8.84 Vertical Acceleration Time-History at Node 13; S-I Method

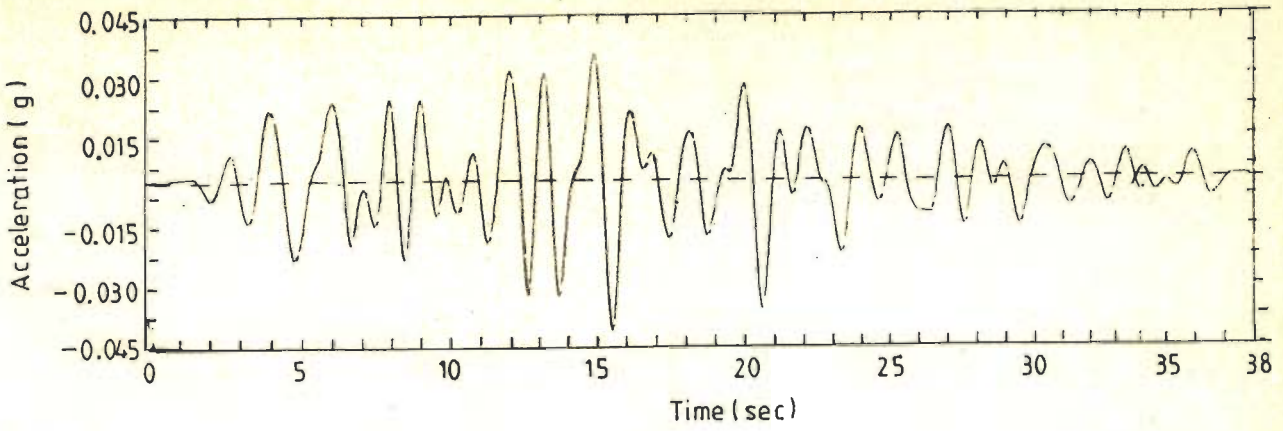


Fig. 8.85 Vertical Acceleration Time-History at Node 48; R-O Model

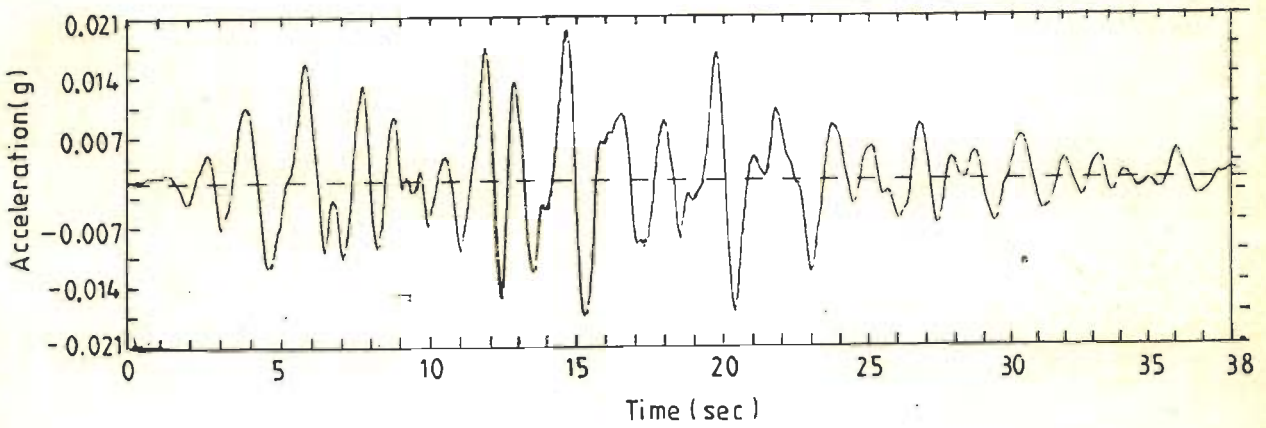


Fig. 8.86 Vertical Acceleration Time-History at Node 48; H-D Model

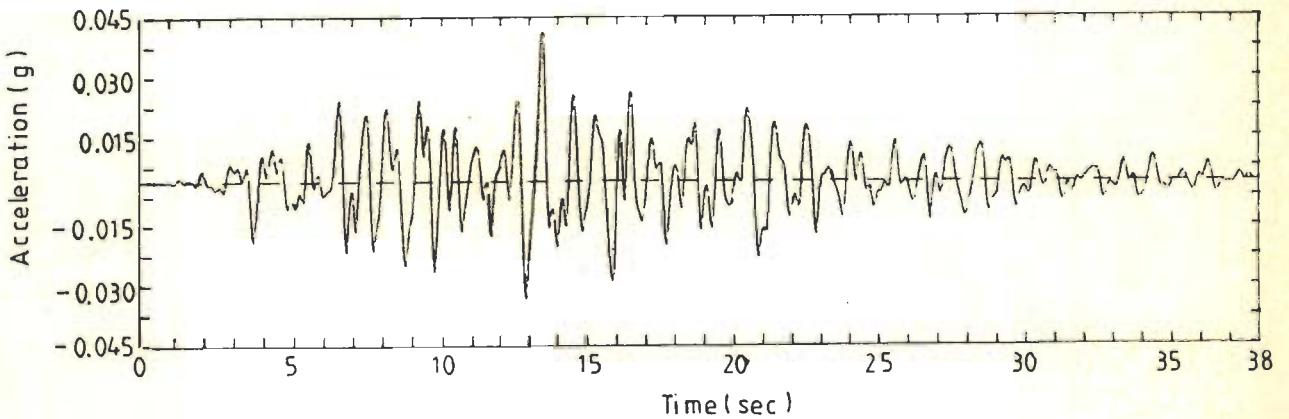


Fig. 8.87 Vertical Acceleration Time-History at Node 48; S-I Method

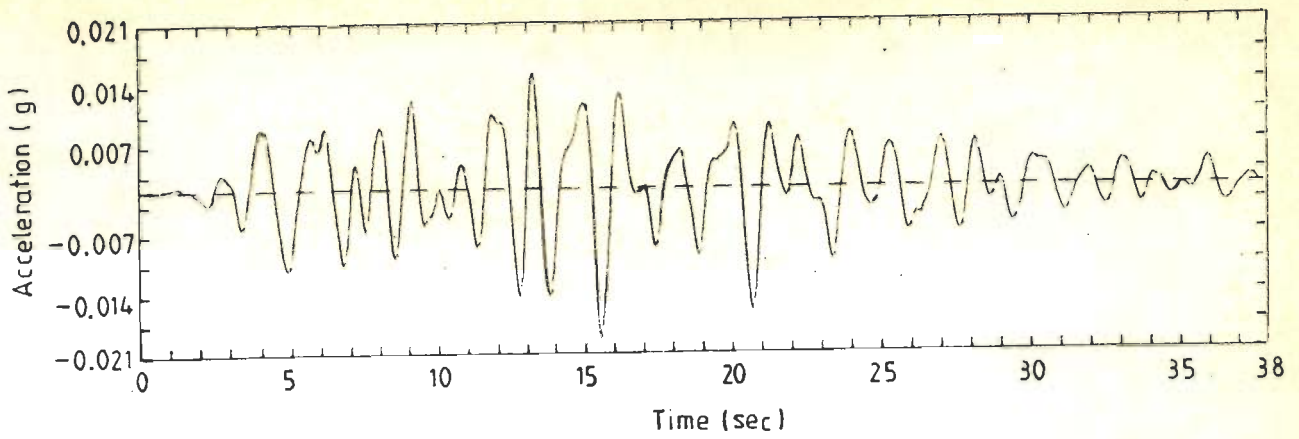


Fig. 8.88 Vertical Acceleration Time-History at Node 223; R-O Model

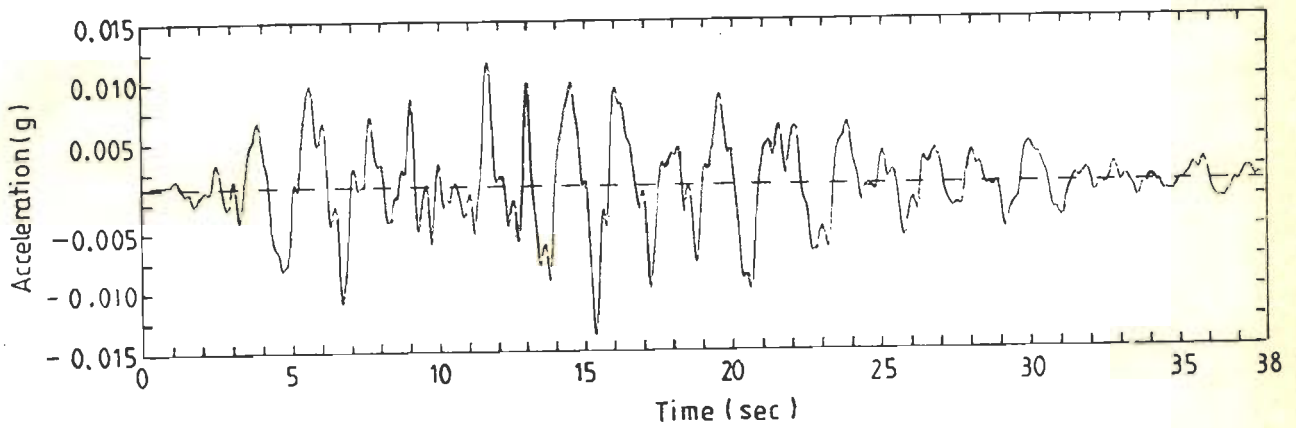


Fig. 8.89 Vertical Acceleration Time-History at Node 223; H-D Model

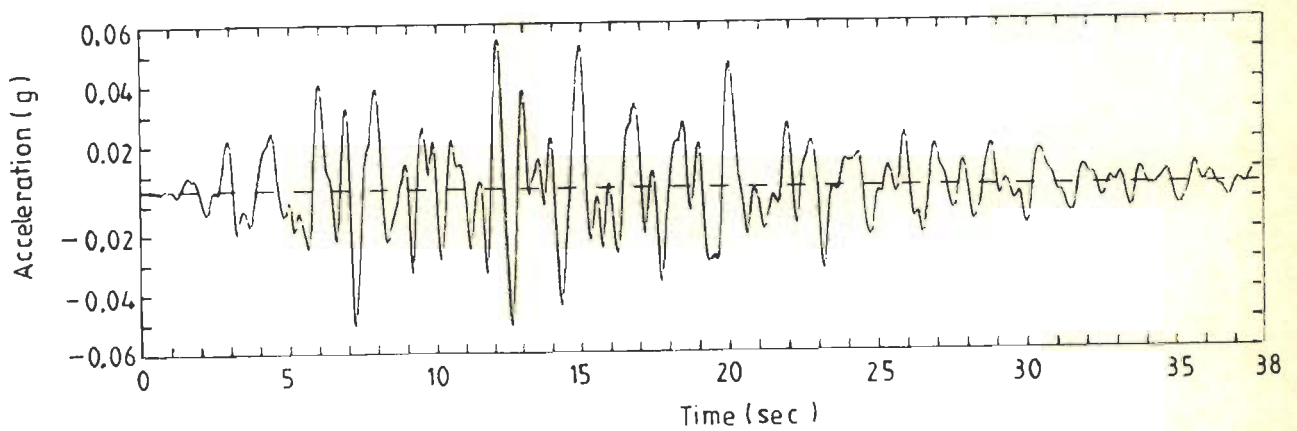


Fig. 8.90 Vertical Acceleration Time-History at Node 223; S-I Method

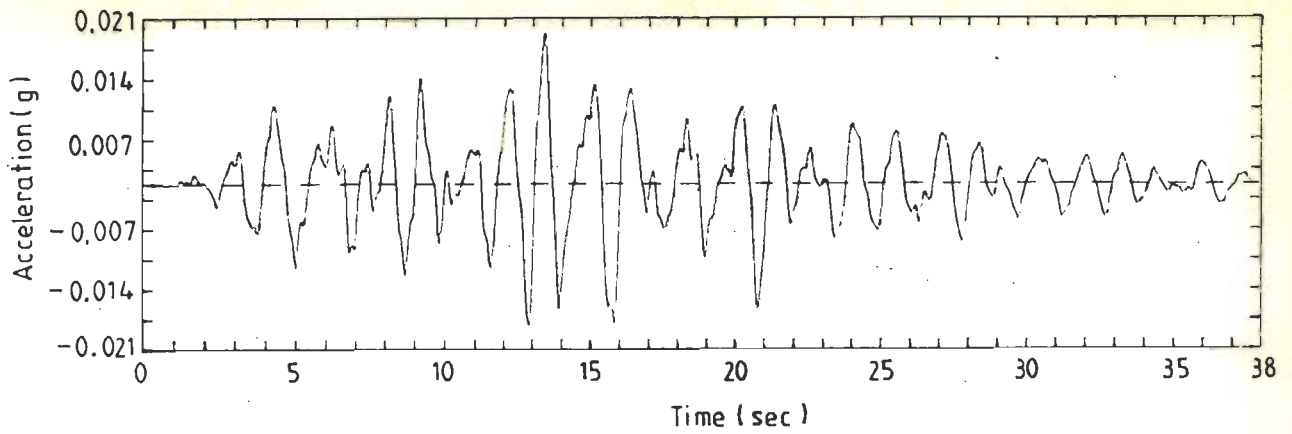


Fig. 8.91 Vertical Acceleration Time-History at Node 328; R-O Model

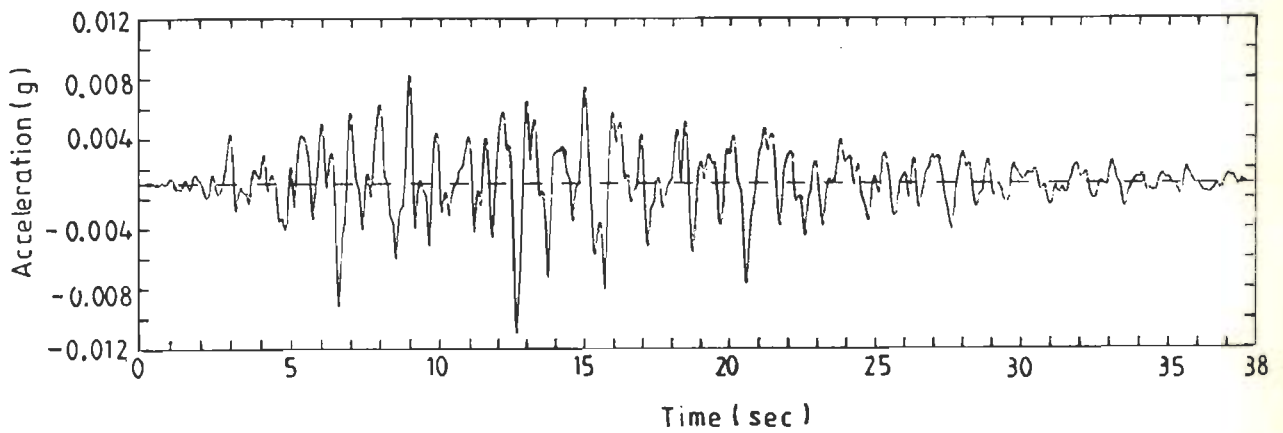


Fig. 8.92 Vertical Acceleration Time-History at Node 328; H-D Model

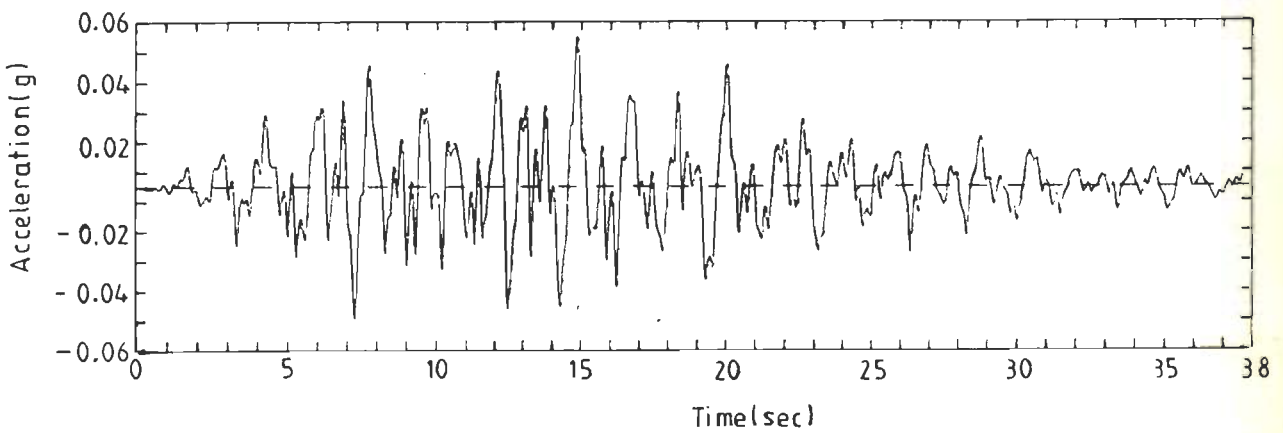


Fig. 8.93 Vertical Acceleration Time-History at Node 328; S-I Method

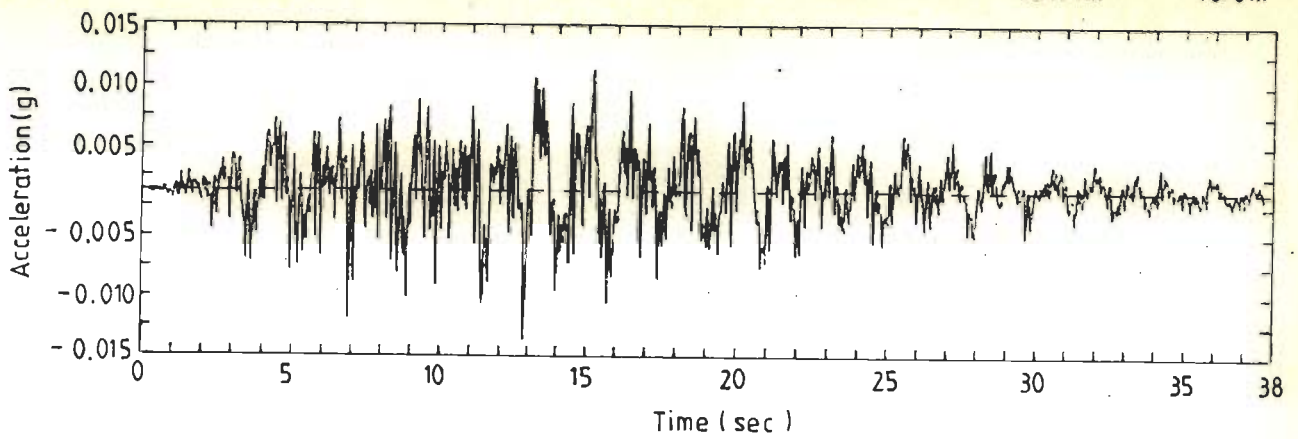


Fig. 8.94 Vertical Acceleration Time-History at Node 468; R-O Model

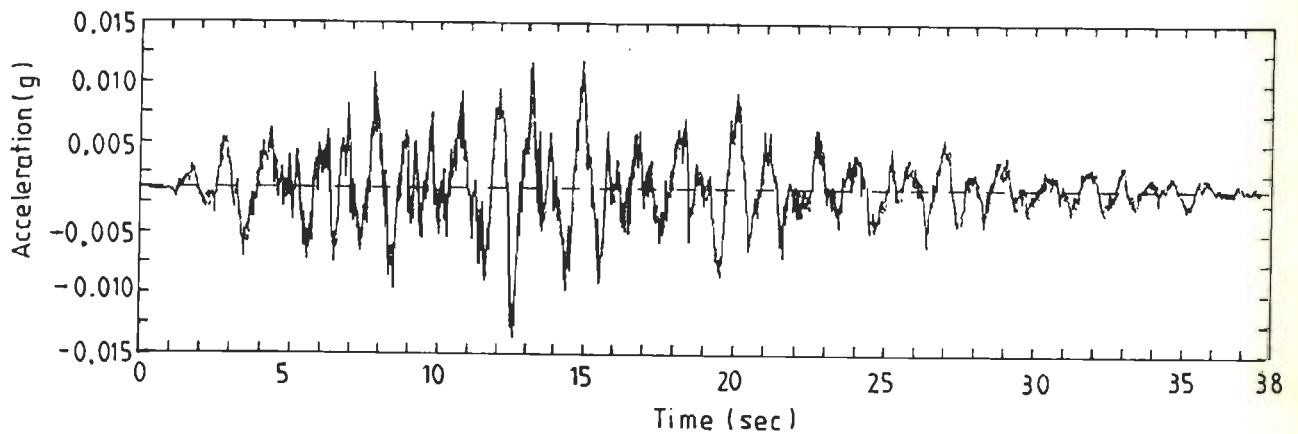


Fig. 8.95 Vertical Acceleration Time-History at Node 468; H-D Model

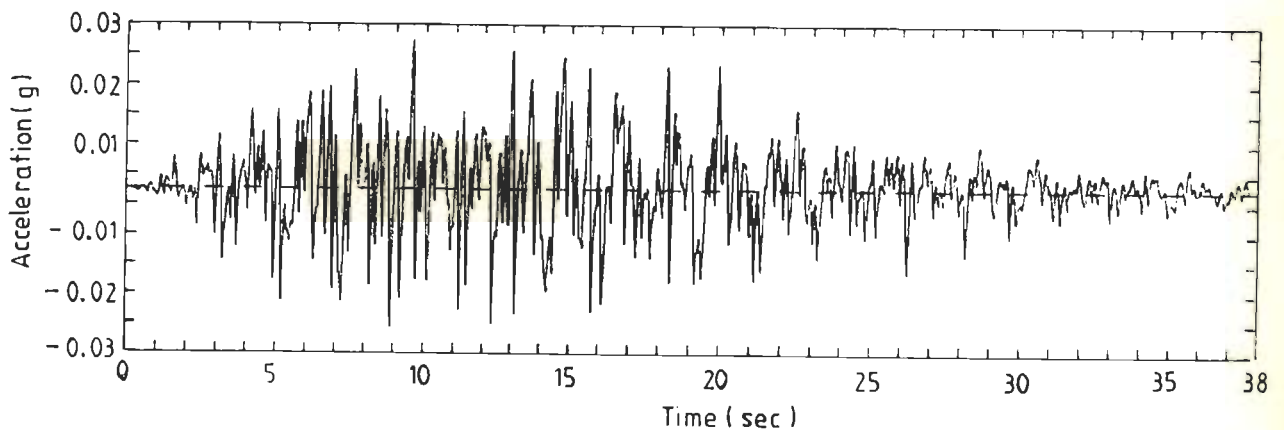


Fig. 8.96 Vertical Acceleration Time-History at Node 468; S-I Method

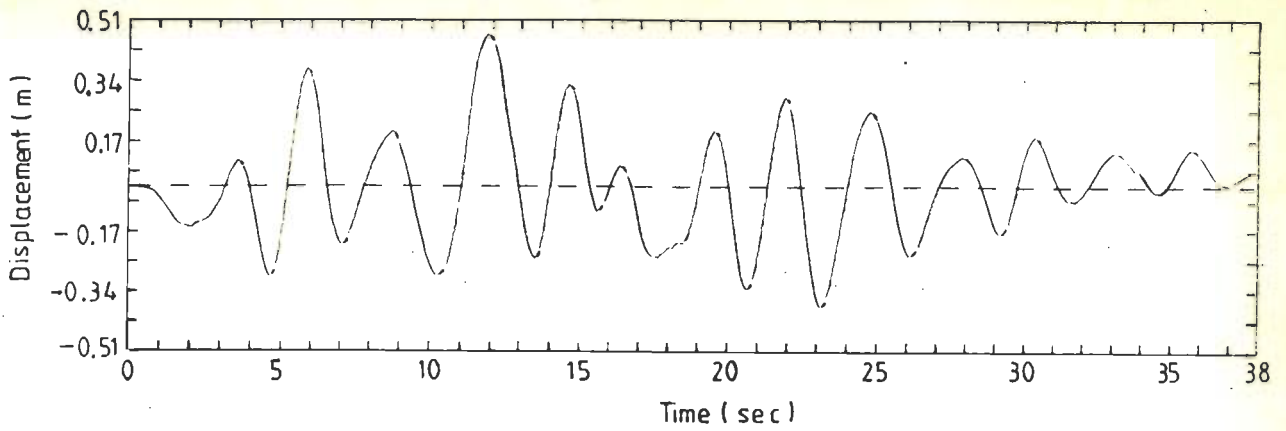


Fig. 8.97 Horizontal Displacement Time-History at Node 13; R-O Model

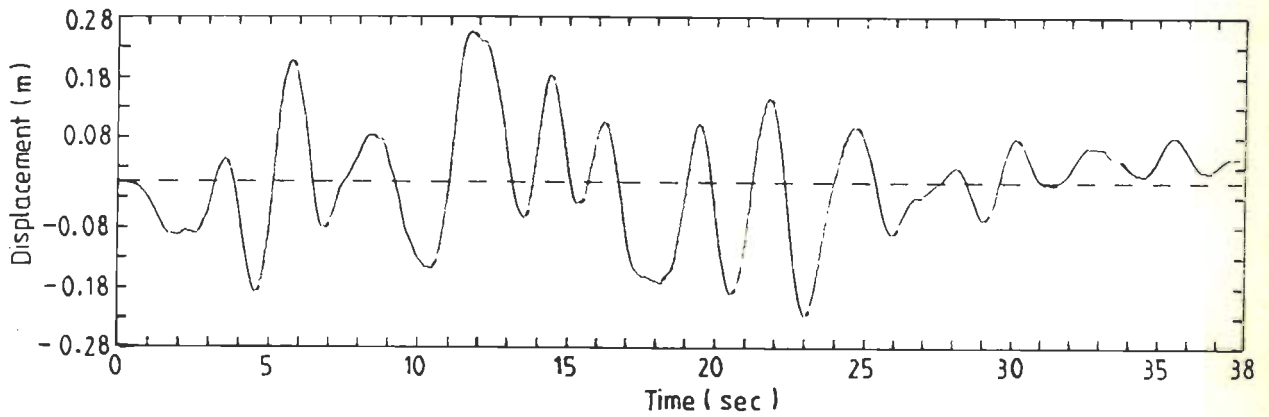


Fig. 8.98 Horizontal Displacement Time-History at Node 13; H-D Model

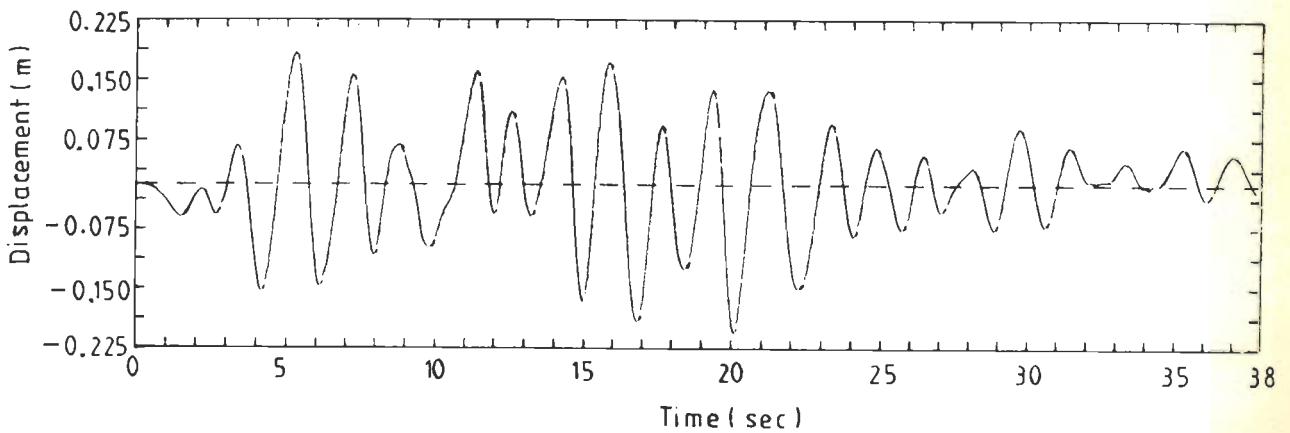


Fig. 8.99 Horizontal Displacement Time-History at Node 13; S-I Method

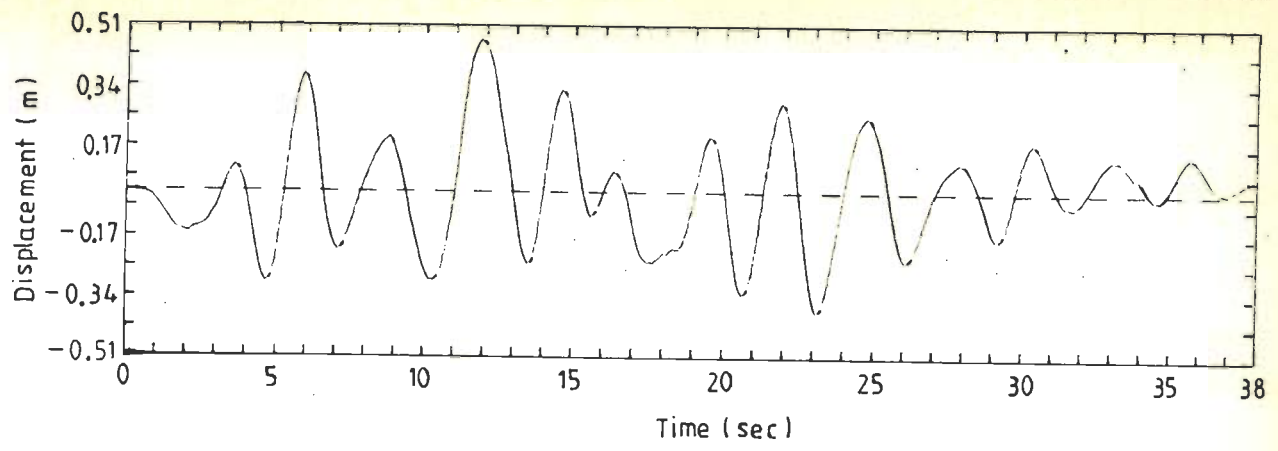


Fig. 8.100 Horizontal Displacement Time-History at Node 48; R-O Model

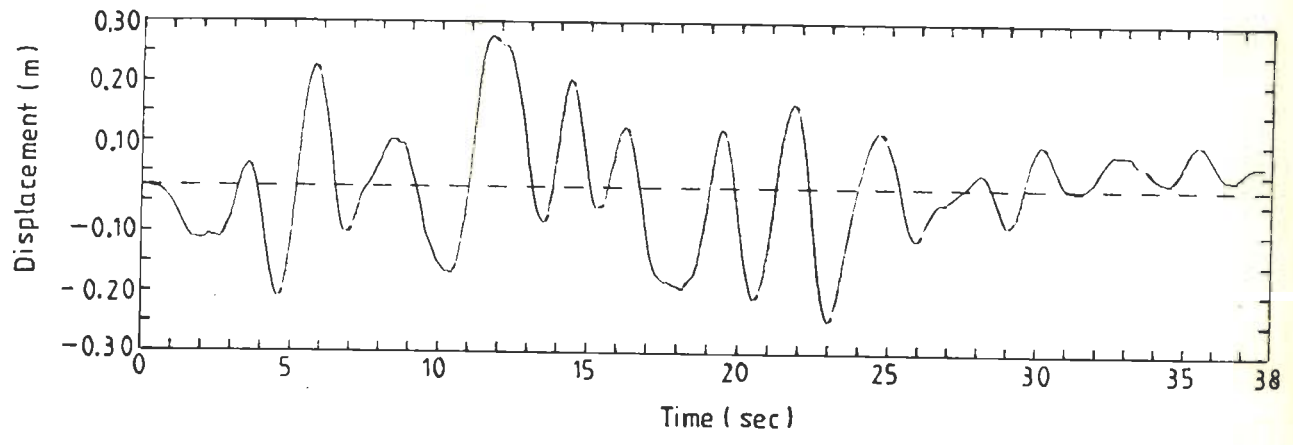


Fig. 8.101 Horizontal Displacement Time-History at Node 48; H-D Model

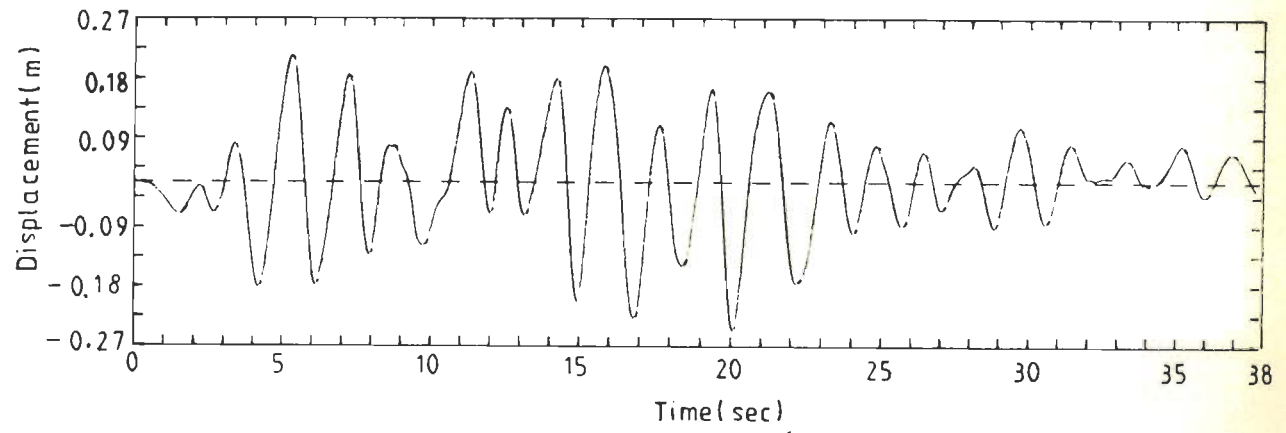


Fig. 8.102 Horizontal Displacement Time-History at Node 48; S-I Methc

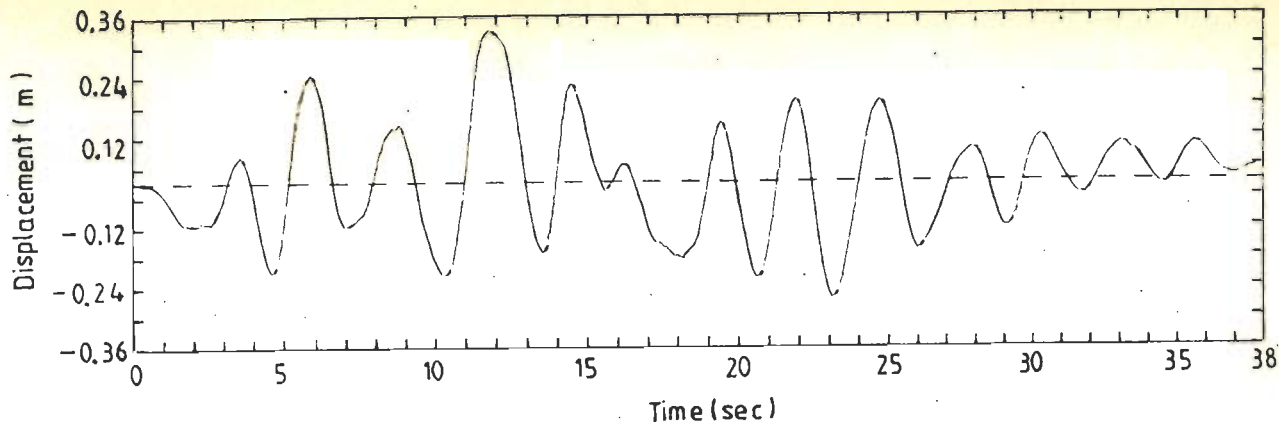


Fig. 8.103 Horizontal Displacement Time-History at Node 223; R-O Model

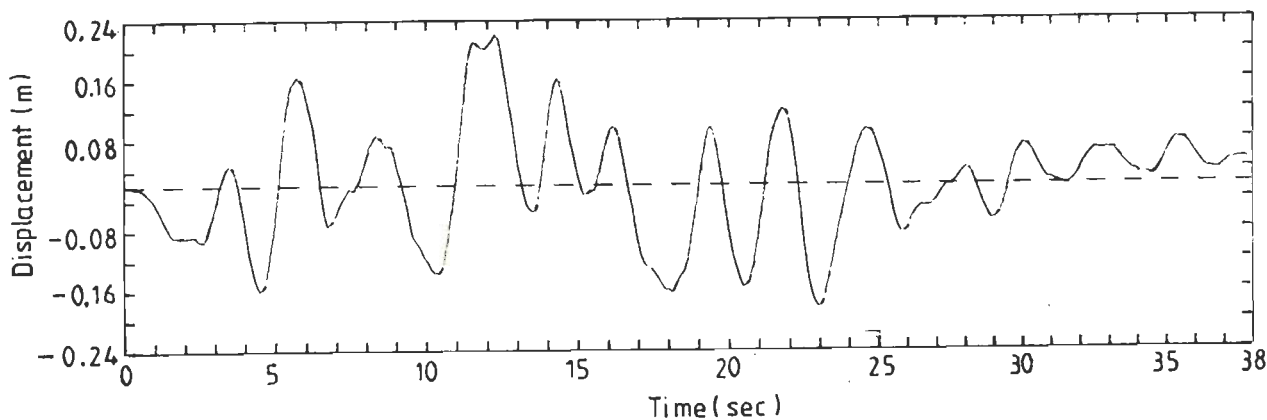


Fig. 8.104 Horizontal Displacement Time-History at Node 223; H-D Model

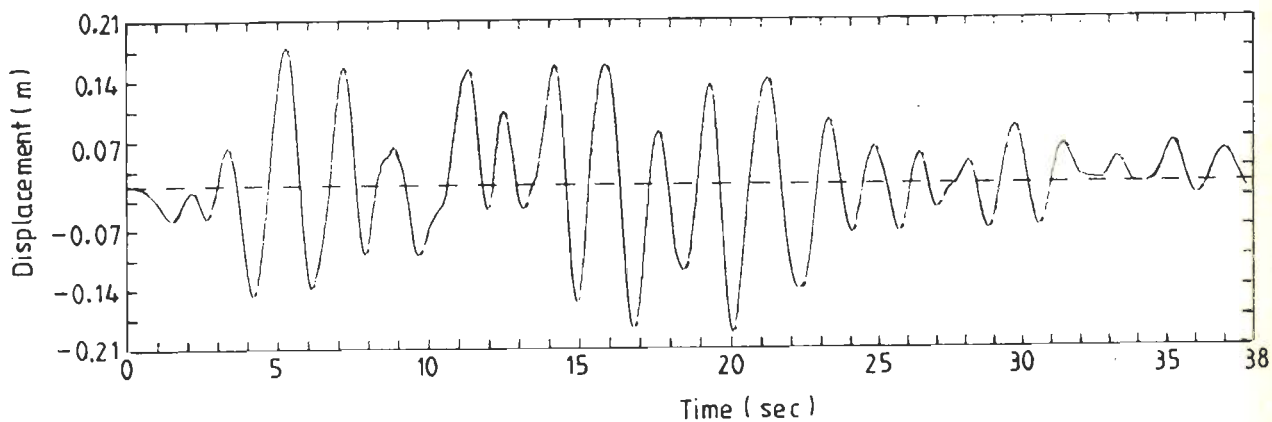


Fig. 8.105 Horizontal Displacement Time-History at Node 223; S-I Method

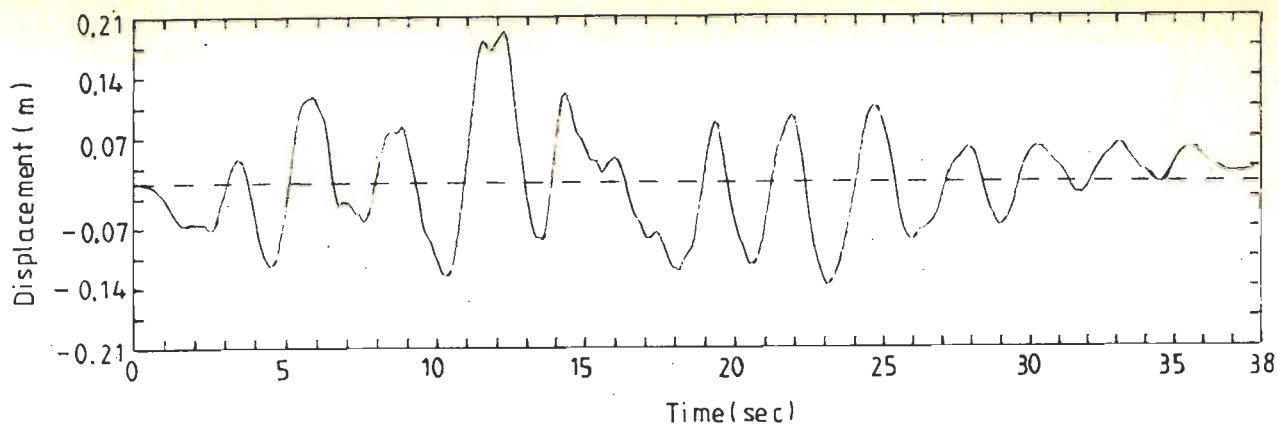


Fig. 8.106 Horizontal Displacement Time-History at Node 328; R-O Model

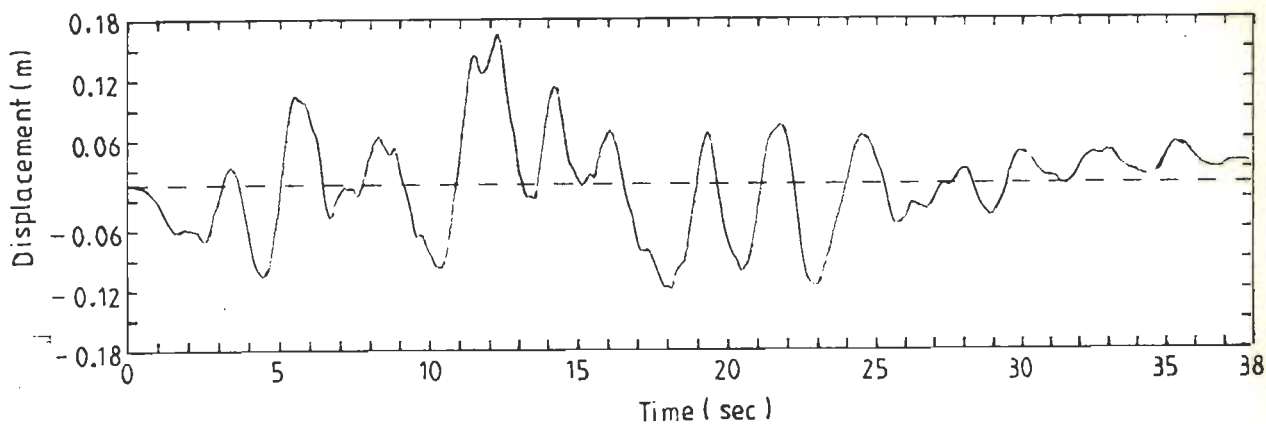


Fig. 8.107 Horizontal Displacement Time-History at Node 328; H-D Model

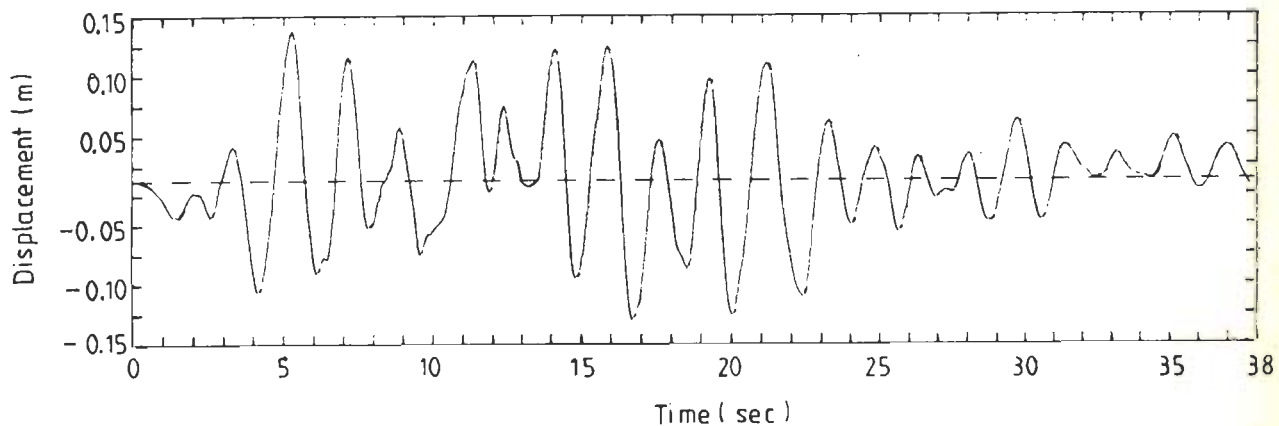


Fig. 8.108 Horizontal Displacement Time-History at Node 328; S-I Method

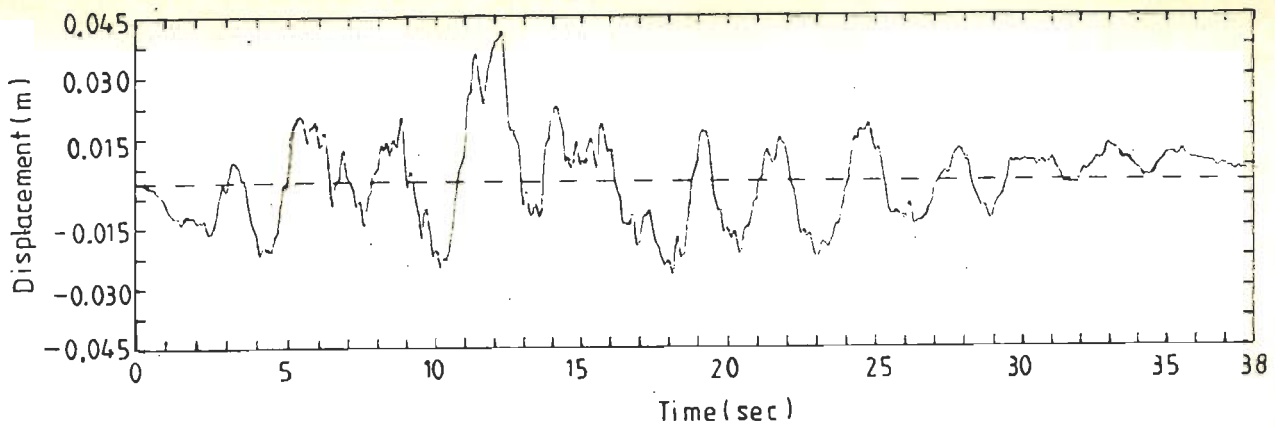


Fig. 8.109 Horizontal Displacement Time-History at Node 468; R-O Model

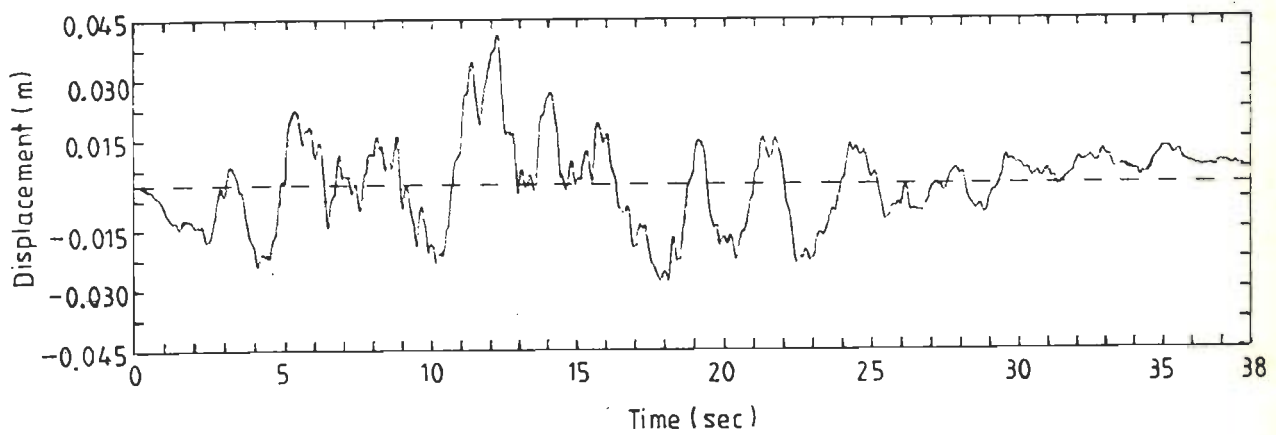


Fig. 8.110 Horizontal Displacement Time-History at Node 468; H-D Model

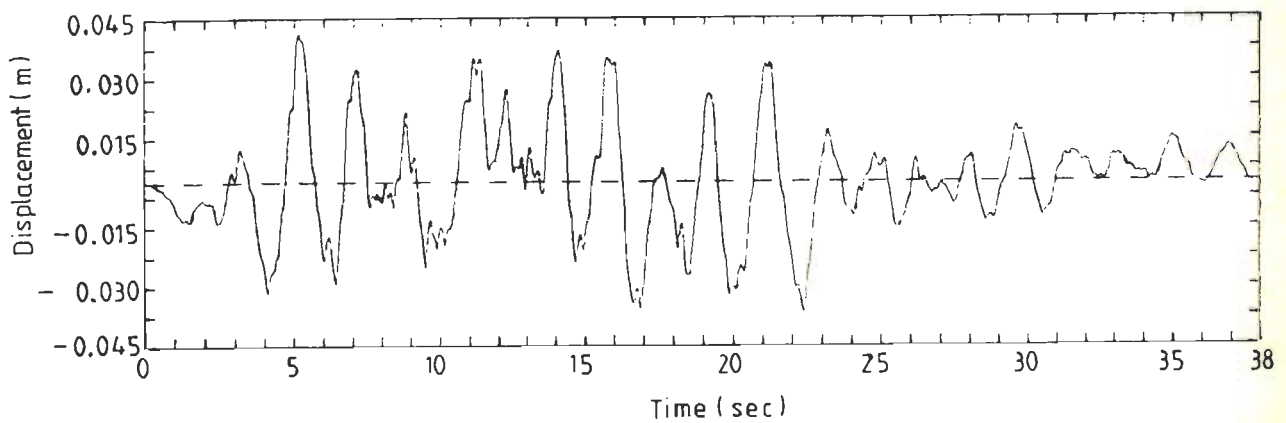


Fig. 8.111 Horizontal Displacement Time-History at Node 468; S-I Method

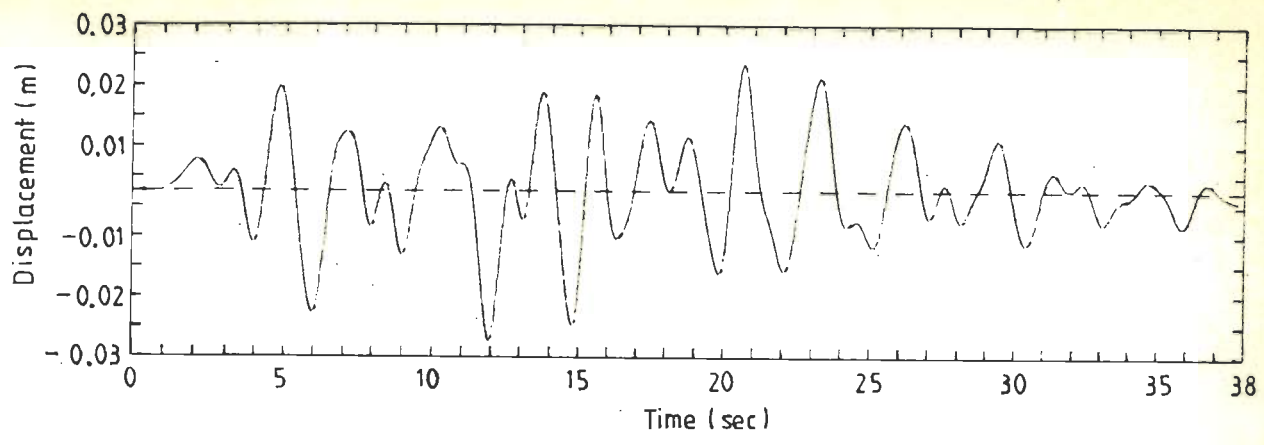


Fig. 8.112 Vertical Displacement Time-History at Node 13; R-O Model

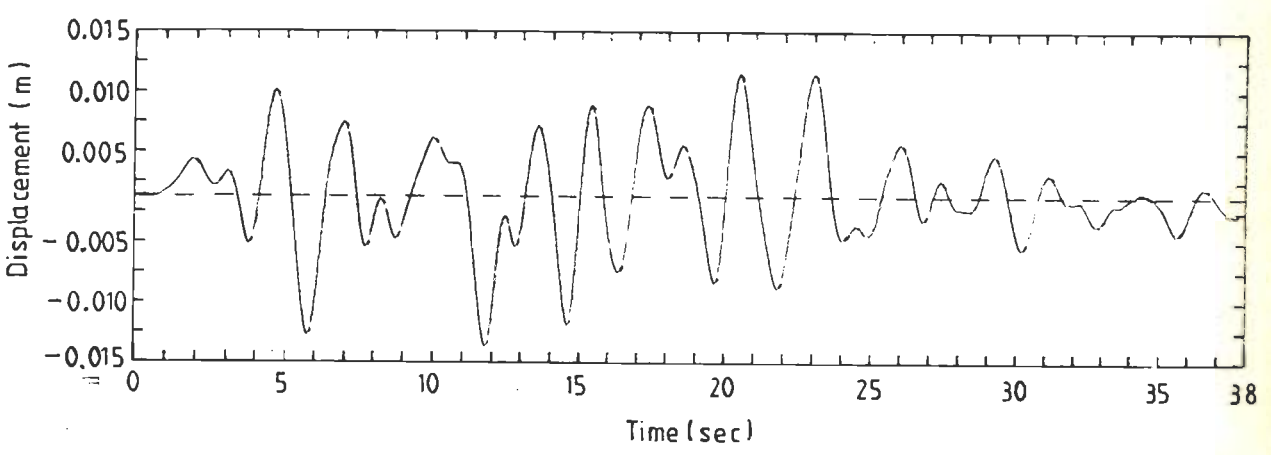


Fig. 8.113 Vertical Displacement Time-History at Node 13; H-D Model

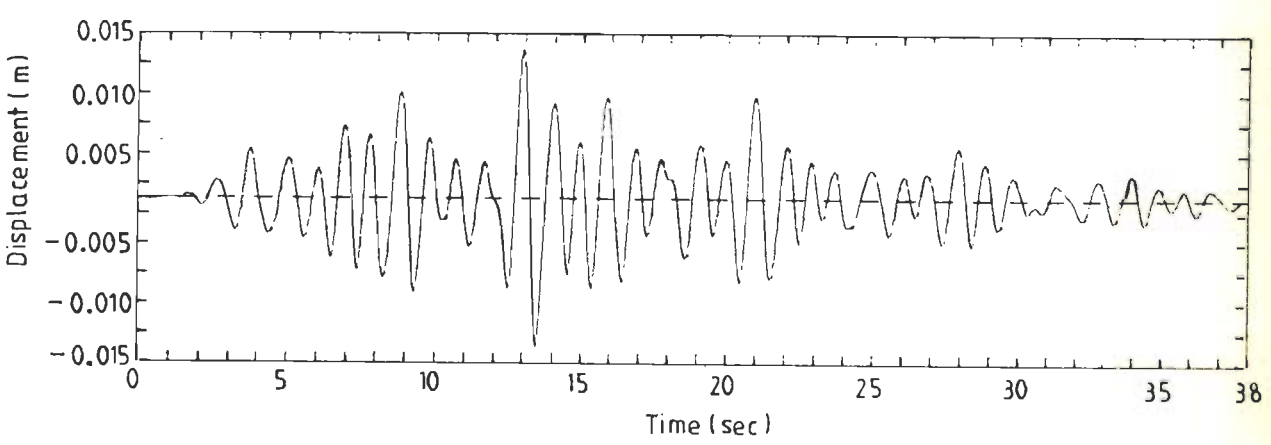


Fig. 8.114 Vertical Displacement Time-History at Node 13; S-I Method

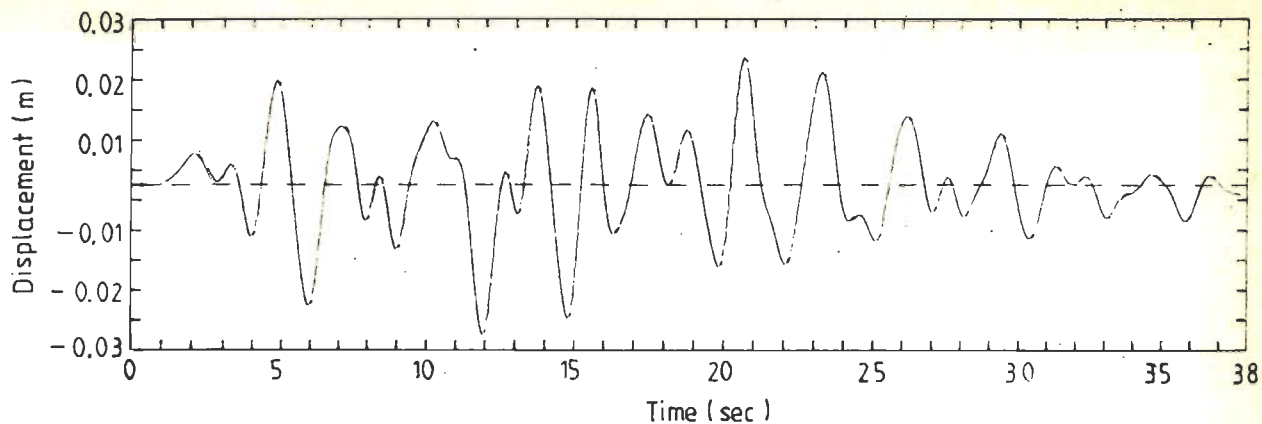


Fig. 8.115 Vertical Displacement Time-History at Node 48; R-O Model

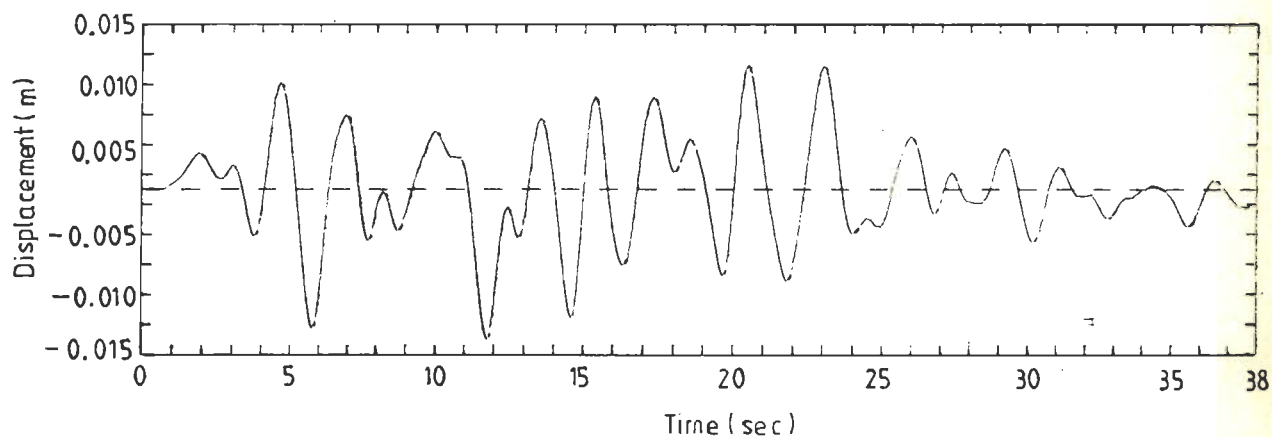


Fig. 8.116 Vertical Displacement Time-History at Node 48; H-D Model

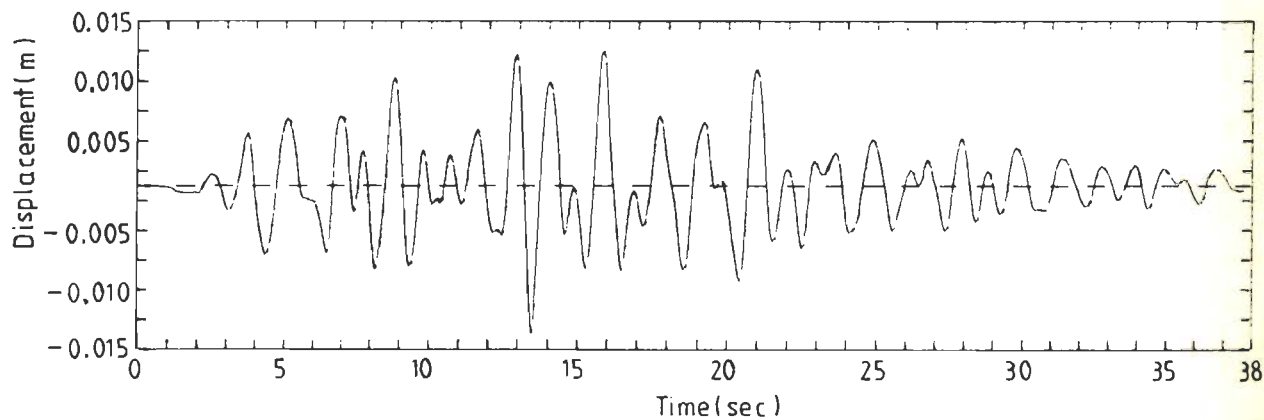


Fig. 8.117 Vertical Displacement Time-History at Node 48; S-I Method

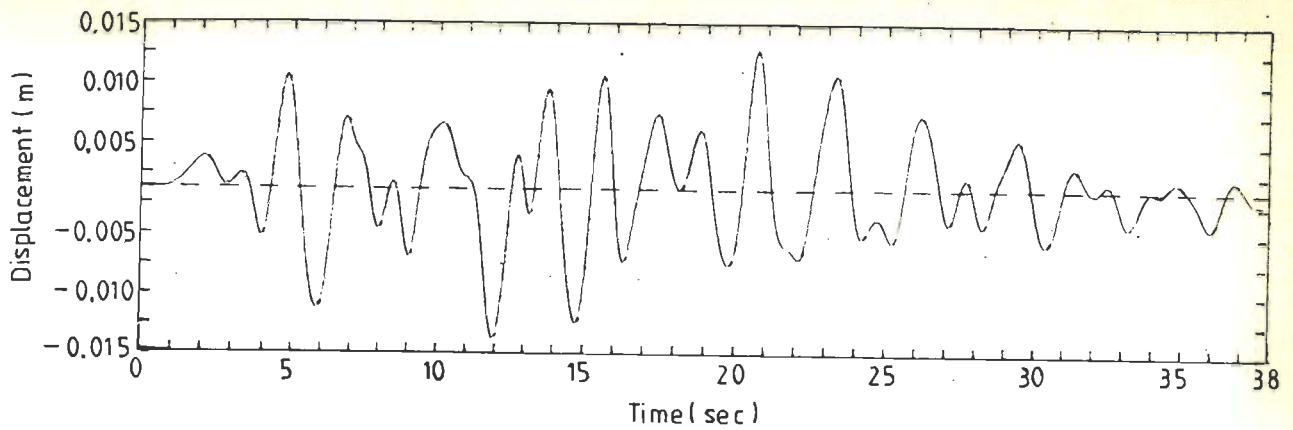


Fig. 8.118 Vertical Displacement Time-History at Node 223; R-O Mode.

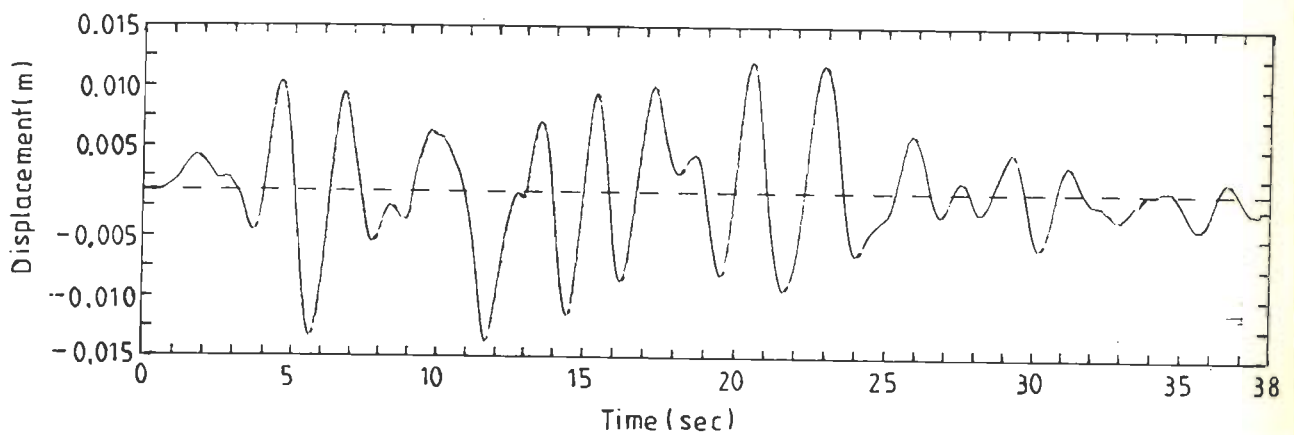


Fig. 8.119 Vertical Displacement Time-History at Node 223; H-D Model

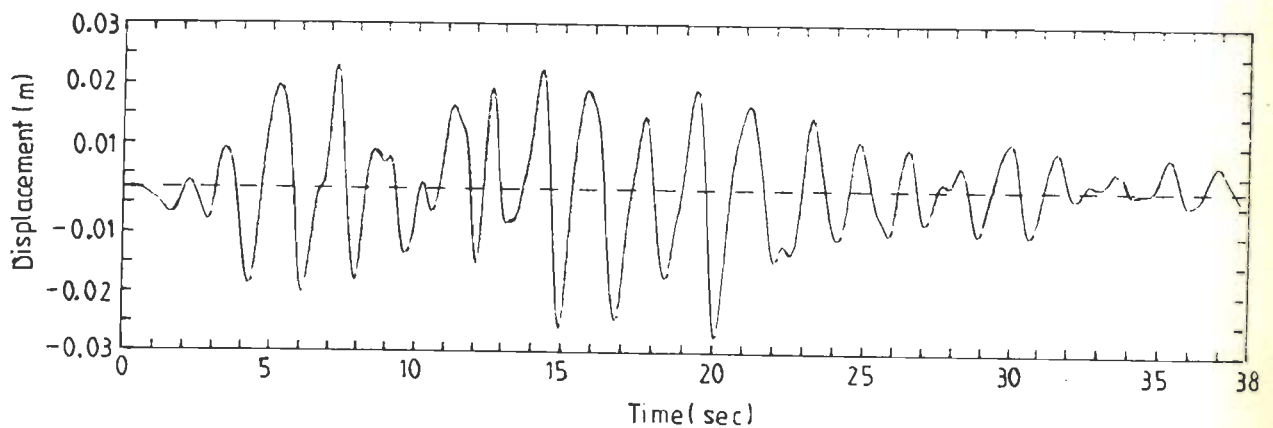


Fig. 8.120 Vertical Displacement Time-History at Node 223; S-I Method

Node x y
328 1625.6 m 182.0m

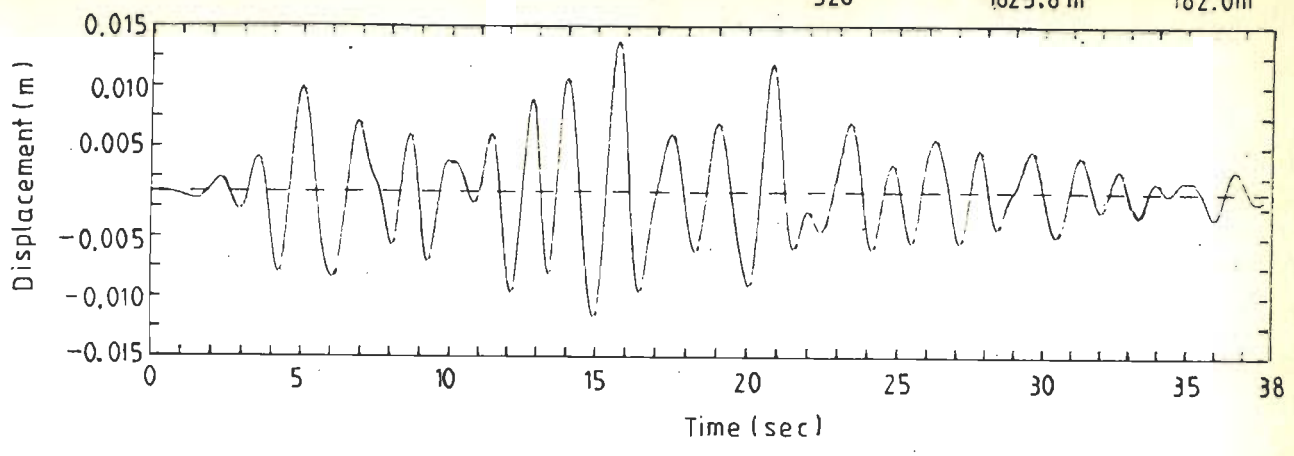


Fig. 8.121 Vertical Displacement Time-History at Node 328; R-O Model

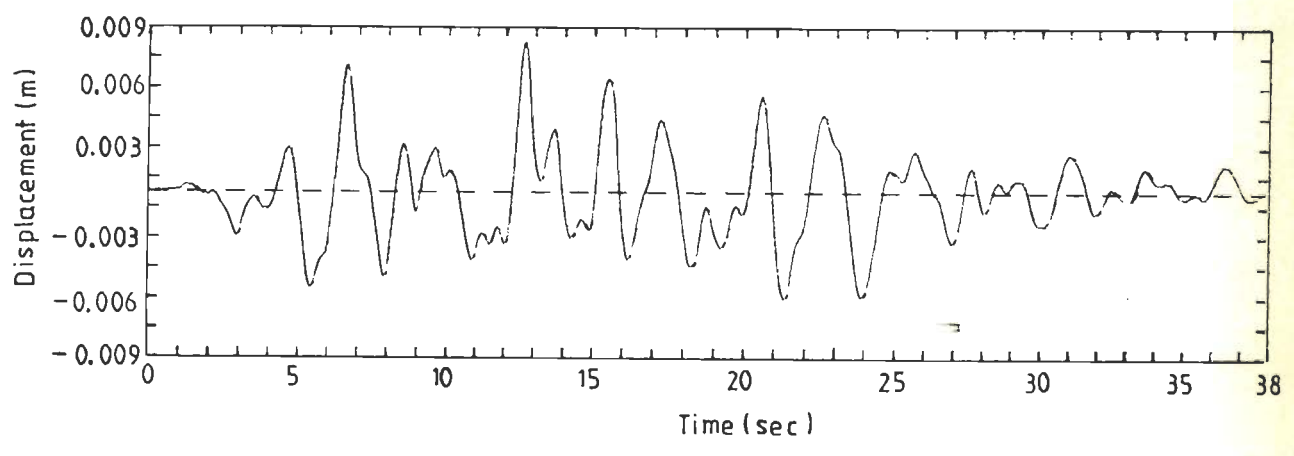


Fig. 8.122 Vertical Displacement Time-History at Node 328; H-D Model

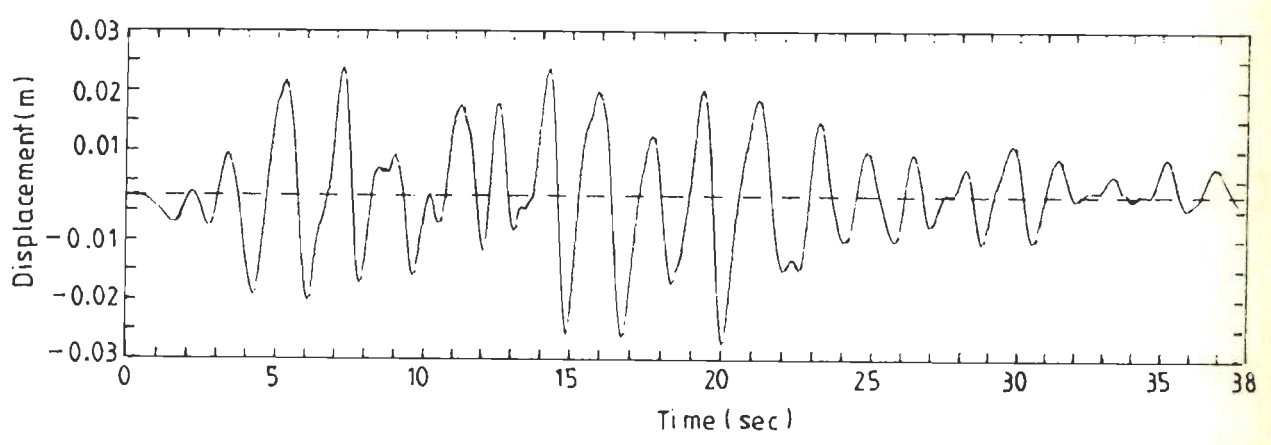


Fig. 8.123 Vertical Displacement Time-History at Node 328; S-I Method

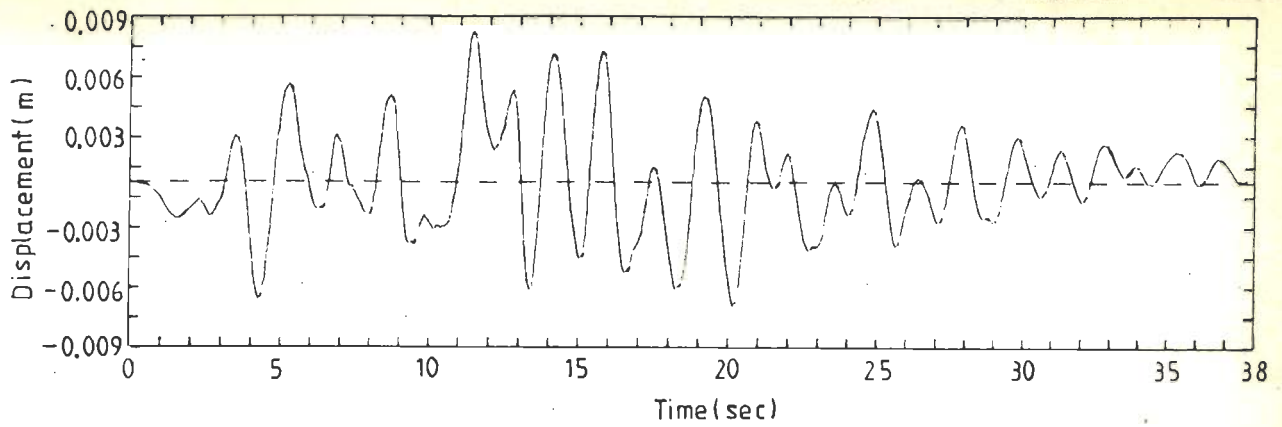


Fig. 8.124 Vertical Displacement Time-History at Node 468; R-O Model

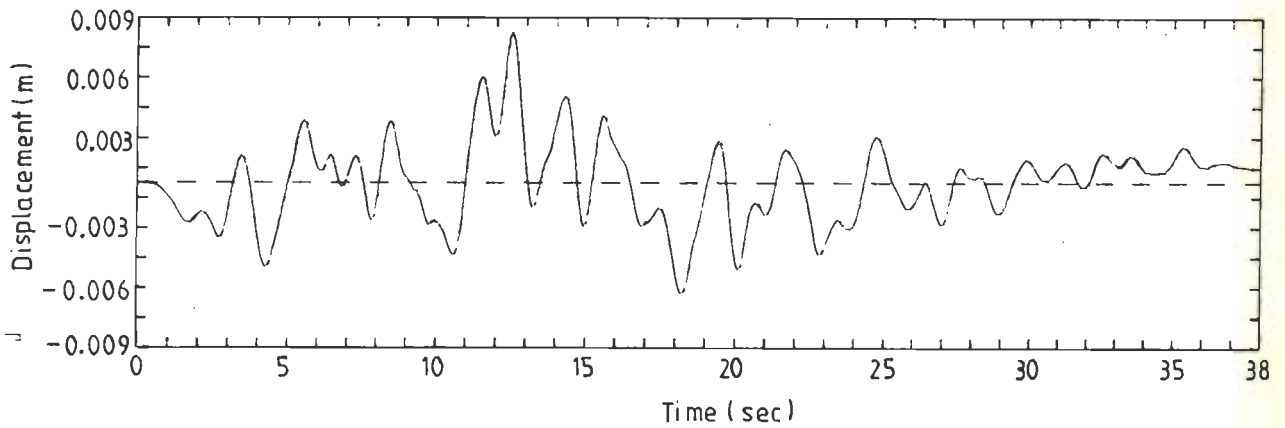


Fig. 8.125 Vertical Displacement Time-History at Node 468; H-D Model

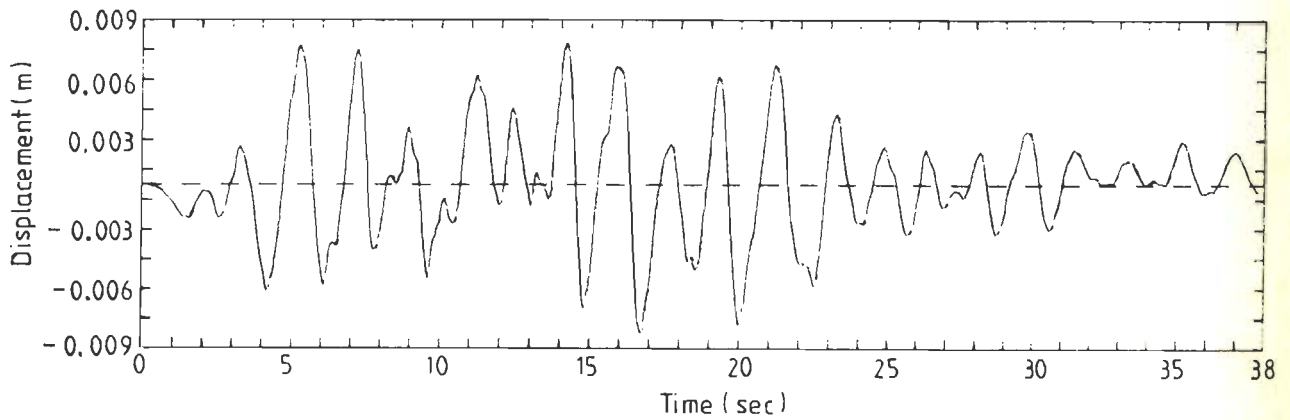


Fig. 8.126 Vertical Displacement Time-History at Node 468; S-I Method

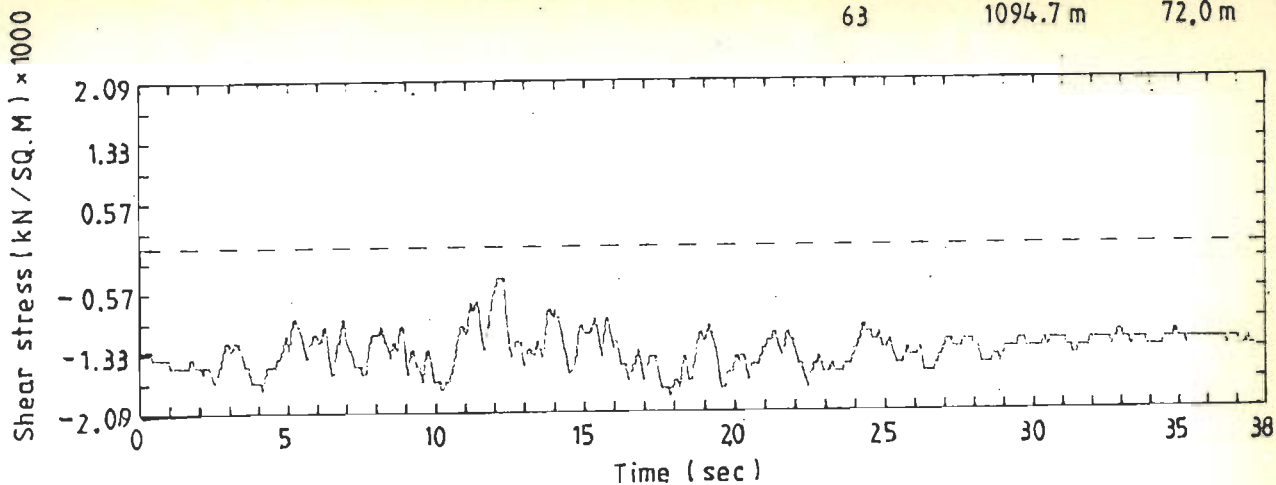


Fig. 8.127 Shear Stress Time-History at Element 63; R-O Model

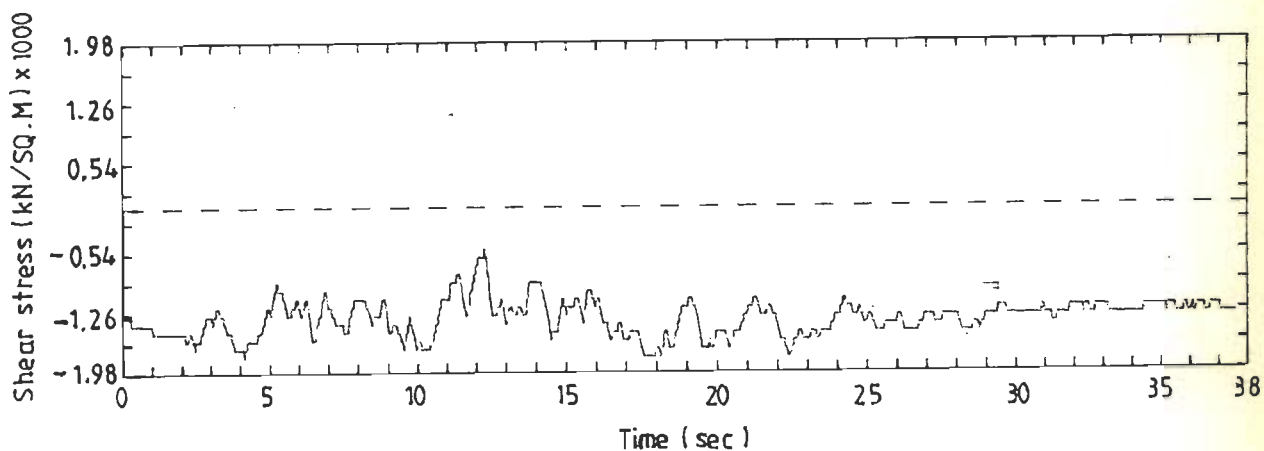


Fig. 8.128 Shear Stress Time-History at Element 63; H-D Model

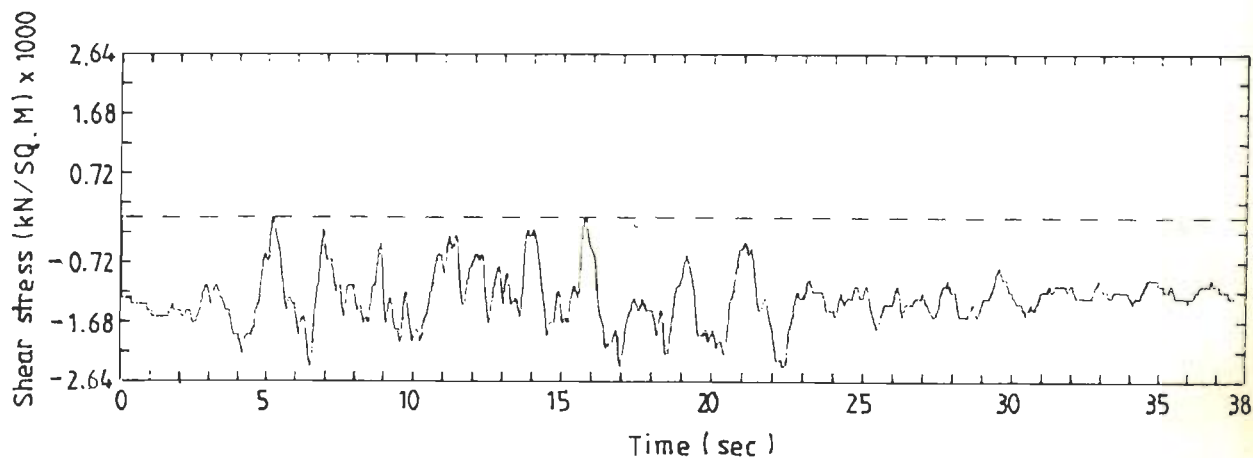


Fig. 8.129 Shear Stress Time-History at Element 63; S-I Method

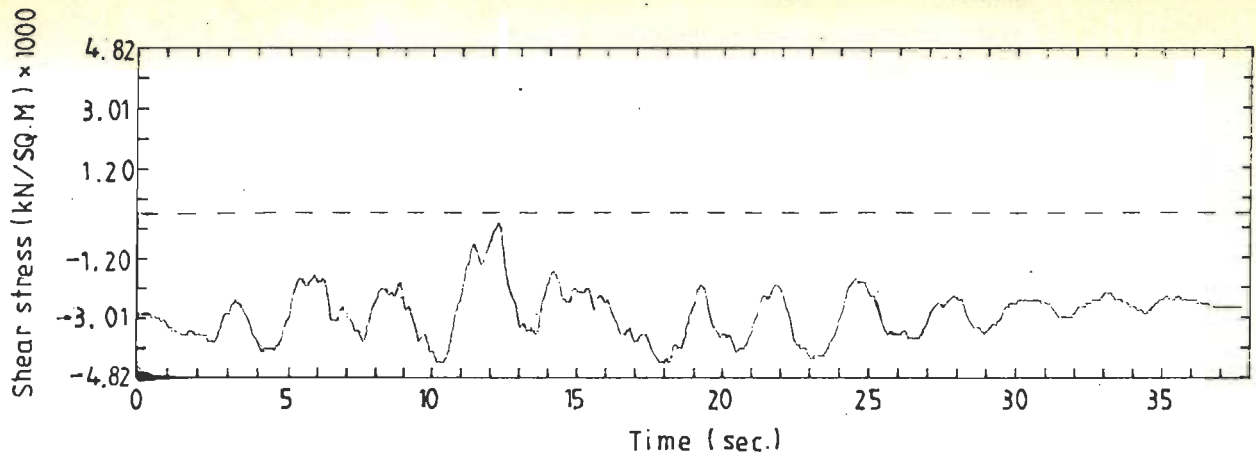


Fig. 8.130 Shear Stress Time-History at Element 66; R-O Model

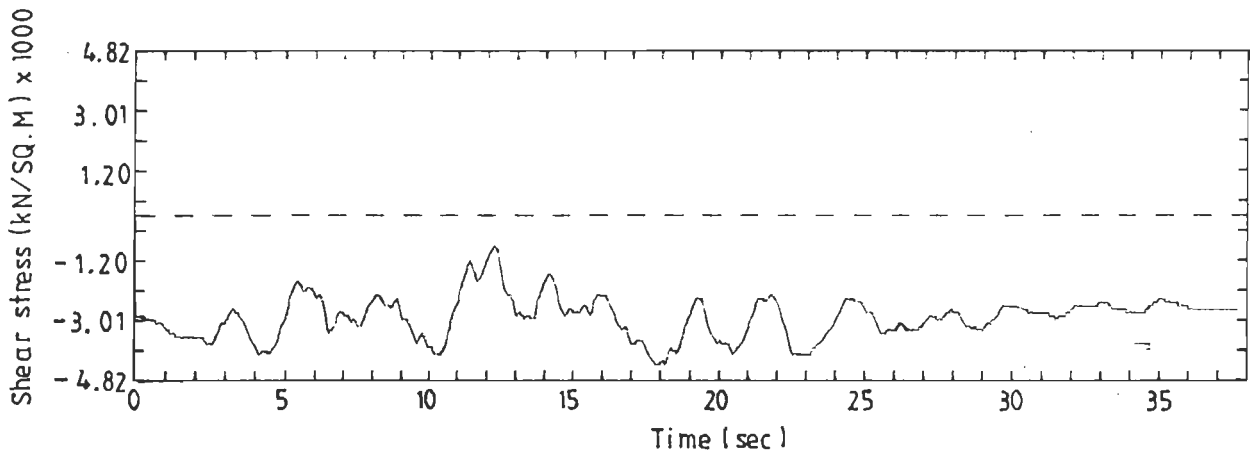


Fig. 8.131 Shear Stress Time-History at Element 66; H-D Model

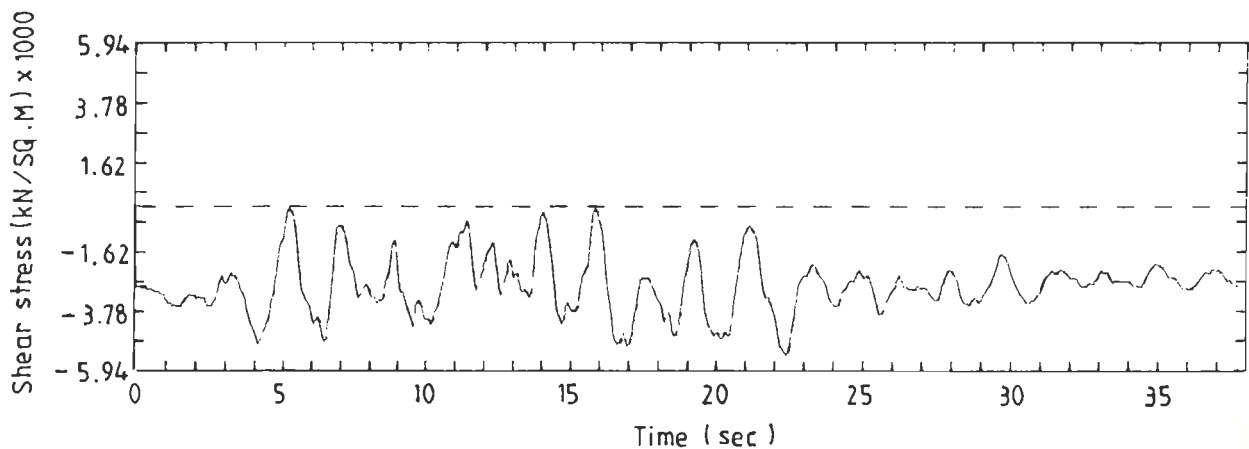


Fig. 8.132 Shear Stress Time-History at Element 66; S-I Method

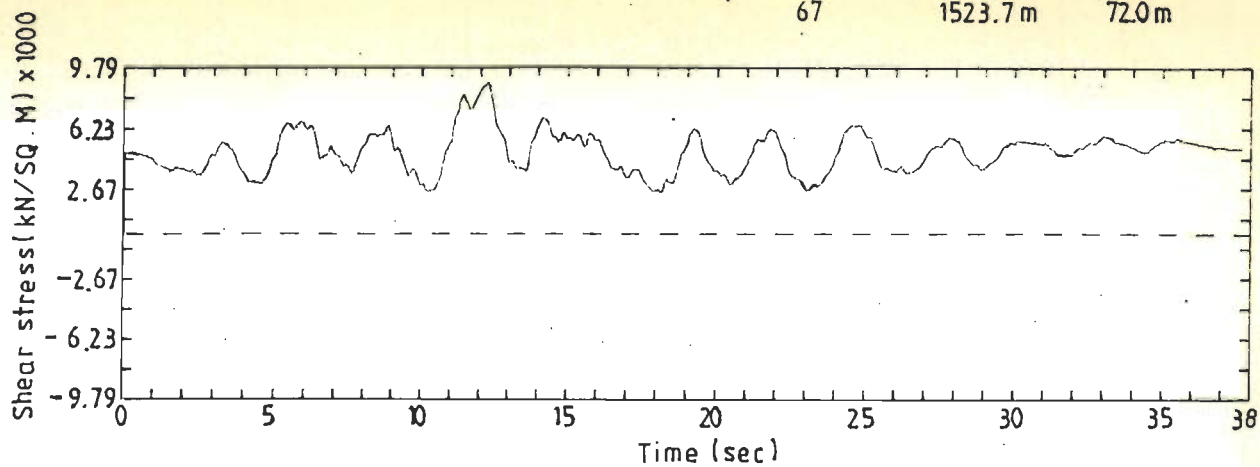


Fig. 8.133 Shear Stress Time-History at Element 67; R-O Model

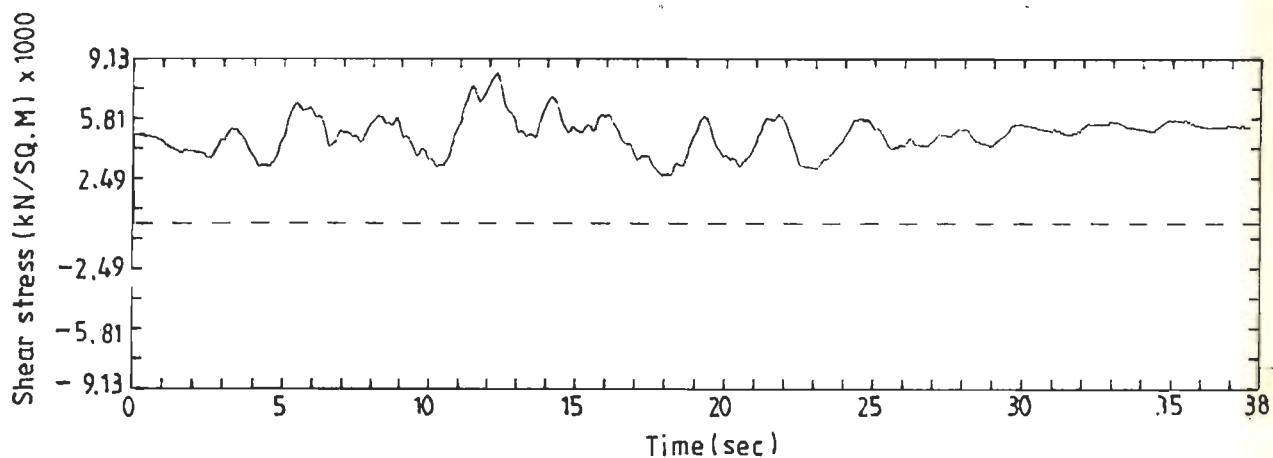


Fig. 8.134 Shear Stress Time-History at Element 67; H-D Model

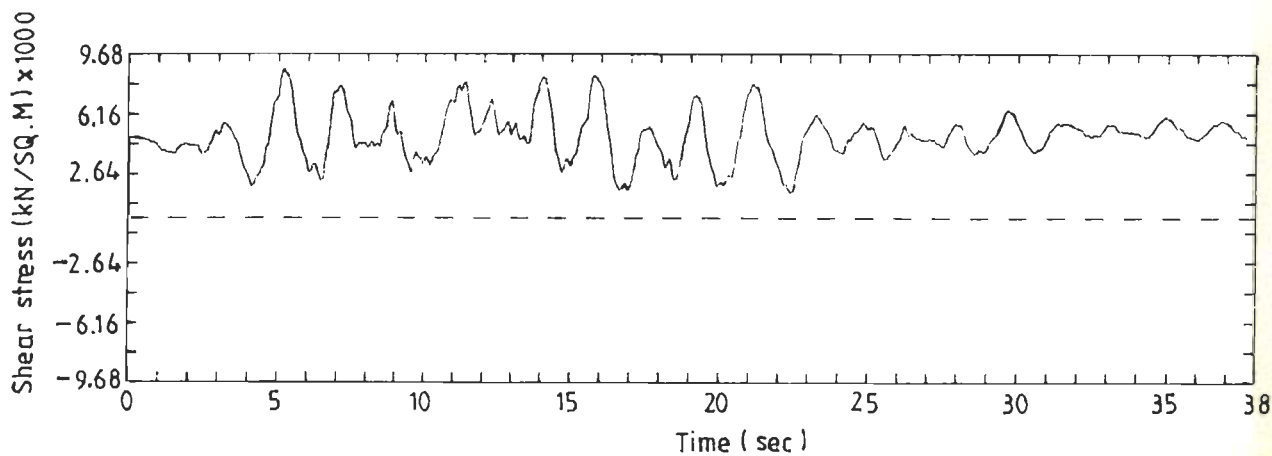


Fig. 8.135 Shear Stress Time-History at Element 67; S-I Method

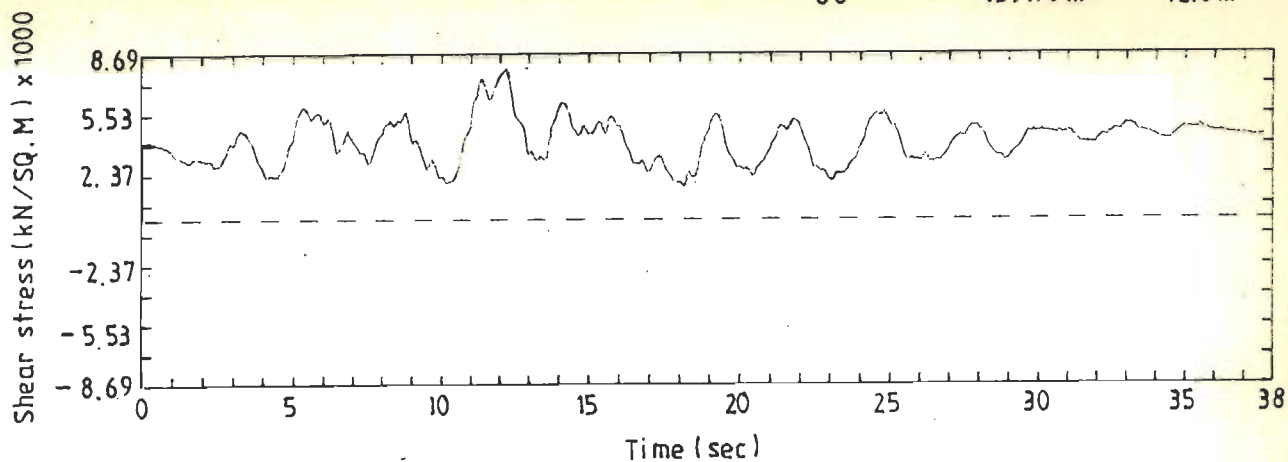


Fig. 8.136 Shear Stress Time-History at Element 68; R-O Model

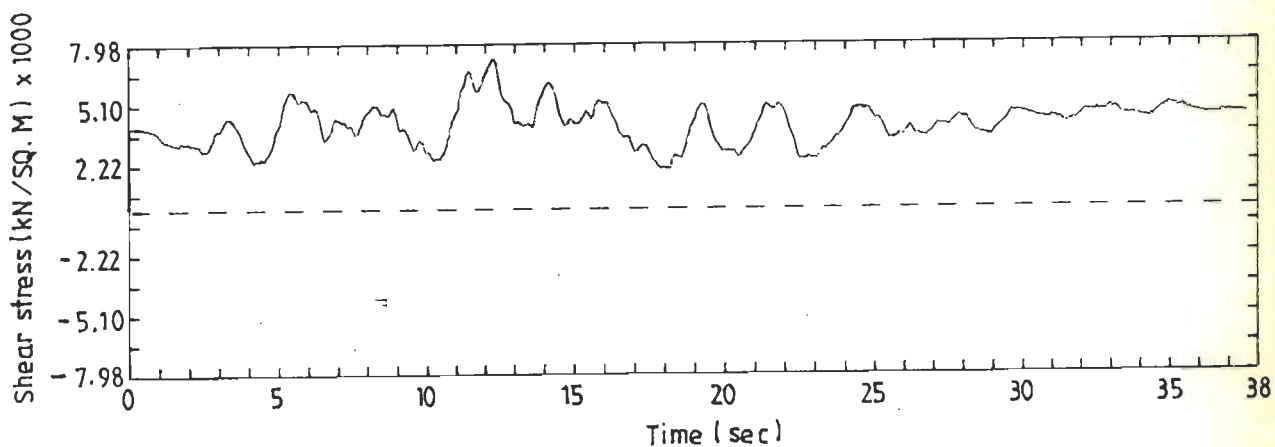


Fig. 8.137 Shear Stress Time-History at Element 68; H-D Model

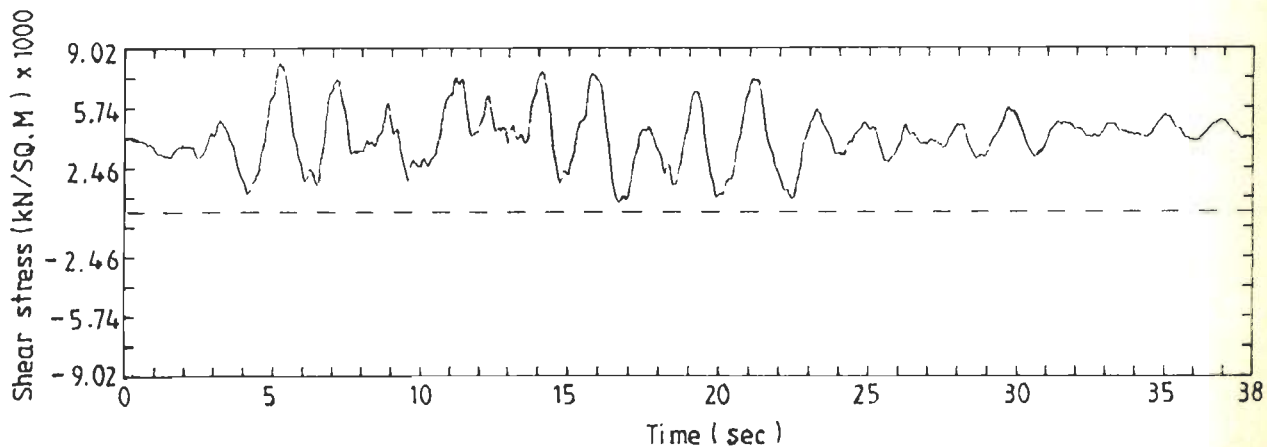


Fig. 8.138 Shear Stress Time-History at Element 68; S-I Method

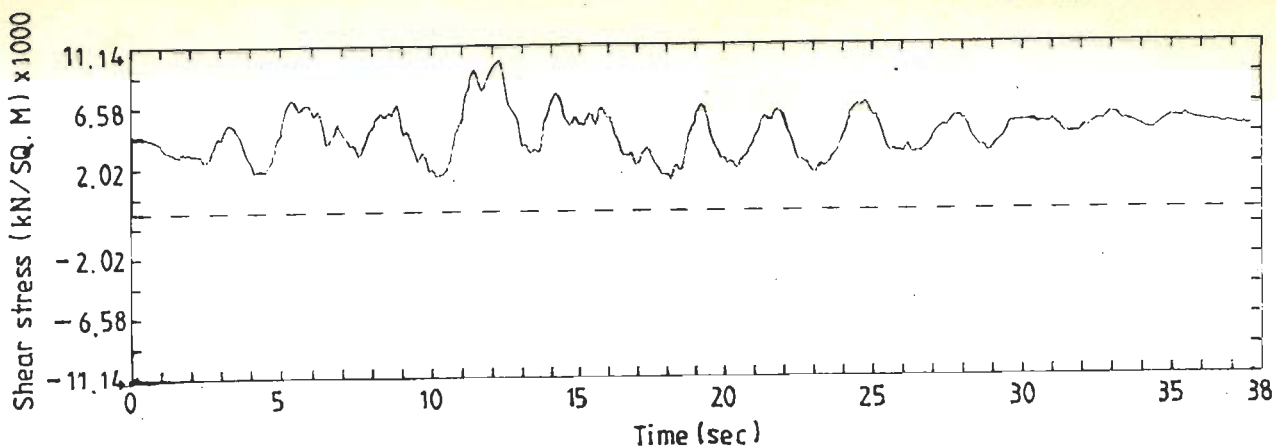


Fig. 8.139 Shear Stress Time-History at Element 69; R-O Model

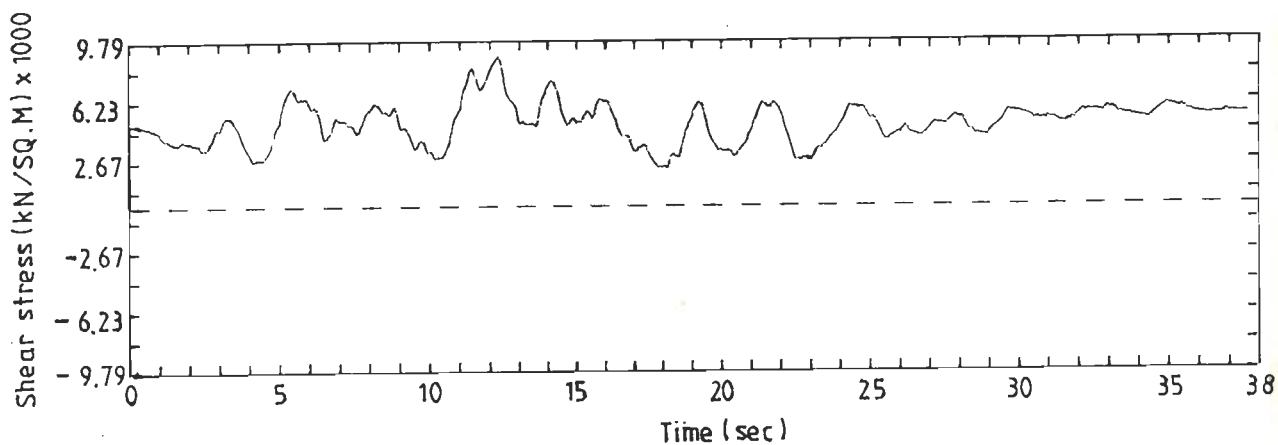


Fig. 8.140 Shear Stress Time-History at Element 69; H-D Model

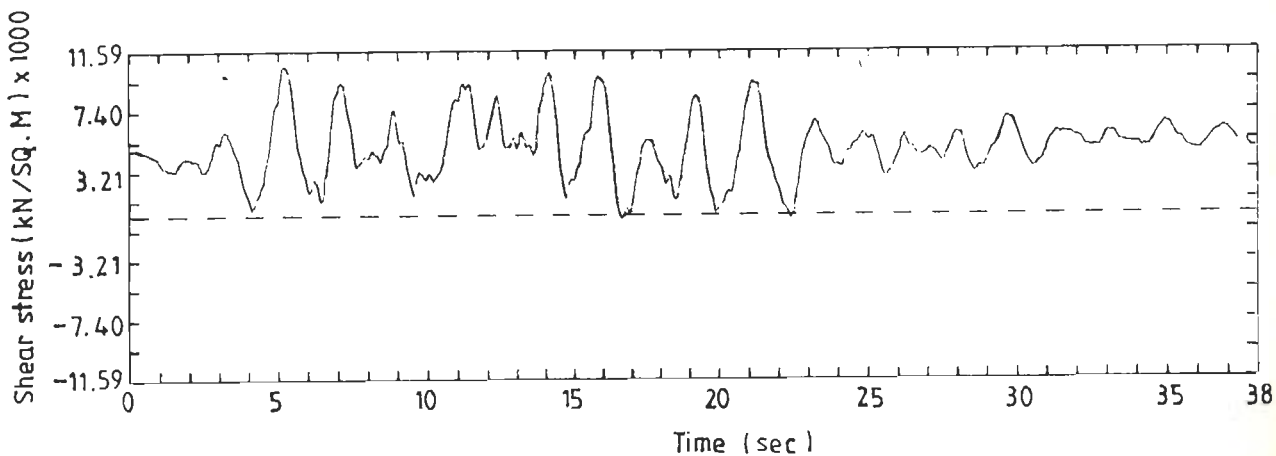


Fig. 8.141 Shear Stress Time-History at Element 69; S-I Method

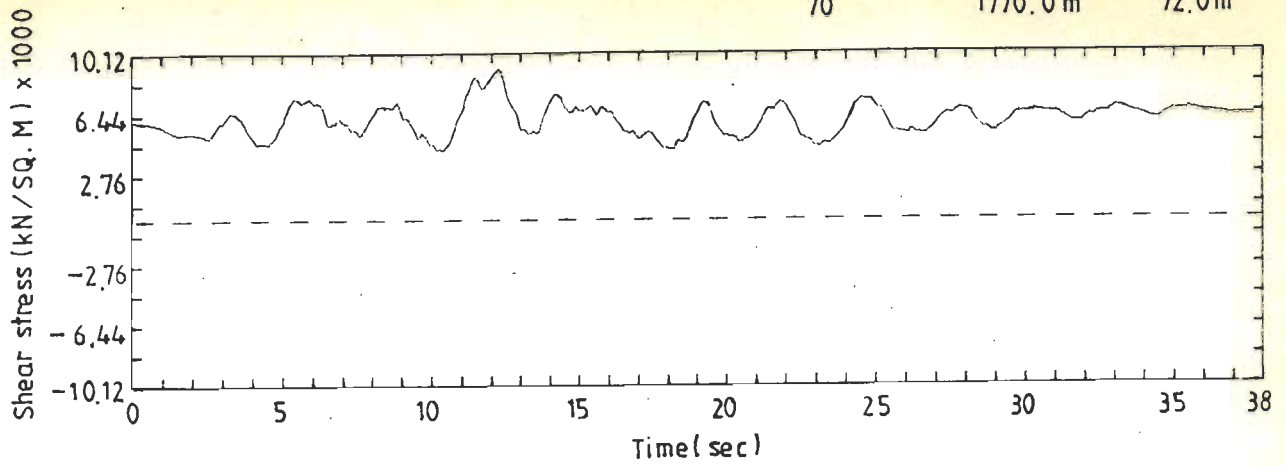


Fig. 8.142 Shear Stress Time-History at Element 70; R-O Model

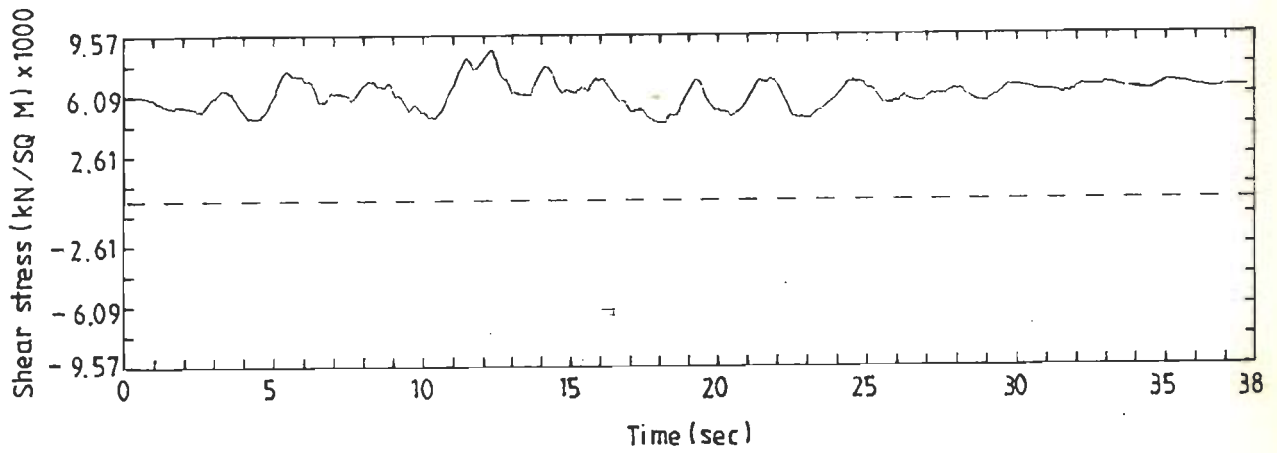


Fig. 8.143 Shear Stress Time-History at Element 70; H-D Model

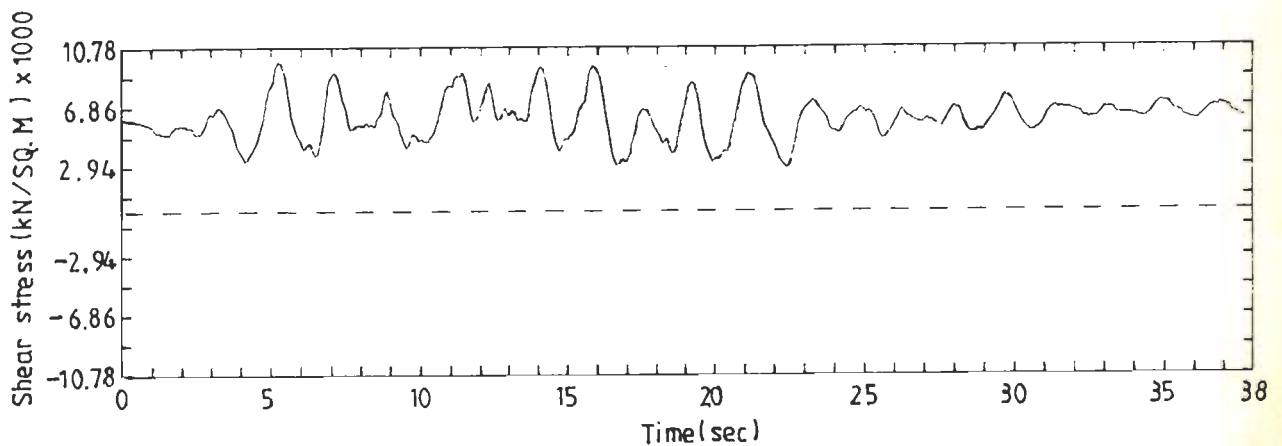


Fig. 8.144 Shear Stress Time-History at Element 70; S-I Method

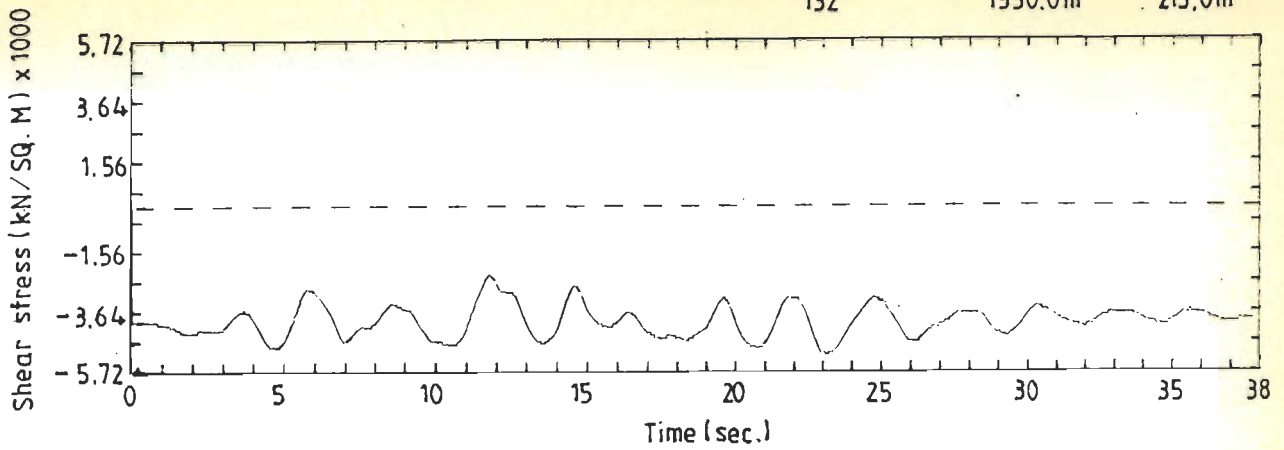


Fig. 8.145 Shear Stress Time-History at Element 132; R-O Model

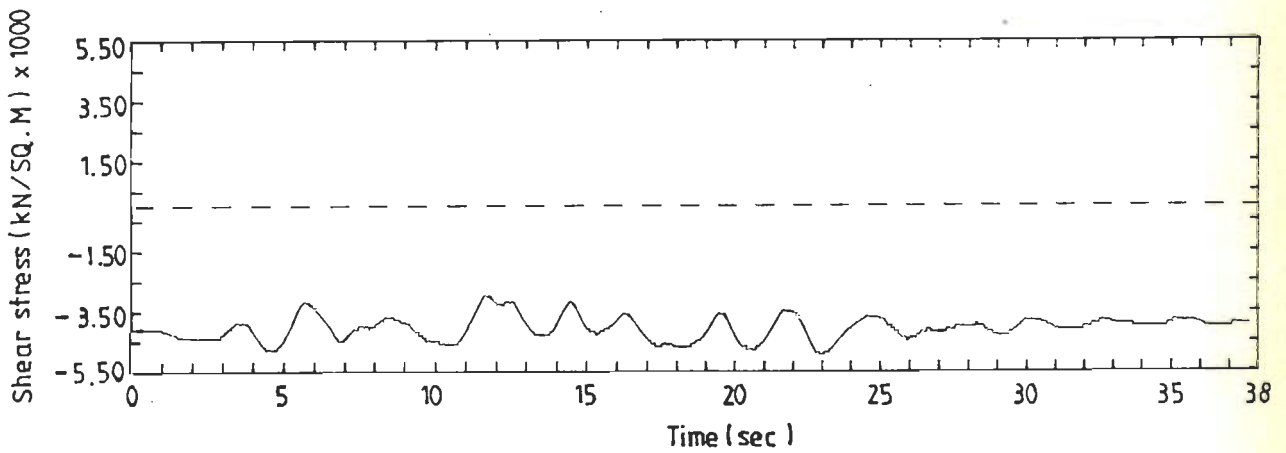


Fig. 8.146 Shear Stress Time-History at Element 132; H-D Model

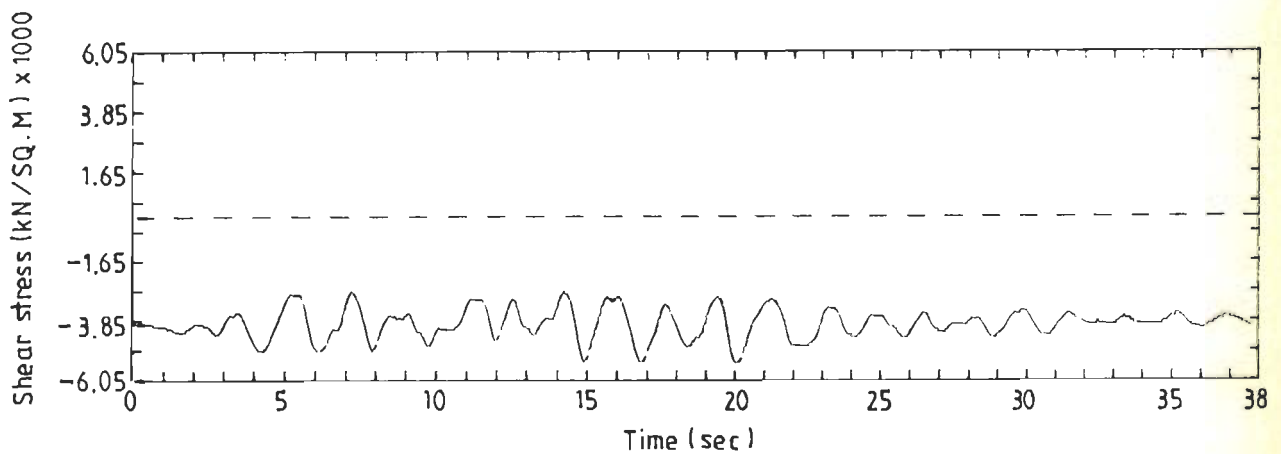


Fig. 8.147 Shear Stress Time-History at Element 132; S-I Method

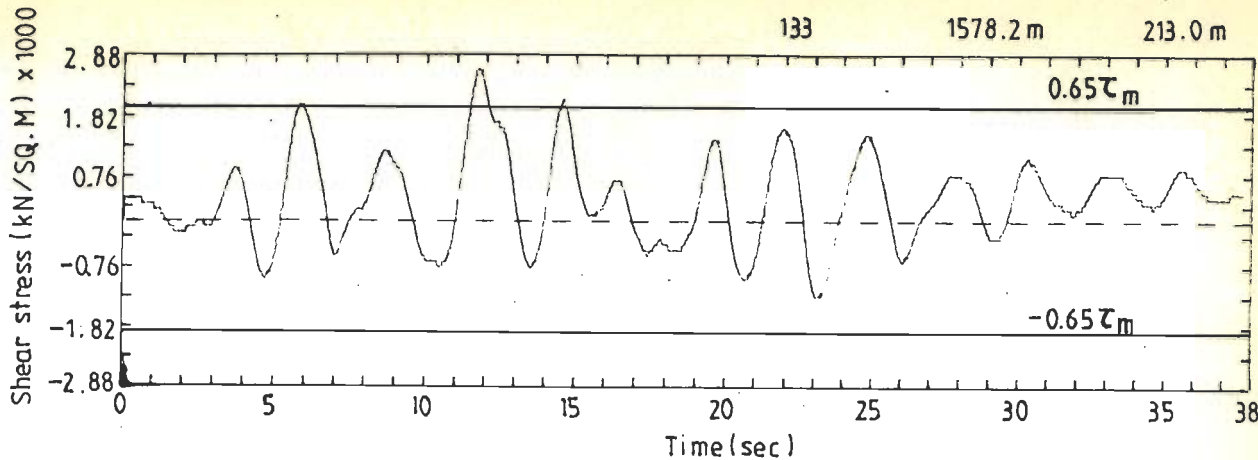


Fig. 8.148 Shear Stress Time-History at Element 133; R-O Model

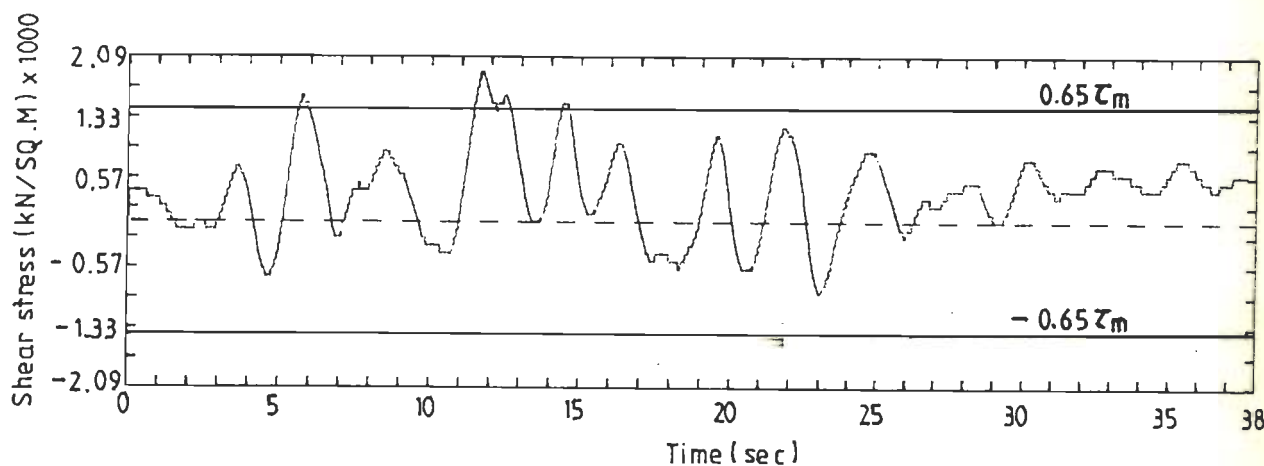


Fig. 8.149 Shear Stress Time-History at Element 133; H-D Model

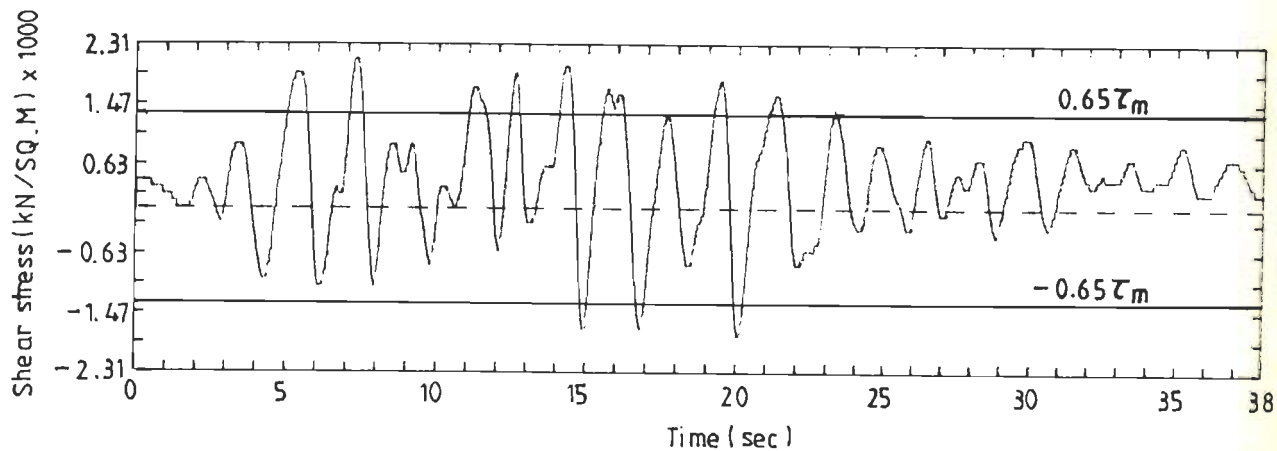


Fig. 8.150 Shear Stress Time-History at Element 133; S-I Method

134

1610.5m

213.0m

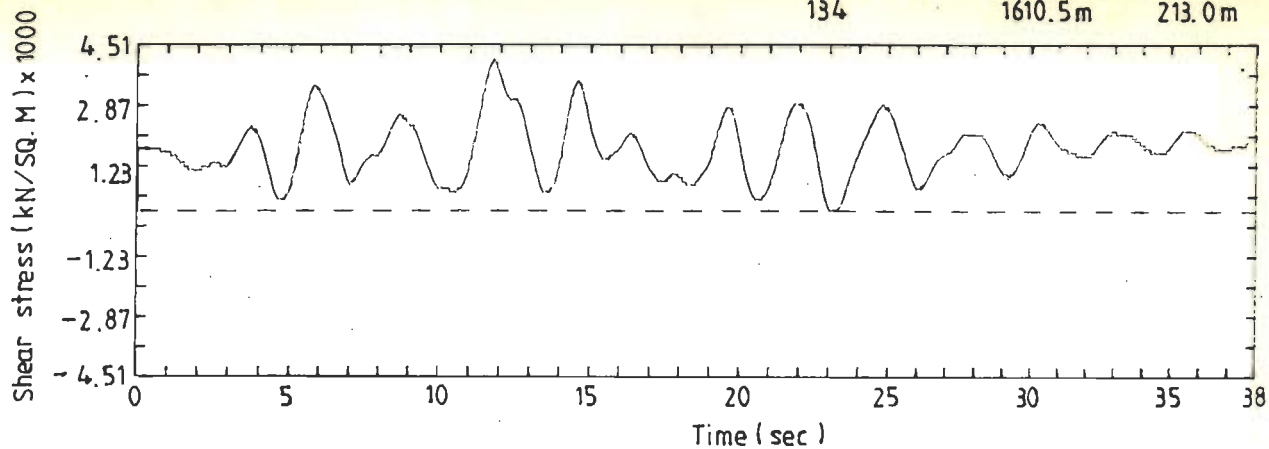


Fig. 8.151 Shear Stress Time-History at Element 134; R-O Model

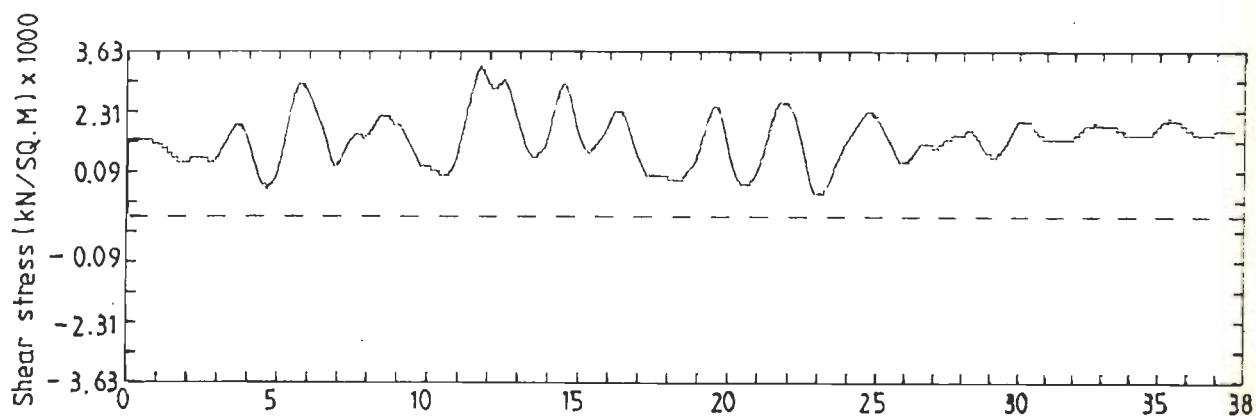


Fig. 8.152 Shear Stress Time-History at Element 134; H-D Model

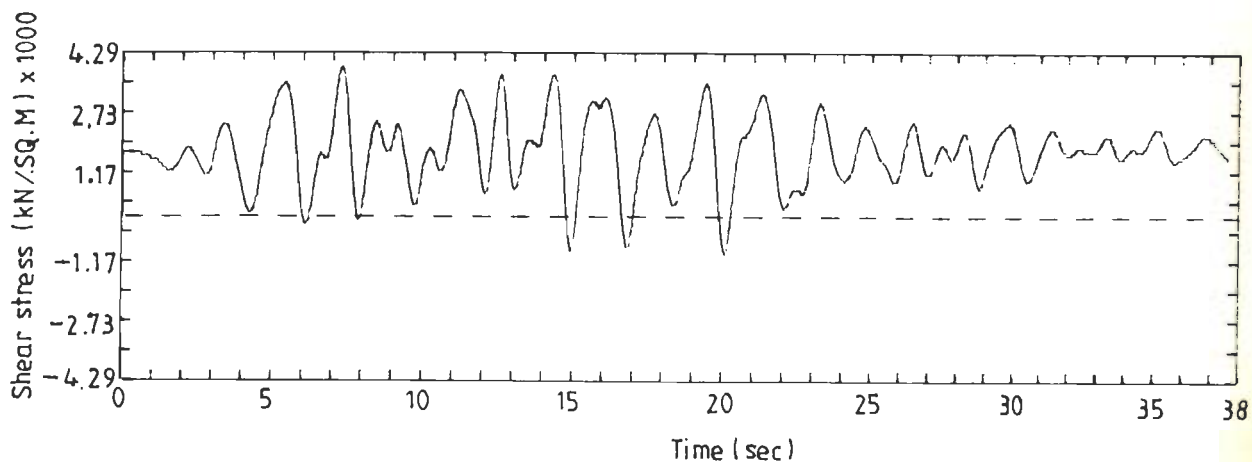


Fig. 8.153 Shear Stress Time-History at Element 134; S-I Method

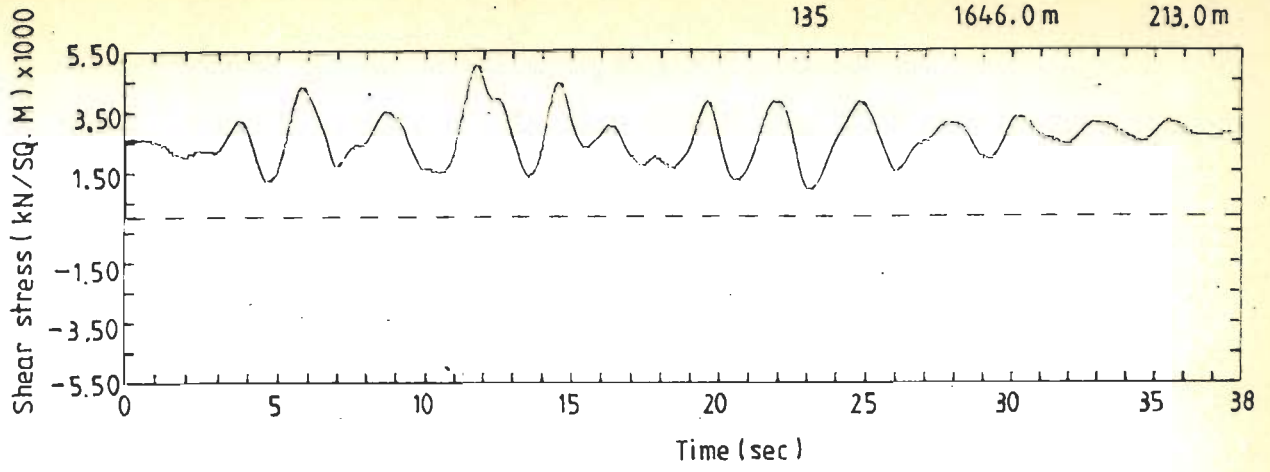


Fig. 8.154 Shear Stress Time-History at Element 135; R-O Model

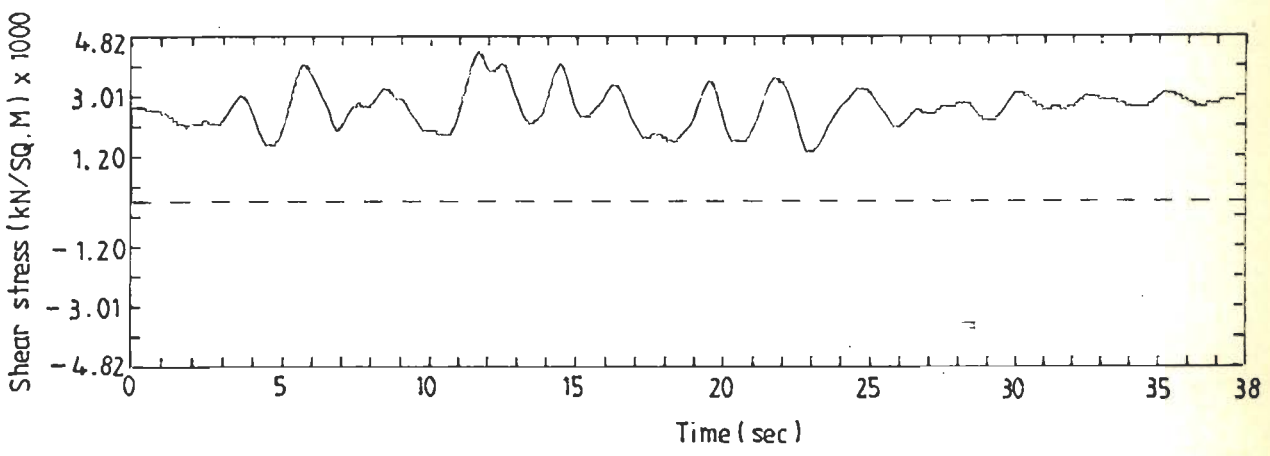


Fig. 8.155 Shear Stress Time-History at Element 135; H-D Model

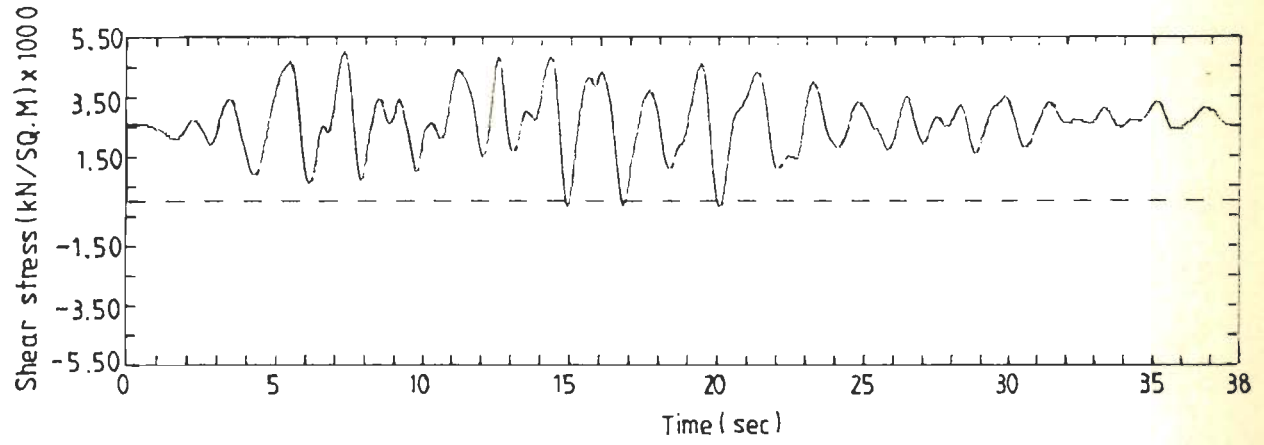


Fig. 8.156 Shear Stress Time-History at Element 135; S-I Method

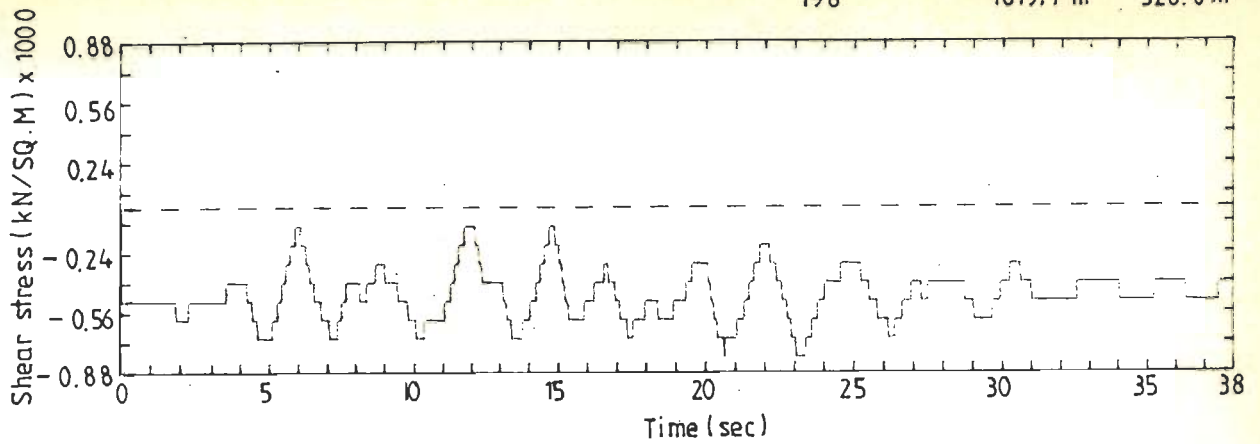


Fig. 8.157 Shear Stress Time-History at Element 198; R-O Model

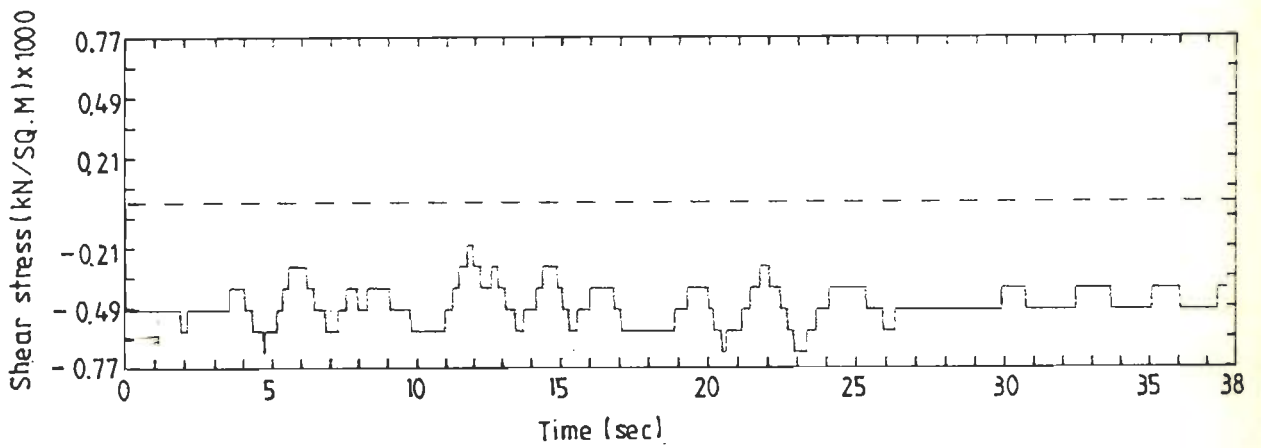


Fig. 8.158 Shear Stress Time-History at Element 198; H-D Model

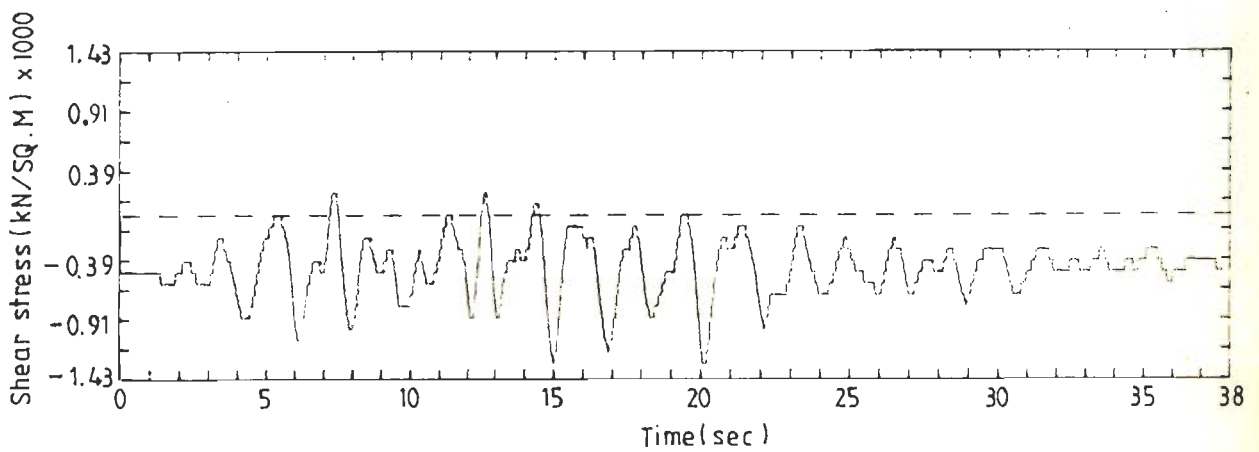


Fig. 8.159 Shear Stress Time-History at Element 198; S-I Method

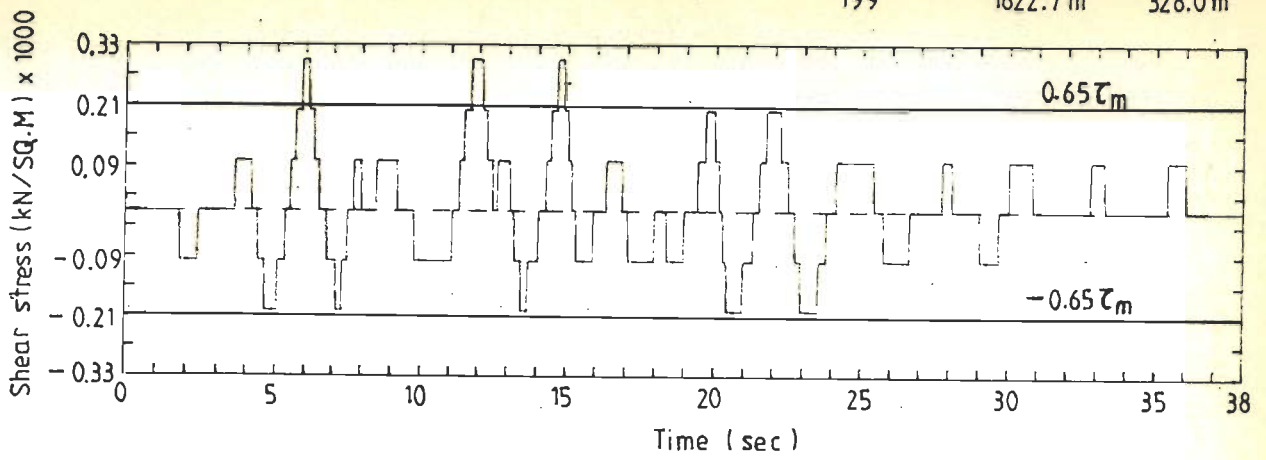


Fig. 8.160 Shear Stress Time-History at Element 199; R-O Model

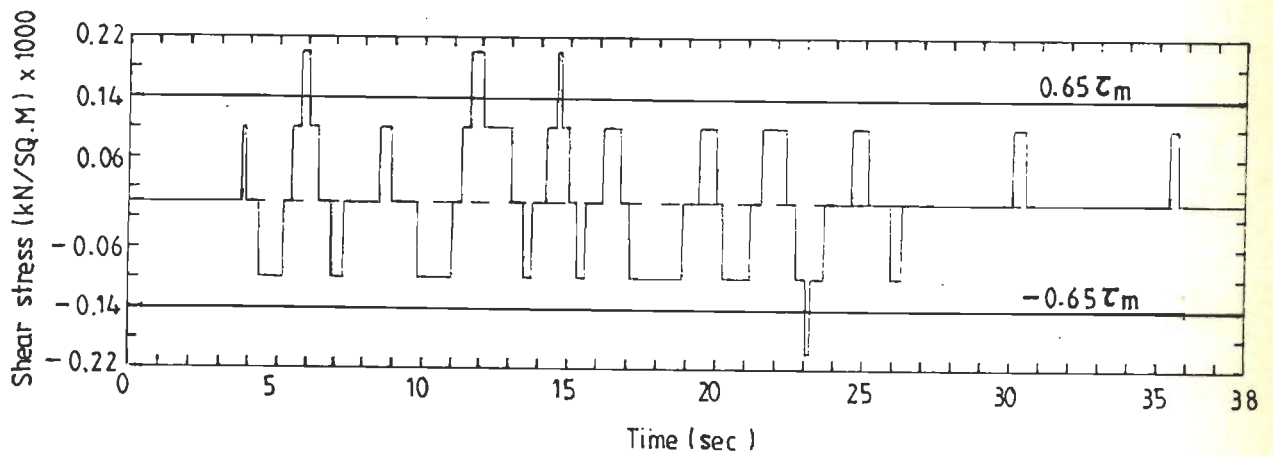


Fig. 8.161 Shear Stress Time-History at Element 199; H-D Model

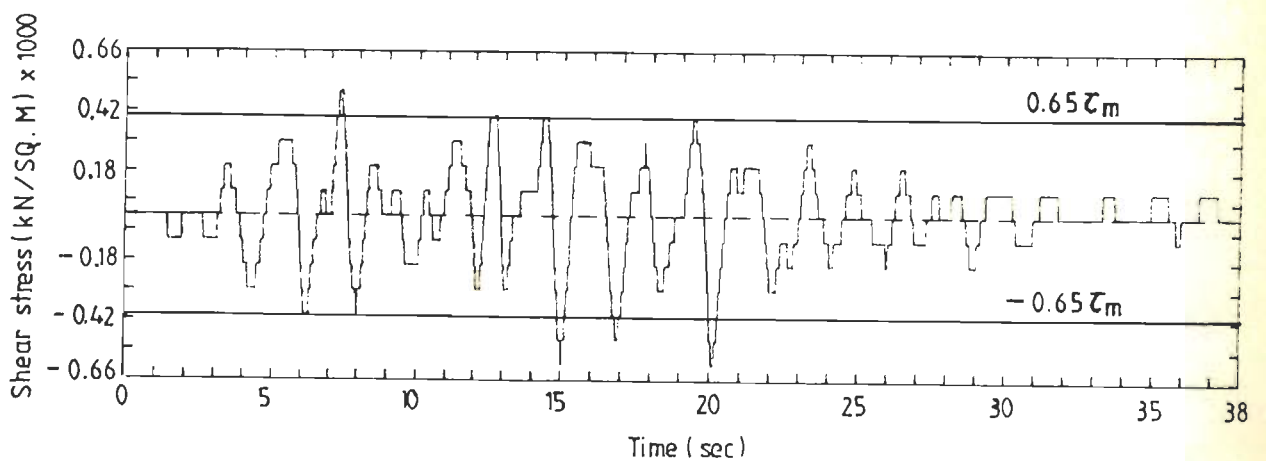


Fig. 8.162 Shear Stress Time-History at Element 199; S-I Method

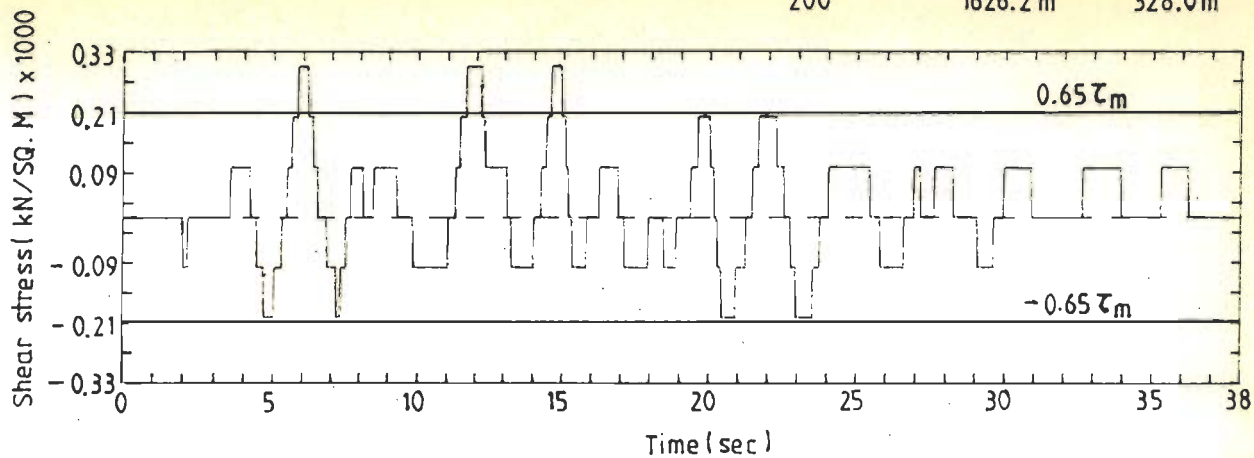


Fig. 8.163 Shear Stress Time-History at Element 200; R-O Model

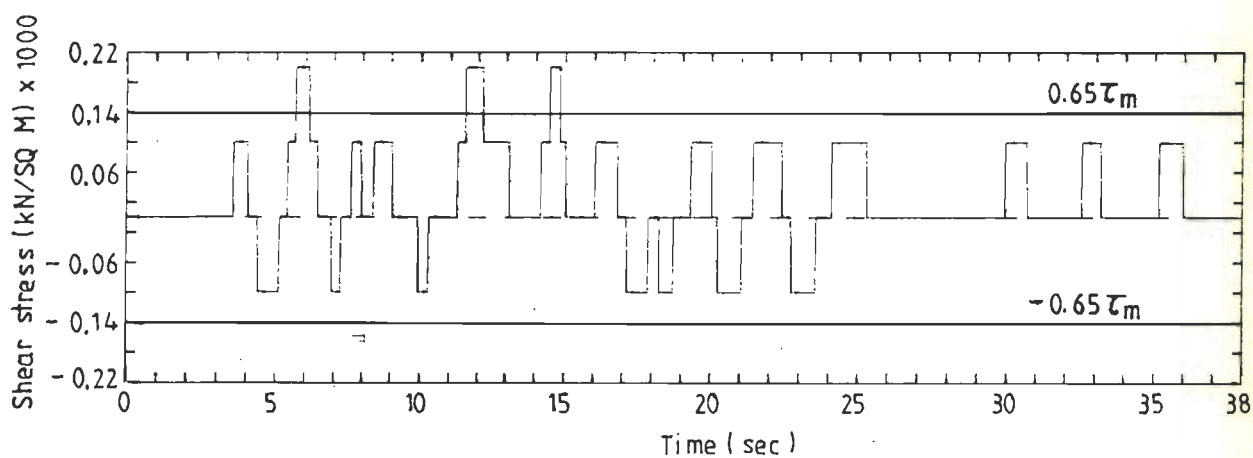


Fig. 8.164 Shear Stress Time-History at Element 200; H-D Model

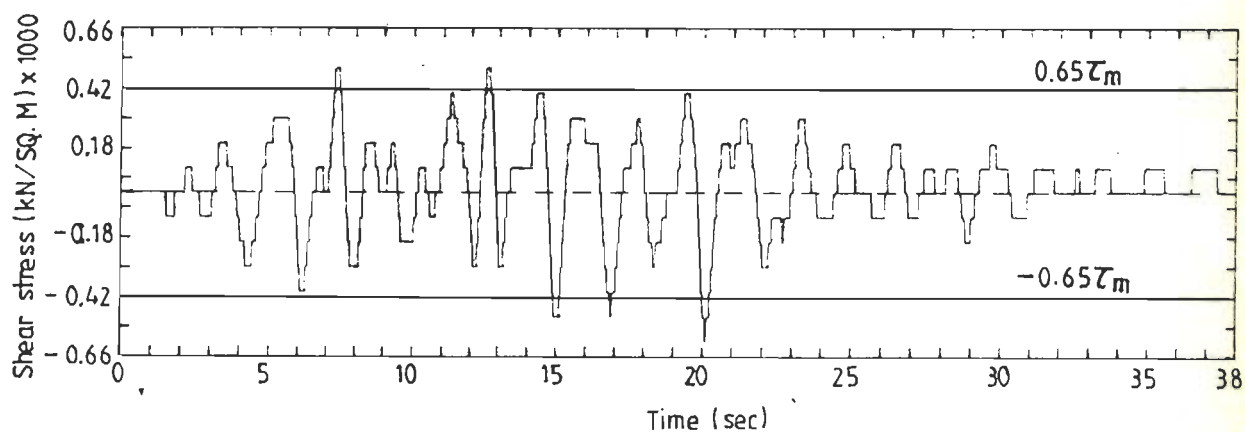


Fig. 8.165 Shear Stress Time-History at Element 200; S-I Method

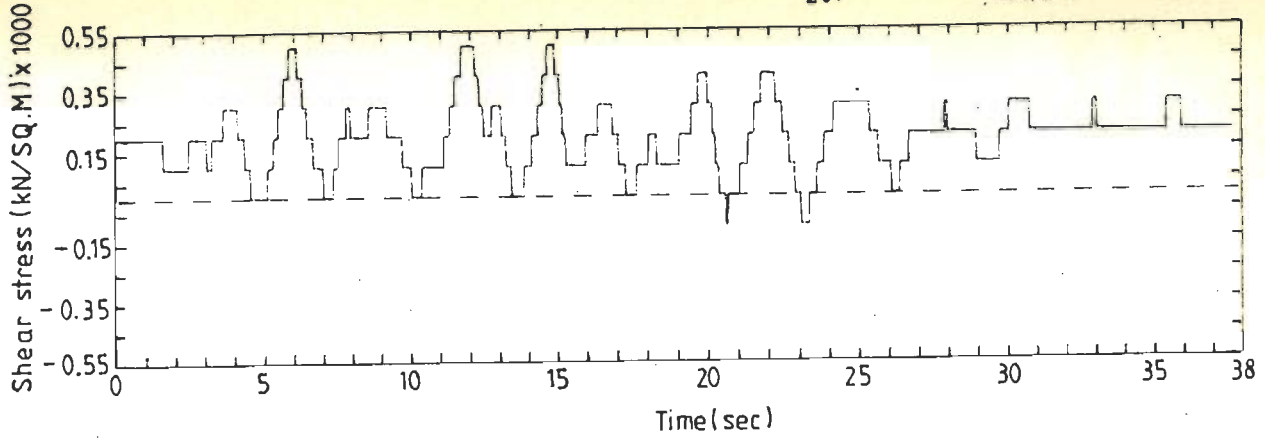


Fig. 8.166 Shear Stress Time-History at Element 201; R-O Model

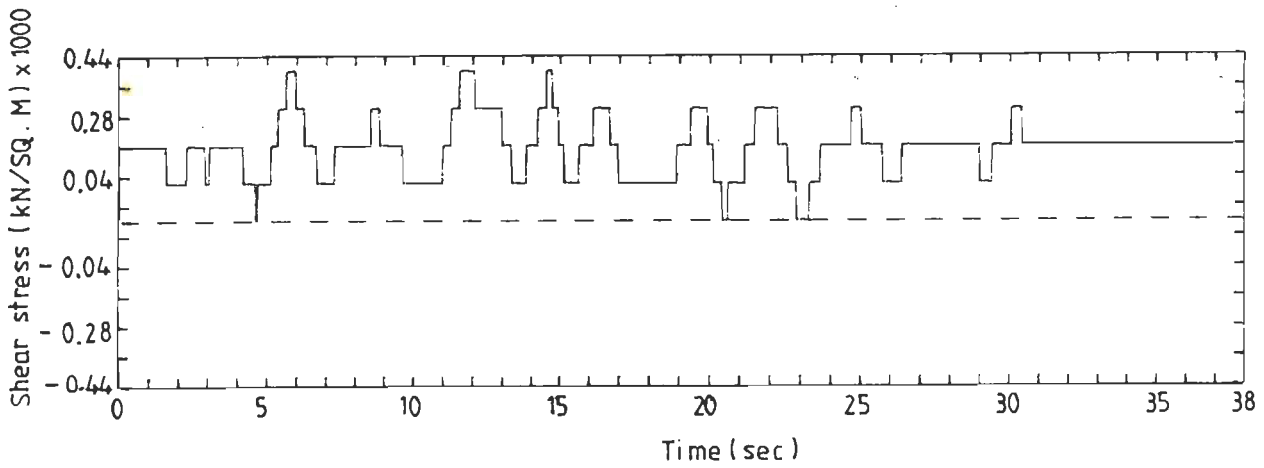


Fig. 8.167 Shear Stress Time-History at Element 201; H-D Model

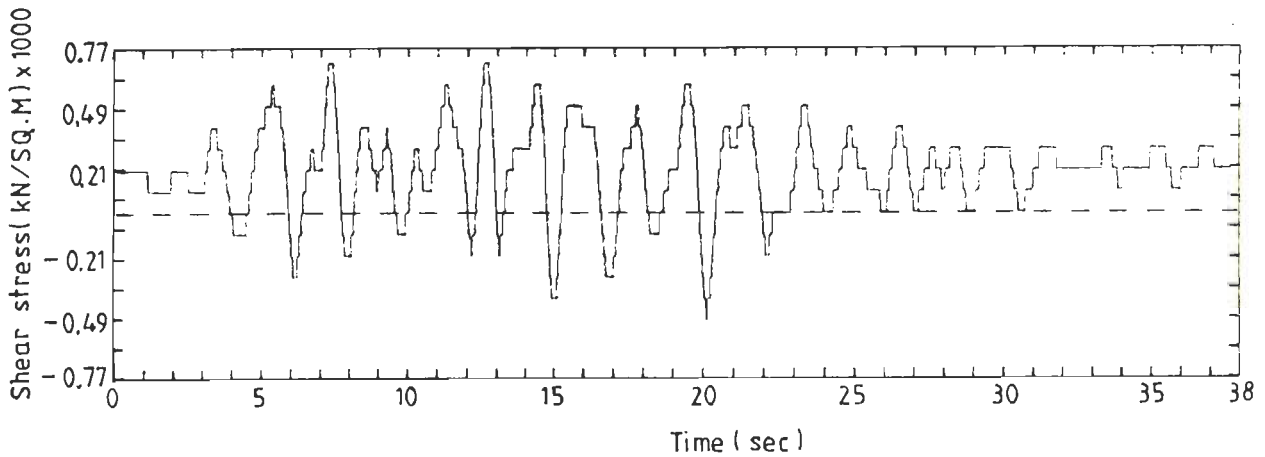


Fig. 8.168 Shear Stress Time-History at Element 201; S-I Method

acceleration values at specified nodes, the maximum values of shear strain at a few element centres and the displacement at the crest have been given in Tables 8.26 to 8.33 respectively.

8.11.8.1 Acceleration

From the peak acceleration values obtained by the Ramberg-Osgood model corresponding to GM1, the crest acceleration at three locations (nodes 1, 13 and 23) is of the order of 0.15g, 0.15g and 0.16g (Column 4, Table 8.26) respectively. These acceleration values are less than the base input motion (= 0.25g) and deamplification of the order of 40, 40 and 36 percent is noticed. However, along the axis at a location immediately below the crest (node 48), the maximum value of acceleration is 0.17g.

At an elevation, $0.75H$ (H is the total height of the dam from the base), the acceleration values at the upstream slope surface, along the axis and at the downstream slope surface are 0.13g, 0.07g and 0.10g which shows the deamplification phenomenon to a greater extent.

At half the height, the acceleration values at the three locations (nodes 316, 328 and 338) are of the order of 0.22g, 0.09g and 0.15g where deamplification is more along the axis in comparison to the two extreme slope surfaces. The acceleration value is larger in the upstream slope surface than in the downstream slope surface. At $0.25H$ from the base, the acceleration values are 0.32g, 0.23g and 0.31g (nodes 456, 468 and 478), in which deamplification is observed

only at the axis to a very low extent. The acceleration value obtained at node 456 ($=0.32g$) is the highest value for the ground motion GM1. At the top of foundation (66 m from the base) and in the body of the foundation (44 m from base) no deamplification is seen. The computed acceleration values below the dam and in the body of the foundation at two elevations (66 m and 44 m) are of the order of 0.30g, 0.25g and 0.29g (nodes 511, 523 and 533; 66 m from the base) and 0.31g, 0.26g and 0.30g (nodes 606, 618 and 628; 44 m from the base) respectively. This shows that the foundation experiences larger acceleration values than the body of the dam. The acceleration value at the two extreme toes of the foundation, at different heights from the base (nodes 491, 553, 586 and 648) is 0.25g.

Similar trend in the distribution of acceleration values have been reported in the dynamic analysis of Fort Peck Dam by Marcuson and Krinitzsky (1976). Similar observation, in the distribution of acceleration is noticed due to the artificial accelerogram (Column 5, Table 8.26) and the Taft earthquake record (Column 6, Table 8.26). In these two cases, the peak acceleration values corresponding to the two input motions (GM2 and GM3) are of the order of 0.33g and 0.32g respectively occurring immediately below the crest along the axis (node 48), and not at the crest. The acceleration value at the crest is 0.25g which shows non-occurrence of deamplification phenomenon.

For both the ground motions between a height of 0.75H and 0.50H deamplification is noticed at all the

locations and to a larger degree along the axis at $0.25H$ from the base as well. Identically, at the other locations, the same type of distribution, similar to that of GM1 is observed as shown in Table 8.26.

At all the elevations from the crest to the base, the upstream of the dam experiences higher values of acceleration than the corresponding locations in the downstream. This indicates that the presence of a full reservoir makes a rockfill dam more disaster prone in the event of a strong ground shaking.

Using the Ramberg-Osgood model and the three base input motions as earthquake load vectors, in Figs. 8.169 to 8.171, at a few locations where only amplification of acceleration has taken place are plotted.

The distribution of acceleration based on the Hardin-Drnevich model is similar to the distribution observed in the Ramberg-Osgood model, except for an appreciable amount of deamplification between the crest and $0.50H$ for all the three ground motions. From $0.25H$ to the base of the foundation the distribution pattern of acceleration is more or less the same as the distribution noticed in the Ramberg-Osgood model. In all the locations along the axis, lower values of acceleration are seen than the two extreme slope surfaces. The body of the dam along the axis experiences lesser value of acceleration than the base. As before, the nodes in the upstream experience more acceleration values than the corresponding nodes in the downstream as noticed in Table 8.27.

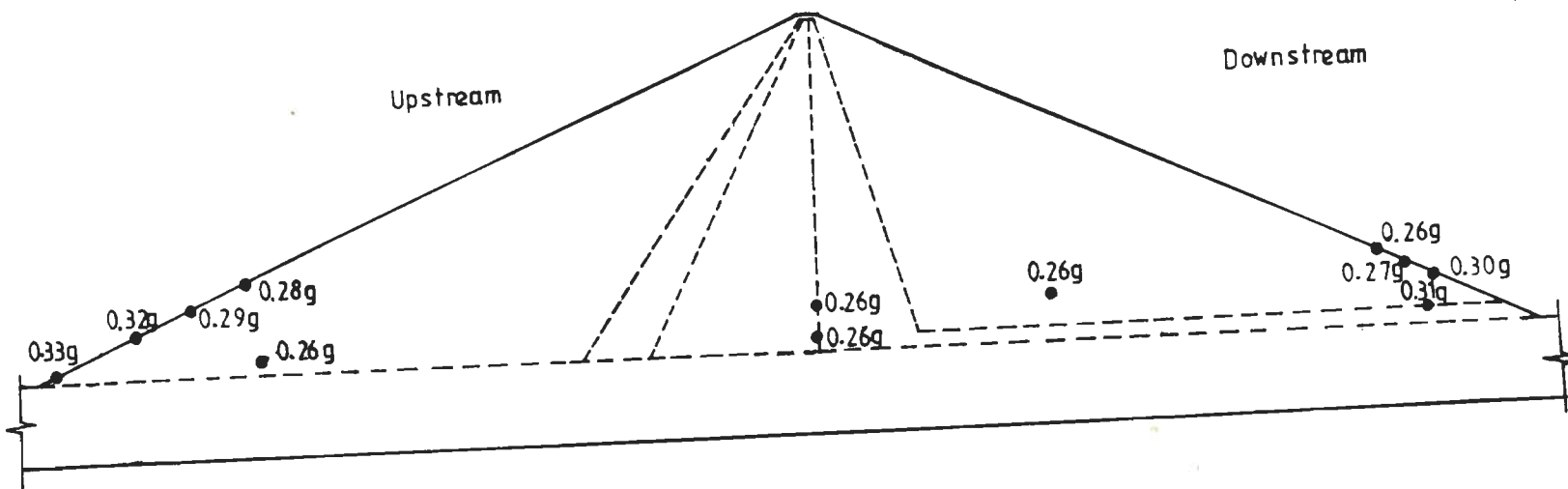


Fig. 8.169 Dam DC; Amplified Acceleration Values at a few Locations; R-O Model; GM1

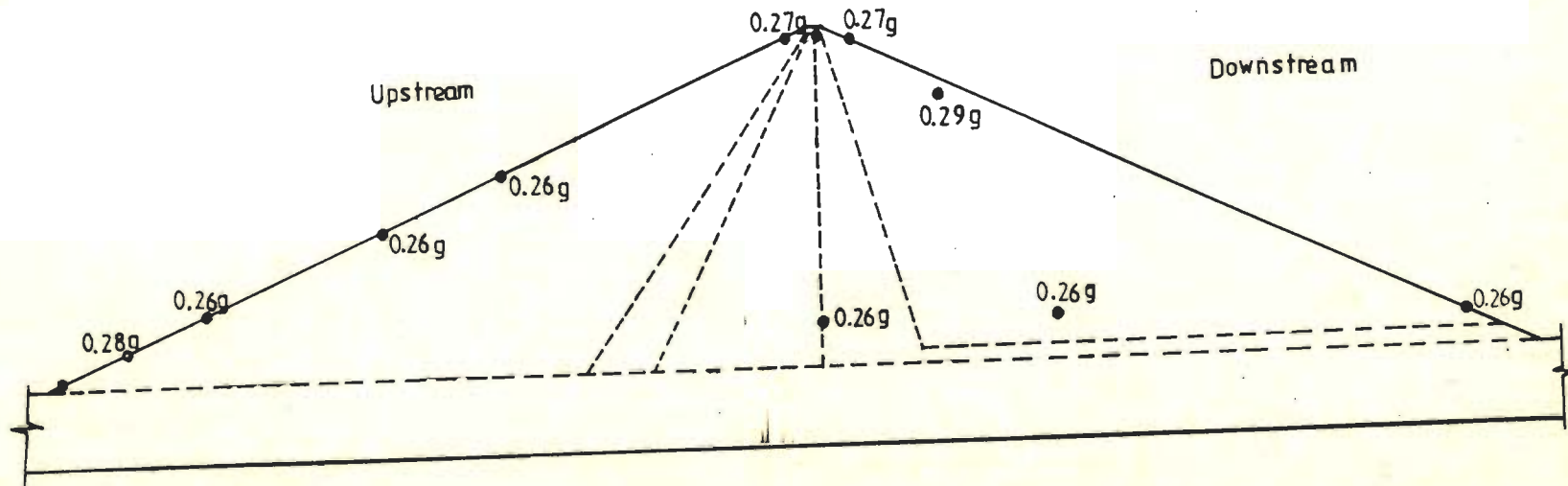


Fig. 8.170 Dam DC; Amplified Acceleration Values at a few Locations; R-O Model; GM2

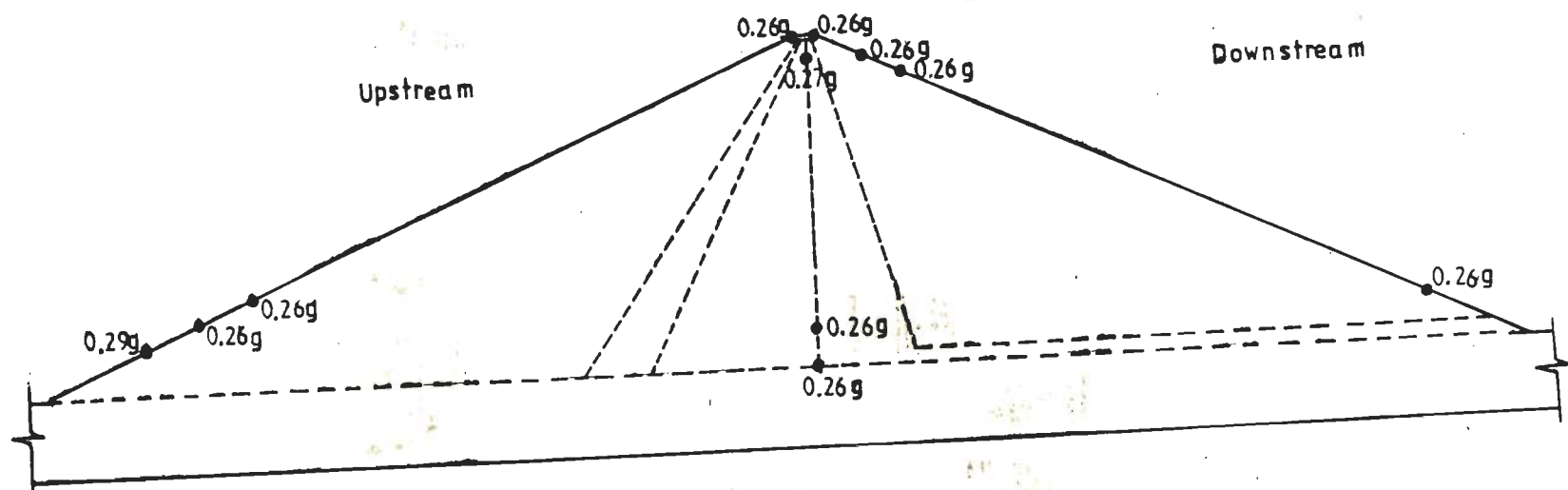


Fig. 8.171 Dam DC; Amplified Acceleration Values at a few Locations; R-O Model; GM3

Based on the Hardin-Drnevich model, in Figs. 8.172 to 8.174, at a few locations where only amplification is noticed, the values of acceleration are displayed for the three ground motions respectively.

From the dynamic analysis based on the Seed-Idriss method the least degree of deamplification is noticed at the crest when compared to the previous two models. The maximum acceleration values of the order of 0.32g, 0.37g and 0.36g respectively for the three ground motions are obtained at node 23 (Table 8.28).

Deamplification to a lesser degree is noticed at an elevation of $0.75H$ from the base (nodes 211, 223 and 233) for all the three ground motions. At the same elevation ($0.75H$ from the base), the computed values of acceleration along the axis (node 223) are larger than the values obtained in the downstream (node 233). Such a behaviour was noticed in the other two models and in the previous dynamic analyses of the El Infiernillo Dam and dam DB.

At elevations between $0.50H$ and $0.25H$ from the base, the acceleration values along the axis are lower than the acceleration values in the downstream. Between $0.25H$ and the base of the foundation, the distribution of acceleration is similar to the distribution described in the Ramberg-Osgood and Hardin-Drnevich models, except for a variation in the magnitude of acceleration. In all the cases, as before, higher values of acceleration are obtained in the upstream than the downstream of the dam.

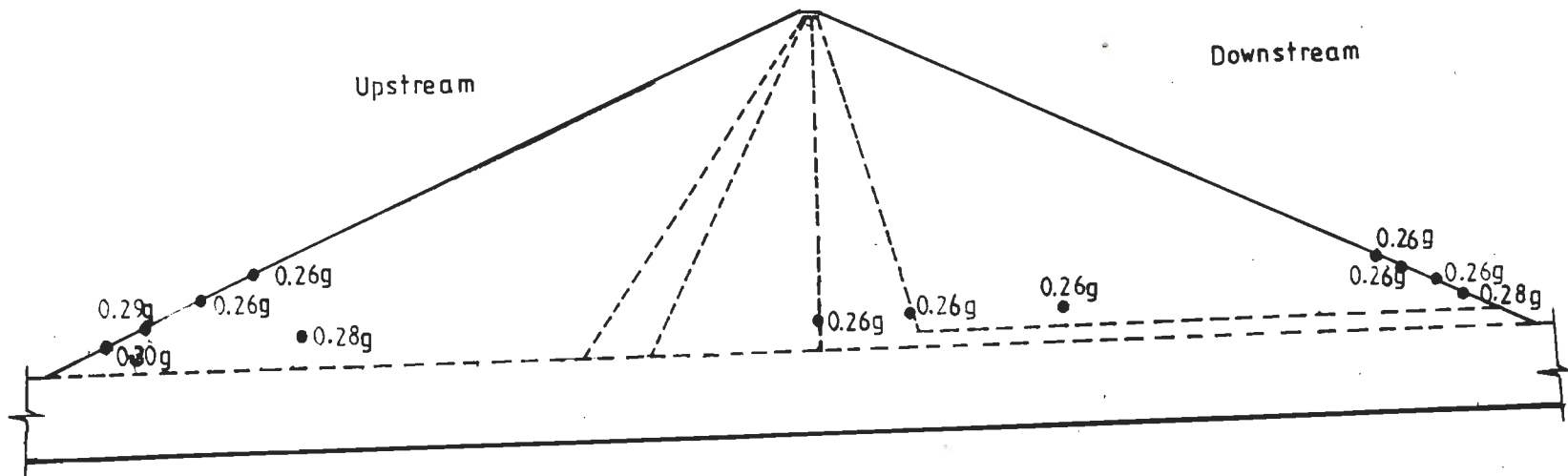


Fig. 8.172 Dam DC; Amplified Acceleration Values at a few Locations; H-D Model; GM1

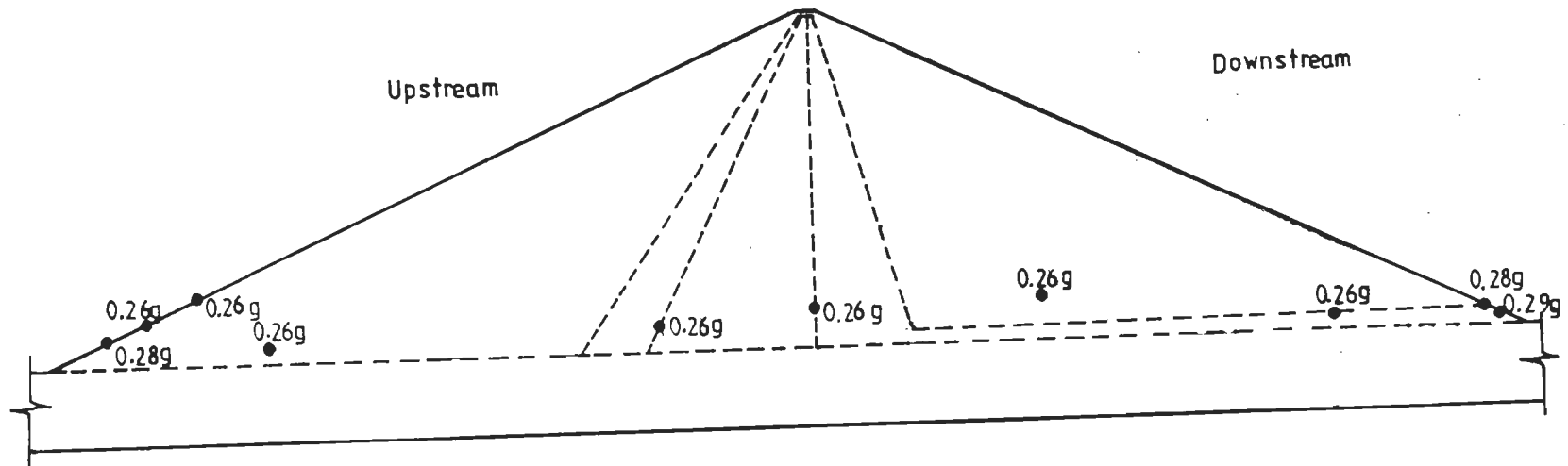


Fig. 8.173 Dam DC; Amplified Acceleration Values at a few Locations; H-D Model; GM2

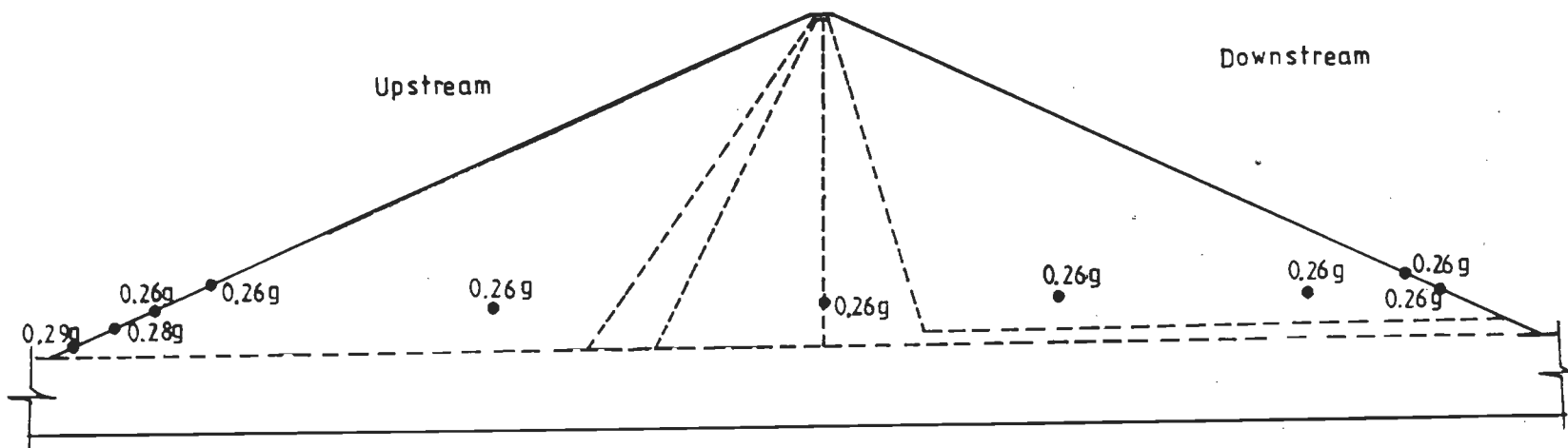


Fig. 8.174 Dam DC; Amplified Acceleration Values at a few Locations; H-D Model; GM3

Based on the Seed-Idriss method, Figs. 8.175 to 8.177 display the locations at which only amplification of acceleration has been noticed for the three input motions.

In general, the Ramberg-Osgood and the Hardin-Drnevich models show lower and higher degree of deamplification phenomena respectively. The Seed-Idriss method shows the least degree of deamplification. In all the three methods of analysis and for the three ground motions, between an elevation $0.25H$ and the bottom of the foundation of dam DC, the distribution of acceleration is more or less the same. In all the cases, higher values of acceleration are noticed in the foundation than the body of the dam. These analysis results conform with that of the dynamic analysis of the Fort Peck Dam (Marcuson and Krinitzsky, 1976). The presence of water makes a rockfill dam more vulnerable to earthquakes. Out of all the three ground motions, the synthetic waveform is more severe than the other two accelerograms corresponding to the two actual earthquake records.

8.11.8.2 Shear strain

From Table 8.29 at any elevation, it can be seen that the shear strain values obtained by the Ramberg-Osgood model using GM1 are less than 1.0 percent. The maximum value of dynamic shear strain is of the order of 0.542 percent and the value of total shear strain is 4.013 percent occurring at element 200, which lies at the top of the impervious core (Fig. 8.64, second layer from the crest). At other locations,

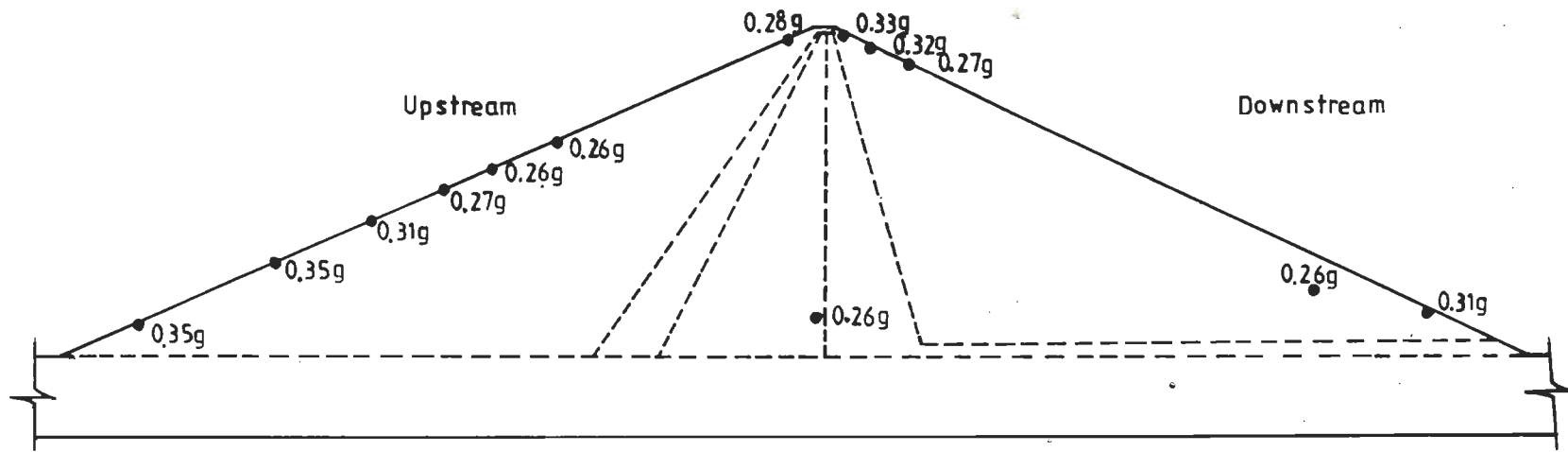


Fig. 8.175 Dam DC; Amplified Acceleration Values at a few Locations; S-I Method; GM1

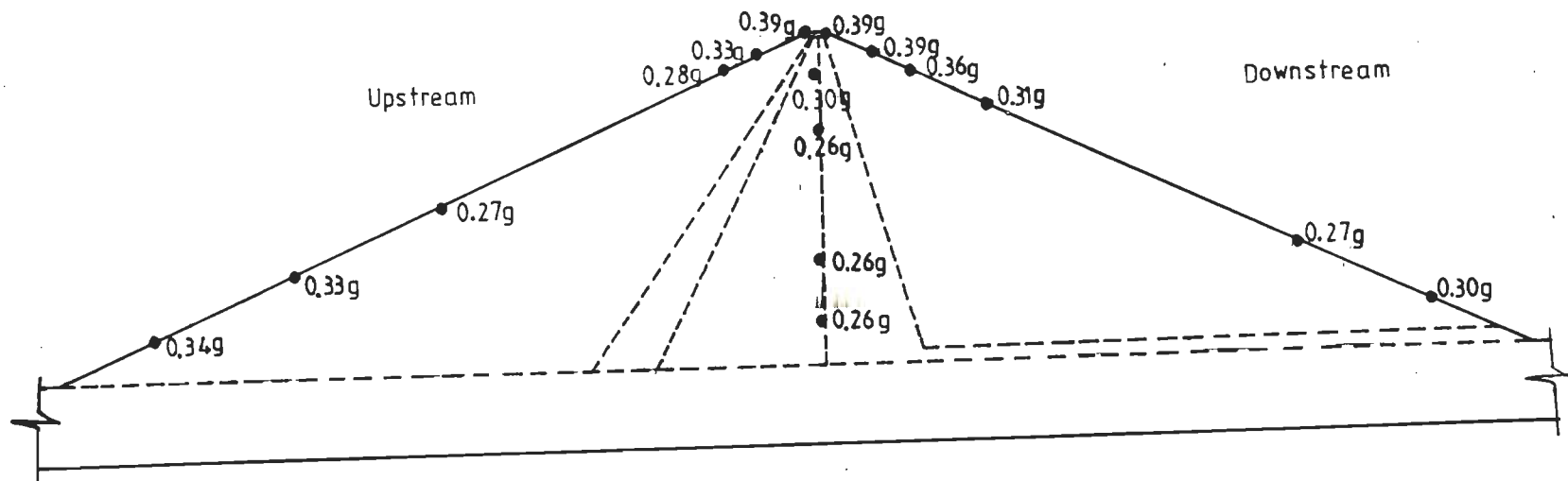


Fig. 8.176 Dam DC; Amplified Acceleration Values at a few Locations; S-I Method; GM2

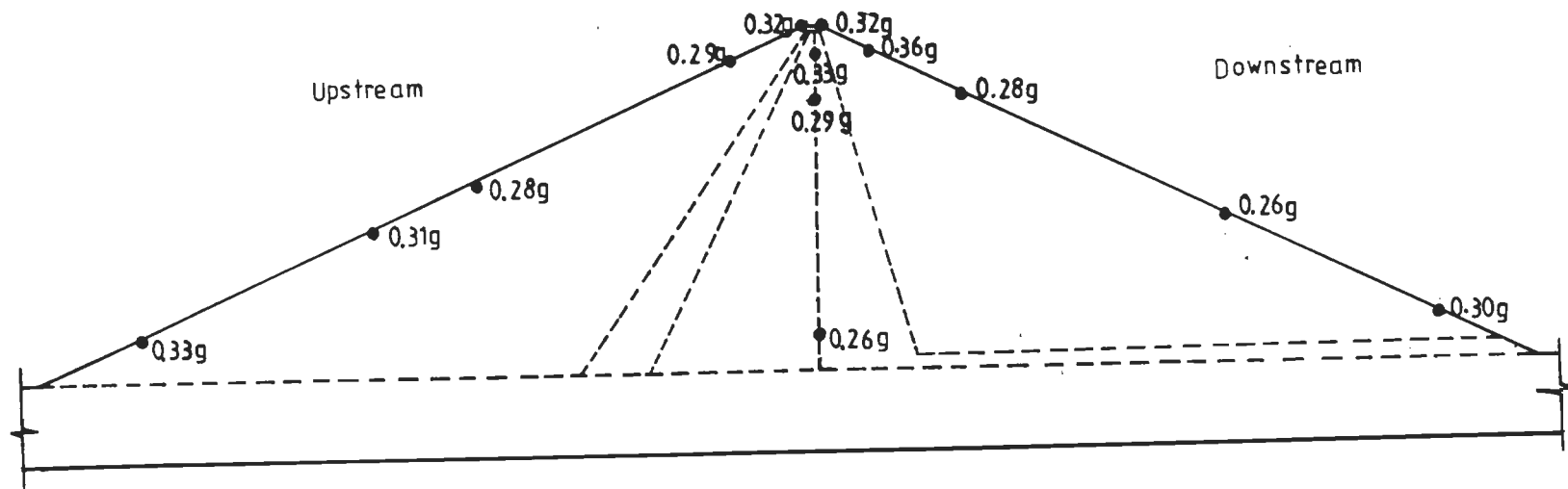


fig. 8.177 Dam DC; Amplified Acceleration Values at a few Locations; S-I Method; GM3

the elements lying in the upstream transition zone yield larger values of shear strain than the downstream transition zone. This behaviour could possibly be due to transfer of load from upstream shell zone to the core and low stiffness zones of the filter. The value of shear strain in the core is lower than the adjacent filter zones in the upstream and the downstream except at element 200.

Corresponding to the artificial accelerogram and the Taft earthquake record the peak values of dynamic shear strain are of the order of 8.491 and 3.265 and the total values of shear strain are 10.162 and 4.936 percent respectively, occurring at element 199 in the core (second layer from the crest), at an elevation of 328 metres from the base. At all other elevations, the value of shear strain in the upstream filter zone is larger than that in the downstream filter zone, demonstrating the transfer of load from the high stiff shell zone to the relatively low stiff filter material.

Further, as described in the analysis of El Infiernillo Dam based on a 5 percent shear strain as the failure criteria, the dam DC reaches the threshold level of failure at the top portion of the core (elements 199 and 200), when the artificial accelerogram is used as the base input motion.

The distribution of shear strain values obtained at the few element centres using the Hardin-Drnevich model (Table 8.30), are similar to the distribution observed using the Ramberg-Osgood model (Table 8.29), except that the peak values of dynamic shear strain of the order of 1.829 percent

and 2.739 percent and the total values of shear strain as 3.847 and 4.757 percent are obtained corresponding to GM1 and the artificial accelerogram (GM2) respectively and taking place at element 66 (72 m from the base). However, in the analysis using the Taft earthquake record, the peak value of dynamic shear strain of the order of 2.251 percent and the total value of shear strain as 4.269 percent are noticed at element 66. As before, the transition in the upstream experiences higher values of shear strain than that in the downstream.

From the shear strain values shown in Table 8.31 by the Seed-Idriss method, the peak value of dynamic shear strain is noticed at element 199, which is of the order of 2.712 percent and the total value of shear strain as 6.073 percent when GM1 has been used as the base input motion. For this input motion, in all the three methods of analysis, the Seed-Idriss method yields the largest value of shear strain in comparison to the other two models. This behaviour has not been observed in the analysis of the El Infiernillo Dam and dam DB. Similarly, another peak value of dynamic shear strain is noticed at element 156 which is lying in the downstream. At all other elevations the largest value of shear strain is noticed in the upstream filter zone only.

For the analysis based on the synthetic accelerogram the largest value of dynamic shear strain by the Seed-Idriss method is of the order of 6.137 percent (element 199) and the total value of shear strain as 8.984 percent occurring at element 200, which are less than the values

predicted by the Ramberg-Osgood model for the same input motion and at the same elevation. At all other elevations, the shear strain values in the upstream filter zone are larger than that of the corresponding downstream filter zone for which the reason has been previously cited.

A similar pattern of distribution of dynamic shear strain is noticed when the Taft earthquake record is used as the base input motion. The peak value of dynamic shear strain is of the order of 3.067 percent and the total value of shear strain as 4.738 percent occurring in element 199, which is less than the value obtained by the Ramberg-Osgood model at the same location. At other elevations, a similar type of distribution of dynamic shear strain as described in the previous paragraph is observed. In the dynamic analysis of the dam DC, the values of shear strain in the upstream filter are larger than that in the downstream filter zone. The peak value of shear strain is obtained by the Ramberg-Osgood model for the synthetic ground motion as the earthquake load vector followed by the Seed-Idriss method for the same input motion at the top portion of the impervious core. The top part of the core lies in a region, consisting of shell, filter and core materials with varying stiffnesses.

For all the three ground motions, the Ramberg-Osgood model and the Seed-Idriss method predict the peak value of shear strain at the same elevation except in one case (GM1, Column 5 of Table 8.31, element 199). The Hardin-Drnevich model predicts the lowest values of shear strain in comparison to the other two methods of analysis.

The 336 m high dam reaches the threshold level of failure corresponding to the artificial waveform, based on the 5 percent failure criterion as predicted by the Ramberg-Osgood model and the Seed-Idriss method. The region of failure is the top portion of the core which is the zone consisting of low to high stiffness materials. Out of the three ground motions, the artificial earthquake record is more severe than the other two records pertaining to actual earthquakes.

As done previously in the case of El Infiernillo Dam and dam DB, to evaluate the stability of dam DC, the dynamic and total shear strain values have been computed using the Ramberg-Osgood model and the modified artificial accelerogram with the peak ground acceleration of 0.40g as the base input motion. These shear strain values are shown in Table 8.32. From this table it is seen that the peak value of dynamic shear strain as 12.325 percent and the value of total shear strain as 15.386 percent. As can be noticed in this table, under the postulated artificial ground motion with a peak ground acceleration value of 0.40g, approximately 50 percent of the elements lie in the threshold level of failure (value of shear strain is between 5 and 15 percent). However, this conclusion is qualitative in nature, since laboratory determined cyclic shear stress values were not available for an exact prediction of the failure phenomenon.

8.11.8.3 Displacement

The computed displacements at the crest (node 13, top of axis), for the Ramberg-Osgood and Hardin-Drnevich models and the Seed-Idriss method of analyses are of the order of 6.91, 5.99 and 9.02 cm respectively, corresponding to the base input motion, GM1 (Table 8.33). For the artificial waveform (GM2), the crest displacements for the three methods of analysis are 49.26, 27.55 and 20.85 cm respectively. And for the Taft earthquake record these values are 20.50, 13.66 and 15.69 cm respectively. As before, for the synthetic ground motion, the largest values of crest displacements are obtained irrespective of the method of analysis adopted. In all the cases, the Ramberg-Osgood model predicts the highest value of displacement of the order of 49.26 cm.

The deformed shape of the dam DC, using the Ramberg-Osgood model corresponding to the three ground motions are shown in Figs. 8.178 to 8.180. Using the Hardin-Drnevich model the deformed plots are shown in Figs. 8.181 to 8.183 and based on the Seed-Idriss method these plots are displayed in Figs. 8.184 to 8.186. These deformed shapes are obtained by connecting the displaced nodes at specific locations only.

8.11.8.4 Time-history of acceleration

From the time-history of acceleration values plotted at five locations along the axis, from the crest to

Table 8.33 Displacement at the Crest (Node 13)
 Dam DC; PGA = 0.25g

Sl. No.	Crest Displacement (cm)			Method of Analysis
	Applied Ground Motion			
	GM1 (2)	GM2 (3)	GM3 (4)	
(1)				(5)
1	6.91	49.26	20.50	Ramberg-Osgood Model
2	5.99	27.55	13.66	Hardin-Drnevich Model
3	9.02	20.85	15.69	Seed-Idriss Method

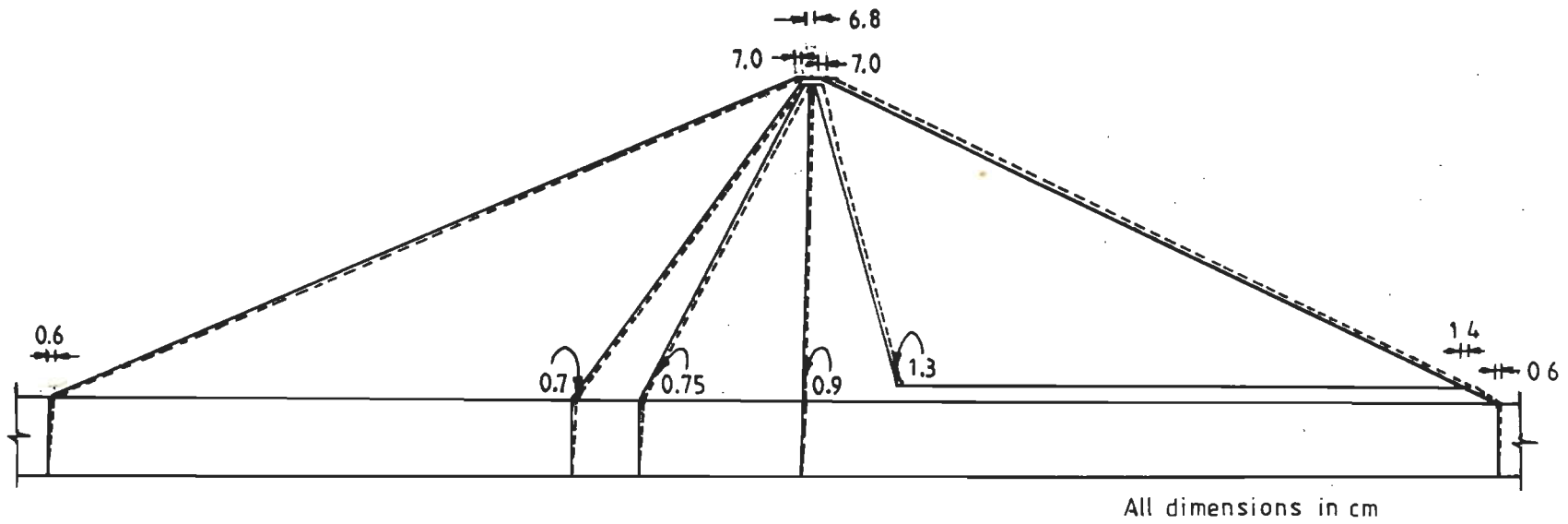
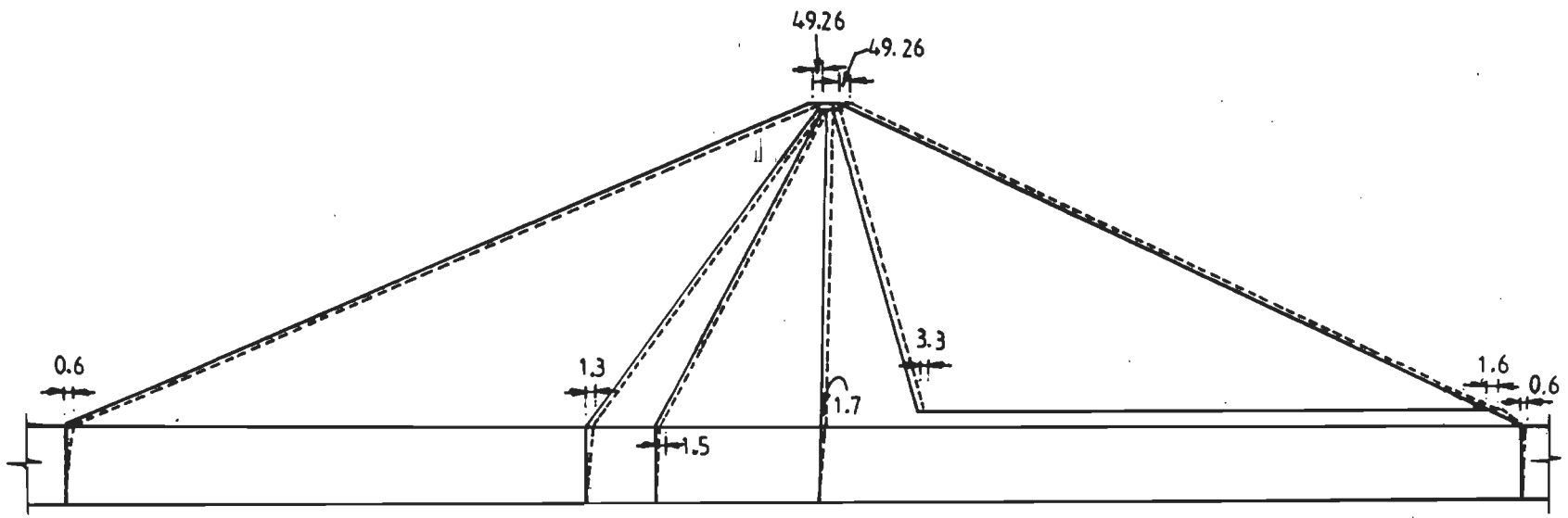


Fig. 8.178 Dam DC; Displacement Values at a few Locations; R-O Model; GM1



All dimensions in cms

Fig. 8.179 Dam DC; Displacement Values at a few Locations: R-O Model; GM2

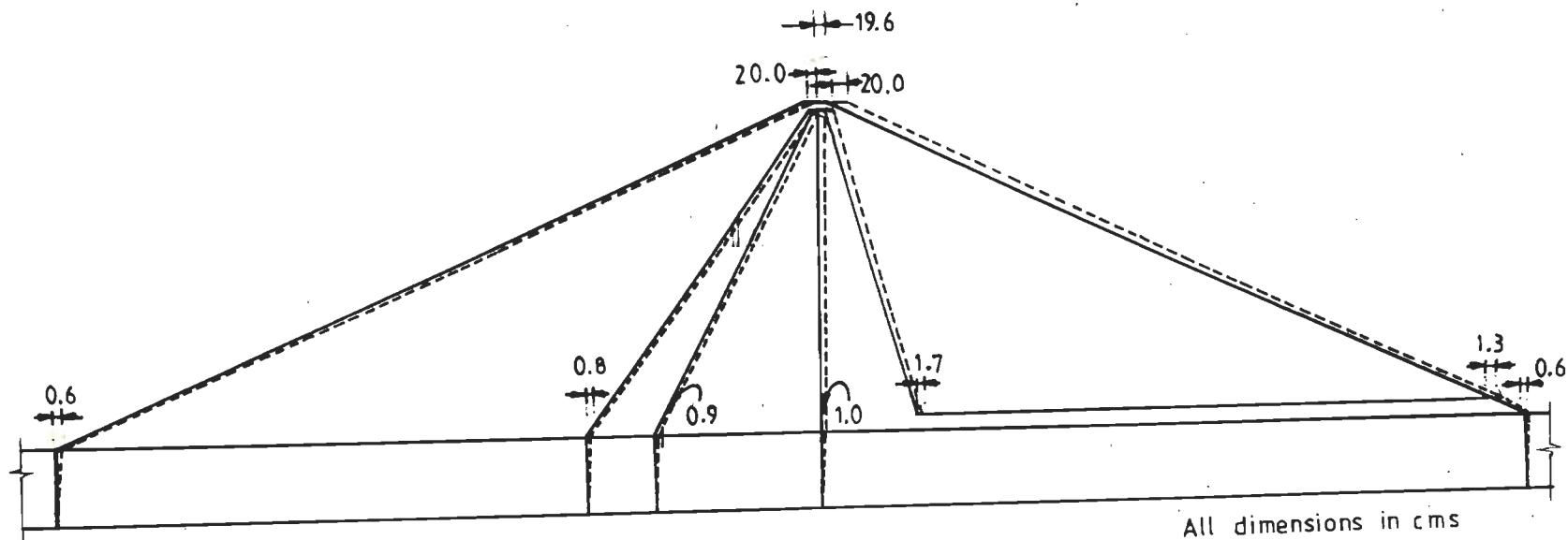


Fig. 8.180 Dam DC; Displacement Values at a few Locations; R-O Model; GM3

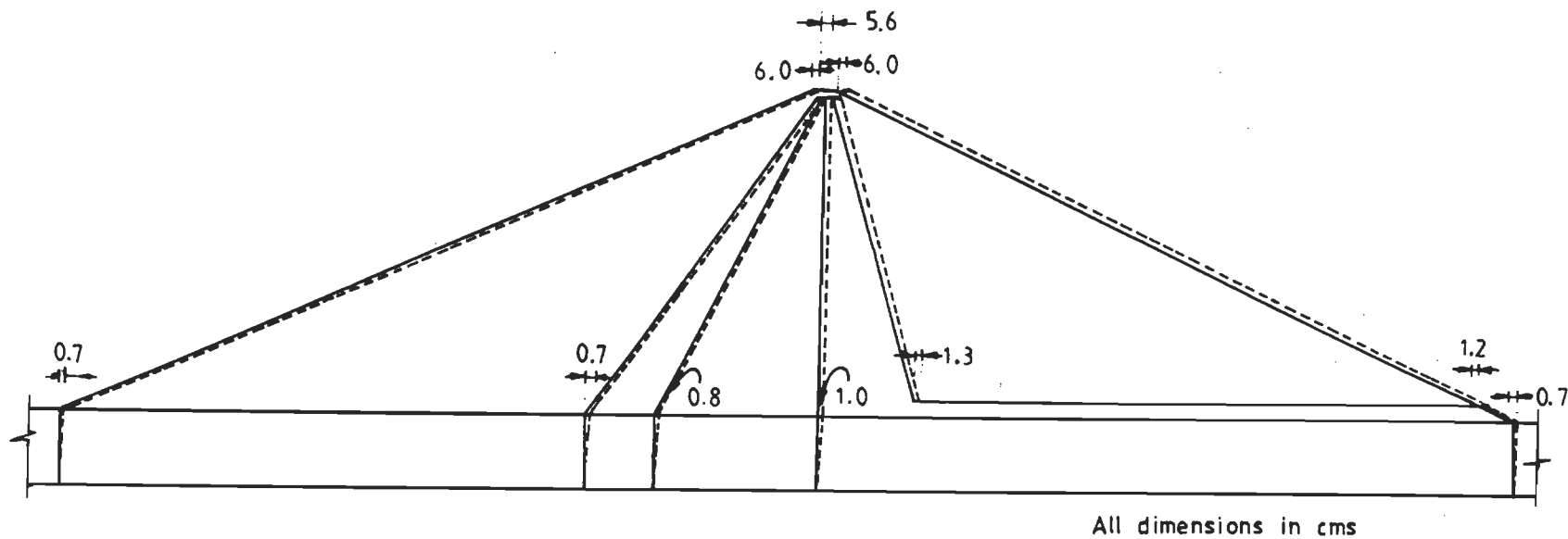


Fig. 8.181 Dam DC; Displacement Values at a few Locations; H-D Model; GM1

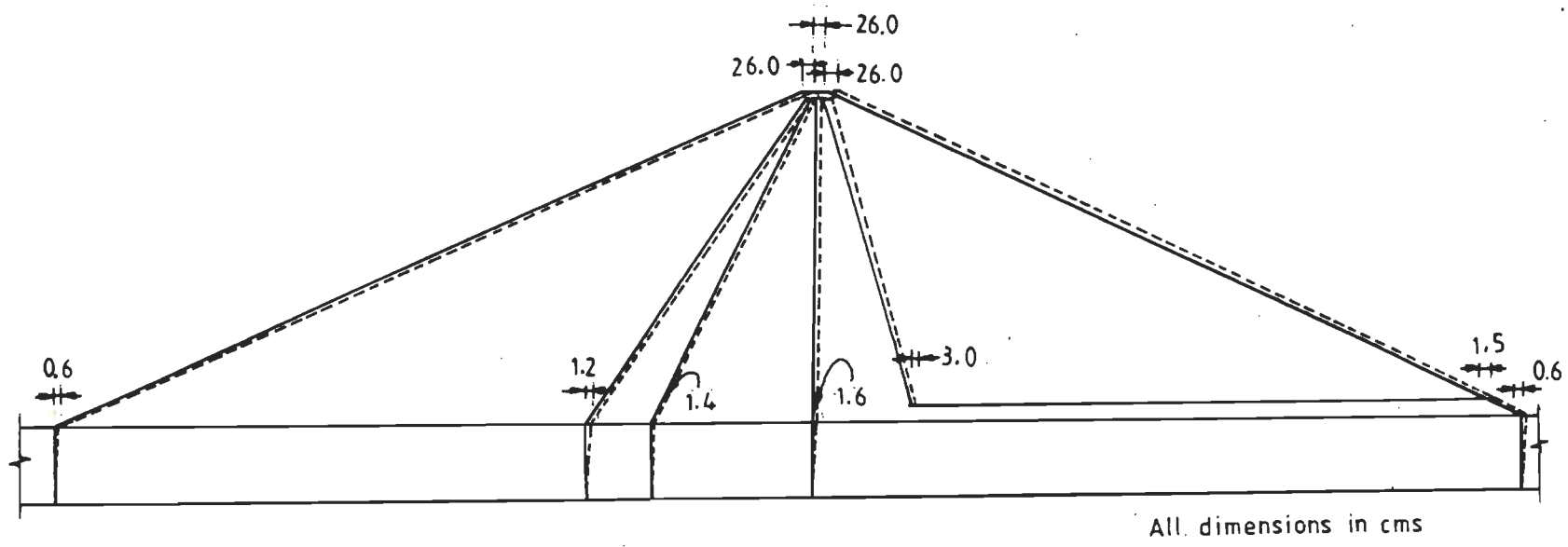


Fig. 8.182 Dam DC; Displacement Values at a few Locations; H-D Model; GM2

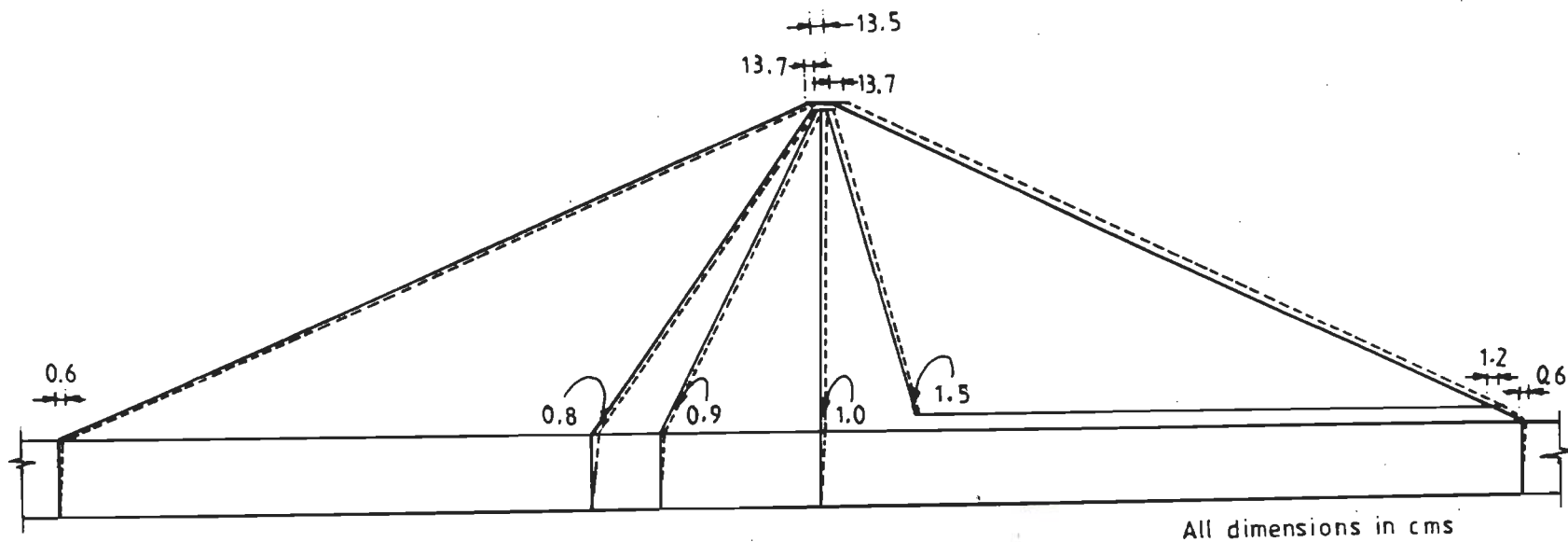
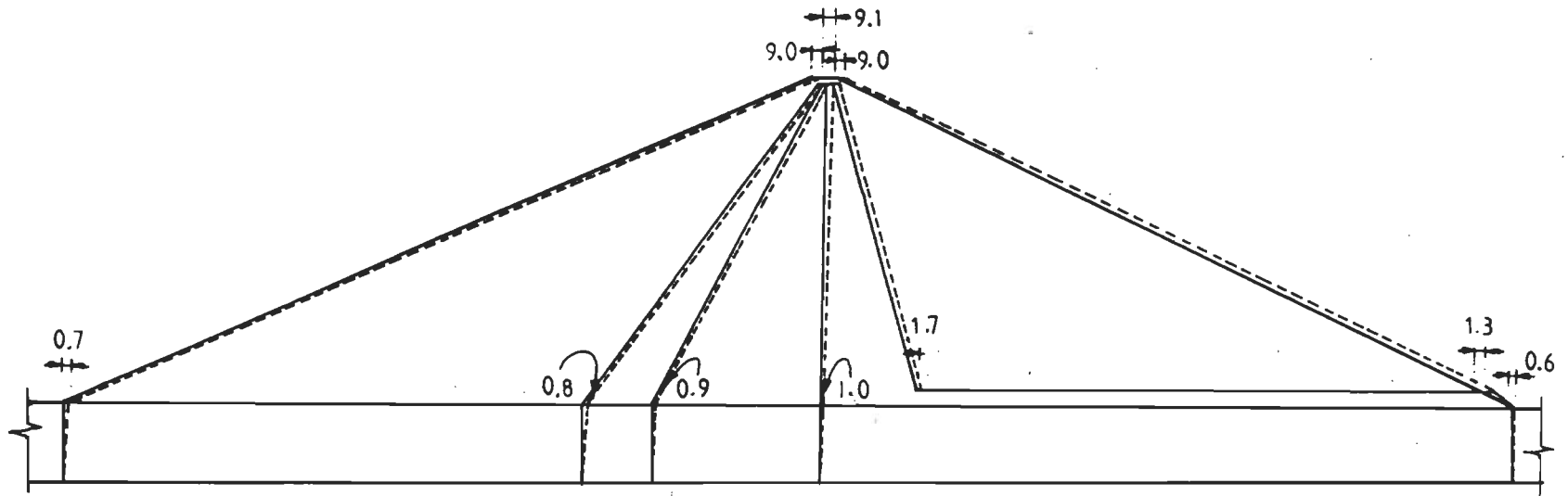


Fig. 8.183 Dam DC; Displacement Values at a few Locations; H-D Model; GM3



All dimensions in cms

Fig. 8.184 Dam DC; Displacement Values at a few Locations; S-I Method; GM1

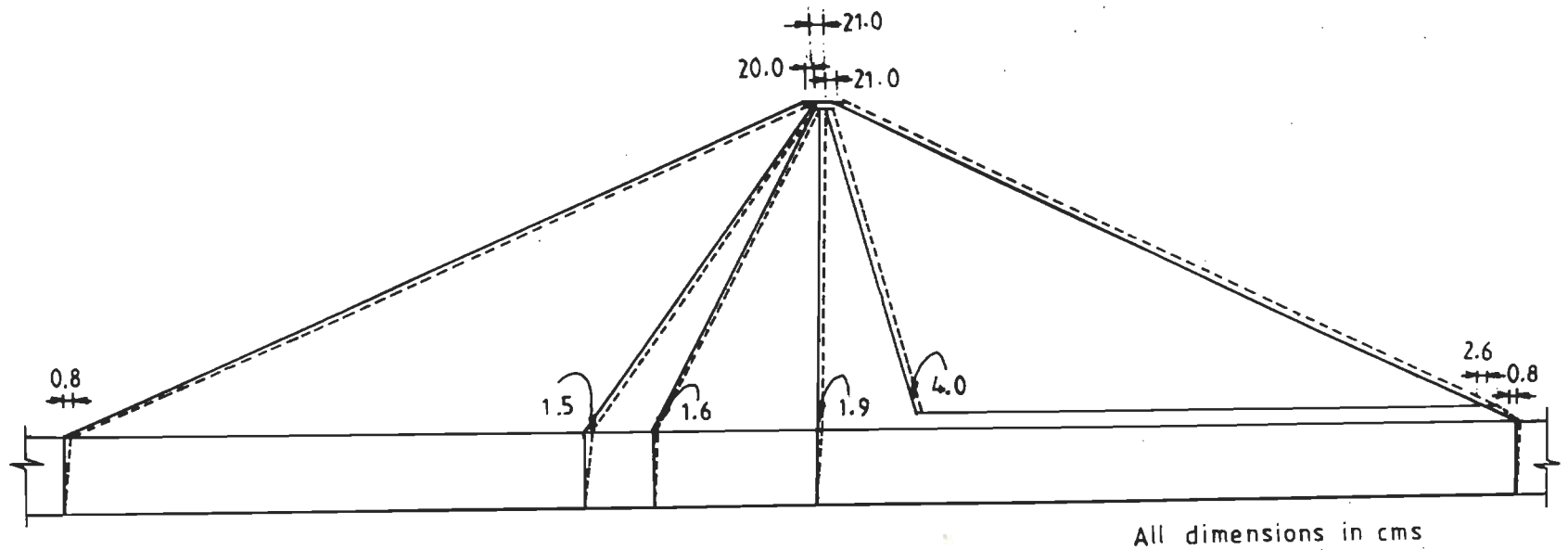


Fig. 8.185 Dam DC; Displacement Values at a few Locations; S-I Method; GM2

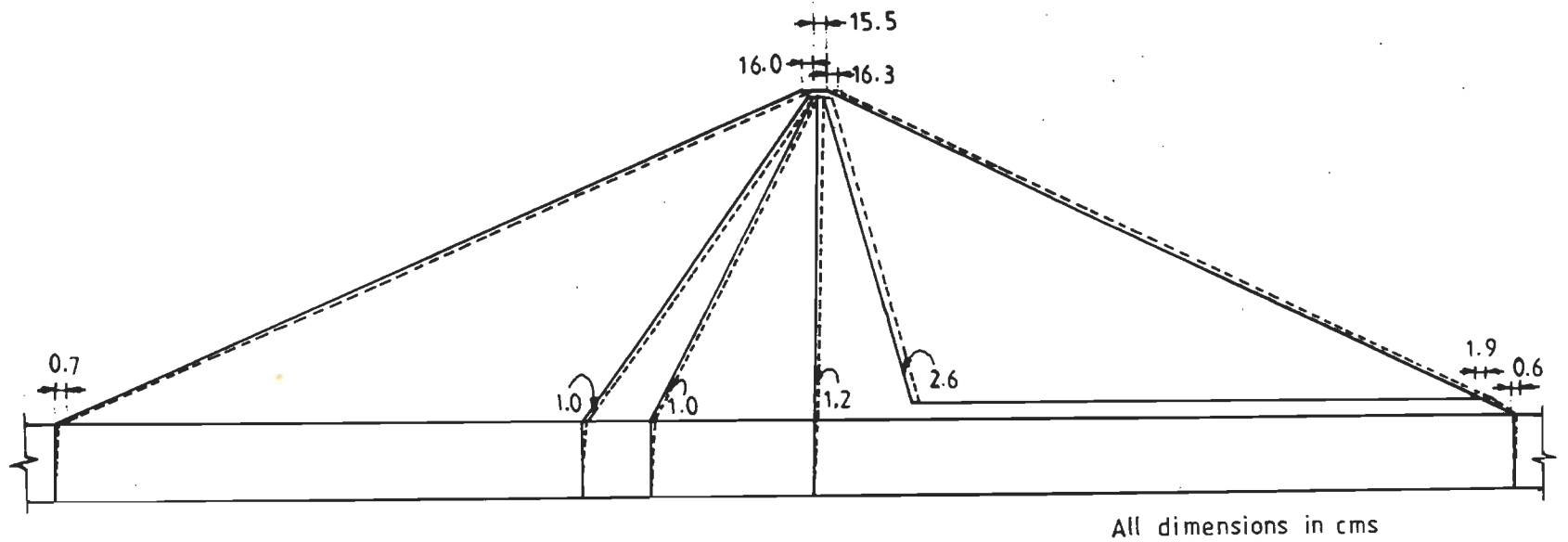


Fig. 8.186 Dam DC; Displacement Values at a few Locations; S-I Method; GM3

the base (nodes 13, 48, 223, 328 and 468) in the horizontal direction by the Ramberg-Osgood and Hardin-Drnevich models and the Seed-Idriss method shown in Figs. 8.67 to 8.81, corresponding to the synthetic accelerogram, it can be seen that lower acceleration values at the crest (node 13) are obtained than the acceleration values obtained at node 48. Out of these three methods of analysis, the acceleration values predicted by the Ramberg-Osgood model are larger than the values predicted by the Hardin-Drnevich model. However, the Seed-Idriss method gives the highest value of acceleration among the three methods of analysis.

At node 223 (approximately $0.75H$ from the base), Ramberg-Osgood and Hardin-Drnevich models yield time-history of acceleration with an appreciable degree of deamplification. Whereas, the Seed-Idriss method does not show such a phenomenon at node 223.

At node 328 (approximately $0.50H$ from the base), the time-history of acceleration plotted by all the three methods of analysis shows deamplification phenomenon. At node 468 (which is in the body of the foundation, along the axis), a very low degree of deamplification is noticed in the three methods of analysis.

Identically, the acceleration time-histories plotted corresponding to the vertical direction for the same five nodes, using the three methods of analysis (Figs. 8.82 to 8.96), corresponding to the synthetic accelerogram show the same distribution pattern with deamplification phenomenon. The vertical acceleration values are very low in

magnitude.

From the displacement time-histories plotted at the same locations, corresponding to the horizontal direction where acceleration time-histories have been computed, and shown in Figs. 8.97 to 8.111, in all the three methods of analysis, the Ramberg-Osgood model yields the highest values of displacement time-histories followed by the Seed-Idriss method. The Hardin-Drnevich model yields the lowest values of displacement time-histories. In all the three methods of analysis, the horizontal displacement is larger at the crest and decreases towards the base of the foundation.

The displacement time-histories plotted in Figs. 8.112 to 8.126 for the vertical direction show the same trend as the horizontal direction ones with very low values of displacement.

8.11.8.5 Time-history of shear stress

The time-histories of shear stress obtained at a few element centres, namely, at elements 63, 66 to 70, 132 to 135 and 198 to 201 are shown in the form of time-history plots in Figs. 8.127 to 8.168, corresponding to the artificial accelerogram for the three methods of analysis used.

It can be seen from Figs. 8.127 to 8.132 corresponding to elements 63 and 66 and in Figs. 8.145 to 8.147 corresponding to element 132 that the time-histories of shear stress are compressive in nature during the entire

duration of the accelerogram. In elements 67 to 70 (Figs. 8.133 to 8.144), the shear stress time-histories are tensile in nature showing that the base of the dam is prone to undergo excessive deformation in the event of a strong ground shaking possessing the characteristics of the synthetic earthquake. In the absence of cyclic triaxial shear stresses as determined from a laboratory testing schedule, the described failure criterion is qualitative only.

In elements 133, 199 and 200, the time-histories of shear stress are continuously changing (Figs. 8.148 to 8.150 and Figs. 8.160 to 8.165), between compressive and tensile stresses and the resulting equivalent uniform number of cycles are 4 to 6 only for the Ramberg-Osgood model and the Seed-Idriss method. However, in the Hardin-Drnevich model the number of equivalent uniform cycles are of the order of 1 to 2. The continuously varying cyclic shear stresses have been converted into equivalent uniform stress cycles by drawing straight lines in the positive and the negative directions, corresponding to 0.65 times the peak shear stress (τ_m) value (Carrera et al., 1979).

In elements 134 and 135 (Figs. 8.151 to 8.156), the shear stress history is only tensile in nature for the Ramberg-Osgood and Hardin-Drnevich models and in the Seed-Idriss method, they are mostly tensile and compressive between the time interval of 14 to 22 seconds duration. In element 134, the magnitude of compressive stresses are larger than that of the compressive stresses occurring in element 135.

In element 198 (Figs. 8.157 to 8.159), the time-history of shear stress is compressive in nature based on the Ramberg-Osgood and Hardin-Drnevich models and they are crossing the zero line of stress during a time interval of 6 to 15 seconds in the Seed-Idriss method of analysis.

In element 201, the Ramberg-Osgood model shows compressive stresses only to a very low extent between the duration of 20 and 24 seconds, as can be seen in Fig. 8.166. The Hardin-Drnevich model predicts only tensile stresses during the entire duration of the ground motion (Fig. 8.167) and the Seed-Idriss method yields tensile stresses of low magnitude and compressive stresses of large magnitude than the other two models (Fig. 8.168) predict at the same location. Thus, in the event of a strong ground motion which is similar to the artificial earthquake and with a peak ground acceleration of 0.25g, large tensile cracks are likely to occur at element 201, as per the predictions of the two models. Such predictions should be supplemented with the laboratory tested cyclic shear stress values, and in the absence of these laboratory data, predictions made are qualitative only. In Fig. 8.168, it can be seen that the Seed-Idriss method shows the presence of equivalent uniform stress cycles of the order of 1 to 2 and the other two models do not show the availability of any such equivalent uniform stress cycle.

8.11.9 Comments on the Analysis of Dam DC

Based on the detailed dynamic analysis of the 336 m high rockfill dam DC, including its foundation, using the three methods of analysis and the three different ground motions as base input motion the following conclusions are arrived at:

- 1 The crest acceleration is of the order of 0.17g, 0.33g and 0.32g by the Ramberg-Osgood model; 0.12g, 0.16g and 0.17g by the Hardin-Drnevich model and 0.32g, 0.37g and 0.36g by the Seed-Idriss method for the three ground motions, GM1, GM2 and GM3 respectively. The Hardin-Drnevich model gives the lowest values of acceleration and the Seed-Idriss method gives the highest values of acceleration.
- 2 In the acceleration response evaluation, from the base of the foundation to 0.50H of the dam DC, all the three methods of analysis yield nearly the same values of acceleration and identical distribution pattern for all the three ground motions. Between 0.50H and the crest of the dam the distribution of acceleration is different for the three ground motions and the three methods of analysis.
- 3 The upstream of the dam is more critical under the reservoir full condition when subjected to a strong ground shaking.
- 4 The foundation experiences higher values of acceleration than the body of the dam. Along the

axis of the dam, except at the crest and immediately below the crest, the computed acceleration values are of very low in magnitude. Similar observations have been made in the past by other researchers as well.

- 5 In all the three methods of analysis, the maximum value of shear strain is noticed at the same location which is at the top of the impervious core with an exception in the Hardin-Drnevich model for GM1 and GM2 ground motions. For all the three ground motions, the transition zone in the upstream experiences higher shear strain values than the downstream transition zone, demonstrating that the dam is more earthquake prone under reservoir full condition.
- 6 The dam DC reaches the threshold level of failure in the Ramberg-Osgood model and the Seed-Idriss method of analysis, corresponding to the postulated artificial accelerogram with the peak ground acceleration value of 0.25g. The Hardin-Drnevich model does not predict any similar failure criterion.
- 7 Among the three methods of analysis, the Ramberg-Osgood model yields intermediate values of acceleration and the largest values of shear strain. A reverse trend can be noticed when the Seed-Idriss method is adopted. The Hardin-Drnevich model yields the lowest values of acceleration at the crest and in the body of the dam and the lowest shear strain values, possibly due to the convergence towards a

larger value of damping, which is not experienced in practice.

- 8 The dam DC reaches the threshold level of failure for the artificial accelerogram as the base input motion with a peak ground acceleration value of 0.40g when the Ramberg-Osgood model has been adopted.
- 9 The highest value of the crest displacement of dam DC is obtained using the Ramberg-Osgood model corresponding to the artificial accelerogram. The Hardin-Drnevich model and the Seed-Idriss method respectively yield crest displacement values in the descending order corresponding to the same accelerogram. For the Taft earthquake record, the Ramberg-Osgood model predicts the highest value of displacement at the crest followed by the Seed-Idriss method and the Hardin-Drnevich model in sequence.
- 10 The acceleration time-histories obtained show deamplification in all the three methods of analysis and for all the three ground motions under the postulated peak ground acceleration value of 0.25g. Acceleration time-histories obtained in the vertical direction are of very low-magnitude.
- 11 The magnitude of the displacement time-histories of both the directions increase from the base towards the crest.
- 12 The number of equivalent uniform stress cycles observed are 4 to 6 in the Ramberg-Osgood model and

- in the Seed-Idriss method.
- 13 The continuously changing tensile and compressive shear stress time-histories demonstrate the likely occurrence of tensile cracks in the event of a strong ground shaking as that of the synthetic ground motion with a peak ground acceleration of 0.25g.
 - 14 The accuracy of the different computed parameters, such as the peak acceleration, crest displacement and maximum shear strain can be verified only in the event of a strong ground motion supplemented with detailed instrumentation, for recording the acceleration and other parameters.
 - 15 In the absence of laboratory determined cyclic shear stress data, the failure phenomenon based on the computed 5 to 15 percent shear strain criteria is qualitative only.
 - 16 The artificial waveform is much severe than the other two actually recorded ground motions.
 - 17 Below 0.25H from the base, the distribution of acceleration is more or less same in the three methods of analysis and for the three strong ground motions used.

8.12 CLOSURE

The case-history study of the 146 m high El Infiernillo Dam and nonlinear static and nonlinear dynamic analysis of two other rockfill dams of height 108 m and 336 m including their respective foundations which were proposed to

be built in earthquake prone areas in India, with moderate and severe seismicity respectively have been described in detail in this chapter. Under the static case, the pre-earthquake stresses of the three rockfill dams corresponding to the reservoir full condition have been evaluated using the nonlinear static model based on the hyperbolic law. The pre-earthquake stresses computed at the Gaussian sampling points have been used as the initial conditions for the nonlinear dynamic analyses. For the 336 m high dam, the different nonlinear static stresses have been presented in the form of stress contours. The minor and the major principal stress ratio is also plotted in the form of contours.

The nonlinear dynamic analyses of the three rockfill dams have been performed using the Ramberg-Osgood model, for curve fitting the strain dependent shear modulus values obtained after carrying out numerous field tests at different sites in India. For comparing the predictions made by the Ramberg-Osgood model, the dynamic analysis has also been carried out using the Hardin-Drnevich model and the very widely used Seed-Idriss method. In the dynamic analysis of each dam, three accelerograms with a total duration of 120, 38 and 30 seconds respectively have been used as the earthquake load vectors. These three ground motions cover a wide range of duration. Out of the three ground motions, the first and the last accelerograms were actually recorded ones and the second accelerogram was an artificially generated motion. For all the three strong ground motions, the peak

ground acceleration was of the order of 0.25g. This was done because of the peak ground acceleration value of the March 14, 1979, Mexico earthquake was also of 0.25g only.

The dynamic response of the El Infiernillo Dam as evaluated in the present thesis has been compared with the actually recorded/measured response due to the March 14, 1979, Mexico earthquake. It has been observed that the Ramberg-Osgood model as proposed in the present thesis predicts a behaviour which is in close agreement in comparison to the recorded/measured value of acceleration/displacement. The effect of a stiff foundation has also been studied in the case of the El Infiernillo Dam.

In the dynamic analysis of two rockfill dams, namely, DB and DC, the low-amplitude shear modulus has been computed based on the Nose's equation and the damping values for the first iteration has been adopted from the damping ratio curves proposed by Seed and Idriss.

For dam DC, time-histories of acceleration and displacement in the horizontal and vertical directions at a few selected nodes and time-histories of shear stress at a few element centres have been presented in the form of time-history plots using the Ramberg-Osgood model, Hardin-Drnevich model and the Seed-Idriss method.

The failure criteria in all the three dams has been estimated on the basis of 5 percent shear strain phenomenon. In this procedure, the El Infiernillo Dam reaches the threshold level of failure corresponding to the artificially generated accelerogram with a peak ground

acceleration of 0.40g. Dam DB does not reach the failure level corresponding to the peak ground acceleration values of 0.25g and 0.40g and in Dam DC only the top part of the core attains the threshold failure level under the postulated artificial ground motion with peak ground acceleration of 0.25g. However, a major portion of the dam DC experiences the threshold level of failure corresponding to the peak ground acceleration value of 0.40g. The reported failure criteria for all the three dams is of qualitative type due to the non-availability of laboratory tested cyclic shear stress data.

From the numerous results presented and the discussions made thereupon the following conclusions are drawn:

- 1 The pre-earthquake stresses are mostly compressive in nature.
- 2 The Ramberg-Osgood model as used in the present study predicts acceleration value and displacement value which are close to the actually recorded/measured values of acceleration/displacement in the case-history analysis of the El Infiernillo Dam. The Hardin-Drnevich model and the very widely used Seed-Idriss method do not yield either acceleration or displacement values which are close to the actual values.
- 3 In all the three dams analysed, the Hardin-Drnevich model predicts the lowest values of acceleration

possibly due to the utilization of damping of the order of 63.7 percent. The Ramberg-Osgood model and the Seed-Idriss method yield intermediate and the largest values of acceleration respectively.

- 4 The computed values of crest displacement do not follow the same trend as the distribution of acceleration.
- 5 The Hardin-Drnevich model shows deamplification phenomenon to a very great extent from the base of the dam (and not at the foundation) towards the crest. The Ramberg-Osgood model and the Seed-Idriss method also, show deamplification phenomenon in a descending order. The reason for the deamplification phenomenon is not known and needs to be investigated.
- 6 The Ramberg-Osgood model predicts the highest values of shear strain followed by the Seed-Idriss method and the Hardin-Drnevich model yields the lowest values.
- 7 The location of the maximum shear strain values obtained in the three methods of analysis for the three ground motions are same, which is at the top of the impervious core, with the exception of the Hardin-Drnevich model (corresponding to dam DC and ground motion GM1). The top portion of the impervious core is a zone with values of lowest stiffness, perhaps due to the transfer of load, from the adjacent transition zones, shell materials from the crest and the water pressure on the upstream face

of the core.

- 8 For convergence purposes, the Ramberg-Osgood and Hardin-Drnevich models need approximately 50 to 60 percent of the computer time required by the very widely used Seed-Idriss method. The reduction in computer time could possibly be due to the fact, that the former two models employ a functional expression for the strain dependent shear modulus and damping values at every time step, whereas, the Seed-Idriss method uses a limited number of digitized values as the modulus reduction factor and damping ratio.
- 9 The observed peak acceleration values are larger on the upstream face of the three dams than the corresponding elevations in the downstream, which demonstrates that the presence of a full reservoir makes a rockfill dam more disaster prone in the event of a strong ground shaking.
- 10 At any elevation above the top surface of the foundation in a horizontal plane intersecting the axis of the dam, the acceleration values along the axis are the lowest in comparison to the computed acceleration values along the upstream and the downstream slope surfaces. The reason for such low values of acceleration along the axis is not known and needs to be investigated.
- 11 The foundation experiences more acceleration values than the centre part of the dam.
- 12 Inclusion of a stiff foundation does not alter the

- response of a dam significantly.
- 13 The upstream filter zone experiences larger values of shear strain than the corresponding filter zone in the downstream. This again shows that the impounded water on the upstream makes a dam less stable against a strong ground shaking.
 - 14 Under the postulated peak ground acceleration of 0.40g using the artificial waveform and the Ramberg-Osgood model, the El Infiernillo Dam shows a small zone undergoing excessive deformation. Dam DB did not show any such behaviour and dam DC shows an appreciable region in the dam experiencing the threshold level of failure strain.
 - 15 In the absence of laboratory tested cyclic shear stress values, the established failure criterion based on a 5 percent shear strain value should be considered as qualitative only, subjected to a peak ground acceleration of any intensity.
 - 16 The dynamic response of a rockfill dam depends upon a few of the important parameters such as geometry, dynamic material properties and the characteristics of the input motion and the method of analysis adopted.
 - 17 Out of the three ground motions used for the dynamic analysis of the three rockfill dams, the artificially generated waveform is more severe than the other two actually recorded ground motions.

- 18 The number of equivalent uniform stress cycles observed are 4 to 6 in the Ramberg-Osgood model and in the Seed-Idriss method of analysis. The Hardin-Drnevich model does not predict the presence of equivalent uniform stress cycles.
- 19 The time-history of shear stress plot which is tensile in nature, is an indication of the likelihood of occurrence of tension cracks at that location, in the event of a strong ground shaking.
- 20 Out of the three methods of analysis the Ramberg-Osgood model is the best suited for the dynamic analysis of rockfill dams and for the simulation of nonlinear stress-strain characteristics of different soils. Also, the Ramberg-Osgood model is more economical than the very widely used Seed-Idriss method of analysis.

CONCLUSIONS AND RECOMMENDATIONS

9.1 GENERAL

Rockfill dams of height 250 m or more are increasingly being constructed in overseas countries and in India. In such tall rockfill dams due to increase in height, the confining pressure also increases appreciably and at this state the induced shear strain value reaches the failure limit, and the behaviour of the dam-materials is nonlinear. The dynamic response of the dam is based upon the strain dependent dynamic characteristics of the different materials constituting the dam. For a detailed dynamic response evaluation of a rockfill dam subjected to a strong ground shaking, the nonlinear stress-strain characteristics of the different materials constituting the dam should be considered in the analysis, based on elaborate experimental studies. The nonlinear stress-strain characteristics of the different soils should be simulated through an appropriate model. The selected model should be able to predict the dynamic nonlinear material behaviour, at large and failure levels of strain, and not at low or medium strain levels only. The nonlinear dynamic analysis of such high rockfill dams using the Ramberg-Osgood model to simulate the stress-strain characteristics, based on in-situ test to determine the

dynamic properties of various dam materials is rarely available in Geotechnical-Earthquake Engineering discipline. The dynamic analyses available till today have been performed mostly on hydraulic fill dams and rockfill dams of medium height of the order of 50 m to 150 m, and soil-structure interaction problems using the Hardin-Drnevich model, based upon the hyperbolic law or the Seed-Idriss method to account for strain dependent dynamic properties of sand and clay materials only. The existing literature on the dynamic analysis of very high dams of the order of 200 m or more is scanty. In these very limited cases of analysis, the ground motions used as the earthquake load vectors are a maximum of 60 to 70 secs. duration only. Any dynamic analysis that has been done for an earthquake accelerogram of duration 120 secs is not immediately available in the literature.

The Hardin-Drnevich model, based on two parameters, namely, shear modulus at low-amplitude strain level and shear strength of soils, predicts unreasonably very high value of damping at large and failure strain levels. The prediction of very large amount of damping, absolutely misleads the dynamic response of an earth structure or soil-structure interaction problem during the occurrence of a severe earthquake or a blast. The Seed-Idriss method which is based on tests carried out by different investigators yields low values of shear modulus and damping ratios in comparison with the actual tests.

In view of the afore mentioned limitations

different type of in-situ and laboratory tests have been carried out to determine the shear modulus of various soils, representing a rockfill dam. From the field tests, damping values have been determined at strain values ranging from low to medium values as a function of strain. Laboratory tests for determining the shear modulus have been conducted only, at large strain values. Using the field determined shear moduli of different soils, ranging between strain values of low to medium and then to large and failure levels, the modulus reduction curves have been obtained based on the Ramberg-Osgood model. Using the same model, the damping values have also been computed as a function of strain. Knowing the two important strain-dependent dynamic properties of different soils representing a rockfill dam, the case history study of the 146 m high El Infiernillo Dam has been carried out using the Ramberg-Osgood model. In the case history analysis, due to the very close agreement between the computed and the recorded/measured values of crest acceleration and displacement, by the Ramberg-Osgood model, two other rockfill dams of height 108m and 336 m, including their respective foundations have been analysed using the same model. Out of these two dams the former (108 m height) was proposed to be built in a region with moderate seismicity and the latter in a region with severe seismicity. Once the 336 m high dam is completed its construction, this dam would be one among the first ten tallest dams of the world. For the purpose of comparison, the dynamic analysis of all the three dams has been carried out using the Hardin-Drnevich model and

the very widely used Seed-Idriss method as well.

In the dynamic analysis, three different ground motions of total durations 120, 38 and 30 secs. have been used as the earthquake load vectors for each dam. Out of these three ground motions, the first ground motion was recorded recently in the North-Eastern Region of India, the second ground motion was an artificially generated and the last accelerogram adopted was recorded during the 1952, Kern County (Taft) earthquake. All the three ground motions have been normalized to a peak ground acceleration of 0.25g, because the intensity of the March 14, 1979, Mexico earthquake was also of 0.25g only.

For the dynamic response evaluation, the pre-earthquake stresses have been used as the initial conditions. These initial stresses have been computed using a computer program based on the finite element method with eight-noded isoparametric elements and reduced integration technique, developed in the present study, incorporating the nonlinear hyperbolic model accounting for volume change characteristics and considering the method of sequential construction. The dynamic analysis has been performed using a computer coding developed on the basis of the finite element method in the present work, incorporating the Ramberg-Osgood model, Hardin-Drnevich model and the very widely used Seed-Idriss method for modulus reduction and damping ratio curves. The dynamic analysis computer coding employs a step-by-step time integration scheme in the time domain with the capabilities of pre-processing.

A failure criteria evaluated on the basis 5 percent shear strain phenomenon is qualitative in nature due to nonavailability of laboratory determined cyclic shear stress values.

9.2 CONCLUSIONS

The significant conclusions drawn from the extensive studies carried out are presented in the following paragraphs.

9.2.1 Shear Modulus

9.2.1.1 Secondary time effects on shear modulus

- 1 Shear modulii determined in the laboratory for all the soils at the end of primary consolidation is larger than the shear modulus values determined without accounting for primary consolidation to take place.
- 2 The percentage increase in shear modulus due to secondary time effect is of the order of 3 to 28 percent or more depending on the type of soil and increases from coarse grained soil to fine grained soil.
- 3 The secondary time effect on shear modulus is negligible for soils having the mean grain diameter is more than 0.038 mm.

9.2.1.2 Relation between field and laboratory determined shear moduli

- 1 The ratio between field shear modulus and laboratory shear modulus at a common strain level called the disturbance factor is greater than 1.0 for the tested soils.
- 2 The field shear modulus curve cannot be arbitrarily obtained from the laboratory determined shear modulus.
- 3 The disturbance factor computed is a function of strain and increases as the value of strain decreases.
- 4 The value of the disturbance factor is larger when the shear modulus is determined without considering the primary consolidation.
- 5 The value of the disturbance factor is not a constant for all type of soils.

9.2.1.3 Prediction of in-situ high-amplitude shear modulus

- 1 The predicted value of in-situ high-amplitude shear modulus using the disturbance factor method, for a site consisting of dense sand is lower than the predicted values obtained by the arithmetic method and the percentage method.
- 2 To obtain the in-situ shear modulus value using the disturbance factor method, only the laboratory shear modulus and the associated value of shear strain are the two parameters needed.

9.2.2 Nonlinear Dynamic Stress-Strain Relationship

9.2.2.1 Ramberg-Osgood model

- 1 The Ramberg-Osgood model which is based on four parameters, namely, shear modulus at low-amplitude strain value and the shear strength corresponding to the low-amplitude shear modulus and the two constants, α and R gives a better fit to experimentally obtained values of shear modulus.
- 2 The Ramberg-Osgood model simulates the shear modulus and damping ratio as closely as possible to the actual value at large and failure strain levels.
- 3 The two constants of the Ramberg-Osgood model, α and R differs from soil to soil and assuming the dynamic properties of gravel and sand to be identical would mislead.
- 4 The Ramberg-Osgood model predicts a damping value of zero at which the modulus reduction curve (G/G_{\max}) is unity. This can be overcome by assigning the experimentally determined damping value at G/G_{\max} equal to unity or a very low value of damping of the order of 0.05.
- 5 The modulus reduction factors reported herein are generally larger than the values proposed by Seed and Idriss for sand and clay type of soils. For silty soils the obtained modulus attenuation curves are in good agreement with that of the curves proposed by Grant and Brown.

- 6 The Ramberg-Osgood model uses a functional expression for the shear moduli and damping ratios which is an essential requirement for a dynamic analysis based on a step-by-step time integration technique.

9.2.2.2 Hardin-Drnevich model

- 1 The Hardin-Drnevich model is based on two parameters, namely, the low-amplitude shear modulus and the shear strength of a soil at failure level.
- 2 At large strain levels the Hardin-Drnevich model tends to give intolerably large damping values of the order of 63.7 percent, which is not experienced in actual situation.
- 3 The Hardin-Drnevich model uses a functional expression for the shear moduli and damping ratios which is an essential requirement for a dynamic analysis based on a step-by-step time integration technique.

9.2.2.3 Seed-Idriss method

The Seed-Idriss method uses a maximum of 11 digitized values of shear modulus and damping ratios as a function of strain over a range of 10^{-4} to 10 percent. The Seed-Idriss method does not employ a functional expression for representing the dynamic soil properties.

9.2.3 Computer Programs

Two specific purpose computer codings, one for static sequential analysis, with material nonlinearity and the other for dynamic analysis in the time domain, incorporating two nonlinear models and one method using the finite element method based on the versatile eight-noded isoparametric element concept with reduced integration scheme have been developed. The following conclusion is drawn.

Two computer programs based on the finite element method with graphics pre-processing facilities have been developed and these programs have been applied to carry out the nonlinear static and nonlinear dynamic analysis of three rockfill dams. For two dams, the interaction of foundation has also been considered. The static nonlinear analysis computer program incorporates the hyperbolic model with volume change characteristics and construction sequence operations. The nonlinear dynamic analysis computer program incorporates the Ramberg-Osgood model, Hardin-Drnevich model and the Seed-Idriss method of modulus reduction curves and damping ratios.

9.2.4 Nonlinear Static Analysis

The following conclusions are arrived at, based on the nonlinear static analysis of the three rockfill dams corresponding to the reservoir full condition.

- 1 The phenomenon of arching, between the upstream

- 455
- shell, filter and the core materials has been observed in the analysis of the three dams.
- 2 The horizontal displacement increases towards downstream of the dam.
 - 3 The horizontal stresses are larger than the hydrostatic pressure, showing the dams are safe against hydraulic fracture.
 - 4 All the principal stresses are compressive in nature.

9.2.5 Nonlinear Dynamic Analysis

The nonlinear dynamic analysis of the three rockfill dams has been carried out under the full reservoir condition. In each case, the pre-earthquake stresses have been used as the initial condition. From the nonlinear dynamic analysis performed the following conclusions are arrived at.

- 1 In the case history analysis of the El Infiernillo Dam, the predicted values of crest acceleration and the crest displacement by the Ramberg-Osgood model are very close to that of the recorded and measured values of acceleration and displacement respectively, due to the March 14, 1979, Mexico earthquake. The differences in the computed values of acceleration and displacement are 2.8 percent less and 1.0 percent more respectively than the actually measured values. The Hardin-Drnevich model and the Seed-Idriss method of analysis do not predict any value that is nearest to the recorded/measured value. The Hardin-Drnevich

model and the Seed-Idriss method give the lowest and the highest values of acceleration and displacement respectively, which shows that the Ramberg-Osgood model is the best suited for the dynamic analysis involving nonlinear stress-strain characteristics of soils.

- 2 The Hardin-Drnevich model is unsuitable for dynamic analysis due to the convergence towards a very high value of damping at large strain levels.
- 3 The Seed-Idriss method gives very high values of acceleration and uneconomical.
- 4 The Ramberg-Osgood and Hardin-Drnevich models require less computer time due to lesser number of iterations than the Seed-Idriss method needs.
- 5 The degree of deamplification is the largest in the Hardin-Drnevich model followed by the Ramberg-Osgood model and the Seed-Idriss method in sequence.
- 6 The base of the dam, base of the foundation, upstream slope surface, and the crest experience more acceleration values than the body of the dam and the downstream slope surface.
- 7 The transition zone in the upstream shows higher values of shear strain than that the downstream transition zone.
- 8 The reservoir full condition is less stable in the event of a strong ground motion.
- 9 The El Infiernillo Dam attains the threshold level of failure, based on the 5 percent shear strain criteria

due to a peak ground acceleration of 0.40g. Dam DB does not show any such failure under the postulated peak ground acceleration values of 0.25g and 0.40g. Dam DC is likely to deform to a large extent, when subjected to an earthquake with a peak ground acceleration of 0.40g with the characteristics similar to that of the artificial earthquake.

- 10 Due to nonavailability of laboratory tested cyclic shear stress data the established failure criteria based on the 5 percent shear strain phenomenon for the three dams is qualitative only.
- 11 At the top of the impervious core larger values of shear strain are noticed than any other location.
- 12 All the three methods of analysis identically predict the same location, namely, the top of the impervious core as the weakest zone of deformation.
- 13 The number of equivalent uniform stress cycles is 3 to 4 in the Ramberg-Osgood and Hardin-Drnevich models and 4 to 5 in the Seed-Idriss method of analysis, in the case of dam DC.
- 14 The vertical acceleration component is negligible in comparison to the value of the horizontal acceleration.
- 15 The time-history of shear stress which is tensile in the whole duration of the input motion predicts the likelihood of occurrence of tension cracks when subjected to a strong ground motion.

- 16 The failure criteria of a rockfill dam should be established on the basis of some important parameters, such as the shear strain, displacement and acceleration and not on the basis of the absolute value of the acceleration alone.
- 17 The synthetic waveform is more stronger than the other two actually recorded accelerograms.

9.3 SUGGESTIONS FOR FURTHER WORK

9.3.1 Dynamic Properties of Soils

- 1 At large confining pressure the shear modulus and damping ratio are influenced to a greater extent by the number of cycles of load application and this should be investigated.
- 2 The degradation of shear modulus may be studied.
- 3 More field and laboratory tests should be carried out at medium strain levels to establish the disturbance factor as a function of strain, other than the large strain levels.
- 4 Shear modulus and damping ratio of boulder or rock materials should be established as a function of strain at high-amplitude values in the field and in the laboratory.
- 5 For all type of soils the Ramberg-Osgood model parameters should be evaluated.

9.3.2 Nonlinear Static Stress-Strain Models

The minor principal stress dependent nonlinear

elastic stress-strain model, based on the hyperbolic law, which has been used in the present thesis to compute the pre-earthquake stresses, possesses inherent limitations as listed below.

- 1 The hyperbolic model is suitable for the analysis of stresses and movements prior to failure, and cannot be applied to earth masses during and after failure. This model is not applicable when plastic deformation is present.
- 2 The hyperbolic relationship does not account for volume changes due to the variation in shear stress or shear dilatancy.
- 3 The hyperbolic model can predict deformations in dilatant soils, such as dense sands under low-confining pressure only.
- 4 The different parameters involved in the hyperbolic model are difficult to determine in the laboratory and these parameters are not fundamental soil properties, but only values of empirical coefficients, which represent the behaviour of the soil under a limited range of conditions.
- 5 The model is sensitive to variation of the soil characteristics and gives a schematic representation of real behaviour.
- 6 A small relative error in the intensity of stresses can lead to large variations of the principal stress ratio.

Thus investigations for an improved stress-strain model is essential.

9.3.3 Nonlinear Dynamic Stress-Strain Model

- 1 Loading, unloading and re-loading sequences should be included in the analysis using the Ramberg-Osgood model combined with the Masing Criteria.
- 2 One particular problem associated with the rockfill dam is the tendency for crushing and breakage at points of inter-granular contact, which leads to decrease in volume. In saturated materials stress is transferred to the pore water and the effective stress and the strength are reduced. In view of this, investigation should be conducted for a mathematical model taking explicitly into account the pore pressure as well as the plasticity of the material in the stress-strain relationship.

9.4 SIGNIFICANT CONTRIBUTIONS

In the present work, the dynamic response evaluation of three rockfill dams including the widely instrumented El Infiernillo Dam subjected to three different ground motions of widely varying total durations, based on the Ramberg-Osgood, Hardin-Drnevich models and the Seed-Idriss method have been studied in great detail. The significant contributions made in the accomplishment of this thesis are:

- 1 Two types of disturbance factors as a function of strain, one corresponding to the end of primary consolidation and the other corresponding to the before the start of primary consolidation have been proposed. Using the disturbance factors corresponding to the end of primary consolidation case, in-situ high-amplitude shear modulus of a particular site consisting of dense sand has been predicted without performing field tests to determine the value of shear modulus at that site.
- 2 Ramberg-Osgood model parameters have been evaluated for four different type of soils, based on extensive in-situ tests carried out in India. This is one of the pioneering investigation in India.
- 3 Two different computer programs, one for nonlinear static analysis and the other for nonlinear dynamic analysis have been developed based on the versatile eight-noded isoparametric elements and reduced integration technique.
- 4 The nonlinear static and nonlinear dynamic analysis of the three rockfill dams based on the strain dependent shear moduli and damping, and using three different methods of analysis and subjected to three different ground motions is one of the first study carried out in India.

9.5 MISCELLANEOUS

9.5.1 Shear Wave Velocity in Rockfill Dams

The shear wave velocity of different materials used in the analysis of two dams is based upon the method proposed by Nose and his co-workers, after carrying out extensive prototype vibratory tests on three existing rockfill dams in Japan, of medium height of the order of 100 to 150 m only. The validity of the Nose's method should be verified by conducting detailed in-situ vibratory tests on high rockfill dams of height more than 200 m or so.

9.5.2 Shape of Valley

In most of the analysis performed, the shape of the foundation considered is rectangular only. When the valley is narrow, in which due to construction of a high rockfill dam, transfer of load would take place to either sides of the valley. In such cases, the influence of different valley shapes needs to be investigated.

9.5.3 Three-Dimensional Analysis

The very widely used two-dimensional (plane strain) analysis of earth and rockfill dams is applicable for dams with large crest length to height ratio. A two-dimensional analysis does not consider the cross-valley movements. For a detailed study of the stresses during a strong ground shaking of a rockfill dam, three dimensional analysis needs to be carried out.

REFERENCES

- 1 Abdel-Ghaffar, A. M. and Scott, R. F. (1978), "An Investigation of the Dynamic characteristics of an Earth Dam," Report No. EERL: 78-02, Earthquake Engineering Research Laboratory, California Institute of Technology, August, 200 p.
- 2 Abdel-Ghaffar, A. M. and Scott, R. F. (1979), "Analysis of Earth Dam Response to Earthquakes," Journal of Geotechnical Engineering Division, Proceedings, ASCE, Vol. 105, GT12, Paper 15033, December, pp. 1379-1404.
- 3 Adams, J. (1981), "Earthquakes, Landslides and Large Dams in New Zealand," Bulletin of the New Zealand National Society for Earthquake Engineering, Vol. 14, No. 2, June, pp. 93-95.
- 4 Afifi, S. S. and Woods, R. D. (1971), "Long-Term Pressure Effects on Shear Modulus of Soils," Journal, Soil Mechanics and Foundation Division, ASCE, Vol. 97, No. SM10, pp. 1445-1460.
- 5 Afifi, S. S. and Richart, F. E., Jr. (1973), "Stress-History Effects on Shear Modulus of Soils," Soils and Foundations, Vol. 13, No. 1, pp. 77-95.
- 6 Aisiks, E. G. and Tarshansky, L. W. (1968), "Soil Studies for Seismic Design of San Francisco Transbay Tube," Vibration Effects of Earthquakes on Soils and Foundations, ASTM STP 450, Special Technical Publication, American Society for Testing and Materials.
- 7 Alberro, J. (1972), "Stress-Strain Analysis of El Infiernillo Dam," ASCE Speciality Conference on Performance of Earth and Earth Supported Structures, Purdue University, June.
- 8 Alonso, L., Prince, J. and Hauskov, J. (1980), "General Characteristics of the 14 March 1979 Earthquake," Centro Editorial de la Commission Federal de Electricidad, Rodano, Mexico, pp. 27-31.
- 9 Ambrassey, N. N. (1960a), "On the Shear Response of a Two-Dimensional Truncated Wedge Subjected to an Arbitrary Disturbance," Bulletin of the Seismological Society of America, Vol. 50, No. 7, January, pp. 45-60.

VITA

Subramaniam Suppiah was born in Kandy, Sri Lanka and passed the G. C. E. (O/L) Examination. He graduated from the Government College of Technology, Coimbatore (Tamil Nadu) in B. E. (Civil) and the Master's Degree in Earthquake Engineering, at the Roorkee University, Roorkee (U. P), India. He was in the faculty of the Earthquake Engineering upto 1985 and he is presently working as a Principal Systems Analyst in the Computer Aided Design Group, National Informatics Centre, New Delhi, India.